DINITROGEN FUNCTIONALIZATION: EXPLORING DINITROGEN CLEAVAGE AND NITROGEN-CARBON BOND FORMING REACTIONS WITH GROUP 4 METALLOCENE COMPOUNDS.

A Dissertation

Presented to the Faculty of the Graduate School

of Cornell University

In Partial Fulfillment of the Requirements for the Degree of

Doctor of Philosophy

by

Donald John Knobloch

January 2011

DINITROGEN FUNCTIONALIZATION: EXPLORING DINITROGEN CLEAVAGE AND NITROGEN-CARBON BOND FORMING REACTIONS WITH GROUP 4 METALLOCENE COMPOUNDS.

Donald John Knobloch, Ph. D.

Cornell University 2011

A family of zirconocene and hafnocene compounds bearing side-on bound dinitrogen ligands were prepared and studied for their capability to promote a variety of nitrogen-carbon bond forming reactions. Most notably, these N_2 compounds underwent N-N cleavage coupled with C-N and C-C bond formation upon addition of excess carbon monoxide, forming unprecedented oxamidide complexes. For each zirconium example dissociation of N_2 and formation of the corresponding dicarbonyl species competes with N-N cleavage. For chiral *ansa*-metallocene examples, two stereoisomeric oxamidide products were observed in a ratio dependent on the pressure of CO added. In all cases, protonolysis liberated free oxamide, demonstrating synthesis of a useful organic product directly from N_2 and CO. For the *ansa*-hafnocene, observation and isolation of a bridging isocyanate species at short reaction times prompted a kinetic study of the mechanism for oxamidide formation. Kinetic and isotopic exchange studies are consistent with a mechanism whereby N_2 cleavage is fast and precedes C-C bond formation. When stoichiometric CO was added to the hafnocene N_2 compounds, new products arising from N-N cleavage coupled with C-H activation of a cyclopentadienyl substituent were observed, suggesting the intermediacy of a μ-nitride species. This reactive intermediate was also intercepted

with added dihydrogen and terminal acetylenes. The hafnocene oxamidide products were elaborated by the addition of various heterocumulenes, alkyl halides, and silanes resulting in new nitrogen-carbon or nitrogen-silicon bonds. Subsequent protonoylsis of the functionalized hafnocene oxamidato species liberated the corresponding substituted oxamides in high yield. In addition to CO-induced N_2 cleavage, other methods of N_2 functionalization were also explored. Addition of two equivalents carbon dioxide to *ansa*-metallocene dinitrogen compounds resulted in selective insertion into each metal-nitrogen bond, forming C_2-symmetric *N*,*N*'-dicarboxylated hydrazido compounds. These compounds could be elaborated by the addition of trimethyliodosilane or methyl triflate to form additional N-C or N-Si bonds, and protonolysis released the corresponding carboxylated hydrazines. Finally, for one hafnocene dinitrogen compound, methyl triflate addition resulted in formation of a monomeric hafnocene diazenide species arising from direct alkylation of coordinated N_2. Further exposure to methyl triflate resulted in additional N-C formation, furnishing a rare triflate hafnocene hydrozanato compound.

BIOGRAPHICAL SKETCH

Donald Knobloch was born and raised in Greensburg, PA. Donald began manipulating matter at an early age as an avid fan of Lego building blocks, often discarding the included recipes and crafting the wild products of his imagination instead. He attended elementary, middle, and high school at Greensburg Salem School District. During his high-school chemistry class he instantly fell in love with chemistry due to the hands-on nature of the subject, and of course for the opportunities it granted for creating explosions under the auspices of the scientific method. He was also captivated by the prospect of, as one chemist put it perfectly, "bringing into existence new molecules and knowledge."[*] Despite a childhood utterly consumed by video games, street hockey and rock and roll music, Donald managed to graduate high school with highest honors, and was also awarded a scholarship to Saint Vincent College in Latrobe, PA, which he attended in the fall of 2002.

At St. Vincent, Donald gained a valuable chemistry foundation imparted by a department of talented professors, most notably Dr. David Vohs, who introduced him to the glory of organometallic chemistry. Donald graduated from St. Vincent summa cum laude with a B.S. in Chemistry in May 2006. The countless unforgettable experiences he enjoyed during his college years at SVC were bookended by two especially consequential events: the chance encounter with a beautiful girl who would later become his wife, and the (admittedly on-a-whim) decision to attend Cornell University for graduate school.

In hindsight he could not be more grateful for this decision. It was at Cornell where his study of chemistry, and in particular his research career, began in earnest.

---

[*] Cummins, C. C. *Angew. Chem. Int. Ed.* **2009**, *48*, 845.

Under the supervision of Professor Paul Chirik, Donald studied dinitrogen functionalization with early transition metal compounds. After a fruitful and fulfilling 4.5 years of intense education and research, culminating in the production of the manuscript before you, Donald obtained his PhD from Cornell in December 2010 with the distinction of departmental thesis of the year.

Upon graduating Donald chose to respectfully depart from the ivory tower of academia (although he couldn't escape the harsh winter climate) to begin an industrial position as a synthetic chemist for the Lubrizol Corporation in Wickliffe, OH. Donald is happily married to the same beautiful girl, and together they eagerly await the arrival of their first child. He is also still a sucker for Legos.

John and Joan Knobloch

Margaret Knobloch

You may not understand a word of this

But you are in no small way responsible for it

ACKNOWLEDGMENTS

Many people whom I am thankful for have contributed directly or indirectly to the creation of this manuscript. First, I thank my advisor, Professor Paul Chirik, for the opportunity to conduct research in his group. When I joined in 2006 I had virtually no previous synthetic chemistry experience and little knowledge of the organometallics field, but Paul's passion for research coupled with his concern for his students' development naturally drew me to the group. Over the past 4.5 years I have learned an incredible amount from Paul about chemistry, laboratory technique, data analysis, scientific writing, work ethic and professionalism. I have grown as a scientist more than I could have ever imagined, and for that he has my sincerest gratitude. In addition I thank Paul for procuring the necessary financial resources through grants from the U.S. Department of Energy (DE-FG02-05ER15659) and the Frasch Foundation, administered by the American Chemical Society.

I would also like to thank my other committee members, Professor Pete Wolczanski and Professor Stephen Lee. In particular, I thank Pete for his seemingly limitless knowledge of inorganic and organometallic chemistry, and for imparting to me a small fraction of that knowledge through his skillful lecturing. I also thank Pete for many enlightening Lit Lunch sessions, and for handily solving the research-related problems that had me stumped for weeks or even months prior. I thank Stephen Lee for offering a unique perspective to my research and for showing me new ways to think about fundamental concepts in chemistry during the time I worked as his TA.

I am extremely grateful for those who laid the foundation for and/or contributed to the projects discussed in this thesis: especially Dr. Wes Bernskoetter, Dr. Tamara Hannah, Dr. Jaime Pool, Dr. David Benito Garagorri, and Hannah Toomey. I thank Wes in particular for helpful insights and for putting up with my

pestering e-mails over the years.

Many other people have helped to make this manuscript a reality and are deserving of acknowledgment. Dr. Emil Lobkovsky collected data for and solved the X-ray crystallographic structures presented in this work. My thesis would be pretty wimpy without them and I am very grateful for his efforts (and also for putting up with the many duds, "porcupines", shards of glass, and other non-diffracting material that I brought him). Many thanks to Ivan Keresztes and Tony Condo for their expertise in NMR spectroscopy, for helping me devise and setup many of the NMR experiments, and especially for help with data interpretation. I must thank Dave Wise, a phenomenal glass blower, for the construction of (and the many subsequent repairs of) our custom vacuum lines and for fixing countless snapped, dropped, chipped, exploded, or otherwise broken J. Young NMR tubes and other assorted pieces of glassware. I also thank Dave Neish for helping to make the transition between lab spaces a smooth one.

Of course I could not have made it through without such a fine cohort of colleagues along the way. To all of my labmates past and present, especially Aaron, Kevin, Sarah, Jon, Andrew, Crisita, Doris, Mandy, Scott, Chantal, Bastian, and Carsten: Thank you for all of the support and plenty of memorable moments throughout the years and best of luck to those of you at Princeton. To my classmates Aaron and Sarah, a special thanks for helping me survive Pete's classes and for setting the research bar so high that it constantly kept me motivated to strive harder. To my box-mates Kevin and Andrew, I thank you for the camaraderie and the many laughs, even if the humor did sink to a high-school crudeness level at times… okay, pretty much all of the time. Whenever Foreigner plays on the radio I will always think of you guys.

Doris, thank you for training me in the ways of Group 4, and for the many

helpful discussions over the years. Scott, you're carrying the Group 4 torch now, and I have no doubts that you will be highly successful doing unspeakable things to dinitrogen. I'm also sure you'll experience as much joy as I have in disposing the mercury waste (or do they have a special drain for that at Princeton?). Carsten, thanks for the calculations and EPR simulations as well as various thoughtful discussions and the ORCA crash course.

Most importantly, I would like to acknowledge those truly responsible for guiding me to this point: my parents and my wife. As long as I can remember my parents have pushed me to succeed and provided continuous support and love. They taught me through both words and actions that there is simply no substitute for hard work, and I hope that is something that is reflected in this manuscript and the degree it represents. I really cannot thank them enough for their support and dedication to me. I also must thank my dear wife Margaret, for her compassion, love, and sacrifice, which were invaluable during this journey. She has offered unconditional support every step of the way; she was there to celebrate the small victories and to pick me up after the epic failures. Now it's my turn to return the favor as we get ready to welcome Eleanor into the world. Finally I thank the rest of my family and my friends for their support and encouragement, and for helping to keep life in perspective as I toiled away in the laboratory. I am very blessed to have such an amazing network of support. As I prepare to take the plunge into the real world, I can only hope that my growth as a professional scientist continues at the same pace and caliber that it has over the past 4.5 years at Cornell. Although, a little more sleep would be nice, too!

TABLE OF CONTENTS

Chapter 2: CO-Induced N_2 Cleavage, Part II: Coupling Dinitrogen Cleavage to Hydrogenation, Intra- and Intermolecular C-H Bond Activation, and CO Deoxygenation

Chapter 3: CO-Induced N_2 Cleavage, Part III: Functionalization of Hafnocene Oxamidide Complexes Prepared from Carbon Monoxide-Induced Dinitrogen Cleavage

LIST OF FIGURES

LIST OF TABLES

CHAPTER 1

CO-Induced N_2 Cleavage, Part I. Dinitrogen Functionalization by Carbon Monoxide Promoted by a Family of Group 4 Metallocene Compounds.*

Abstract

Several zirconocene and hafnocene complexes bearing side-on bound dinitrogen ligands underwent N-N cleavage coupled with C-N and C-C bond formation upon addition of excess carbon monoxide, forming unprecedented oxamidide complexes. In each zirconium example, dissociation of N_2 and formation of the corresponding dicarbonyl species was competitive with oxamidide formation, highlighting the importance of the activation of the N_2 ligand. With *ansa*-metallocenes, two oxamidide stereoisomers were observed in a ratio dependent on the pressure of CO added; lower pressure (~1 atm) favored a C_1 symmetric isomer whereas higher pressure (~4 atm) favored a C_2 symmetric isomer. For the *ansa*-hafnocene, an intermediate species was observed at short reaction times and low (< 10 ºC) temperatures, prompting a study of the kinetics of oxamidide formation. Based on the kinetics and spectroscopic data, as well as isotopic exchange studies, a mechanism was proposed whereby N_2 cleavage follows insertion of a single equivalent of CO to form a transient μ-nitrido intermediate. Rapid trapping by a second equivalent of CO leads to an observable μ-(NCO) intermediate. Rearrangement and C-C bond formation form the final oxamidide product.

* Portions of this work were taken with permission from: (a) Knobloch, D. J.; Lobkovsky, E.; Chirik, P. *Nature Chem.* **2010**, *2*, 30. (b) Knobloch, D. J.; Lobkovsky, E.; Chirik, P. J. *J. Am. Chem. Soc.* **2010**, *132*, 10533.

Introduction

Elemental nitrogen, N_2, is an attractive synthon due to its atmospheric abundance, non-toxicity and its utility as a versatile N-atom source for a variety of chemical applications ranging from fertilizers to materials to pharamaceuticals.[1] However, its strong, non-polar bond (225 kcal/mol) poses significant challenges from a synthetic perspective and N_2 is typically resistant to reduction and functionalization.[1,2] While dinitrogen fixation occurs in nature *via* nitrogenase enzymes, virtually the only industrial process that utilizes dinitrogen as a reagent is the Haber-Bosch process for ammonia synthesis, which supports approximately 40% of the world's population through fertilizer production.[3,4] This process, which combines N_2 and H_2 in the presence of a multiple-component iron-based catalyst, has been in use—and nearly unchanged from its original form—for the past century.[4,5] In addition to its application in synthetic fertilizers and explosives, Haber-Bosch ammonia is the primary nitrogen source for many nitrogen-containing organic targets of the materials, commodity chemical, and pharmaceutical industries.

Despite its widespread use, the Haber-Bosch process suffers from extreme temperature and pressure requirements.[6] Furthermore, while dinitrogen is an abundant and readily accessible feedstock, the hydrogen required for the process is predominantly produced via steam reformation of methane and the water gas shift reaction, thus linking industrial ammonia production to fossil fuel availability and prices.[3,7] The prospect of nitrogen-carbon bond formation directly from dinitrogen and small organic molecules is attractive given its potential independence from both Haber-Bosch ammonia synthesis and the large fossil fuel requirements of hydrogen production. Several fundamental N_2 fixation alternatives have been the subject of intense investigations in the past few decades.[8]

Carbon monoxide, like N_2, contains a strong triple bond of 257 kcal/mol (the strongest known in chemistry), and is widely used as an industrial gas in processes such as hydroformylation, the Monsanto acetic acid synthesis, and the Fischer-Tropsch hydrocarbon synthesis.[9] Although CO is primarily derived from coal, tying it to the fossil fuels market, it is an attractive feedstock due to its abundance and its potential for use in both C-N bond forming reactions as well as CO homologation reactions. During the past few decades, investigations by Cloke[10,11] and Evans[12] have demonstrated the ability of f-block metal sandwich complexes to promote homologation of carbon monoxide, forming bridging deltate $[C_3O_3]^{2-}$, squarate $[C_4O_4]^{2-}$, and ketenecarboxylate $[O_2CCCO]^{2-}$ dianions under mild conditions (Figure 1.1).[13]

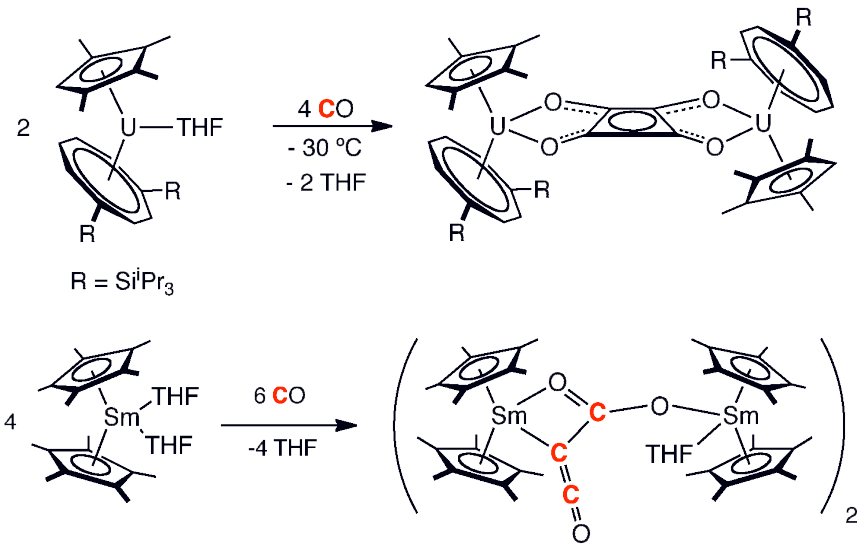

Figure 1.1. Examples of CO homologation reported by Cloke (top) and Evans (bottom)

Examples of ligand-induced N-N cleavage have also emerged in recent years. Fryzuk reported treatment of an unusual side-on, end-on tantalum dinitrogen complex with boranes, silanes, and alanes resulted in N_2 cleavage and yielded new tantalum

imides and nitrides.[14] Carbonylative cleavage of N-N bonds (not directly from N_2) has also been observed (Figure 1.2). Evans reported in an early example of samarocene-promoted homologation of CO coupled with N-C bond formation and cleavage of the N=N bond in azobenzene.[15] Bergman[16] and Gade[17] have reported a number of examples in which exposure of early metal hydrazides to CO resulted in N-N cleavage concomitant with N-C formation. Together these reports demonstrate the susceptibility of weakened N-N bonds to undergo reactions with small substrates, especially CO, to form oxamidate, terminal isocyanate, and other ligands resulting from new N-C bond formation (Figure 1.2).

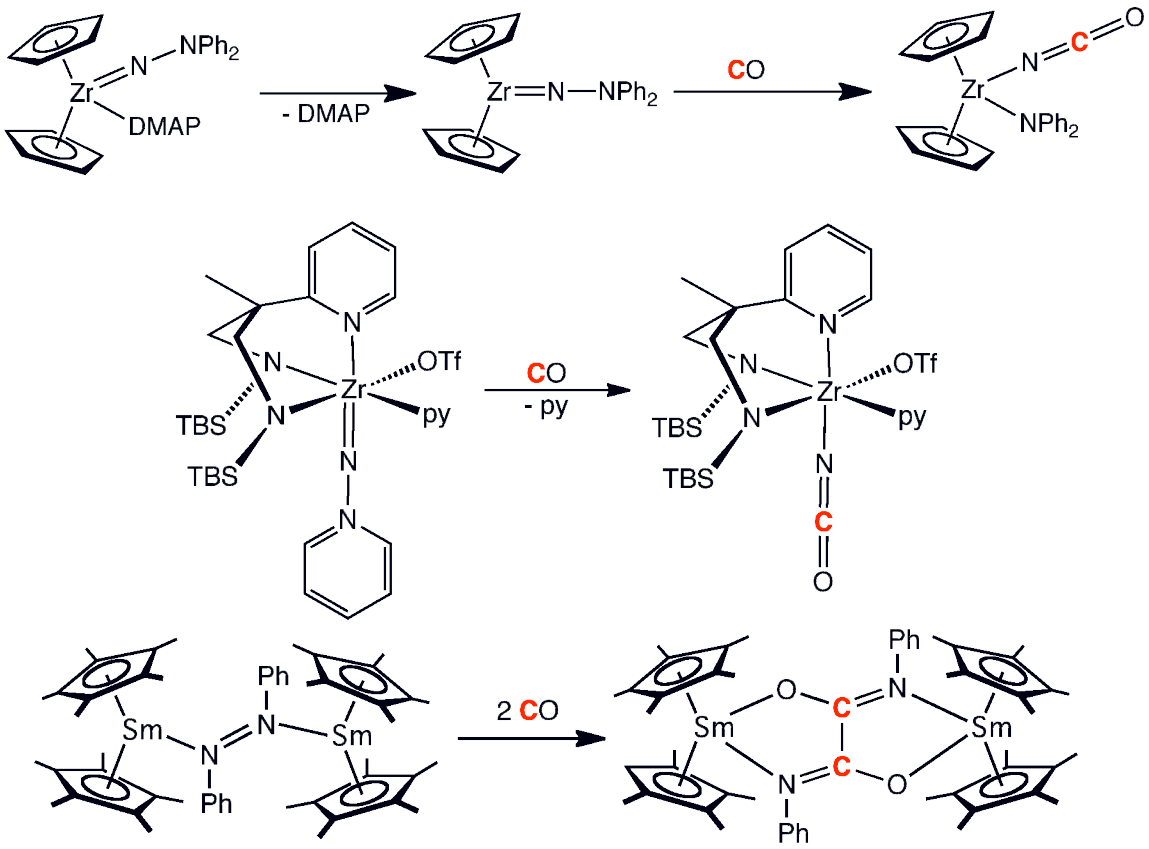

Figure 1.2. Examples of CO-induced N-N cleavage by Bergman (top), Gade (center), and Evans (bottom).

Transition metal dinitrogen complexes offer great potential for N_2 functionalization with a variety of small molecule substrates.[18,19] In particular, group 4 metallocene complexes synthesized in our laboratory are well suited for transformations involving N-C formation due to their side-on bound, highly activated dinitrogen ligands which may be viewed as having hydrazide character in one resonance form (Figure 1.3). These compounds have exhibited a fairly wide range of N_2 functionalization chemistry including hydrogenation,[20,21,22,23] 1,2-addition of C-H bonds,[22,24] and protonolysis with Brønsted acids,[23,25,26] as well as N-C bond formation by cycloaddition,[27,28] insertions,[29,30] and alkylation with small organic substrates.[31,32,33] In this chapter the unprecedented carbon monoxide-induced cleavage of dinitrogen promoted by a series of group 4 metallocene complexes is reported, and a general mechanism of the reaction is proposed based on experimental findings.

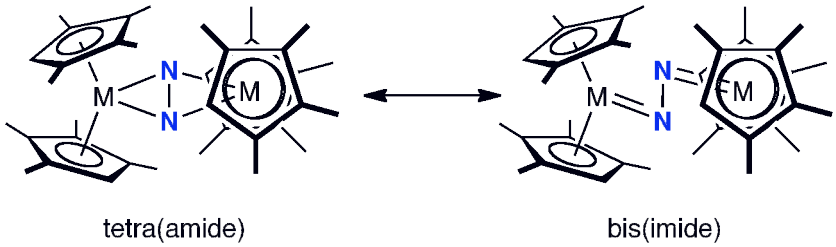

Figure 1.3. Resonance forms of group 4 metallocene dinitrogen complexes.

Results and Discussion

Synthesis and characterization of a side-on bound *ansa*-hafnocene dinitrogen complex and comparison to previously reported compounds. The highly activated dinitrogen ligand as well as the unique reactivity of the *ansa*-zirconocene dinitrogen compound, $(Me_2Si(\eta^5\text{-}C_5Me_4)(\eta^5\text{-}C_5H_3\text{-}3\text{-}^tBu)Zr)_2(\mu_2,\eta^2,\eta^2\text{-}N_2)$ (**3-N₂**),[34] prompted exploration of the chemistry of the hafnium congener. Previous

studies of early metal dinitrogen complexes established that substitution of the second row metal with its third row congener results in elongation of the N-N bond and often enables new types of reactivity.[22]

The *ansa*-hafnocene dichloride complex, $Me_2Si(\eta^5\text{-}C_5Me_4)(\eta^5\text{-}C_5H_3\text{-}3\text{-}{}^tBu)HfCl_2$ (**4-Cl$_2$**), was prepared analogously to its zirconium congener[34] and was isolated as a pale yellow solid in 67% yield. This compound was characterized by multinuclear NMR spectroscopy and single crystal X-ray diffraction. A representation of the structure of the (*S*) enantiomer of **4-Cl$_2$** is presented in Figure 1.4, and the (*R*)-enantiomer is reported in Appendix C.

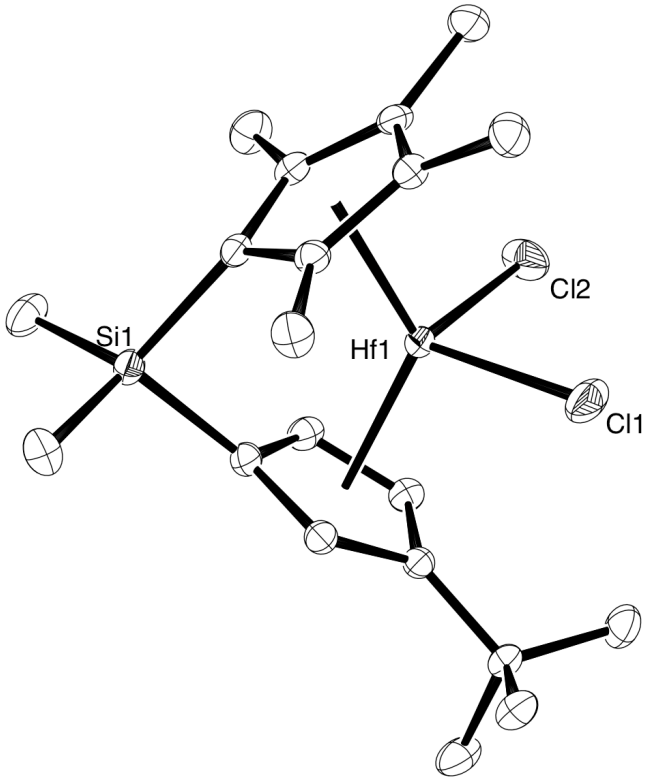

Figure 1.4. Molecular structure of **4-Cl$_2$** at 30% probability ellipsoids. The (*S*) enantiomer is presented. Hydrogen atoms are omitted for clarity.

All attempts at chemical reduction of **4-Cl$_2$** using various amounts of either 0.5% sodium amalgam, potassium graphite, or sodium/potassium alloy were unsuccessful, yielding complicated inseparable mixtures and no evidence for dinitrogen coordination. This result was unsurprising as hafnium dichloride complexes are typically more difficult to reduce than their zirconium congeners due to their more negative reduction potentials. This issue was addressed by synthesizing the corresponding diiodide complex, $Me_2Si(\eta^5\text{-}C_5Me_4)(\eta^5\text{-}C_5H_3\text{-}3\text{-}^tBu)HfI_2$ (**4-I$_2$**), which was readily prepared by treating a toluene solution of **4-Cl$_2$** with excess iodotrimethylsilane followed by solvent removal and washing with pentane, yielding a bright yellow solid in 93% yield (Figure 1.5).

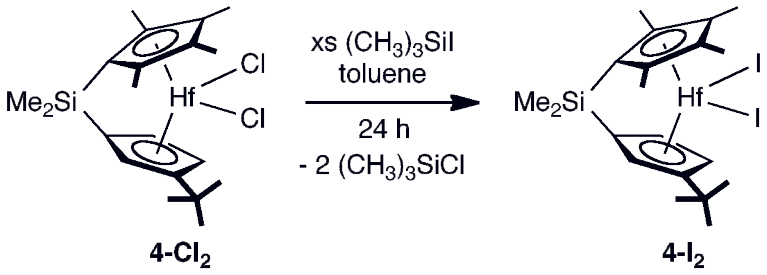

Figure 1.5. Synthesis of **4-I$_2$**.

Replacement of the chloride ligands with iodide ligands renders **4-I$_2$** susceptible to clean reduction chemistry. Initially, a toluene solution of **4-I$_2$** under an N_2 atomsphere was treated with 5 equivalents KC_8 as a toluene slurry. After several minutes, the solution had turned a vivid purple color although NMR spectroscopy suggested only minimal consumption of the starting diiodide. Monitoring the course of the reaction over several hours by analyzing aliquots by ^{1}H NMR spectroscopy established complete consumption of **4-I$_2$** and formation of a single diastereomer of $((Me_2Si(\eta^5\text{-}C_5Me_4)(\eta^5\text{-}C_5H_3\text{-}3\text{-}^tBu)Hf)_2(\mu_2,\eta^2,\eta^2\text{-}N_2)$ (**4-N$_2$**) after about 8 hours (Figure

1.6). Unfortunately, this procedure was plagued by very poor yields due to the formation of significant quantities of a paramagnetic impurity tentatively assigned as the monochloride dimeric anion, $\mathbf{[4\text{-}(I)]_2(N_2)^-}$ (Figure 1.6). This complex, which interestingly yields ammonium chloride upon protonolysis with HCl, did not undergo further reduction by KC_8, complicating efficient synthesis of $\mathbf{4\text{-}N_2}$ by this method. At longer reaction times and larger quantities of KC_8, decomposition of $\mathbf{4\text{-}N_2}$ was competitive with $\mathbf{4\text{-}I_2}$ consumption. Because of these complications, different methods of reduction were explored.

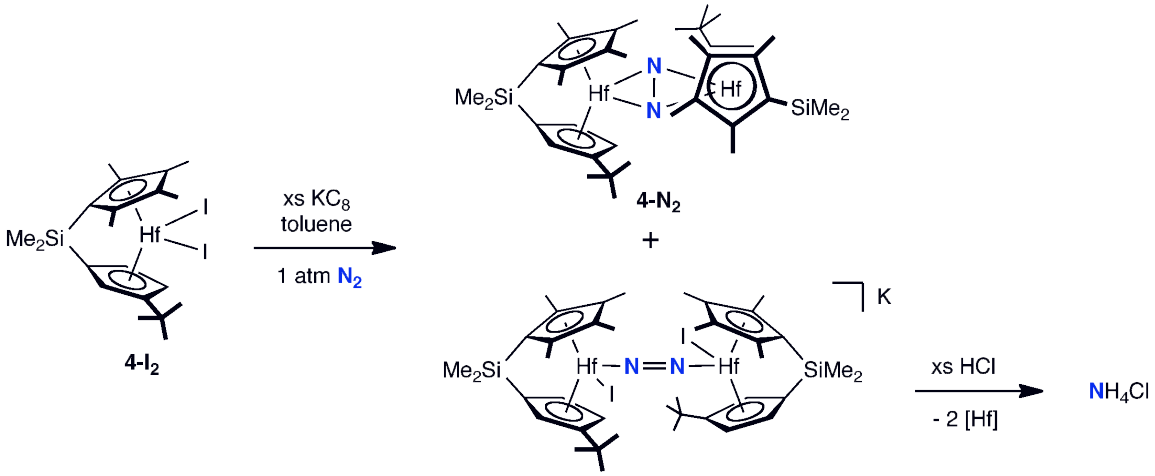

Figure 1.6. Reduction of $\mathbf{4\text{-}I_2}$ with KC_8.

A more successful reduction protocol was found for $\mathbf{4\text{-}I_2}$ using eight equivalents of 0.5% Na(Hg) under an atmosphere of N_2 for exactly one week, forming $\mathbf{4\text{-}N_2}$ in 61% yield (Figure 1.7). As observed in chemistry of the related zirconium congener,[34] only one isomer of $\mathbf{4\text{-}N_2}$ was isolated. Characterization of $\mathbf{4\text{-}N_2}$ by multinuclear (^{1}H, ^{13}C, ^{15}N) NMR spectroscopy as well as single crystal X-ray diffraction established exclusive formation of the *syn*, homochiral diastereomer as an equimolar mixture of the (*S*,*S*) and (*R*,*R*) enantiomers.[35] The ^{1}H NMR and ^{13}C NMR

spectra of **4-N_2** exhibit the number of resonances consistent with a single metallocene environment, indicative of the idealized C_2 symmetry of the molecule.

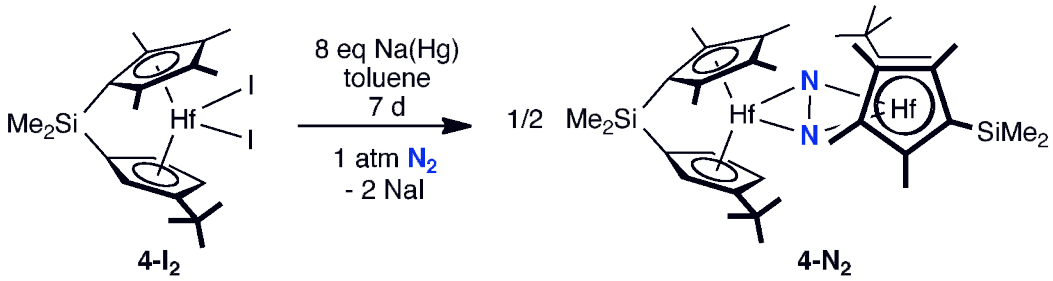

Figure 1.7. Reduction of **4-I_2** with Na(Hg).

Performing the reduction of **4-I_2** using similar reaction conditions under an atmosphere of $^{15}N_2$ enabled the synthesis of the ^{15}N-labeled isotopologue, **4-$^{15}N_2$**. The benzene-d_6 ^{15}N NMR spectrum of **4-$^{15}N_2$** contains a single resonance at 576.8 ppm, consistent with a symmetric dinitrogen ligand with a chemical shift in good agreement with other group 4 metallocene dinitrogen compounds previously synthesized in our laboratory.[21,22,34]

The solid-state X-ray structure of **4-N_2** (Figure 1.8) confirms side-on coordination of the dinitrogen ligand and *syn*-homochirality of the dimer. A representation of the (*S*,*S*) enantiomer is presented in Figure 1.8, and a representation of the (*R*,*R*) enantiomer is reported in Appendix C. The N-N bond length of 1.457(5) Å is the longest observed for any group 4 metallocene N_2 complex prepared to date, although several non-metallocene complexes reported by Sita[32] and Fryzuk[18,36,37] contain longer N-N bonds. The two hafnocene subunits are rotated with respect to each other with a dihedral angle (defined as the angle between the planes of the cyclopentadienyl centroids and the hafnium center of each monomer) of 54.0º. As has been shown for related complexes, this dihedral "twist" facilitates overlapping of the

metallocene out-of-phase linear combination orbital ($1a_1$-$1a_1$) with the N_2 π^* orbital, resulting in a four electron reduced, $[N_2]^{4-}$ ligand.[38] It should be noted the solid-state structure of **4-N_2** is a static view of the molecule, and that in solution the structure is likely dynamic due to rocking of the hafnocene subunits with respect to each other. Overall **4-N_2** is structurally similar to **3-N_2** with the key difference being the elongated dinitrogen ligand. Table 1.1 compares spectroscopic and X-ray crystallographic parameters of the dinitrogen complexes featured in this study.

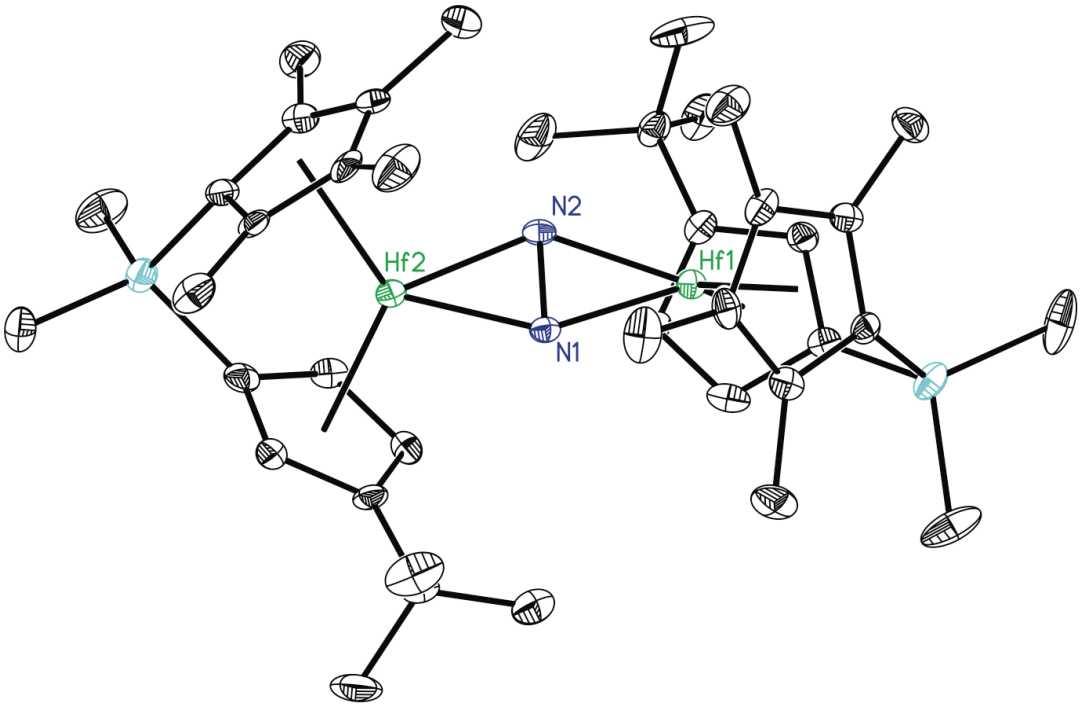

Figure 1.8. Molecular structure of **4-N_2** at 30% probability ellipsoids. Hydrogen atoms omitted for clarity. (*S*,*S*)-enantiomer pictured.

Table 1.1. Comparison of spectroscopic and crystallographic measurements of the compounds in this study.

Compound	d(N-N) (Å)	d(M-N) (Å)	d(M-M) (Å)	dihedral angle (°)	δ ^{15}N (ppm)
1-N_2	1.377(3)	2.118(1)	4.020	65.3	621.1
		2.131(1)			
2-N_2	1.423(11)	2.072(3)	3.910	65.3	590.5
		2.089(4)			
3-N_2	1.406(4)	2.090(3)	3.911	54.1	608.4
		2.087(3)			
		2.079(3)			
		2.102(3)			
4-N_2	1.457(5)	2.043(4)	3.820	54.0	576.8
		2.057(4)			
		2.059(4)			
		2.059(4)			

Reactivity of Group 4 Metallocene Dinitrogen Compounds with Carbon Monoxide. With a family of group 4 metallocenes bearing strongly activated N_2 ligands in hand, including the newly synthesized **4-N_2**, new N-C forming reactions that would take advantage of an elongated N-N bond were sought. Carbon monoxide was chosen due to its abundance and importance as a chemical feedstock. Sobota has reported successful nitrogen carbonylation for a reduced titanium species, which yielded dimethylformamide from N_2, CO, and CH_3I, demonstrating that lighter group 4 congeners are able to promote the desired CO-induced N_2 cleavage chemistry.[39] In addition, CO has recently proven to exhibit an exciting array of reactivity in transition

metal compounds, including carbonylation of terminal metal nitrides,[40,41] homologation promoted by mixed-ring actinide complexes,[10-13] and CO-induced N-N cleavage in several compounds where the N-N bond is not N_2-derived.[15-17] The ease of use of CO as well as the availability of its ^{13}C-labeled isotopologue make it an especially attractive reagent from a synthetic perspective. The reactivity of the four metallocene dinitrogen complexes presented in Table 1.1 with carbon monoxide will be presented, starting with *ansa*-metallocenes and following with the unlinked metallocenes.

Addition of 4 atm CO to a toluene solution of $((Me_2Si(\eta^5\text{-}C_5Me_4)(\eta^5\text{-}C_5H_3\text{-}3\text{-}^tBu)Hf)_2(\mu_2,\eta^2,\eta^2\text{-}N_2)$ (**4-N_2**), the compound with the most activated N_2 ligand in the series, resulted in a color change from purple to light brown. A single product was formed which was identified as the C_2-symmetric hafnium oxamidide complex **4-($N_2C_2O_2$)-*C_2*** (Figure 1.9). This compound, bearing an unusual $[N_2C_2O_2]^{4-}$ core, was coined "oxamidide" due to the relationship of this bridging ligand to the organic molecule oxamide, $H_2NC(O)\text{-}C(O)NH_2$. Repeating the above reaction with a reduced pressure of 1 atm CO furnished exclusively an isomeric, C_1-symmetric hafnium oxamidide product, **4-($N_2C_2O_2$)-*C_1*** (Figure 1.9). When intermediate pressures of CO were used, inseparable mixtures of **4-($N_2C_2O_2$)-*C_1*** and **4-($N_2C_2O_2$)-*C_2*** were obtained in varying ratios. The CO pressure dependence of the reaction is an interesting feature that will be discussed in detail in a later section of this chapter. The C_1 and C_2-symmetric hafnocene oxamidide complexes were isolated as crystalline yellow solids in 73% and 82% yield, respectively. The oxamidide ligand of both isomers arises from cleavage of coordinated N_2 coupled to N-C bond formation and CO homologation. This is an unprecedented reaction among transition metal dinitrogen complexes, as the addition of CO typically results in N_2 dissociation and formation of the corresponding metal (di)carbonyl compound.[42]

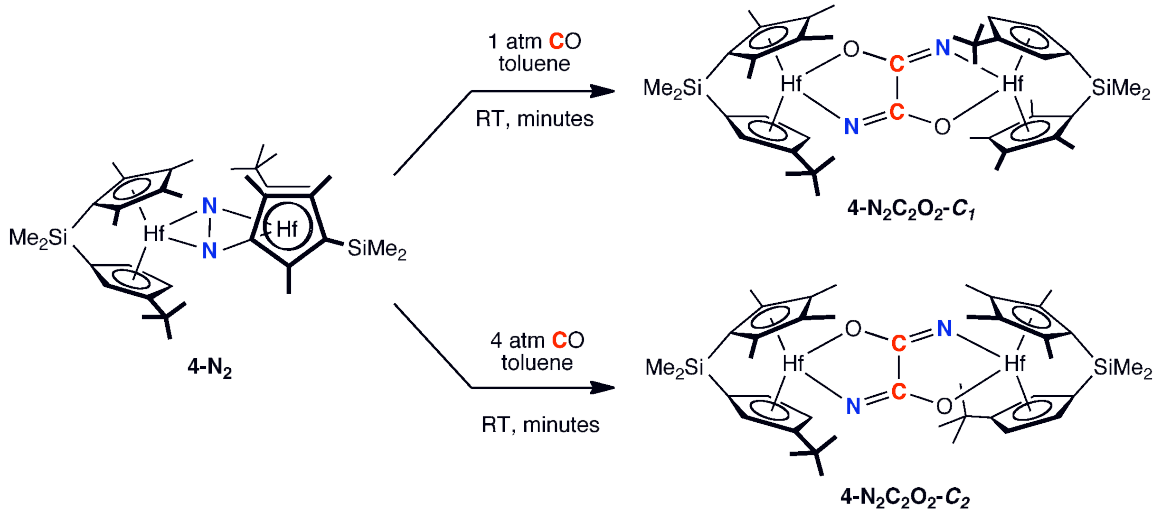

Figure 1.9. Addition of 1-4 atm CO to **4-N_2**.

The oxamidide complexes, **4-($N_2C_2O_2$)-*C1*** and **4-($N_2C_2O_2$)-*C2***, were fully characterized by multinuclear (^{1}H, ^{13}C, ^{15}N) NMR spectroscopy, infrared spectroscopy, single crystal X-ray diffraction and protonolysis studies. A summary of the key NMR spectroscopic features for these and related compounds is presented in Table 1.2. The availability of $^{15}N_2$ and ^{13}CO enabled the preparation of various combinations of ^{13}C- and ^{15}N-enriched isotopologues. The benzene-d_6 ^{1}H NMR spectra of **4-($N_2C_2O_2$)-*C1*** and **4-($N_2C_2O_2$)-*C2*** exhibit the number of resonances consistent with two chemically unique cyclopentadienyl ligand environments and a single cyclopentadienyl environment, respectively. The ^{13}C and ^{15}N NMR spectra of **4-($N_2C_2O_2$)-*C1*** and **4-($N_2C_2O_2$)-*C2*** are presented in Figure 1.10 and Figure 1.11, respectively, and confirm N_2 cleavage and N-C and C-C bond formation in these compounds. The {^{1}H}^{13}C NMR spectrum of **4-($N_2{}^{13}C_2O_2$)-*C1*** exhibits two leaning doublets ($^1J_{CC}$ = 61.7 Hz) centered at 159.9 and 161.4 ppm for the two inequivalent carbons. The large magnitude of the coupling constant is consistent with a newly formed sp^2-sp^2 C-C bond resulting from CO homologation. Upon additional isotopic

enrichment with ^{15}N to afford **4-($^{15}N_2{}^{13}C_2O_2$)-*C1***, both doublets undergo additional splitting with coupling constants ($^1J_{CN}$ = 5.0 Hz; $^2J_{CN}$ = 3.0 Hz) consistent with the formation of two new N-C bonds. Similar observations were made by ^{15}N NMR spectroscopy. Two singlets were observed corresponding to the inequivalent nitrogen atoms in **4-($^{15}N_2C_2O_2$)-*C1***, which split into pseudo triplets for the doubly labeled isotopologue **4-($^{15}N_2{}^{13}C_2O_2$)-*C1*** (Figure 1.10).

Table 1.2. Selected NMR data of metallocene oxamidide compounds.

Compound	δ ^{13}C (ppm)[a]	δ ^{15}N (ppm)[b]	Coupling Constants[c]
1-$N_2C_2O_2$	162.89	400.4	$^1J_{C\text{-}N}$, $^2J_{C\text{-}N}$ = 3.7[d]
2-$N_2C_2O_2$	160.21	376.4	$^1J_{C\text{-}N}$, $^2J_{C\text{-}N}$ = 3.9[d]
3-$N_2C_2O_2$-*C1*	162.76	392.4	$^1J_{C\text{-}N}$ = 4.0, $^2J_{C\text{-}N}$ = 4.0
	164.07	396.5	$^1J_{C\text{-}C}$ = 60.9
3-$N_2C_2O_2$-*C2*	165.39	397.2	$^1J_{C\text{-}N}$, $^2J_{C\text{-}N}$ = 3.8[d]
4-$N_2C_2O_2$-*C1*	159.93	369.4	$^1J_{C\text{-}N}$ = 5.0, $^2J_{C\text{-}N}$ = 3.0
	161.46	370.3	$^1J_{C\text{-}C}$ = 61.4
4-$N_2C_2O_2$-*C2*	162.65	371.3	$^1J_{C\text{-}N}$, $^2J_{C\text{-}N}$ = 3.9[d]

[a.] Benzene-d_6 ^{13}C NMR shift in ppm of the $[N_2C_2O_2]^{4-}$ core. [b.] Benzene-d_6 ^{15}N NMR shift in ppm of the $[N_2C_2O_2]^{4-}$ core referenced to NH_3. [c.] Values reported in Hz. [d.] Values reported as an average due to AA'XX' spin system. See Experimental Section for details.

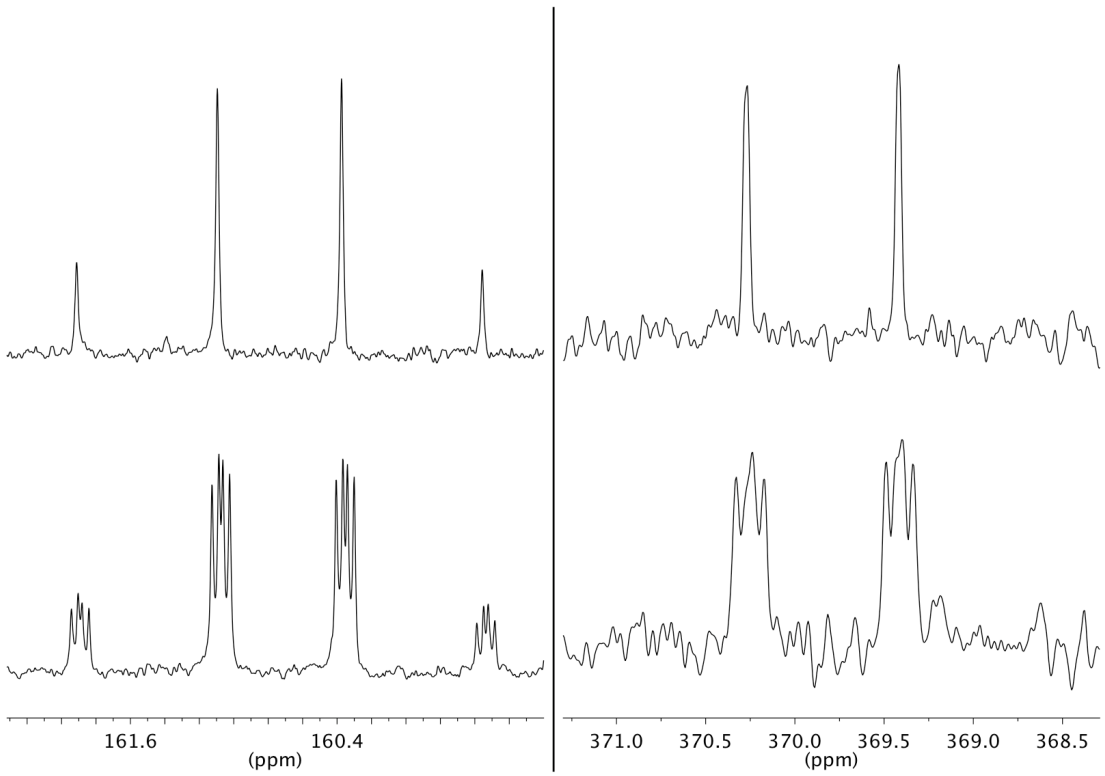

Figure 1.10. $\{^{1}H\}^{13}C$ NMR spectra of **4-$N_2{}^{13}C_2O_2$-*C1*** (top left), **4-$^{15}N_2{}^{13}C_2O_2$-*C1*** (bottom left), and ^{15}N NMR spectra of **4-$^{15}N_2C_2O_2$-*C1*** (top right) and **4-$^{15}N_2{}^{13}C_2O_2$-*C1*** (bottom right). All spectra measured in benzene-d_6 at 23 °C.

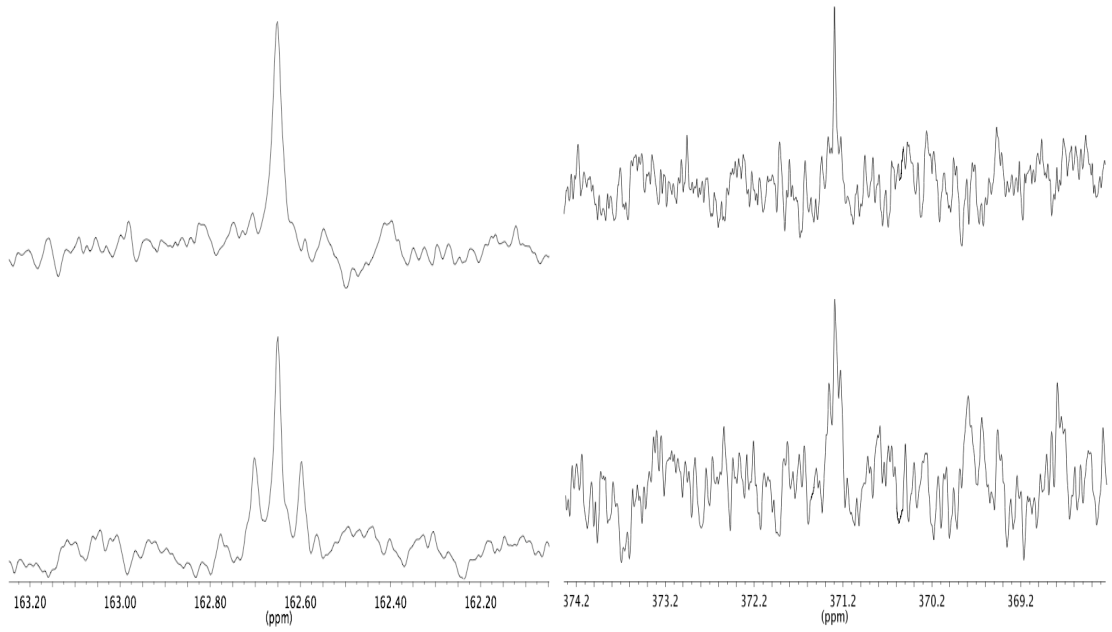

Figure 1.11. $\{^1H\}^{13}C$ NMR spectra of **4-$N_2{}^{13}C_2O_2$-*C_2*** (top left), **4-$^{15}N_2{}^{13}C_2O_2$-*C_2*** (bottom left), and ^{15}N NMR spectra of **4-$^{15}N_2C_2O_2$-*C_2*** (top right) and **4-$^{15}N_2{}^{13}C_2O_2$-*C_2*** (bottom right). All spectra measured in benzene-d_6 at 23 °C.

For the C_2 symmetric isomer, **4-($N_2{}^{13}C_2O_2$)-*C_2***, the oxamidide region of the $\{^1H\}^{13}C$ NMR spectrum exhibits a single resonance at 162.7 ppm assigned to the symmetric oxamidide ligand (Figure 1.11). Doubly labeling the compound to form **4-($^{15}N_2{}^{13}C_2O_2$)-*C_2*** produces a non-first order AA'XX' spin system which resembles a pseudo-triplet in the ^{13}C NMR spectrum with an average coupling constant of $^1J_{CN} = {}^2J_{CN} = 3.9$ Hz, as determined by simulation.[43] Likewise, the ^{15}N NMR spectrum consists of a single resonance at 371.3 ppm that splits into an apparent pseudo-triplet as a result of the AA'XX' system (Figure 1.11). These NMR spectroscopic observations for **4-($N_2{}^{13}C_2O_2$)-*C_1*** and **4-($N_2{}^{13}C_2O_2$)-*C_2*** confirm N_2 and CO as the exclusive source of the bridging core in these unprecedented hafnocene oxamidide complexes.

The solid-state structures of both the C_2 and the C_1 symmetric isomers of **4-$N_2C_2O_2$** were determined by X-ray diffraction (Figure 1.12 and Figure 1.13, respectively) and confirm the formation of an $[N_2C_2O_2]^{4-}$ core arising from N_2 cleavage and CO homologation with C-N bond formation. The (*S*,*S*) enantiomers are presented in Figure 1.12 and Figure 1.13, and the (*R*,*R*) enantiomers are reported in Appendix C. In each case the hafnocene wedges are nearly coplanar with dihedral angles of 5.8° (C_2 isomer) and 12.5° (C_1 isomer), and the principal symmetry axis in **4-$N_2C_2O_2$-*C_2*** bisects the C41-C42 bond in the planar oxamidide ligand. The key distinction between the two structures pertains to the orientation of the cycopentadienyl ring substituents with respect to the atoms in the oxamidide core. In the C_2 symmetric isomer, the rings are oriented such that the *tert*-butyl substituents are *syn* to each other. This orientation situates both *tert*-butyl groups *syn* to a nitrogen atom of the oxamidide ligand. The nitrogen and oxygen atoms in the C_1 symmetric isomer, **4-$N_2C_2O_2$-*C_1***, could not be absolutely distinguished crystallographically and are labeled "E" in Figure 1.13; however, core bond distances (d(E-C) = 1.297(4)-1.320(4) Å) as well as spectroscopic data clearly establish that E1 and E2 have the same identity, as do E3 and E4. The *tert*-butyl groups in **4-$N_2C_2O_2$-C_1** are geared *anti*, placing one *tert*-butyl group *syn* to oxygen and the other *syn* to nitrogen. This orientation gives rise to the overall C_1 symmetry of the compound. The metrical parameters of the bridging $[N_2C_2O_2]^{4-}$ ligand in the C_2 symmetric isomer are consistent with formation of C=N double bonds (1.270(3) and 1.275(3) Å), C-O single bonds (1.341(3) and 1.339(3) Å) and a C-C single bond (1.534(3) Å).

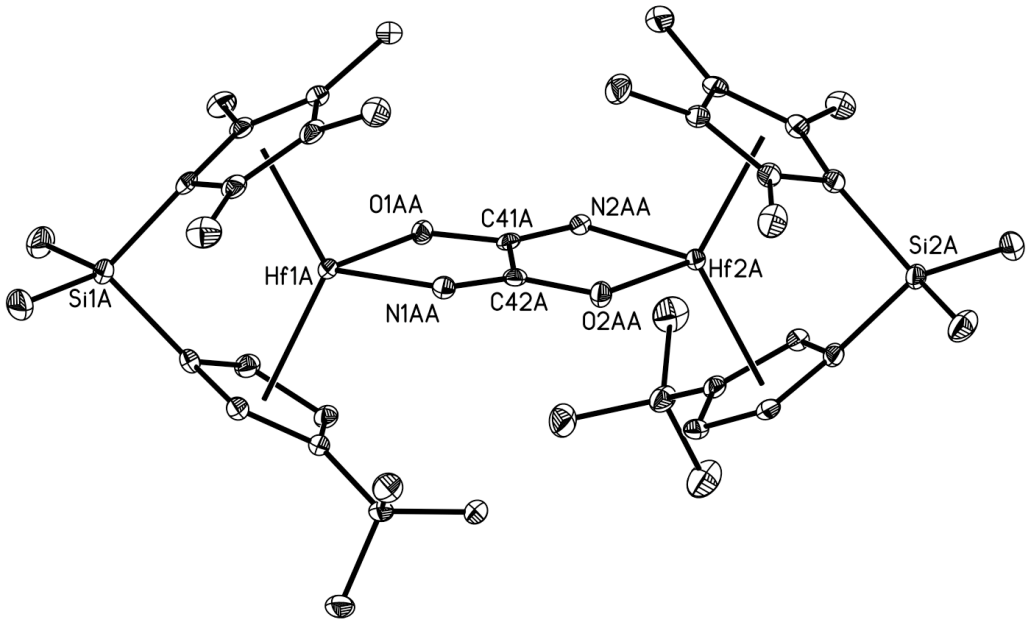

Figure 1.12. Molecular structure of **4-$N_2C_2O_2$-*C*$_2$** at 30% probability ellipsoids. Hydrogen atoms omitted for clarity. The (*S*,*S*)-enantiomer is shown.

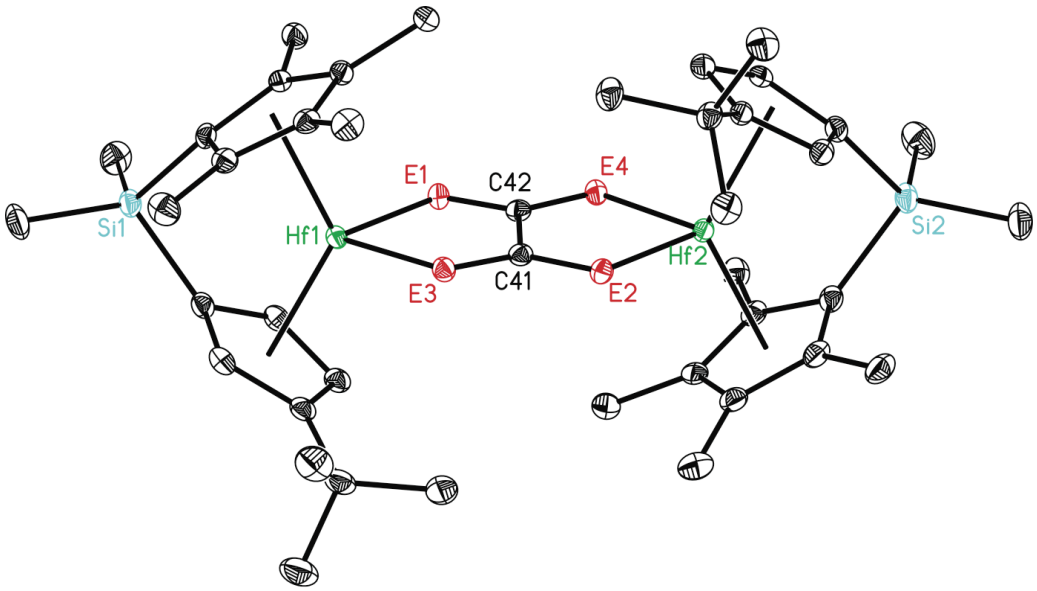

Figure 1.13. Molecular structure of **4-$N_2C_2O_2$-*C*$_1$** at 30% probability ellipsoids. Hydrogen atoms omitted for clarity. The (*S*,*S*)-enantiomer is shown. Nitrogen and oxygen atoms in the $[N_2C_2O_2]^{4-}$ core could not be distinguished and are labeled "E".

The discovery of CO-induced N_2 cleavage promoted by **4-N_2** prompted exploration into the reactivity of the less activated metallocene dinitrogen complexes of the series (Table 1.1). The generality of oxamidide formation as a function of N-N length and metal (zirconium vs. hafnium) was explored, as well as the effect, if any, of the bis(cyclopentadienyl) ligand on outcome of the reaction.

Addition of 1 to 4 atm CO to $((Me_2Si(\eta^5\text{-}C_5Me_4)(\eta^5\text{-}C_5H_3\text{-}3\text{-}^tBu)Zr)_2(\mu_2,\eta^2,\eta^2\text{-}N_2)$ (**3-N_2**), the zirconium congener of **4-N_2** having a slightly contracted N-N bond distance,[34] resulted in a color change from green to red, signaling full consumption of **3-N_2** in approximately one minute. As was observed for the hafnium congener, the observed products were the *C_1*-symmetric zirconocene oxamidide (favored at lower pressures, e.g. ~1 atm), **3-($N_2C_2O_2$)-*C_1***, and the *C_2*-symmetric zirconocene oxamidide (favored at higher pressures, e.g. ~4 atm) **3-($N_2C_2O_2$)-*C_2***, in yields of 42% and 46%, respectively (Figure 1.14). At all pressures, small quantities (< 5%) of the previously reported zirconocene dicarbonyl species, **3-$(CO)_2$**,[34] were observed by NMR and IR spectroscopies. The formation of the dicarbonyl compound accounts for the red color of the reaction solution and suggests that N_2 carbonylation is sensitive to changes in bond length of the coordinated N_2 ligand. Representative NMR spectra of **3-($N_2C_2O_2$)-*C_1*** and **3-($N_2C_2O_2$)-*C_2*** are presented in Figure 1.15 and are comparable to those of the isomers of **4-($N_2C_2O_2$)**. Diagnostic chemical shifts and coupling constants obtained upon isotopic labeling confirm formation of the oxamidide ligand in each case (Table 1.2).

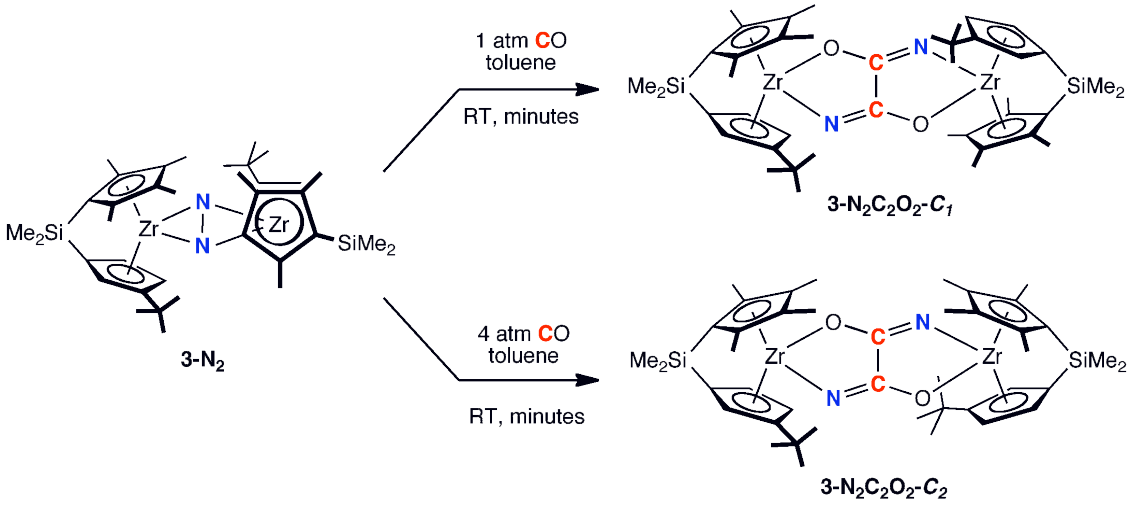

Figure 1.14. Addition of 1 or 4 atm CO to **3-N_2**.

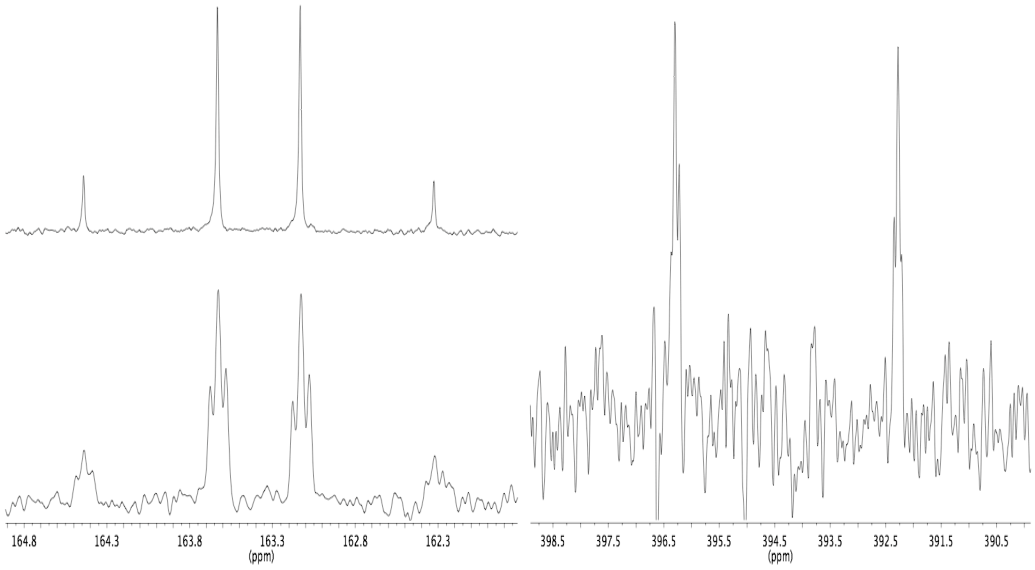

Figure 1.15. Benzene-d_6 $\{^1H\}^{13}C$ NMR spectra of **3-$N_2{}^{13}C_2O_2$-*C1*** (top left) and **3-$^{15}N_2{}^{13}C_2O_2$-*C1*** (bottom left), and benzene-d_6 ^{15}N NMR spectrum of **3-$^{15}N_2{}^{13}C_2O_2$-*C1*** (right).

The more symmetric (idealized C_{2h}) unlinked metallocene variants, $[(\eta^5\text{-}C_5Me_4H)_2Zr]_2(\mu_2,\eta^2,\eta^2\text{-}N_2)$ (**1-N_2**) and $[(\eta^5\text{-}C_5Me_4H)_2Hf]_2(\mu_2,\eta^2,\eta^2\text{-}N_2)$ (**2-N_2**), were also treated with carbon monoxide. In the latter case, exposure of **2-N_2** to 1-4 atm CO resulted in a color change from purple to red-brown and selective formation of the corresponding hafnocene oxamidide species, **2-$N_2C_2O_2$** in 75% yield (Figure 1.16). No evidence for hafnocene dicarbonyl (**2-$(CO)_2$**) formation was obtained using NMR and IR spectroscopies. As a consequence of the symmetric and homoleptic metallocene in this case, only a single isomer of **2-$N_2C_2O_2$**, exhibiting idealized C_{2h} symmetry, was formed at all CO pressures between 1 and 4 atm.

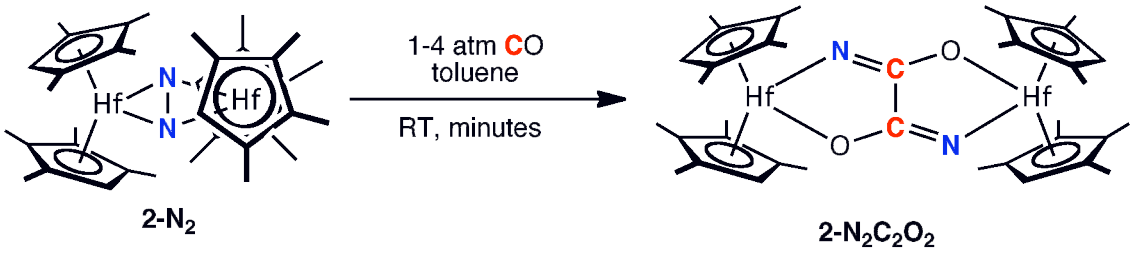

Figure 1.16. Addition of 1-4 atm CO to **2-N_2**.

The ^{13}C NMR spectrum of **2-$N_2{}^{13}C_2O_2$**, presented in Figure 1.17, exhibits the diagnostic feature for a symmetric oxamidide complex, specifically a single resonance at 160.2 ppm that splits into a pseudo triplet due to the AA'XX' spin system that results from additional labeling with ^{15}N to form **2-$^{15}N_2{}^{13}C_2O_2$**. Other key NMR spectroscopic data for the compound are presented in Table 1.2. The solid state structure of **2-$N_2C_2O_2$** was determined by single-crystal X-ray diffraction and has the familiar bent metallocene geometry with an essentially planar, bridging metallocene core (Figure 1.18). The nitrogen and oxygen atoms of the $[N_2C_2O_2]^{4-}$ core in this structure could not be distinguished and are labeled "E" in this depiction. The

structure exhibits the typical distance for a C-C bond (1.531(8) Å) and the core oxamidide distances of 1.297(7)/1.299(7) Å and 1.303(7)/1.320(8) Å for C(37)-E(2)/E(4) and C(38)-E(1)/E(3) are similar to those found in the *ansa*-hafnocene oxamidides **4-$N_2C_2O_2$-*C1*** and **4-$N_2C_2O_2$-*C2***.

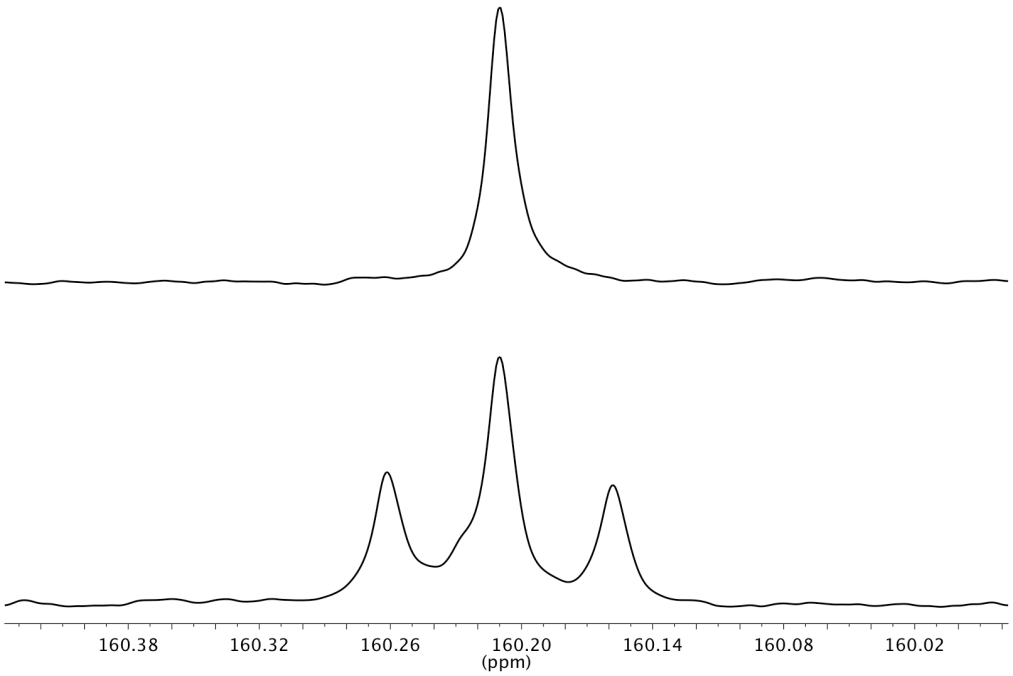

Figure 1.17. Benzene-d_6 $\{^1H\}^{13}C$ NMR spectra of **2-$N_2{}^{13}C_2O_2$** (top) and **2-$^{15}N_2{}^{13}C_2O_2$** (bottom).

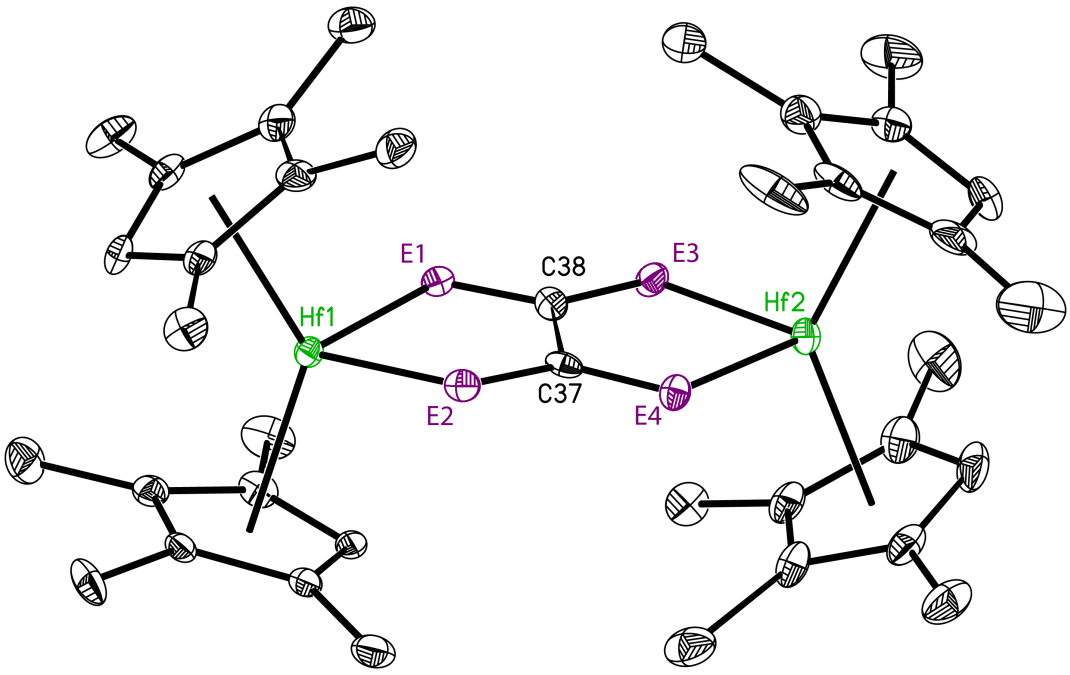

Figure 1.18. Molecular structure of **2-$N_2C_2O_2$** at 30% probability ellipsoids. Hydrogen atoms omitted for clarity. N and O atoms were not distinguished and are labeled "E".

To complete the carbonylation of the series of N_2 compounds in Table 1.1, the compound with the least activated N_2 ligand in the series, $[(\eta^5\text{-}C_5Me_4H)_2Zr]_2(\mu_2,\eta^2,\eta^2\text{-}N_2)$ (**1-N_2**),[21] was treated with 4 atm CO, resulting in two products, formed in a 3:1 ratio (Figure 1.19). The major product was identified as the C_{2h}-symmetric zirconocene oxamidide complex, **1-$N_2C_2O_2$**, arising from CO-induced N_2 cleavage. As shown in Table 1.2 and Figure 1.20, **1-$N_2C_2O_2$** exhibits NMR spectroscopic features diagnostic of an oxamidide ligand. An average C-N coupling,[43] simulated for the AA'XX' spin system, of $^1J_{CN} = {}^2J_{CN} = 3.7$ Hz[43] was observed for the doubly labeled isotopologue **1-$^{15}N_2{}^{13}C_2O_2$**, confirming C-N formation from CO and N_2.

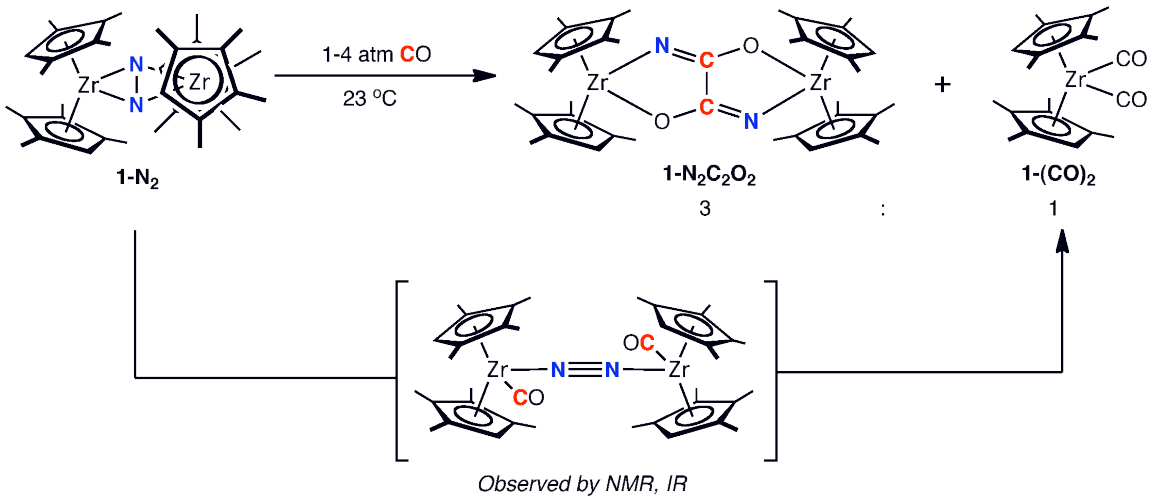

Figure 1.19. Addition of 1-4 atm CO to **1-N_2**.

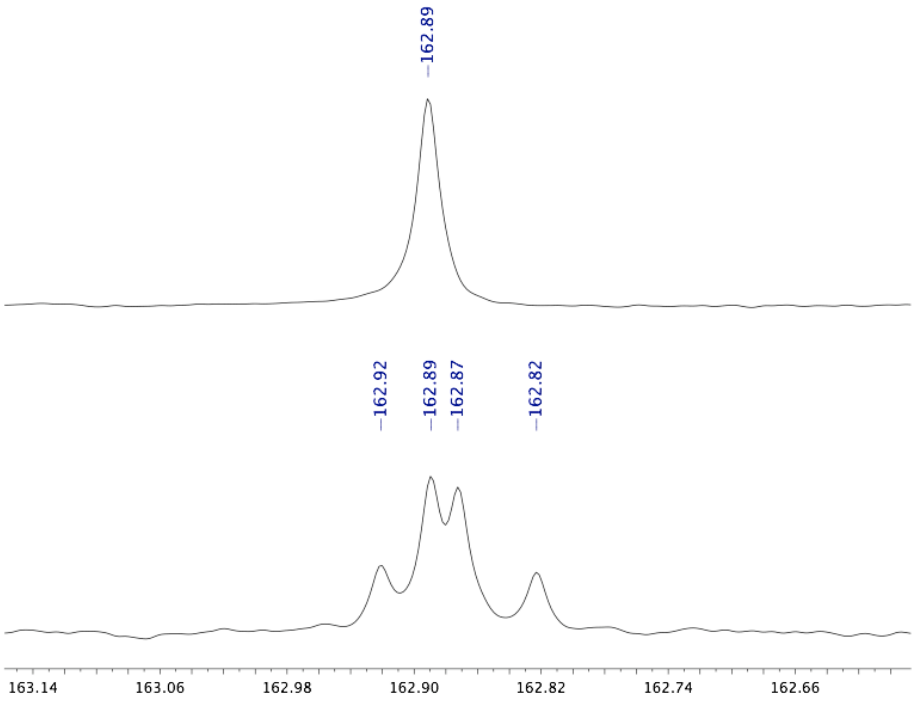

Figure 1.20. Benzene-d_6 $\{^1H\}^{13}C$ NMR spectra of **1-$N_2{}^{13}C_2O_2$** (top) and **1-$^{15}N_2{}^{13}C_2O_2$** (bottom). The bottom spectrum also contains some **1-$N_2{}^{13}C_2O_2$** (162.89 ppm) due to incomplete ^{15}N isotopic enrichment.

The minor product of CO addition to **1-N_2** was identified as (η^5-$C_5Me_4H)_2Zr(CO)_2$ (**1-$(CO)_2$**),[44] indicating N_2 dissociation becomes competitive with N-N bond cleavage for this less activated dinitrogen compound (Figure 1.19). Varying the pressure of CO employed in the reaction did not alter the final ratio of products, although monitoring the course of the reaction over time by ^1H and ^{13}C NMR spectroscopy allowed the observation of an intermediate identified as [(η^5-$C_5Me_4H)_2Zr(CO)]_2(\mu_2,\eta^2,\eta^2$-$N_2)$, which converted to the product mixture over the course of 1 h at 23 ºC (Figure 1.19). This intermediate was characterized by multinuclear NMR and infrared spectroscopies, and is analogous to the permethylzirconocene complex, [(η^5-$C_5Me_5)_2Zr(CO)]_2(\mu_2,\eta^2,\eta^2$-$N_2)$, prepared in a similar manner and previously reported by Bercaw and co-workers.[42] Key spectroscopic features include the downfield ^{13}C chemical shift for the carbonyl carbons at 283.02 ppm and the intense CO bands in the IR spectrum at 1844 and 1907 cm^{-1}.

Protonolysis studies were performed on each of the oxamidide complexes in the series. For example, treatment of a benzene-d_6 solution of **4-$N_2C_2O_2$-*C_2*** with 20 eq HCl (in a dioxane solution) furnished the corresponding hafnocene dichloride, **4-Cl_2**, with liberation of oxamide, $H_2NC(O)$-$C(O)NH_2$, in 95% yield (Figure 1.21). Oxamide is an important compound with applications as a slow-release fertilizer and as an additive to rocket propellant. This molecule was readily identified by a diagnostic ^{13}C NMR resonance at 162.5 ppm in dimethylsulfoxide-d_6 and by comparison to an authentic sample. Protonolysis was also performed with ethanol or water, releasing oxamide and forming the corresponding hafnocene bis(ethoxide) or bis(hydroxide) complexes, respectively. A similar protonolysis procedure was used for the remaining oxamidide complexes, **1-$N_2C_2O_2$**, **2-$N_2C_2O_2$**, and **3-$N_2C_2O_2$-*C_1*/*C_2***, and in all cases the reaction produced free oxamide and the expected metallocene byproducts in very high

yields. Importantly, these results demonstrate that a useful organic molecule can be synthesized from N_2 and CO, abundant diatomic molecules with the strongest known chemical bonds.

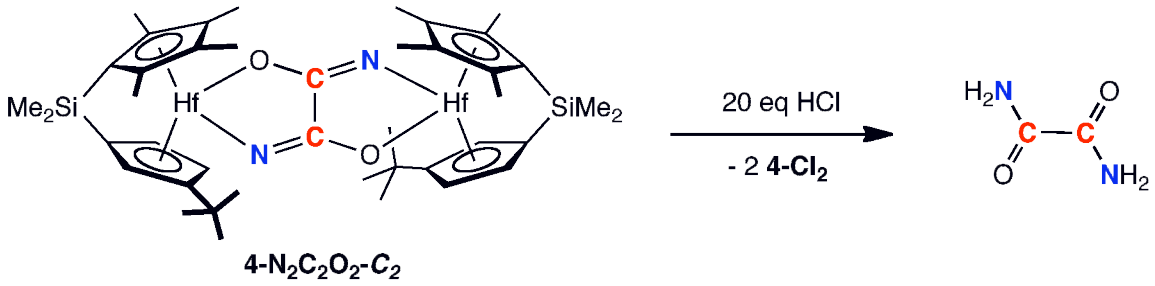

Figure 1.21. Protonolysis of **4-$N_2C_2O_2$-*C_2***.

Observation of intermediate to oxamidide formation. Monitoring the course of the reaction depicted in Figure 1.9, *i.e.* exposure of **4-N_2** to CO, over time was quite revealing. A frozen benzene-d_6 solution of **4-N_2** was treated with 4 atm CO, thawed with shaking, and quickly inserted into the probe of the NMR spectrometer. The ^{1}H NMR spectrum acquired after a few minutes showed no evidence for either isomer of **4-$N_2C_2O_2$**, although **4-N_2** had been completely consumed. The spectrum exhibited the number of resonances consistent with a new C_1 symmetric dihafnocene complex. This compound was identified as the intermediate, **4-(μ-NCO)(CO)(NCO)** (Figure 1.22), which after several minutes under 4 atm CO, converted fully to **4-$N_2C_2O_2$-*C_2*** (Figure 1.23). Under an evacuated headspace, a benzene-d_6 solution of **4-(μ-NCO)(CO)(NCO)** converted to a roughly 3:1 mixture of **4-$N_2C_2O_2$-*C_2*** to **4-$N_2C_2O_2$-*C_1*** (Figure 1.23). Notably, conversion of **4-(μ-NCO)(CO)(NCO)** to exclusively **4-$N_2C_2O_2$-*C_1*** was not observed over a range of reaction conditions.

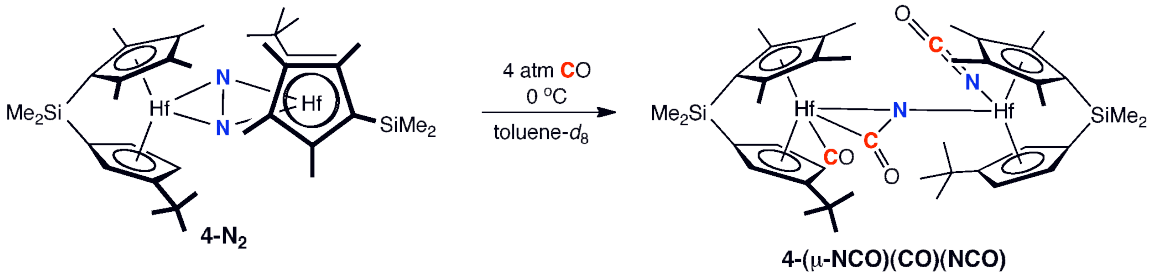

Figure 1.22. Observation of intermediate **4-(μ-NCO)(CO)(NCO)**.

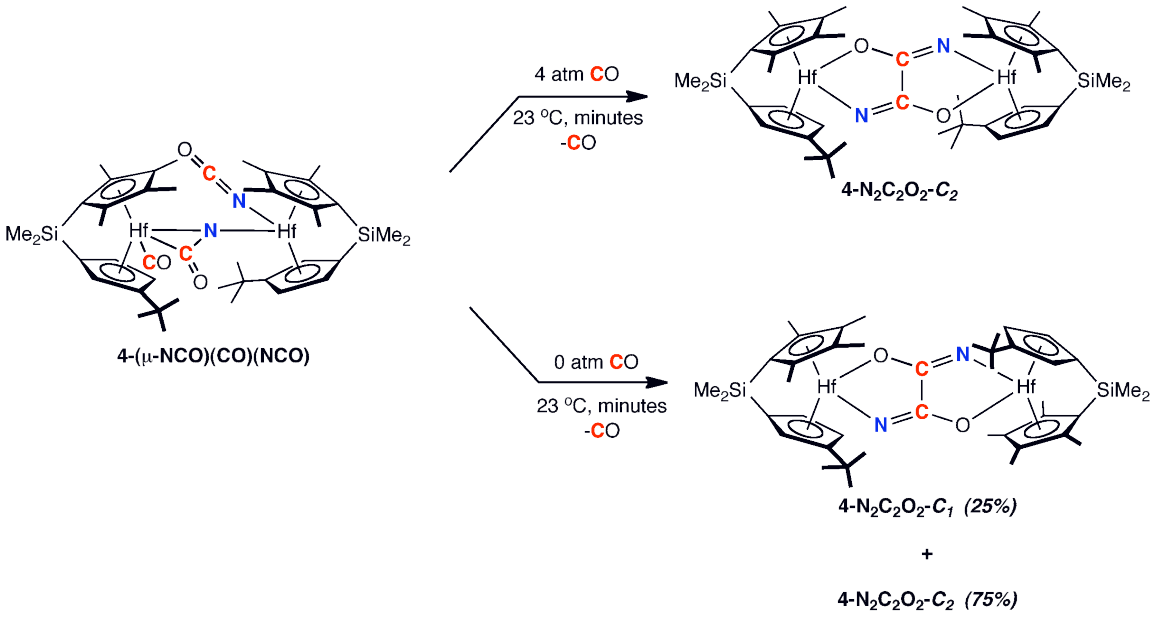

Figure 1.23. Conversion of **4-(μ-NCO)(CO)(NCO)** to **4-($N_2C_2O_2$)-C_1/C_2**.

Characterization of **4-(μ-NCO)(CO)(NCO)** was accomplished using multinuclear (^{1}H, ^{13}C, ^{15}N) NMR spectroscopies and infrared spectroscopy. The synthesis of various isotopologues of **4-(μ-NCO)(CO)(NCO)** was also useful for structural elucidation. Unfortunately, the transient nature of **4-(μ-NCO)(CO)(NCO)** in solution (discussed below), even at low temperatures, precluded growth of single crystals suitable for X-ray diffraction. Because of this, the stereochemical configuration of the terminal CO and NCO ligands and of the bridging NCO ligand

with respect to the cyclopentadienyl substituents is unknown. A representation of other possible isomers of **4-(μ-NCO)(CO)(NCO)** is presented in Figure 1.24 with proposed pathways to formation (see mechanistic discussion below and Chapter 2 for details). The isomer with terminal and bridging carbonyl groups both *syn* to the cyclopentadienyl *tert*-butyl substituent is used for the purpose of this discussion, although the other three possibilities have not been definitively ruled out. The bridging isocyanate group in **4-(μ-NCO)(CO)(NCO)** is unusual but similar compounds are known for early metallocene compounds[45] as well as for late metal compounds.[46] Examples of this structural type are presented in Figure 1.25.

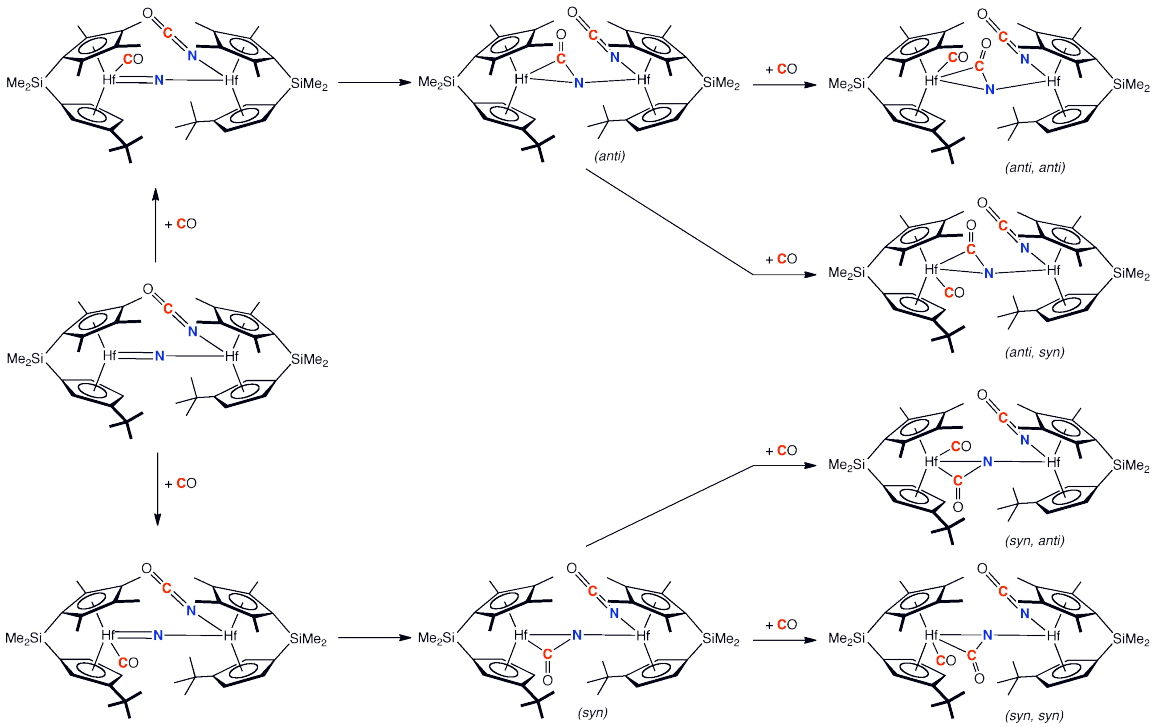

Figure 1.24. Possible structures of **4-(μ-NCO)(CO)(NCO)**.

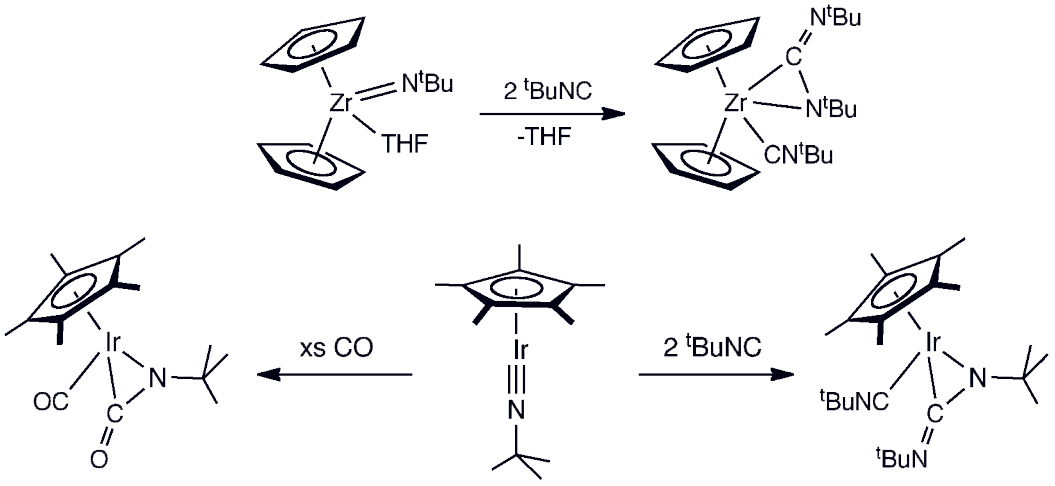

Figure 1.25. Examples by Bergman of migratory insertion of CO and RNC into metal imido bonds. Reproduced with permission from references 45 and 46a.

Due to the rapid decay of **4-(μ-NCO)(CO)(NCO)** in solution at 23 ºC, all NMR spectroscopic characterization was carried out in toluene-d_8 at 0 ºC, at which temperature the conversion to **4-$N_2C_2O_2$** proceeded over the course of several hours. Also, **4-(μ-NCO)(CO)(NCO)** was isolated as a powder by carefully subliming the solvent from frozen benzene solutions of **4-(μ-NCO)(CO)(NCO)** on the high vacuum line. The toluene-d_8 ^{13}C NMR spectrum of ^{13}C-,^{15}N-enriched **4-(μ-^{15}N^{13}CO)(^{13}CO)(^{15}N^{13}CO)** is presented in Figure 1.26 and establishes the presence of three unique carbon environments derived from ^{13}CO. Two of these carbon atoms are bonded to nitrogen atoms derived from $^{15}N_2$, as evidenced by $^1J_{CN}$ couplings, and correspond to a bridging isocyanate (δ = 192.50 ppm, $^1J_{CN}$ = 9.6 Hz) and a terminal isocyanate (δ = 134.48 ppm, $^1J_{CN}$ = 32.9 Hz), the latter having a chemical shift, coupling constant, and infrared stretch (ν_{NCO} = 2220 cm^{-1} for the natural abundance isotopologue in KBr) all diagnostic of a terminal isocyanate group. The third carbon environment corresponds to a terminal carbonyl ligand (δ = 247.07 ppm), which is coupled to the carbon of the bridging isocyanate ($^2J_{CC}$ = 13.7 Hz). The terminal

carbonyl also exhibits a diagnostic stretch in the solid state (KBr) infrared spectrum at 1959 cm^{-1}. This is an uncommon example of coupling through a hafnium center, although similar couplings have been observed in related systems.[34,47,48] Specifically, C-H coupling through group 4 metal centers has been reported by Bercaw and coworkers with $Cp^*_2ZrH_2(CO)$ ($^2J_{CH}$ = 25 Hz) and $Cp^*_2HfH_2(CO)$ ($^2J_{CH}$ = 21.5 Hz).[47] In addition, through-metal H-H coupling has been observed with a bis(cyclopentadienyl) zirconium compound in our laboratory ($^2J_{HH}$ = 7 Hz),[34] and with Cp_2TaH_3 ($^2J_{HH}$ = 10 Hz), reported by Wilkinson and coworkers.[48] The ^{15}N NMR spectrum of **4-(μ-$^{15}N^{13}CO$)(^{13}CO)($^{15}N^{13}CO$)** presented in Figure 1.26 exhibits two doublets centered at 89.6 and 241.1 ppm (with appropriate $^1J_{CN}$ couplings) corresponding to the terminal and bridging isocyanate groups, respectively.

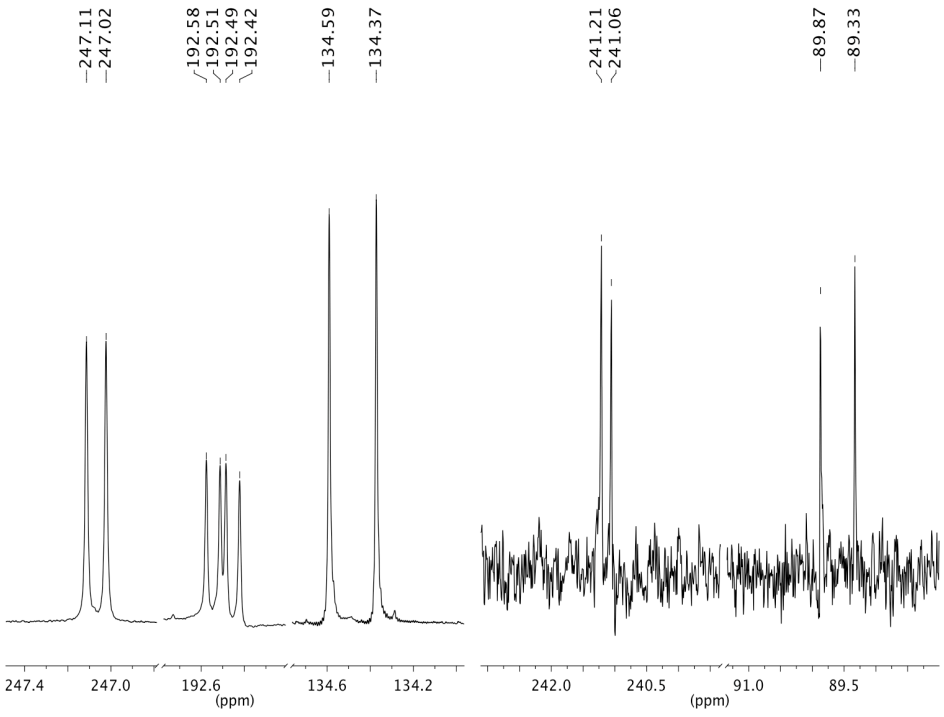

Figure 1.26. Toluene-d_8 $\{^1H\}^{13}C$ (left) and ^{15}N (right) NMR spectra of **4-(μ-$^{15}N^{13}CO$)(^{13}CO)($^{15}N^{13}CO$)**. Only regions corresponding to ^{13}C-enriched nuclei (left) are shown.

According to mass balance, no additional CO is necessary for the conversion of **4-(μ-NCO)(CO)(NCO)** to **4-$N_2C_2O_2$**. Rather, the loss of one equivalent of CO is necessary. This is consistent with experimental observations as monitoring the decay of **4-(μ-NCO)(CO)(NCO)** to **4-$N_2C_2O_2$** in absence of CO established that indeed CO was not required for the reaction to proceed. Additionally, the ^{13}C-labeled isotoplogue **4-(μ-N^{13}CO)(^{13}CO)(N^{13}CO)** converted to **4-$N_2{}^{13}C_2O_2$** with concomitant loss of ^{13}CO, which was detected by ^{13}C NMR spectroscopy.

An isotopic exchange study was conducted to determine which CO environment in **4-(μ-NCO)(CO)(NCO)** is incorporated into the final oxamidide product. Approximately 4 atm of CO was admitted to a J. Young NMR tube containing a frozen toluene-d_8 solution of **4-(μ-N^{13}CO)(^{13}CO)(N^{13}CO)** and the tube was warmed to 0 ºC and monitored by ^{13}C NMR spectroscopy. Over the course of 1.5 h, complete selective exchange at the terminal carbonyl position, forming the new isotopologue, **4-(μ-N^{13}CO)(CO)(N^{13}CO)**, had occurred, signaled by the complete disappearance of the ^{13}C resonance for the terminal carbonyl in **4-(μ-N^{13}CO)(^{13}CO)(N^{13}CO)** (Figure 1.27). As shown in the ^{13}C NMR spectra after 5 min and 1.0 h, incorporation of natural abundance CO into the intermediate to form the isotopologue **4-(μ-N^{13}CO)(CO)(N^{13}CO)** resulted in the disappearance of the terminal carbonyl resonance centered at 247.07 ppm and the loss of $^2J_{CC}$ coupling in the bridging isocyanate resonance.

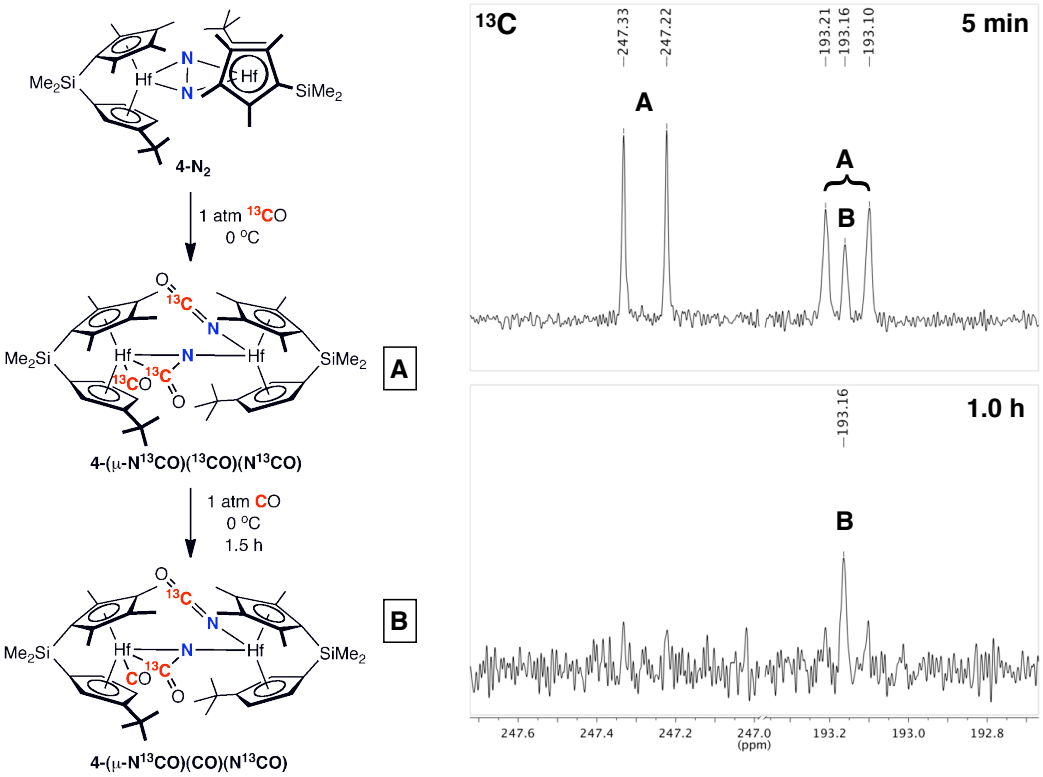

Figure 1.27. Isotopic exchange of CO into **4-(μ-N^{13}CO)(^{13}CO)(N^{13}CO)**.

Subsequently, to determine the origin of the oxamidide carbon atoms, the contents of the reaction tube were frozen and the headspace was evacuated. Finally the tube was thawed to 23 ºC and after 30 minutes the ^{13}C NMR spectrum was collected. Notably, only the $^{13}C_2$-isotopologue, **4-($N_2^{13}C_2$$O_2$)-*$C_1$***, was observed in the ^{13}C NMR spectrum, and **4-(N_2(^{13}C)CO_2)-*C_1*** was not observed. In addition, a substantial quantity of **4-($N_2C_2O_2$)-*C_2*** was observed, although the isotopologues for this isomer are spectroscopically indistinguishable. Overall, these results establish that it is the bridging isocyanate in **4-(μ-NCO)(CO)(NCO)**, and not the terminal CO, that is incorporated into the oxamidide product, **4-$N_2C_2O_2$-*C_1***. Since a similar mechanism is likely operative for both the C_1 and C_2 symmetric hafnocene oxamidide products, it is likely the bridging isocyanate is also incorporated into **4-($N_2C_2O_2$)-*C_2***.

To evaluate the lability of the terminal CO and bridging NCO ligands in **4-(μ-NCO)(CO)(NCO)**, a second isotopic exchange experiment was conducted similar to the one described above over prolonged times. Specifically, a frozen solution of the ^{13}C-labeled isotopologue **4-(μ-N^{13}CO)(^{13}CO)(N^{13}CO)** (prepared from **4-N$_2$** and ^{13}CO) was degassed and subsequently exposed to 1 atm of natural abundance CO, thawed to 0 ºC and monitored by ^{13}C NMR spectroscopy for several hours. Over the course of about 1.5 hours, virtually exclusive isotopic exchange into the terminal carbonyl position was observed, as described above. Over longer times (2-4 hours) partial isotopic exchange into the bridging isocyanate position was also detected by ^{13}C NMR spectroscopy. After 4 hours of exchange at 0 ºC, the solution was warmed to room temperature allowing complete conversion to hafnocene oxamidide product(s). The *C$_1$*-symmetric oxamidide was targeted so that the various possible isotopologues and isotopomers could easily be distinguished by ^{13}C NMR spectroscopy. The entire process described above is represented in Figure 1.28. The ^{13}C NMR spectrum of the resulting solution is presented in Figure 1.29 and establishes formation of predominantly **4-N$_2$^{13}C$_2$O$_2$-*C$_1$*** as well as an additional isotopologue, **4-N$_2$(^{13}C)CO$_2$-*C$_1$*** where one carbon in the oxamidide core is ^{13}C-labeled and the other is natural abundance.

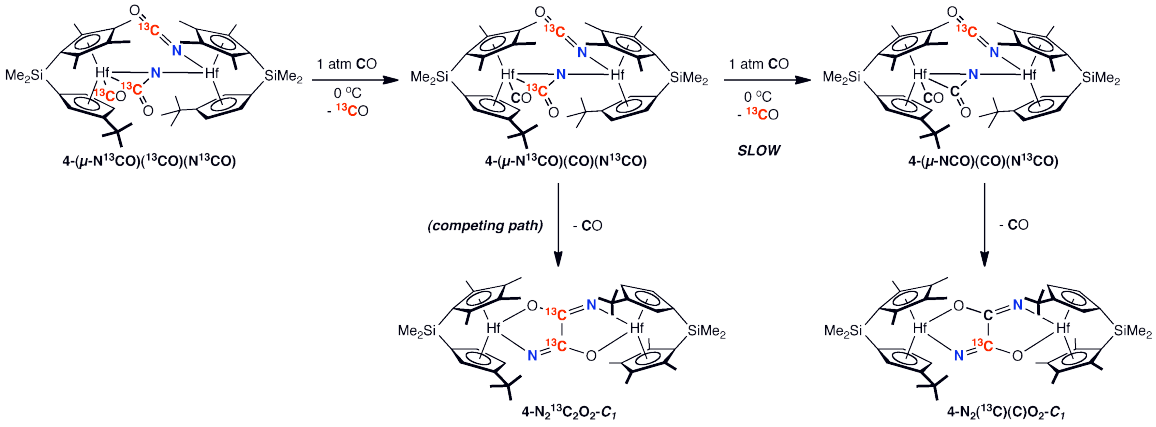

Figure 1.28. Incorporation of natural abundance CO into two positions of **4-(μ-N^{13}CO)(^{13}CO)(N^{13}CO)** and subsequent conversion to hafnocene oxamidide products.

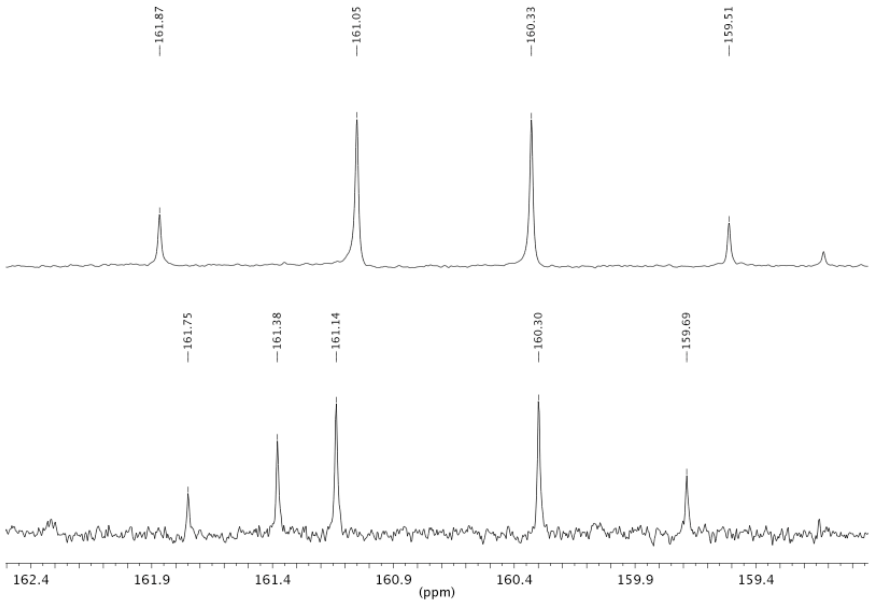

Figure 1.29. Benzene-d_6 {^{1}H}^{13}C NMR spectra of **4-N$_2$C$_2$O$_2$-*C*$_1$** (top), for reference, and the mixture of isotopologues resulting from CO exchange into **4-(μ-N^{13}CO)(^{13}CO)(N^{13}CO)** (bottom). Resonance at 161.4 ppm corresponds to **4-N$_2$(^{13}C)CO$_2$-*C*$_1$**.

The selective incorporation of an unlabeled carbon into a single position (out of two possible chemically inequivalent positions) of the oxamidide product confirms the lability of the bridging CO moiety (as well as the terminal CO) in the intermediate and implies a series of equilibria leading to formation of **4-(μ-NCO)(CO)(NCO)**. A probable exchange pathway to account for the formation of **4-N_2(^{13}C)CO_2-C_1** involves dissociation of the terminal ^{13}CO ligand, followed by deinsertion and subsequent dissociation of ^{13}CO from the bridging N^{13}CO group to form the bridging nitrido species as shown in Figure 1.37 (*vide infra)*. Natural abundance CO could then be incorporated via the microscopic reverse of these steps, leading to the experimentally observed isotopologue, **4-N_2(^{13}C)CO_2-C_1**. Notably, the terminal isocyanate is unperturbed throughout this process and retains its isotopic label, consistent with the observed product. As mentioned, a significant amount of **4-$N_2{}^{13}C_2O_2$-C_1** was also observed in the above experiment, and this is due to incomplete exchange as a consequence of the competing rates of isotopic exchange and oxamidide formation (Figure 1.29).

Isotopic exchange into the terminal carbonyl position was also monitored by infrared spectroscopy. A solution of **4-(μ-NCO)(CO)(NCO)** was treated with 1 atm ^{13}CO at 0 ºC for 5 min and 1.0 h and the resulting solid-state KBr infrared spectra were collected (Figure 1.30). The IR spectra exhibit complementary disappearance and growth of the CO and ^{13}CO stretches at 1959 and 1913 cm^{-1}, respectively, over the course of 1 h, supporting the spectroscopic assignment and confirming the lability of the terminal carbonyl ligand in **4-(μ-NCO)(CO)(NCO)**.

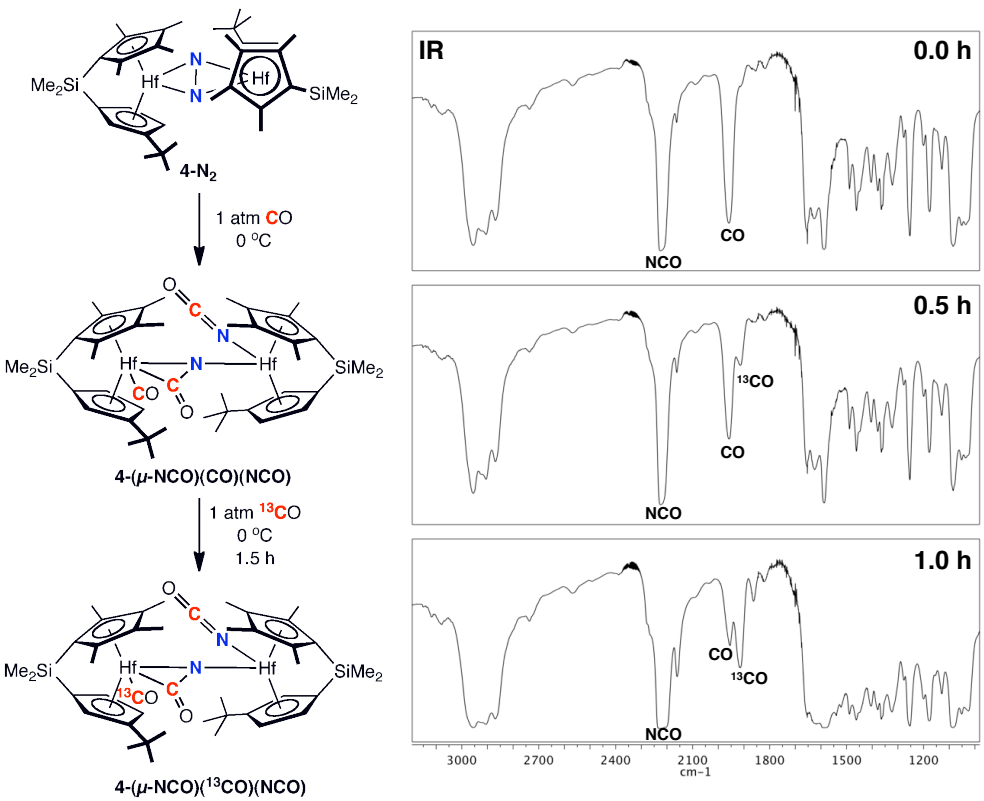

Figure 1.30. Isotopic exchange study to monitor ^{13}C exchange into the terminal CO position of **4-(μ-NCO)(CO)(NCO)** by infrared spectroscopy.

Kinetics of oxamidide formation from 4-(μ-NCO)(CO)(NCO). The discovery of **4-(μ-NCO)(CO)(NCO)** as an intermediate on the pathway to hafnocene oxamidide formation prompted a mechanistic study of the process. The half-life of the transformation shown in Figure 1.23 at room temperature is on the order of several minutes, making the system conducive to a kinetics study using variable temperature NMR spectroscopy. We sought to determine the observed rate constants for the conversion of **4-(μ-NCO)(CO)(NCO)** to **4-$N_2C_2O_2$-*C*$_2$** at various temperatures, and in turn the activation parameters of this transformation. We were also interested in the

pressure dependence of CO on the rate of the reaction and on the ratio of C_1 and C_2-symmetric oxamidide products at completion.

To determine the rate constants for oxamidide formation, the following experimental procedure was used. In a typical run, 0.015 of **4-N_2** was dissolved in 0.600 mL benzene-d_6 in a J. Young NMR tube and treated with approximately 1 atm CO. The contents of the tube were thawed and shaken until the solution turned clear and red-brown in color, signaling conversion to **4-(μ-NCO)(CO)(NCO)**, at which point the contents of the tube were quickly re-frozen and the headspace evacuated. To avoid isomeric misctures, and to ensure exclusive formation of the C_2-symmetric isomer and efficient mixing, the tube was pressurized with 4 atm CO. The thawing tube was quickly transferred to the NMR spectrometer probe (preset to the desired temperature) for data collection. An arrayed 1D ^{1}H NMR experiment was performed whereby spectra were recorded at approximately 60 second intervals for the duration of the reaction. Each kinetic run was repeated in triplicate, and the kinetics of the reaction were measured over a range of temperatures from 10 to 40 ºC at 5 ºC intervals. Representative plots of concentration versus time are presented in Figure 1.31, showing the decay of **4-(μ-NCO)(CO)(NCO)** and the evolution **4-$N_2C_2O_2$-*C_2*** with respect to time at 15 ºC. A comprehensive set of plots are presented in Appendix B. Relative concentrations of **4-(μ-NCO)(CO)(NCO)** and **4-$N_2C_2O_2$-*C_2*** were determined based on the integrations of their Cp*H* resonances, and absolute concentrations were calculated based on the known starting concentration of **4-(μ-NCO)(CO)(NCO)**. The decay of **4-(μ-NCO)(CO)(NCO)** and the growth of **4-$N_2C_2O_2$-*C_2*** were both clearly observable by this method, providing reliable and reproducible data for interpretation. A slight erosion (~10-15%) of total concentration ([**4-(μ-NCO)(CO)(NCO)**] + [**4-$N_2C_2O_2$-*C_2***]) was observed during each run, attributed to the formation of several minor, unidentified byproducts.

Monitoring the disappearance of the CpH benzene-d_6 ^{1}H NMR resonance of **4-(μ-NCO)(CO)(NCO)** at 5.16 ppm under the above reaction conditions established first-order behavior for the conversion to the C_2-symmetric oxamidide product. Plots of ln([**4-(μ-NCO)(CO)(NCO)**]) versus time and -1/([**4-(μ-NCO)(CO)(NCO)**]) versus time at 15 ºC are presented in Figure 1.32 and clearly establish a first-order dependence on [Hf].

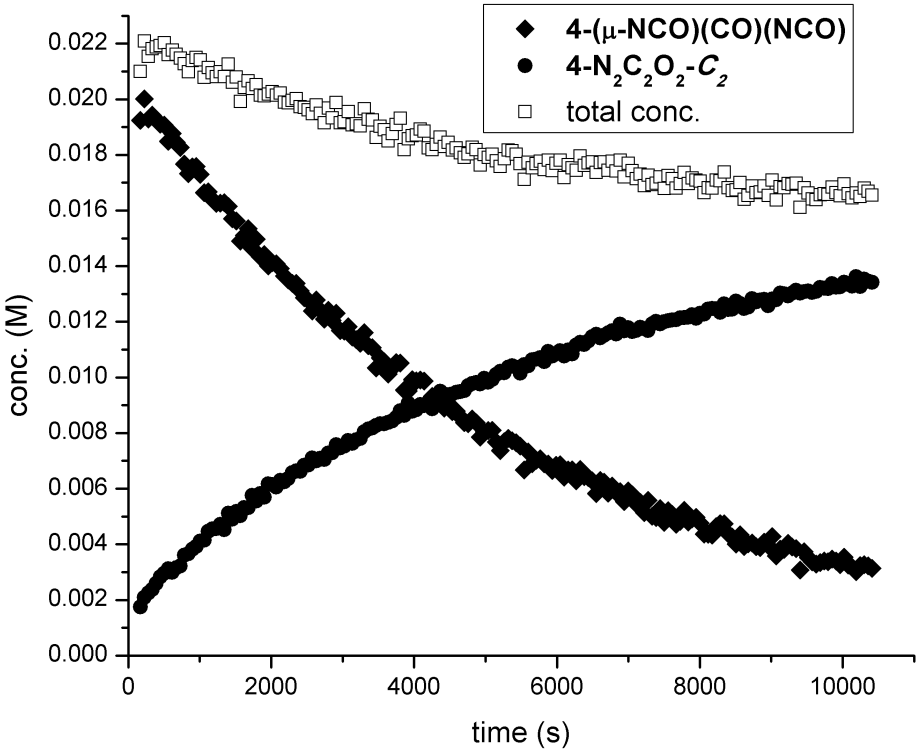

Figure 1.31. Representative plot of concentration versus time at 15 ºC. Note: total conc. = [**4-(μ-NCO)(CO)(NCO)**] + [**4-$N_2C_2O_2$-C_2**]

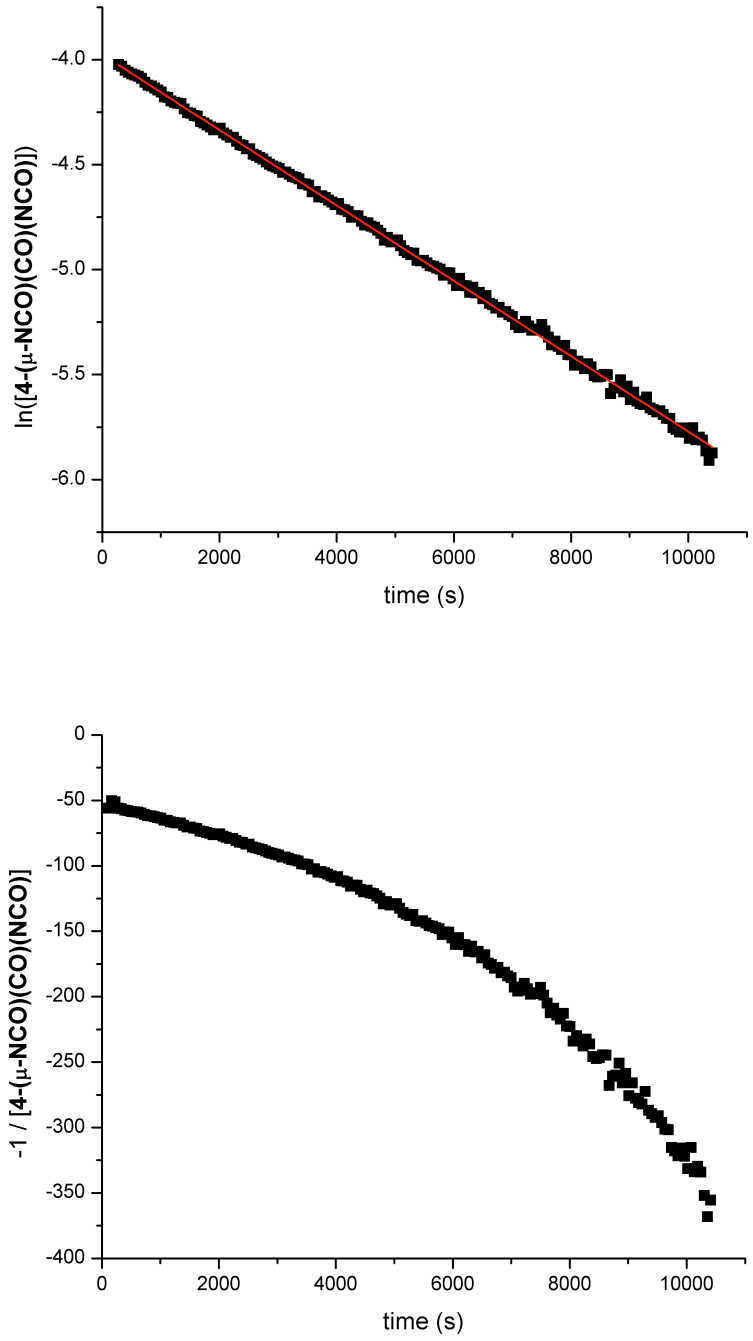

Figure 1.32. First-order (top) and second-order (bottom) plots for disappearance of **4-(μ-NCO)(CO)(NCO)** at 15 ºC.

To determine the activation parameters for the process in Figure 1.23 (C_2-symmetric path), rate constants for the reaction were measured over a 30 ºC temperature range. The first-order plots of these reactions are presented in Figure 1.33 and their respective observed rate constants are reported in Table 1.3. An Eyring plot was constructed from these results and is presented in Figure 1.34, and activation parameters of $\Delta H^{\ddagger} = 20.5(3)$ kcal/mol and $\Delta S^{\ddagger} = -4.4(8)$ eu were obtained from the data, giving a total activation barrier of $\Delta G^{\ddagger} = 21.8(5)$ kcal/mol at 20 ºC.

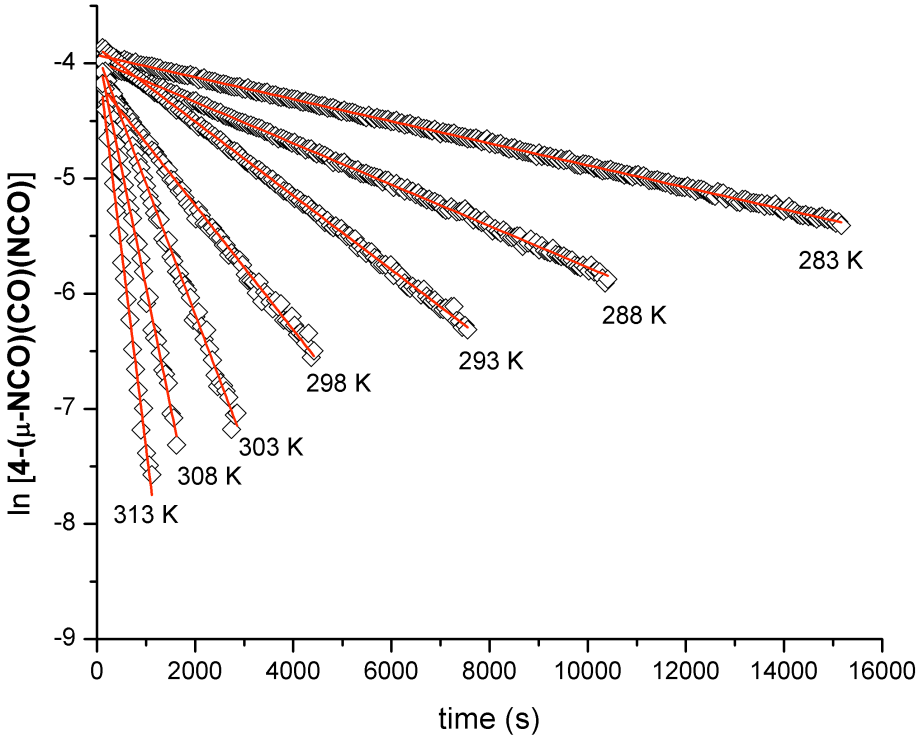

Figure 1.33. First-order kinetic plots of representative runs for T = 283-313 K.

Table 1.3. Rate constants, k_{obs}, for the first-order decay of **4-(μ-NCO)(CO)(NCO)** at various temperatures.

Temperature (K)	k_{obs} (10^4 s^{-1})
283	1.02
288	1.80
293	3.32
298	5.85
303	11.7
308	20.4
313	35.7

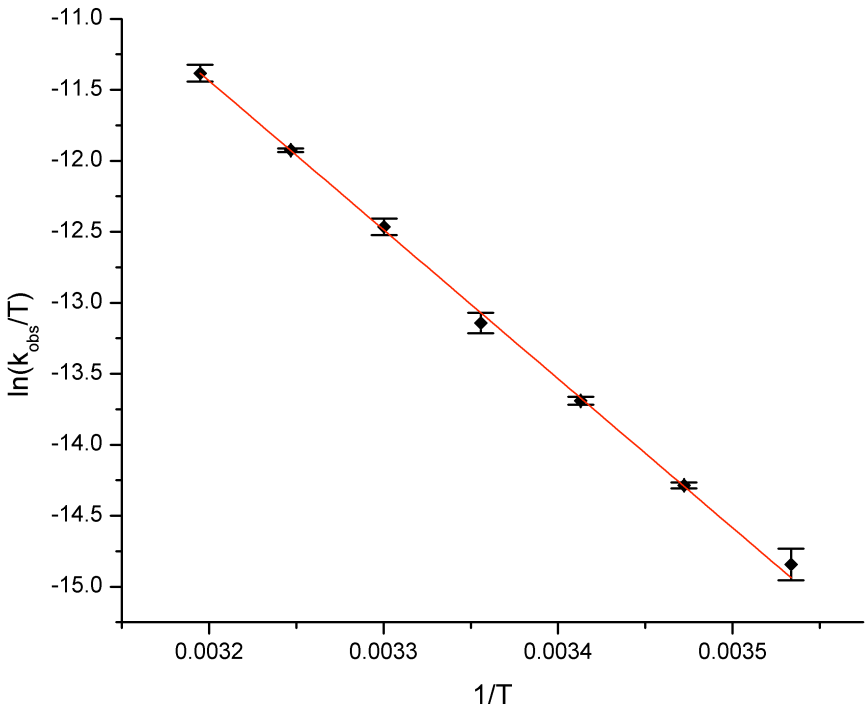

Figure 1.34. Eyring plot for the first-order decay of **4-(μ-NCO)(CO)(NCO)**.

Dependence of oxamidide formation on carbon monoxide concentration.

Upon inspection of the observed intermediate species shown Figure 1.22, it was expected that the rate of formation of **4-$N_2C_2O_2$-*C*$_2$** might be inhibited by [CO] as one equivalent of CO is lost on the way to oxamidide formation. Thus, to determine the effect, if any, of [CO] on the rate of oxamidide evolution, rate constants were measured under 1 atm of CO and 0 atm CO while maintaining a constant temperature of 20 ºC. The first-order plots of these kinetic data are presented in Figure 1.35, and the observed first-order rate constants with respect to CO concentration are presented in Table 1.4. In general, little change in k_{obs} was observed for 1 atm CO and 0 atm CO compared to 4 atm CO, over full conversion of **4-(μ-NCO)(CO)(NCO)**. Interestingly, for [CO] = 0 atm, at short reaction times (t = 0 to t = 5 min) a slight increase in k_{obs} was observed, followed by a decrease in rate. The increased rate at short times also coincides with increased production of **4-($N_2C_2O_2$)-*C*$_1$**, which eventually is suppressed as **4-($N_2C_2O_2$)-*C*$_2$** becomes favored (t > 5 min for the [CO] = 0 atm run). In the corresponding first-order kinetic plot this phenomenom is manifested as a slight curvature at short reaction times (Figure 1.35). The increased rate at short times is therefore likely not a true inverse dependence on [CO], but rather a consequence of the pathway to the C_1-symmetric isomer, **4-($N_2C_2O_2$)-*C*$_1$**, becoming accessible at short reaction times when the decay of **4-(μ-NCO)(CO)(NCO)** occurs in the absence of additional CO. Eventually enough CO is liberated *in situ* to shift the equilibrium (see Figure 1.39, *vide infra*) in favor of the C_2 regime and the observed rate of reaction slows accordingly. These observations also suggest that the pathways to **4-($N_2C_2O_2$)-*C*$_1$** and **4-($N_2C_2O_2$)-*C*$_2$** likely diverge at **4-(μ-NCO)(NCO)** (Figure 1.39) and that the formation of **4-($N_2C_2O_2$)-*C*$_1$** is faster than that of **4-($N_2C_2O_2$)-*C*$_2$**.

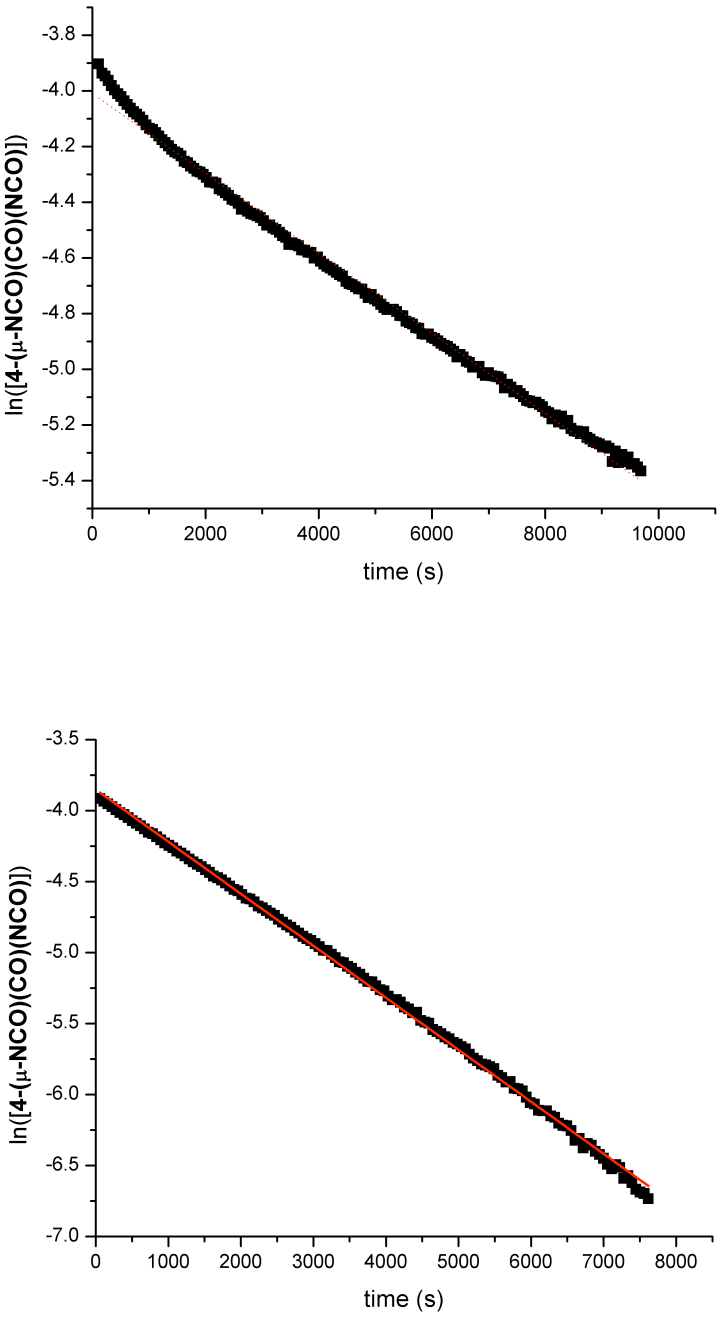

Figure 1.35. Representative first-order kinetic plots for the conversion of [**4-(μ-NCO)(CO)(NCO)**] to **4-$N_2C_2O_2$-*C*$_2$** under 0 atm CO (top) and 1 atm CO (bottom) at 15 ºC.

Table 1.4. Experimental rate constants as a function of CO pressure for the conversion of **4-(μ-NCO)(CO)(NCO)** to **4-$N_2C_2O_2$-C_2** at 20 ºC.

Approximated headspace CO pressure (atm)[b]	k_{obs} (10^4 s^{-1})[a]
4	3.32
1	3.52
0	3.75

a) Rate constants taken as an average of at least three consistent independent trials.

b) CO concentrations determined based on solubility data in reference 49.

All of the collected data are consistent with an overall first-order reaction with the following rate law: Rate = k_{obs}[**4-(μ-NCO)(CO)(NCO)**]. This is summarized in Figure 1.36.

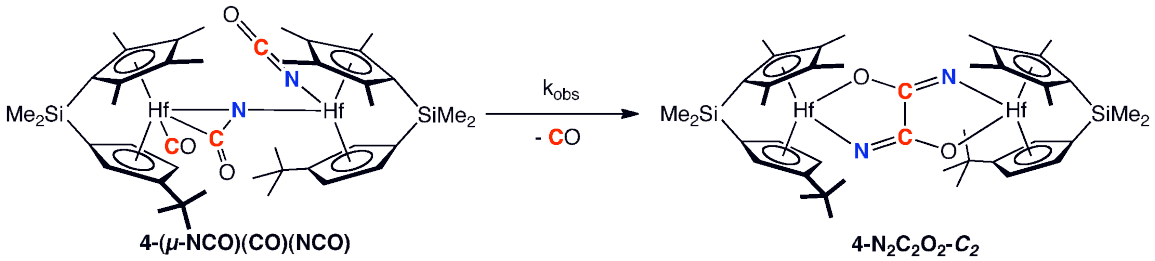

Figure 1.36. Observed rate law for the conversion of **4-(μ-NCO)(CO)(NCO)** to **4-$N_2C_2O_2$-C_2**.

Mechanistic proposal. The lack of observable species combined with the likelihood of a relatively complicated sequence of interrelated CO-

dissociation/coordination equilibria with branching pathways to different isomers makes proposing a definitive mechanism for the overall process quite tenuous. Still, all of our findings combined form a reasonably complete picture of the reaction between **4-N_2** and carbon monoxide, and a simplified mechanism for the reaction is proposed in Figure 1.37 and Figure 1.38. What is quite clear, and perhaps the most striking feature of the reaction, is that *N-N cleavage occurs rapidly and precedes CO homologation and C-C bond formation* in the mechanism.

The proposed mechanism begins (Figure 1.37) with insertion of one equivalent of CO into a Hf-N bond, followed by retro-[2+2] addition or β-elimination, forming a bridging nitrido species with a terminal isocyanate ligand. The trapping of this species with various reagents will be discussed at length in the following chapter. The isotopic exchange studies discussed earlier implicate a series of equilibria linking this hafnium μ-nitrido intermediate and **4-(μ-NCO)(CO)(NCO)**, the observable hafnocene compound, by a series of CO coordination and insertion events.

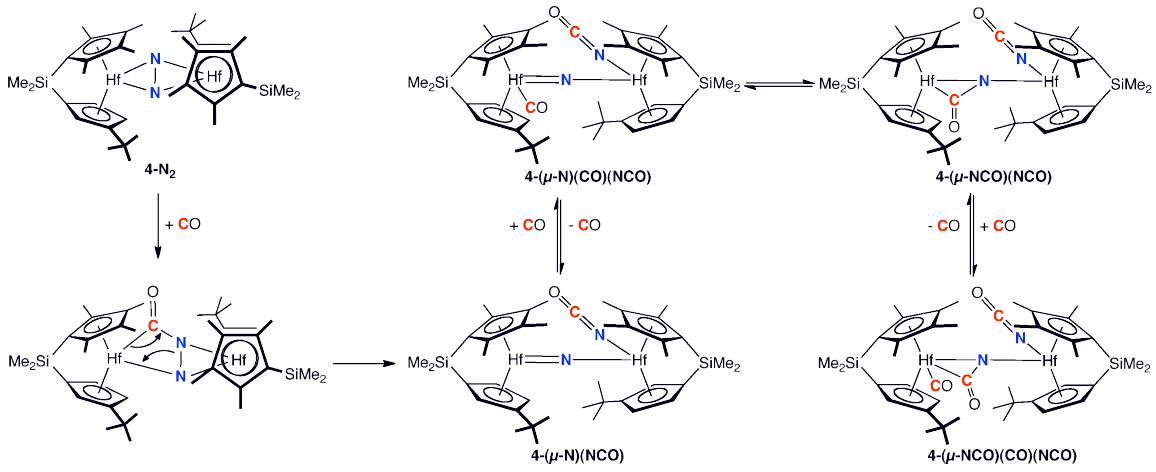

Figure 1.37. Proposed mechanism for formation of **4-(μ-NCO)(CO)(NCO)**.

A proposed mechanism for conversion of **4-(μ-NCO)(CO)(NCO)** to **4-($N_2C_2O_2$)-C_2** is presented in Figure 1.38. Rearrangement of the bridging isocyanate ligand forms a Hf-O bond. The details of this rearrangement are currently under investigation, and two possibilities are presented in Figure 1.38. This step is likely rate-determining due to the independence of the rate on the pressure of CO. In a series of fast, subsequent steps (or, alternatively, a single concerted step) the isocyanate ligands couple, forming a new C-C bond, and CO dissociation furnishes the observed product, **4-($N_2C_2O_2$)-C_2**. A recent computational study on the mechanism of formation of **4-($N_2C_2O_2$)-C_2** has been reported by Schwarz and coworkers, and also is consistent with rapid N-N cleavage and subsequent C-C bond formation *via* an isocyanate coupling mechanism, although the details of the isocyanate rearrangement were not computed.[50] Also, while the experimentally observed intermediate **4-(μ-NCO)(CO)(NCO)** was not calculated, the CO-free bridging isocyanate compound, **4-(μ-NCO)(NCO)**, was calculated and lies on the computed reaction coordinate in Schwarz's proposed mechanism.[50]

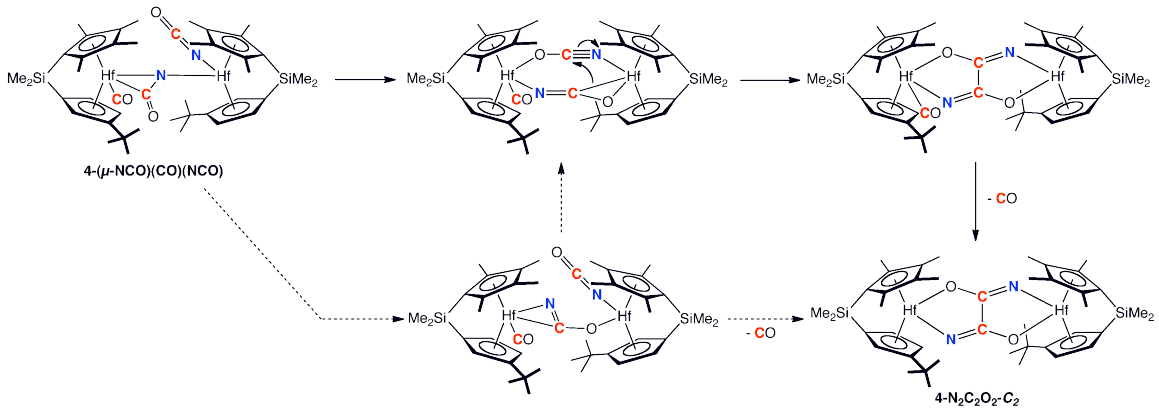

Figure 1.38. Proposed mechanism for the conversion of **4-(μ-NCO)(CO)(NCO)** to **4-$N_2C_2O_2$-C_2**.

The C_1-symmetric product must also be accounted for. Isotopic exchange studies discussed above have established a series of equilbria between **4-(μ-NCO)(CO)(NCO)** and the proposed bridging nitrido species **[4-(μ-N)(NCO)** + 2 CO]. It is likely that rotation about the Hf-N bond in **[4-(μ-N)(NCO)]** gears the cyclopentadienyl ligands into the appropriate configuration on the pathway to **4-($N_2C_2O_2$)-C_1** formation (Figure 1.39). This is supported by the fact that **4-($N_2C_2O_2$)-C_1** is favored at lower CO pressure and higher temperature. It is also possible that bond rotation occurs in the proposed bridging isocyanato intermediate, [**4-(μ-NCO)(NCO)]**, although such a transformation would not preserve the relative stereochemistry of the bridging and terminal isocyanate ligands with respect to each other and would necessitate an alternative mechanism for formation of the C_1-symmetric oxamidide product. Also, the kinetic experiments discussed above suggest that conversion from either **[4-(μ-N)(NCO)]** or **[4-(μ-NCO)(NCO)]** to **4-($N_2C_2O_2$)-C_1** is rapid, possibly explaining why an additional stereoisomer of **4-(μ-NCO)(CO)(NCO)** was never observed.

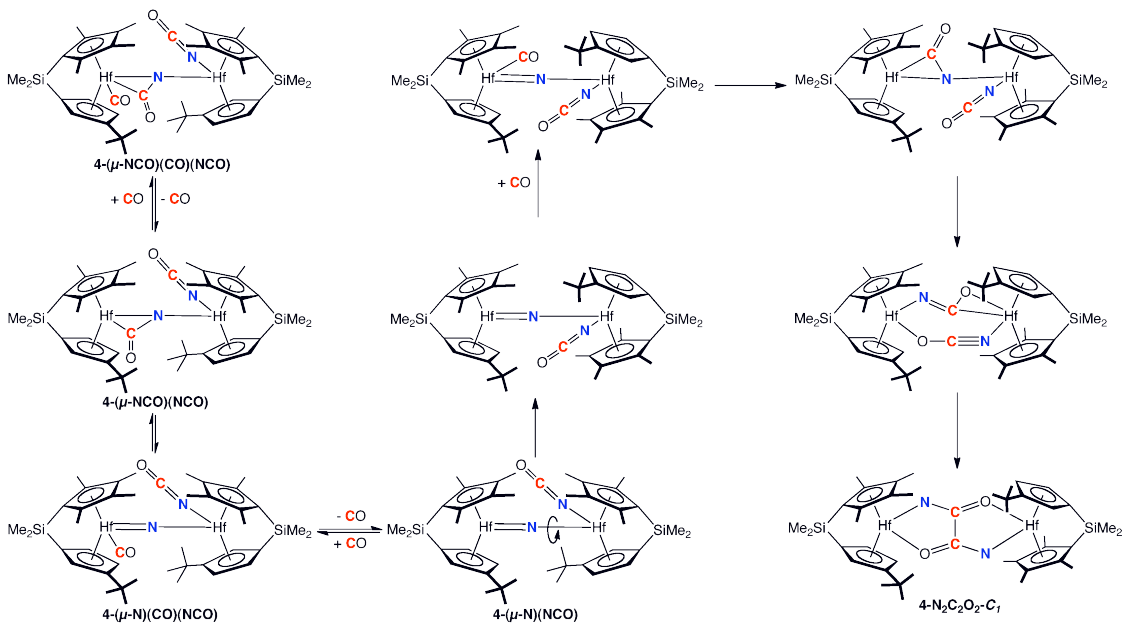

Figure 1.39. Proposed mechanism for the conversion of **4-(μ-NCO)(CO)(NCO)** to **4-$N_2C_2O_2$-*C_1***.

Reactivity of 4-(μ-NCO)(CO)(NCO) with methyl iodide, *tert*-butylisocyanate, and carbon dioxide. The intermediate **4-(μ-NCO)(CO)(NCO)** was treated with excess methyl iodide in a two-fold effort to intercept it in an isolable form and to form a new nitrogen-carbon bond from an external reagent following the N-N cleavage step. (A complete study of oxamidide reactivity with a variety of substrates will be presented in Chapter 3). Addition of 5 equivalents CH_3I to a benzene solution of **4-(μ-NCO)(CO)(NCO)** resulted in clean, rapid conversion to a new C_1 symmetric product identified as **5** (Figure 1.40). This new complex contains a new C-N and C-C bond, resulting from formal 1,2-addition of CH_3 across the Hf-N bond and concomitant CO homologation. The structure was characterized by NMR (^{1}H, ^{13}C, ^{15}N) and infrared spectroscopic studies, and the {^{1}H}^{13}C NMR spectra of isotopically

enriched **5-$^{15}N_2{}^{13}C_3$** is presented in Figure 1.42 (top spectrum). Interestingly, the most downfield chemical shift in the benzene-d_6 ^{13}C NMR spectrum was assigned as the carbon in the beta position, and not the acyl carbon. The assignment was given on the basis of relative N-C and C-C coupling constants, reported in Table 1.5. To determine the origin of the beta carbon, **4-(μ-NCO)(^{13}CO)(NCO)** was prepared and treated with CH_3I. This procedure is represented in Figure 1.41, and the benzene-d_6 ^{13}C NMR spectrum of the resulting product is presented in Figure 1.42 (bottom spectrum). This spectrum establishes that the beta carbon in **5** is derived from the terminal carbonyl ligand in **4-(μ-NCO)(CO)(NCO)**. This is an unexpected result, and further support of the unusual spectroscopic assignment and its mechanistic implications are the focus of ongoing studies in our laboratory.

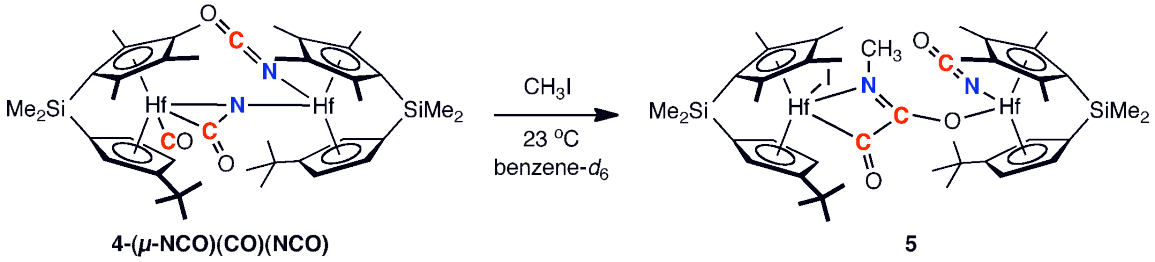

Figure 1.40. Addition of CH_3I to **4-(μ-NCO)(CO)(NCO)**.

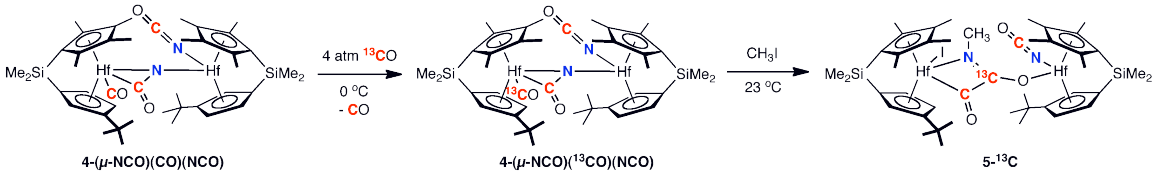

Figure 1.41. Selective isotopic labeling of **5**.

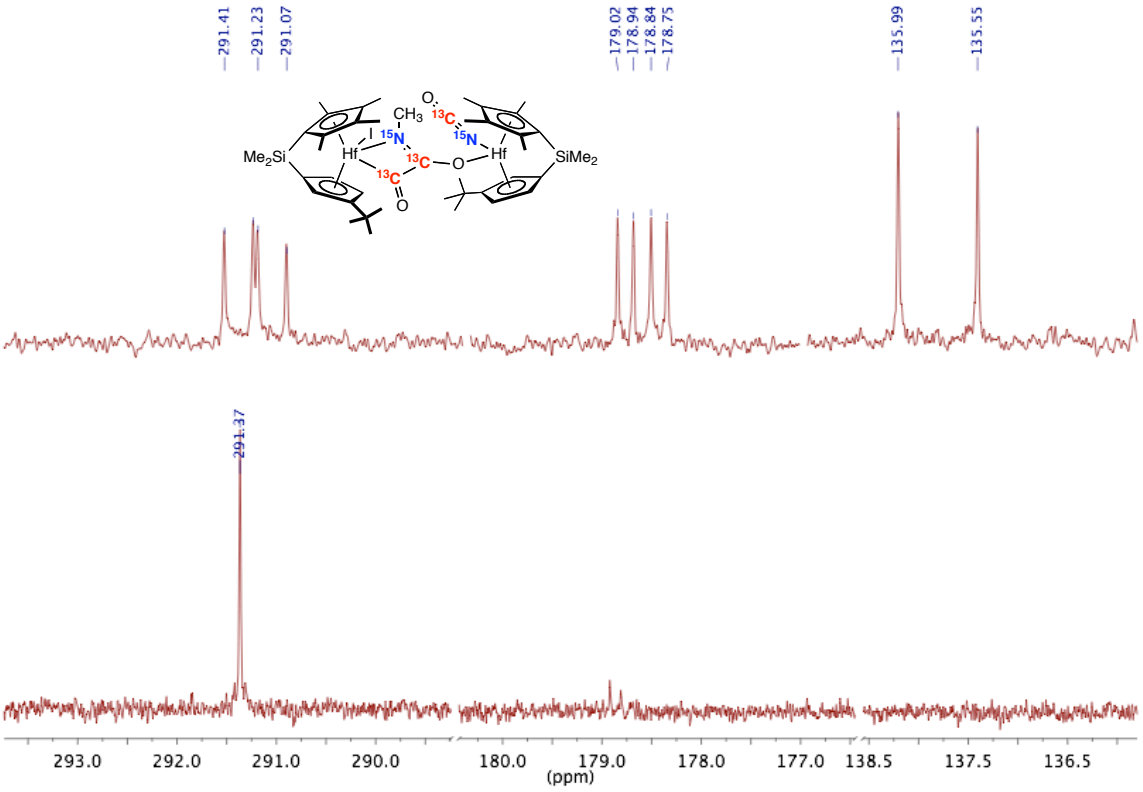

Figure 1.42. Partial benzene-d_6 ^{13}C NMR spectra of **5-$^{15}N_2{}^{13}C_3$** (top) and **5-$N_2{}^{13}C_1$** (bottom) at 23 ºC.

Table 1.5. Selected benzene-d_6 (23 ºC) NMR data for **5**, **6**, and **4-(μ-O)(NCO)$_2$**.

Compound	$\{^1H\}^{13}C$ NMR ∂ (ppm)	^{15}N NMR ∂ (ppm)
5	38.83 (N***C***H$_3$) $^2J_{CC}$ = 6.2 Hz $^3J_{CC}$ = 3.2 Hz 135.77 (HfN***C***O) $^1J_{CN}$ = 32.9 178.89 (Hf(***C***O)C=N) $^1J_{CC}$ = 13.8 Hz $^2J_{CN}$ = 6.6 Hz 291.24 (Hf(CO)***C***=N) $^1J_{CN}$ = 11.9 Hz	91.4 (Hf***N***CO) $^1J_{CN}$ = 32.9 Hz 227.3 (Hf(CO)C=***N***) $^1J_{CN}$ = 11.9 Hz $^2J_{CN}$ = 6.6 Hz
6	134.07 (HfN***C***O) $^1J_{CN}$ = 33.9 176.15 (Hf(***C***O)C=N) $^1J_{CC}$ = 10.9 Hz $^2J_{CN}$ = 1.3 Hz 303.60 (Hf(CO)***C***=N) $^1J_{CN}$ = 13.8 Hz	91.1 (Hf***N***CO) $^1J_{CN}$ = 33.9 Hz 205.7 (Hf-(CO)-C=***N***) $^1J_{CN}$ = 13.8 Hz $^2J_{CN}$ = 1.3 Hz
4-(μ-O)(NCO)$_2$	135.76 (HfN***C***O) $^1J_{CN}$ = 33.8	94.6 (Hf***N***CO) $^1J_{CN}$ = 33.8 Hz

The molecular structure of **5** was confirmed by single crystal X-ray diffraction. A representation of the structure of the (*S*,*S*)-enantiomer is presented in Figure 1.43, and the (*R*,*R*)-enantiomer is reported in Appendix C. The crystal structure confirms new N-C and C-C bond formation in the core of the molecule, giving rise to an unusual bridging imidate and a planar four-membered cyclometallate. The terminal isocyanate and hafnium acyl groups are both *syn* to *tert*-butyl substituents on the cyclopentadienyl rings. Selected metrical paramters are reported in Table 1.6. The reaction demonstrates that the intermediate species **4-(μ-NCO)(CO)(NCO)** can be intercepted by an appropriate substrate and that additional N-C bond formation is possible.

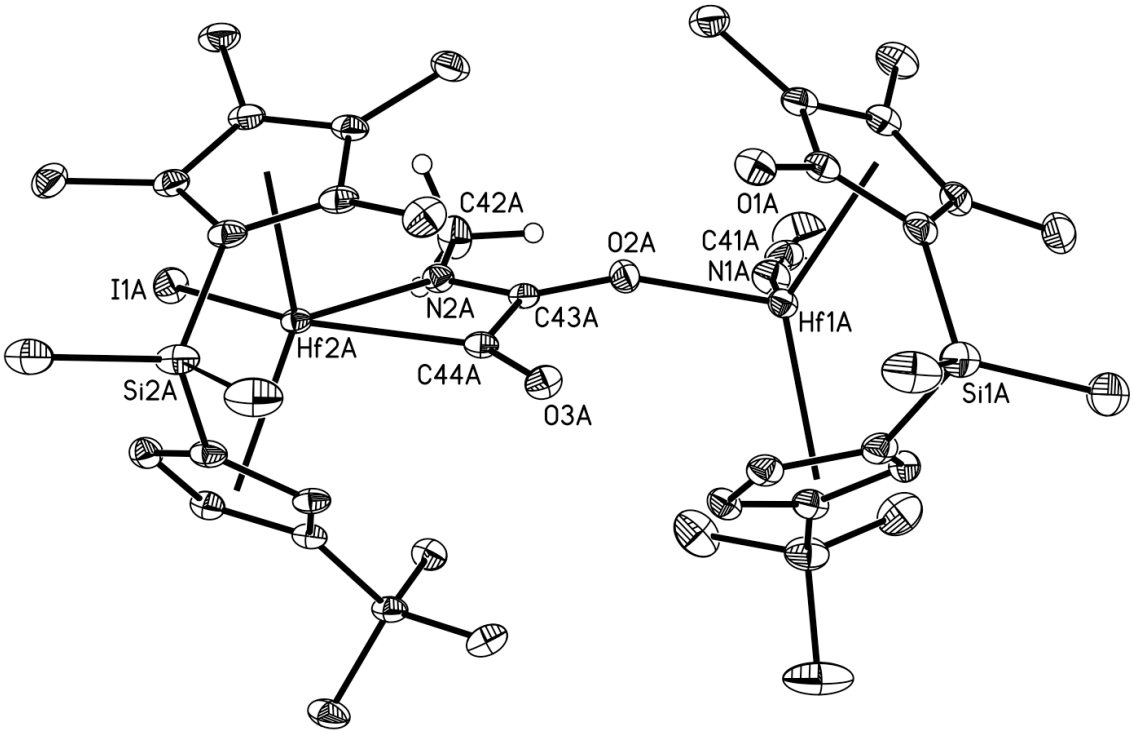

Figure 1.43. Molecular structure of **5** at 30% probability ellipsoids. Hydrogen atoms, except those on the N-CH_3 group, omitted for clarity. The (*S,S*) enantiomer is shown.

Table 1.6. Selected distances and angles in **5**.

Bond / Angle	Distance (Å) / Angle (º)
Hf1A-O2A	2.0149(19)
Hf2A-N2A	2.354(2)
Hf2A-C44A	2.338(3)
O2A-C43A	1.292(3)
O3A-C44A	1.214(3)
N2A-C43A	1.29(3)
N2A-C42A	1.462(3)
C43A-C44A	1.533(5)
Hf1A-O2A-C43A	159.86(17)

Similar reactivity was observed when **4-(μ-NCO)(CO)(NCO)** was treated with *tert*-butyl isocyanate (Figure 1.44). The resulting product, **6**, arising from cycloaddition of the heterocumulene across the Hf-N bond, was characterized by multinuclear NMR and infrared spectroscopies. Selected NMR data are reported in Table 1.5. The benzene-d_6 ^{13}C NMR spectrum of the ^{15}N-/^{13}C-enriched isotopologue, **6-$^{15}N_2{}^{13}C_2$**, is presented in Figure 1.45 and confirms N-C and C-C bond formation. The absolute stereochemistry of **6** is unknown, although it likely adopts a configuration analogous to that of **5**, with the hafnium acyl and terminal isocyanate groups both *syn* to the cyclopentadienyl *tert*-butyl substituents. As with **5**, the carbon atom in the beta position is most likely derived from the carbonyl group in the terminal position in **4-(μ-NCO)(CO)(NCO)**, although further isotopic labeling studies are necessary for definitive assignment.

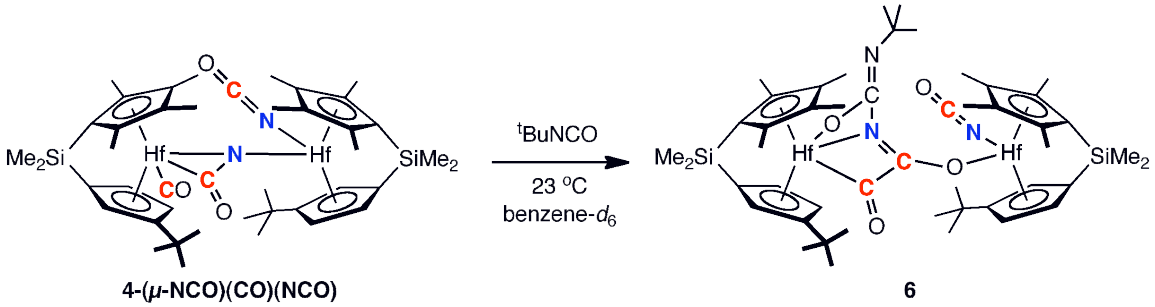

4-(μ-NCO)(CO)(NCO) 6

Figure 1.44. Treatment of **4-(μ-NCO)(CO)(NCO)** with ^{t}BuNCO.

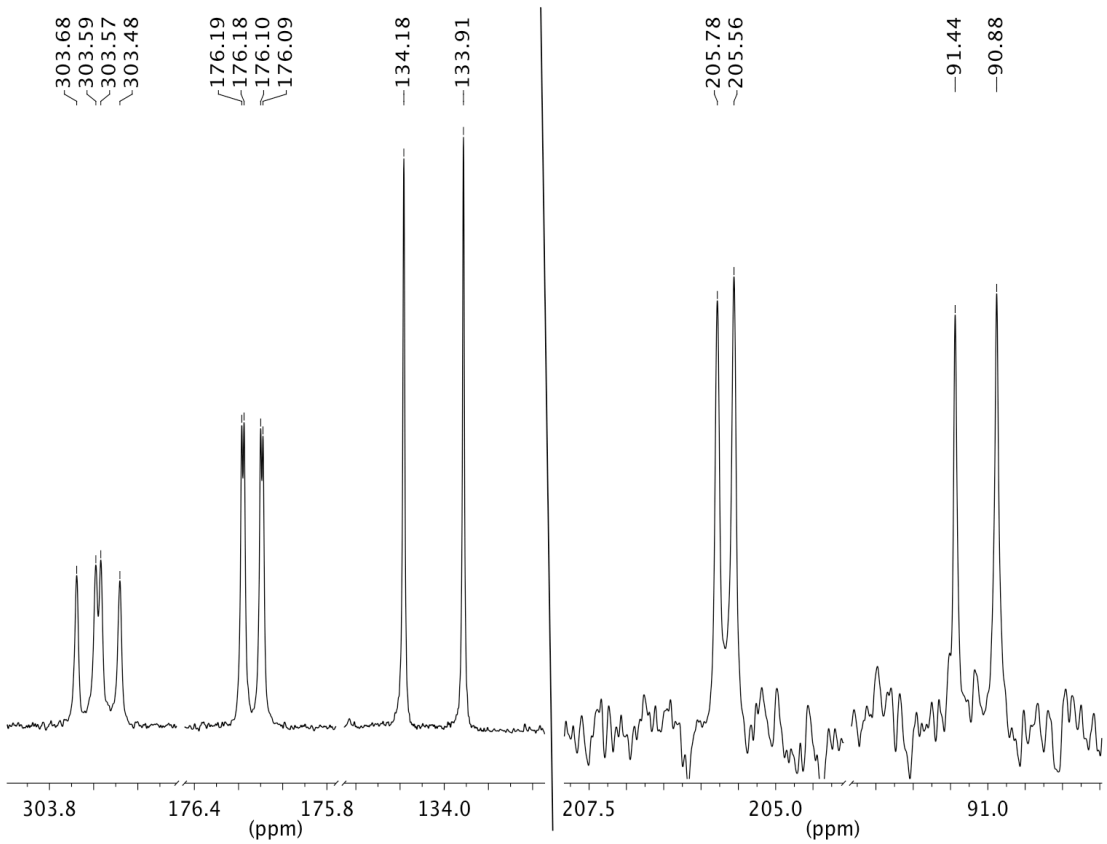

Figure 1.45. Benzene-d_6 ^{13}C (left) and ^{15}N (right) NMR spectra of **6-$^{15}N_2{}^{13}C_3$** at 23 ºC.

The successful interception of **4-(μ-NCO)(CO)(NCO)** with CH_3I and *tert*-butylisocyanate prompted the addition of carbon dioxide to **4-(μ-NCO)(CO)(NCO)** with the expectation of an analogous product. Surprisingly, treatment of **4-(μ-NCO)(CO)(NCO)** resulted in exclusive formation of a new C_2-symmetric product identified as the μ-oxo dihafnocene bis(isocyanato) compound, **4-(μ-O)(NCO)$_2$** along with concomitant loss of two equivalents of carbon monoxide (Figure 1.46).

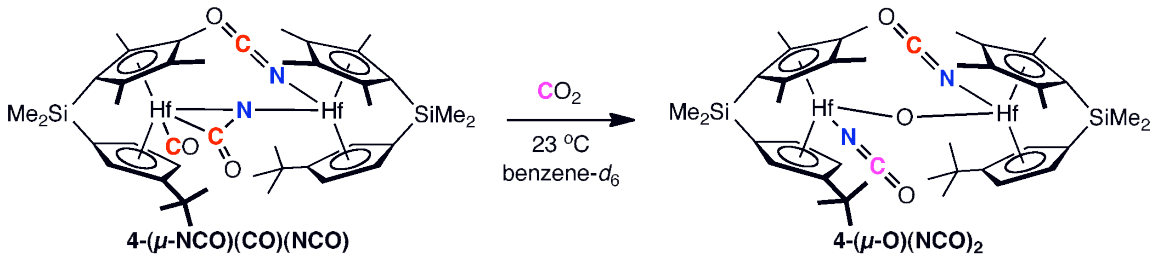

Figure 1.46. Treatment of **4-(μ-NCO)(CO)(NCO)** with CO_2.

The structure of **4-(μ-O)(NCO)$_2$** was established by multinuclear (^{1}H, ^{13}C, ^{15}N) NMR and infrared spectroscopies and single crystal X-ray diffraction. Selected NMR data are reported in Table 1.5. To determine the origin of the terminal isocyanate ligands (i.e. CO-derived versus CO_2-derived), the ^{15}N-enriched isotopologue of the starting material, **4-(μ-^{15}NCO)(CO)(NCO)**, was treated with $^{13}CO_2$. The benzene-d_6 ^{15}N spectrum of the product of this reaction is presented in Figure 1.47, and establishes a roughly 1:1 ratio of $^{15}N^{13}CO$ groups to ^{15}NCO groups based on integration, consistent with the formation of the product isotopologue **4-(μ-O)(^{15}N^{13}CO)(^{15}NCO)**, where one isocyanate group is derived from carbon monoxide, and the other from carbon dioxide. It is also likely the bridging oxo group is derived from deoxygenation of added carbon dioxide, although the possibility that it originates

from carbon monoxide has not been definitively ruled out. Importantly, the spectroscopic data confirm additional N-C bond formation from carbon dioxide.

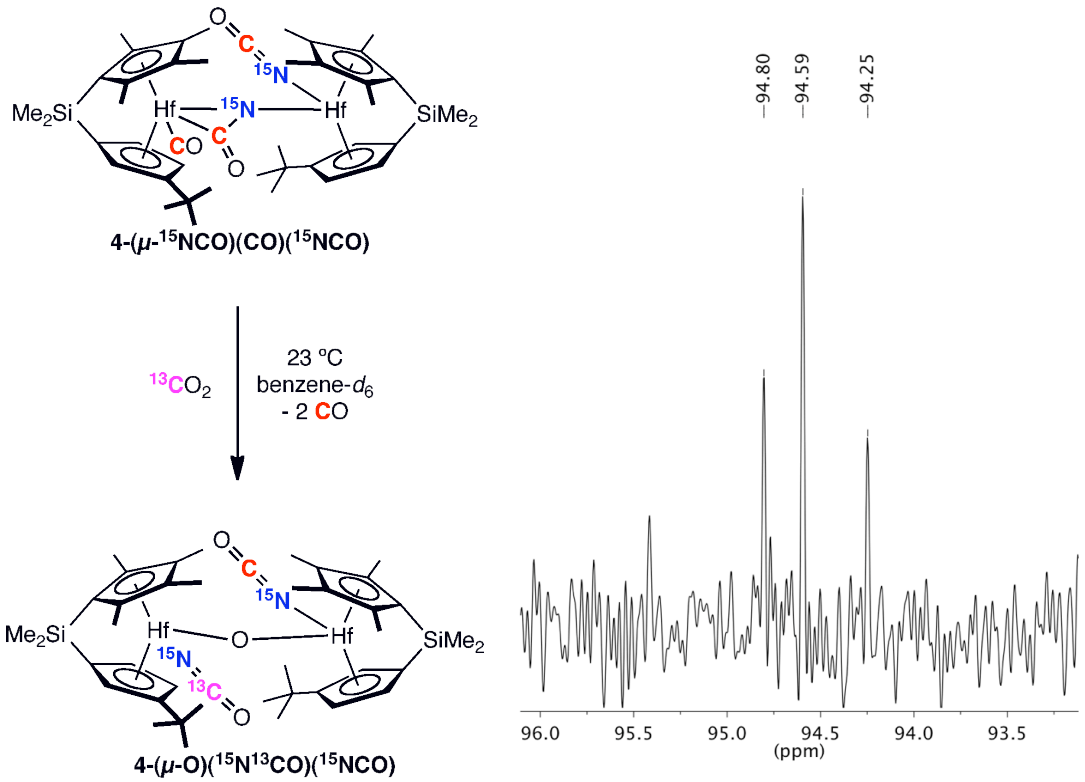

Figure 1.47. Formation of **4-(μ-O)(^{15}N^{13}CO)(^{15}NCO)** and corresponding ^{15}N NMR spectrum collected in benzene-d_6 at 23 ºC.

Single crystals of **4-(μ-O)(NCO)$_2$** suitable for X-ray diffraction were obtained and a representation of the molecular structure is presented in Figure 1.48. The (*S*,*S*)-enantiomer is shown here, and the (*R*,*R*)-enantiomer is reported in Appendix C. The structure confirms the presence of a bridging oxygen atom as well as the equivalent terminal isocyanate groups. Notably the Hf-O-Hf angle is effectively linear in accordance with the idealized C_2-symmetry of the molecule. Other selected metrical data are reported in Table 1.7. Overall the interception experiments with CH_3I, -

^{t}BuNCO, and CO_2 demonstrate the potential of **4-(μ-NCO)(CO)(NCO)** as a platform for additional N-C bond forming reactions with a variety of substrates.

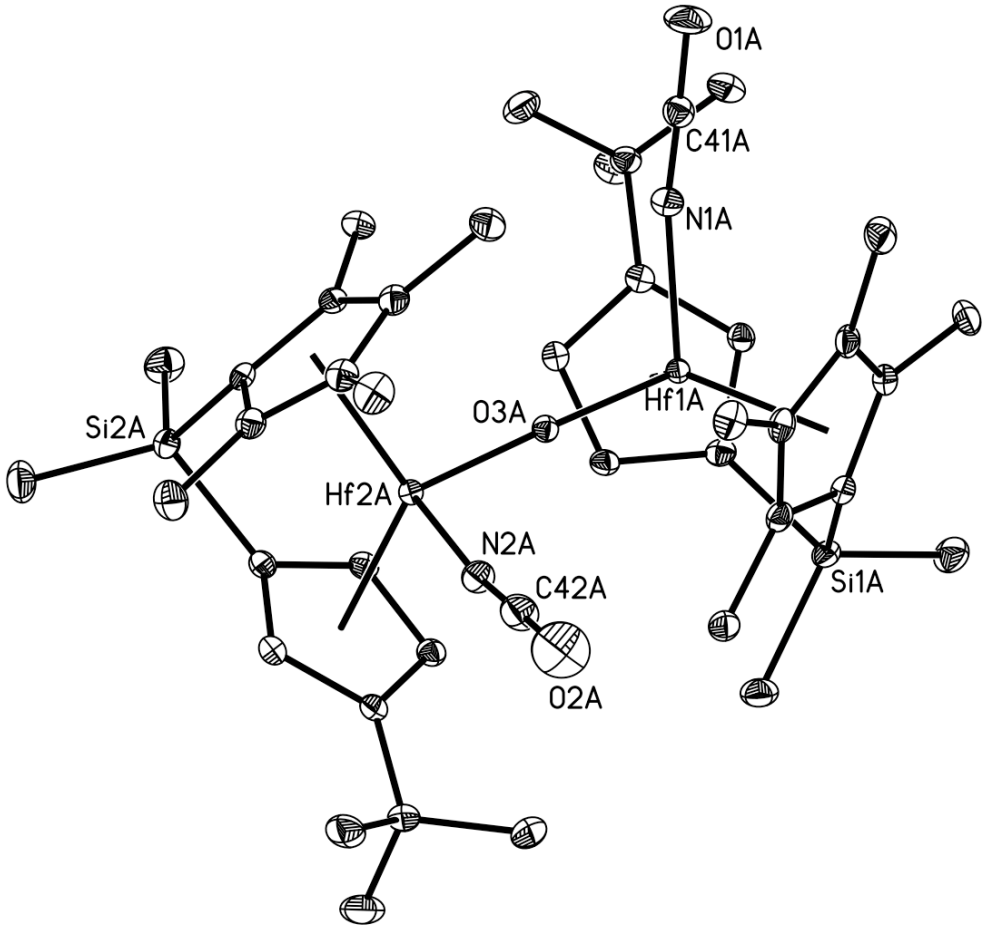

Figure 1.48. Molecular structure of **4-(μ-O)(NCO)$_2$** at 30% probability ellipsoids. H-atoms are omitted for clarity. The (*S*,*S*)-enantiomer is shown.

Table 1.7. Selected metrical parameters for **4-(μ-O)(NCO)$_2$**.

Bond / Angle	Distance (Å) / Angle (°)
Hf1A-O3A	1.9747(14)
Hf1A-N1A	2.1035(19)
Hf2A-O3A	1.9647(14)
Hf2A-N2A	2.1034(18)
Hf1A-O3A-Hf2A	175.91(8)
N1A-C41A-O1A	178.6(3)
N2A-C42A-O2A	179.0(4)

Conclusions

The successful synthesis of **4-N$_2$** completed a family group 4 metallocene dinitrogen compounds (**1-N$_2$**, **2-N$_2$**, **3-N$_2$**, and **4-N$_2$**). Addition of carbon monoxide to these complexes resulted in N_2 cleavage and formation of unprecedented oxamidide complexes; higher purities and yields were obtained from the more activated hafnium congeners. For the *ansa*-metallocene examples, two isomeric oxamidide products were observed in a ratio dependent on the pressure of added CO. In the case of **4-N$_2$**, at shorter reaction times an unusual bridging isocyanate intermediate, **4-(μ-NCO)(CO)(NCO)**, was observed en route to oxamidide formation. The kinetics of this transformation were studied, establishing a rate law that is overall first-order, with activation parameters of $\Delta H^{\ddagger} = 20.5(3)$ kcal/mol and $\Delta S^{\ddagger} = -4.4(8)$ eu, and no inhibition by CO. The kinetics, in combination with isotopic exchange studies, are consistent with a mechanism in which N-N cleavage is fast and precedes a series of equilibria that incorporate two additional equivalents of CO into the molecule prior to C-C bond formation.

Experimental Section

General Considerations. All air- and moisture-sensitive manipulations were carried out using standard high vacuum line, Schlenk or cannula techniques or in an M. Braun inert atmosphere drybox containing an atmosphere of purified nitrogen. The M. Braun drybox was equipped with a cold well designed for freezing samples in liquid nitrogen. Solvents for air- and moisture-sensitive manipulations were dried and deoxygenated using literature procedures.[51] Toluene, benzene, pentane and heptane were further dried by distillation from "titanocene".[52] Deuterated solvents for NMR spectroscopy were distilled from sodium metal under an atmosphere of argon and stored over 4 Å molecular sieves. Argon and hydrogen gas were purchased from Airgas Incorporated and passed through a column containing manganese oxide on vermiculite and 4 Å molecular sieves before admission to the high vacuum line. Carbon monoxide was also dried over 4 Å molecular sieves before admission to the high vacuum line. The metallocene dinitrogen complexes, **1-N_2**,[21] **2-N_2**,[22] and **3-N_2**[34] were prepared according to literature procedures.

^{1}H NMR spectra were recorded on a Varian Inova 400 Spectrometer operating at 399.860 MHz. All chemical shifts are reported relative to $SiMe_4$ using ^{1}H (residual) chemical shifts of the solvent as a secondary standard. ^{2}H, ^{13}C, ^{29}Si, and ^{15}N NMR spectra were recorded on a Varian Inova 500 Spectrometer operating at 76.848, 125.716, 161.83, 99.320 and 50.663 MHz, respectively. ^{2}H, ^{29}Si, and ^{13}C chemical shifts are reported relative to $SiMe_4$ using chemical shifts of the solvent as a secondary standard where applicable. ^{15}N chemical shifts are reported relative liquid to NH_3 using an external standard. The N-C coupling constants for **1-$N_2C_2O_2$**, **2-$N_2C_2O_2$**, and **3-$N_2C_2O_2$-*C_2*** are reported as an average of $^1J_{N\text{-}C}$ and $^2J_{N\text{-}C}$; these AA'XX' spin systems appear as effective triplets by ^{13}C NMR spectroscopy and this lack of detail in the spectra prevented accurate simulation. Infrared spectroscopy was conducted on a

Mattson RS-10500 Research Series FT-IR spectrometer calibrated with a polystyrene standard. Elemental analyses were performed at Robertson Microlit Laboratories, Inc., in Madison, NJ.

Preparation of $((\eta^5\text{-}C_5Me_4H)_2Zr)_2(N_2C_2O_2)$ (1-$(N_2C_2O_2)$). In a drybox, a J. Young NMR tube was charged with 0.020 g (0.027 mmol) of **1-N_2** and approximately 0.5 mL of benzene-d_6 was added. On a high vacuum line, the tube was submerged in liquid nitrogen, degassed and 1 atm of carbon monoxide was admitted at -196 °C. The contents of the tube were thawed and the resulting reaction monitored over the course of several hours. Initially, the starting dinitrogen compound was converted to a roughly (1:1) mixture of **1-$N_2C_2O_2$** and $[(\eta^5\text{-}C_5Me_4H)_2Zr(CO)]_2(\mu_2\text{-}N_2)$. Over the course of several hours, $[(\eta^5\text{-}C_5Me_4H)_2Zr(CO)]_2(\mu_2\text{-}N_2)$ had fully converted to **1-$(CO)_2$**,[44] affording a final **1-$N_2C_2O_2$** to **1-$(CO)_2$** ratio of approximately (1:0.7). ^{1}H NMR (benzene-d_6): ∂ = 1.87 (s, 12H, Cp*Me*$_4$H), 1.88 (s, 12H, Cp*Me*$_4$H), 2.02 (s, 12H, Cp*Me*$_4$H), 2.07 (s, 12H, Cp*Me*$_4$H), 5.76 (s, 4H, CpMe$_4$*H*). $\{^1H\}^{13}$C NMR (benzene-d_6): ∂ = 12.05 (Cp*Me*), 12.36 (Cp*Me*), 13.25 (Cp*Me*), 13.42 (Cp*Me*), 111.66, 119.40, 119.94, 124.62, 124.65 (*Cp*), 162.89 ($N_2C_2O_2$). ^{15}N NMR (benzene-d_6): ∂ = 400.4 ($^{15}N_2C_2O_2$) ($^1J_{CN}$, $^2J_{CN}$ = 3.7 Hz (average)). IR (KBr): ν = 1590 cm^{-1} (C=N).

Spectroscopic Identification of $[(\eta^5\text{-}C_5Me_4H)_2Zr(CO)]_2(\mu_2\text{-}N_2)$. ^{1}H NMR (benzene-$d_6$): ∂ = 1.73 (s, 6H, Cp*Me*$_4$H), 1.85 (s, 6H, Cp*Me*$_4$H), 1.87 (s, 6H, Cp*Me*$_4$H), 1.89 (s, 6H, Cp*Me*$_4$H), 1.90 (s, 6H, Cp*Me*$_4$H), 1.91 (s, 6H, Cp*Me*$_4$H), 1.92 (s, 6H, Cp*Me*$_4$H), 1.93 (s, 6H, Cp*Me*$_4$H), 4.70 (s, 2H, CpMe$_4$*H*), 4.71 (s, 2H, CpMe$_4$*H*). $\{^1H\}^{13}$C NMR (benzene-d_6): ∂ = 11.53 (Cp*Me*), 11.54 (Cp*Me*), 11.79 (Cp*Me*), 11.94 (Cp*Me*), 13.23 (Cp*Me*), 13.53 (Cp*Me*), 13.62 (Cp*Me*), 14.63 (Cp*Me*), 100.77, 100.99, 107.22, 107.62, 108.41, 108.45, 108.67, 109.95, 114.71, 116.70 (*Cp*), 283.02 (*C*O). ^{15}N NMR

(benzene-d_6): ∂ = 533.2 ($^{15}N_2$). IR (KBr): ν = 1608 cm^{-1} (N_2); 1844 cm^{-1}, 1907 cm^{-1} (CO).

Preparation of [(η^5-$C_5Me_4H)_2Hf]_2(\mu_2$-$^{15}N_2)$ (2-$^{15}N_2$). This compound was prepared in a similar manner to **2-(N_2)**[22] with the exception that the reaction mixture was quickly frozen and degassed prior to stirring. The headspace was then charged with $^{15}N_2$ and the reaction vessel was thawed and stirred as usual. **2-$^{15}N_2$** may also be prepared via exchange from **2-N_2**, but in smaller quantities and poorer isotopic enrichment.[22]

Preparation of [(η^5-$C_5Me_4H)_2Hf]_2(N_2C_2O_2)$ (2-$N_2C_2O_2$). In a drybox, a thick-walled glass vessel was charged with 0.150 g (0.172 mmol) of **2-N_2** dissolved in about 20 mL of toluene. On a high vacuum line, the vessel was degassed and 1 atm of carbon monoxide was admitted at -196 °C for a total pressure of 4 atm at 23 ºC. The vessel was thawed and its contents stirred for 2 hours after which time excess gas and solvent were removed *in vacuo*. In a drybox, the resulting burgundy oil was washed with cold pentane furnishing a yellow solid. This solid was dissolved in toluene and recrystallized at -35 °C affording pale yellow crystals of the desired product **2-$N_2C_2O_2$** in 75% yield. Anal. Calcd for $C_{38}H_{52}N_2O_2Hf_2$: C, 49.30; H, 5.66; N, 3.03. Found: C, 49.45; H, 5.75; N, 2.92. ^{1}H NMR (benzene-d_6): d = 1.92 (s, 24H, CpMe_4H (2 coincident environments)), 2.02 (s, 12H, CpMe_4H), 2.07 (s, 12H, CpMe_4H), 5.73 (s, 4H, CpMe$_4H$). {^{1}H}^{13}C NMR (benzene-d_6): d = 11.99 (Cp*Me*), 12.34 (Cp*Me*), 13.17 (Cp*Me*), 13.26 (Cp*Me*), 111.34, 117.89, 118.32, 123.65, 123.68 (*Cp*), 160.2 ($N_2C_2O_2$). ^{15}N NMR (benzene-d_6): d = 376.2 ($^{15}N_2C_2O_2$) ($^1J_{CN}$, $^2J_{CN}$ = 3.9 Hz (average)). IR (KBr): ν = 1593 cm^{-1} (C=N), 1560 cm^{-1} (^{13}C=N).

Preparation of ([$Me_2Si(\eta^5$-$C_5Me_4)(\eta^5$-C_5H_3-3-$^tBu)$]Zr)$_2(N_2C_2O_2)$ (3-$N_2C_2O_2$-C_1) (C_1 symmetric isomer). In a drybox, a thick-walled glass vessel was charged with 0.100 g (0.124 mmol) of **3-N_2**[34] dissolved in approximately 10 mL of toluene. On a high vacuum line, the vessel was degassed and 1 atm of carbon monoxide was admitted at -196 °C. The contents of the vessel were thawed and stirred for 2 hours at which time excess gas and solvent were removed *in vacuo*. In a drybox, the resulting deep red oil was washed with cold pentane to remove the small amounts of the byproduct zirconocene dicarbonyl, **3-$(CO)_2$**.[34] The remaining yellow solid was dissolved in diethyl ether and recrystallized at -35 °C affording pale yellow crystals of **3-$N_2C_2O_2$-C_1** in 42% yield. Anal. Calcd for $C_{42}H_{60}O_2N_2Si_2Zr_2$: C, 58.41; H, 7.00; N, 3.24. Found: C, 58.08; H, 7.10; N, 3.08. ^{1}H NMR (benzene-d_6): ∂ = 0.47 (s, 3H, SiMe_2), 0.48 (s, 3H, SiMe_2), 0.65 (s, 3H, SiMe_2), 0.66 (s, 3H, SiMe_2), 1.32 (s, 9H, $C_5H_3CMe_3$), 1.41 (s, 9H, $C_5H_3CMe_3$), 1.90 (s, 3H, C_5Me_4), 1.96 (s, 3H, C_5Me_4), 2.02 (s, 3H, C_5Me_4), 2.04 (s, 3H, C_5Me_4), 2.07 (s, 3H, C_5Me_4), 2.10 (s, 3H, C_5Me_4), 2.19 (s, 3H, C_5Me_4), 2.21 (s, 3H, C_5Me_4), 5.75 (m, 1H, $C_5H_3CMe_3$), 5.76 (m, 1H, $C_5H_3CMe_3$), 5.92 (m, 1H, $C_5H_3CMe_3$), 5.98 (m, 1H, $C_5H_3CMe_3$), 6.60 (m, 1H, $C_5H_3CMe_3$), 6.64 (m, 1H, $C_5H_3CMe_3$). {^{1}H}^{13}C NMR (benzene-d_6): ∂ = -0.93 (SiMe_2), -0.87 (SiMe_2), 1.31 (SiMe_2), 1.44 (SiMe_2), 11.41 (CpMe), 11.60 (CpMe), 11.81 (CpMe), 12.22 (CpMe), 14.61 (CpMe), 15.01 (CpMe), 15.18 (CpMe), 15.68 (CpMe), 31.48 (CMe_3), 31.53 (CMe_3), 33.53 (CMe$_3$), 33.72 (CMe$_3$), 102.26, 104.50, 109.96, 111.34, 113.39, 114.01, 115.06, 118.77, 119.36, 120.84, 122.28, 126.03, 126.97, 129.54, 129.66, 132.48, 133.47, 134.41, 152.45, 153.23 (*Cp*), 162.76 ($N_2C_2O_2$), 164.07 ($N_2C_2O_2$). ^{15}N NMR (benzene-d_6): ∂ = 392.4 ($^{15}N_2C_2O_2$), 396.5 ($^{15}N_2C_2O_2$). ($^1J_{CC}$=60.9 Hz, $^1J_{CN}$=4.0 Hz, $^2J_{CN}$ = 4.0 Hz). IR (KBr): ν = 1574 cm^{-1} (C=N); ν = 1535 cm^{-1} (^{13}C=N).

Preparation of ([$Me_2Si(\eta^5$-$C_5Me_4)(\eta^5$-C_5H_3-3-$^tBu)$]$Zr)_2(N_2C_2O_2)$ (3-$(N_2C_2O_2)$-C_2) (C_2 symmetric isomer). This compound was prepared in a similar manner to **3-$(N_2C_2O_2)$-C_1** with 4 atm of carbon monoxide at -196 °C. After washing the resulting deep red oil with pentane to remove **3-$(CO)_2$**, the remaining yellow solid was dissolved in diethyl ether and recrystallized at -35 °C yielding pale yellow crystals of the C_2 symmetric compound **3-$(N_2C_2O_2)$-C_2** in 46% yield. ^{1}H NMR (benzene-d_6): ∂ = 0.51 (s, 3H, SiMe_2), 0.63 (s, 3H, SiMe_2), 1.54 (s, 9H, $C_5H_3CMe_3$), 1.77 (s, 3H, C_5Me_4), 1.95 (s, 3H, C_5Me_4), 2.06 (s, 3H, C_5Me_4), 2.09 (s, 3H, C_5Me_4), 5.69 (m, 1H, $C_5H_3CMe_3$), 5.76 (m, 1H, $C_5H_3CMe_3$), 6.69 (m, 1H, $C_5H_3CMe_3$). {^{1}H}^{13}C NMR (benzene-d_6): ∂ = -0.51 (SiMe_2), 0.86 (SiMe_2), 12.00 (CpMe), 12.29 (CpMe), 14.26 (CpMe), 14.64 (CpMe), 31.29 (CMe_3), 33.92 (CMe$_3$), 104.22, 109.91, 113.27, 116.23, 116.95, 121.70, 126.62, 130.22, 133.04, 152.24 (Cp), 165.39 ($N_2C_2O_2$). IR (KBr): ν = 1585 cm^{-1} (C=N); ν = 1544 cm^{-1} (^{13}C=N).

Preparation of [$Me_2Si(\eta^5$-$C_5Me_4)(\eta^5$-C_5H_3-3-$^tBu)$]$HfCl_2$ (4-Cl_2). In a drybox, a 250 mL round bottomed flask was charged with 4.40 g (14.1 mmol) of Li_2[$Me_2Si(h^5$-$C_5Me_4)(h^5$-C_5H_3-3-^{t}Bu)], 4.51 g (14.1 mmol) of $HfCl_4$, and approximately 125 mL of toluene. A reflux condenser and 180° needle valve were attached, and the reaction assembly was transferred to a high vacuum line. The reaction mixture was heated to reflux for 3 days with stirring. After this time, the solvent was removed *in vacuo*, leaving a yellow oil. The oil was dissolved in diethyl ether and the lithium chloride precipitate was removed by filtration through Celite. Recrystallization from a pentane/diethyl ether mixture furnished **4-Cl_2** as a pale yellow solid in 67% yield. Anal. Calcd for $C_{20}H_{30}SiHfCl_2$: C, 43.84; H, 5.52; N, 0.00. Found: C, 43.57; H, 5.37; N, <0.02. ^{1}H NMR (benzene-d_6): ∂ = 0.38 (s, 3H, SiMe_2), 0.42 (s, 3H, SiMe_2), 1.44 (s, 9H, $C_5H_3CMe_3$), 1.80 (s, 3H, C_5Me_4), 1.83 (s, 3H, C_5Me_4), 2.01 (s, 6H, C_5Me_4), 5.44

(m, 1H, $C_5H_3CMe_3$), 5.51 (m, 1H, $C_5H_3CMe_3$), 6.81 (m, 1H, $C_5H_3CMe_3$). $\{^1H\}$ ^{13}C NMR (benzene-d_6): ∂ = -0.56 (Si*Me*$_2$), 0.21 (Si*Me*$_2$), 12.41 (Cp*Me*), 12.62 (Cp*Me*), 15.12 (Cp*Me*), 15.14 (Cp*Me*), 31.18 (C*Me*$_3$), 34.04 (*C*Me$_3$), 99.57, 106.76, 108.45, 111.70, 121.29, 124.24, 125.92, 133.64, 134.74, 150.27 (*Cp*).

Preparation of [Me$_2$Si(η^5-C$_5$Me$_4$)(η^5-C$_5$H$_3$-3-^{t}Bu)]HfI$_2$ (4-I$_2$). A 20 mL scintillation vial was charged with 1.00 g (1.82 mmol) of **4-Cl$_2$** dissolved in approximately 10 mL of toluene. To the vial 3.65 g (18.2 mmol) of iodotrimethylsilane was added with stirring. The reaction was stirred at room temperature for approximately 24 hours. Excess iodotrimethylsilane and toluene were removed *in vacuo*, yielding a yellow solid which was washed with cold pentane to furnish **4-I$_2$** in 93% yield. Anal. Calcd for $C_{20}H_{30}SiHfI_2$: C, 32.87; H, 4.14; N, 0.00. Found: C, 32.59; H, 4.08; N, 0.00. ^1H NMR (benzene-d_6): ∂ = 0.34 (s, 3H, Si*Me*$_2$), 0.37 (s, 3H, Si*Me*$_2$), 1.43 (s, 9H, C_5H_3C*Me*$_3$), 1.72 (s, 3H, C_5*Me*$_4$), 1.74 (s, 3H, C_5*Me*$_4$), 1.97 (s, 3H, C_5*Me*$_4$), 2.36 (s, 3H, C_5*Me*$_4$), 5.16 (m, 1H, $C_5H_3CMe_3$), 5.49 (m, 1H, $C_5H_3CMe_3$), 7.37 (m, 1H, $C_5H_3CMe_3$). $\{^1H\}$ ^{13}C NMR (benzene-d_6): ∂ = -0.49 (Si*Me*$_2$), -0.05 (Si*Me*$_2$), 12.67 (Cp*Me*), 15.76 (Cp*Me*), 16.00 (2 Cp*Me*), 31.14 (C*Me*$_3$), 34.06 (*C*Me$_3$), 98.73, 105.29, 108.65, 111.50, 121.77, 124.50, 126.53, 134.24, 135.13, 150.16 (*Cp*).

Preparation of ([Me$_2$Si(η^5-C$_5$Me$_4$)(η^5-C$_5$H$_3$-3-^{t}Bu)]Hf)$_2$N$_2$ (4-N$_2$). A 100 mL round bottomed flask was charged with 25.33 g (8 equivalents) of 0.5% sodium amalgam and approximately 10 mL of toluene. With vigorous stirring, 0.500 g (0.684 mmol) of **4-I$_2$** was added as a yellow toluene solution and the resulting reaction mixture was stirred for seven days at ambient temperature. The resulting purple solution was filtered through Celite to remove excess sodium amalgam and sodium iodide, and the solvent was removed *in vacuo* leaving a purple solid. Recrystallization from pentane

furnished **4-N_2** as purple crystals in 61% yield. Anal. Calcd for $C_{40}H_{60}N_2Si_2Hf_2$: C, 48.92; H, 6.16; N, 2.85. Found: C, 48.48; H, 6.08; N, 2.44. ^{1}H NMR (benzene-d_6): ∂ = 0.57 (s, 3H, SiMe_2), 0.70 (s, 3H, SiMe_2), 1.39 (s, 9H, $C_5H_3C$$Me_3$), 1.87 (s, 3H, $C_5$$Me_4$), 2.11 (s, 3H, $C_5$$Me_4$), 2.16 (s, 3H, $C_5$$Me_4$), 2.22 (s, 3H, $C_5$$Me_4$), 5.64 (m, 1H, $C_5H_3$$CMe_3$), 5.80 (m, 1H, $C_5H_3$$CMe_3$), 6.02 (m, 1H, $C_5H_3$$CMe_3$). {^{1}H} ^{13}C NMR (benzene-d_6): ∂ = -0.38 (SiMe_2), 1.31 (SiMe_2), 12.30 (CpMe), 13.39 (CpMe), 14.61 (CpMe), 14.84 (CpMe), 32.13 (CMe_3), 33.20 ($C$$Me_3$), 107.74, 107.85, 109.01, 110.00, 110.40, 116.68, 117.17, 120.27, 130.19, 146.42 (Cp). ^{15}N NMR (benzene-d_6): ∂ = 576.8 ($^{15}N_2$).

Preparation of ([$Me_2Si(\eta^5$-$C_5Me_4)(\eta^5$-C_5H_3-3-^{t}Bu)]Hf)$_2$($N_2C_2O_2$) (4-($N_2C_2O_2$)-C_1) (C_1 symmetric isomer). In a drybox, a thick-walled glass vessel was charged with 0.100 g (0.102 mmol) of **4-N_2** dissolved in about 10 mL of toluene. On a high vacuum line, the vessel was degassed and 1 atm of carbon monoxide was admitted at -196 °C. The vessel was thawed and its contents stirred for 2 hours after which time excess gas and solvent were removed *in vacuo*. In a drybox, the resulting light brown oil was washed with cold pentane furnishing a yellow solid. This solid was dissolved in diethyl ether and recrystallized at -35 °C affording pale yellow crystals of the C_1 symmetric compound, **4-($N_2C_2O_2$)-C_1** in 73% yield. Anal. Calcd for $C_{42}H_{60}O_2N_2Si_2Hf_2$: C, 48.59; H, 5.83; N, 2.70. Found: C, 48.38; H, 5.60; N, 2.61. ^{1}H NMR (benzene-d_6): ∂ = 0.46 (s, 3H, SiMe_2), 0.48 (s, 3H, SiMe_2), 0.65 (s, 3H, SiMe_2), 0.66 (s, 3H, SiMe_2), 1.32 (s, 9H, $C_5H_3C$$Me_3$), 1.40 (s, 9H, $C_5H_3C$$Me_3$), 1.97 (s, 3H, $C_5$$Me_4$), 1.99 (s, 3H, $C_5$$Me_4$), 2.09 (s, 3H, $C_5$$Me_4$), 2.10 (s, 3H, $C_5$$Me_4$), 2.13 (s, 3H, $C_5$$Me_4$), 2.15 (s, 3H, $C_5$$Me_4$), 2.20 (s, 3H, $C_5$$Me_4$), 2.21 (s, 3H, $C_5$$Me_4$), 5.72 (m, 1H, $C_5H_3$$CMe_3$), 5.76 (m, 1H, $C_5H_3$$CMe_3$), 5.95 (m, 1H, $C_5H_3$$CMe_3$), 5.99 (m, 1H, $C_5H_3$$CMe_3$), 6.52 (m, 1H, $C_5H_3$$CMe_3$), 6.57 (m, 1H, $C_5H_3$$CMe_3$). {^{1}H} ^{13}C NMR

(benzene-d_6): ∂ = -1.07 (Si*Me*$_2$), -0.97 (Si*Me*$_2$), 1.43 (Si*Me*$_2$), 1.53 (Si*Me*$_2$), 11.29 (Cp*Me*), 11.81 (Cp*Me*), 11.90 (Cp*Me*), 12.26 (Cp*Me*), 14.52 (Cp*Me*), 14.94 (Cp*Me*), 15.10 (Cp*Me*), 15.54 (Cp*Me*), 31.54 (C*Me*$_3$), 31.60 (C*Me*$_3$), 33.50 (*C*Me$_3$), 33.74 (*C*Me$_3$), 103.02, 104.75, 105.47, 108.66, 110.32, 112.35, 113.08, 113.88, 114.15, 117.77, 118.03, 119.03, 120.61, 125.61, 126.03, 127.19, 130.94, 133.37, 151.46, 152.60 (*Cp*), 159.93 (N*C*O), 161.46 (N*C*O). ^{15}N NMR (benzene-d_6): ∂ = 369.4 (^{15}*N*CO), 370.3 (^{15}*N*CO). ($^1J_{CC}$=61.4 Hz, $^1J_{CN}$=5.0 Hz, $^2J_{CN}$=3.0 Hz). IR (KBr): ν = 1590 cm^{-1} (C=N); ν = 1556 cm^{-1} (^{13}C=N); 1536 (^{13}C=^{15}N).

Preparation of ([Me$_2$Si(η^5-C$_5$Me$_4$)(η^5-C$_5$H$_3$-3-^{t}Bu)]Hf)$_2$(N$_2$C$_2$O$_2$) (4-(N$_2$C$_2$O$_2$)-*C*$_2$) (*C*$_2$ symmetric isomer). This compound was prepared in a similar manner to **4-(N$_2$C$_2$O$_2$)-*C*$_1$** using 4 atm of carbon monoxide at -196 °C. The product was dissolved in diethyl ether and recrystallized at -35 °C yielding pale yellow crystals of the C_2 symmetric compound **4-(N$_2$C$_2$O$_2$)-*C*$_2$** in 82 % yield. ^{1}H NMR (benzene-d_6): ∂ = 0.50 (s, 3H, Si*Me*$_2$), 0.62 (s, 3H, Si*Me*$_2$), 1.53 (s, 9H, C$_5$H$_3$C*Me*$_3$), 1.81 (s, 3H, C$_5$*Me*$_4$), 2.01 (s, 3H, C$_5$*Me*$_4$), 2.07 (s, 3H, C$_5$*Me*$_4$), 2.09 (s, 3H, C$_5$*Me*$_4$), 5.72 (m, 2H, C$_5$*H*$_3$CMe$_3$), 6.63 (m, 1H, C$_5$*H*$_3$CMe$_3$). {^{1}H}^{13}C NMR (benzene-d_6): ∂ = -0.56 (Si*Me*$_2$), 0.92 (Si*Me*$_2$), 11.93 (Cp*Me*), 12.35 (Cp*Me*), 14.14 (Cp*Me*), 14.49 (Cp*Me*), 31.28 (C*Me*$_3$), 33.93 (*C*Me$_3$), 105.11, 108.20, 114.46, 114.75, 116.18, 119.32, 124.83, 126.03, 132.09, 151.86 (*Cp*), 162.65 (N*C*O). ^{15}N NMR (benzene-d_6): ∂ = 371.3 (^{15}*N*CO). IR (KBr): ν = 1588 cm^{-1} (C=N); ν = 1560 cm^{-1} (^{13}C=N).

Preparation of ([Me$_2$Si(η^5-C$_5$Me$_4$)(η^5-C$_5$H$_3$-3-^{t}Bu)]Hf)$_2$(μ-NCO)(CO)(NCO) (4-(μ-NCO)(CO)(NCO). In a drybox, a J. Young NMR tube was charged with 0.020 g (0.020 mmol) of **4-N$_2$** dissolved in about 0.6 mL of benzene-d_6. On a high vacuum line, the vessel was degassed and 4 atm of carbon monoxide was admitted at -196 °C.

The vessel was thawed and its contents shaken for 20 seconds until the solution turned red-brown and clear, signaling the formation of **4-(μ-NCO)(CO)(NCO)**. The tube was cooled to 0 ºC and the solvent was sublimed on the high vacuum line. The tube was transferred to the glove box and the solid was transferred to a vial for storage. In solution, **4-(μ-NCO)(CO)(NCO)** converts to **4-$N_2C_2O_2$** over the course of minutes. Anal. Calcd for $C_{43}H_{60}O_3N_2Si_2Hf_2$: C, 48.44; H, 5.67; N, 2.63. Found: C, 48.17; H, 5.87; N, 2.27. ^{1}H NMR (benzene-d_6): ∂ = 0.44 (s, 3H, SiMe_2), 0.52 (s, 3H, SiMe_2), 0.57 (s, 3H, SiMe_2), 0.63 (s, 3H, SiMe_2), 1.28 (s, 9H, $C_5H_3C$$Me_3$), 1.50 (s, 3H, $C_5$$Me_4$), 1.51 (s, 9H, $C_5H_3C$$Me_3$), 1.85 (s, 3H, $C_5$$Me_4$), 1.86 (s, 3H, $C_5$$Me_4$), 1.94 (s, 3H, $C_5$$Me_4$), 2.05 (s, 3H, $C_5$$Me_4$), 2.13 (s, 3H, $C_5$$Me_4$), 2.30 (s, 3H, $C_5$$Me_4$), 2.33 (s, 3H, $C_5$$Me_4$), 5.17 (m, 1H, $C_5$$H_3$$CMe_3$), 5.47 (m, 1H, $C_5$$H_3$$CMe_3$), 5.61 (m, 1H, $C_5$$H_3$$CMe_3$), 5.83 (m, 1H, $C_5$$H_3$$CMe_3$), 5.93 (m, 1H, $C_5$$H_3$$CMe_3$), 7.14 (m, 1H, $C_5$$H_3$$CMe_3$). ^{1}H NMR (toluene-$d_8$): ∂ = 0.45 (s, 3H, SiMe_2), 0.55 (s, 3H, SiMe_2), 0.59 (s, 3H, SiMe_2), 0.64 (s, 3H, SiMe_2), 1.24 (s, 9H, $C_5H_3C$$Me_3$), 1.42 (s, 3H, $C_5$$Me_4$), 1.46 (s, 9H, $C_5H_3C$$Me_3$), 1.82 (s, 3H, $C_5$$Me_4$), 1.86 (s, 3H, $C_5$$Me_4$), 1.93 (s, 3H, $C_5$$Me_4$), 2.02 (s, 3H, $C_5$$Me_4$), 2.10 (s, 3H, $C_5$$Me_4$), 2.24 (s, 3H, $C_5$$Me_4$), 2.28 (s, 3H, $C_5$$Me_4$), 5.12 (m, 1H, $C_5$$H_3$$CMe_3$), 5.43 (m, 1H, $C_5$$H_3$$CMe_3$), 5.51 (m, 1H, $C_5$$H_3$$CMe_3$), 5.71 (m, 1H, $C_5$$H_3$$CMe_3$), 5.82 (m, 1H, $C_5$$H_3$$CMe_3$), 7.06 (m, 1H, $C_5$$H_3$$CMe_3$). {^{1}H} ^{13}C NMR (toluene-d_8): ∂ = -0.81 (SiMe_2), -0.48 (SiMe_2), -0.06 (SiMe_2), 0.11 (SiMe_2), 11.13 (CpMe), 11.27 (CpMe), 11.72 (CpMe), 13.88 (CpMe), 14.00 (CpMe), 14.13 (CpMe), 14.31 (CpMe), 14.60 (CpMe), 30.78 (CMe_3), 32.13 (CMe_3), 33.06 ($C$$Me_3$), 33.38 ($C$$Me_3$), 90.94, 97.30, 98.26, 99.53, 107.52, 107.89, 112.12, 114.71, 115.17, 115.26, 117.68, 117.88, 118.23, 118.73, 123.89, 127.05, 128.18, 129.08, 132.28, 152.61 (Cp), 134.48 (NCO, $^1J_{CN}$ = 32.9 Hz), 192.50 (μ-NCO, $^1J_{CN}$ = 9.6 Hz, $^2J_{CC}$ = 13.7 Hz), 247.07 (Hf-CO, $^2J_{CC}$ = 13.7 Hz). ^{15}N NMR (toluene-d_8): ∂ = 89.60 (^{15}NCO,

$^{1}J_{CN}$ = 32.9 Hz), 241.14 (μ-^{15}*N*CO, $^{1}J_{CN}$ = 9.6 Hz). IR (KBr): ν = 2220 cm^{-1} (NCO); ν = 1959 cm^{-1} (CO); ν = 1914 (^{13}CO); ν = 1588 cm^{-1} (μ-NCO).

Preparation of ([Me$_2$Si(η^5-C$_5$Me$_4$)(η^5-C$_5$H$_3$-3-^{t}Bu)]Hf)$_2$((NCH$_3$)C$_2$O$_2$)(I)(NCO) (5). In a drybox, a J. Young NMR tube was charged with 0.020 g (0.020 mmol) of **4-N$_2$** dissolved in about 0.6 mL of benzene-d_6. On a high vacuum line, the vessel was degassed and 4 atm of carbon monoxide was admitted at -196 °C. The vessel was thawed and its contents shaken for 20 seconds until the solution turned red-brown and clear, signaling the formation of **4-(μ-NCO)(CO)(NCO)**. The tube was degassed, and 0.100 mmol of CH_3I were admitted via calibrated gas bulb. The tube was thawed and shaken and complete conversion to **5** after several minutes was confirmed by NMR spectroscopy. The solvent was evacuated and the remaining red oil was washed with pentane furnishing pure **5** in 61% yield (from 3 combined batches). ^{1}H NMR (benzene-d_6): ∂ = 0.41 (s, 3H, Si*Me$_2$*), 0.48 (s, 3H, Si*Me$_2$*), 0.53 (s, 3H, Si*Me$_2$*), 0.64 (s, 3H, Si*Me$_2$*), 1.23 (s, 9H, C$_5$H$_3$C*Me$_3$*), 1.42 (s, 9H, C$_5$H$_3$C*Me$_3$*), 1.49 (s, 3H, C$_5$*Me$_4$*), 1.65 (s, 3H, C$_5$*Me$_4$*), 1.76 (s, 3H, C$_5$*Me$_4$*), 1.89 (s, 6H, C$_5$*Me$_4$*, 2 coincident), 2.06 (s, 3H, C$_5$*Me$_4$*), 2.29 (s, 3H, C$_5$*Me$_4$*), 2.49 (s, 3H, C$_5$*Me$_4$*), 3.37 (s, 3H, N-C*H$_3$*, $^{1}J_{CH}$ = 137.8 Hz, $^{2}J_{NH}$ = 1.5 Hz), 5.27 (m, 1H, C$_5$*H$_3$*CMe$_3$), 5.33 (m, 1H, C$_5$*H$_3$*CMe$_3$), 5.96 (m, 1H, C$_5$*H$_3$*CMe$_3$), 6.18 (m, 1H, C$_5$*H$_3$*CMe$_3$), 6.24 (m, 1H, C$_5$*H$_3$*CMe$_3$), 7.54 (m, 1H, C$_5$*H$_3$*CMe$_3$). {^{1}H} ^{13}C NMR (benzene-d_6): ∂ = -1.26 (Si*Me$_2$*), -0.99 (Si*Me$_2$*), 0.58 (Si*Me$_2$*), 1.00 (Si*Me$_2$*), 11.30 (Cp*Me*), 11.99 (Cp*Me*), 12.25 (Cp*Me*), 14.64 (Cp*Me*), 14.89 (Cp*Me*), 15.91 (Cp*Me*), 17.00 (Cp*Me*), 30.83 (C*Me$_3$*), 31.22 (*C*Me$_3$), 32.70 (C*Me$_3$*), 33.71 (*C*Me$_3$), 38.83 (N-*C*H$_3$, $^{1}J_{CN}$= 3.0 Hz, $^{2}J_{CC}$ = 6.2 Hz, $^{3}J_{CC}$ = 3.2 Hz) 100.11, 100.36, 105.26, 107.10, 109.27, 110.72, 111.84, 113.99, 114.56, 116.30, 116.53, 119.98, 123.51, 125.60, 126.03, 127.60, 127.80, 129.67, 130.66, 156.47 (*Cp*), 135.77 (N*C*O, $^{1}J_{CN}$ = 32.9 Hz), 178.89 (Hf-(*C*=O)-C=N, $^{1}J_{CC}$ = 13.8 Hz, $^{2}J_{CN}$ = 6.6

Hz, $^{3}J_{CC}$ = 3.2 Hz), 291.24 (Hf-(C=O)-*C*=N, $^{1}J_{CC}$ = 13.8 Hz, $^{1}J_{CN}$ = 11.9 Hz, $^{2}J_{CC}$ = 6.2 Hz), one Cp*Me* resonance not located. ^{15}N NMR (benzene-d_6): ∂ = 91.4 (^{15}*N*CO), 227.3 (^{15}*N*-CH_3). IR (KBr): ν = 2218 cm^{-1} (NCO); ν = 1605 cm^{-1} (Hf-C=O).

Preparation of ([$Me_2Si(\eta^5$-$C_5Me_4)(\eta^5$-C_5H_3-3-^{t}Bu)]Hf)$_2$(($N(^t$BuNCO))C_2O_2)(I)(NCO) (6). In a drybox, a J. Young NMR tube was charged with 0.020 g (0.020 mmol) of **4-N_2** dissolved in about 0.6 mL of benzene-d_6. On a high vacuum line, the vessel was degassed and 4 atm of carbon monoxide was admitted at -196 °C. The vessel was thawed and its contents shaken for 20 seconds until the solution turned red-brown and clear, signaling the formation of **4-(μ-NCO)(CO)(NCO)**. The tube was degassed, and 0.100 mmol of *tert*-butylisocyanate were admitted *via* calibrated gas bulb. The tube was thawed and shaken and complete conversion to **6** after several minutes was confirmed by NMR spectroscopy. The solvent was evacuated and the remaining brown oil was washed with pentane furnishing pure **6** in 40% yield (from 3 combined batches). ^{1}H NMR (benzene-d_6): ∂ = 0.44 (s, 3H, SiMe_2), 0.48 (s, 3H, SiMe_2), 0.54 (s, 6H, SiMe_2, 2 coincident), 1.26 (s, 9H, $C_5H_3CMe_3$), 1.43 (s, 9H, $C_5H_3CMe_3$), 1.52 (s, 9H, C=NCMe_3), 1.56 (s, 3H, C_5Me_4), 1.62 (s, 3H, C_5Me_4), 1.68 (s, 3H, C_5Me_4), 2.03 (s, 3H, C_5Me_4), 2.05 (s, 3H, C_5Me_4), 2.16 (s, 3H, C_5Me_4), 2.18 (s, 3H, C_5Me_4), 2.20 (s, 3H, C_5Me_4), 5.57 (m, 1H, $C_5H_3CMe_3$), 5.59 (m, 1H, $C_5H_3CMe_3$), 5.63 (m, 1H, $C_5H_3CMe_3$), 5.91 (m, 1H, $C_5H_3CMe_3$), 6.36 (m, 1H, $C_5H_3CMe_3$), 6.51 (m, 1H, $C_5H_3CMe_3$). {^{1}H} ^{13}C NMR (benzene-d_6): ∂ = -0.87 (SiMe_2), -0.51 (SiMe_2), 0.11 (SiMe_2), 0.63 (SiMe_2), 12.69 (Cp*Me*), 12.78 (Cp*Me*), 12.97 (Cp*Me*), 14.63 (Cp*Me*), 14.89 (Cp*Me*), 14.99 (Cp*Me*), 15.36 (Cp*Me*), 15.72 (Cp*Me*), 31.92 (CMe_3), 32.19 (CMe_3), 32.93 (N-CMe_3), 33.46 (*C*Me_3), 34.18 (*C*Me_3), 106.75, 107.07, 108.20, 108.47, 110.62, 110.93, 111.72, 112.57, 114.80, 116.93, 119.13, 121.22, 122.57, 123.52, 124.48, 125.94, 127.80,

129.66, 150.28, 151.68 (*Cp*), 134.07 (N*C*O, $^{1}J_{CN}$ = 33.9 Hz), 176.15 (Hf-(*C*=O)-C=N, $^{1}J_{CC}$ = 10.9 Hz, $^{2}J_{CN}$ = 1.3 Hz), 303.60 (Hf-(C=O)-*C*=N, $^{1}J_{CC}$ = 10.9 Hz, $^{1}J_{CN}$ = 13.8 Hz) . ^{15}N NMR (benzene-d_6): ∂ = 91.1 (^{15}*N*CO, $^{1}J_{NC}$ = 33.9 Hz), 205.7 (Hf-(CO)-C=^{15}*N*, $^{1}J_{CN}$ = 13.8 Hz, $^{2}J_{CN}$ = 1.3 Hz).

Preparation of ([Me$_2$Si(η^5-C$_5$Me$_4$)(η^5-C$_5$H$_3$-3-^{t}Bu)]Hf)$_2$(μ-NCO)(NCO)$_2$ (4-(μ-O)(NCO)$_2$). In a drybox, a J. Young NMR tube was charged with 0.020 g (0.020 mmol) of **4-N$_2$** dissolved in about 0.6 mL of benzene-d_6. On a high vacuum line, the vessel was degassed and 4 atm of carbon monoxide was admitted at -196 °C. The vessel was thawed and its contents shaken for 20 seconds until the solution turned red-brown and clear, signaling the formation of **4-(μ-NCO)(CO)(NCO)**. The tube was degassed, and 0.03 mmol of carbon dioxide were admitted *via* calibrated gas bulb. The tube was thawed and shaken and complete conversion to **4-(μ-O)(NCO)$_2$** was confirmed by NMR spectroscopy. The solvent was evacuated and the remaining brown oil was washed with pentane furnishing pure **6** in 56% yield (from 3 combined batches). Anal. Calcd for $C_{42}H_{60}O_3N_2Si_2Hf_2$: C, 47.85; H, 5.74; N, 2.66. Found: C, 47.58; H, 5.55; N, 2.38. ^{1}H NMR (benzene-d_6): ∂ = 0.51 (s, 3H, Si*Me$_2$*), 0.60 (s, 3H, Si*Me$_2$*), 1.40 (s, 9H, C$_5$H$_3$C*Me$_3$*), 1.93 (s, 3H, C$_5$*Me$_4$*), 1.97 (s, 3H, C$_5$*Me$_4$*), 2.00 (s, 3H, C$_5$*Me$_4$*), 2.12 (s, 3H, C$_5$*Me$_4$*), 5.47 (m, 1H, C$_5$*H$_3$*CMe$_3$), 5.99 (m, 1H, C$_5$*H$_3$*CMe$_3$), 6.57 (m, 1H, C$_5$*H$_3$*CMe$_3$). {^{1}H}^{13}C NMR (benzene-d_6): ∂ = -0.34 (Si*Me$_2$*), 0.27 (Si*Me$_2$*), 11.84 (Cp*Me*), 12.20 (Cp*Me*), 14.42 (Cp*Me*), 14.96 (Cp*Me*), 31.30 (C*Me$_3$*), 32.32 (*C*Me$_3$), *Cp* resonances not located. 135.76 (N*C*O, $^{1}J_{CN}$ = 33.8 Hz). ^{15}N NMR (benzene-d_6): ∂ = 94.6 (^{15}*N*CO, $^{1}J_{CN}$ = 33.8 Hz). IR (KBr): ν = 2222 cm^{-1} (NCO).

REFERENCES

[1] Shaver, M. P.; Fryzuk, M. D. *Adv. Synth. Catal.* **2003**, *345*, 1061.

[2] (a) Mori, M. *J. Organomet. Chem.* **2004**, *689*, 4210. (b) Fryzuk, M. D. *Chem. Rec.* **2003**, *3*, 2.

[3] V. Smil *Enriching the Earth: Fritz Haber, Carl Bosch, and the Transformation of World Food Production*; MIT Press, Cambridge, MA, 2001.

[4] Hager, T. in *The Alchemy of Air*, Three Rivers Press, NY, 2008.

[5] Ertl, G. *Angew. Chem. Int. Ed.* **2008**, *47*, 3524.

[6] (a) Schlögl, R. *Angew. Chem. Int. Ed.* **2003**, *42*, 2004. (b) K. Tamaru in *Catalytic Ammonia Synthesis.* J. R. Jennings, Ed.; Plenum, NY 1991. (c) D. Pimentel, T. W. Patzek, *Nat. Resources Res.* **2005**, *14*, 65.

[7] Holladay, J. D.; Hu, J.; King, D. L.; Wang, Y. *Catalysis Today* **2009**, *139*, 244.

[8] (a) Henderickx, H.; Kwakkenbos, G.; Peters, A.; van der Spoel, J.; de Vries, K. *Chem. Commun.* **2003**, 2050. (b) Komori, K.; Oshita, H.; Mizobe, Y.; Hidai, M. *J. Am. Chem. Soc.* **1989**, *111*, 1939. (c) Rocklage, S. M.; Schrock, R. R. *J. Am. Chem. Soc.* **1982**, *104*, 3077. (d) Betley, T. E.; Peters, J. C. *J. Am. Chem. Soc.* **2003**, *125*, 10782. (e) Figueroa, J. S. Piro, N. A.; Clough, C. R.; Cummins, C. C. *J. Am. Chem. Soc.* **2006**, *128*, 940.

[9] (a) Thomas, J. M.; Thomas, W. J. Fischer-Tropsch Catalysis, In: *Principles and Practice of Heterogeneous Catalysis* (VCH Verlagsgessellschaft, Weinheim 1996). (b) Macho, V.; Kralik, M.; Komora, L. *Pet. Coal* **1997**, *39*, 6.

[10] (a) Summerscales, O. T.; Cloke, F. G. N.; Hitchcock, P. B.; Green, J. C.; Hazari, N. *Science* **2006**, *311*, 829. (b) Summerscales, O. T.; Cloke, F. G. N.; Hitchcock, P. B.; Green, J. C.; Hazari, N. *J. Am. Chem. Soc.* **2006**, *128*, 9602.

[11] Frey, A. S.; Cloke, F. G. N.; Hitchcock, P. B.; Day, I. J.; Green, J. C.; Aitken, G. *J. Am. Chem. Soc.* **2008**, *130*, 13816.

[12] Evans, W. J.; Grate, J. W.; Hughes, L. A.; Zhang, H.; Atwood, J. L. *J. Am. Chem. Soc.* **1985**, *107*, 3728.

[13] An additional example of CO homologation and subsequent C-H activation using a uranium complex was very recently reported: Arnold, P. L.; Turner, Z. R.; Bellabarba, R. M.; Tooze, R. P. *Chem. Sci.* **2011**, 77.

[14] Fryzuk, M. D. *Acc. Chem. Res.* **2009**, *42*, 127.

[15] a) Evans, W. J.; Drummond, D. K. *J. Am. Chem. Soc.* **1986**, *108*, 7440. b) Evans, W. J.; Drummond, D. K.; Chamberlain, L. R.; Doedens, R. J.; Bott, S. G.; Zhang, H.; Atwood, J. L. *J. Am. Chem. Soc.* **1988**, *110*, 4983.

[16] Walsh, P. J.; Carney, M. J.; Bergman, R. G. *J. Am. Chem. Soc.* **1991**, *113*, 6343.

[17] Herrmann, H.; Fillol, J. L.; Wadepohl, H.; Gade, L. H. *Organometallics* **2008**, *27*, 172.

[18] MacLachlan, E. A.; Fryzuk, M. D. *Organometallics* **2006**, *25*, 1530.

[19] Chirik, P. J. *Dalton Trans.* **2007**, 16.

[20] Fryzuk, M. D.; Love, J. B.; Rettig, S. J.; Young, V. G. *Science* **1997**, *275*, 1445.

[21] Pool, J. A.; Lobkovsky, E.; Chirik, P. J. *Nature* **2004**, *427*, 527.

[22] Bernskoetter, W. H.; Olmos, A. V.; Lobkovsky, E.; Chirik, P. J. *Organometallics* **2006**, *25*, 1021.

[23] Pun, D.; Bradley, C. A.; Lobkovsky, E.; Keresztes, I.; Chirik, P. J. *J. Am. Chem. Soc.* **2008**, *130*, 14046.

[24] Bernskoetter, W. H.; Lobkovsky, E.; Chirik, P. J. *J. Am. Chem. Soc.* **2005**, *127*, 14051.

[25] Bernskoetter, W. H.; Pool, J. A.; Lobkovsky, E.; Chirik, P. J. *J. Am. Chem. Soc.* **2005**, *127*, 7901.

[26] Morello, L.; Ferreira, M. J.; Patrick, B. O.; Fryzuk, M. D. *Inorg. Chem.* **2008**, *47*, 1319.

[27] Morello, L.; Love, J. B.; Patrick, B. O.; Fryzuk, M. D. *J. Am. Chem. Soc.* **2004**, *126*, 9480.

[28] Bernskoetter, W. H.; Olmos, A. V.; Pool, J. A.; Lobkovsky, E.; Chirik, P. J. *J. Am. Chem. Soc.* **2006**, *128*, 10696.

[29] Bernskoetter, W. H.; Lobkovsky, E.; Chirik, P. J. *Angew. Chem. Int. Ed.* **2007**, *119*, 2858.

[30] For a full discussion of this work, see Chapter 4 of this Thesis. Knobloch, D. J.; Toomey, H. E.; Chirik, P. J. *J. Am. Chem. Soc.* **2008**, *130*, 4248.

[31] Benito-Garagorri, D.; Bernskoetter, W. H.; Lobkovsky, E.; Chirik, P. J. *Organometallics* **2009**, *28*, 4807.

[32] Hirotsu, M.; Fontaine, P. P.; Zavalij, P. Y.; Sita, L. R. *J. Am. Chem. Soc.* **2007**, *129*, 12690.

[33] For a full discussion of this work, see Chapter 5 of this Thesis. Knobloch, D. J.; Benito-Garagorri, D.; Bernskoetter, W. H.; Keresztes, I.; Lobkovsky, E.; Toomey, H.; Chirik, P. J. *J. Am. Chem. Soc.* **2009**, *131*, 14903.

[34] Hanna, T. E.; Keresztes, I.; Lobkovsky, E.; Chirik, P. J. *Inorg. Chem.* **2007**, *46*, 1675.

[35] For a discussion of this nomenclature, see ref. 34.

[36] Fryzuk, M. D.; Haddad, T. S.; Rettig, S. J. *J. Am. Chem. Soc.* **1990**, *112*, 8185.

[37] Cohen, J. D.; Fryzuk, M. D.; Loehr, T. M.; Mylvaganam, M.; Rettig, S. J. *Inorg. Chem.* **1998**, *37*, 112.

[38] Pool, J. A.; Bernskoetter, W. H.; Chirik, P. J. *J. Am. Chem. Soc.* **2004**, *126*, 14326.

[39] Sobota, P.; Janas, Z. *J. Organomet. Chem.* **1984**, *276*, 171.

[40] Silvia, J. S.; Cummins, C. C. *J. Am. Chem. Soc.* **2009**, *131*, 446.

[41] Tran, B. L.; Pink, M.; Gao, X.; Park, H.; Mindiola, D. J. *J. Am. Chem. Soc.* **2010**, *132*, 1458.

[42] Manriquez, J. M.; McAlister, D. R.; Rosenberg, E.; Shiller, A. M.; Williamson, K. L.; Chan, S. I.; Bercaw, J. E. *J. Am. Chem. Soc.* **1978**, *100*, 3078.

[43] See general experimental considerations for details.

[44] Courtot, P.; Labed, V.; Pichon, R.; Salaun, J.Y. *J. Organomet. Chem.* **1989**, *359*, C9.

[45] Walsh, P. J.; Hollander, F. J.; Bergman, R. G. *Organometallics* **1993**, *12*, 3705.

[46] (a) Glueck, D. S.; Wu, J.; Hollander, F. J.; Bergman, R. G. *J. Am. Chem. Soc.* **1991**, *113*, 2041. (b) Mindiola, D. J.; Hillhouse, G. L. *Chem. Commun.* **2002**, 1840.

[47] (a) Marsella, J.; Curtis, C. J.; Bercaw, J. E.; Caulton, K. G. *J. Am. Chem. Soc.* **1980**, *102*, 7244. (b) Roddick, D. M.; Fryzuk, M. D.; Seidler, P. F.; Hillhouse, G. L.; Bercaw, J. E. *Organometallics* **1985**, *4*, 97.

[48] Green, M. L. H.; McCleverty, J. A.; Pratt, L.; Wilkinson, G. *J. Chem. Soc. A* **1961**, 4854.

[49] Cargill, R. W. *IUPAC Solubility Series (Carbon Monoxide-Aromatic Solvent System)*, **1990**, *43*, 110.

[50] Zhang, X.; Butschke, B.; Schwarz, H. *Chem. Eur. J.* **2010**, *16*, 12564.

[51] Pangborn, A.B.; Giardello, M.A.; Grubbs, R.H.; Rosen, R.K.; Timmers, F.J. *Organometallics* **1996**, 15, 1518.

[52] Marvich, R.H.; Brintzinger, H. H. *J. Am. Chem. Soc.* **1971**, *93*, 2046.

CHAPTER 2

CO-Induced N_2 Cleavage, Part II: Coupling Dinitrogen Cleavage to Hydrogenation, Intra- and Intermolecular C-H Bond Activation, and CO Deoxygenation.*

Abstract

Carbon monoxide-induced dinitrogen cleavage was coupled to N-H bond formation by hydrogenation and intra- and intermolecular C-H bond activation for a series of group 4 metallocene dinitrogen complexes bearing side-on bound N_2 ligands. Slow addition of a slight excess of CO to the hafnocene dinitrogen complexes resulted in N-N cleavage coupled to intramolecular C-H bond activation and formation of new μ-NH and terminal NCO ligands. Carbonylation of the dinitrogen complexes in the presence of H_2 or phenylacetylene also furnished isocyanato metallocene complexes with bridging imido ligands, arising from formal 1,2-addition of H_2 or the acetylenic C-H bond, respectively, across the Hf=N bond of a transient bridging nitrido intermediate. In the case of the *ansa*-hafnocene dinitrogen complex, replacing the hydrogen atmosphere with various primary silanes yielded an isocyanato hafnocene μ-oxo hydride resulting from cleavage of both N_2 and CO, the diatomics with the two strongest bonds in chemistry.

Introduction

Chemical processes that couple cleavage of atmospheric dinitrogen, N_2, and nitrogen-heteroatom bond formation, are highly attractive given the ubiquity of N-C and N-H bonds in synthetic fertilizers, commodity and specialty chemicals, and

* Portions of this work were taken with permission from: (a) Knobloch, D. J.; Lobkovsky, E.; Chirik, P. *Nature Chem.* **2010**, *2*, 30. (b) Knobloch, D. J.; Lobkovsky, E.; Chirik, P. J. *J. Am. Chem. Soc.* **2010**, *132*, 10533.

pharmaceuticals.[1,2] The Haber-Bosch process has been the industrial benchmark for such processes for the past century. From N_2 and H_2, this process generates the ammonia supply for the production of more elaborate nitrogen-containing chemical structures. The downsides to Haber-Bosch, as discussed in the previous chapter, include the harsh reaction conditions and the dependence on natural gas availability.[1,3,4,5,6] Therefore the direct conversion of dinitrogen to small nitrogen-containing organics would provide a more energetically sustainable and fossil-fuel efficient alternative to Haber-Bosch.[7,8] Well-defined, homogeneous organometallic systems have demonstrated potential in this context although the majority of these transformations are currently stoichiometric and far from industrially viable. Most notable is the Chatt-inspired cycle developed by Schrock and co-workers which catalytically couples dinitrogen cleavage and hydrogenation to ammonia using a series of successive reductions and protonations of N_2 coordinated to a [Mo] complex (Figure 2.1).[9] Unfortunately, while catalytic, the reaction suffers from low turn-over.[9] Examples of catalytic N-C bond formation from dinitrogen are exceedingly rare,[10] although stoichiometric examples have been reported by Cummins, Mori, Fryzuk, Kawaguchi, and our own laboratory, as well as several others.[11,12,13,14,15,16,20-23] Key to each of these studies is a fundamental understanding of the reactivity of dinitrogen as it is coordinated to a particular organometallic framework. In addition to the Chatt-inspired proton coupled electron transfer model utilized by the Schrock system (Figure 2.1), several other paradigms for N_2 cleavage have recently emerged.

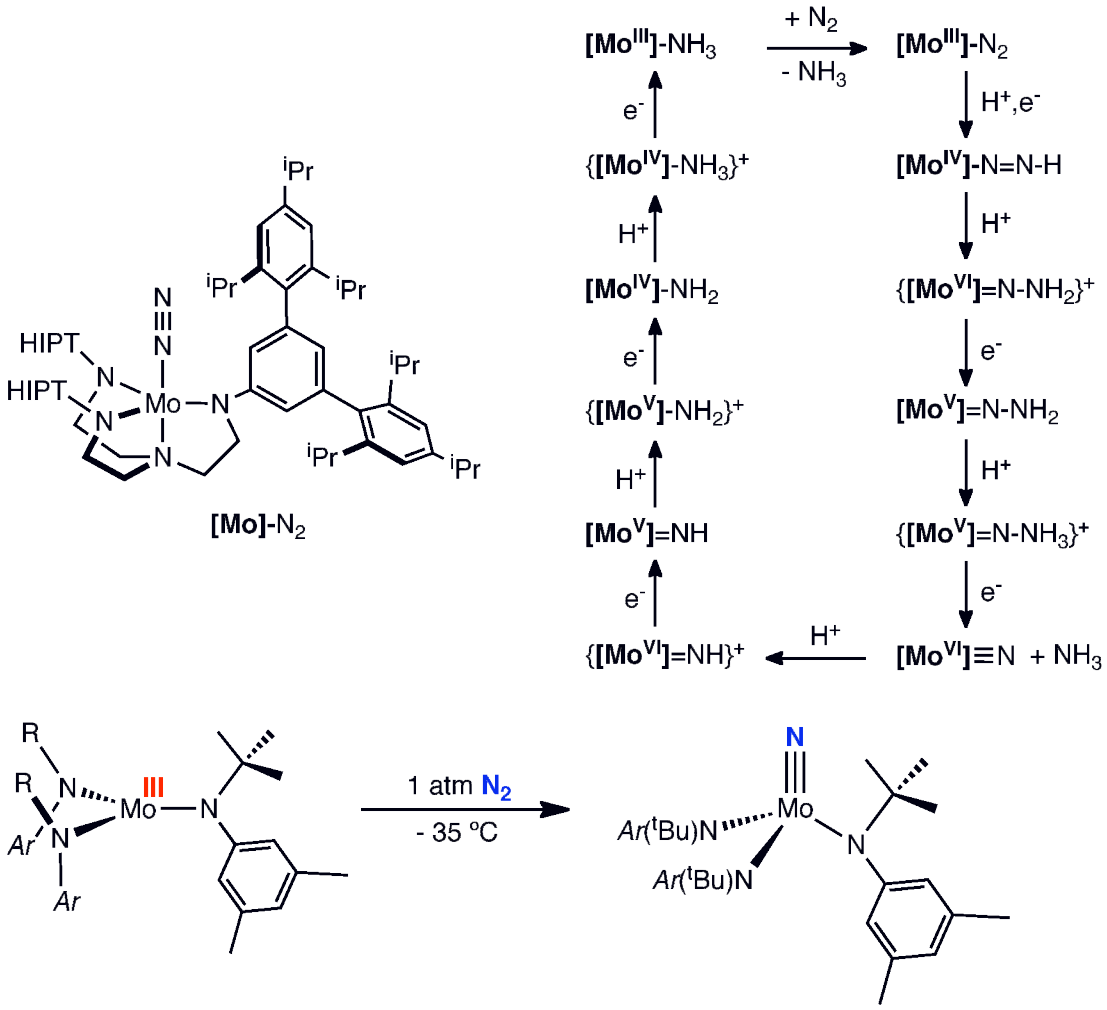

Figure 2.1. Paradigms for dinitrogen cleavage. Schrock's catalytic cycle for N_2 to NH_3 utilizing proton-coupled electron transfer (top) and Cummins' system for N_2 cleavage where the six reducing equivalents are provided by two d^3 metal centers. Reproduced with permission from references 9 and 11.

Cleavage of N_2 by a soluble transition metal complex under mild conditions to form two equivalents of the corresponding terminal metal nitride was first accomplished by Laplaza and Cummins.[11] In this system, the six electrons required for N_2 scission are provided by two d^3 molybdenum centers, establishing an N_2

cleavage strategy whereby reducing equivalents are provided exclusively by the transition metal centers (Figure 2.1). Other examples have since been reported.[17]

A third paradigm is the supply of electrons from metal-metal as well as metal-hydride bonds in addition to the metal centers. This approach has been exploited by the group of Kawaguchi with a triaryloxide-supported niobium tetrahydride dimeric dianion that underwent reductive elimination of hydrogen to effect N_2 cleavage and yield a dimeric bridging nitrido complex (Figure 2.2).[14]

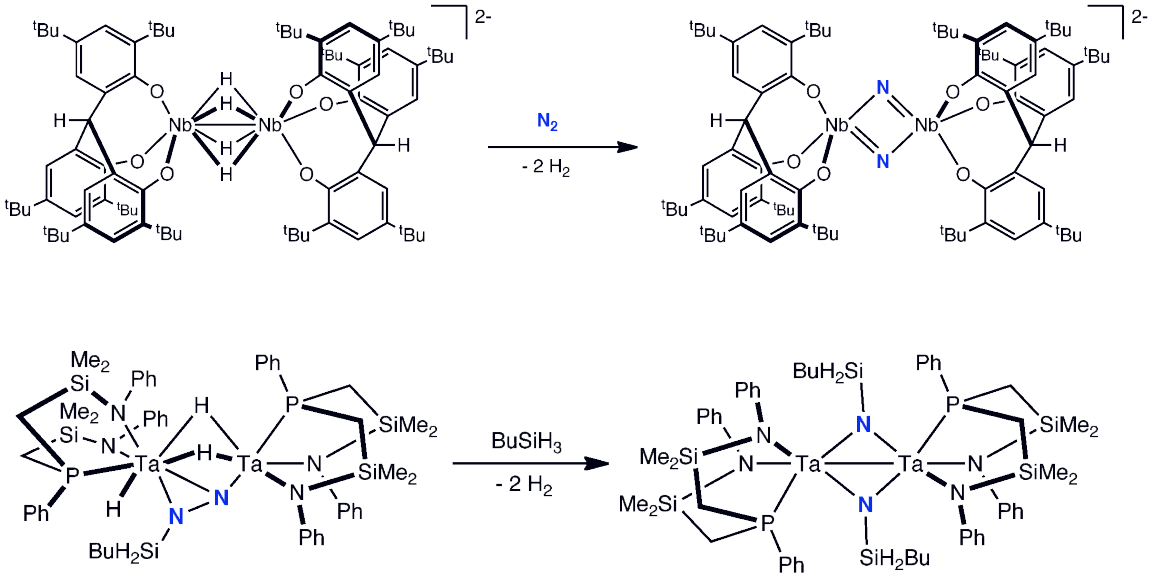

Figure 2.2. Paradigms for dinitrogen cleavage. Kawaguchi's niobium system where the reducing equivalents required for N_2 cleavage are stored in M-M and M-H bonds (top) and Fryzuk's example of ligand-induced N_2 cleavage (bottom). Reproduced with permission from references 14 and 13.

Another approach to N_2 cleavage by soluble transition metal complexes is the addition of a ligand that provides reducing equivalents required for cleavage of coordinated N_2. Fryzuk and co-workers have demonstrated this technique with a rare

side-on, end-on bound dinitrogen complex of tantalum that undergoes N_2 cleavage upon the addition of hydridic sources such as boranes, alanes, silanes, and metal hydrides (Figure 2.2).[13]

Our group has also contributed to this method of ligand-induced dinitrogen cleavage. Dinitrogen compounds synthesized in our laboratory[15,16] have been shown to participate in a variety of N-H bond forming[18,19] and N-C bond forming[20,21,22,23] functionalization reactions, due to their strongly activated, side-on bound $[N_2]^{4-}$ ligands.[24,25] We recently discovered that the addition of carbon monoxide to a series of group 4 metallocene dinitrogen complexes resulted in N-N bond cleavage and assembly of one C-C and two new N-C bonds (Figure 2.3).[26] Reactivity and mechanistic studies implicated a μ-nitrido intermediate along the pathway to oxamidide formation. A recent computational study conducted by Schwarz and co-workers also proposes an intermediate μ-nitrido species.[27] The transient existence of this highly reactive compound provides a unique opportunity for new nitrogen-heteroatom bond formation. In this chapter we continue our exploration of the CO-induced bond N_2 cleavage chemistry, with primary focus on the intra- and intermolecular interception and functionalization of the putative bridging nitride intermediate in the mechanism for oxamidide formation presented in the previous chapter (see Figure 1.22).

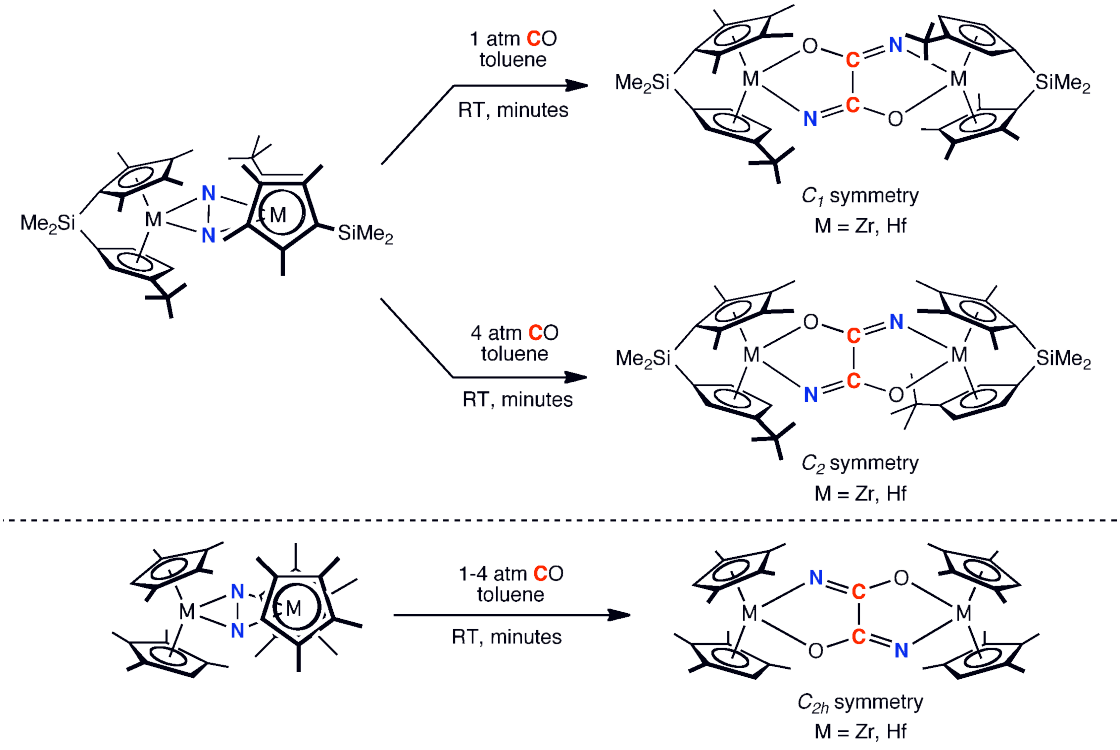

Figure 2.3. Carbon-monoxide induced N-N cleavage promoted by group 4 metallocene complexes.

Results and Discussion

Stoichiometric addition of CO to hafnocene dinitrogen complexes. As reported in the previous chapter, exposure of the strongly activated hafnocene dinitrogen complex, $(Me_2Si(\eta^5\text{-}C_5Me_4)(\eta^5\text{-}C_5H_3\text{-}3\text{-}^tBu)Hf)_2(\mu_2,\eta^2,\eta^2\text{-}N_2)$ (**4-N_2**), to 1-4 atm carbon monoxide resulted in N-N cleavage coupled to C-N and C-C bond formation yielding the hafnocene oxamidide complexes **4-($N_2C_2O_2$)-*C_1*** and **4-($N_2C_2O_2$)-*C_2*** (Figure 2.3). To observe potential intermediates on the N_2 cleavage pathway or to possibly alter the outcome of the reaction, **4-N_2** was treated with a slight excess of CO. Slow diffusion over the course of 12 hours of 1.5 eq CO into a benzene-*d_6* solution of **4-N_2** resulted in clean conversion to a new *C_1* symmetric product having inequivalent metallocene subunits (Figure 2.4) as determined by ^{1}H NMR

spectroscopy. This pale yellow compound, identified as the cyclometalated dihafnocene, **5**, bears a terminal isocyanate (NCO) ligand and a bridging imido (μ-NH) ligand as well as a cyclometalated *tert*-butyl substituent of one of the cyclopentadienyl rings.

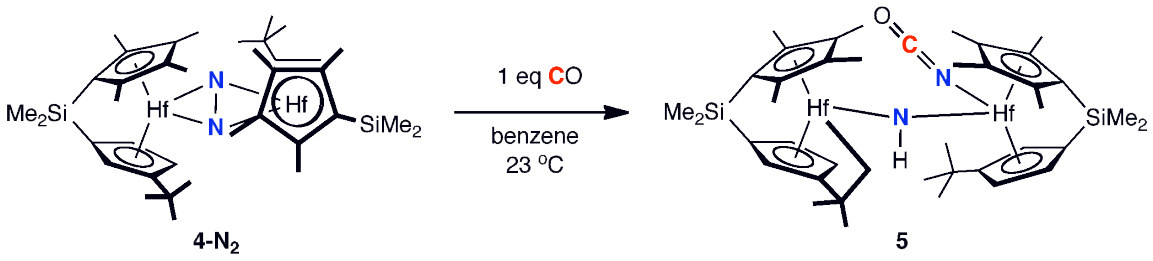

Figure 2.4. Reaction of **4-N_2** with 1 equivalent CO.

The cyclometalated product **5** was fully characterized by multinuclear (^{1}H, ^{13}C, ^{15}N) NMR spectroscopy, infrared spectroscopy and X-ray diffraction. The availability of ^{13}CO and $^{15}N_2$ gases enabled the synthesis of various ^{13}C and ^{15}N-enriched isotopologues of **5**. The ^{13}C and ^{15}N NMR spectra of **5** are presented in Figure 2.5 and Figure 2.6, respectively, and confirm N-N cleavage and N-C and N-H bond formation. Specifically, the ^{13}C NMR chemical shift of 135.26 ppm and the N-C coupling constant of $^{1}J_{NC}$ = 33.1 Hz observed in the terminal isocyanate ligand of the ^{13}C/^{15}N-labeled isotopologue are diagnostic for this group. In addition, the ^{15}N NMR spectrum exhibits two distinct ^{15}N environments at 82.7 ppm and 315.5 ppm, corresponding to the terminal isocyanate and bridging imido groups, respectively. In the proton coupled spectrum, the resonance at 315.5 ppm splits into a doublet with an N-H coupling constant of $^{1}J_{NH}$ = 40.8 Hz. The KBr infrared spectrum of **5** was also informative, exhibiting an N-H stretch at 3577 cm^{-1} and an isocyanate stretch at 2222 cm^{-1} that red shifts to 2159 cm^{-1} and 2147 cm^{-1} for the ^{13}C-labeled and doubly labeled (^{13}C and ^{15}N)

isotopologues, respectively.

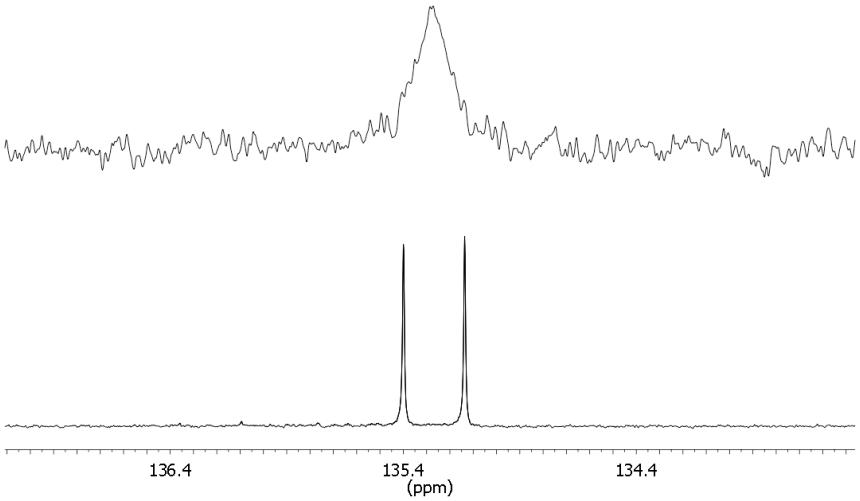

Figure 2.5. Benzene-d_6 {^{1}H} ^{13}C NMR spectra of **5-^{13}C** (top) and **5-^{13}C^{15}N$_2$** (bottom) at 23 °C.

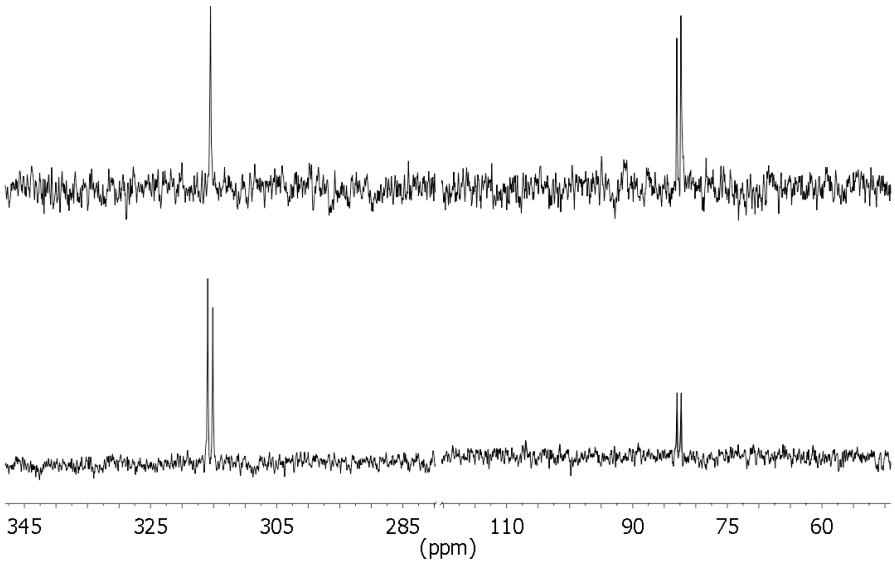

Figure 2.6. Benzene-d_6 {^{1}H}^{15}N NMR spectrum (top) and ^{15}N spectrum (bottom) of **5** at 23 °C.

Single crystals of **5** suitable for X-ray diffraction were obtained and a representation of the molecular structure is presented in Figure 2.7. The (*S*,*S*) enantiomer is shown, and a representation of the (*R*,*R*) enantiomer is presented in Appendix C. The structure confirms N-N cleavage, isocyanate formation, and cyclometalation with one of the cyclopentadienyl *tert*-butyl substituents. The angle between the two hafnium atoms and the imido nitrogen is near linear (172.5(3)°) and the imido ligand is equidistant between the hafnium centers.

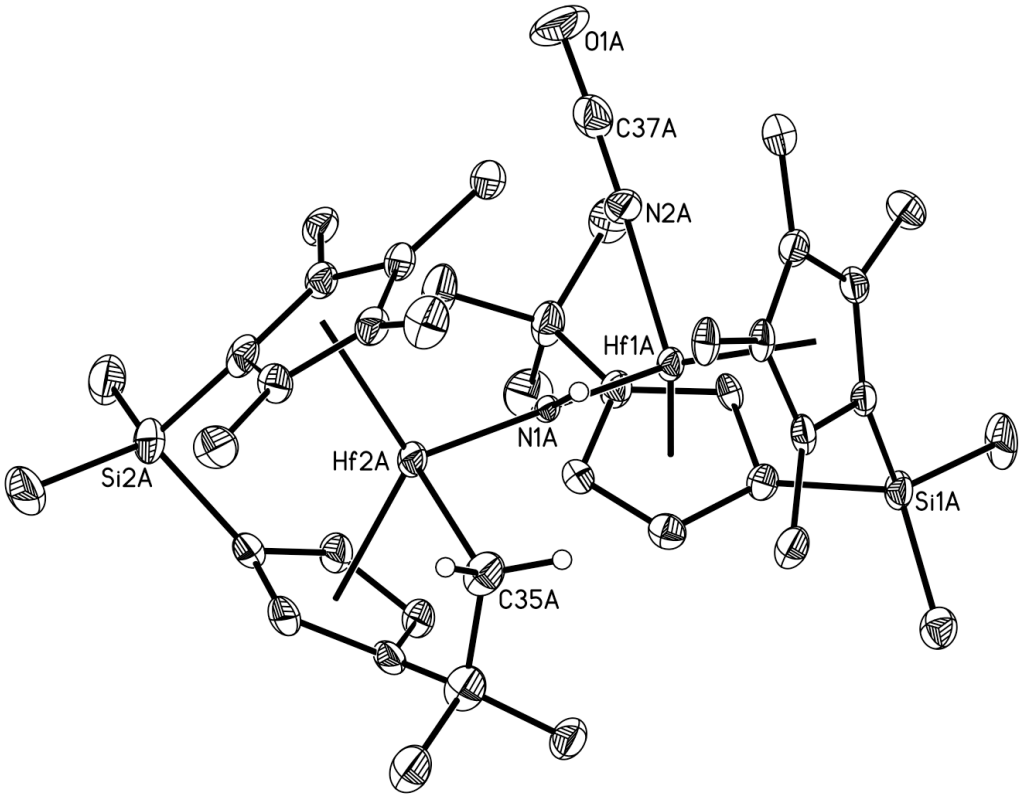

Figure 2.7. Molecular structure of **5** at 30% probability ellipsoids. Hydrogen atoms omitted for clarity. The (*S*,*S*) enantiomer is shown.

The reactivity of **5** was also consistent N-N cleavage and bridging imido formation. Protonolysis of **5** with anhydrous, gaseous HCl produced NH_4Cl in 96%

yield per μ-NH (as judged by ^{1}H NMR spectroscopy in dimethylsulfoxide-d_6 and phenol-hypochlorite titration)[28] along with the corresponding hafnocene dichloride complex (**4-Cl$_2$**) (Figure 2.8). Trace isocyanic acid (HNCO) was also detected by ^{13}C NMR spectroscopy after carefully transferring the volatiles to a clean J. Young NMR tube under anhydrous conditions following protonolysis.

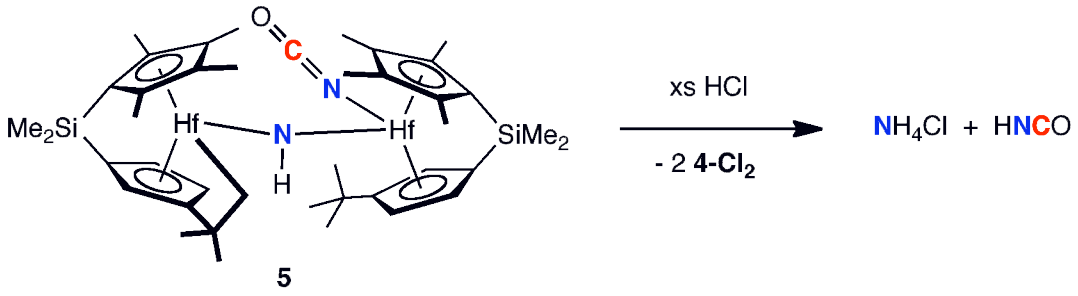

Figure 2.8. Protonolysis of **5** with hydrochloric acid.

To ensure clean formation of **5**, CO must be slowly diffused into solutions of **4-N$_2$**. Otherwise, formation of **4-N$_2$C$_2$O$_2$-*C$_1$*** competes with the cyclometalation pathway. A proposed mechanism for the formation of **5** is presented in Figure 2.9. This mechanism is derived from that proposed for oxamidide formation in the previous chapter (see Figure 1.37), and begins with insertion of CO into a Hf-N bond. Retro-[2+2] cycloaddition relieves strain in the four-membered ring and furnishes the terminal isocyanate, along with a bridging nitrido species. The bridging nitrido, due to its multiple bonding to hafnium,[29] promotes the rapid, intramolecular 1,2-addition of a C-H bond from the *tert*-butyl substituent on the same hafnocene subunit across the Hf=N bond, yielding the observed cyclometalated species **5**. While the proposed bridging nitrido species has not yet been direcly observed, its transient existence is strongly implied as the theoretical product of the microscopic reverse of the process leading to μ-NH formation (i.e. 1,2-elimination).

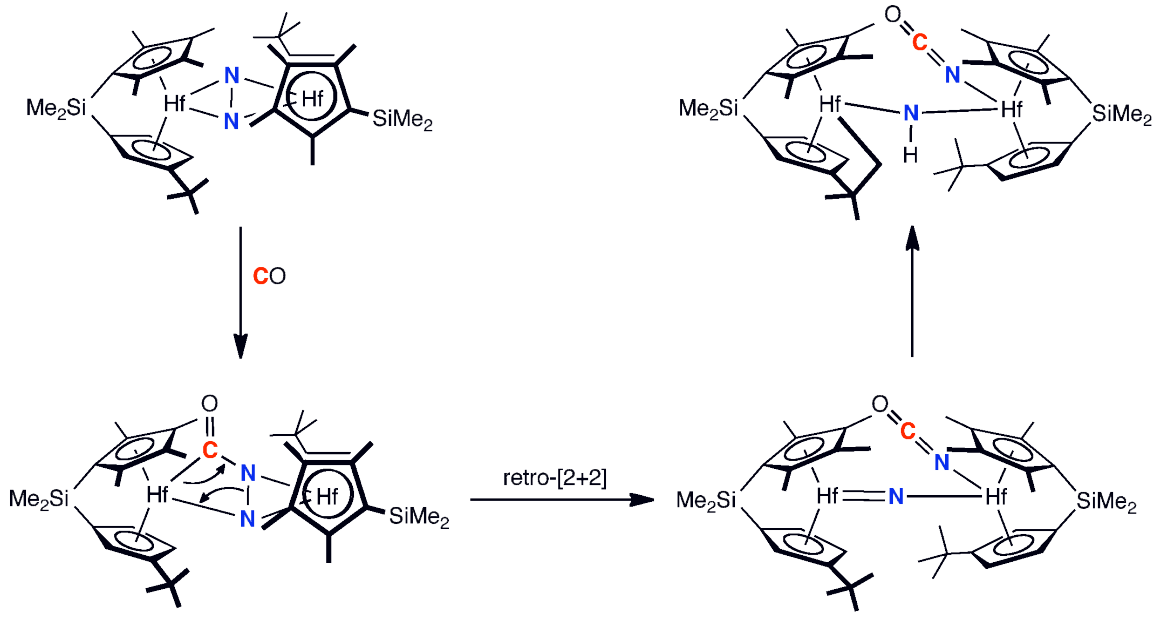

Figure 2.9. Proposed mechanism for the formation of **5**.

The transformation of **4-N_2** to **5** is analogous to previously reported chemistry from the laboratories of Bergman and Gade with group 4 hydrazide complexes.[30,31,32] Carbonylation of these zirconium hydrazides resulted in N-N cleavage and C-N formation to give terminal isocyanate and amido ligands. The $[NR_2]^-$ fragment in these compounds is isolobal to the $[Hf{=}N]^-$ fragment in **5**, and the resulting zirconium isocyanate amido complexes are directly analogous to the purported bridging nitrido intermediate in Figure 2.9. Gade cites the bent nature of the hydrazide ligand as the origin of carbonylation and N-N cleavage in these species.[30] This observation is also consistent with carbonylation of the hafnocene species, **4-N_2**, as in one resonance extreme, the dinitrogen complex can be viewed as a bent bis(imido) species, analagous to Gade's starting hydrazide complex (Figure 2.10).

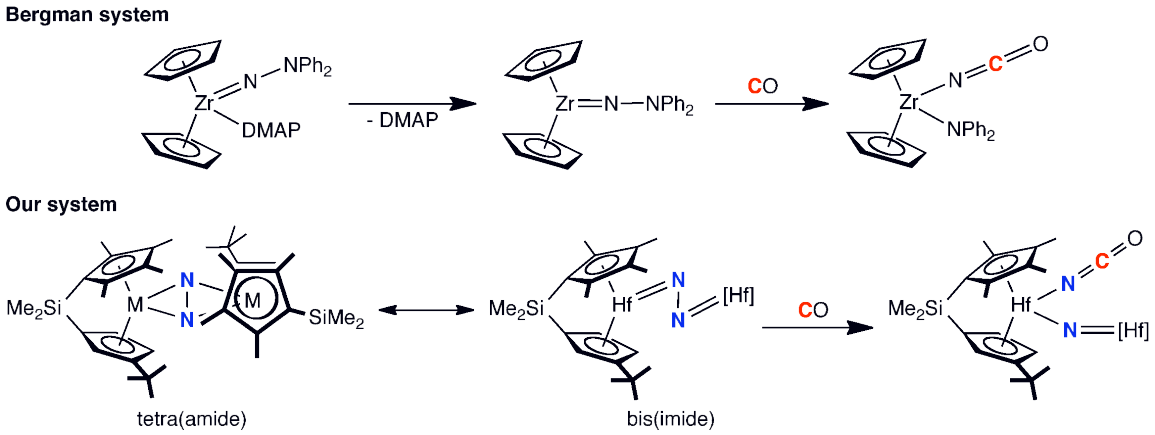

Figure 2.10. Comparison of **4-N_2** carbonylation to previously reported zirconium hydrazide carbonylation.

Stoichiometric, slow CO addition experiments were also attempted with the unlinked hafnocene variant, **2-N_2** to determine whether analogous cyclometalated products would result when the cyclopentadienyl rings were substituted with methyl groups rather than the *tert*-butyl substituent present in **4-N_2**. Slow diffusion of 1.1 eq CO into a benzene-d_6 solution of **2-N_2** over the course of 16 h at 23 °C resulted in a color change from purple to yellow. ^{1}H NMR spectroscopy established the formation of two C_1 symmetric hafnocene products in a 1.5:1 ratio (Figure 2.11). These products were identified as isomers of a cyclometalated dihafnocene isocyanate complex, **6**, by multinuclear (^{1}H, ^{13}C, ^{15}N) NMR spectroscopy, infrared spectroscopy and in one case X-ray diffraction. On a preparative scale, several samples were independently synthesized in NMR tubes and combined and the isomeric mixture was isolated. Attempts to separate the isomers of **6** on a preparative scale via recrystallization have been unsuccessful.

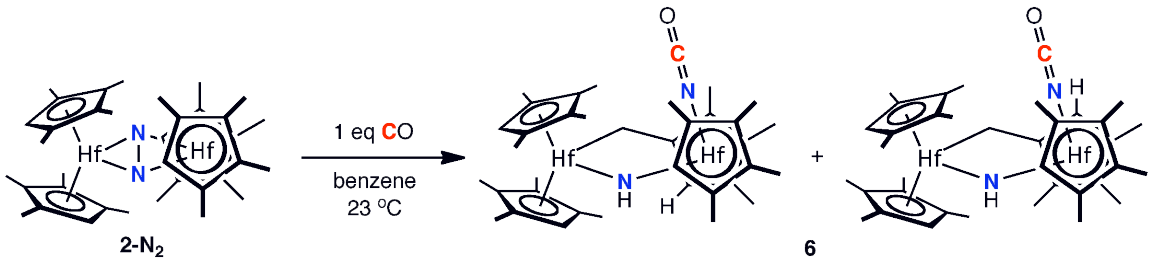

Figure 2.11. Formation of **6** from stoichiometric CO addition to **2-N_2**.

The $\{^1H\}^{13}C$ and ^{15}N NMR spectra of the ^{13}C, ^{15}N-labeled isotopologue of the isomeric mixture, **6**, are presented in Figure 2.12 and Figure 2.13, respectively, and confirm the presence of isocyanate and μ-imido ligands in both isomers. As with **5**, the isocyanate groups in **6** have diagnostic upfield chemical shifts and coupling constants in the ^{15}N spectrum of 86.8 ppm ($^1J_{CN}$ = 32.4 Hz) (major) and 84.2 ppm ($^1J_{CN}$ = 32.6 Hz) (minor) as well as a diagnostic stretch in the KBr infrared spectrum at 2220 cm^{-1}. The bridging imido ligands appear downfield at 289.4 ppm ($^1J_{NH}$ = 55.7 Hz) (major) and 296.2 ppm ($^1J_{NH}$ = 55.7 Hz) (minor) and exhibit a broad overlapping stretch in the infrared spectrum at 3564 cm^{-1}.

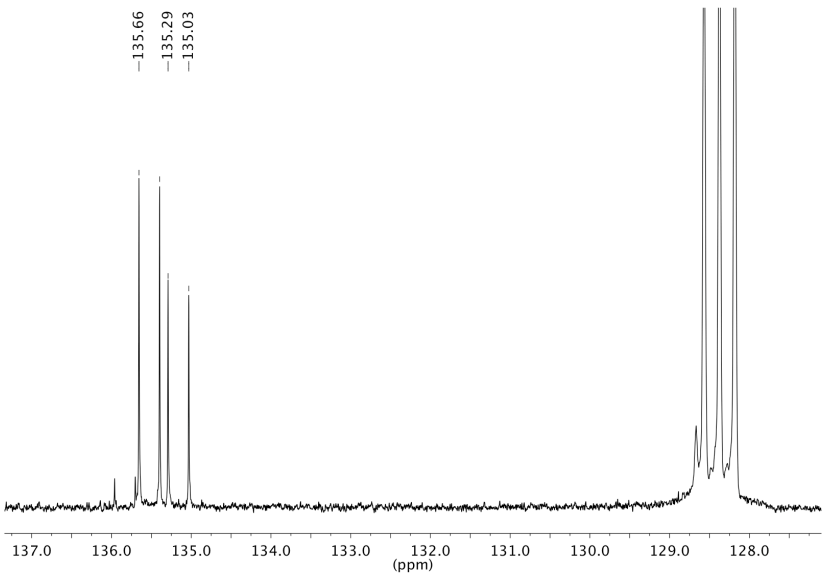

Figure 2.12. Benzene-d_6 $\{^1H\}$ ^{13}C NMR spectrum of the isocyanate region of the mixture of isomers of **6-$^{15}N_2{}^{13}C$** at 23 °C.

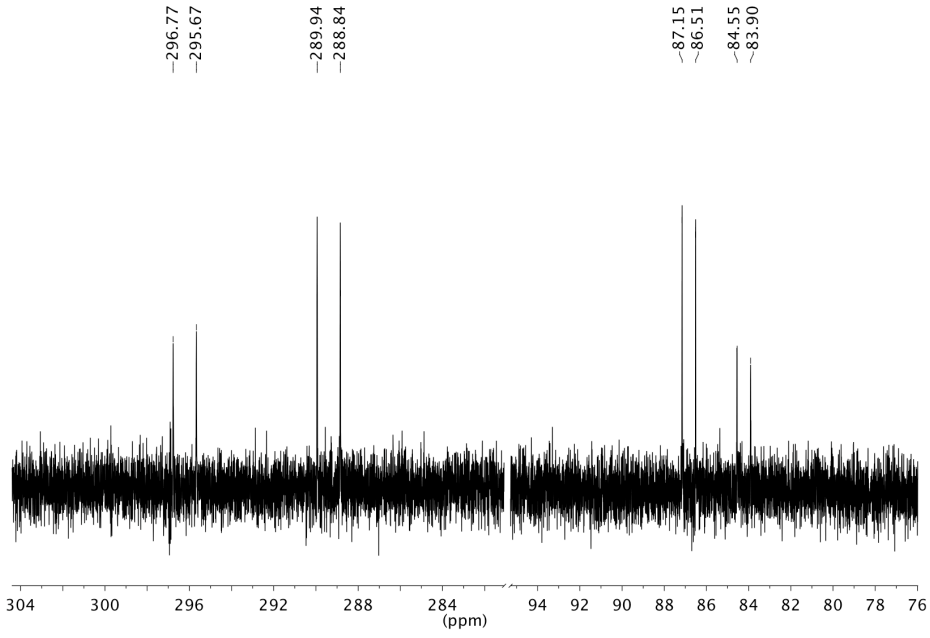

Figure 2.13. Benzene-d_6 ^{15}N NMR spectrum of the μ-imido region (downfield) and isocyanate region (upfield) of the mixture of isomers of **6-$^{15}N_2{}^{13}C$** at 23 °C.

To determine which methyl substituent(s) on the cyclopentadiene were involved in cyclometalation, the mixture of isomers **6** was treated with excess gaseous DCl, furnishing the corresponding hafnocene dichloride, **2-Cl$_2$-*d*$_1$**, along with liberation of (deuterium enriched) ammonium chloride and isocyanic acid (Figure 2.14). The hafnocene dichloride product was analyzed by ^{2}H NMR spectroscopy and a single peak centered at 1.82 ppm was observed (Figure 2.15), indicating that cyclometalation occurred exclusively at the cyclopentadienyl methyl group adjacent to the hydrogen substituent.[16] From this result it was concluded that the two observed products likely result from cyclometalation of the diastereotopic methyl group across the dihafnocene complex, forming two diastereomers of a so-called "tuck-over" complex as shown in Figure 2.14.[33] It is also possible that one isomer is a "tuck-in" complex where the methyl group cyclometalates on the same side of the dihafnocene compound.

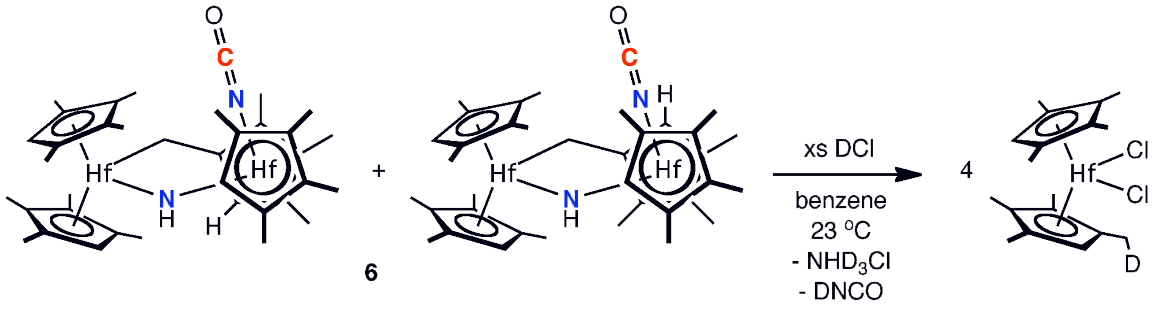

Figure 2.14. Protonoylsis of **6** with DCl.

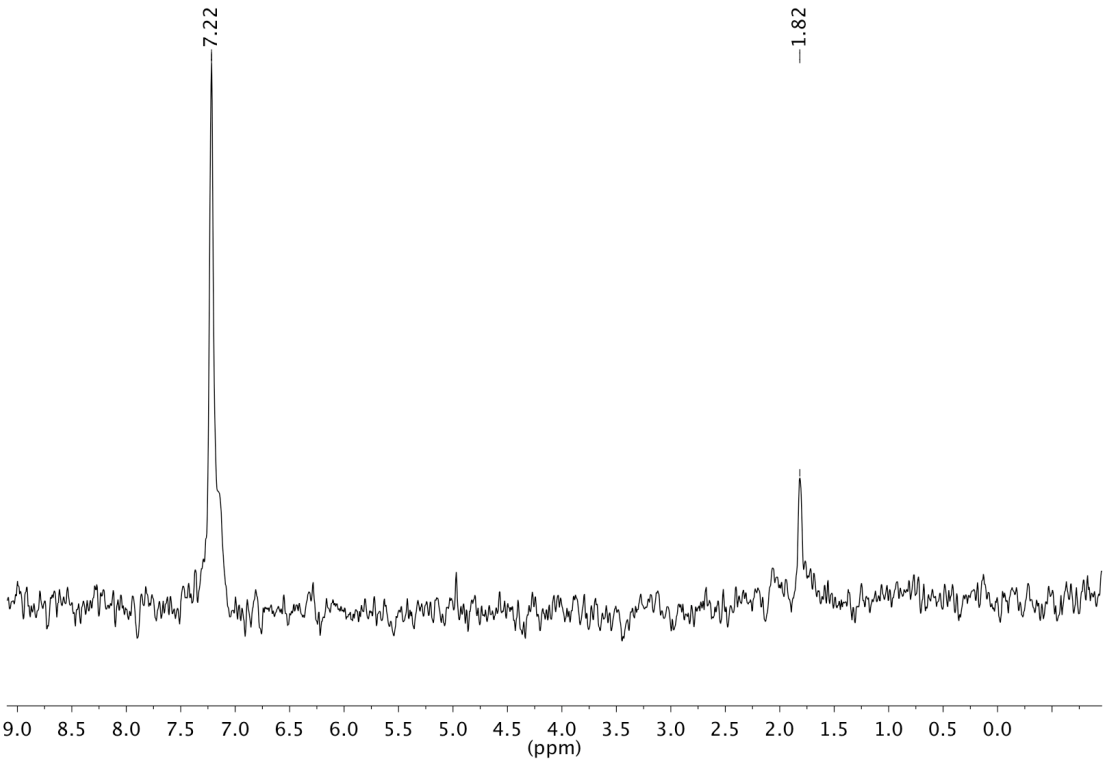

Figure 2.15. Benzene ^{2}H NMR spectrum of **2-Cl$_2$-*d$_1$*** establishing exclusive deuterium incorporation into the methyl groups adjacent to the Cp hydrogen.

The solid-state structure of one of the isomers of **6** was obtained and a representation is presented in Figure 2.16. The structural data confirms N_2 cleavage giving rise to terminal isocyanate and bridging imido formation. The structure also supports the spectroscopic identification of a cyclometalated methyl group that bridges the two hafnocene fragments in a "tuck-over" fashion, providing the hydrogen for imido formation. The Hf1−N1 and Hf2−N1 distances of 2.034(4) and 2.059(3) Å, respectively, are elongated for an imido species and more consistent with hafnium−nitrogen single bonds. The Hf1−N1−Hf2 linkage is bent with an angle of 131.47(17)°. This distortion contrasts with the nearly linear angle of 172.5(3)° in the bridging imido formed from addition of 1 equivalent of CO to **4-N$_2$**.

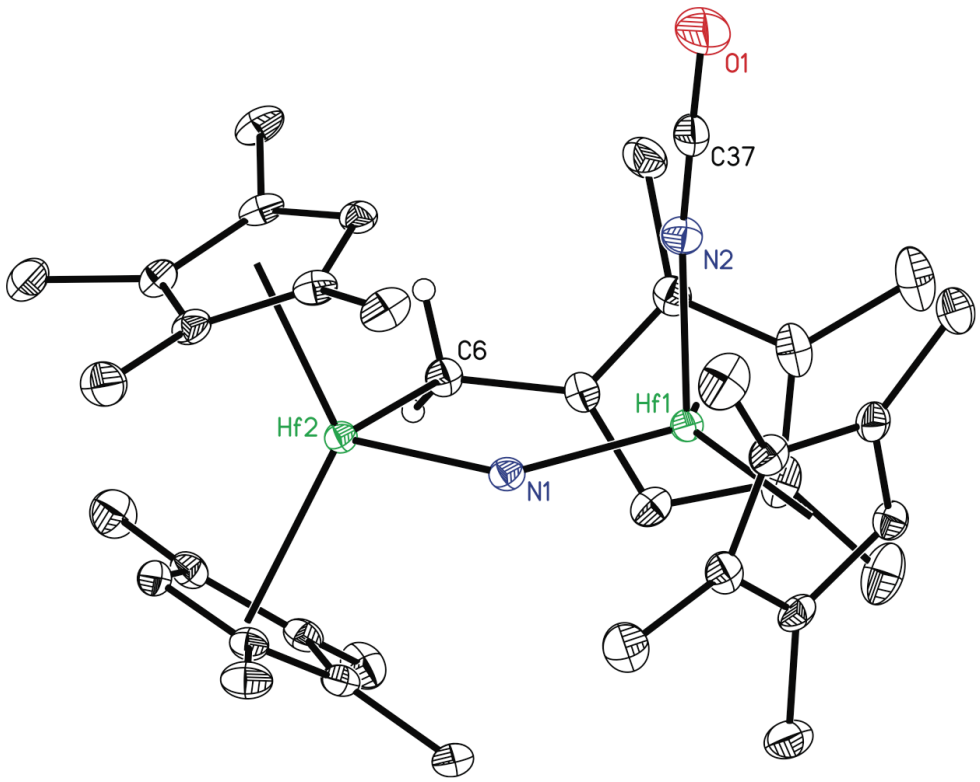

Figure 2.16. Molecular structure of one isomer of **6** at 30% probability ellipsoids. Hydrogen atoms, except those attached to C6, have been omitted for clarity.

A similar mechanism to that for the formation of **5** was also proposed for the formation of **6**, and is shown in Figure 2.17. Similarly no intermediates were observed during the transformation of **2-N$_2$** to **6**. The mechanism starts with CO insertion followed by N-N cleavage via retro-[2+2] cycloaddition to yield the terminal isocyanate and bridging nitrido ligands. The bridging nitrido species is rapidly trapped by 1,2-addition of a cyclopentadienyl methyl C-H bond across the Hf=N bond on the opposite side of the molecule, affording the observed diastereomers of **6**.

Similar "tuck-over" fulvalene chemistry was observed previously in our laboratory following the hydrogenation of **2-N$_2$** to form the diazenido hafnocene hydride complex [(η^5-$C_5Me_4H)_2HfH$](μ_2,η^2,η^2-N_2H_2) (**2-N$_2$H$_4$**). Heating a benzene-d_6

solution of this compound to 65 °C resulted in loss of 1 equivalent of H_2 and initially furnished the fulvalene complex where cyclometalation occurred on the same hafnium center. Additional heating at 65 °C resulted in loss of a second equivalent of H_2 and a second cyclometalation event in which both fulvalenes were metalated across the dimer.[16]

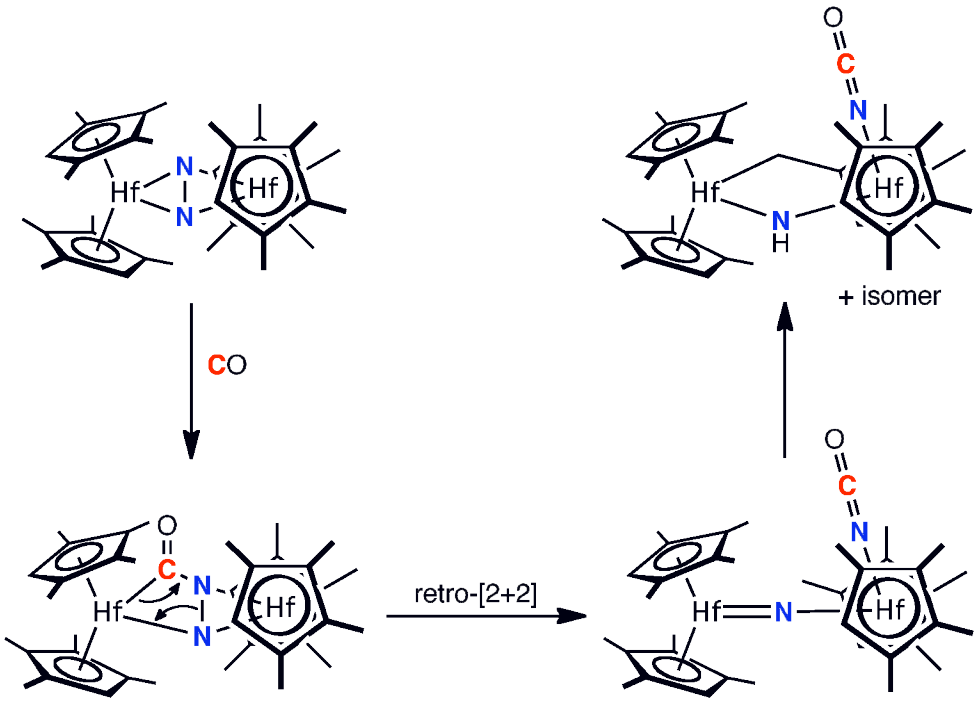

Figure 2.17. Mechanism for the formation of **6**.

Coupling CO-induced N2 cleavage to N-H formation via hydrogenation.

The observation of CO-induced N_2 cleavage concomitant with intramolecular C-H activation promoted by a putative bridging nitrido intermediate for both hafnocene dinitrogen complexes, **2-N_2** and **4-N_2**, prompted an exploration into the interception of these μ-nitrido species with other non-polar and polar reagents. Dihydrogen was initially selected because of its potential for the desired 1,2-addition chemistry and for

the possibility of coupling N_2 cleavage with hydrogenation. One potential challenge with these experiments is the ratio of reagents used, as the reaction of H_2 with the starting dinitrogen compound[15,16,25] must be slower than the initial carbonylation and 1,2-addition of H_2 must be faster than the subsequent CO addition step.

Exposure of a benzene-d_6 solution of **2-N$_2$** to a gaseous mixture of CO and H_2 in an approximate ratio of P_{CO}:P_{H2} = 3:1 (1 atm total) with vigorous shaking at 23 °C resulted in a rapid color change from purple to pale yellow, signaling consumption of **2-N$_2$** and conversion to a new C_1 symmetric organometallic product identified as **2-(μ-NH)(H)(NCO)** (Figure 2.18). The "modified syngas" mixture was prepared using the mixing station of a high vacuum line prior to addition to the reaction vessel. To ensure that **2-(μ-NH)(H)(NCO)** was not simply a product of the hydrogenation of **6**, a control experiment in which a benzene-d_6 solution of **6** was exposed to 4 atm H_2 was conducted. No change was observed after heating to 100 °C for 24 h, establishing that **2-(μ-NH)(H)(NCO)** was indeed a unique product formed from modified syngas addition to **2-N$_2$**. Interestingly, this result demonstrates the cleavage and hydrogenation of coordinated dinitrogen in a single transformation.

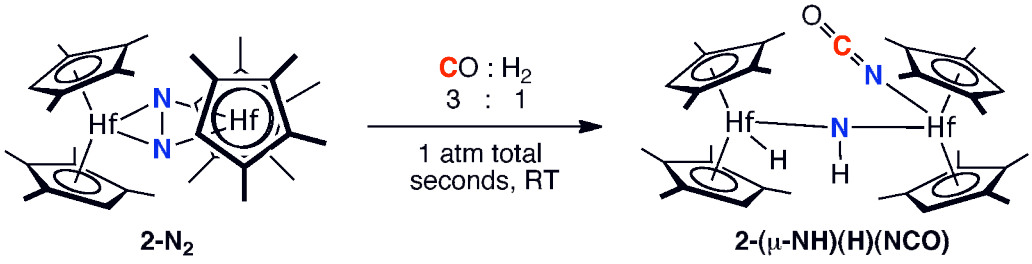

2-N$_2$ **2-(μ-NH)(H)(NCO)**

Figure 2.18. Addition of a gaseous mixture of CO and H_2 to **2-N$_2$**.

The structure of **2-(μ-NH)(H)(NCO)** was definitively established by multi-nuclear (^{1}H, ^{13}C, ^{15}N) NMR spectroscopy, infrared spectroscopy and X-ray crystallography. Selected NMR features for **2-(μ-NH)(H)(NCO)** and analogous compounds studied in this work are presented in Table 2.1. The benzene-d_6 ^{1}H NMR spectrum of **2-(μ-NH)(H)(NCO)** contains the number of resonances consistent with a C_1 symmetric dihafnocene complex with a diagnostic downfield hydride resonance at 10.50 ppm. The ^{13}C and ^{15}N-enriched isotopologues of **2-(μ-NH)(H)(NCO)** were readily prepared and selected regions of the benzene-d_6 ^{13}C and ^{15}N NMR spectra of **2-(μ-^{15}NH)(H)(^{15}N^{13}CO)** are presented in Figure 2.19. Two doublets were observed in the ^{15}N NMR spectrum at 319.1 ($^{1}J_{NH}$ = 45.6 Hz) and 104.3 ($^{1}J_{NC}$ = 32.9 Hz) ppm and assigned to the bridging imido and isocyanate nitrogens, respectively. The benzene-d_6 ^{13}C NMR spectrum also exhibits a broad resonance at 135.45 ppm for the terminal NCO ligand, which splits into a sharp doublet upon ^{15}N labeling (Figure 2.19). The presence of both the μ-NH and NCO groups was confirmed by IR spectroscopy, as bands were observed at 3590 and 2224 cm^{-1} (KBr), respectively.

The product of syngas addition, **2-(μ-NH)(H)(NCO)**, could only be reproducibly prepared in NMR tubes. By combining several independent samples, single crystals suitable for X-ray diffraction were obtained. The solid state structure of **2-(μ-NH)(H)(NCO)** is presented in Figure 2.20 and confirms the spectroscopic identification.

Table 2.1. NMR spectroscopic data for the products of CO-induced N_2 bond cleavage coupled to N-H bond formation by hydrogenation.

Compound	δ M-H[a]	δ N-H[a,b]	δ ^{13}C[c]	δ ^{15}N[d]	IR (cm^{-1})[e]
2-(μ-NH)(H)(NCO)	10.50	4.05	135.45	89.5	3590
		(45.6)	(32.9)	304.5	2224
3-(μ-NH)(H)(NCO)	4.84	6.78	133.65	82.5	3610
		(40.6)	(30.9)	372.0	2215
4-(μ-NH)(H)(NCO)	9.39	4.66	135.29	N/D	3580
		(40.9)	(32.9)	326.5	2223
4-(μ-NH)(CCPh)(NCO)	---	5.17	135.52	N/D	3577
				324.1	2222
					2084[f]
4-(μ-O)(H)(NCO)	9.23	---	136.24	91.4	2220[g]
			(33.9)	---	1560

[a.] Benzene-d_6 ^{1}H NMR shift in ppm. [b.] The $^1J_{N\text{-}H}$ coupling constant is reported in Hz in parentheses. [c.] ^{13}C NMR shift of the M-N*C*O ligand in ppm recorded in benzene-d_6. The $^1J_{C\text{-}N}$ coupling constant in Hz is reported in parenthesis. [d.] ^{15}N NMR shifts of the isocyanate (listed first) and μ-NH (second) ligands. [e.] Recorded in KBr. The N-H stretch is listed first followed by the NCO band. [f.] IR band for C≡CPh [g.] IR bands for the terminal NCO ligand (top) and Hf-H (bottom). N/D = not determined.

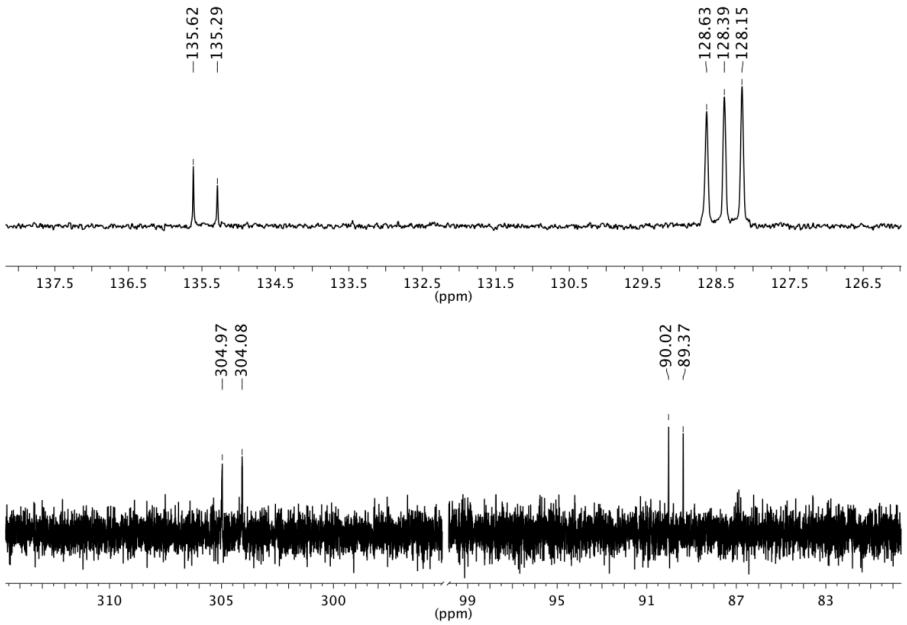

Figure 2.19. Benzene-d_6 $\{^1H\}$ ^{13}C NMR spectrum (top) and ^{15}N NMR spectrum (bottom) of **2-(μ-^{15}NH)(H)(^{15}N^{13}CO)**.

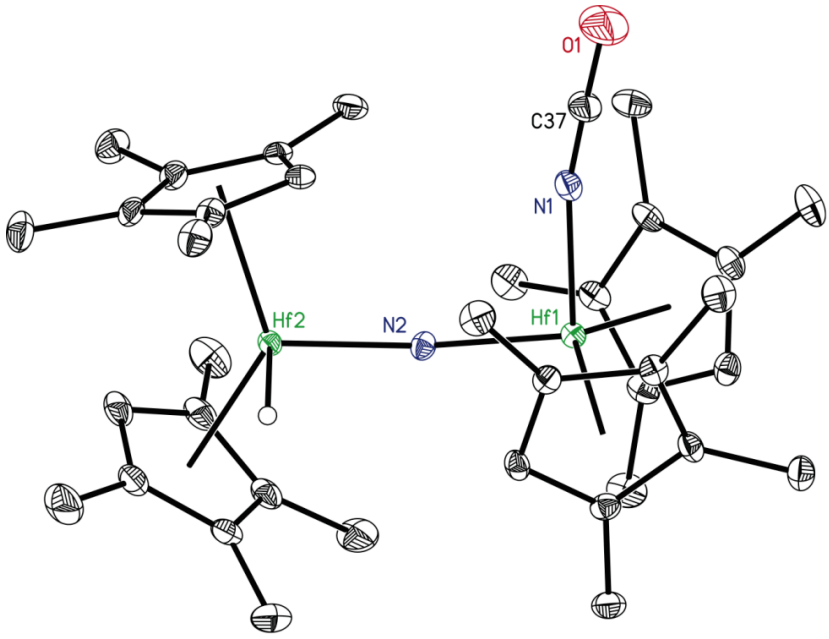

Figure 2.20. Molecular structure of **2-(μ-NH)(H)(NCO)** at 30% probability ellipsoids. Hydrogen atoms, expect for the one bound to hafnium, have been omitted for clarity. The imido hydrogen was not located.

Selected metrical parameters for **2-(μ-NH)(H)(NCO)** (and other related compounds in this study) are reported in Table 2.2. The hafnium hydride was located in the difference map but the imido hydrogen was not. The two hafnocene subunits are canted with respect to each other, forming a dihedral angle of 92.4° between the idealized planes of the two metallocene wedges. The bridging imido ligand is slightly bent, with a Hf1−N2−Hf2 angle of 151.0(2)°. The nitrogen atom is nearly equidistant from the two metal centers with statistically indistinguishable Hf1−N2 and Hf2−N2 distances of 2.042(4) and 2.053(4) Å, respectively. These values are slightly elongated relative to the values of 1.950(4) and 1.987(5) Å reported for the cyclometalated μ-imido ansa-hafnocene isocyanate shown in Figure 2.7.

Table 2.2. Selected bond distances (Å) and angles (deg) for **2-(μ-NH)(H)(NCO)**, **4-(μ-NH)(H)(NCO)** and **4-(μ-O)(H)(NCO)**.

	2-(μ-NH)(H)(NCO)	**4-(μ-NH)(H)(NCO)**	**4-(μ-O)(H)(NCO)**
Hf-(μ-*N*H)	2.053(4) Hf(1)	2.065(3) Hf(1)	1.976(2) (Hf1)
(or μ-*O*)	2.042(4) Hf(2)	2.048(3) Hf(2)	1.956(2) (Hf2)
Hf-H	2.06(5)	1.88(3)	1.88(5)
Hf-*N*CO	2.141(4)	2.120(4)	2.093(4)
N=*C*O	1.157(7)	1.114(6)	1.154(6)
N*C*=*O*	1.197(7)	1.255(14)	1.190(6)
Hf-E-Hf[a]	151.0(2)	169.79(18)	147.88(16)
Hf-N-C	167.7(4)	174.1(4)	177.8(4)
N-C-O	178.7(7)	171(2)	179.3(6)

[a.] E = NH or O**.**

The CO-induced cleavage of N_2 coupled to hydrogenation was also successful for the *ansa*-hafnocene **4-N$_2$**. Addition of 3:1 CO:H_2 "syngas" to a benzene-d_6 solution of **4-N$_2$** and vigorous shaking for several seconds resulted in complete conversion to the C_1 symmetric bridging imido product, **4-(μ-NH)(H)(NCO)** (Figure 2.21). Despite the possibility for multiple isomers, only one isomer was observed spectroscopically. In this case, the reaction was complicated by the formation of white, insoluble, unidentified byproduct. Unfortunately, adjusting the gas ratio did not reduce the amount of this impurity and the reaction suffered from low yields of the desired product, **4-(μ-NH)(H)(NCO)**. Combining, filtering and recrystallizing several independent samples afforded quantities of **4-(μ-NH)(H)(NCO)** sufficient for full characterization by multinuclear (^{1}H, ^{13}C, ^{15}N) NMR spectroscopy, infrared spectroscopy as well as single crystal X-ray diffraction.

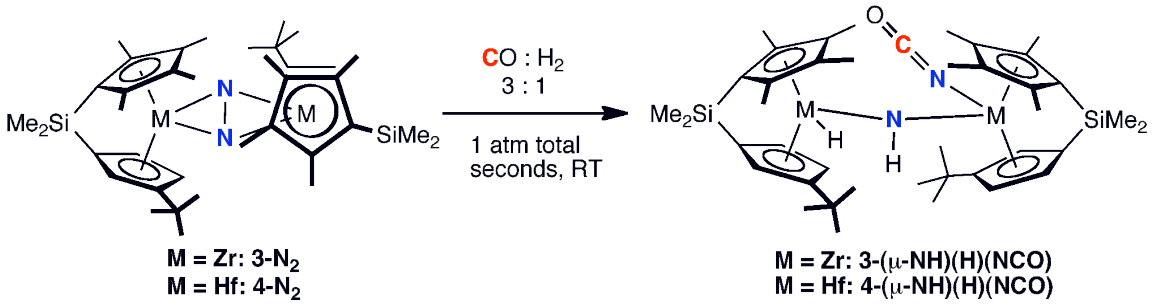

Figure 2.21. Addition of syngas to **3-N$_2$** and **4-N$_2$**

Selected NMR data for **4-(μ-NH)(H)(NCO)** are reported in Table 2.1 and are consistent with the formation of new terminal isocyanate (^{13}C δ = 135.29 ppm, $^1J_{NC}$ = 32.9 Hz), bridging imido (^{15}N δ = 326.5 ppm, $^1J_{NH}$ = 40.9 Hz), and terminal hydride (^{1}H δ = 9.39 ppm) ligands. The molecular structure of **4-(μ-NH)(H)(NCO)** is represented in Figure 2.22; the (*S*,*S*) enantiomer is pictured and a representation of the (*R*,*R*) enantiomer is reported in Appendix C. Selected metrical parameters for **4-(μ-**

NH)(H)(NCO) are reported in Table 2.2, and in general, bond distances similar to those found in **2-(μ-NH)(H)(NCO)** were observed. Importantly, the structure establishes the stereochemistry of the ligands with respect to the *ansa*-metallocene framework. The preferred isomer has both the hafnium hydride and the isocyanate ligand oriented *syn* to the *tert*-butyl substituents on the cyclopentadienyl rings, and like rings are *syn* across the dimer with the *tert*-butyl groups directed *anti*.

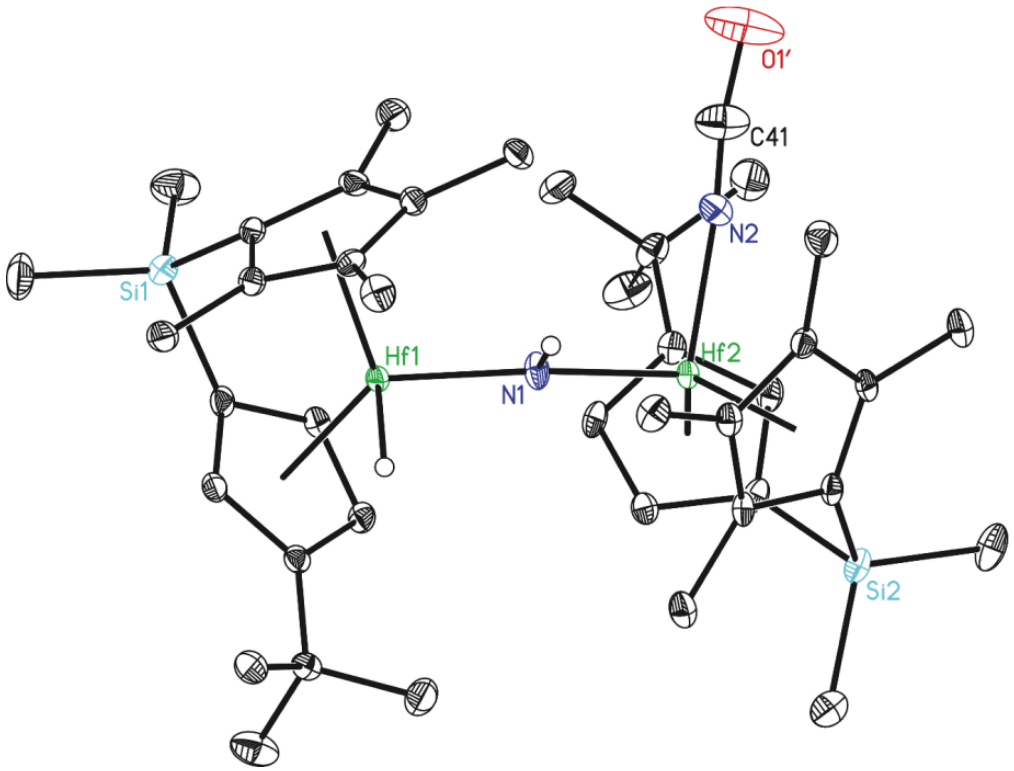

Figure 2.22. Molecular structure of **4-(μ-NH)(H)(NCO)** at 30% probability ellipsoids. Hydrogen atoms, except for those in the Hf-H and N-H bonds, have been omitted for clarity. The (*S*,*S*) enantiomer is shown.

The successful outcomes of modified syngas addition to the hafnocene dinitrogen complexes **2-N_2** and **4-N_2** prompted exploration of similar chemistry with

the zirconium congeners, **1-N_2** and **3-N_2**. Attempts to achieve clean chemistry with the unlinked compound **1-N_2** were unsuccessful. Addition of a 3:1 CO/H_2 mixture (1 atm total) to solutions of **1-N_2** resulted in the formation of a mixture of several products, including the zirconocene oxamidide complex **1-$N_2C_2O_2$**, the zirconocene dicarbonyl complex **1-$(CO)_2$**, and several other unidentified products. Varying the ratio of gases did not significantly change the outcome of the reaction, and separation attempts were unsuccessful.

Repeating a similar gas addition protocol with the *ansa*-zirconocene complex **3-N_2** resulted in formation of the desired isocyanato hydrido μ-imide product, **3-(μ-NH)(H)(NCO)** (Figure 2.21). As with the hafnium congener, the reaction of **3-N_2** with syngas also produced a significant quantity of insoluble precipitate, substantially lowering the yield of **3-(μ-NH)(H)(NCO)**. Key spectroscopic data for this compound and its ^{13}C and ^{15}N isotopologues are reported in Table 2.1. As expected, these data are similar to those of **4-(μ-NH)(H)(NCO)** except for the more upfield chemical shift of the zirconium hydride at 4.84 ppm. This Zr-*H* resonance was distinguished from the N-*H* resonance by ^{15}N and ^{2}H labeling experiments. Weakly diffracting single crystals of **3-(μ-NH)(H)(NCO)** were obtained, and a structural representation of the (*S,S*) enantiomer is presented in Figure 2.23. The (*R,R*) enantiomer is reported in Appendix C. Despite the poor quality of the data, connectivity and stereochemistry could be determined and the sole isomer formed was identified as the *syn* homochiral[34] dizirconocene structure in which the terminal hydride and isocyanate ligands are positioned over the *tert*-butyl substituents. This is the same diastereomeric preference as in the hafnium congener.

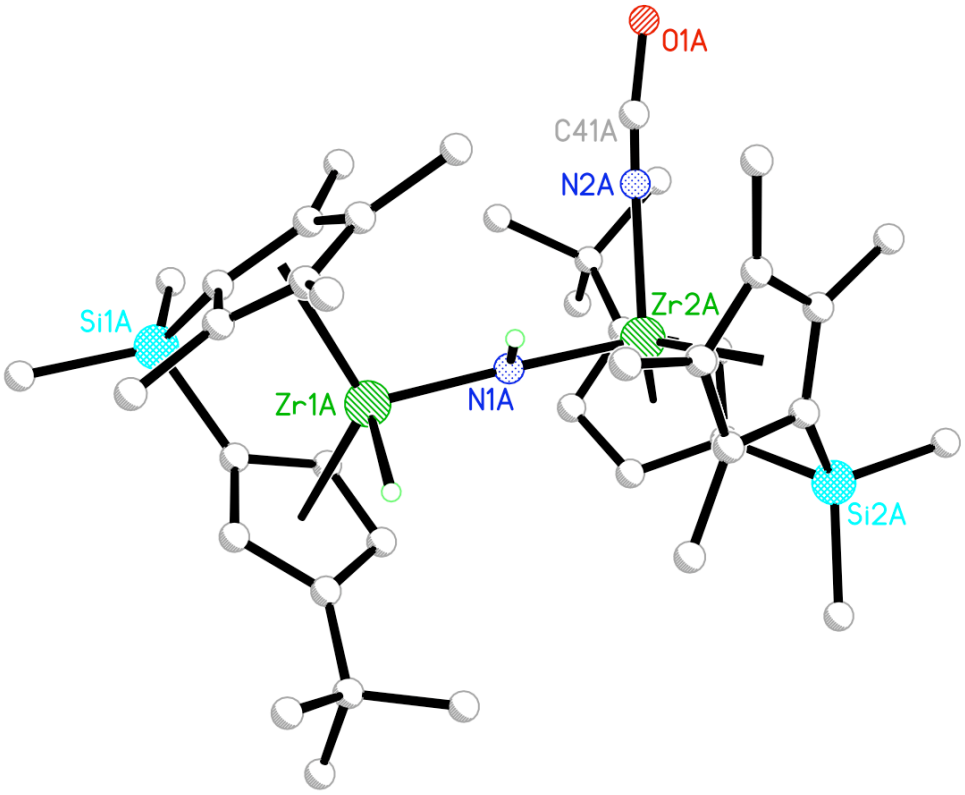

Figure 2.23. Molecular representation of **3-(μ-NH)(H)(NCO)**. The (*S*,*S*) enantiomer is shown.

Coupling CO-induced N_2 cleavage to N-H formation via intermolecular C-H activation. Given the effectiveness of hydrogen as an intermolecular trapping reagent for the putative μ-nitrido intermediate, we were inspired to explore other reagents that could serve a similar purpose. Alkynes were chosen due to their potential to serve as substrates for both 1,2-addition and cycloaddition across metal-nitrogen bonds. Our laboratory, as well as the labs of Fryzuk and others have previously demonstrated this possibility in N_2 functionalization chemistry and early metal imido and hydrazido chemistry.[35,36,37] Unfortunately, internal alkynes such as 2-butyne were inert with respect to the μ-nitrido intermediate, and exposing solutions of **4-N_2** to a mixture of 1 atm CO and 10 equivalents 2-butyne resulted in exclusive oxamidide

formation (**4-$N_2C_2O_2$-C_1/C_2**) with no evidence for cycloaddition across the Hf=N bond. Varying the ratio of reagents did not change the outcome.

Thus, we sought to trap the putative μ-nitrido intermediate formed after addition of 1 equivalent of CO by C-H activation of a terminal alkyne. Allowing a frozen benzene-d_6 solution of **4-N_2** containing 10 equiv of PhC≡CH to thaw in the presence of 1 atm CO furnished a single new C_1-symmetric hafnocene product identified as **4-(μ-NH)(CCPh)(NCO)** arising from functionalization of the putative μ-nitrido by 1,2-addition of the acetylenic C−H bond (Figure 2.24). The compound was definitively characterized by multinuclear (^{1}H, ^{13}C, ^{15}N) NMR spectroscopy and infrared spectroscopy. Key spectroscopic features of **4-(μ-NH)(CCPh)(NCO)** (and its ^{13}C/^{15}N-enriched isotopologues) include bridging N-*H* resonances in the ^{1}H NMR (δ = 5.17 ppm) and ^{15}N NMR (δ = 324.1 ppm) spectra, with a coupling constant of $^1J_{NH}$ = 40.4 Hz, determined by ^{1}H-^{15}N HSQC experiments. The isocyanate was clearly identified by a diagnostic ^{13}C NMR resonance at 135.52 ppm and infrared stretch at 2222 cm^{-1}.

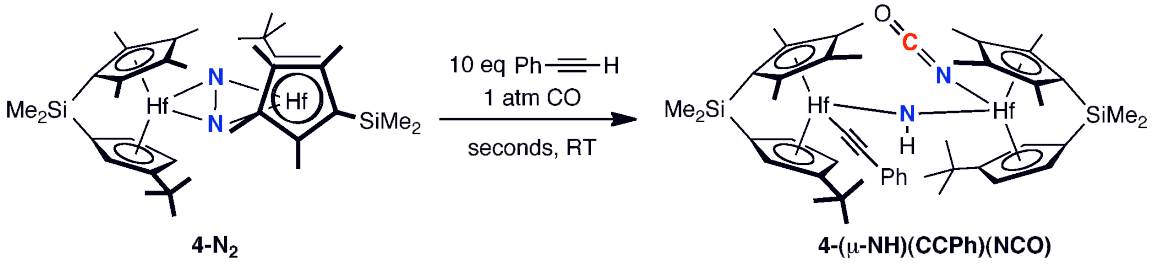

Figure 2.24. Addition of CO/phenyl acetylene to **4-N_2**.

Coupling N-N cleavage with CO deoxygenation promoted by silanes.

Silanes were also targeted as possible substrates for intercepting the μ-nitrido intermediate, as they have been used successfully by Fryzuk in N_2 functionalization

and cleavage chemistry with group 4 and 5 complexes.[38,39] We were also hoping to access routes to form new nitrogen-heteroatom bonds other than N-H bonds and ultimately incorporate the functionalized N-containing fragment into useful small molecules.

Treatment of a frozen benzene-d_6 solution of **4-N$_2$** with 5 equivalents ^{n}HexylSiH$_3$ followed by 1 atm CO produced, after thawing and vigorous shaking for 30 seconds, a color change from purple to yellow, signaling formation of a single new C_1 symmetric dihafnocene compound. Analysis of the product by multinuclear (^{1}H, ^{13}C, ^{15}N) NMR spectroscopy, infrared spectroscopy, single crystal X-ray diffraction, and protonolysis studies, definitively established its identity as the μ-oxo hydrido isocyanate complex, **4-(μ-O)(H)(NCO)** (Figure 2.25). Notably, **4-(μ-O)(H)(NCO)** was also formed when ^{n}BuSiH$_3$ or PhSiH$_3$ were used instead of ^{n}HexylSiH$_3$, establishing that the silyl fragment was not a component of the final organometallic product. The formation of **4-(μ-O)(H)(NCO)** was surprising and arises from deoxygenation of coordinated CO.

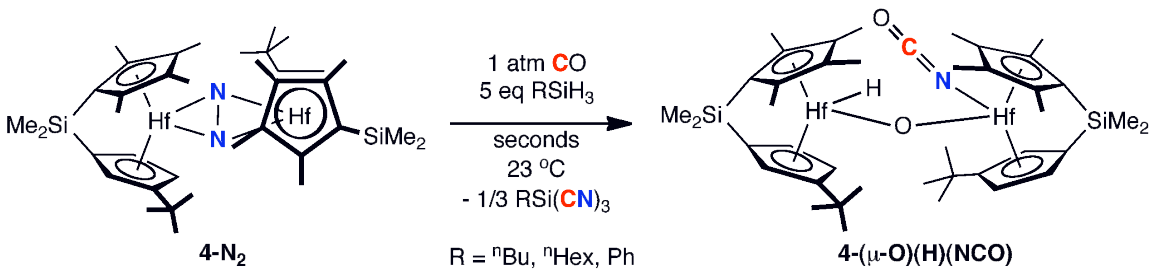

Figure 2.25. Addition of a mixture of CO and primary silane to **4-N$_2$**.

The same product was observed when 1 equivalent of silane was used, but in this case a small but significant quantity of ^{n}HexylSi(CN)H$_2$ was detected by ^{1}H NMR, ^{13}C NMR, and IR spectroscopies, which was consumed over time.[40] The

formation of ^{n}HexylSi(CN)$_3$ from the ligand redistribution reaction of ^{n}HexylSi(CN)H$_2$ with excess ^{n}HexylSiH$_3$ is the most likely explanation, and was supported by the observation of new cyano bands in the infrared spectrum of the product mixture and comparison to an independently prepared sample. The formation of 1/3 equivalents of ^{n}Hexyl(CN)$_3$ therefore accounts for the fate of silyl fragment during and following the formation of **4-(μ-O)(H)(NCO)**.

With such an unusual reaction,[41] it was important to unequivocally identify the bridging ligand as a bridging oxo (and rule out a bridging imido as seen in the previous cases). Several key pieces of experimental data were necessary to definitively establish the identity of the bridging ligand as a μ-oxo, and rule out all other possibilities. First, no N-*H* resonance was observed by ^{1}H NMR spectroscopy, and only a Hf-*D* signal, and no N-*D* signal, was observed by ^{2}H NMR spectroscopy upon preparation of the deuterated isotopologue **4-(μ-O)(D)(NCO)** from ^{n}HexylSiD$_3$. Similarly, no ^{15}*N*-H resonance was observed by ^{15}N NMR spectroscopy for the ^{15}N-enriched isotopologue **4-(μ-O)(H)(^{15}NCO)**; only one resonance is observed at 91.4 ppm corresponding to the terminal isocyanate ligand, that split into a doublet ($^{1}J_{CN}$ = 33.9 Hz) for the doubly labeled isotopologue **4-(μ-O)(H)(^{15}N^{13}CO)** (Figure 2.26). The isocyanate ligand was also observed in the ^{13}C NMR spectrum at 136.24 ppm (Figure 2.26). Additional spectroscopic details supporting this linkage are presented in Table 2.1. Attempts to collect mass spectral data using either electrospray ionization (EI) or matrix-assisted laser desorption ionization (MALDI) techniques were unsuccessful.

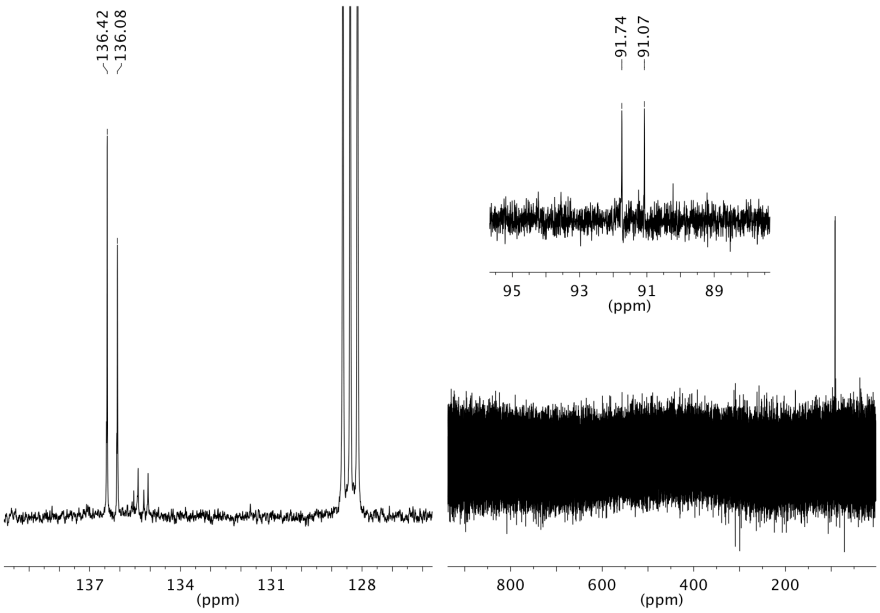

Figure 2.26. Benzene-d_6 $\{^1H\}$ ^{13}C NMR (left) and ^{15}N NMR (right) spectra of **4-(μ-O)(H)($^{15}N^{13}CO$)** at 23 °C.

In addition to spectroscopic evidence for the formation of **4-(μ-O)(H)(NCO)**, single crystal X-ray diffraction was used to corroborate the assignment. Single crystals of **4-(μ-O)(H)(NCO)** were obtained from slow evaporation of a benzene solution, and a representation of the solid state structure is presented in Figure 2.27. The (*S*,*S*) enantiomer is presented in the Figure and the (*R*,*R*) enantiomer is reported in Appendix C. It should be noted that data collected on two independently grown single crystals reproduced an identical crystallographic disorder. A large (~10 e/Å^3) difference Fourier peak was located near (0.9 Å from) the Hf1 atom, consistent with whole-molecule disorder. All of the other atoms were invisible and the minor hafnium component constituted one-ninth of the mixture. Despite these complications, the X-ray data confirm a bimetallic structure with terminal isocyanate and hydride ligands as well as a bridging oxo ligand. The orientation of the terminal ligands contrasts that of

4-(μ-NH)(H)(NCO), which has both terminal ligands *syn* to *tert*-butyl substituents. In **4-(μ-O)(H)(NCO)** while the isocyanate is *syn* to a *tert*-butyl group, the hydride ligand is orientated *anti* with respect to the remaining Cp *tert*-butyl substituent. The Hf1−O2 and Hf2−O2 distances of 1.976(2) and 1.956(2) Å are contracted relative to the corresponding lengths of 2.065(3) and 2.048(3) Å found in the related μ-imide **4-(μ-NH)(H)(NCO)**. Additional crystallographic parameters are reported in Table 2.2.

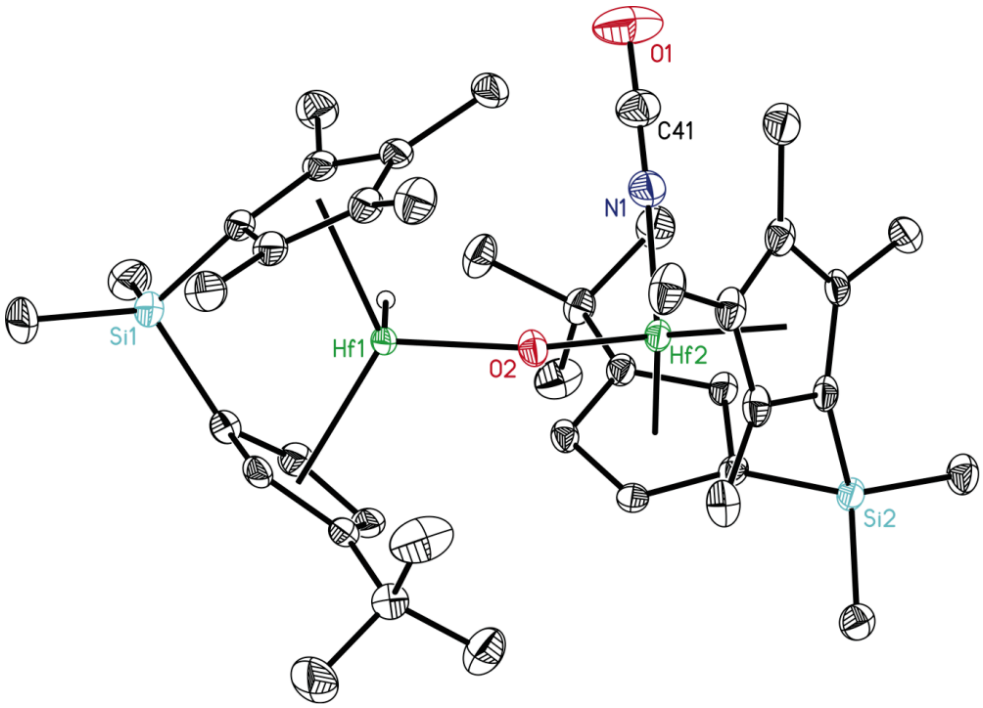

Figure 2.27. Molecular structure of **4-(μ-O)(H)(NCO)** at 30% probability ellipsoids. Hydrogen atoms except for the one in the Hf-H bond have been omitted for clarity. The (*S*,*S*) enantiomer is shown.

To further support the assigned structure, protonolysis studies were undertaken. For **4-(μ-NH)(H)(NCO)** and the other μ-NH compounds prepared in this work, the expected protonolysis products would be HNCO and NH_3. In principle, the

bridging oxo complex **4-(μ-O)(H)(NCO)** should produce no NH_3 upon protonolysis; however, HNCO is known to hydrolyze to NH_3 and CO_2.[42] The results of protonolysis of **4-(μ-O)(H)(NCO)** and several other compounds are reported in Table 2.3. The percentage NH_3 reported in the table assumes that the bridging ligand is the only potential source of NH_3. For the compounds containing both a μ-NH and terminal NCO ligand, the yield of ammonia is inflated to significantly greater than 100 percent. Importantly, the yield for **4-(μ-O)(H)(NCO)** is only 71.8 percent, significantly lower than compounds containing a μ-NH and around the observed "excess" for these compounds that can be attributed to hydrolysis of released HNCO.

Table 2.3. Amount of ammonia detected following treatment with 20 equivalents of HCl and aqueous digestion. The NH_3 was quantified by the method described in ref 28.

Compound	% NH_3[a]
2-(μ-NH)(H)(NCO)	147.4
3-(μ-NH)(H)(NCO)	175.2
4-(μ-NH)(H)(NCO)	166.8
4-(μ-O)(H)(NCO)	71.8

[a.] The percent yields are reported with respect to the μ-NH ligand. Thus, yields in excess of 100 % take into account the ammonia produced from the hydrolysis of HNCO.

Furthermore, in subsequent experiments the HNCO generated upon protonolysis was rigorously removed from the product mixture *in vacuo* and colorimetric quantitation was repeated. Using this procedure, the bridging imido complex **4-(μ-NH)(H)(NCO)** yielded 75.7% ammonia, consistent with a single μ-NH

moiety. On the other hand **4-(μ-O)(H)(NCO)** produced only 8.0% ammonia, thus supporting the presence of a μ-O rather than a μ-NH ligand in **4-(μ-O)(H)(NCO)**. All of the experimental data are therefore consistent with CO deoxygenation and liberation from the hafnium coordination sphere of a cyanosilane formed from dinitrogen and carbon monoxide in a single clean transformation. The reaction likely proceeds through the anticipated hydrido hafnocene silyl-imide complex, followed by additional CO insertion and release of the silyl isocyanide (which tautomerizes in solution to the cyanosilane) to furnish the observed bridging oxo product.

Conclusions

The coupling of CO-induced N_2 cleavage with intramolecular and intermolecular bond activation was accomplished. Treatment of the hafnocene nitrogen compounds **2-N_2** and **4-N_2** with 1 equivalent of CO afforded the bridging imido hafnocene isocyanate complexes arising from C-H activation of the Cp ligand substituent and cyclometalation. These results support a putative μ-nitrido intermediate, which inspired further reactivity studies. Addition of mixtures of CO with other substrates afforded a variety of different species resulting from successful trapping of this μ-nitrido intermediate. In this manner, CO-induced N_2 cleavage was coupled to N-H bond formation via hydrogenation and C-H activation of terminal alkynes. Attempts to intercept the bridging nitrido intermediate with primary silanes resulted in an unexpected bridging oxo complex arising from CO deoxygenation and the release of functionalized dinitrogen as a cyanosilane. In general, these results demonstrate the ability of group 4 metallocene complexes to cleanly promote the cleavage of dinitrogen coupled to hydrogenation and other useful nitrogen-heteroatom bond forming processes.

Experimental Section

General Considerations. All air- and moisture-sensitive manipulations were carried out using standard high vacuum line, Schlenk or cannula techniques or in an M. Braun inert atmosphere drybox containing an atmosphere of purified nitrogen. The M. Braun drybox was equipped with a cold well designed for freezing samples in liquid nitrogen. Solvents for air- and moisture-sensitive manipulations were dried and deoxygenated using literature procedures.[43] Toluene, benzene, pentane and heptane were further dried by distillation from "titanocene".[44] Deuterated solvents for NMR spectroscopy were distilled from sodium metal under an atmosphere of argon and stored over 4 Å molecular sieves. Argon and hydrogen gas were purchased from Airgas Incorporated and passed through a column containing manganese oxide on vermiculite and 4 Å molecular sieves before admission to the high vacuum line. Carbon monoxide was also dried over 4 Å molecular sieves before admission to the high vacuum line. The metallocene dinitrogen complexes, **1-N_2**,[15] **2-N_2**,[16] **3-N_2,**[25] and **4-N_2**[26] were prepared according to literature procedures.

^{1}H NMR spectra were recorded on a Varian Inova 400 Spectrometer operating at 399.860 MHz. All chemical shifts are reported relative to $SiMe_4$ using ^{1}H (residual) chemical shifts of the solvent as a secondary standard. ^{2}H, ^{13}C, ^{29}Si, and ^{15}N NMR spectra were recorded on a Varian Inova 500 Spectrometer operating at 76.848, 125.716, 161.83, 99.320 and 50.663 MHz, respectively. ^{2}H, ^{29}Si, and ^{13}C chemical shifts are reported relative to $SiMe_4$ using chemical shifts of the solvent as a secondary standard where applicable. ^{15}N chemical shifts are reported relative liquid to NH_3 using an external standard. Infrared spectroscopy was conducted on a Mattson RS-10500 Research Series FT-IR spectrometer calibrated with a polystyrene standard. Elemental analyses were performed at Robertson Microlit Laboratories, Inc., in Madison, NJ.

Preparation of ([$Me_2Si(\eta^5\text{-}C_5Me_4)(\eta^5\text{-}C_5H_3\text{-}3\text{-}^tBu)$]Hf)(NCO)(NH)(Hf[$Me_2Si(\eta^5\text{-}C_5Me_4)(\eta^5\text{-}C_5H_3\text{-}3\text{-}(C(CH_3)_2(CH_2))$]) (5). A J. Young NMR tube was charged with 0.020 g (0.020 mmol) of **4-N_2** and 1 mL of benzene-d_6. On a high vacuum line, the contents of the tube were degassed and approximately 17.8 torr of CO (0.030 mmol) were admitted to an attached 31.6 mL calibrated gas bulb. The solution was thawed and the CO gas was slowly diffused from the gas bulb into the solution over 24 hours yielding a light brown solution. The solvent was removed *in vacuo* and the resulting brown oil was washed with cold pentane, affording a white solid identified as **5** without further purification. Protonolysis of **5** with excess hydrochloric acid afforded one equivalent of ammonium chloride (per μ-NH) in 96% yield confirmed by quantitative analysis,[28] along with formation of one equivalent of isocyanic acid (HNCO) and two equivalents of the corresponding hafnocene dichloride as judged by ^{1}H and ^{13}C NMR spectroscopy.[26] ^{1}H NMR (benzene-d_6): δ = -1.27 (d, 1H, $C_5H_3C(CH_3)_2(CH_2)$), -0.43 (d, 1H, $C(CH_3)_2(CH_2)$), 0.48 (s, 3H, $SiMe_2$), 0.49 (s, 3H, $SiMe_2$), 0.54 (s, 3H, $SiMe_2$), 0.60 (s, 3H, $SiMe_2$), 1.44 (s, 9H, $C_5H_3CMe_3$), 1.61 (s, 3H, C_5Me_4), 1.62 (s, 3H, C_5Me_4), 1.75 (s, 3H, C_5Me_4), 1.86 (s, 3H, C_5Me_4), 1.87 (s, 3H, C_5Me_4), 1.88 (s, 6H, $C_5H_3C(CH_3)_2(CH_2)$), 2.00 (s, 3H, C_5Me_4), 2.10 (s, 3H, C_5Me_4), 4.65 (s, 1H, HfN*H*), 5.46 (m, 1H, Cp*H*), 5.56 (m, 1H, Cp*H*), 5.76 (m, 1H, Cp*H*), 6.24 (m, 1H, Cp*H*), 6.39 (m, 1H, Cp*H*), 6.99 (m, 1H, Cp*H*), One Cp*Me* not found. {^{1}H} ^{13}C NMR (benzene-d_6): δ = -0.79 ($SiMe_2$), -0.10 ($SiMe_2$), 0.02 ($SiMe_2$), 1.32 ($SiMe_2$), 11.18 (Cp*Me*), 11.46 (Cp*Me*), 11.97 (Cp*Me*), 14.23 (Cp*Me*), 14.60 (Cp*Me*), 14.98 (Cp*Me*), 15.60 (Cp*Me*), 15.68 (Cp*Me*), 29.47 ($CpCMe_2(CH_2)$), 31.70 (CMe_3), 33.60 ($CpCMe_2(CH_2)$), 34.91 (CMe_3), 35.36 (CMe_3), 99.48, 104.69, 107.32, 108.13, 108.41, 109.76, 111.51, 114.31, 115.16, 116.72, 119.41, 123.50, 125.58, 126.27, 126.63, 129.66, 131.27, 136.09, 136.36, 150.59 (*Cp*), 135.26 (N*C*O). {^{1}H} ^{15}N NMR

(benzene-d_6): δ = 82.7 (^{15}NCO), 315.5 (^{15}NH) ($^{1}J_{CN}$=33.1 Hz, $^{1}J_{NH}$=40.8 Hz). IR (KBr): ν = 2222 cm^{-1} (N=C); ν = 2159 cm^{-1} (N=^{13}C), ν = 2147 cm^{-1} (^{15}N=^{13}C), ν = 3577 cm^{-1} (NH).

Preparation of [(η^5-$C_5Me_4H)_2Hf]_2(\mu_2$-$^{15}N_2$) (2-$^{15}N_2$). This compound was prepared in a similar manner to **2-(N_2)**[4] with the exception that the reaction mixture was quickly frozen and degassed prior to stirring. The headspace was then charged with $^{15}N_2$ and the reaction vessel was thawed and stirred as usual. **2-$^{15}N_2$** may also be prepared via exchange from **2-N_2**, but in smaller quantities and poorer isotopic enrichment.[16]

Preparation of ((η^5-$C_5Me_4H)_2Hf$)((CH_2-η^5-C_5Me_3H)(η^5-C_5Me_4H)Hf)(μ-NH)(NCO) (6). In a drybox, a J. young NMR tube was charged with 0.015 g (0.016 mmol) of **2-N_2** and approximately 0.5 mL of benzene-d_6. The contents of the tube were frozen and the tube evacuated. To an attached calibrated gas bulb, 1.1 equivalents (25 torr, 13.1 mL) of carbon monoxide were admitted. The contents of the tube were thawed and the CO was slowly diffused into the solution over 16 hours at room temperature, during which time a color change from purple to yellow was observed. ^{1}H NMR spectroscopy established complete conversion to two isomers of **6**. This process was repeated in several independent NMR tubes and the products combined, and the solvent was removed *in vacuo*. The resulting oil was dissolved in toluene and single crystals of a single isomer were obtained via slow evaporation of the solvent. The reaction was reproducible with **2-$^{15}N_2$** and ^{13}CO enabling the synthesis and characterization of various ^{15}N and ^{13}C isotopologue combinations of **5**. ^{1}H NMR (benzene-d_6) (Mixture of two isomers): δ = 1.55 (s, 3H, CpMe_4H), 1.56 (s, 3H, CpMe_4H), 1.61 (s, 3H, CpMe_4H), 1.62 (s, 3H, CpMe_4H), 1.68 (s, 3H, CpMe_4H), 1.69 (s, 3H, CpMe_4H), 1.70 (s, 3H, CpMe_4H), 1.71 (s, 3H, CpMe_4H), 1.73 (2

coincident, m, 2H, Hf-CH_2), 1.74 (s, 3H, CpMe_4H), 1.75 (s, 3H, CpMe_4H), 1.77 (s, 3H, CpMe_4H), 1.78 (s, 3H, CpMe_4H), 1.79 (s, 3H, CpMe_4H), 1.82 (s, 3H, CpMe_4H), 1.83 (3 coincident, s, 9H, CpMe_4H), 1.86 (s, 3H, CpMe_4H), 1.87 (s, 3H, CpMe_4H), 1.88 (2 coincident, s, 6H, CpMe_4H), 1.92 (s, 3H, CpMe_4H), 1.95 (s, 3H, CpMe_4H), 1.97 (s, 3H, CpMe_4H), 1.99 (s, 3H, CpMe_4H), 2.00 (s, 3H, CpMe_4H), 2.02 (s, 3H, CpMe_4H), 2.06 (s, 3H, CpMe_4H), 2.07 (s, 3H, CpMe_4H), 2.10 (s, 3H, CpMe_4H), 2.21 (s, 3H, CpMe_4H), 2.40 (s, 3H, CpMe_4H), 2.56 (2 coincident, m, Hf-CH_2), 4.60 (s, 1H, CpMe$_4$*H*), 5.07 (s, 1H, CpMe$_4$*H*), 5.10 (s, 1H, CpMe$_4$*H*), 5.17 (s, 1H, CpMe$_4$*H*), 5.19 (2 coincident, s, 2H, CpMe$_4$*H*), 5.68 (s, 1H, CpMe$_4$*H*), 5.69 (br s, 1H, μ-N*H* (major)), 5.73 (br s, 1H, μ-N*H* (minor)), 6.19 (s, 1H, CpMe$_4$*H*). ^{13}C NMR (benzene-d_6): δ = 11.21, 11.52, 11.70, 12.03, 12.16, 12.20, 12.24, 12.32, 12.45, 12.69, 12.85, 12.92, 13.02, 13.19, 13.29, 13.36, 13.41, 13.47, 13.59, 13.66, 13.69, 13.76, 14.04, 14.21, 14.45, 14.55, 14.59, 15.36, 15.69, 15.79 (Cp*Me*), 23.05 (Hf-*C*H$_2$ (major)), 36.65 (Hf-*C*H$_2$ (minor)), 101.66, 101.73, 107.09, 107.14, 108.07, 108.46, 108.58, 108.99, 109.14, 109.24, 109.72, 109.85, 110.96, 111.04, 111.47, 112.16, 112.35, 112.51, 112.76, 113.57, 113.83, 114.00, 117.12, 118.13, 118.77, 118.97, 119.35, 119.52, 119.81, 112.13, 120.61, 120.90, 121.93, 122.50, 124.14, 124.32, 126.02, 130.16, 131.93, 136.58 (*Cp*), 135.18 (N*C*O, $^1J_{N\text{-}C}$ = 32.6 Hz (minor)), 135.54 (N*C*O, $^1J_{N\text{-}C}$ = 32.4 Hz (major)). ^{15}N NMR (benzene-d_6): δ = 289.4 (μ-*N*H) ($^1J_{N\text{-}H}$ = 55.7 Hz) (major), 296.2 (μ-*N*H) ($^1J_{N\text{-}H}$ = 55.7 Hz) (minor), 86.8 (*N*CO) (major), 84.2 (*N*CO) (minor). IR (KBr): ν = 2220 cm^{-1} (CNO), 3564 cm^{-1} (NH).

Preparation of ($(\eta^5$-$C_5Me_4H)_2Hf)_2$(μ-NH)(H)(NCO) (2-(μ-NH)(H)(NCO)). In a drybox, a J. young NMR tube was charged with 0.015 g (0.016 mmol) of **2-N$_2$** and approximately 0.5 mL benzene-d_6. The contents of the tube were frozen and the tube evacuated. A mixture carbon monoxide and hydrogen (P_{CO}:P_{H2} = 3:1, ~ 1 atm total)

was admitted to the tube at liquid nitrogen temperature. The contents of the tube were thawed with vigorous shaking and a color change to yellow was observed over the course of 30 seconds at room temperature. Monitoring the reaction by ^{1}H NMR spectroscopy established complete conversion to **2-(μ-NH)(H)(NCO)** after 1 hour. This process was repeated in several independent NMR tubes and the products combined the solvent was removed *in vacuo*. The resulting oil was washed with pentane and furnished an analytically pure pale yellow solid identified as **2-(μ-NH)(H)(NCO)**. The reaction was reproducible with **2-^{15}N$_2$** and ^{13}CO enabling the synthesis and characterization of various ^{15}N and ^{13}C isotopologue combinations. Anal. Calcd for $C_{37}H_{54}O_1N_2Hf_2$: C, 49.38; H, 6.05; N, 3.11. Found: C, 49.66; H, 5.99; N, 2.89. ^{1}H NMR (benzene-d_6): δ = 1.70 (s, 3H, Cp*Me*$_4$H), 1.73 (s, 3H, Cp*Me*$_4$H), 1.80 (s, 3H, Cp*Me*$_4$H), 1.83 (s, 3H, Cp*Me*$_4$H), 1.84 (s, 3H, Cp*Me*$_4$H), 1.87 (s, 3H, Cp*Me*$_4$H), 1.88 (s, 3H, Cp*Me*$_4$H), 1.95 (s, 3H, Cp*Me*$_4$H), 1.99 (s, 3H, Cp*Me*$_4$H), 2.00 (s, 3H, Cp*Me*$_4$H), 2.05 (s, 3H, Cp*Me*$_4$H), 2.06 (s, 3H, Cp*Me*$_4$H), 2.10 (s, 3H, Cp*Me*$_4$H), 2.27 (s, 3H, Cp*Me*$_4$H), 2.33 (s, 3H, Cp*Me*$_4$H), 2.41 (s, 3H, Cp*Me*$_4$H), 4.05 (s, 1H, μ-N*H*), 5.16 (s, 1H, CpMe$_4$*H*), 5.23 (s, 1H, CpMe$_4$*H*), 5.30 (s, 1H, CpMe$_4$*H*), 6.08 (s, 1H, CpMe$_4$*H*), 10.50 (s, 1H, Hf*H*). ^{13}C NMR (benzene-d_6): δ = 11.80, 11.90, 12.06, 12.23, 12.97, 13.10, 13.40, 13.60, 13.86, 14.16, 14.39, 14.47, 14.61, 14.71, 14.73, 14.91 (Cp*Me*), 108.73, 110.32, 110.86, 112.81, 113.18, 113.40, 114.26, 114.66, 116.09, 116.19, 117.38, 118.48, 120.33, 120.57, 120.78, 121.09, 121.18, 121.82, 125.25, 126.03 (*Cp*), 135.45 (N*C*O). ^{15}N NMR (benzene-d_6): δ = 319.1 (μ-*N*H) ($^{1}J_{N\text{-}H}$ = 45.6 Hz), 104.3 (*N*CO) ($^{1}J_{N\text{-}C}$ = 32.9 Hz). IR (KBr): ν = 2224 cm^{-1} (C=N), 3590 cm^{-1} (NH).

Preparation of [Me$_2$Si(η^5-C$_5$Me$_4$)(η^5-C$_5$H$_3$-3-^{t}Bu)Hf]$_2$(μ-NH)(CCPh)(NCO) (4-(μ-NH)(CCPh)(NCO)). In a drybox, a J. young NMR tube was charged with 0.010 g

(0.010 mmol) of **4-N_2** and approximately 0.5 mL benzene-d_6. The contents of the tube were frozen in a cold well and phenylacetylene (10 μL, 0.091 mmol) was layered on top of the frozen solution. The tube was sealed and quickly transferred to a high vacuum line where the headspace of the tube was degassed. Carbon monoxide (1 atm) was admitted to the tube at liquid nitrogen temperature. The contents of the tube were thawed with vigorous shaking and a color change to light orange was observed over the course of 30 seconds at ambient temperature. Monitoring the reaction by ^{1}H NMR spectroscopy established complete conversion to **4-(μ-NH)(CCPh)(NCO)**. This process was repeated in several independent NMR tubes, the products were combined and the solvent and excess phenylacetylene were removed *in vacuo*. The resulting oil was washed with pentane and furnished analytically pure **4-(μ-NH)(CCPh)(NCO)**. The reaction was also conducted with **4-$^{15}N_2$** and ^{13}CO enabling the synthesis and characterization of various ^{15}N and ^{13}C isotopologues. ^{1}H NMR (benzene-d_6): δ = 0.49 (s, 3H, SiMe_2), 0.51 (s, 3H, SiMe_2), 0.58 (s, 3H, SiMe_2), 0.62 (s, 3H, SiMe_2), 1.45 (s, 9H, $C_5H_3C$$Me_3$), 1.63 (s, 9H, $C_5H_3C$$Me_3$), 1.84 (s, 3H, $C_5$$Me_4$), 1.94 (s, 3H, $C_5$$Me_4$), 1.95 (s, 3H, $C_5$$Me_4$), 1.96 (s, 3H, $C_5$$Me_4$), 2.00 (s, 3H, $C_5$$Me_4$), 2.07 (s, 3H, $C_5$$Me_4$), 2.16 (s, 3H, $C_5$$Me_4$), 2.27 (s, 3H, $C_5$$Me_4$), 5.17 (s, 1H, μ-N$H$) 5.46 (m, 1H, $C_5H_3CMe_3$), 5.54 (m, 1H, $C_5H_3CMe_3$), 6.03 (m, 1H, $C_5H_3CMe_3$), 6.18 (m, 1H, $C_5H_3CMe_3$), 6.93 (m, 1H, $C_5H_3CMe_3$), 6.96 (m, 1H, $C_5H_3CMe_3$), 7.11-7.22 (m, 1H, *Ph*), 7.54-7.68 (m, 4H, *Ph*). $\{^1H\}^{13}$C NMR (benzene-d_6): δ = -0.17 (SiMe_2), -0.05 (SiMe_2), 0.18 (SiMe_2), 0.22 (SiMe_2), 11.32 (CpMe), 12.00 (CpMe), 12.07 (CpMe), 13.65 (CpMe), 14.24 (CpMe), 15.00 (CpMe), 15.24 (CpMe), 15.31 (CpMe), 31.41 (CMe_3), 31.85 (CMe_3), 33.66 (CMe$_3$), 33.80 (CMe$_3$), 98.71, 99.82 (CCPh), 105.30, 107.70, 108.12, 108.23, 108.63, 111.96, 112.67, 116.39, 116.63, 120.90, 121.71, 123.13, 126.33, 127.27, 127.39, 127.53, 128.68, 128.98, 129.01, 130.76, 131.23, 132.33, 151.16, 151.94 (*Cp* and *Ph*), 135.52 (NCO). IR (KBr): ν = 2084 cm^{-1} (CCPh),

ν = 2222 cm^{-1} (CNO); ν = 3577 cm^{-1} (NH).

Preparation of ([$Me_2Si(\eta^5$-$C_5Me_4)(\eta^5$-C_5H_3-3-$^tBu)]Zr)_2(\mu$-NH)(H)(NCO) (3-(μ-NH)(H)(NCO)). This molecule was prepared in a similar manner to the methods used to synthesize **2-(μ-NH)(H)(NCO)** using 0.010 g (0.012 mmol) of **3-N_2** and a P_{CO}:P_{H2} = 3:1, ~1 atm total of CO:H_2 gas and yielded an analytically pure yellow solid identified as **3-(μ-NH)(H)(NCO)**. Anal. Calcd for $C_{41}H_{62}O_1N_2Si_2Zr_2$: C, 58.79; H, 7.46; N, 3.35. Found: C, 59.12; H, 7.43; N, 3.50. ^{1}H NMR (benzene-d_6): δ = 0.50 (s, 3H, SiMe_2), 0.51 (s, 3H, SiMe_2), 0.55 (s, 3H, SiMe_2), 0.62 (s, 3H, SiMe_2), 1.48 (s, 9H, $C_5H_3C$$Me_3$), 1.49 (s, 9H, $C_5H_3C$$Me_3$), 1.77 (s, 3H, $C_5$$Me_4$), 1.79 (s, 3H, $C_5$$Me_4$), 1.81 (s, 3H, $C_5$$Me_4$), 1.87 (s, 3H, $C_5$$Me_4$), 1.91 (s, 3H, $C_5$$Me_4$), 1.98 (s, 3H, $C_5$$Me_4$), 2.12 (s, 3H, $C_5$$Me_4$), 2.29 (s, 3H, $C_5$$Me_4$), 4.84 (s, 1H, Zr*H*), 5.24 (m, 1H, C_5*H*$_3$$CMe_3$), 5.54 (m, 1H, C_5*H*$_3$$CMe_3$), 5.86 (m, 1H, C_5*H*$_3$$CMe_3$), 6.34 (m, 1H, C_5*H*$_3$$CMe_3$), 6.60 (m, 1H, C_5*H*$_3$$CMe_3$), 6.78 (s, 1H, μ-N*H*), 6.97 (s, 1H, C_5*H*$_3$$CMe_3$). {^{1}H}^{13}C NMR (benzene-d_6): δ = -0.45 (SiMe_2), -0.07 (SiMe_2), 0.12 (SiMe_2), 0.78 (SiMe_2), 12.07 (Cp*Me*), 12.60 (Cp*Me*), 14.08 (Cp*Me*), 14.43 (Cp*Me*), 14.60 (Cp*Me*), 15.06 (Cp*Me*), 15.79 (Cp*Me*), 15.87 (Cp*Me*), 31.70 (CMe_3), 32.82 (*C*Me_3), 32.97 (CMe_3), 33.64 (*C*Me_3), 101.61, 105.92, 109.38, 109.84, 109.90, 110.30, 110.47, 115.88, 118.21, 120.63, 122.21, 122.98, 123.39, 124.85, 126.03, 129.67, 130.16, 132.27, 152.18, 151.61 (*Cp*), 133.65 (N*C*O). ^{15}N NMR (benzene-d_6): δ = 372.0 (μ-^{15}*N*H) ($^1J_{NH}$ = 40.6 Hz), 82.5 (^{15}*N*CO) ($^1J_{NC}$ = 30.9 Hz). IR (KBr): ν = 2215 cm^{-1} (NCO); ν = 3610 cm^{-1} (NH).

Preparation of ([$Me_2Si(\eta^5$-$C_5Me_4)(\eta^5$-C_5H_3-3-$^tBu)]Hf)_2(\mu$-NH)(H)(NCO) (4-(μ-NH)(H)(NCO)). This molecule was prepared in a similar manner to the methods used to synthesize **2-(μ-NH)(H)(NCO)** using 0.015 g (0.015 mmol) of **4-N_2** and a P_{CO}:P_{H2} = 3:1, ~1 atm total of CO:H_2 gas and yielded an analytically pure yellow solid

identified as **4-(μ-NH)(H)(NCO)**. Anal. Calcd for $C_{41}H_{62}O_1N_2Si_2Hf_2$: C, 48.65; H, 6.18; N, 2.77. Found: C, 48.25; H, 6.09; N, 2.43. ^{1}H NMR (benzene-d_6): δ = 0.49 (s, 3H, Si*Me*$_2$), 0.50 (s, 3H, Si*Me*$_2$), 0.53 (s, 3H, Si*Me*$_2$), 0.62 (s, 3H, Si*Me*$_2$), 1.46 (s, 9H, C_5H_3C*Me*$_3$), 1.49 (s, 9H, C_5H_3C*Me*$_3$), 1.75 (s, 3H, C_5*Me*$_4$), 1.85 (s, 3H, C_5*Me*$_4$), 1.86 (s, 3H, C_5*Me*$_4$), 1.90 (s, 3H, C_5*Me*$_4$), 1.92 (s, 3H, C_5*Me*$_4$), 1.99 (s, 3H, C_5*Me*$_4$), 2.16 (s, 3H, C_5*Me*$_4$), 2.35 (s, 3H, C_5*Me*$_4$), 4.66 (s, 1H, μ-N*H*, $^1J_{NH}$ = 40.9 Hz), 5.25 (m, 1H, C_5*H*$_3$CMe$_3$), 5.57 (m, 1H, C_5*H*$_3$CMe$_3$), 5.79 (m, 1H, C_5*H*$_3$CMe$_3$), 6.27 (m, 1H, C_5*H*$_3$CMe$_3$), 6.45 (m, 1H, C_5*H*$_3$CMe$_3$), 6.92 (m, 1H, C_5*H*$_3$CMe$_3$), 9.39 (s, 1H, Hf*H*). {^{1}H}^{13}C NMR (benzene-d_6): δ = -0.56 (Si*Me*$_2$), 0.92 (Si*Me*$_2$), -0.56 (Si*Me*$_2$), 0.92 (Si*Me*$_2$), 11.93 (Cp*Me*), 12.35 (Cp*Me*), 14.14 (Cp*Me*), 14.49 (Cp*Me*), 11.93 (Cp*Me*), 12.35 (Cp*Me*), 14.14 (Cp*Me*), 14.49 (Cp*Me*), 31.28 (C*Me*$_3$), 31.28 (C*Me*$_3$), 33.93 (*C*Me$_3$), 33.93 (*C*Me$_3$), 105.11, 108.20, 114.46, 114.75, 116.18, 119.32, 124.83, 126.03, 132.09, 151.86 (*Cp*), 135.27 (N*C*O, $^1J_{NC}$ = 32.9 Hz). IR (KBr): ν = 2223 cm^{-1} (NCO); ν = 3580 cm^{-1} (NH).

Preparation of ([Me$_2$Si(η^5-C$_5$Me$_4$)(η^5-C$_5$H$_3$-3-^{t}Bu)]Hf)$_2$(μ-O)(H)(NCO) (4-(μ-O)(H)(NCO)). In a drybox, a J. young NMR tube was charged with 0.020 g (0.020 mmol) of **4-N$_2$** and approximately 0.75 mL C_6D_6. The tube was frozen and degassed on the vacuum line, and with a calibrated gas bulb 5 equivalents (60 torr, 31.6 mL) of hexylsilane were admitted to the tube. Subsequently (prior to thawing) 1 atm of carbon monoxide was admitted to the tube. The tube was thawed with vigorous shaking and the solution turned yellow over the course of 30 seconds. ^{1}H NMR spectroscopy revealed clean conversion to **4-(μ-O)(H)(NCO)** after a few minutes. Several of these NMR tube scale samples were combined and the solvent was removed *in vacuo*. The remaining oil was washed with pentane, precipitating pure **4-(μ-O)(H)(NCO)** as a pale yellow solid suitable for analysis. The reaction was

reproducible with **4-$^{15}N_2$** and ^{13}CO enabling the synthesis and characterization of various ^{15}N and ^{13}C isotopologue combinations. Anal. Calcd for $C_{41}H_{61}O_2N_1Si_2Hf_2$: C, 48.61; H, 6.07; N, 1.38. Found: C, 48.36; H, 6.20; N, 1.63. ^1H NMR (benzene-d_6): δ = 0.34 (s, 3H, SiMe_2), 0.47 (s, 3H, SiMe_2), 0.48 (s, 3H, SiMe_2), 0.57 (s, 3H, SiMe_2), 1.21 (s, 9H, $C_5H_3CMe_3$), 1.63 (s, 9H, $C_5H_3CMe_3$), 1.69 (s, 3H, C_5Me_4), 1.81 (s, 3H, C_5Me_4), 1.93 (s, 3H, C_5Me_4), 2.03 (s, 3H, C_5Me_4), 2.04 (s, 3H, C_5Me_4), 2.21 (s, 3H, C_5Me_4), 2.28 (s, 3H, C_5Me_4), 2.51 (s, 3H, C_5Me_4), 5.67 (m, 2H, $C_5H_3CMe_3$), 5.84 (m, 2H, $C_5H_3CMe_3$), 6.62 (m, 1H, $C_5H_3CMe_3$), 6.87 (m, 1H, $C_5H_3CMe_3$), 9.23 (s, 1H, Hf*H*). $\{^1H\}^{13}C$ NMR (benzene-d_6): δ = -0.56 (SiMe_2), 0.92 (SiMe_2), -0.56 (SiMe_2), 0.92 (SiMe_2), 11.93 (Cp*Me*), 12.35 (Cp*Me*), 14.14 (Cp*Me*), 14.49 (Cp*Me*), 11.93 (Cp*Me*), 12.35 (Cp*Me*), 14.14 (Cp*Me*), 14.49 (Cp*Me*), 31.28 (CMe_3), 31.28 (CMe_3), 33.93 (*C*Me_3), 33.93 (*C*Me_3), 105.11, 108.20, 114.46, 114.75, 116.18, 119.32, 124.83, 126.03, 132.09, 151.86 (*Cp*), 136.24 (N*C*O). ^{15}N NMR (benzene-d_6): δ = 91.4 (^{15}NCO) ($^1J_{NC}$ = 33.9 Hz). IR (KBr): ν = 2220 cm^{-1} (NCO); ν = 1560 cm^{-1} (HfH).

Spectroscopic Identification of n-hexylcyanosilane. Prepared according to previously reported synthesis for n-heptylcyanosilane.[45] ^1H NMR (benzene-d_6): δ = 0.39 (m, 2H, C_6H_{13}), 0.82 (t, 3H, C_6H_{13}), 1.02-1.23 (m, 8H, C_6H_{13}), 3.55 (t, 2H, SiH_2), $\{^1H\}^{13}C$ NMR (benzene-d_6): δ = 7.67, 14.52, 23.10, 24.87, 31.85, 32.53 (C_6H_{13}), 122.16 (Si*C*N). IR (KBr): ν = 2143 cm^{-1} (CN); ν = 2190 cm^{-1} (SiH).

REFERENCES

[1] Shaver, M. P.; Fryzuk, M. D. *Adv. Synth. Catal.* **2003**, *345*, 1061.

[2] (a) Mori, M. *J. Organomet. Chem.* **2004**, *689*, 4210. (b) Fryzuk, M. D. *Chem. Rec.* **2003**, *3*, 2.

[3] V. Smil *Enriching the Earth: Fritz Haber, Carl Bosch, and the Transformation of World Food Production*; MIT Press, Cambridge, MA, 2001.

[4] Hager, T. in *The Alchemy of Air*, Three Rivers Press, NY, 2008.

[5] Ertl, G. *Angew. Chem. Int. Ed.* **2008**, *47*, 3524.

[6] Holladay, J. D.; Hu, J.; King, D. L.; Wang, Y. *Catalysis Today* **2009**, *139*, 244.

[7] (a) Schlögl, R. *Angew. Chem. Int. Ed.* **2003**, *42*, 2004. (b) K. Tamaru in *Catalytic Ammonia Synthesis*. J. R. Jennings, Ed.; Plenum, NY 1991. (c) D. Pimentel, T. W. Patzek, *Nat. Resources Res.* **2005**, *14*, 65.

[8] (a) Henderickx, H.; Kwakkenbos, G.; Peters, A.; van der Spoel, J.; de Vries, K. *Chem. Commun.* **2003**, 2050. (b) Komori, K.; Oshita, H.; Mizobe, Y.; Hidai, M. *J. Am. Chem. Soc.* **1989**, *111*, 1939. (c) Rocklage, S. M.; Schrock, R. R. *J. Am. Chem. Soc.* **1982**, *104*, 3077. (d) Betley, T. E.; Peters, J. C. *J. Am. Chem. Soc.* **2003**, *125*, 10782. (e) Figueroa, J. S. Piro, N. A.; Clough, C. R.; Cummins, C. C. *J. Am. Chem. Soc.* **2006**, *128*, 940.

[9] (a) Yandulov, D. V.; Schrock, R. R. *Science* **2003**, *301*, 76. (b) Schrock, R. R. *Acc. Chem. Res.* **2005**, *38*, 955.

[10] Curley, J. J.; Sceats, E. L.; Cummins, C. C. *J. Am. Chem. Soc.* **2006**, *128*, 14306.

[11] Laplaza, C. E.; Cummins, C. C. *Science* **1995**, *268*, 861. (b) Laplaza, C. E. et al. *J. Am. Chem. Soc.* **1996**, *118*, 8623.

[12] Mori, M. *Heterocycles* **2009** *78*, 281.

[13] Fryzuk, M. D. *Acc. Chem. Res.* **2009**, *42*, 127.

[14] Akagi, F.; Matsuo, T.; Kawaguchi, H. *Angew. Chem. Int. Ed.* **2007**, *46*, 8778.

[15] Pool, J. A.; Lobkovsky, E.; Chirik, P. J. *Nature* **2004**, *427*, 527.

[16] Bernskoetter, W. H.; Olmos, A. V.; Lobkovsky, E.; Chirik, P. J. *Organometallics* **2006**, *25*, 1021.

[17] Clentsmith, G. K. B.; Bates, V. M. E.; Hitchcock, P. B.; Cloke, F. G. N. *J. Am. Chem. Soc.* **1999**, *121*, 10444.

[18] Pun, D.; Bradley, C. A.; Lobkovsky, E.; Keresztes, I.; Chirik, P. J. *J. Am. Chem. Soc.* **2008**, *130*, 14046.

[19] Bernskoetter, W. H.; Lobkovsky, E.; Chirik, P. J. *J. Am. Chem. Soc.* **2005**, *127*, 14051.

[20] Bernskoetter, W. H.; Olmos, A. V.; Pool, J. A.; Lobkovsky, E.; Chirik, P. J. *J. Am. Chem. Soc.* **2006**, *128*, 10696.

[21] Bernskoetter, W. H.; Lobkovsky, E.; Chirik, P. J. *Angew. Chem. Int. Ed.* **2007**, *119*, 2858.

[22] For a full discussion of this work, see Chapter 4 of this Thesis. Knobloch, D. J.; Toomey, H. E.; Chirik, P. J. *J. Am. Chem. Soc.* **2008**, *130*, 4248.

[23] For a full discussion of this work, see Chapter 5 of this Thesis. Knobloch, D. J.; Benito-Garagorri, D.; Bernskoetter, W. H.; Keresztes, I.; Lobkovsky, E.; Toomey, H.; Chirik, P. J. *J. Am. Chem. Soc.* **2009**, *131*, 14903.

[24] Chirik, P. J. *Dalton Trans.* **2007**, 16.

[25] Hanna, T. E.; Keresztes, I.; Lobkovsky, E.; Chirik, P. J. *Inorg. Chem.* **2007**, *46*, 1675.

[26] For a full discussion of this work, see Chapter 1 of this Thesis. Knobloch, D. J.; Lobkovsky, E.; Chirik, P. J. *Nature Chemistry* **2010**, *2*, 30.

[27] Zhang, X.; Butschke, B.; Schwarz, H. *Chem. Eur. J.* **2010**, *16*, 12564.

[28] Weatherburn, M. W. *Anal. Chem.* **1967**, *39*, 971.

[29] Duncan, A. P.; Bergman, R. G. *Chem. Rec.* **2002**, *2*, 431.

[30] Walsh, P. J.; Carney, M. J.; Bergman, R. G. *J. Am. Chem. Soc.* **1991**, *113*, 6343.

[31] Herrmann, H.; Fillol, J. L.; Wadepohl, H.; Gade, L. H. *Organometallics* **2008**, *27*, 172.

[32] Herrmann, H.; Fillol, J. L.; Wadepohl, H.; Gade, L. H. *Angew. Chem. Int. Ed.* **2007**, *46*, 8426.

[33] Montalvo, E.; Ziller, J. W.; DiPasquale, A. G.; Rheingold, A. L.; Evans, W. J. *Organometallics* **2010**, *29*, 2104.

[34] For a discussion of this nomenclature, see ref. 25.

[35] Morello, L; Love, J. B.; Patrick, B. O.; Fryzuk, M. D. *J. Am. Chem. Soc.* **2004**, *126*, 9480.

[36] (a) Guiducci, A. E.; Boyd, C. L.; Mountford, P. *Organometallics* **2006**, *25*, 1167. (b) Dunn, S. C.; Hazari, N.; Cowley, A. R.; Green, J. C.; Mountford, P. *Organometallics* **2006**, *25*, 1755. (c) Zuckerman, R. L.; Bergman, R. G. *Organometallics* **2001**, *20*, 1792. (d) Zuckerman, R. L.; Bergman, R. G. *Organometallics* **2000**, *19*, 4795. (e) Thorman, J. E.; Guzei, I. A.; Young, V. G.; Woo, L. K. *Inorg. Chem.* **1999**, *38*, 3814. (f) Polse, J. L.; Andersen, R. A.; Bergman, R. G. *J. Am. Chem. Soc.* **1998**, *120*, 13405.

[37] Bernskoetter, W. H.; Pool, J. A.; Lobkovsky, E.; Chirik, P. J. *J. Am. Chem. Soc.* **2005**, *127*, 7901.

[38] Fryzuk, M. D.; Love, J. B.; Rettig, S. J.; Young, V. G. *Science* **1997**, *275*, 1445.

[39] (a) Fryzuk, M. D.; MacKay, B. A.; Patrick, B. O. *J. Am. Chem. Soc.* **2003**, *125*, 3234. (b) MacKay, B. A.; Munha, R. F.; Fryzuk, M. D. *J. Am. Chem. Soc.* **2006**, *128*, 9472.

[40] See Experimental Section for details.

[41] For other examples of CO deoxygenation, see: (a) Wood, C. D.; Schrock, R. R. *J. Am. Chem. Soc.* **1979**, *101*, 5421. (b) Mayer, J. M.; Bercaw, J. E. *J. Am. Chem. Soc.* **1982**, *104*, 2157. (c) Planalp, R. P.; Andersen, R. A. *J. Am. Chem. Soc.* **1983**, *105*, 7774. (d) LaPointe, R. T.; Wolczanski, P. T.; Mitchell, J. F. *J. Am. Chem. Soc.* **1986**, *108*, 6382.

[42] Belson, D. J.; Strachan, A. N. *Chem. Soc. Rev.* **1982**, *11*, 41.

[43] Pangborn, A.B.; Giardello, M.A.; Grubbs, R.H.; Rosen, R.K.; Timmers, F.J. *Organometallics* **1996**, *15*, 1518.

[44] Marvich, R.H.; Brintzinger, H. H. *J. Am. Chem. Soc.* **1971**, *93*, 2046.

[45] Anderson, H. H.; Hendifar, A. *J. Org. Chem.* **1961**, *26*, 3033.

CHAPTER 3

CO-Induced N_2 Cleavage, Part III: Functionalization of Hafnocene Oxamidide Complexes Prepared from Carbon Monoxide-Induced Dinitrogen Cleavage*

Abstract

Functionalization of the nitrogen atoms in the hafnocene oxamidide complexes, $[(\eta^5\text{-}C_5Me_4H)_2Hf]_2(N_2C_2O_2)$ and $[Me_2Si(\eta^5\text{-}C_5Me_4)(\eta^5\text{-}C_5H_3\text{-}3\text{-}^tBu)Hf]_2(N_2C_2O_2)$, prepared from CO-induced N_2 bond cleavage, was explored by formal 1,2 addition and by cycloaddition chemistry. Alkylation of the oxamidide ligand in $[(\eta^5\text{-}C_5Me_4H)_2Hf]_2(N_2C_2O_2)$ was explored due to the high symmetry of the complex. A host of sequential 1,2-addition reactions with various alkyl halides was discovered and both *N*- and *N, N'*-alkylated products were obtained. Treatment with Brønsted acids such as HCl or ethanol liberates the free oxamides, $H(R^1)NC(O)C(O)N(R^2)H$, which are useful precursors for *N, N'*-diamines, *N*-heterocyclic carbenes and other heterocycles. Oxamidide functionalization in $[(\eta^5\text{-}C_5Me_4H)_2Hf]_2(N_2C_2O_2)$ was also accomplished with silanes and terminal alkynes, resulting in additional N-Si and N-H bond formation, respectively. The *ansa*-hafnocene variant, $[Me_2Si(\eta^5\text{-}C_5Me_4)(\eta^5\text{-}C_5H_3\text{-}3\text{-}^tBu)Hf]_2(N_2C_2O_2)$, undergoes facile cycloaddition with heterocumulenes such as ^{t}BuNCO and CO_2 to form new N-C and Hf-O bonds. Both products were crystallographically characterized and the latter reaction demonstrates that an organic ligand can be synthesized from three abundant and often inert small molecules: N_2, CO and CO_2. Treatment of either $[(\eta^5\text{-}C_5Me_4H)_2Hf]_2(N_2C_2O_2)$ or $[Me_2Si(\eta^5\text{-}C_5Me_4)(\eta^5\text{-}C_5H_3\text{-}3\text{-}^tBu)Hf]_2(N_2C_2O_2)$ with I_2 yielded the corresponding monomeric iodo hafnocene isocyanate products, $(\eta^5\text{-}$

* Portions of this were taken with permission from: Knobloch, D. J.; Lobkovsky, E.; Chirik, P. J. *J. Am. Chem. Soc.* **2010**, *132*, 15340.

$C_5Me_4H)_2Hf(I)(NCO)$ and $Me_2Si(\eta^5\text{-}C_5Me_4)(\eta^5\text{-}C_5H_3\text{-}3\text{-}^tBu)Hf(I)(NCO)$, respectively, demonstrating that C-C bond formation is reversible.

Introduction

The Haber-Bosch process, which has reigned as the industrial standard of N_2 fixation for nearly a century, has limitations in terms of fossil-fuel efficiency and scope with respect to the commodity scale synthesis of N-containing organic molecules.[1,2,3,4,5,6] Consequently, there is a need for new processes that complement the Haber-Bosch process and offer new ways for the direct cleavage and incorporation of atmospheric nitrogen into useful organic molecules.[7,8]

For example, the simple N-containing molecule formamide is industrially prepared by the reaction of Haber-Bosch ammonia with methyl formate (which itself is prepared from carbonylation of methanol), in an energy-inefficient, multi-step, multi-catalyst process.[9] A similar strategy is applied to nearly all other commodity chemicals containing N-C bonds, being derived indirectly from N_2 that has first been reduced fully to ammonia via the Haber-Bosch process.[10]

A more elegant and energy efficient synthetic approach to formamide and related compounds would be to directly combine N_2, CO (or other appropriate carbon-based feedstocks) in a one-pot synthesis using a single catalyst. With this strategy, the required reducing equivalents for cleavage of N_2 bond may be provided by the metal centers as well as the added carbon-based substrate, coupling cleavage with new N-C bond formation and circumventing the need for intermediate ammonia production. Ideally the addition of water or hydrogen would serve to release the final product and to regenerate the active catalyst (or catalyst precursor) for turnover in the cycle. A general cycle representing this overall approach is presented in Figure 3.1. Several examples relevant to this general approach have been recently reported.[11,12,13,14,15]

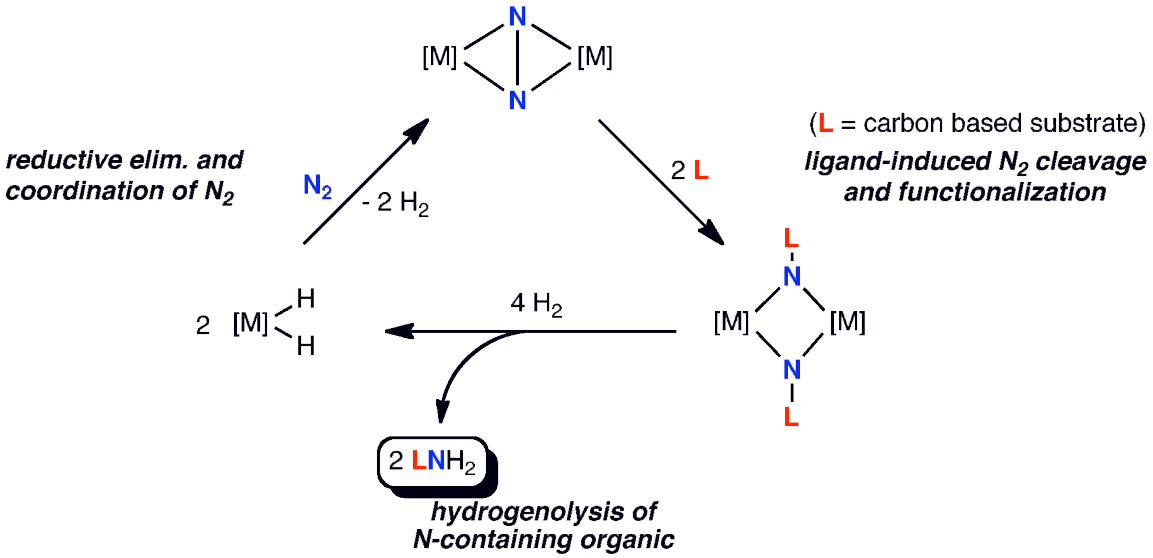

Figure 3.1. Idealized catalytic cycle for the synthesis N-containing organic molecules.

As discussed in the preceding chapters, we have discovered a method to cleave the strong triple bond of dinitrogen, which concomitantly forms two new nitrogen-carbon bonds and one new carbon-carbon bond (Figure 3.2).[16] The reaction appears to be general with dimeric group 4 metallocene complexes that facilitate strong, side-on binding of dinitrogen (i.e. $[N_2]^{4-}$)[17,18,19] and several examples have been reported.[20] As shown in Figure 3.2, the concentration of carbon monoxide determines the type and stereochemistry of the products formed.[16,20] With several metallocene oxamidide complexes in hand, our focus was shifted to the prospect of elaborating the $[N_2C_2O_2]^{4-}$ core and devising new routes to a host of useful N-containing organic molecules from N_2, CO, and other abundant feedstocks. If these strategies evolve into catalytic reactions in the future they may ultimately serve as promising avenues to industrially viable processes. Such processes would be attractive and potentially more versatile alternatives to today's industrial standard, the Haber-Bosch process.

In this chapter the functionalization of metallocene oxamidide complexes prepared from CO-induced N_2 cleavage is reported. A primary focus of this work is

the formation of additional nitrogen-carbon bonds, with the ultimate goal of synthesizing value-added organic products. Toward this end, a range of substrates has been used for elaboration of the $[N_2C_2O_2]^{4-}$ core including heterocumulenes, alkyl halides, silanes, and terminal acetylenes. In some cases, subsequent protonolysis liberated the functionalized oxamide from the metal centers. Currently these studies are a fundamental demonstration that useful N-containing organics can be synthesized directly from N_2 without the prerequisite of ammonia synthesis. Although our methods are currently stoichiometric, a long-term goal is to develop catalytic, industrially applicable systems.

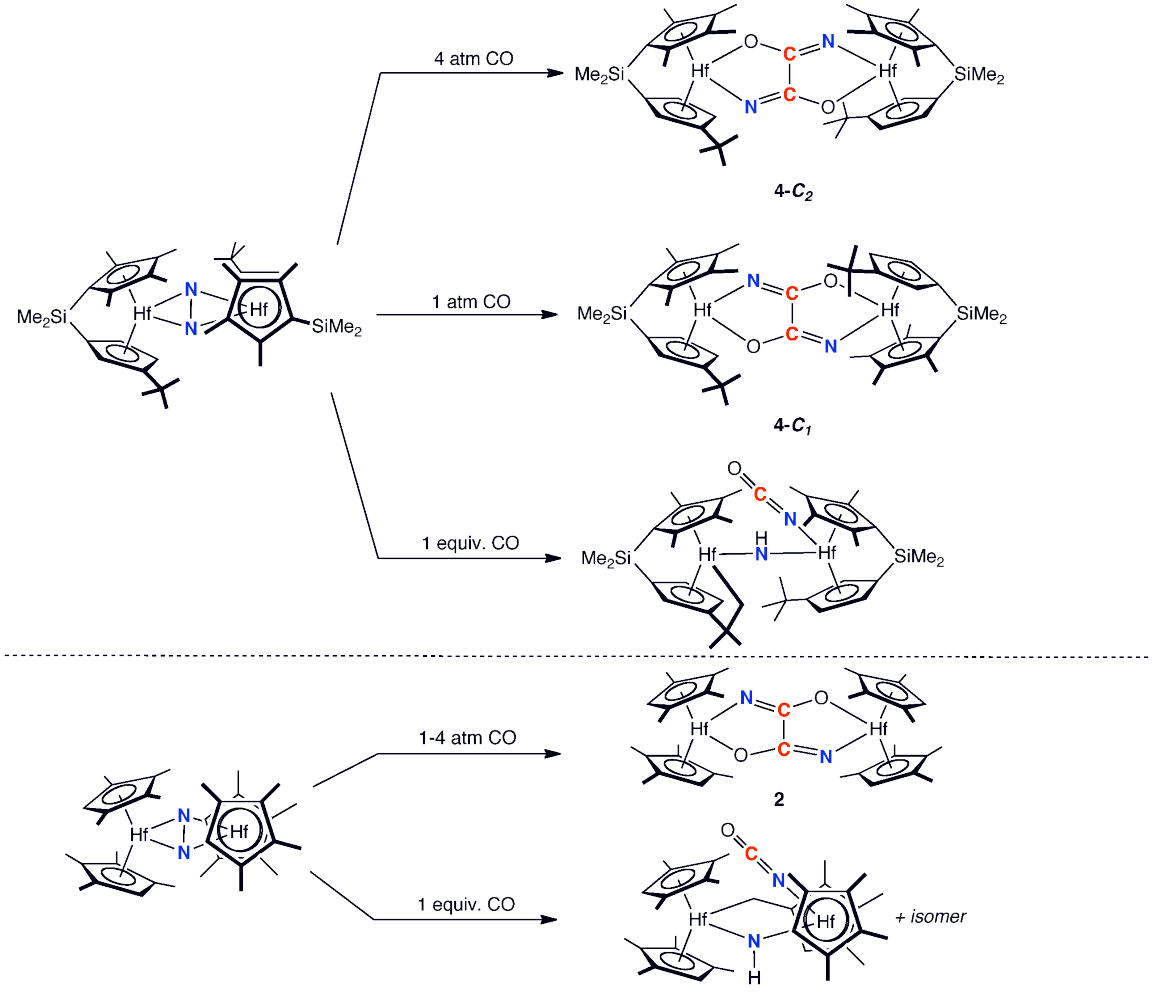

Figure 3.2. CO-induced N_2 cleavage by hafnocene dinitrogen complexes.

Results and Discussion

Electronic structure of hafnocene oxamidide complex (2). Full molecule density function theory (DFT) calculations were performed on the hafnocene oxamidide complex, $((\eta^5\text{-}C_5Me_4H)_2Hf)_2(N_2C_2O_2)$ (**2**), to provide insight into the electronic structure of the molecule as well as to guide reactivity strategies for this and other metallocene oxamidide compounds. The full molecule calculations were carried out at the B3LYP level of theory. A representation of **2** following geometry optimization, along with selected Mayer bond orders determined from the calculations, is presented in Figure 3.3. The Hf-N bond orders of 1.231 and 1.225 are indicative of multiple bond character due to donation from the lone pair of the of the oxamidide nitrogen atom into the $1a_1$ hafnocene orbital (see Figure 3.3). This multiple bond character predicted by theory suggests that the oxamidide complexes might be elaborated *via* cycloaddition of heterocumulenes across the Hf-N bond.[21,22,23]

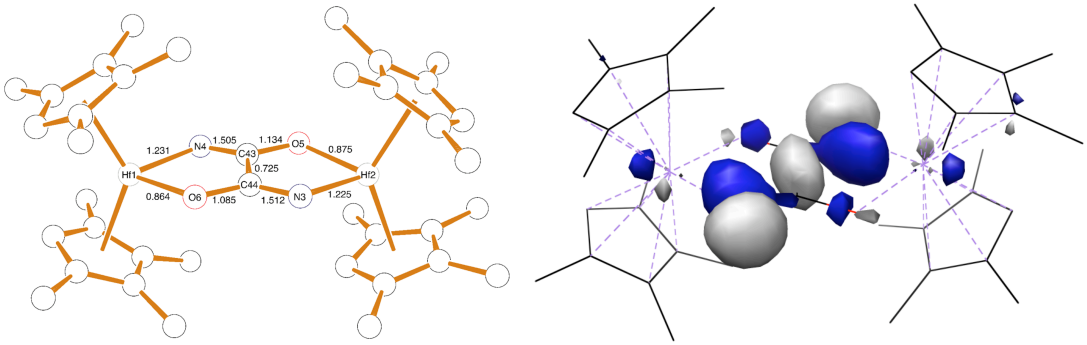

Figure 3.3. DFT-computed (B3LYP functional) geometry-optimized structure of **2**: selected Mayer bond orders (left) and highest occupied molecular orbital (right).

Selected molecular orbitals of **2** are presented in Figure 3.4. The highest occupied molecular orbital (HOMO) of **2** consists predominantly of a lone pair of electrons on each of the nitrogen atoms in the oxamidide core. This predicted lone-pair

HOMO suggests that **2** (and other oxamidide complexes by comparison) might exhibit nucleophilic character at nitrogen and be susceptible to formal 1,2-addition reactions with acidic and/or highly electrophilic substrates.

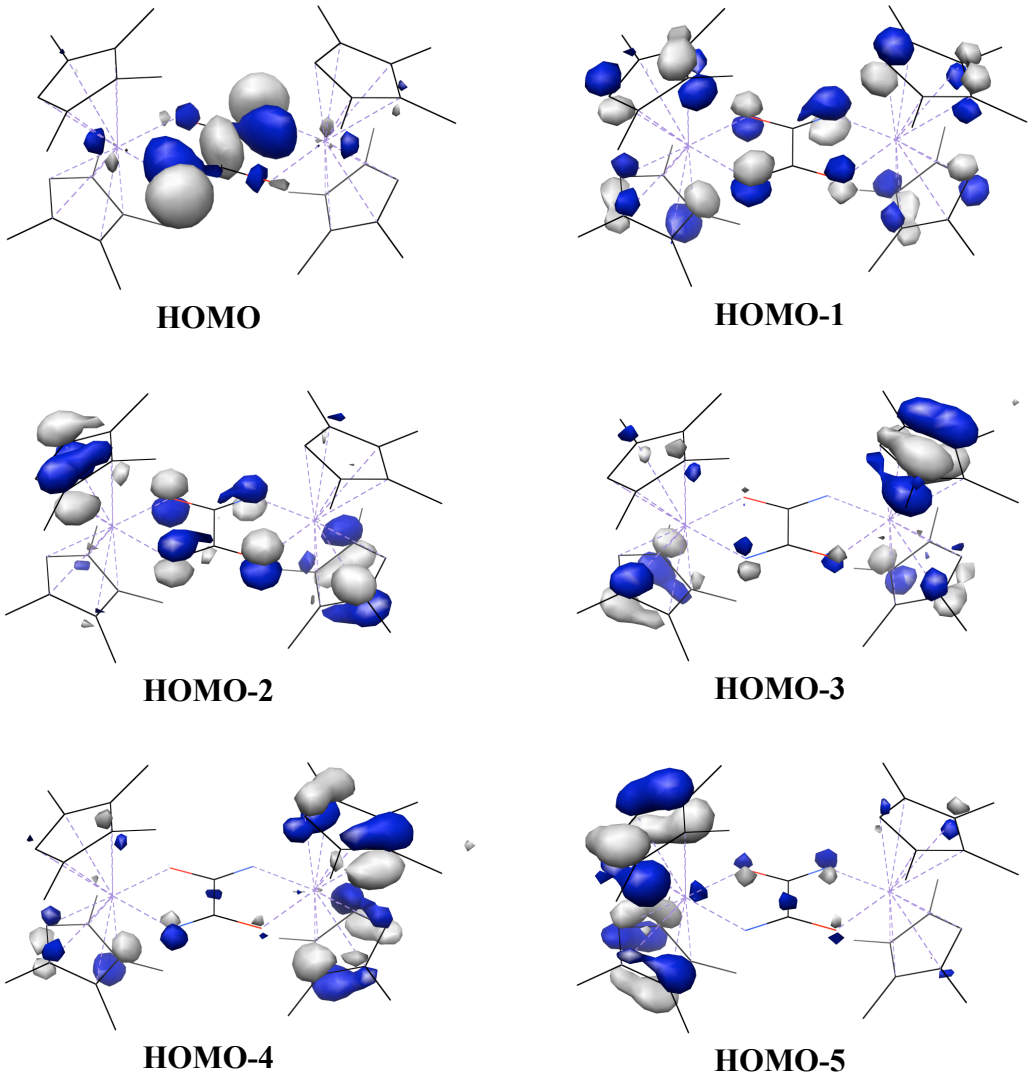

Figure 3.4. Selected DFT-computed (B3LYP functional) highest occupied molecular orbitals of **2**.

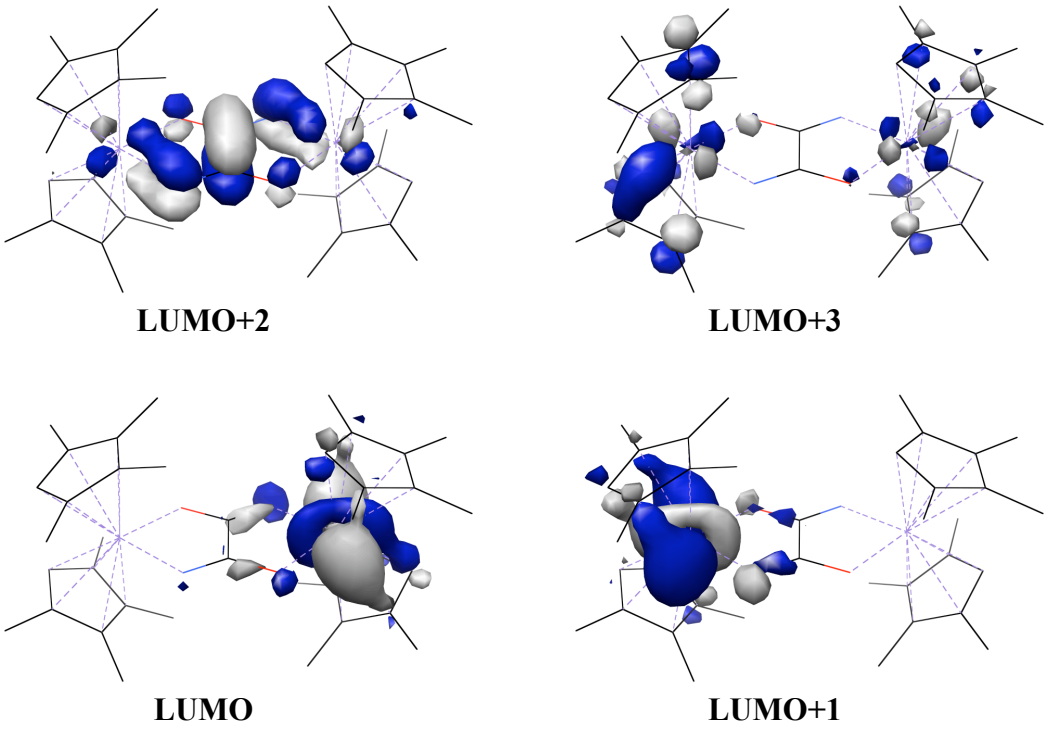

Figure 3.5. Selected DFT-computed (B3LYP functional) lowest occupied molecular orbitals of **2**.

The lowest unoccupied molecular orbital (LUMO) and the molecular orbital labeled LUMO+1 both essentially consist of non-bonding hafnocene $1a_1$ character. Importantly, the unoccupied orbital labeled LUMO+2 exhibits an overlap between the p_z nitrogen orbital and the b_1, comprising an π-interaction reminiscent of the π bond observed in early metallocene imido complexes.[24,25] The vacancy of this orbital predicted by calculation suggests that the bonding in **2** and similar oxamidide complexes is not imido-like and may therefore render these compounds inert to non-polar 1,2-addition substrates such as hydrogen and saturated hydrocarbons.

Oxamidide functionalization attempts with internal and terminal alkynes. Functionalization reactions were explored only with the hafnocene oxamidide complexes, $(Me_2Si(\eta^5\text{-}C_5Me_4)(\eta^5\text{-}C_5H_3\text{-}3\text{-}^tBu)Hf)_2(N_2C_2O_2)$ (**1**) and $((\eta^5\text{-}C_5Me_4H)_2Hf)_2(N_2C_2O_2)$ (**2**), as the zirconium congeners suffer from deleterious N_2 loss chemistry that is competitive with carbonylation. Initial attempts at functionalizing compound **2** with internal alkynes were unsuccessful. Treatment of **2** with 10-fold excess of either 2-butyne, diphenylacetylene, or 1-phenyl-1-propyne produced no reaction, even after prolonged heating at temperatures up to 100 °C for 24 h, under which conditions gradual decomposition of the starting material was observed. These results are consistent with the DFT prediction that the group 4 metallocene oxamidide complexes exhibit reactivity that contrasts with group 4 metallocene complexes bearing imido or hydrazido ligands. It has been well documented that the latter complexes react with internal alkynes *via* cycloaddition[23,26] and in some instances, *via* insertion.[27] In light of these unsuccessful attempts at functionalization of **2** with internal alkynes, terminal alkynes were targeted in hopes of accessing products of carbon-hydrogen bond activation. Our laboratory has also seen success with this approach in the functionalization of zirconocene and hafnocene dinitrogen compounds[19,28] and transient μ-nitrido compounds (see Chapter 2 of this Thesis).

Addition of two equivalents of phenylacetylene to **2** resulted in clean conversion, after 1 h at 65 °C, to the C_{2h}-symmetric oxamidato dihafnocene acetylide product, **2-(PhCCH)$_2$** (Figure 3.6), arising from formal 1,2-addition of the acetylenic C-H bond across the hafnium-nitrogen bond. Full spectroscopic characterization of the compound was achieved using multinuclear (^{1}H, ^{13}C, ^{1}H-^{15}N HSQC) NMR and infrared spectroscopies. The benzene-d_6 ^{1}H NMR spectrum contains the number of resonances consistent with the proposed C_{2h}-symmetric structure. The formation of a

new N-H bond was evidenced by coupling of the N-H proton (^{1}H NMR) and the $N_2{}^{13}C_2O_2$ carbon (^{13}C NMR) in an AA'XX' non-first-order spin system[29] observed in the oxamidiate region of the benzene-d_6 ^{13}C NMR spectrum (Figure 3.7) upon isotopic labeling of the oxamidate core with ^{13}CO. Diagnostic stretches for the N-H and acetylide functional groups were identified by infrared spectroscopy at 3371 cm^{-1} and 2087 cm^{-1}, respectively. Activation of the acidic carbon-hydrogen bond in phenylacetylene by **2** demonstrates the nucleophilic character of the oxamidide core nitrogen atom, consistent with the theoretical prediction.

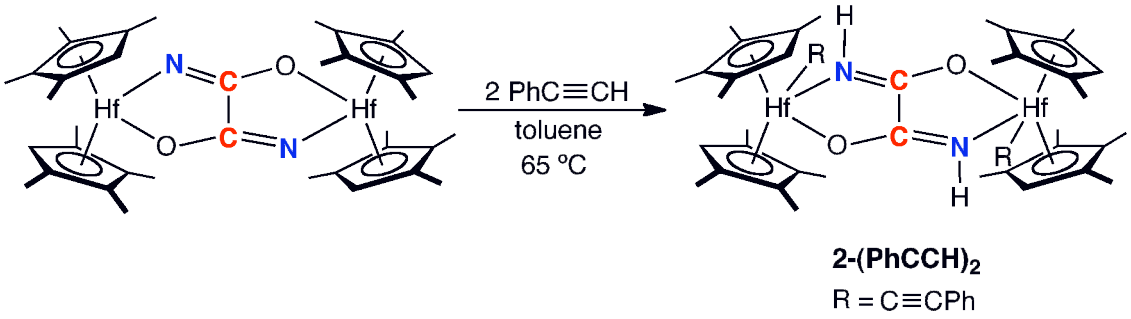

Figure 3.6. Addition of terminal acetylenes to **2**.

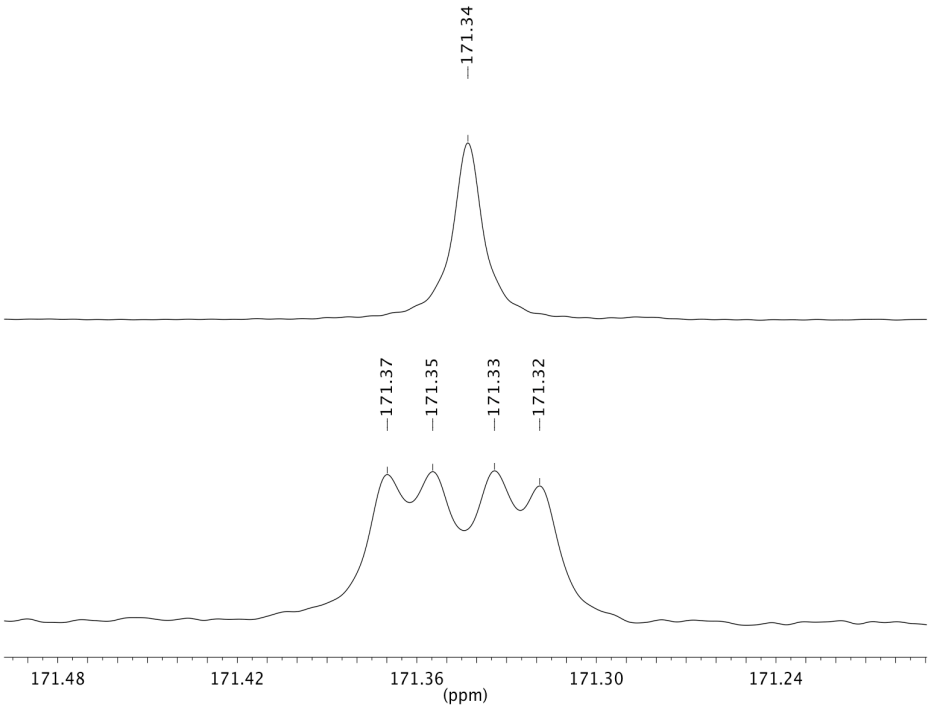

Figure 3.7. Oxamidate region of the benzene-d_6 $\{^1H\}^{13}C$ NMR (top) and (proton-coupled) ^{13}C NMR (bottom) spectra of **2-(PhCCH)$_2$-^{13}C$_2$** at 23 ºC.

Hafnocene Oxamidide Functionalization with Alkyl Halides and Silanes. The C-H activation chemistry observed with **2** and terminal alkynes prompted study into the possibility of other formal 1,2-addition reactions in hopes of applying this chemistry to the synthesis of new nitrogen-carbon and nitrogen-heteroatom bonds. The 1,2-additions of carbon-hydrogen bonds,[21,30,31] dihydrogen,[32] and alkyl halides[21,22] are all well-established reactions for group 4 transition metal compounds with metal-nitrogen bonds.[33] Unfortunately, the oxamidide complex **2** is unreactive with dihydrogen and simple alkanes over a wide range of reaction conditions. This lack of reactivity with nonpolar reagents is consistent with the computed molecular orbital diagram, which suggests little imido-like character. Therefore our attention became focused on the alkylation and silylation of the oxamidide core by using more polar

substrates, namely alkyl halides as well as primary and secondary silanes. Subsequent protonolysis to release the functionalized oxamidate core could offer a useful route to substituted oxamides, which, in addition to their direct applicability as agrochemicals, also serve as synthons for a wide variety of nitrogen containing organic molecules such as diamines, *N*-heterocyclic carbenes, and *N*-heterocycles.[38-40]

Our attention focused on the alkylation and silylation of the hafnocene oxamidide complex, **2**, due to its higher symmetry and relative ease of synthesis compared to **4**. The zirconium congeners were not studied due to competitive N_2 loss chemistry.

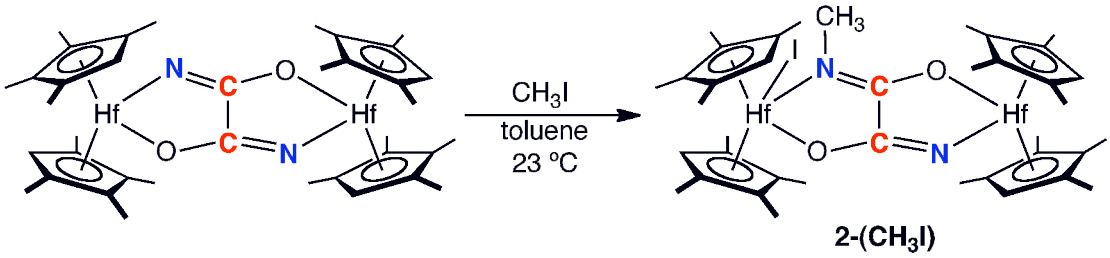

Figure 3.8. Addition of methyl iodide to **2**.

Addition of 1 equiv of CH_3I to a toluene solution of **2** at 23 °C, followed by solvent removal and washing with cold pentane furnished a yellow solid, identified as **2-(CH_3I)**, the product of a single 1,2-addition of the alkyl halide across a Hf-N bond (Figure 3.8). Nitrogen-carbon bond formation was confirmed by preparing various isotopologues of **2-(CH_3I)**, conveniently accessed with isotopically labeled reagents, ^{13}CO, $^{15}N_2$ and $^{13}CH_3I$. The multinuclear (^1H, ^{13}C, ^{15}N) NMR spectroscopic data of these isotopologues are fully consistent with the assigned structure. The benzene-d_6 $\{^1H\}^{13}C$ NMR spectrum of **2-$^{13}C_2$-($^{13}CH_3I$)** is presented in Figure 3.9 (left, center spectra) as a mixture with the dimethylated oxamidate product, **2-$^{13}C_2$-($^{13}CH_3I)_2$** (*vide infra*), and exhibits chemical shifts and coupling constants consistent with a C_s-

symmetric molecule bearing a unique $[N(^{13}CH_3)N^{13}C_2O_2]^{3-}$ core. In addition, the $\{^1H\}^{13}C$ NMR spectrum of the $^{15}N/^{13}C$-labeled isotopologue **2-$^{15}N_2$-($^{13}CH_3I$)** confirms N-C bond formation with an N-C coupling constant of $^1J_{CN}$ = 5.3 Hz (Figure 3.9, right). The features of the benzene-d_6 ^1H NMR spectrum are also diagnostic. The C_{2h}-symmetric starting material, **2**, was cleanly and quantitatively converted to a C_s-symmetric molecule with inequivalent hafnocene subunits.

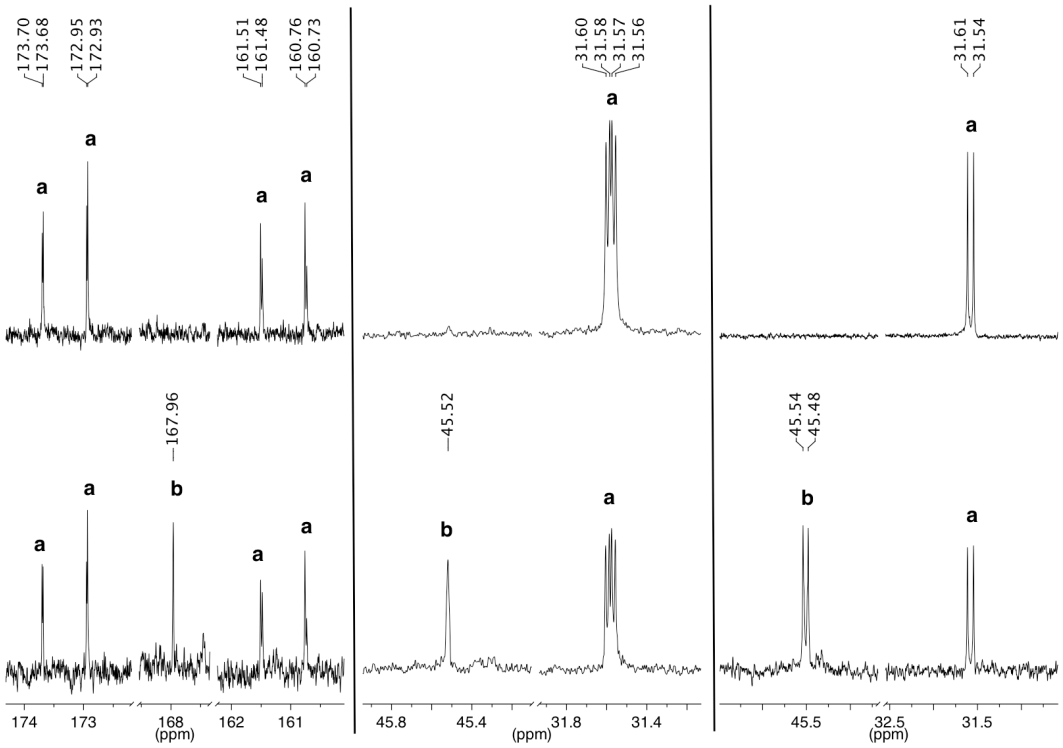

Figure 3.9. $N_2C_2O_2$ region (left) and N-CH_3 region (center) of the benzene-d_6 ^{13}C NMR spectrum of the reaction of **2** (^{13}C labeled) with excess $^{13}CH_3I$ in benzene-d_6 after 5 minutes (top spectra) and after 8 hours (bottom spectra); Peaks labeled "**a**" correspond to **2-$^{13}C_2$-($^{13}CH_3I$)** and peaks labeled "**b**" correspond to **2-$^{13}C_2$-($^{13}CH_3I)_2$**. (Right): N-*C*H3 region of the benzene-d_6 ^{13}C NMR spectrum of the reaction of **2** (^{15}N labeled) with excess $^{13}CH_3I$ in benzene-d_6 after 5 minutes (top spectra) and after 8 hours (bottom spectra).

Other products of a single hafnocene oxamidide alkylation were also prepared. Addition of 1 equiv of ethyl iodide to a benzene-d_6 solution of **2** resulted in rapid 1,2-addition to form exclusively the *N*-ethylated product, **2-(CH_3CH_2I)**, in quantitative yield as judged by NMR spectroscopy (Figure 3.10). The compound was characterized by ^1H and ^{13}C NMR as well as infrared spectroscopies, and the data are fully consistent with a C_s symmetric molecule arising from a single ethylation of an oxamidide nitrogen atom. The benzylated analog, **2-($PhCH_2Br$)** was also prepared by addition of 1 equiv $PhCH_2Br$ to **2** (Figure 3.10). In the *N*-benzylated case, the NMR spectroscopic data was consistent with a molecule having C_1 symmetry rather than the expected C_s symmetry. This is possibly due to steric constraints imparted by the bulkier benzyl substituent. Full conversion to each of these products (**2-(CH_3CH_2I)** and **2-($PhCH_2Br$)**) occurred over the course of 1 h at 23 °C.

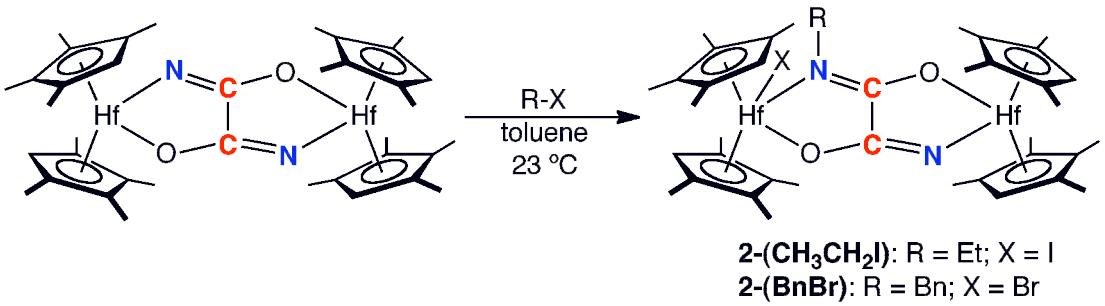

Figure 3.10. Addition of alkyl halides to **2**.

The successful syntheses of *N*-monoalkylated hafnocene oxamidide complexes inspired further alkylation studies with the goal of synthesizing various homo- and heterosubstituted *N*, *N*'-oxamidate complexes. Subsequent protonolysis of these compounds would liberate the corresponding alkylated oxamides in their free forms. Because **2-(CH_3I)** could be cleanly isolated on a preparative scale, it was targeted for the synthesis of heterosubstituted oxamidate complexes. Treatment of **2-(CH_3I)** with a

slight excess of ethyl bromide for 48 h at 23 ºC resulted in full conversion to the disubstituted dihafnocene oxamidate complex, **2-(CH_3I)(CH_3CH_2Br)** arising from a second 1,2-addition event (Figure 3.11). A similar outcome was achieved after treating **2-(CH_3I)** with excess benzyl bromide, forming the disubstituted hafnocene oxamidate, **2-(CH_3I)($PhCH_2Br$)**. In the case of benzyl bromide addition, heating to 65 °C for 16 h was required for complete conversion.

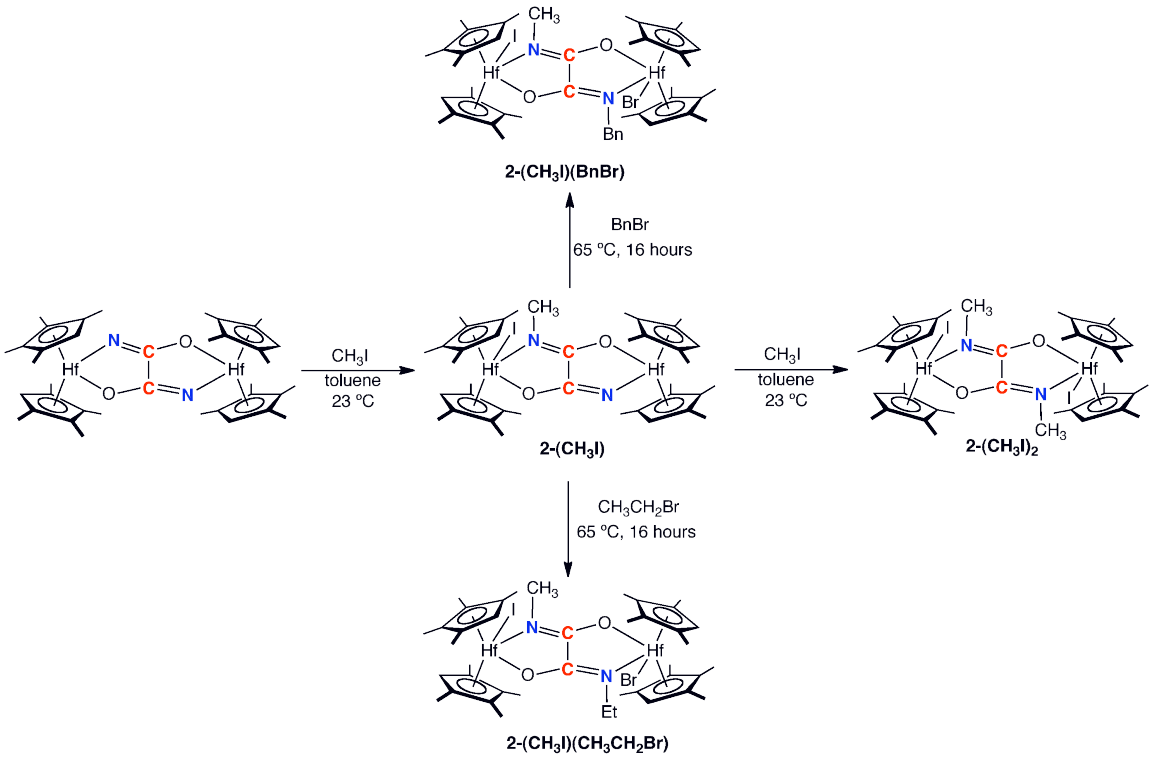

Figure 3.11. Methylation and subsequent alkylation of **2**.

The heterosubstituted oxamidate complexes (**2-(CH_3I)(CH_3CH_2Br)** and **2-(CH_3I)($PhCH_2Br$)**) were characterized by multinuclear (^1H and ^{13}C) NMR spectroscopy as well as infrared spectroscopy. In both cases the ^1H and ^{13}C NMR spectra exhibit the number of resonances consistent with a C_s symmetric dihafnium

complex with inequivalent subunits arising from the formal 1,2-addition of the carbon-halogen bond.

Homosubstituted oxamidate complexes were also synthesized. Dimethylation of the oxamidide ligand was accomplished either by addition of a second equivalent of methyl iodide to **2-(CH_3I)** (Figure 3.11) or by direct treatment of **2** with 2 equiv (or a large excess) of CH_3I (Figure 3.12). The latter procedure proved more convenient and yielded, following workup, analytically pure iodohafnocene dimethyl oxamidate, **2-(CH_3I)$_2$**, in 92% yield. The formation of two N-CH_3 bonds via methylation of the hafnocene oxamidide was readily established by ^1H and ^{13}C NMR spectroscopy as the number of resonances consistent with a C_{2h}-symmetric dimeric hafnocene oxamidate complex was observed. The straightforward synthesis of various isotopologues of **2-(CH_3I)$_2$** from $^{15}N_2$, ^{13}CO, and $^{13}CH_3I$ provided a convenient tool for NMR spectroscopic characterization. Figure 3.9 (right) presents a representation of the ^{13}C NMR spectrum of the product of the reaction of **2-$^{15}N_2$** with excess $^{13}CH_3I$ after 5 min and 8 h, and analysis of these data established a $^1J_{CN}$ of 4.3 Hz, consistent with N-C bond formation from the added methyl iodide.

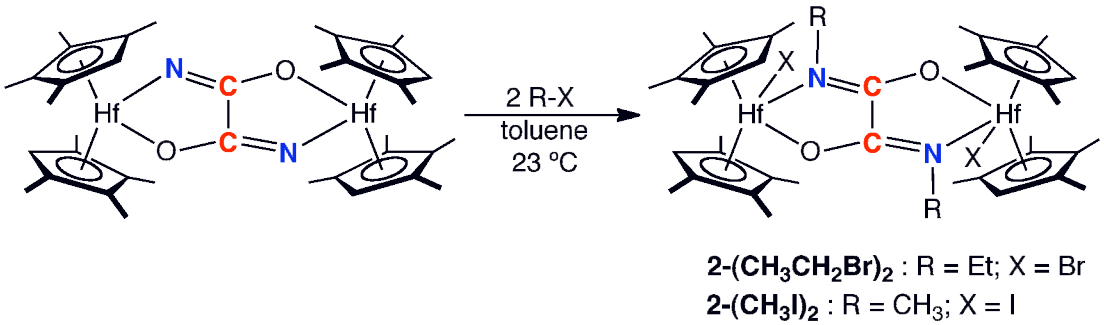

Figure 3.12. Synthesis of homosubstituted *N*,*N*'-oxamidate complexes.

The solid-state structure of **2-(CH_3I)$_2$** was established by X-ray diffraction and a representation of the molecule is presented in Figure 3.13. Selected metrical parameters are presented in Table 3.1. Important features include the elongation of the Hf-N and Hf-O bonds, consistent with a change in the formal oxidation state of the core ligand from $[N_2C_2O_2]^{4-}$ to $[(NCH_3)_2C_2O_2]^{2-}$. Notably, the hafnium centers retain contact to both the oxygen and nitrogen and the C-N and C-O distances in the core are comparable to the values in the parent oxamidide **2**, suggesting only subtle geometrical changes in the overall transformation of **2** to **2-(CH_3I)$_2$**. The core of the molecule is essentially planar, and the dihedral angle between the hafnocene subunits (defined by the plane containing each Hf and two bound Cp centroids) is 0.0 °.

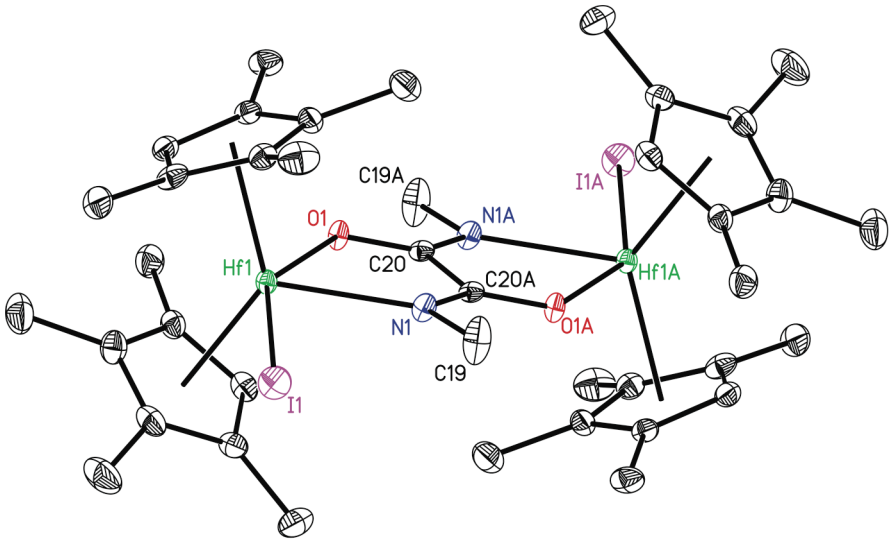

Figure 3.13. Molecular structure of **2-(CH_3I)$_2$** at 30% probability ellipsoids. Hydrogen atoms omitted for clarity.

Another example of a homosubstituted hafnocene dialkyoxamidate complex was obtained from treatment of **2** with excess ethyl bromide for several days at 23 °C or for 16 h at 65 °C, furnishing **2-(CH_3CH_2Br)$_2$** in quantitative yield (Figure 3.12).

Spectroscopic characterization of **2-(CH_3CH_2Br)$_2$** is consistent with a molecule of idealized C_{2h} symmetry and two N-C bond forming events. Unfortunately, the dibenzylated complex was not obtained, as addition of excess benzyl bromide to **2-($PhCH_2Br$)** resulted in no further reaction up to 100 °C, at which temperature gradual decomposition occurred.

Table 3.1. Crystallographic data summary.

	1-*C*$_2$	**1-(^{t}BuNCO)$_2$**	**1-(CO_2)$_2$**	**2**[c]	**2-($PhSiH_3$)$_2$**[d]	**2-(CH_3I)$_2$**[d]
d(Hf-N)	2.062(2)	2.165(2)	2.174(2)	2.043(5) (E3)	2.322(4)	2.358(6)
	2.0557(19)	2.175(2)	2.186(2)	2.057(4) (E1)		
d(Hf-O)	2.0570(16)	2.2440(18)	2.2528(18)	2.058(5) (E4)	2.253(3)	2.211(4)
	2.0584(17)	2.2115(18)	2.2432(17)	2.062(4) (E2)		
d(C-C)	1.534(3)	1.506(4)	1.524(4)	1.531(8)	1.499(8)	1.468(9)
d(C-N)	1.270(3)	1.295(3)	1.299(3)	1.299(7) (E3)	1.317(5)	1.295(9)
	1.275(3)	1.302(3)	1.300(3)	1.320(8) (E1)		
d(C-O)	1.341(3)	1.267(3)	1.258(3)	1.303(7) (E4)	1.273(5)	1.277(9)
	1.339(3)	1.269(3)	1.259(3)	1.297(7) (E2)		
d(N-E)[a]	-	1.417(3)	1.420(3)	-	1.786(4)	1.47(1)
		1.407(3)	1.429(3)			
d(Hf-X)[b]	-	2.2054(18)	2.1880(18)	-	1.91(4)	2.9788(7)
		2.1970(19)	2.2081(19)			

[a]"E" denotes heteroatom in the newly formed bond to nitrogen (eg. C, Si)

[b]"X" denotes heteroatom in newly formed bond to hafnium (eg. I, H, O)

[c]E1/E3 and E2/E4 indistinguishable by crystallography

[d]centrosymmetry relates both halves of the molecule

The successful alkylation of **2** with a series of alkyl halides prompted studies into releasing the functionalized core from the resulting hafnocene oxamidate compounds. In previous chapters of this thesis, we have reported that treatment of **2**[34] or treatment of the *ansa*-hafnocene oxamidide complex, **4-*C*$_1$** and **4-*C*$_2$**[35] with excess ethanol, water, or anhydrous HCl released free oxamide in nearly quantitative yield. On the basis of these results, the reactivity of each of the newly synthesized hafnocene oxamidate complexes with Brønsted acids was studied. A summary of these results is presented in Figure 3.14. In each case, free *N*-monoalkyl or *N*, *N*'-dialkyl oxamides were liberated and their identities confirmed by ^{1}H NMR, ^{13}C NMR, and infrared spectroscopies. The products obtained from the dinitrogen functionalization studies were compared to materials prepared by independent synthesis or to previously reported data where possible.[36,37]

These *N*-monoalkyl- and *N*, *N*'-dialkyloxamides are known synthons for a variety of important small molecules and heterocycles (Figure 3.14).[38,39,40] In particular, *N*, *N*'-dimethyloxamide obtained on a preparatory scale from protonolysis of the corresponding oxamidate compound and subsequent separation from the hafnocene byproduct was of suitable purity and quantity for further reactivity. Treatment of this isolated oxamide with PCl_5, according to an adopted procedure,[41] resulted in, following workup, 5-chloro-1-methyl-imidazole in reasonable yield. This example illustrates the utility of our method for application in certain small-scale syntheses. While the process is limited to stoichiometric chemistry, it should at least be noted that the organometallic byproduct of protonolysis (i.e. the corresponding hafnocene dichloride, **2-Cl$_2$**) is recoverable in high yield and can be recycled back into the synthesis of the oxamidide compound, **2**.

Importantly, the ease of ^{15}N and ^{13}C isotopic labeling into these complexes provides a convenient route to the small-scale synthesis of specifically labeled

isotopologues of various nitrogen-containing small molecules and heterocycles. There is also considerable interest in the synthesis of substituted oxamides for their coordination properties, in particular their interesting electronic properties, when bound to late transition metals.[42]

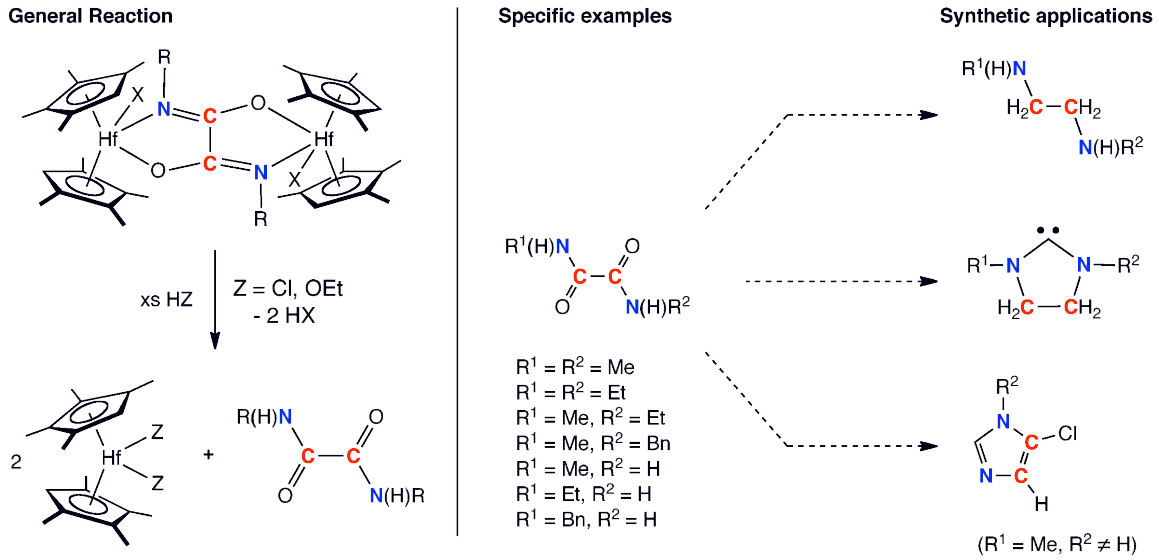

Figure 3.14. Liberation of substituted oxamides and synthetic applications.

Functionalization of oxamidides via 1,2-addition of silanes. The successful 1,2-addition chemistry observed with **2** and various alkyl halides suggested that related 1,2-addition processes might be accessible for **2** with primary and secondary silanes. Additional motivation for these studies was derived from the observation by Fryzuk and coworkers of dinitrogen functionalization[43] and cleavage upon addition of silanes.[44,45] Our laboratory has also recently observed silane-induced N_2 cleavage with a related hafnocene dinitrogen compound, $((\eta^5\text{-}C_5Me_3H)_2Hf)_2(\mu_2, \eta^2, \eta^2\text{-}N_2)$.[46] We have also observed that dinitrogen carbonylation in the presence of primary silanes resulted in cleavage of the N≡N and C≡O bonds with release of free cyanosilanes, reported in the previous chapter of this thesis.[20]

Treatment of a toluene solution of **2** with a slight excess (2.2 equiv) of $PhSiH_3$ and stirring the resulting mixture for 1 h at 23 °C furnished, following solvent removal and recrystallization, a pale yellow solid identified as **2-(PhSiH$_3$)$_2$** in 86% yield (Figure 3.15). Attempts to isolate the monosilylated intermediate product were unsuccessful, as at short reaction times and with sub-stoichiometric quantities of the silane, only **2** and **2-(PhSiH$_3$)$_2$** were observed by ^{1}H NMR spectroscopy. In contrast to the previously discussed PhCCH addition reaction, which favors N-H and Hf-R (R=CCPh) formation, the outcome of silane addition is Hf-H and N-[Si] ([Si]=$SiPhH_2$) formation. These constitutional differences in the products are consistent with deprotonation of PhCCH by the oxamidide nitrogen atom in the former case and nucelophilic attack by nitrogen at silicon in the latter case. The benzene-d_6 ^{1}H NMR spectrum exhibits the number of peaks consistent with a C_{2h}-symmetric molecule arising from two formal 1,2-additions of Si-H bonds across the Hf-N bonds. A diagnostic hafnium hydride resonance was observed at 9.54 ppm.

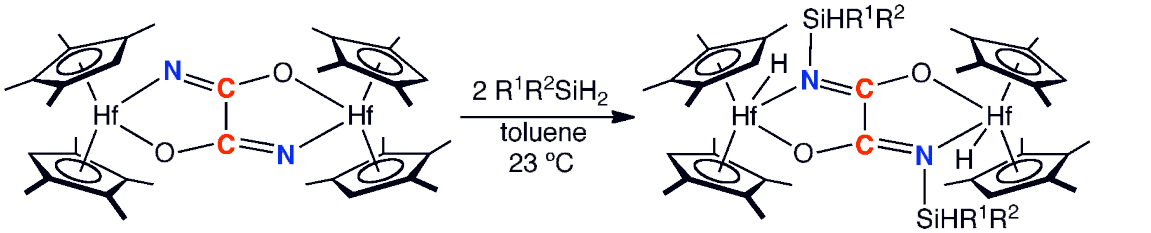

Figure 3.15. Addition of primary and secondary silanes to **2**.

The solid-state structure of **2-(PhSiH$_3$)$_2$** was determined by X-ray diffraction. A representation of the molecule is presented in Figure 3.16 and selected bond distances are reported in Table 3.1. The data were of sufficient quality that the

hafnium and silyl hydrides were located. The crystallographic data confirm Si-N bond formation and a disilylated oxamidate core. Similar to **2-$(CH_3I)_2$**, the Hf-O and Hf-N bonds in **2-$(PhSiH_3)_2$** are slightly elongated with respect to the parent oxamidide, **2**, consistent with oxamidate ($[(NSiH_2Ph)_2C_2O_2]^{2-}$) formation. The Hf-H bond is comparable with those reported previously in this thesis for related compounds.[20] The oxamidate core is essentially planar and the dihedral angle between the hafnocene subunits is 24.1°.

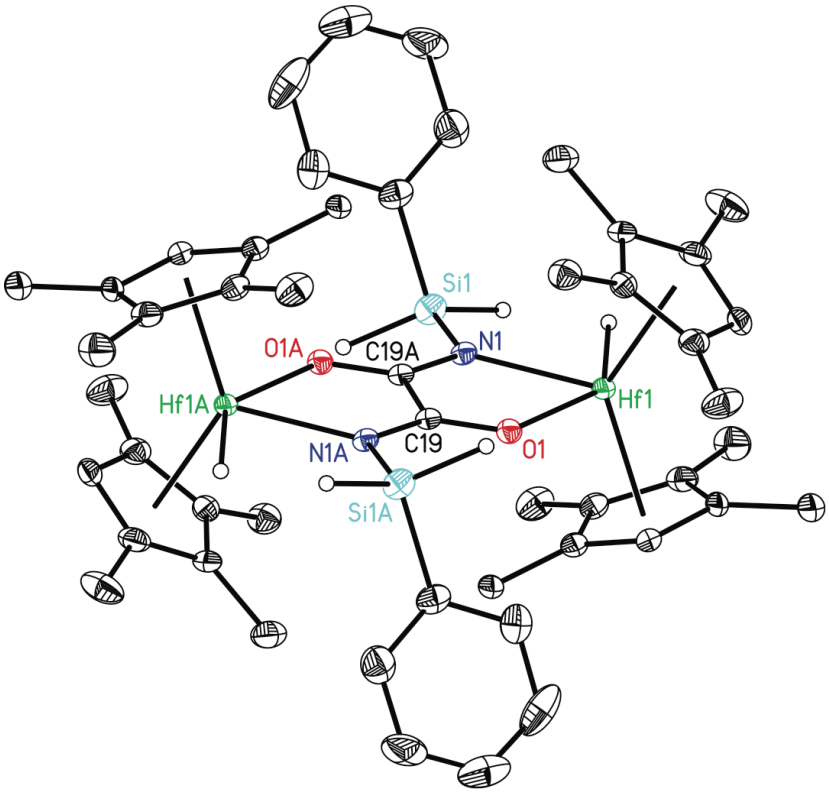

Figure 3.16. Molecular structure of **2-$(PhSiH_3)$** at 30% probability ellipsoids. Hydrogen atoms, except for the hafnium and silyl hydrides, are omitted for clarity.

Similar idealized C_{2h}-symmetric silylated hafnocene oxamidate complexes were synthesized from addition of ^{n}HexylSiH$_3$ and the secondary silane Ph_2SiH_2 to **2** (Figure 3.15). Diagnostic hafnium hydride resonances were located for these

complexes, **2-(^{n}HexSiH$_3$)$_2$** and **2-(Ph$_2$SiH$_2$)$_2$** by ^{1}H NMR spectroscopy at 9.95 ppm and 9.80 ppm, respectively. Attempts to functionalize **2** with triethylsilane were unsuccessful, resulting in no reaction at either 23 °C or 100 °C.

Functionalization of the oxamidide core in **2** with both alkyl halides and silanes prompted exploration of a combined strategy where additional nitrogen-element bond formation was accomplished with both reagent types. A benzene-d_6 solution of the monomethylated complex, **2-(CH$_3$I)**, was treated with 1.2 equiv of PhSiH$_3$. Complete conversion to the idealized C_s-symmetric compound **2-(CH$_3$I)(PhSiH$_3$)** was observed immediately (Figure 3.17). Full characterization of **2-(CH$_3$I)(PhSiH$_3$)** was accomplished using multinuclear (^{1}H, ^{13}C) NMR and infrared spectroscopies.

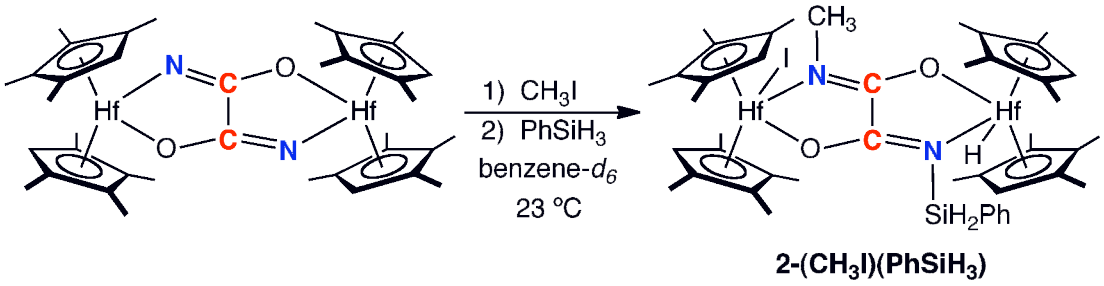

Figure 3.17. Sequential alkylation and silylation of **2**.

Characterization by ^{1}H and ^{13}C NMR spectroscopy established methyl iodide and silane addition to the oxamidide core. The benzene-d_6 ^{1}H NMR spectrum exhibited the number of peaks consistent with formation of two inequivalent metallocene subunits along with a diagnostic Hf-H resonance at 9.38 ppm. The new N-CH$_3$ group was located at 3.67 ppm ($^3J_{CH}$ = 4.4 Hz), while the Si-H resonance for the newly formed N-Si bond was assigned at 4.89 ppm. The benzene-d_6 ^{13}C NMR spectrum of **2-(CH$_3$)(PhSiH$_3$)-^{13}C$_2$**, prepared from ^{13}CO, is presented in Figure 3.18,

and exhibits diagnostic peaks for an oxamidate core functionalized with two different groups. Inequivalent carbons were observed at 170.33 and 173.05 ppm ($^{1}J_{CC}$ = 72.5 Hz). In addition, C=N and Si-H bands were observed at 1558 and 2119 cm^{-1}, respectively, in the solid-state (KBr) infrared spectrum.

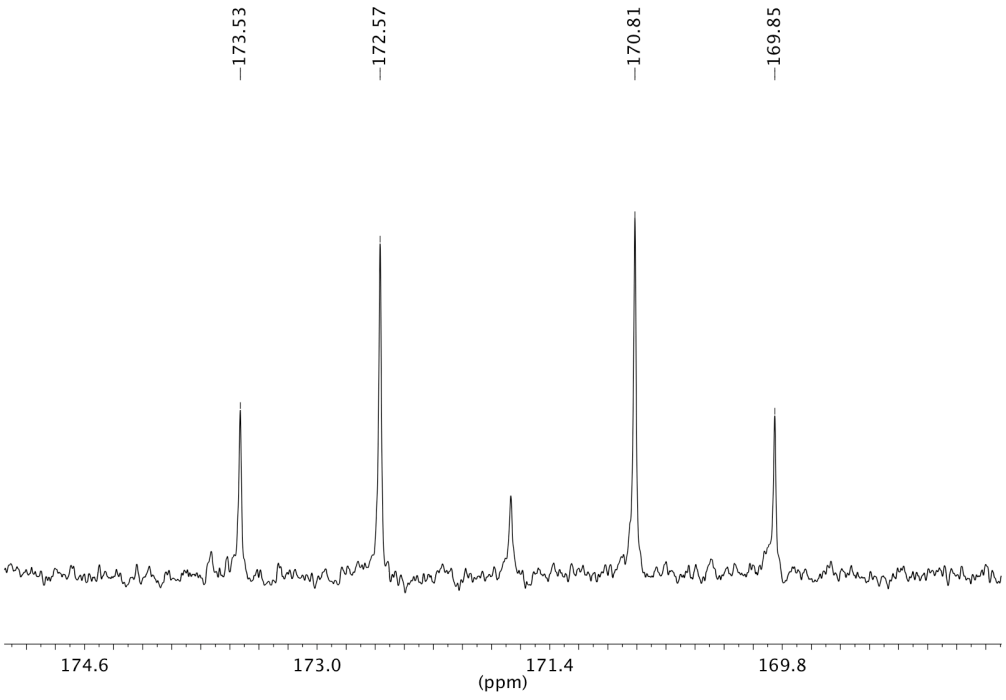

Figure 3.18. Oxamidate region of the benzene-d_6 ^{13}C NMR spectrum of **2-(CH_3)($PhSiH_3$)-$^{13}C_2$**, collected at 23 ºC.

Oxamidide functionalization via cycloaddition of heterocumulenes. The modest Hf-N multiple bond character in **2** predicted by theory (*vide supra*) suggested that cycloaddition reactivity to elaborate the oxamidide nitrogen may be possible.[21-23] The possibility of cycloaddition-type reactivity with the metallocene oxamidides was explored by the addition of heterocumulenes.

Our laboratory previously reported that addition of isocyanates to [(η^5-$C_5Me_4H)_2Hf]_2(\mu_2,\eta^2,\eta^2$-$N_2$) resulted in formation of nitrogen-carbon bonds arising from both insertion and cycloaddition reactions with the hafnium-nitrogen bonds in the dinitrogen complex with the heterocumulene.[47] Inspired by this result, similar reactivity was explored with metallocene oxamidide complexes. Only the hafnocene oxamidide complexes **2** and **4** were studied, as the zirconium congeners (**1** and **3**) suffer from chemistry derived from N_2 loss that is competitive with dinitrogen carbonylation.

Initial studies of the reactivity of **2** with various heterocumulenes were hampered due to poor yields of the desired products and by the concomitant formation of insoluble, intractable byproducts. As a result, the *ansa*-hafnocene oxamidide, **4**, was chosen for the focus of these studies. As described in Chapter 1 of this thesis,[16] this complex can be synthesized as either the C_1- or C_2-symmetric isomer, depending on the pressure of CO used for dinitrogen carbonylation and cleavage. Due to its relative ease of scalable synthesis and its higher symmetry the C_2-symmetric isomer, **4-*C*$_2$** (as a racemic mixture), was used for these studies. Addition of an excess (~5 equiv) of *tert*-butyl isocyanate to a toluene solution of **4-*C*$_2$**, followed by removal of the volatiles and recrystallization from diethyl ether at -35 °C, furnished a yellow solid identified as **4-(^{t}BuNCO)$_2$**, arising from double isocyanate cycloaddition across the oxamidide Hf-N bonds, in 56% yield (Figure 3.19).

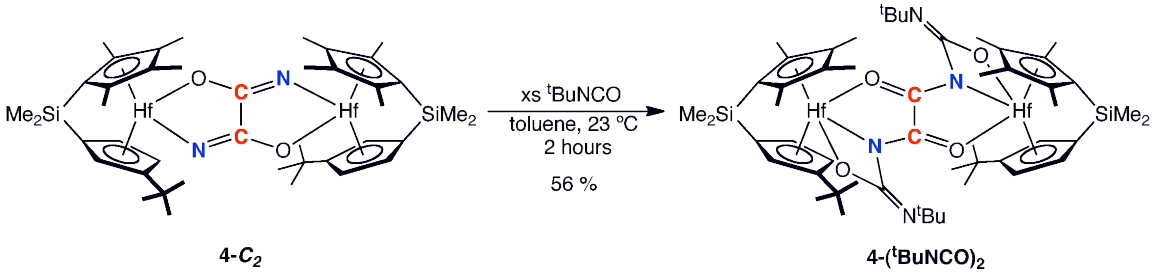

Figure 3.19. Addition of *tert*-butylisocyanate to **4-*C*$_2$**.

The molecule was fully characterized by multinuclear (^{1}H and ^{13}C) NMR spectrosocopy, infrared spectroscopy and single crystal X-ray diffraction. The benzene-d_6 ^{1}H and ^{13}C NMR spectra of **4-(^{t}BuNCO)$_2$** exhibit the number of peaks consistent with formation of a single, C_2-symmetric product. Diagnostic bands at 1673 and 1647 cm^{-1} were observed in the solid-state (KBr) infrared spectrum. The identity of the preferred diastereomers was established by X-ray diffraction. A representations of the (*S*, *S*) enantiomer is presented in Figure 3.20, and a representation of the (*R*, *R*) enantiomer is reported in Appendix C. Selected bond distances and angles of this complex are given in Table 3.1. The crystallographic data are consistent with the solution NMR spectroscopic studies and establish formation of a C_2-symmetric product arising from cycloaddition of the C=O portion of the heterocumulene. Key features are the elongated C-N bonds and contracted C-O bonds in the oxamidate core in comparison to the parent oxamidide, **4-*C*$_2$**, consistent with increased C-N single bond and C=O double bond character. The stereochemistry of the starting hafnocene is preserved in the cycloaddition product, placing the *tert*-butyl groups of the isocyanate groups *syn* to the *tert*-butyl substituents on the cyclopentadienyl ligand. The newly formed core maintains a nearly planar configuration, and the hafnocene subunits are slightly twisted with respect to each other with a dihedral angle of 1.7°.

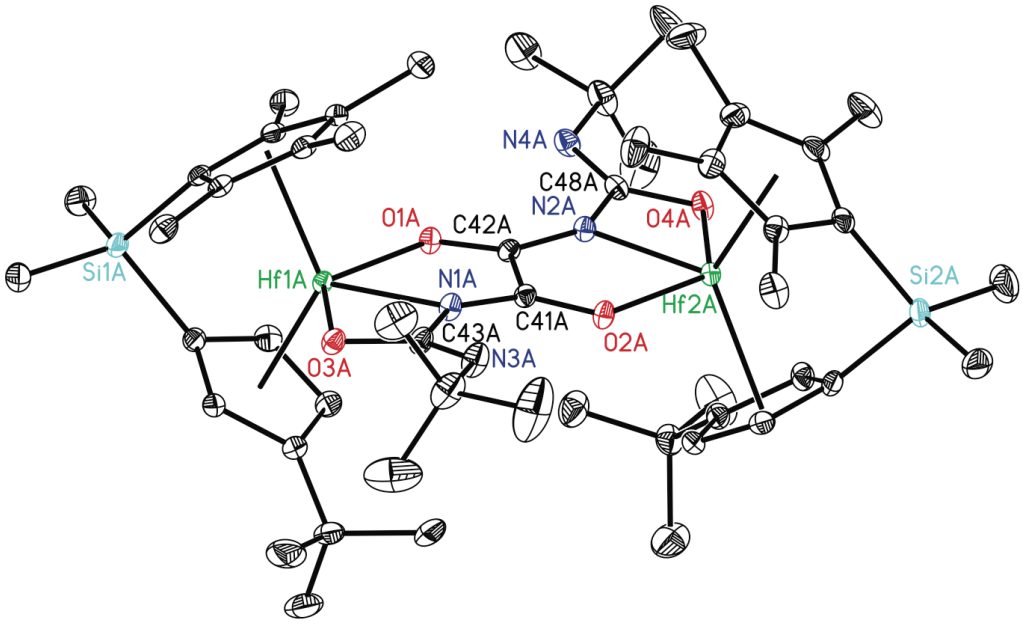

Figure 3.20. Molecular structure of the (*S*, *S*) enantiomer of **4-(^{t}BuNCO)$_2$** at 30% probability ellipsoids. Hydrogen atoms omitted for clarity.

The clean and facile cycloaddition of ^{t}BuNCO to **4-*C*$_2$** prompted exploration of related chemistry with carbon dioxide. Our laboratory has previously reported dinitrogen functionalization with CO_2 to yield various dicarboxylated metallocene hydrazide complexes. For $[(\eta^5\text{-}C_5Me_4H)_2Hf]_2(\mu_2,\eta^2,\eta^2\text{-}N_2)$,[48] an 85:15 mixture of *N*, *N*- and *N*, *N*'- insertion products was obtained, while for the *ansa*-zirconocene, $[Me_2Si(\eta^5\text{-}C_5Me_4)(\eta^5\text{-}C_5H_3\text{-}3\text{-}^t\text{Bu})Zr]_2(\mu_2,\eta^2,\eta^2\text{-}N_2)$, exclusive *N*, *N*'-insertion was observed.[49] In each case the hydrazide cores could be further elaborated by the addition of the appropriate electrophile to yield various dicarboxylated hydrazines. This work will be discussed at length in Chapter 4 of this thesis.[50]

Addition of 2 equivalents of CO_2 gas to a frozen toluene solution of **4-*C*$_2$**, followed by warming to ambient temperature and stirring for 1 h, produced a yellow solution from which a yellow solid identified as **4-(CO$_2$)$_2$** was isolated in 88% yield (Figure 3.21). The benzene-d_6 ^{1}H and ^{13}C NMR spectra exhibit the number of peaks

consistent with formation of a single diastereomers of a C_2-symmetric product. Isotopic labeling with both ^{13}CO and $^{13}CO_2$ gases produced multiplets in the ^{13}C NMR spectrum arising from an AA'XX' spin system centered at 163.18 and 150.54 ppm with $^2J_{CC} = {}^3J_{CC} = 1.5$ Hz,[51] confirming CO_2 incorporation (Figure 3.22).

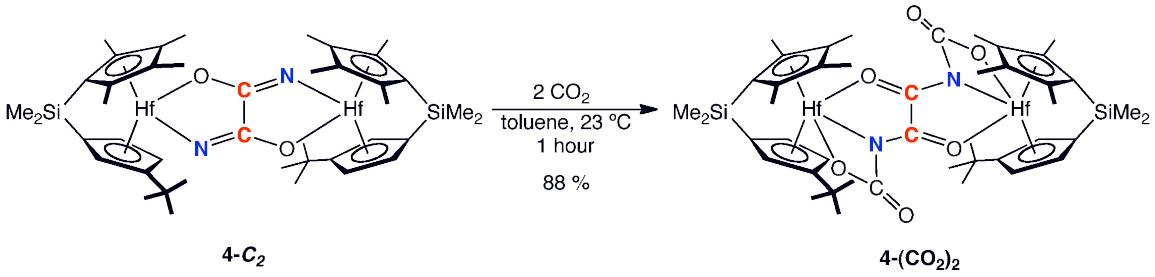

Figure 3.21. Addition of CO_2 to **4-*C*$_2$**.

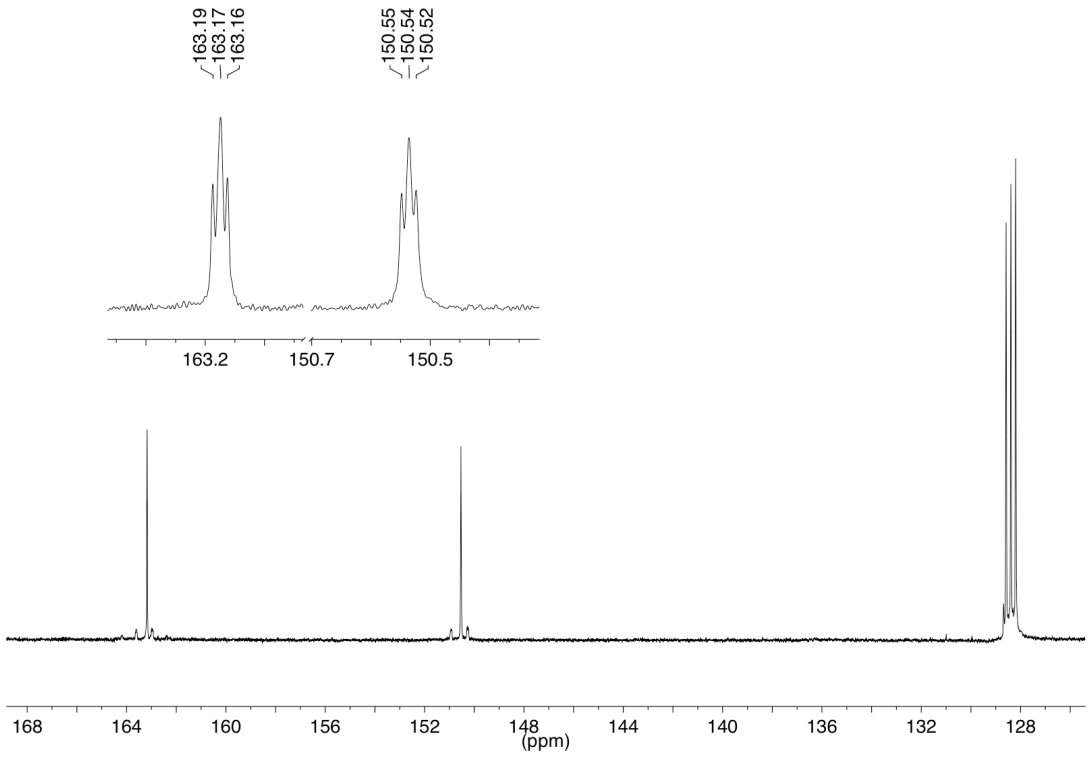

Figure 3.22. Benzene-d_6 ^{13}C NMR spectrum of **4-$^{13}C_2$-($^{13}CO_2$)$_2$**.

Single crystals suitable for X-ray diffraction were obtained and a representation of the (*S*, *S*) enantiomer in the solid-state is presented in Figure 3.23. A representation of the (*R*,*R*) enantiomer is reported in Appendix C. Selected metrical parameters are reported in Table 3.1. Similar to **4-(^{t}BuNCO)$_2$**, the crystallographic data establish cycloaddition of two molecules of CO_2 across the Hf-N bonds in the starting oxamidide with concomitant formation of new N-C and Hf-O bonds. The metrical parameters for **4-(CO$_2$)$_2$** demonstrate that in the solid state the compound exhibits C-N elongation and C=O contraction similar to that observed with **4-(^{t}BuNCO)$_2$**. The core is nearly planar and the dihedral angle between the hafnocene subunits is 3.0°.

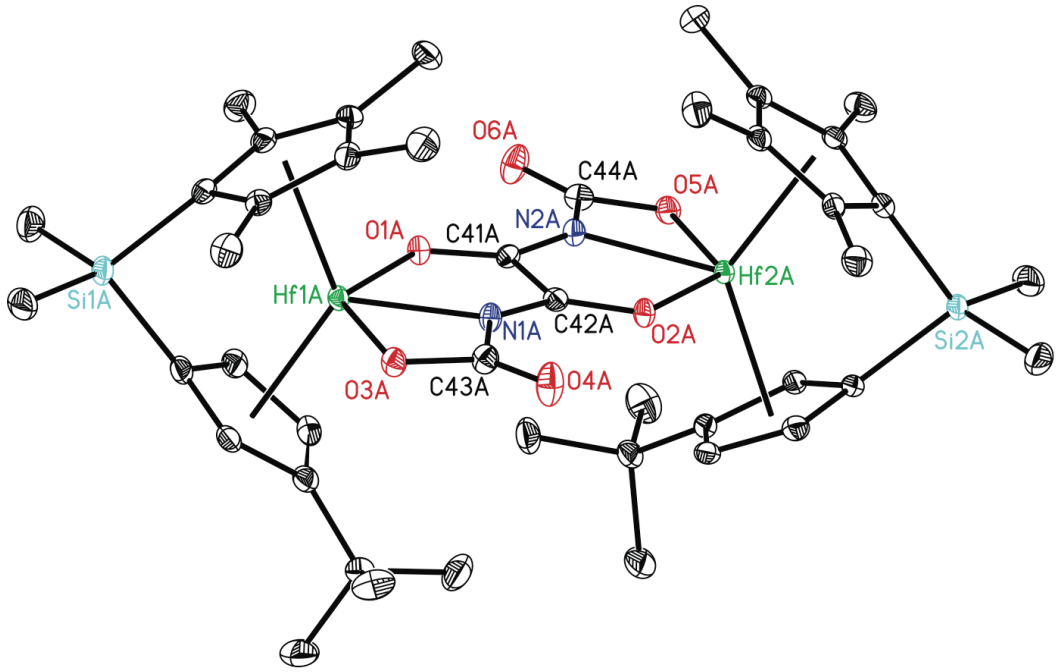

Figure 3.23. Molecular structure of the (*S*, *S*) enantiomer of **4-(CO$_2$)$_2$** at 30% probability ellipsoids. Hydrogen atoms omitted for clarity.

The cycloaddition reactivity of the hafnocene oxamidide complex with carbon dioxide contrasts the CO_2 insertion chemistry observed from direct carboxylation of the hafnocene and zirconocene N_2 compounds.[48,49] Perhaps most notably, the synthesis of **4-(CO_2)$_2$** demonstrates that an organic ligand can be synthesized from three typically inert and abundant small molecules: N_2, CO, and CO_2. Unfortunately, attempts to liberate the functionalized core from the molecule by either protonolysis or the addition of various electrophiles were unsuccessful. Only oxamide and free CO_2 were observed spectroscopically in these experiments, suggesting decarboxylation occurs rapidly either during or following release of the oxamidate core.

Oxidative C-C cleavage of hafnocene oxamidides with iodine. In addition to heterocumulenes, the reactivity of the hafnocene oxamidide complexes with iodine was also explored. Treatment of a toluene solution of **2** with 1 equivalent of I_2 resulted in oxidative cleavage of the oxamidide C-C bond to form the monomeric iodo hafnocene isocyanate product, **2-(I)(NCO)** (Figure 3.24). Due to complications arising from the concomitant formation of an unidentified insoluble byproduct, as well as the formation of small amounts of the corresponding diiodide complex (**2-I_2**), the yield of this reaction was quite low (22%). Nevertheless, full characterization of **2-(I)(NCO)** was accomplished with multinuclear (^{1}H, ^{13}C, ^{15}N) NMR and infrared spectroscopies. A diagnostic chemical shifts and splitting of the isocyanate resonance for the isotopically enriched species, **2-(I)(^{15}N^{13}CO)**, was observed in the ^{13}C NMR spectrum at 136.41 ppm ($^1J_{CN}$ = 32.6 Hz). The isocyanate functionality also exhibits a diagnostic stretch at 2220 cm^{-1} in the solid state (KBr) infrared spectrum. The formation of **2-(I)(NCO)** was also confirmed by comparison to a sample independently synthesized from the reaction of (η^5-$C_5Me_4H)_2HfI_2$ (**2-I_2**) with 1 equiv AgOCN (Figure 3.24) at 80 °C in THF for several days.

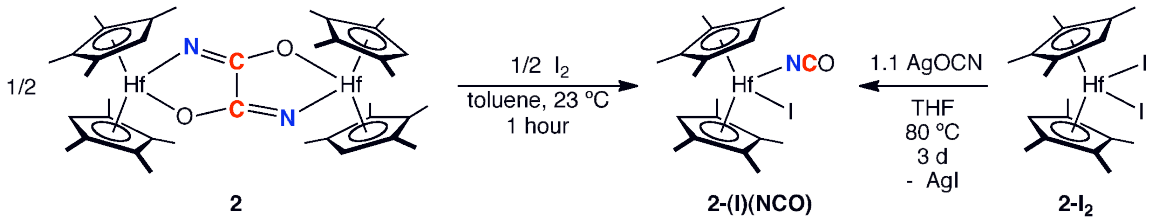

Figure 3.24. Formation of **2-(I)(NCO)** from the addition of iodine to **2** and from independent synthesis.

Oxidative C-C cleavage was also observed in the case of the *ansa*-hafnocene oxamidide complex, **4**. Addition of 1 equiv of I_2 to a toluene solution of **4** (either isomer or a mixture of C_1 and C_2 isomers) yielded a single new C_1-symmetric product, identified as the monomeric iodo *ansa*-hafnocene isocyanate, **4-(I)(NCO)**, as a pale yellow solid (Figure 3.25). Fortunately, in this case the reaction was very clean and the yield was not diminished due to the formation of insoluble byproducts. Only small quantities (< 5%) of the corresponding diiodide complex, **4-I_2**, were observed, which could be separated by recrystallization.

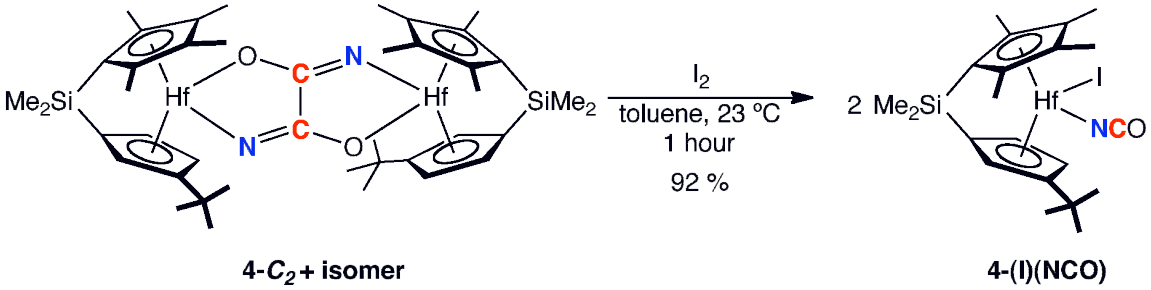

Figure 3.25. Addition of iodine to **4**.

The presence of a terminal isocyanate ligand formed from oxidative C-C cleavage of the oxamidide core was established by a combination of IR spectroscopy, multinuclear NMR experiments, and X-ray diffraction. The solid-state infrared

spectrum (KBR) exhibits a strong band centered at 2229 cm^{-1}, diagnostic of a hafnocene terminal isocyanate.[16,20] The ^{13}C NMR spectrum of **4-(I)(N^{13}CO)** presented in Figure 3.26 exhibits a broad peak centered at 136.81 ppm due to broadening from the quadrupolar ^{14}N nucleus. In the ^{15}N-labeled isotopologue, **4-(I)(^{15}N^{13}CO)**, this peak splits into a well-resolved doublet ($^{1}J_{NC}$ = 33.0 Hz), confirming the presence of an N-C bond assembled from N_2 and CO.

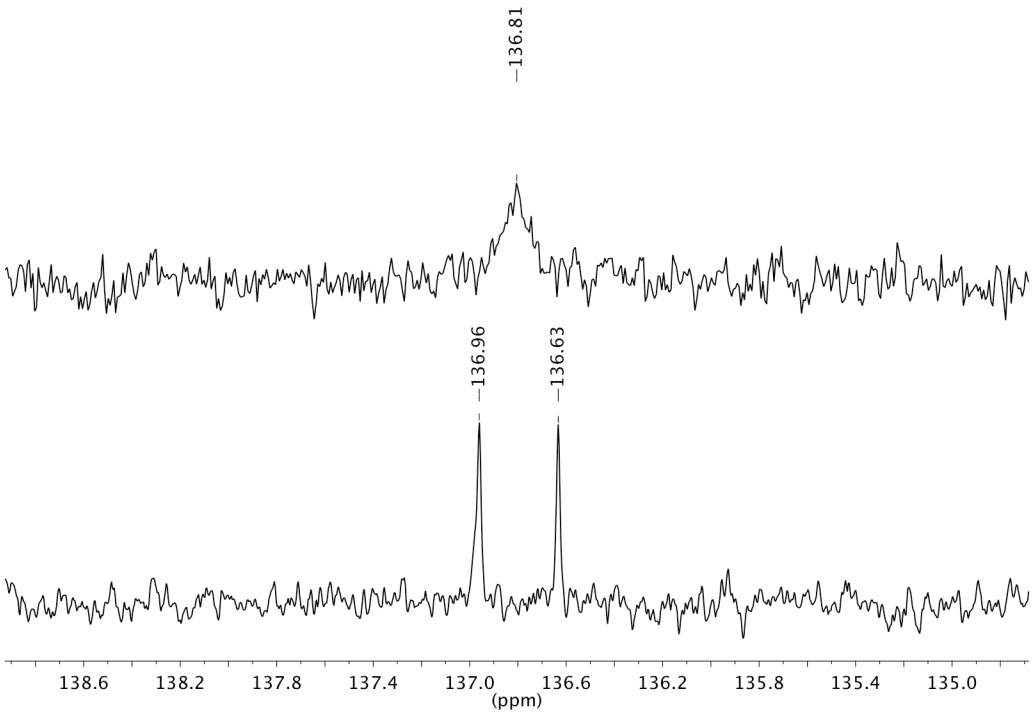

Figure 3.26. Isocyanate region of the ^{13}C NMR spectrum of **4-(I)(N^{13}CO)** (top) and **4-(I)(^{15}N^{13}CO)** (bottom) in benzene-d_6.

The identity of the observed diastereomer was confirmed by single-crystal X-ray diffraction. A representation of the (*S*) enantiomer is presented in Figure 3.27 and a representation of the (*R*) enantiomer is reported in Appendix C. The crystallographic data confirm the formation of the terminal isocyanate *syn* to the *tert*-

butyl ligand. The distances and angle for the terminal hafnocene isocyanate ligand are statistically indistinguishable from the corresponding values in the bimetallic hafnocene μ-imide isocyanate compound, and comparable to those in related hafnium isocyanate complexes, discussed in the previous chapter.[34] As with **2-(I)(NCO)**, independent synthesis of **4-(I)(NCO)** was also achieved by stirring a THF slurry of **4-I_2** and AgOCN at 80 °C for 3 days. Analysis of the product by ^{1}H and ^{13}C NMR spectroscopy established formation of the same diastereomer as from C-C bond cleavage of the C_1- and C_2- symmetric *ansa*-hafnocene oxamidides.

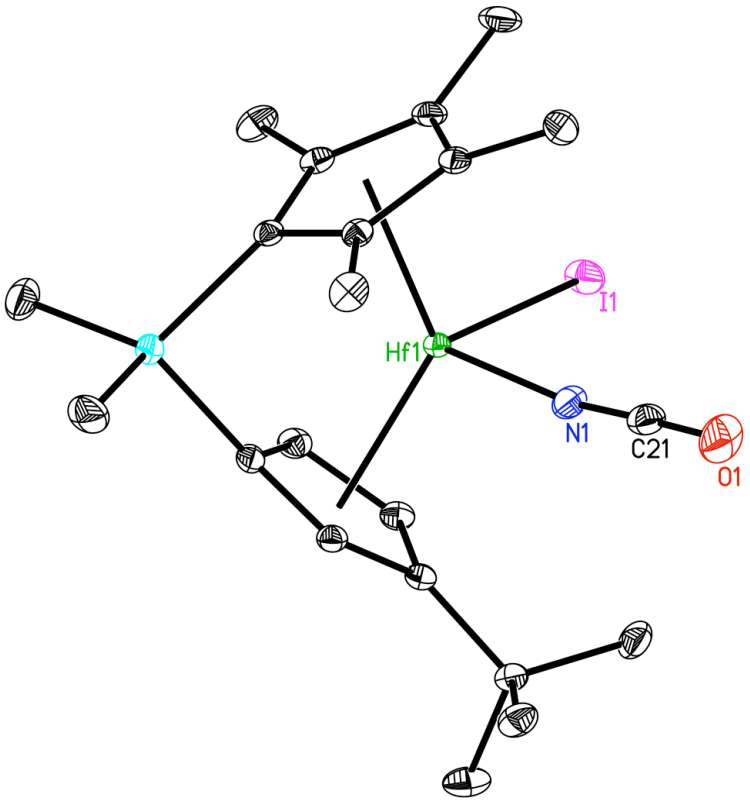

Figure 3.27. Molecular structure of the *S* enantiomer of **4-(I)(NCO)** at 30% probability ellipsoids. Hydrogen atoms omitted for clarity.

Conclusions

Methods for the functionalization of hafnocene oxamidide cores, prepared from CO-induced N_2 bond cleavage, were discovered that exploit the nucleophilicity and basicity of the hafnium-nitrogen bonds. DFT investigations into the nature of the Hf-N bonding in the oxamidide complexes provided a general guide into reactivity studies and established Hf-N multiple bond character that might be exploited by cycloaddition reactions, as well as nucleophilic nitrogen atoms that could facilitate functionalization with the appropriate polar substrates. For **2**, sequential 1,2-addition of alkyl halides was observed, resulting in the synthesis of, following protonolysis, free *N*, *N*'-disubstituted oxamides that are useful precursors for the preparation of *N*, *N*'-diamines, *N*-heterocyclic carbenes, and various heterocycles. Given the availability of ^{13}CO and $^{15}N_2$, isotopically labeled variants of these molecules are also synthetically accessible. In addition to alkyl halides, elaboration of the hafnocene oxamidides was also accomplished with primary and secondary silanes and terminal alkynes. For the *ansa*-hafnocene, **4**, cycloaddition of heterocumulenes such as ^{t}BuNCO and CO_2 resulted in additional N-C bond assembly with concomitant formation of hafnium-oxygen bonds. The latter functionalization reaction demonstrates that organic molecules, in the form of a coordinated ligand, can be synthesized from three abundant and often inert small molecule feedstocks: N_2, CO, and CO_2.

Experimental Section

General Considerations. All air- and moisture-sensitive manipulations were carried out using standard high vacuum line, Schlenk or cannula techniques or in an M. Braun inert atmosphere drybox containing an atmosphere of purified nitrogen. The M. Braun drybox was equipped with a cold well designed for freezing samples in liquid nitrogen. Solvents for air- and moisture-sensitive manipulations were dried and deoxygenated using literature procedures.[52] Toluene, benzene, pentane and heptane were further dried by distillation from "titanocene".[53] Deuterated solvents for NMR spectroscopy were distilled from sodium metal under an atmosphere of argon and stored over 4 Å molecular sieves. Argon and hydrogen gas were purchased from Airgas Incorporated and passed through a column containing manganese oxide on vermiculite and 4 Å molecular sieves before admission to the high vacuum line. Carbon dioxide was also dried over 4 Å molecular sieves before admission to the high vacuum line.

^{1}H NMR spectra were recorded on a Varian Inova 400 Spectrometer operating at 399.860 MHz. All chemical shifts are reported relative to $SiMe_4$ using ^{1}H (residual) chemical shifts of the solvent as a secondary standard. ^{2}H, ^{13}C, ^{29}Si, and ^{15}N NMR spectra were recorded on a Varian Inova 500 Spectrometer operating at 76.848, 125.716, 161.83, 99.320 and 50.663 MHz, respectively. ^{2}H, ^{29}Si, and ^{13}C chemical shifts are reported relative to $SiMe_4$ using chemical shifts of the solvent as a secondary standard where applicable. ^{15}N chemical shifts are reported relative liquid to NH_3 using an external standard. The C-C coupling constants for **4-$(CO_2)_2$** in the main text are reported as an average of $^{2}J_{C\text{-}C}$ and $^{3}J_{C\text{-}C}$; these AA'XX' spin systems appear as effective triplets by ^{13}C NMR spectroscopy and this lack of detail in the spectra prevented accurate simulation.

Mass spectra were acquired using a JEOL GCMate II mass spectrometer operating at 500 (LRMS) resolving power (20% FWHM) in positive ion mode and an electron ionization (EI) potential of 70 eV. Samples were introduced via a GC inlet using an Agilent HP 6890N GC equipped with a 30 m (0.25 mm i.d.) HP-5ms capillary GC column. The carrier gas is helium with a flow rate of 1 mL/min. Samples were introduced into the GC using a split/splitless injector at 230 ºC with a split ratio of 50:1. Infrared spectroscopy was conducted on a Mattson RS-10500 Research Series FT-IR spectrometer calibrated with a polystyrene standard. Elemental analyses were performed at Robertson Microlit Laboratories, Inc., in Madison, NJ.

Computational Details. All DFT calculations were performed with the ORCA program package.[54] The geometry optimizations of the complexes and single-point calculations on the optimized geometries were carried out at the B3LYP level[55,56,57] of DFT. Relativistic effects were accounted for by including the zeroth-order regular approximation (ZORA).[58,59,60,61] The def2-TZVP(-f) basis set in the scalar relativistic recontraction reported by Neese et al. (segmented all-electron relativistic basis sets, SARC) was applied.[62,63] For all elements up to bromine, the SARC basis sets are simply scalar relativistic recontractions of the basis sets developed by the Karlsruhe group,[64,65] while for heavier elements, the primitives and contraction patterns were designed in refs 60 and 61. The Coulomb fitting basis set of Weigend[66] was used in uncontracted form in all calculations. The RIJCOSX[67,68,69] approximation was used to accelerate the calculations.

Preparation of $[(\eta^5\text{-}C_5Me_4H)_2Hf]_2(CCPh)_2((NH)_2C_2O_2)$ (2-$(PhCCH)_2$). A J. Young NMR tube was charged with 0.015 g (0.016 mmol) of **2** and approximately 0.5 mL benzene-d_6. A slight excess of phenylacetylene (2.2 equivalents, 0.035 mmol) was added via syringe and the resulting reaction mixture was shaken and heated at 65 ºC

for 1 h. After this time, complete conversion to **2-(PhCCH)$_2$** was observed as judged by ^{1}H NMR spectroscopy. ^{1}H NMR (benzene-d_6): δ = 1.75 (s, 12H, Cp*Me*$_4$H), 2.06 (s, 12H, Cp*Me*$_4$H), 2.10 (s, 12H, Cp*Me*$_4$H), 2.12 (s, 12H, Cp*Me*$_4$H), 5.09 (s, 4H, CpMe$_4$*H*), 6.66 (s, 2H, N*H*), 7.10-7.15 (m, 6H, CC*Ph*), 7.55-7.60 (m, 4H, CC*Ph*). {^{1}H} ^{13}C NMR (benzene-d_6): δ = 12.38, 13.14, 13.94, 14.48 (Cp*Me*), 95.01 (*CC*Ph), 110.29, 114.47, 114.90, 117.42, 120.75, 122.12, 126.25, 128.27, 128.88, 131.49, 132.73 (*Cp* and CC*Ph*), 171.34 ((NH)$_2$*C*$_2$O$_2$), 1 *Cp*/CC*Ph* not found. IR (KBr): ν = 2087 cm^{-1} (CC), 3371 cm^{-1} (NH).

Preparation of [(η^5-C$_5$Me$_4$H)$_2$Hf]$_2$(I)(N(CH$_3$)NC$_2$O$_2$) 2-(CH$_3$I). In a drybox a 100 mL round bottom flask was charged with 0.100 g (0.11 mmol) of **2** and 20 mL of toluene. A 180º needle valve was attached and the contents of the assembly were degassed on a high vacuum line. While frozen at liquid nitrogen temperature, 23.9 torr of CH_3I was added via a 100.1 mL calibrated gas bulb. The contents of the flask were warmed to ambient temperature and stirred for one hour. The excess methyl iodide and solvent were removed in vacuo and the flask transferred into the dry box. The resulting yellow oil was washed with cold pentane and furnished 0.093 g (81 %) of a yellow solid identified as **2-(N$_2$C$_2$O$_2$)(CH$_3$I)**. ^{1}H NMR (benzene-d_6): δ = 1.66 (s, 6H, Cp*Me*$_4$H), 1.67 (s, 6H, Cp*Me*$_4$H), 1.73 (s, 6H, Cp*Me*$_4$H), 1.95 (s, 6H, Cp*Me*$_4$H), 2.06 (s, 6H, Cp*Me*$_4$H), 2.22 (s, 6H, Cp*Me*$_4$H), 2.44 (s, 6H, Cp*Me*$_4$H), 2.48 (s, 6H, Cp*Me*$_4$H), 2.49 (s, 3H, N*CH$_3$*), 5.50 (s, 2H, CpMe$_4$*H*), 5.55 (s, 2H, CpMe$_4$*H*). {^{1}H}^{13}C NMR (benzene-d_6): δ = 11.24 (Cp*Me*), 12.18 (Cp*Me*), 13.01 (Cp*Me*), 13.26 (Cp*Me*), 13.36 (Cp*Me*), 14.75 (Cp*Me*), 14.88 (Cp*Me*), 15.96 (Cp*Me*), 31.58 (N*CH$_3$*) ($^1J_{CN}$ = 5.3 Hz, $^2J_{CC}$ = 3.0 Hz, $^3J_{CC}$ = 1.8 Hz), 109.60, 112.29, 114.61, 117.37, 118.19, 120.85, 123.07, 123.56, 126.95 (*Cp*), 161.12 (N(CH$_3$)(*C*O)NCO), 173.31 (N(CH$_3$)(CO)N*C*O), ($^1J_{CC}$ = 75.3 Hz), (1 *Cp* resonance not located). IR (KBr): ν = 1618 cm^{-1} (C=N).

Preparation of ((η^5-$C_5Me_4H)_2Hf)_2(I)_2(N_2(CH_3)_2C_2O_2$) (2-($CH_3I)_2$). In a drybox, a thick walled glass vessel was charged with 0.120 g (0.13 mmol) of **2** and approximately 20 mL of toluene. On a high vacuum line, the vessel was degassed and 59.8 torr of methyl iodide was added via a 100.1 mL calibrated gas bulb. The contents of the vessel were thawed and stirred at 65 ºC for 16 hours. After this time, the excess methyl iodide and solvent were removed *in vacuo*. The vessel was transferred into the dry box and the resulting yellow oil washed with cold pentane and furnished 0.144 g (92 %) of a yellow solid identified as **2-($CH_3I)_2$**. Anal. Calcd for $C_{40}H_{58}O_2N_2I_2Hf_2$: C, 39.71; H, 4.83; N, 2.32. Found: C, 39.98; H, 4.90; N, 2.29. ^{1}H NMR (benzene-d_6): δ = 1.55 (s, 12H, CpMe_4H), 1.86 (s, 12H, CpMe_4H), 2.12 (s, 12H, CpMe_4H), 2.15 (s, 12H, CpMe_4H), 3.58 (s, 6H, NCH_3), 5.40 (s, 4H, CpMe$_4H$). {^{1}H}^{13}C NMR (benzene-d_6): δ = 12.14 (Cp*Me*), 14.52 (Cp*Me*), 15.12 (Cp*Me*), 16.32 (Cp*Me*), 45.50 (NCH_3) ($^1J_{CN}$ = 4.3 Hz), 112.62, 116.07, 120.08, 122.43, 127.50 (*Cp*), 167.94 ($N_2(CH_3)_2C_2O_2$). IR (KBr): ν = 1606 cm^{-1} (C=N).

Spectroscopic characterization of [(η^5-$C_5Me_4H)_2Hf]_2(I)(N(CH_2CH_3)NC_2O_2$) (2-$CH_3CH_2I$). This compound was prepared in a similar manner to **2-(CH_3I)** using 0.010 g (0.011 mmol) of **2** and 0.055 mmol of ethyl iodide admitted *via* calibrated gas bulb, and required 1 h for complete conversion to **2-(CH_3CH_2I)**. ^{1}H NMR (benzene-d_6): δ = 1.39 (t, 3H, NCH_2CH_3), 1.76 (s, 6H, CpMe_4H), 1.77 (s, 6H, CpMe_4H), 1.78 (s, 6H, CpMe_4H), 1.98 (s, 6H, CpMe_4H), 2.05 (s, 6H, CpMe_4H), 2.22 (s, 6H, CpMe_4H), 2.40 (s, 6H, CpMe_4H), 2.45 (s, 6H, CpMe_4H), 2.93 (q, 2H, NCH_2CH_3), 5.53 (s, 2H, CpMe$_4H$), 5.55 (s, 2H, CpMe$_4H$). {^{1}H}^{13}C NMR (benzene-d_6): δ = 11.73 (NCH_2CH_3), 12.54 (Cp*Me*), 13.16 (Cp*Me*), 13.33 (Cp*Me*), 13.34 (Cp*Me*), 13.59 (Cp*Me*), 14.66 (Cp*Me*), 14.74 (Cp*Me*), 14.85 (Cp*Me*), 39.97 (NCH_2CH_3), 109.71, 112.71, 114.69,

117.32, 118.96, 120.21, 123.29, 123.64, 126.78, 127.00 (*Cp*), (N(CH_2CH_3)(*C*O)N*C*O resonances not located). IR (KBr): ν = 1618 cm^{-1} (C=N).

Spectroscopic characterization of [(η^5-$C_5Me_4H)_2Hf]_2(Br)_2(N_2(CH_2CH_3)_2C_2O_2$) (2-($CH_3CH_2Br)_2$). This molecule was prepared in a similar manner to **2-($CH_3I)_2$** with 0.010 g (0.011 mmol) of **2** and 0.11 mmol of ethyl bromide added via calibrated gas bulb on a vacuum line. After 24 hours at 65 ºC complete conversion to **2-($CH_3CH_2Br)_2$** was observed by NMR spectroscopy. ^{1}H NMR (benzene-d_6): δ = 1.33 (t, 6H, NCH_2CH_3), 1.72 (s, 12H, CpMe_4H), 2.03 (s, 12H, CpMe_4H), 2.07 (s, 12H, CpMe_4H), 2.11 (s, 12H, CpMe_4H), 4.14 (q, 6H, NCH_2CH_3), 5.22 (s, 4H, $CpMe_4H$). {^{1}H}^{13}C NMR (benzene-d_6): δ = 11.48 (NCH_2CH_3), 12.87 (Cp*Me*), 13.76 (Cp*Me*), 14.39 (Cp*Me*), 14.78 (Cp*Me*), 58.64 (NCH_2CH_3), 113.34, 114.75, 120.75, 122.70, 125.95 (*Cp*), 169.25 ($N_2(CH_2CH_3)_2C_2O_2$). IR (KBr): ν = 1586, 1621 cm^{-1} (C=N).

Spectroscopic characterization of [(η^5-$C_5Me_4H)_2Hf]_2(Br)(N(CH_2Ph)NC_2O_2$) (2-$PhCH_2Br$). This compound was prepared in a similar manner to **2-(CH_3I)** using 0.010 g (0.011 mmol) of **2** and 6.5 mL (0.055 mmol) of benzyl bromide and required 1 h for complete conversion to **2-($PhCH_2Br$)**. ^{1}H NMR (benzene-d_6): δ = 1.60 (s, 3H, CpMe_4H), 1.67 (s, 3H, CpMe_4H), 1.70 (s, 3H, CpMe_4H), 1.71 (s, 3H, CpMe_4H), 1.79 (s, 3H, CpMe_4H), 1.83 (s, 3H, CpMe_4H), 1.96 (s, 3H, CpMe_4H), 1.97 (s, 3H, CpMe_4H), 2.06 (s, 3H, CpMe_4H), 2.07 (s, 3H, CpMe_4H), 2.09 (s, 3H, CpMe_4H), 2.25 (s, 3H, CpMe_4H), 2.29 (s, 3H, CpMe_4H), 2.31 (s, 3H, CpMe_4H), 2.33 (s, 3H, CpMe_4H), 2.49 (s, 3H, CpMe_4H), 4.39 (s, 1H, NCH_2Ph), 4.92 (s, 1H, NCH_2Ph), 5.25 (s, 1H, $CpMe_4H$), 5.55 (s, 1H, $CpMe_4H$), 5.59 (s, 2H, $CpMe_4H$), 7.07-7.29, 7.56 (m, 5H, NCH_2Ph). {^{1}H}^{13}C NMR (benzene-d_6): δ = 11.25 (Cp*Me*), 11.99 (Cp*Me*), 12.98 (Cp*Me*), 13.00 (Cp*Me*), 13.37 (Cp*Me*), 13.82 (Cp*Me*), 14.10 (Cp*Me*), 14.61 (Cp*Me*),

31.55 (N*CH*$_2$Ph), 33.70 (N*CH*$_3$), 109.28, 112.22, 114.59, 117.20, 118.21, 120.71, 122.09, 122.98, 123.99, 126.87, 126.89, 129.59, 140.05, 138.55 (*Cp,* NCH$_2$*Ph*), (N(CH$_2$Ph)(*C*O)) and (N*C*O) not observed. IR (KBr): ν = 1624, 1653 cm^{-1} (C=N).

Spectroscopic characterization of [(η^5-C$_5$Me$_4$H)$_2$Hf]$_2$(I)(Br)(N(CH$_3$)N(CH$_2$Ph)C$_2$O$_2$) (2-(CH$_3$I)(PhCH$_2$Br)). In a drybox, a J. Young NMR tube was charged with 0.010 g (0.009 mmol) of **2-(CH$_3$I)** dissolved in about 0.5 mL of benzene-d_6. While in the box, 5.5 μL (0.045 mmol) of benzyl bromide was added via syringe. The tube was capped, shaken and the progress of the reaction monitored by ^{1}H NMR spectroscopy. Full conversion occurred after 16 h at 65 ºC. ^{1}H NMR (benzene-d_6): δ = 1.67 (s, 6H, Cp*Me*$_4$H), 1.69 (s, 6H, Cp*Me*$_4$H), 1.71 (s, 6H, Cp*Me*$_4$H), 1.94 (s, 6H, Cp*Me*$_4$H), 2.07 (s, 6H, Cp*Me*$_4$H), 2.24 (s, 6H, Cp*Me*$_4$H), 2.31 (s, 6H, Cp*Me*$_4$H), 2.45 (s, 6H, Cp*Me*$_4$H), 2.51 (s, 3H, N*CH*$_3$), 3.89 (s, 3H, N*CH*$_2$Ph), 5.49 (s, 2H, CpMe$_4$*H*), 5.53 (s, 2H, CpMe$_4$*H*), 6.85-7.00 (m, 5H, NCH$_2$*Ph*). {^{1}H}^{13}C NMR (benzene-d_6): δ = 11.25 (Cp*Me*), 11.99 (Cp*Me*), 12.98 (Cp*Me*), 13.00 (Cp*Me*), 13.37 (Cp*Me*), 13.82 (Cp*Me*), 14.10 (Cp*Me*), 14.61 (Cp*Me*), 31.55 (N*CH*$_2$Ph), 33.70 (N*CH*$_3$), 109.28, 112.22, 114.59, 117.20, 118.21, 120.71, 122.09, 122.98, 123.99, 126.87, 126.89, 129.59, 140.05, 138.55 (*Cp,* NCH$_2$*Ph*), (N(CH$_3$)(*C*O) and (N(CH$_2$Ph)(*C*O)) not determined. IR (KBr): ν = 1603, 1621 cm^{-1} (C=N).

Spectroscopic characterization of [(η^5-C$_5$Me$_4$H)$_2$Hf]$_2$(I)(Br)(N(CH$_3$)N(CH$_2$CH$_3$)C$_2$O$_2$) (2-(CH$_3$I)(CH$_3$CH$_2$Br)). This compound was prepared in a similar manner to **2-(CH$_3$I)(PhCH$_2$Br)** using 0.010 g (0.009 mmol) of **2-(CH$_3$I)** and 0.045 mmol of ethyl bromide added via calibrated gas bulb on a vacuum line, and full conversion to **2-(CH$_3$I)(CH$_3$CH$_2$Br)** was observed

after 48 h at 23 ºC. ^{1}H NMR (benzene-d_6): δ = 1.58 (t, 3H, NCH$_2$*CH$_3$*), 1.67 (s, 6H, Cp*Me*$_4$H), 1.69 (s, 6H, Cp*Me*$_4$H), 1.71 (s, 6H, Cp*Me*$_4$H), 1.94 (s, 6H, Cp*Me*$_4$H), 2.07 (s, 6H, Cp*Me*$_4$H), 2.24 (s, 6H, Cp*Me*$_4$H), 2.32 (s, 6H, Cp*Me*$_4$H), 2.46 (s, 6H, Cp*Me*$_4$H), 2.49 (q, 2H, NC*H$_2$*CH$_3$), 2.51 (s, 3H, NC*H$_3$*), 2.93 (q, 2H, N*CH$_2$*CH$_3$), 5.49 (s, 2H, CpMe$_4$*H*), 5.53 (s, 2H, CpMe$_4$*H*). {^{1}H}^{13}C NMR (benzene-d_6): δ = 11.26 (NCH$_2$*CH$_3$*), 12.00 (Cp*Me*), 13.00 (Cp*Me*), 13.01 (Cp*Me*), 13.37 (Cp*Me*), 13.63 (Cp*Me*), 13.82 (Cp*Me*), 14.11 (Cp*Me*), 14.61 (Cp*Me*), 31.56 (NC*H$_3$*) 40.68 (N*CH$_2$*CH$_3$), 109.29, 112.23, 114.61, 117.21, 118.23, 120.71, 122.98, 123.99, 126.87 (*Cp*), 1 *Cp*, N(CH$_2$CH$_3$)(*C*O) and (N(CH$_3$)*C*O) not determined. IR (KBr): ν = 1605 cm^{-1}, 1623 cm^{-1}(C=N).

Representative oxamidate protonolysis of 2-(CH$_3$I)$_2$. Treatment of the hafnium oxamidide compound **2-(CH$_3$I)$_2$** (0.075 g, 0.062 mmol) with 10 equivalents of HCl (as a dioxane solution) admitted via calibrated gas bulb resulted in liberation of dimethyloxamide in high yield (>95% by ^{1}H NMR spectroscopy), along with formation of 2 equivalents of **2-Cl$_2$**. The product mixture was washed several times with diethyl ether, affording 0.005 g (71%) of pure *N*, *N'*-dimethyloxamide as a white solid, confirmed spectroscopically by comparison to an independently prepared sample (*vide infra*). Similar results were achieved performing the protonolysis with ethanol (10 equiv added via syringe) instead of HCl.

Spectroscopic characterization of *N*-alkyl and *N*, *N'*-dialkyloxamides. The identities of *N*-methyl-*N'*-benzyloxamide,[70] *N*, *N'*-diethyloxamide,[71] and methyloxamide[72] were confirmed by comparison to their previously reported spectroscopic parameters.

Independent synthesis of *N*, *N'*-dimethyloxamide.[73] A 500 mL 3-neck round bottom flask fitted with an addition funnel was charged with 200 mL of THF, added via cannula on a Schlenk line. The flask was cooled to -78 ºC, the headspace was evacuated, and triethylamine (~0.01 mol) was admitted via vacuum transfer, followed by excess methylamine (~0.12 mol). The flask was warmed to 0 ºC and, with stirring, oxalyl chloride (5.2 mL, 0.05 mol) was added dropwise through an addition funnel, causing vigorous generation of HCl. The reaction mixture was slowly warmed to room temperature and stirred for 24 h. After this time the solvent volume was reduced and the insoluble white material was filtered and recrystallized from ethanol, furnishing ~5 g (85%) pure *N*, *N'*-dimethyloxamide. ^{1}H NMR (dimethylsulfoxide-d_6): δ = 2.66 (d, 6H, CH_3) ($^2J_{HH}$=4.9 Hz), 8.67 (br s, 2H, NH). $\{^1H\}^{13}$C NMR (dimethylsulfoxide-d_6): δ = 25.79 (CH$_3$), 160.47 (N$_2C_2$O$_2$).

Spectroscopic characterization of ethyloxamide. ^{1}H NMR (dimethylsulfoxide-d_6): δ = 1.03 (t, 3H, CH_3CH$_2$N) ($^3J_{HH}$=7.2 Hz), 3.13 (m, 2H, CH$_3$CH_2N), 7.74 (br s, 1H, NH_2), 8.02 (br s, 1H, NH_2), 8.70 (br s, 1H, CH$_3$CH$_2$NH). $\{^1H\}^{13}$C NMR (dimethylsulfoxide-d_6): δ = 14.41 (CH$_3$CH$_2$N), 33.66 (CH$_3$$CH_2$N), 159.99, 162.29 (N$_2C_2O_2$).

Spectroscopic characterization of benzyloxamide. ^{1}H NMR (dimethylsulfoxide-d_6): δ = 4.31 (d, 2H, PhCH_2N), 7.2-7.4 (m, 5H, PhCH$_2$N), 7.81 (br s, 1H, NH_2), 8.08 (br s, 1H, NH_2), 9.24 (br s, 1H, PhCH$_2$NH). $\{^1H\}^{13}$C NMR (dimethylsulfoxide-d_6): δ = 42.33 (PhCH$_2$N), 118.14, 120.29, 120.35 (PhCH$_2$N), 160.10, 162.16 (N$_2C_2$O$_2$).

Preparation of [(η^5-C$_5$Me$_4$H)$_2$Hf]$_2$(H)$_2$((NSiH$_2$Ph)$_2$C$_2$O$_2$) (2-(PhSiH$_3$)$_2$)). In a drybox, a 20 mL scintillation vial was charged with 0.100 g (0.11 mmol) of **2** and

approximately 10 mL of toluene. Via syringe, 2.2 equivalents (0.029 mL, 0.24 mmol) of phenylsilane were added with stirring. Once the addition was complete, the resulting reaction mixture was stirred for one hour at 23 ºC after which time excess phenylsilane and solvent were removed *in vacuo*. The resulting yellow oil was washed with cold pentane furnishing 0.106 g (86 %) of a pale yellow solid identified as **2-($PhSiH_3$)$_2$**. The product was recrystallized from toluene at -35 °C and isolated as pale yellow crystals. Anal. Calcd for $C_{50}H_{68}O_2N_2Si_2Hf_2$: C, 52.57; H, 6.00; N, 2.45. Found: C, 52.36; H, 5.80; N, 2.40. ^{1}H NMR (benzene-d_6): δ = 1.72 (s, 12H, CpMe_4H), 1.84 (s, 12H, CpMe_4H), 2.09 (s, 24H, CpMe_4H), 4.93 (s, 4H, NSiCH_2Ph), 5.81 (s, 4H, CpMe$_4H$), 7.22-7.33 (m, 6H, NSiCH$_2$*Ph*), 8.09 (d, 4H, NSiCH$_2$*Ph*), 9.54 (s, 2H, Hf*H*). {^{1}H}^{13}C NMR (benzene-d_6): δ = 12.25 (Cp*Me*), 12.72 (Cp*Me*), 13.74 (Cp*Me*), 15.19 (Cp*Me*), 107.69, 111.78, 115.57, 118.17, 120.50 (*Cp*), 128.26, 130.49, 136.65, 137.95 (SiH$_2$*Ph*), 175.37 (N$_2$(SiCH$_2$Ph)$_2$*C*$_2$O$_2$). IR (KBr): ν = 1552 cm^{-1} (C=N), 2157 cm^{-1} (SiH$_2$).

Preparation of [(η^5-C_5Me_4H)$_2$Hf]$_2$(H)$_2$((NSiH^{n}Hex)$_2$C$_2$O$_2$) (2-(^{n}HexSiH$_3$)$_2$). A J. Young NMR tube was charged with 0.010 g (0.011 mmol) of **2** approximately 0.5 mL benzene-d_6. A slight excess of *n*-hexylsilane (2.2 equivalents, 0.024 mmol) was added via calibrated gas bulb on a vacuum line and the resulting reaction mixture was shaken resulting in complete conversion to **2-(^{n}HexSiH$_3$)$_2$** as judged by ^{1}H NMR spectroscopy. ^{1}H NMR (benzene-d_6): δ = 0.92 (t, 6H, NSiH$_2$(CH$_2$)$_5$CH_3), 1.34 (m, 4H, NSiH$_2$(CH_2)$_5$CH$_3$), 1.52 (m, 4H, NSiH$_2$(CH_2)$_5$CH$_3$), 1.60 (m, 4H, NSiH$_2$(CH_2)$_5$CH$_3$), 1.72 (s, 12H, CpMe_4H), 2.00 (m, 4H, NSiH$_2$(CH_2)$_5$CH$_3$), 2.06 (s, 12H, CpMe_4H), 2.19 (s, 12H, CpMe_4H), 2.20 (s, 12H, CpMe_4H), 4.96 (s, 4H, CpMe$_4H$), 5.22 (t, 4H, NSiH_2(CH$_2$)$_5$CH$_3$), 9.95 (s, 2H, Hf*H*). {^{1}H} ^{13}C NMR (benzene-d_6): δ = 12.42, 12.78, 13.95, 14.77, 15.28 (SiH$_2$(CH$_2$)$_5$*C*H$_3$, Cp*Me*), 23.37, 25.03, 32.49, 33.44

($SiH_2(CH_2)_5CH_3$), 107.37, 111.92, 115.13, 118.47, 119.80 (*Cp*), 175.32 ($N_2(SiH_2(CH_2)_5CH_3)_2C_2O_2$). IR (KBr): ν = 1560 cm^{-1} (C=N), 2188 cm^{-1} (SiH).

Preparation of [(η^5-$C_5Me_4H)_2Hf]_2(H)_2((NSiHPh_2)_2C_2O_2)$ (2-$(Ph_2SiH_2)_2$). This molecule was prepared in a similar manner to **2-(^{n}HexSiH$_3$)$_2$** with 0.010 g (0.011 mmol) of **2** and 4.4 μL (0.024 mmol) of Ph_2SiH_2. Immediate conversion to **2-(Ph_2SiH_2)$_2$** was observed. ^{1}H NMR (benzene-d_6): δ = 1.72 (s, 12H, CpMe_4H), 1.78 (s, 12H, CpMe_4H), 1.86 (s, 12H, CpMe_4H), 2.11 (s, 12H, CpMe_4H), 4.78 (s, 4H, $CpMe_4H$), 6.47 (s, 2H, NSiHPh$_2$), 7.06-7.34 (m, 12H, NSiHPh_2), 8.15 (m, 8H, NSiHPh_2), 9.80 (s, 2H, HfH). {^{1}H}^{13}C NMR (benzene-d_6): δ = 13.35 (CpMe), 13.40 (CpMe), 14.62 (CpMe), 15.29 (CpMe), 108.14, 110.15, 116.55, 116.60, 121.95 (*Cp*), 130.47, 136.39, 137.92, 139.01 (SiHPh_2) 176.15 ($N_2(SiHPh_2)_2C_2O_2$). IR (KBr): ν = 1567 cm^{-1} (C=N), 2194 cm^{-1} (SiH).

Preparation of [(η^5-$C_5Me_4H)_2Hf)_2(H)(I)((NSiH_2Ph)(NCH_3)C_2O_2)$ (2-(CH_3I)($PhSiH_3$)). In a drybox, a J. Young NMR tube was charged with 0.010 g (0.009 mmol) of **2-(CH_3I)** and approximately 0.5 mL of benzene-d_6 was added. Approximately 1.2 equivalents of $PhSiH_3$ (1.3 μL, 0.011 mmol) were added via syringe and the tube shaken thoroughly. Monitoring the reaction by ^{1}H NMR spectroscopy established complete conversion to **2-(CH_3I)($PhSiH_3$)**. ^{1}H NMR (benzene-d_6): δ = 1.56 (s, 6H, CpMe_4H), 1.74 (s, 6H, CpMe_4H), 1.80 (s, 6H, CpMe_4H), 1.97 (s, 6H, CpMe_4H), 1.99 (s, 6H, CpMe_4H), 2.10 (s, 6H, CpMe_4H), 2.16 (s, 6H, CpMe_4H), 2.23 (s, 6H, CpMe_4H), 3.67 (s, 3H, NCH_3, $^3J_{CH}$ = 4.4 Hz), 4.89 (s, 2H, NSiH_2Ph), 5.41 (s, 2H, $CpMe_4H$), 5.86 (s, 2H, $CpMe_4H$), 7.20-7.40 (m, 3H, $NSiH_2Ph$), 8.10 (m, 2H, $NSiH_2Ph$), 9.38 (s, 1H, HfH). {^{1}H}^{13}C NMR (benzene-d_6): δ = 11.99 (CpMe), 12.01 (CpMe), 13.45 (CpMe), 13.56 (CpMe), 14.96 (CpMe), 15.07

(Cp*Me*), 15.20 (Cp*Me*), 16.13 (Cp*Me*), 46.49 (N*CH*$_3$), 107.34, 111.83, 113.43, 115.36, 115.41, 118.24, 120.29, 121.90, 122.34, 127.23 (*Cp*), 130.65, 136.64, 137.04, 138.07 (NSiH$_2$*Ph*), 170.33, 173.05 ((N(CH$_3$)(*C*O), (N(CH$_2$Ph)(*C*O), $^1J_{CC}$ = 72.5 Hz), 1 Cp not found. IR (KBr): ν = 1558 cm^{-1} (C=N), 2119 cm^{-1} (SiH).

Preparation of ([Me$_2$Si(η^5-C$_5$Me$_4$)(η^5-C$_5$H$_3$-3-^{t}Bu)]Hf)$_2$(^{t}BuNCO)$_2$(N$_2$C$_2$O$_2$) (4-(^{t}BuNCO)$_2$). In a drybox, a 20 mL scintillation vial was charged with 0.090 g (0.087 mmol) of **4-*C*$_2$** in approximately 10 mL of toluene. An excess of *tert*-butylisocyanate (50 μL, 0.44 mmol) was added via syringe and the reaction was stirred for 2 hours at ambient temperature. After this time, the solvent and excess isocyanates were removed in vacuo and the resulting orange oil was washed with pentane to yield a pale yellow solid which was purified via recrystallization from a minimal amount of diethyl ether furnishing pale yellow crystals of **4-(^{t}BuNCO)$_2$** in 56% yield. ^{1}H NMR (benzene-*d*$_6$): δ = 0.52 (s, 6H, Si*Me*$_2$), 0.58 (s, 6H, Si*Me*$_2$), 1.41 (s, 18H, C$_5$H$_3$C*Me*$_3$), 1.68 (s, 18H, *Me*$_3$CNCO), 1.85 (s, 6H, C$_5$*Me*$_4$), 1.88 (s, 6H, C$_5$*Me*$_4$), 2.07 (s, 6H, C$_5$*Me*$_4$), 2.31 (s, 6H, C$_5$*Me*$_4$), 5.35 (m, 2H, C$_5$*H*$_3$CMe$_3$), 5.62 (m, 2H, C$_5$*H*$_3$CMe$_3$), 6.27 (m, 2H, C$_5$*H*$_3$CMe$_3$). {^{1}H}^{13}C NMR (benzene-*d*$_6$): δ = -0.65 (Si*Me*$_2$), -0.83 (Si*Me*$_2$), 11.21 (Cp*Me*), 11.89 (Cp*Me*), 14.10 (Cp*Me*), 14.30 (Cp*Me*), 31.85 (CpC*Me*$_3$), 32.63 (*Me*$_3$CNCO), 33.55 (Cp*C*Me$_3$), 55.54 (Me$_3$*C*NCO), 103.28, 109.62, 109.91, 117.86, 121.42, 122.09, 122.90, 129.67, 133.41, 147.32 (*Cp*), 147.55 (Me$_3$CN*C*O), N$_2$(^{t}BuNCO)$_2$*C*$_2$O$_2$ not located. IR (KBr): ν = 1647, 1673 cm^{-1} (C=N).

Preparation of ([Me$_2$Si(η^{5}-C$_5$Me$_4$)(η^{5}-C$_5$H$_3$-3-^{t}Bu)]Hf)$_2$(CO$_2$)$_2$(N$_2$C$_2$O$_2$) (4-(CO$_2$)$_2$). In a drybox, a thick-walled glass vessel was charged with 0.130 g (0.13 mmol) of **4-*C*$_2$** and approximately 10 mL of toluene. On a high vacuum line, the vessel was submerged in liquid nitrogen, degassed and 2.2 equivalents of carbon dioxide were

added to the reaction vessel via a calibrated gas bulb (50.8 torr, 100.1 mL). The contents of the vessel were thawed and stirred for 1 hour after which time excess carbon dioxide and solvent were removed *in vacuo*. The vessel was transferred into a dry box and the resulting yellow oil was washed with cold pentane and furnished 0.124 g (88 %) of a yellow solid identified as **4-$(CO_2)_2$**. Anal. Calcd for $C_{44}H_{60}O_6N_2Si_2Hf_2$: C, 49.76; H, 5.69; N, 2.64. Found: C, 50.06; H, 5.67; N, 2.28. ^{1}H NMR (benzene-d_6): δ = 0.48 (s, 6H, SiMe_2), 0.51 (s, 6H, SiMe_2), 1.37 (s, 18H, $C_5H_3CMe_3$), 1.62 (s, 6H, C_5Me_4), 1.76 (s, 6H, C_5Me_4), 1.97 (s, 6H, C_5Me_4), 2.01 (s, 6H, C_5Me_4), 5.38 (m, 2H, $C_5H_3CMe_3$), 5.57 (m, 2H, $C_5H_3CMe_3$), 6.25 (m, 2H, $C_5H_3CMe_3$). {^{1}H}^{13}C NMR (benzene-d_6): δ = -0.54 (SiMe_2), 0.17 (SiMe_2), 10.69 (Cp*Me*), 11.64 (Cp*Me*), 13.90 (Cp*Me*), 14.06 (Cp*Me*), 31.31 (CMe_3), 34.09 (CMe_3), 102.94, 108.61, 110.13, 111.70, 119.16, 119.29, 119.45, 122.64, 128.68, 129.95 (*Cp*), 150.54 ($N_2(CO_2)_2C_2O_2$) ($^2J_{CC} = {}^3J_{CC}$ = 1.5 Hz, reported as an average[51]), 163.18 ($N_2(CO_2)_2C_2O_2$). IR (KBr): ν = 1637 cm^{-1} (C=N); ν = 1734 cm^{-1} (C=O).

Preparation of ($(\eta^5$-$C_5Me_4H)_2Hf)_2$(I)(NCO) (2-(I)(NCO). In a drybox, a 20 mL scintillation vial was charged with 0.085 g (0.092 mmol) of **2-$N_2C_2O_2$** and approximately 10 mL of toluene. A solution containing 0.023 g (0.092 mmol) of iodine in approximately 5 mL of toluene was added dropwise over several minutes with stirring at room temperature. After 1 hour, solvent and any unreacted iodine were removed *in vacuo*. The remaining yellow solid was extracted with diethyl ether and filtered, removing a highly insoluble byproduct tentatively assigned as $[(\eta^5$-$C_5Me_4H)_2Hf)(NCO)]_n$ **(**based on mass spectrometry and infrared spectroscopy). Excess diethyl ether was removed *in vacuo*, and the resulting yellow residue was recrystallized from pentane at -35 °C, affording 0.024 g (22 %) of pale yellow crystals of **2-(I)(NCO)**. The reaction was reproducible on the NMR scale enabling the

spectroscopic characterization of various ^{15}N and ^{13}C isotopologue combinations (**2-(I)($N^{13}CO$)** and **2-(I)($^{15}N^{13}CO$)**). Anal. Calcd for $C_{19}H_{26}O_1N_1Hf_1$: C, 38.69; H, 4.44; N, 2.38. Found: C, 38.92; H, 4.45; N, 2.24. ^1H NMR (benzene-d_6): δ = 1.69 (s, 6H, CpMe_4H), 1.70 (s, 6H, CpMe_4H), 1.86 (s, 6H, CpMe_4H), 2.28 (s, 6H, CpMe_4H), 5.23 (s, 2H, CpMe$_4H$). $\{^1H\}^{13}C$ NMR (benzene-d_6): δ = 12.08 (Cp*Me*), 14.00 (Cp*Me*), 14.60 (Cp*Me*), 15.80 (Cp*Me*), 109.97, 118.48, 119.38, 127.86, 127.88 (*Cp*), 136.41 (N*C*O) ($^1J_{CN}$=32.6 Hz). IR (KBr): ν = 2220 cm^{-1} (NCO).

Independent preparation of 2-(I)(NCO). A thick-walled glass vessel was charged with 0.200 g (0.30 mmol) of **2-I_2** and approximately 10 mL of tetrahydrofuran. With stirring, a slurry of 0.049 g (0.33 mmol) silver cyanate in approximately 5 mL of tetrahydrofuran was added dropwise to the reaction vessel. The contents of the vessel were frozen and the vessel degassed on the vacuum line, and after thawing, transferred to an 80 °C oil bath and stirred for three days. The volatiles were removed *in vacuo* and the remaining solid was taken up in diethyl ether and filtered through Celite to remove silver iodide byproduct. The filtrate was reduced in volume to about 2 mL, and recrystallized at -35 °C overnight, furnishing 0.119 g of **2-(I)(NCO)** as pale yellow crystals (68 % yield).

Preparation of [$Me_2Si(\eta^5$-$C_5Me_4)(\eta^5$-C_5H_3-3-^{t}Bu)]Hf(I)(NCO) (4-(I)(NCO)). In a drybox, a 20 mL scintillation vial was charged with 0.057 g (0.055 mmol) of **4** (mixture of C_1 and C_2 isomers) dissolved in approximately 10 mL of toluene. A solution containing 0.015 g (0.059 mmol) of iodine in approximately 5 mL of toluene was added dropwise over about one minute with stirring. After 1 hour, the solvent and the unreacted iodine were removed *in vacuo*. The remaining yellow residue was washed with pentane to furnish 0.065 g (92 %) of a pale yellow solid identified as **4-**

(I)(NCO). The reaction was conveniently performed on the NMR scale enabling the synthesis and characterization of the ^{15}N and ^{13}C isotopologues, (**4-(I)($N^{13}CO$)** and **4-(I)($^{15}N^{13}CO$)**). Anal. Calcd for $C_{19}H_{26}N_1O_1I_1Hf_1$: C, 38.69; H, 4.44; N, 2.38. Found: C, 38.92; H, 4.45; N, 2.24. ^1H NMR (benzene-d_6): δ = 0.31 (s, 3H, SiMe_2), 0.36 (s, 3H, SiMe_2), 1.31 (s, 9H, $C_5H_3CMe_3$), 1.58 (s, 3H, C_5Me_4), 1.64 (s, 3H, C_5Me_4), 1.84 (s, 3H, C_5Me_4), 2.31 (s, 3H, C_5Me_4), 5.10 (m, 1H, $C_5H_3CMe_3$), 5.37 (m, 1H, $C_5H_3CMe_3$), 7.25 (m, 1H, $C_5H_3CMe_3$). $\{^1H\}^{13}C$ NMR (benzene-d_6): δ = -0.43 (SiMe_2), -0.25 (SiMe_2), 11.89 (CpMe), 15.08 (CpMe), 15.54 (CpMe), 15.90 (CpMe), 31.20 (CMe_3), 33.42 (CMe$_3$), 98.39, 104.58, 105.39, 108.12, 111.81, 121.95, 123.39, 125.60, 133.51, 149.73 (Cp), 136.81 (NCO) ($^1J_{NC}$ = 33.0 Hz). IR (KBr): ν = 2229 cm^{-1} (NCO).

Independent preparation of 4-(I)(NCO). A thick walled glass vessel was charged with 0.257 g (0.38 mmol) of **4-I_2** and approximately 10 mL of tetrahydrofuran. A slurry of 0.063 g (0.42 mmol) silver cyanate in approximately 5 mL of tetrahydrofuran was added dropwise to the reaction vessel with stirring. The vessel was degassed and then placed in an 80 ºC oil bath for three days. After this time, the volatiles were removed in vacuo and the desired product extracted into diethyl ether. The diethyl ether solution containing the product was concentrated to approximately 2 mL and then stored at -35 ºC. This procedure furnished 0.142 g (81 %) of pale yellow crystals identified as **4-(I)(NCO)**.

REFERENCES

[1] Fryzuk, M. D. *Chem. Rec.* **2003**, *3*, 2.

[2] Schlögl, R. *Angew. Chem. Int. Ed.* **2003**, *42*, 2004.

[3] K. Tamaru in *Catalytic Ammonia Synthesis.* J. R. Jennings, Ed.; Plenum, NY 1991.

[4] Pimentel, D.; Patzek, T. W. *Nat. Resources Res.* **2005**, *14*, 65.

[5] Ertl, G. *Angew. Chem. Int. Ed.* **2008**, *47*, 3524.

[6] Hager, T. in *The Alchemy of Air*, Three Rivers Press, NY, 2008.

[7] MacKay, B. A.; Fryzuk, M. D. *Chem. Rev.* **2004**, *104*, 385.

[8] Chatt J. *Philos. Trans. R. Soc. London, Ser B.* **1977**, *281*, 243.

[9] Maxwell, G. R. in *Kent and Riegel's Handbook of Industrial Chemistry and Biotechnology, Vol. 1.* Kent, J. A., Ed, Springer Science and Business Media, LLC, New York, NY, 2007.

[10] Shaver, M. P.; Fryzuk, M. D. *Adv. Synth. Catal.* **2003**, *345*, 1061.

[11] Henderickx, H.; Kwakkenbos, G.; Peters, A.; van der Spoel, J.; de Vries, K. *Chem. Commun.* **2003**, 2050.

[12] (a) Curley, J. J.; Sceats, E. L.; Cummins, C. C. *J. Am. Chem. Soc.* **2006**, *128*, 14036. (b) Figueroa, J. S. Piro, N. A.; Clough, C. R.; Cummins, C. C. *J. Am. Chem. Soc.* **2006**, *128*, 940.

[13] Hirotsu, M.; Fontaine, P. P.; Epshteyn, A.; Zavalij, P. Y.; Sita, L. R. *J. Am. Chem. Soc.* **2007**, *129*, 9284.

[14] Akagi, F.; Matsuo, T.; Kawaguchi, H. *Angew. Chem. Int. Ed.* **2007**, *46*, 8778.

[15] Sobota, P.; Janas, Z. *J. Organomet. Chem.* **1984**, *276*, 171.

[16] Knobloch, D. J.; Lobkovsky, E.; Chirik, P. J. *Nature Chem.* **2010**, *2*, 30.

[17] Pool, J. A.; Lobkovsky, E. Chirik, P. J. *Nature* **2004**, *427*, 527.

[18] Bernskoetter, W. H.; Olmos, A. V.; Lobkovsky, E.; Chirik, P. J. *Organometallics* **2006**, *25*, 1021.

[19] Chirik, P. J. *Dalton Trans.* **2007**, 16.

[20] Knobloch, D. J.; Lobkovsky, E.; Chirik, P. J. *J. Am. Chem. Soc.* **2010**, *132*, 10553.

[21] Duncan, A. P.; Bergman, R. G. *Chem. Rec.* **2002**, *2* 431.

[22] Hazari, N.; Mountford, P. *Acc. Chem. Res.* **2005**, *38*, 839.

[23] a) Guiducci, A. E.; Boyd, C. L.; Mountford, P. *Organometallics* **2006**, *25*, 1167. b) Dunn, S. C.; Hazari, N.; Cowley, A. R.; Green, J. C.; Mountford, P. *Organometallics* **2006**, *25*, 1755. c) Zuckerman, R. L.; Bergman, R. G. *Organometallics* **2001**, *20*, 1792. d) Zuckerman, R. L.; Bergman, R. G. *Organometallics* **2000**, *19*, 4795. e) Thorman, J. E.; Guzei, I. A.; Young, V. G.; Woo, L. K. *Inorg. Chem.* **1999**, *38*, 3814. f) Polse, J. L.; Andersen, R. A.; Bergman, R. G. *J. Am. Chem. Soc.* **1998**, *120*, 13405.

[24] Pool, J. A.; Bernskoetter, W. H.; Chirik, P. J. *J. Am. Chem. Soc.* **2004**, *126*, 14326.

[25] Cundari, T. R.; Gordon, M. S. *J. Am. Chem. Soc.* **1993**, *115*, 4210.

[26] Walsh, P. J.; Hollander, F. J.; Bergman, R. G. *J. Am. Chem. Soc.* **1988**, *110*, 8729.

[27] Schofield, A. D.; Nova, A.; Selby, J. D.; Manley, C. D.; Schwarz, A. D.; Clot, E.; Mountford, P. *J. Am. Chem. Soc.* **2010**, *132*, 10484.

[28] Bernskoetter, W. H.; Pool, J. A.; Lobkovsky, E.; Chirik, P. J. *J. Am. Chem. Soc.* **2005**, *127*, 7901.

[29] Coupling constants could not be determined because the simulated AA'XX' spectrum generated infinite solutions that fit the experimental data.

[30] Mindiola, D. J. *Acc. Chem. Res.* **2006**, *39*, 813.

[31] a) Bennett, J. L.; Wolczanski, P. T. *J. Am. Chem. Soc.* **1997**, *119*, 10696. b) Schaller, C. P.; Cummins, C. C.; Wolczanski, P. T. *J. Am. Chem. Soc.* **1996**, *118*, 591. c) Hoyt, H. M.; Michael, F. E.; Bergman, R. G. *J. Am. Chem. Soc.* **2004**, *126*, 1018.

[32] Toomey, H. E.; Pun, D.; Veiros, L. F.; Chirik, P. J. *Organometallics* **2008**, *27*, 872.

[33] a) Howard, W. A.; Trnka, T. M.; Waters, M.; Parkin, G. *J. Organomet. Chem.* **1997**, *528*, 95. b) Howard, W. A.; Waters, M.; Parkin, G. *J. Am. Chem. Soc.* **1993**, *115*, 4917.

[34] See Chapter 1 of this thesis and reference 20.

[35] See Chapter 1 of this thesis and reference 16.

[36] Desseyn, H. O.; Perlepes, S. P.; Clou, K.; Blaton, N.; Van der Veken, B. J.; Dommisse, R.; Hansen, P. E. *J. Phys. Chem. A* **2004***, 108*, 5175.

[37] Pfoertner, K.; Daly, J. J. *Helv. Chim. Acta* **1987***, 70*, 171.

[38] Blicke, F. F.; Godt, H. C. *J. Am. Chem. Soc.* **1954**, *76*, 3653.

[39] Denk, M. K.; Hezarkhani, A.; Zheng, F. *Eur. J. Inorg. Chem.* **2007**, 3527.

[40] Lambert, J. B.; Huseland, D. E.; Wang, G. *Synthesis* **1986**, 657.

[41] Mukherjee, A.; Kumar, S.; Seth, M.; Bhaduri, A. P. *Indian Journal of Chemistry, Section B: Organic Chemistry Including Medicinal Chemistry*, **1989**, *28B*, 391.

[42] Ruiz, R.; Faus, J.; Lloret, F.; Julve, M.; Journaux, Y. *Coord. Chem. Rev.* **1999**, *193*, 1069.

[43] Fryzuk, M. D.; Love, J. B.; Rettig, S. J.; Young, V. G. *Science* **1997**, *275*, 1445.

[44] Fryzuk, M. D.; MacKay, B. A.; Patrick, B. O. *J. Am. Chem. Soc.* **2003**, *125*, 3234.

[45] MacKay, B. A.; Munha, R. F.; Fryzuk, M. D. *J. Am. Chem. Soc.* **2006**, *128*, 9472.

[46] Semproni, S. P.; Lobkovsky, E.; Chirik, P. J. *J. Am. Chem. Soc.* Manuscript in progress.

[47] Bernskoetter, W. H.; Olmos, A. V.; Pool, J. A.; Lobkovsky, E.; Chirik, P. J. *J. Am. Chem. Soc.* **2006**, *128*, 10696.

[48] Bernskoetter, W. H.; Lobkovsky, E.; Chirik, P. J. *Angew. Chem. Int. Ed.* **2007**, *46*, 2858.

[49] Knobloch, D. J.; Toomey, H. E.; Chirik, P. J. *J. Am. Chem. Soc.* **2008**, *130*, 4248.

[50] See Chapter 4 for a full discussion of this work.

[51] Values reported as an average for the AA'XX' spin system. See the Experimental Section for details.

[52] Pangborn, A.B.; Giardello, M.A.; Grubbs, R.H.; Rosen, R.K.; Timmers, F.J. *Organometallics* **1996**, 15, 1518.

[53] Marvich, R.H.; Brintzinger, H. H. *J. Am. Chem. Soc.* **1971**, *93*, 2046.

[54] F. Neese, Orca - an ab initio, DFT and Semiempirical Electronic Structure Package, Version 2.7, Revision 0; Institut für Physikalische und Theoretische Chemie, Universität Bonn, Bonn (Germany), August **2009**.

[55] Becke, A. D. *J. Chem. Phys.* **1986**, *84*, 4524.

[56] Becke, A. D. *J. Chem. Phys.* **1993**, *98*, 5648.

[57] Lee, C. T.; Yang, W. T.; Parr, R. G. *Phys. Rev. B* **1988**, *37*, 785.

[58] van Lenthe, E.; Snijders, J. G.; Baerends, E. J. *J. Chem. Phys.* **1993**, *99*, 4597.

[59] van Lenthe, E.; Baerends, E. J.; Snijders, J. G. *J. Chem. Phys.* **1994**, *101*, 9783.

[60] van Lenthe, E.; Snijders, J. G.; Baerends, E. J. *J. Chem. Phys.* **1996**, *105*, 6505.

[61] van Wüllen, C. *J. Chem. Phys.* **1998**, *109*, 392.

[62] Pantazis, D.; Chen, X.-Y.; Landis, C. R.; Neese, F. *J. Chem. Theory Comput.* **2008**, *4*, 908.

[63] Pantazis, D.; Neese, F. *J. Chem. Theory Comput.* **2009**, *5*, 2220–2238.

[64] Schäfer, A.; Huber, C.; Ahlrichs, R. *J. Chem. Phys.* **1994**, *100*, 5829.

[65] Weigend, F.; Ahlrichs, R. *Phys. Chem. Chem. Phys.* **2005**, *7*, 3297.

[66] Weigend, F. *Phys. Chem. Chem. Phys.* **2006**, *8*, 1057.

[67] Neese, F.; Wennmohs, F.; Hansen, A.; Becker, U. *Chem. Phys.* **2009**, *356*, 98.

[68] Kossmann, S.; Neese, F. *Chem. Phys. Lett.* **2009**, *481*, 240.

[69] Neese, F. *J. Comput. Chem.* **2003**, *24*, 1740.

[70] Lambert, J. B.; Huseland, D. E.; Wang, G. *Synthesis* **1986**, 657.

[71] Desseyn, H. O.; Perlepes, S. P.; Clou, K.; Blaton, N.; Van der Veken, B. J.; Dommisse, R.; Hansen, P. E. *J. Phys. Chem. A* **2004***, 108*, 5175.

[72] Pfoertner, K.; Daly, J. J. *Helv. Chim. Acta* **1987***, 70*, 171.

[73] Modified procedure from Santana, D. M.; Garcia, G.; Julve, M.; Lloret, F.; Perez, J.; Liu, M.; Sanz, F.; Cano, J.; Lopez, G. *Inorg. Chem.* **2004**, *43*, 2132.

CHAPTER 4

Carboxylation of *Ansa*-Zirconocene and Hafnocene Dinitrogen Complexes: Regioselective Hydrazine Synthesis from N_2 and CO_2.*

Abstract

Addition of 2 equivalents of carbon dioxide to the *ansa*-zirconocene dinitrogen complex **3-N_2** resulted in selective insertion into each zirconium-nitrogen bond, forming a C_2-symmetric *N,N'*-dicarboxylated hydrazido compound. Treatment with excess Me_3SiI furnished the *ansa*-zirconocene diiodide along with the free *N,N'*-dicarboxylated silylated hydrazine. New nitrogen−carbon bonds were also assembled by addition of methyl triflate. Tri- and tetrasubstituted hydrazines could be formed by treatment with water and Me_3SiI, respectively. The regiochemistry of the N_2 carboxylation is likely controlled by the *ansa*-cyclopentadienyl ligand where the sterically demanding *tert*-butyl substituents and the C_2 symmetry of the dimer determines the stereochemistry of CO_2 insertion. The generality of CO_2 insertion was explored with several other *ansa*-metallocene complexes, and in each case high regioselectivity favoring the *N,N'*-dicarboxylated hydrazide was observed. These results demonstrate the ability of zirconium dinitrogen compounds to participate in heterocumulene insertion chemistry.

---

* Portions of this work were taken with permission from: Knobloch, D. J.; Toomey, H. E.; Chirik, P. J. *J. Am. Chem. Soc.* **2008**, *130*, 4248.

Introduction

Carbon dioxide and dinitrogen are highly desirable as synthons for organic molecules due to their natural abundance in the Earth's atmosphere, relative non-toxicity, and ease of handling.[1] Reactions promoted by—and ideally catalyzed by—transition metal complexes that couple heterocumulenes such as CO_2 to N_2 are attractive as potential alternatives to the harsh energy requirements of the Haber-Bosch process for ammonia synthesis.[2,3,4]

Recent inspiration for nitrogen-carbon bond formation with heterocumulenes has been provided by multiple reports,[5,6,7,8,9,10,11] demonstrating that early metal-nitrogen bonds (not N_2 derived) may be functionalized with heterocumulenes via insertion and cycloaddition pathways. Two examples of such reactivity involving group 4 imido and hydrazido compounds are presented in Figure 4.1. Heterocumulene insertion into metal-nitrogen bonds has also been documented.[12,13] The discovery of four-electron reduced dinitrogen complexes of zirconium and hafnium[14,15,16,17] presents an opportunity to capitalize on the known reactivity between carbon dioxide (as well as other heterocumulenes) and metal-nitrogen single and multiple bonds. In principle this strategy will result in routes to useful organic molecules directly from N_2 and CO_2. Early success using this approach has been recently reported by our laboratory.[18,19] Importantly, strongly activated $[N_2]^{4-}$ ligands are required for functionalization; when N_2 activation is insufficient, competing reductive coupling of CO_2 and dinitrogen loss is observed.[20] Another potential pitfall when studying the reactivity of heterocumulene substrates is deleterious competing reactivity with the supporting ligands.[21]

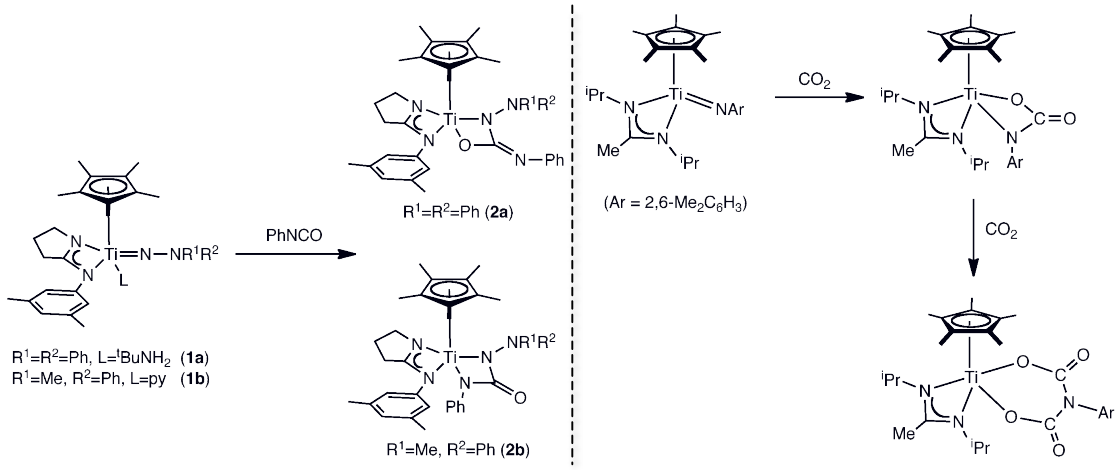

Figure 4.1. Heterocumulene addition to early metal imido and hydrazido complexes; examples by Gade et al. (left) and Mountford et al. (right). Reproduced with permission from references 11 and 7.

In this chapter the addition of carbon dioxide to activated dinitrogen complexes of group 4 transition metals will be presented. Specifically the functionalization of dinitrogen with CO_2 has been extended to include zirconium dinitrogen complexes and, importantly, regioselective *N*,*N*'-dicarboxylation of dinitrogen is reported for first time. Subsequent reactivity studies, including synthetic routes to a family of trisubstituted and tetrasubstituted hydrazines, will also be presented. These results complement the rich N_2 functionalization chemistry involving carbon monoxide reported by our laboratory that has been the main focus of the preceding chapters.[22,23,24,25]

Results and Discussion

Previous studies conducted in our laboratory[19] have demonstrated the successful functionalization of atmospheric dinitrogen with carbon dioxide promoted by the hafnocene dinitrogen compound, $[(\eta^5\text{-}C_5Me_4H)_2Hf]_2(\mu_2, \eta^2, \eta^2\text{-}N_2)$ (**2-N₂**).

When a benzene-d_6 solution of **2-N$_2$** was exposed to 2 equivalents of carbon dioxide, the dicarboxylated derivative was formed as a mixture of regioisomers in an 85:15 ratio (Figure 4.2). The major product was identified as the C_2-symmetric compound, **2-NN(CO$_2$)$_2$**, resulting from *N*,*N*-dicarboxylation, i.e. double functionalization of one nitrogen atom. The minor product was identified as the idealized C_{2h}-symmetric compound, where *N*,*N'* dicarboxylation had occurred.[19]

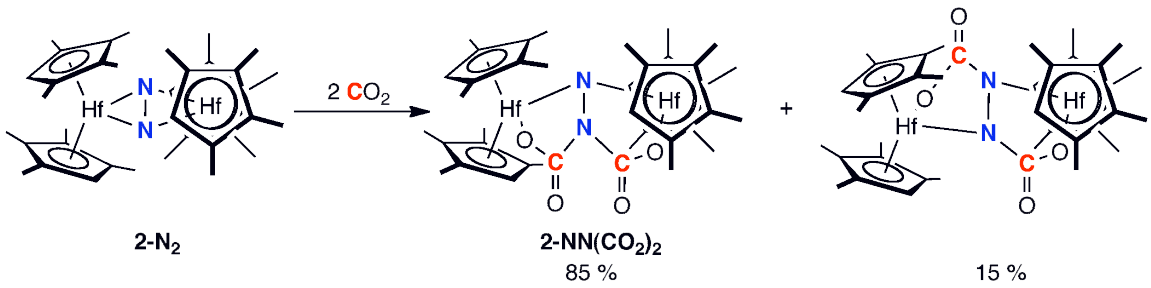

Figure 4.2. Addition of carbon dioxide to **2-N$_2$** previously reported in our laboratory.[19]

Based on this result, we sought to achieve dinitrogen carboxylation with an analogous zirconocene dinitrogen complex, with the additional goal of improving regioselectivity and perhaps favoring the *N*,*N*'-substituted regioisomer. It should be noted that treatment of the zirconium congener of **2-N$_2$**, [(η^5-C$_5$Me$_4$H)$_2$Zr]$_2$(μ_2, η^2, η^2-N$_2$) (**1-N$_2$**)[15] with carbon dioxide resulted in a complicated mixture of products, and no evidence for N-C bond formation. Toepler pump analysis of this reaction indicated 76% of the coordinated dinitrogen was lost upon addition of CO_2 to **1-N$_2$**, confirming the lack of N_2 functionalization.

Turning to a more activated dinitrogen compound, the recently reported *ansa*-zirconocene N_2 compound, [Me$_2$Si(η^5-C$_5$Me$_4$)(η^5-C$_5$H$_3$-3-^{t}Bu)Zr]$_2$(μ_2, η^2, η^2-N$_2$) (**3-N$_2$**),[26] was selected. This complex has well-established electronic properties and

structural configuration.[26,27] **3-N_2** adopts exclusively the *syn*-homochiral dimeric configuration as judged by solution spectroscopic techniques as well as by single crystal X-ray diffraction.[26] It was predicted the idealized C_2-symmetry of **3-N_2** might impart an element of regiocontrol to subsequent reactivity studies.[28]

Initially, the ligand-induced dissociation of N_2 from **3-N_2** was a potential concern, given the N_2 loss chemistry observed with **1-N_2**. However, we were pleased to find that **3-N_2** undergoes very slow exchange with $^{15}N_2$ gas, establishing a high barrier for ligand-induced side-on, end-on isomerization (Figure 4.3). In fact, a more convenient route to the ^{15}N-enriched dinitrogen compound **3-$^{15}N_2$** is reduction of the corresponding diiodide, **3-I_2**, with sodium amalgam under an atmosphere of $^{15}N_2$ gas (Figure 4.4). The diiodide precursor is used to minimize the formation of zirconium(III) monohalide impurities formed during the reduction which interfere with subsequent CO_2 functionalization chemistry.[29]

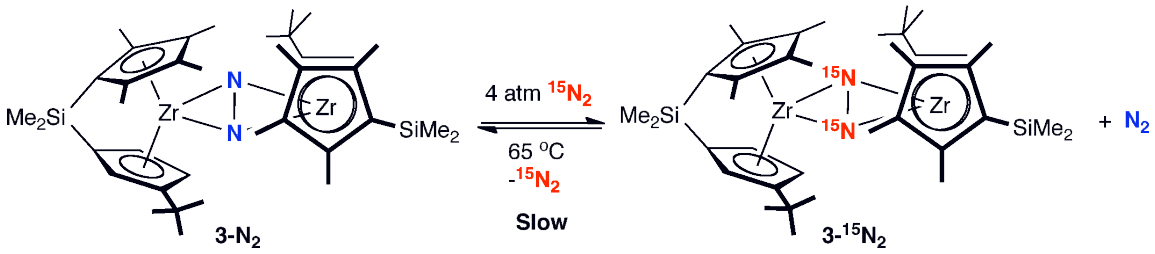

Figure 4.3. Exchange of $^{15}N_2$ into **3-N_2**.

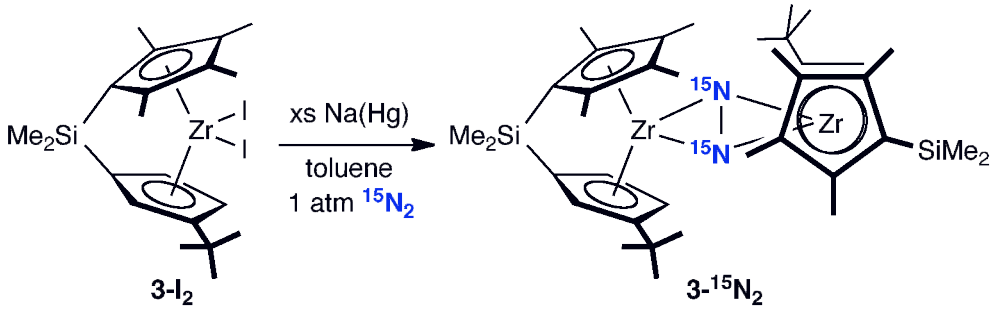

Figure 4.4. Synthesis of **3-$^{15}N_2$** by sodium amalgam reduction of **3-I_2** under $^{15}N_2$ gas.

Exposure of a benzene or toluene solution of **3-N_2** to 2 equivalents of carbon dioxide resulted in rapid consumption of starting materials and formation of the product arising from carboxylation of both nitrogen atoms (Figure 4.5). The product, **3-$(NCO_2)_2$**, is sparingly soluble in benzene and decomposes rapidly to a complicated mixture of unidentified products in solution at room temperature ($t_{1/2} \sim 30$ min). A preferred alternative synthesis, whereby carbon dioxide was added to a pentane slurry of **3-N_2**, followed by vigorous shaking for several minutes, filtration, and cold pentane wash, furnished **3-$(NCO_2)_2$** as an orange solid in 76% yield. Product **3-$(NCO_2)_2$** is stable for weeks at -35 °C in the solid state. Similar behavior was observed for the hafnocene complex, **2-NN$(CO_2)_2$**, although solution decomposition occurred on the time scale of days under similar conditions.[19]

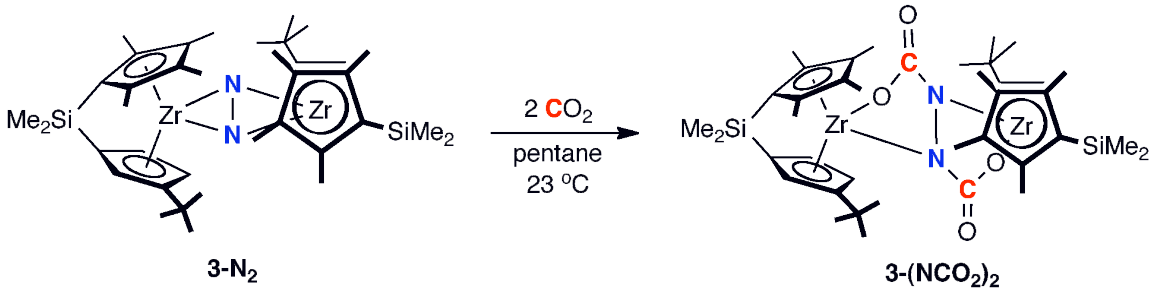

3-N_2 **3-$(NCO_2)_2$**

Figure 4.5. Addition of carbon dioxide to the *ansa*-zirconocene dinitrogen complex **3-N_2**.

Although the instability of **3-$(NCO_2)_2$** has thus far precluded structural determination by X-ray diffraction, multinuclear NMR experiments, IR spectroscopy, combustion analysis, and reactivity studies definitively establish the regiochemistry of dinitrogen carboxylation. The benzene-d_6 ^{1}H NMR spectrum of **3-$(NCO_2)_2$** exhibits the number of resonances expected for a C_2-symmetric dimeric zirconocene. Likewise, a single ^{13}C resonance was observed at 166.0 ppm, which splits into an AA'XX'

pattern upon labeling with $^{15}N_2$ gas (Figure 4.6). Simulating the data (Figure 4.7) yielded coupling constants similar in magnitude to those reported for **2-NN(CO$_2$)$_2$**,[19] confirming N_2 carboxylation.

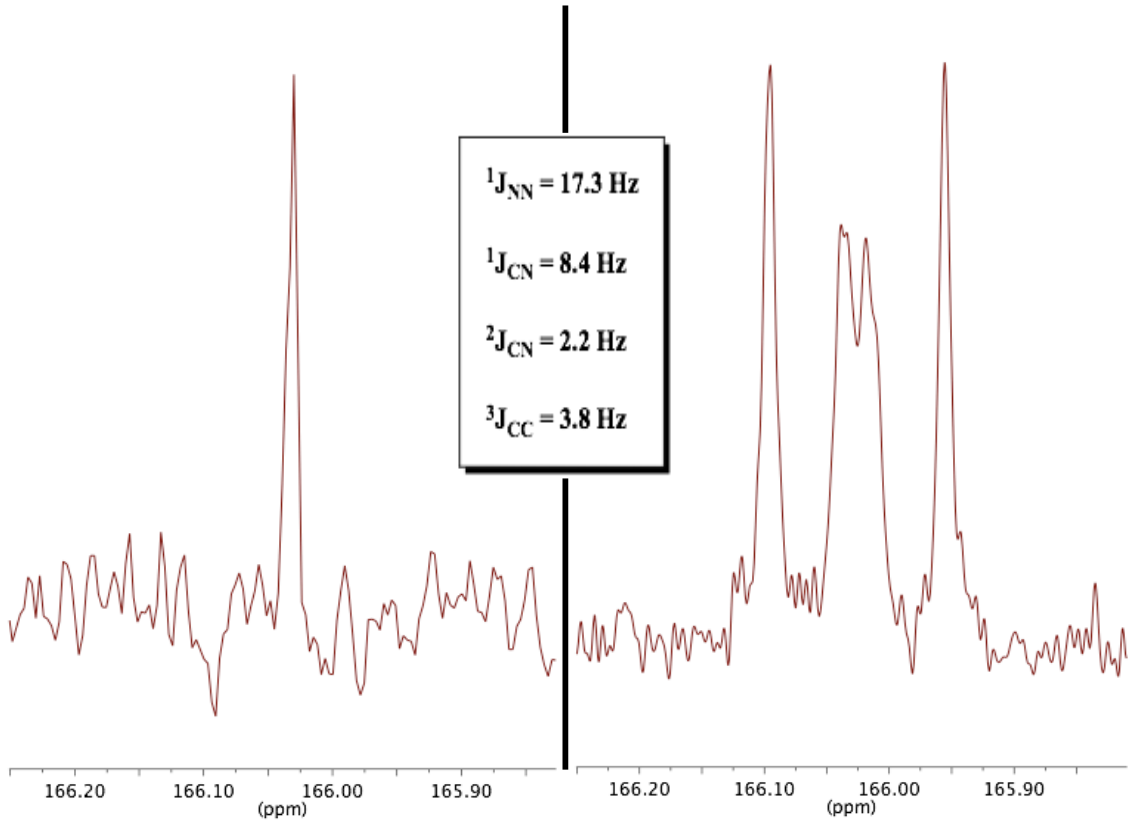

Figure 4.6. Partial benzene-d_6 ^{13}C NMR spectra of **3-(NCO$_2$)$_2$** (left) and **3-(N^{13}CO$_2$)$_2$** (right).

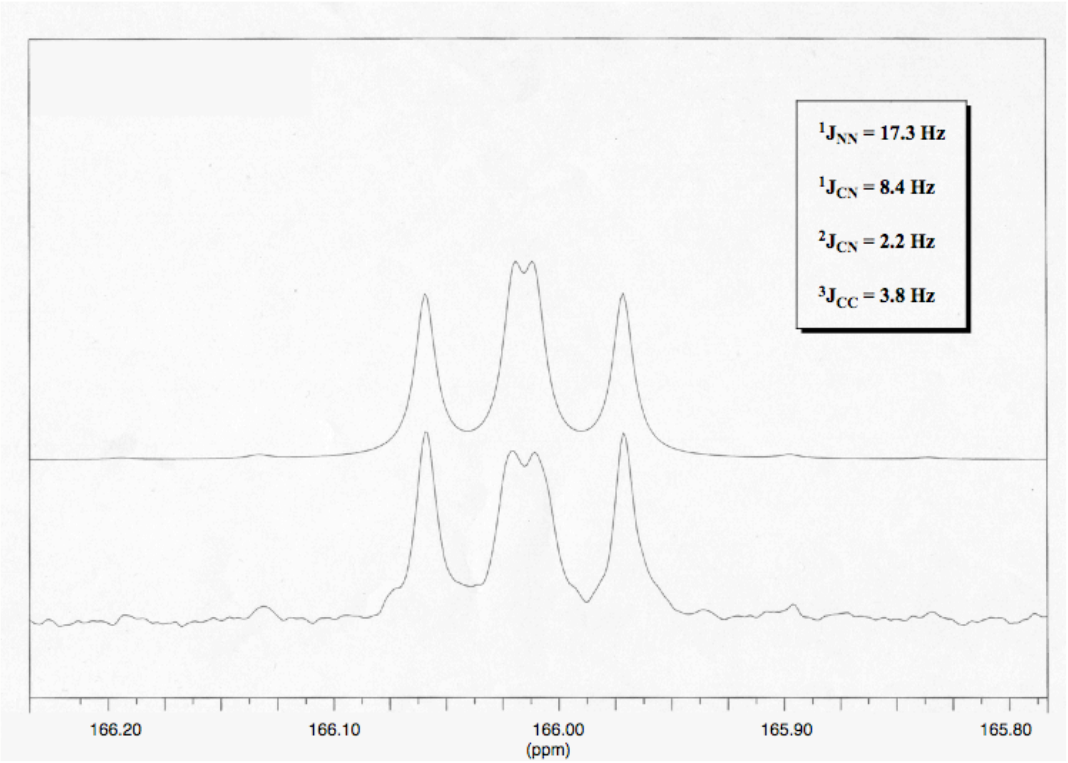

Figure 4.7. Partial experimental (bottom) and simulated (top) benzene-d_6 ^{13}C NMR spectra of **3-(N^{13}CO$_2$)$_2$**.

The ^{15}N NMR spectrum also established functionalization of each nitrogen atom. A single resonance centered at 209.5 ppm was observed, comparable to the value of 184.4 ppm for the carboxylated nitrogen in **2-NN(CO$_2$)$_2$**.[19] If the structure of **3-(NCO$_2$)$_2$** was analogous to the hafnocene compound where one nitrogen atom was functionalized twice, C_2 symmetry and single ^{13}C and ^{15}N NMR resonances would not be observed. Thus, the C_2 symmetry imparted by the *ansa*-zirconocene ligand environment translates onto the regiochemistry of nitrogen carboxylation. The sterically demanding *tert*-butyl substituents likely direct the approach of the inserting CO_2 molecule to the more open lateral positions of the metallocene wedge, although

the opposite configuration, whereby the CO_2 inserts *syn* to the ^{t}Bu, has not been definitively eliminated.

Analogous chemistry was attempted with the hafnium congener of the *ansa*-zirconocene dinitrogen compound, **4-N$_2$**. Treatment of a benzene-d_6 solution of **4-N$_2$** with 2 equivalents of CO_2 resulted in the expected *N*,*N'*-dicarboxylated hydrazido product, **4-(NCO$_2$)$_2$** (Figure 4.8). This compound was characterized by multinuclear NMR spectroscopy as well as infrared spectroscopy. Notably **4-(NCO$_2$)$_2$** exhibits improved solubility and stability in aromatic solvents compared to **3-(NCO$_2$)$_2$**. Unfortunately single crystals of this compound suitable for X-ray diffraction have thus far not been obtained.

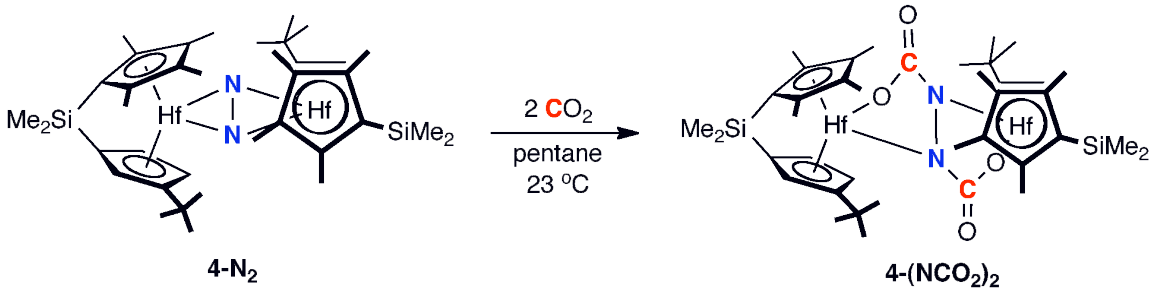

Figure 4.8. Addition of carbon dioxide to the *ansa*-hafnocene dinitrogen complex **4-N$_2$**.

Elaboration of carboxylated dinitrogen complexes. Various electrophilic reagents were targeted for their potential to release the functionalized hydrazido fragment from the metal centers in **3-(NCO$_2$)$_2$** and **4-(NCO$_2$)$_2$**. Treatment of a benzene-d_6 solution of **3-(NCO$_2$)$_2$** with excess Me_3SiI rapidly generated **3-I$_2$** along with *N*,*N'*-dicarboxylated hydrazine, $[(Me_3Si)(Me_3SiO_2C)N]_2$ (**5**) (Figure 4.9). Similarly, treatment of **4-(NCO$_2$)$_2$** with excess Me_3SiI also generated **5** and the corresponding diiodide **4-I$_2$**. While the mass spectral data of **5** and its ^{13}C and ^{15}N

isotopologues generated in these experiments are identical to that previously reported for the *N*,*N*-isomer,[19] the multinuclear NMR spectroscopic data are distinctly different and conclusively establish its identity as the *N*,*N'*-dicarboxylated isomer.

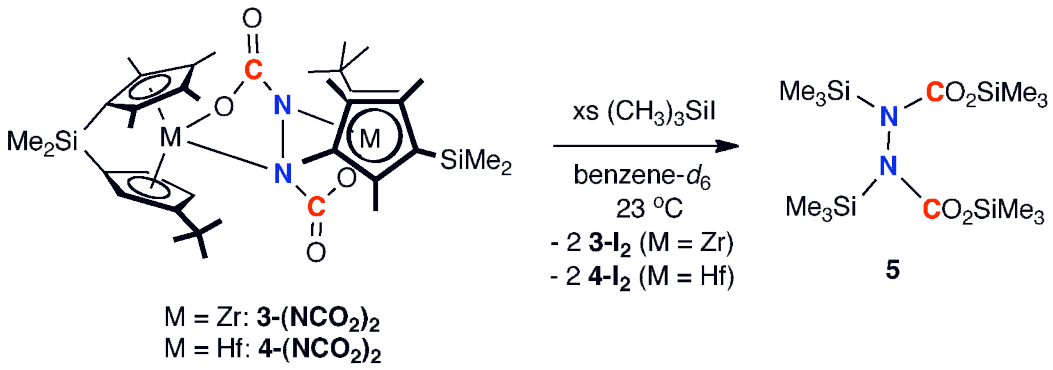

Figure 4.9. Liberation of silylated hydrazine from the metal centers in **3-(NCO$_2$)$_2$** and **4-(NCO$_2$)$_2$**.

The *N*,*N'*-dicarboxylated metallocene products were also treated with the carbon-based electrophile methyl triflate with the goal of additional nitrogen-carbon bond formation. Treatment of a benzene-d_6 solution of **3-(NCO$_2$)$_2$** with 3 equivalents of CH_3OTf furnished a 1:1 ratio of the zirconocene bis(triflate), **3-(OTf)$_2$**, and a second zirconium compound, **6**, containing new nitrogen−carbon bonds (Figure 4.10). The zirconocene bis(triflate), **3-(OTf)$_2$**, was independently prepared in a straightforward manner from **2-I$_2$** and AgOTf, confirming its identity as a byproduct from methyl triflate addition to **3-(NCO$_2$)$_2$** (Figure 4.11).

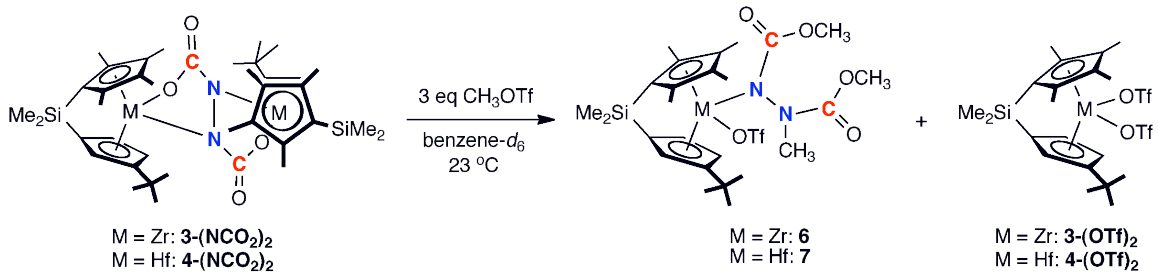

Figure 4.10. Addition of methyl triflate to CO_2-functionalized *ansa*-metallocene complexes.

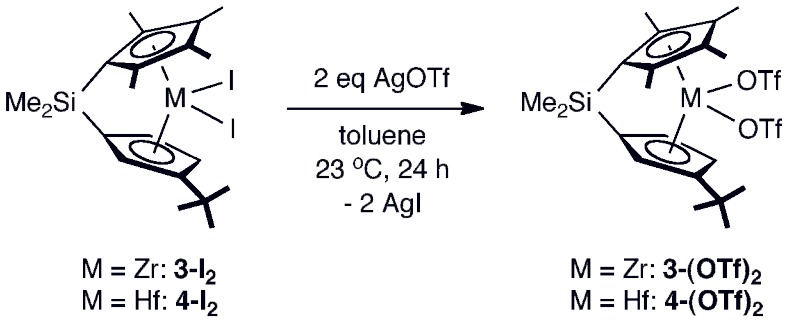

Figure 4.11. Independent synthesis of metallocene bis(triflate) compounds **3-(OTf)$_2$** and **4-(OTf)$_2$** from the corresponding diiodide precursors.

Preparation of various isotopologues of **6** with $^{15}N_2$, $^{13}CO_2$, $^{13}CH_3OTf$, and CD_3OTf along with protonation and 2-D NMR experiments establish the identity of the product as the *ansa*-zirconocene hydrazido where a total of three new N−C bonds (two from CO_2, one from CH_3OTf) have been assembled (Figure 4.10).[30] Presented in Figure 4.12 is the benzene-d_6 ^{1}H NMR spectrum of the product mixture from methyl triflate addition to **3-(N^{13}CO$_2$)$_2$**. The spectrum confirms the presence of three chemically inequivalent methyl groups in the hydrazido ligand. Also from this spectrum, coupling constants of $^3J_{CH}$ = 3.8 and 3.9 Hz for the -OCH_3 groups and $^3J_{CH}$ = 1.9 Hz for the -NCH_3 group were obtained.

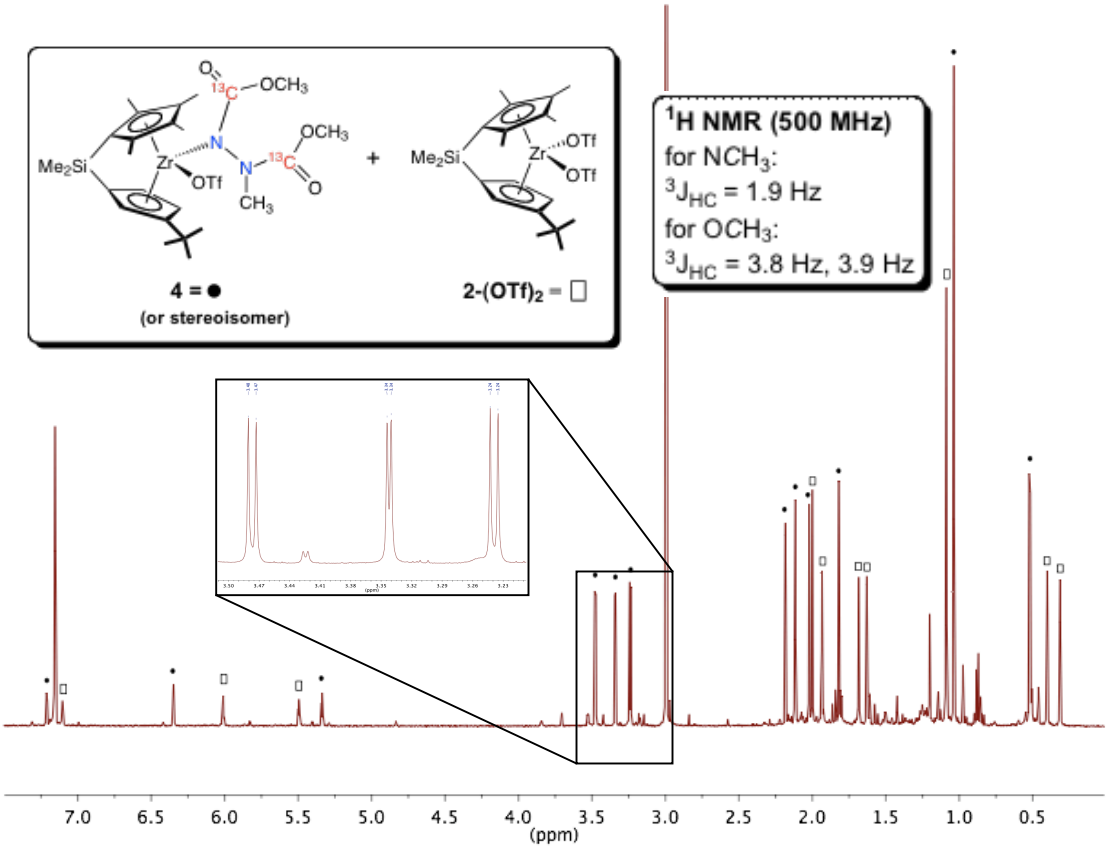

Figure 4.12. ^{1}H NMR spectrum of **6** and **3-(OTf)$_2$** (^{13}C labeled).

In Figures 4.13, 4.14 and 4.15 the ^{13}C NMR spectra of various isotopologues of **6** are presented. These spectra are consistent with the formation of a new nitrogen-carbon bond and two new methoxy groups resulting from three methylation events at the hydrazide core of **3-(NCO$_2$)$_2$**. Coupling constants of $^{1}J_{NC}$ = 11.5 Hz, $^{2}J_{NC}$ = 1.3 Hz for the -NCH$_3$ group were observed, confirming N-C formation. Interestingly, exposure of **6** to excess methyl triflate did not result in a fourth methylation event or liberation of the functionalized hydrazido fragment from the zirconium center. Unfortunately, **6** could not be separated from **3-(OTf)$_2$**, and because we have been unable to obtain X-ray quality crystals of **6**, the hapticity and the relative

stereochemistry of the hydrazido ligand in the zirconocene wedge has not been established.

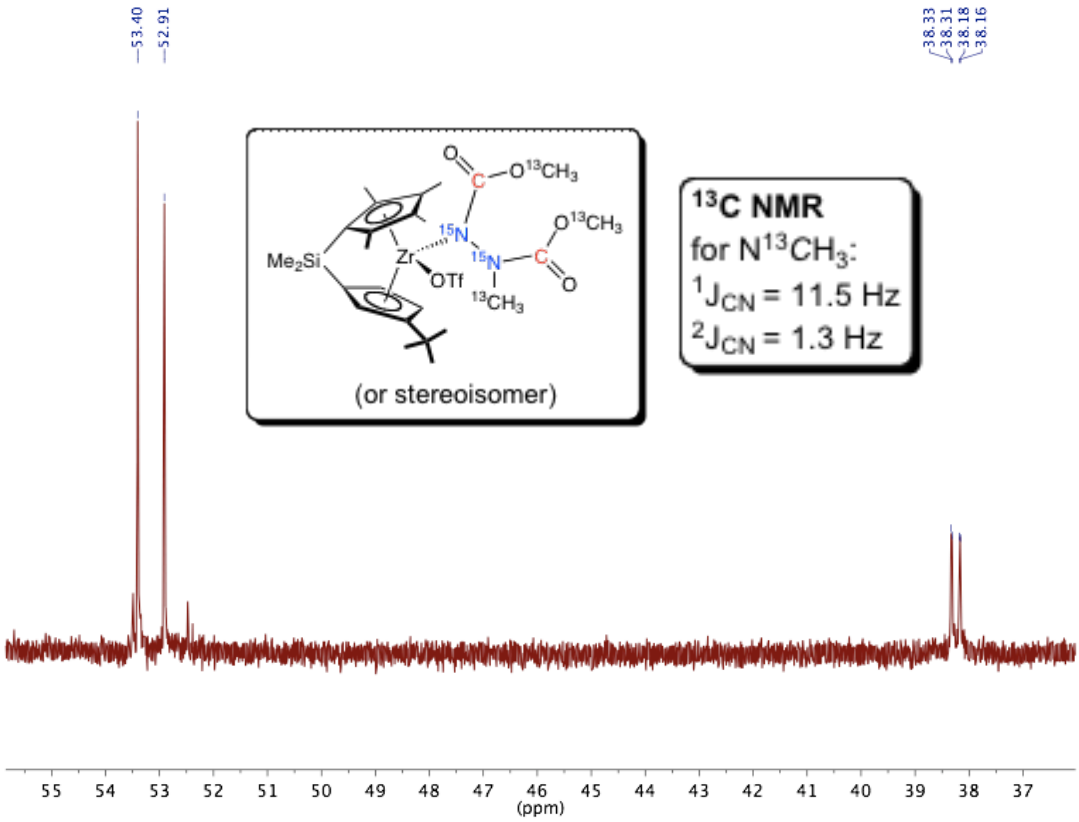

Figure 4.13. Partial benzene-d_6 ^{13}C NMR spectrum of **6** (^{15}N, ^{13}C labeled) at 23 ºC.

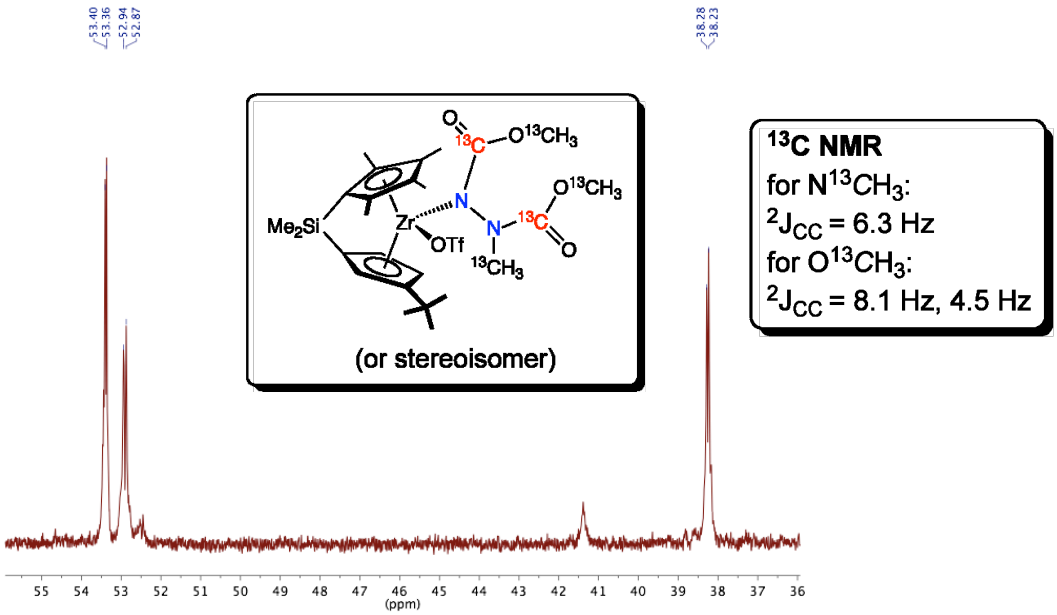

Figure 4.14. Partial benzene-d_6 ^{13}C NMR spectrum of **6** (^{13}C labeled) at 23 ºC.

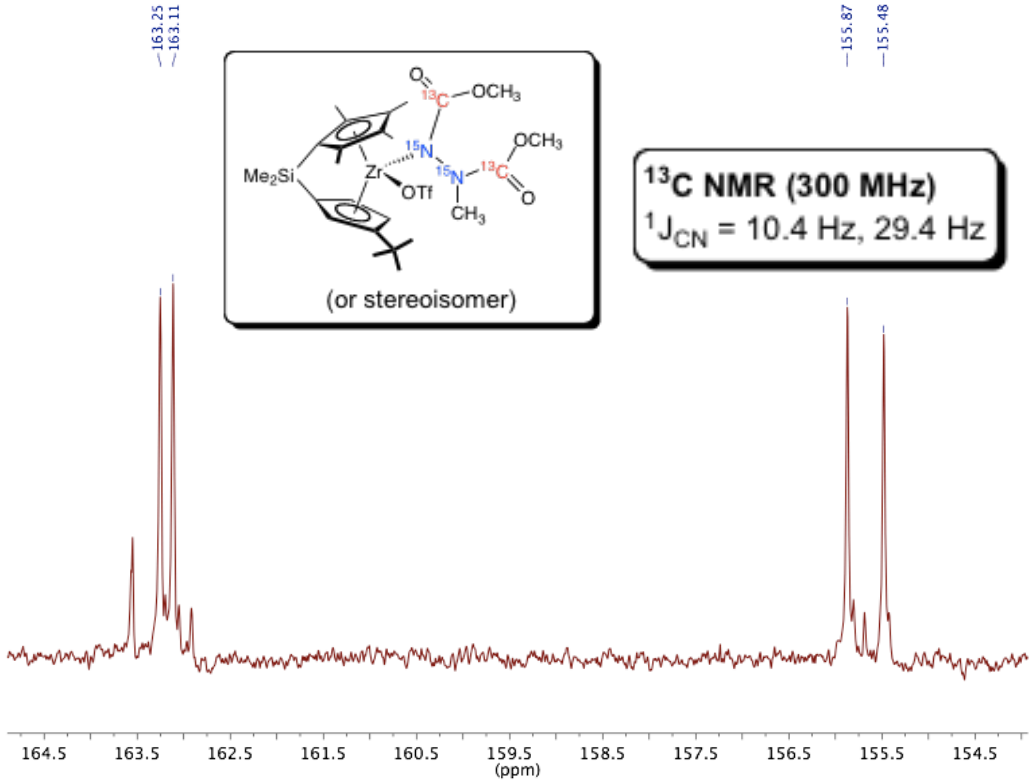

Figure 4.15. Partial benzene-d_6 ^{13}C NMR spectrum of **6** (^{15}N, ^{13}C labeled) at 23 ºC.

Preliminary investigations into the reaction of methyl triflate with the hafnocene congener (**4-$(NCO_2)_2$**) have produced similar results. As observed with zirconium, the hydrazide ligand in **4-$(NCO_2)_2$** is methylated three times, forming **7** and concomitantly the bis(triflate) compound **4-$(OTf)_2$** (Figure 4.10). The reason why these methylation reactions stop after three equivalents is likely kinetic in nature, since formation of the bis(triflate) complexes (**3-$(OTf)_2$** and **4-$(OTf)_2$**) should be favored thermodynamically over **6** and **7**, respectively. However, heating solutions of **6** or **7** to 90 °C in the presence of methyl triflate only resulted in gradual decomposition to complicated mixtures of products, and no tetrasubstituted hydrazines were detected by mass spectrometric analysis.

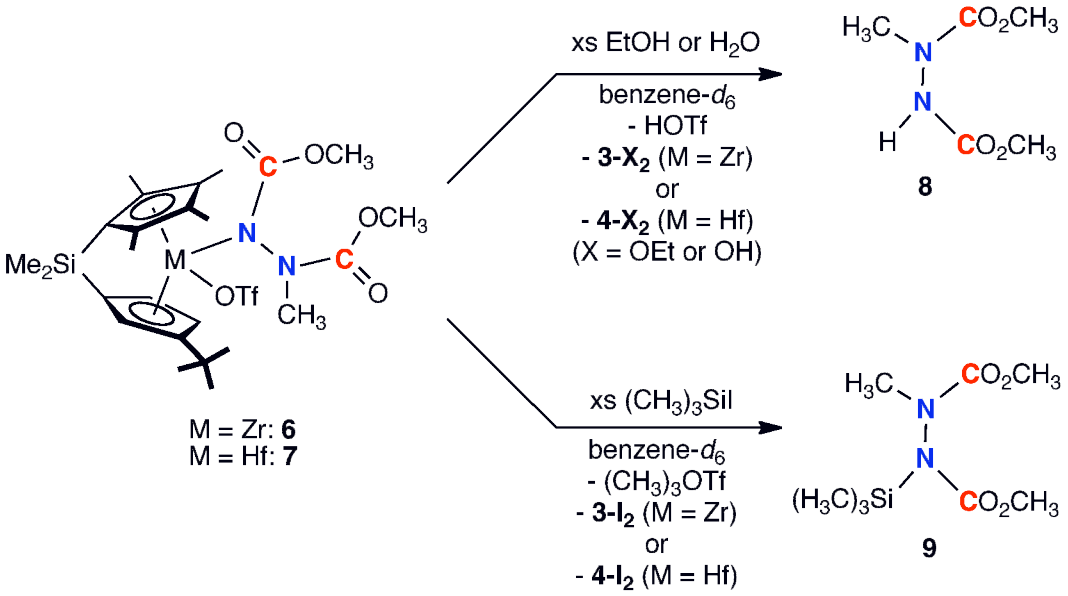

Figure 4.16. Hydrolysis and addition of $(CH_3)_3SiI$ to *ansa*-metallocene hydrazide complexes **6** and **7**.

Although excess methyl triflate is not sufficient to cleave to the Zr−N(hydrazido) bond in **6** and **7**, free hydrazine, **8**, was obtained upon hydrolysis (Figure 4.16). A parent ion peak of 162 amu in the mass spectrum of **8** was observed

for the natural abundance hydrazine, and the appropriate isotopic perturbations were observed upon preparation of the d_9 isotopologue from CD_3OTf, $^{13}C_2$ isotopologues from independent additions of $^{13}CH_3OTf$ and $^{13}CO_2$, respectively, and the $^{13}C_4$ isotopologue from the combination of $^{13}CH_3OTf$ and $^{13}CO_2$. While excess MeOTf and MeI proved ineffective for removing the free hydrazine (even with heating), addition of excess Me_3SiI to **6** produced a mixture of the previously reported silylated hydrazine, **9**,[31] along with **3-I$_2$** and Me_3SiOTf (Figure 4.16).

The successful elaboration and subsequent liberation of *N*,*N'*-dicarboxylated hydrazines from **3-N$_2$** and **4-N$_2$** prompted a similar study with the previously reported *N*,*N*-dicarboxylated hafnocene hydrazido complex, **2-NN(CO$_2$)$_2$**.[19] Treatment of a benzene-d_6 solution of **2-NN(CO$_2$)$_2$** with 3 equivalents of methyl triflate resulted in clean formation of a 1:1 mixture of the previously reported[32] hafnocene bis(triflate), **2-(OTf)$_2$**, and a new product identified as the hydrazido hafnocene triflate compound, **10** (Figure 4.17). Prolonged exposure of **10** to excess methyl triflate resulted in no further reaction at temperatures up to 90 °C, whereupon gradual decomposition was observed. The reaction is therefore akin to those discussed previously (Figure 4.10) and the hafnocene hydrazido product is resistant to Hf-N cleavage by methyl triflate. The structure of compound **10** was established by multinuclear (^{1}H, ^{13}C, ^{15}N) NMR and vibrational spectroscopies.

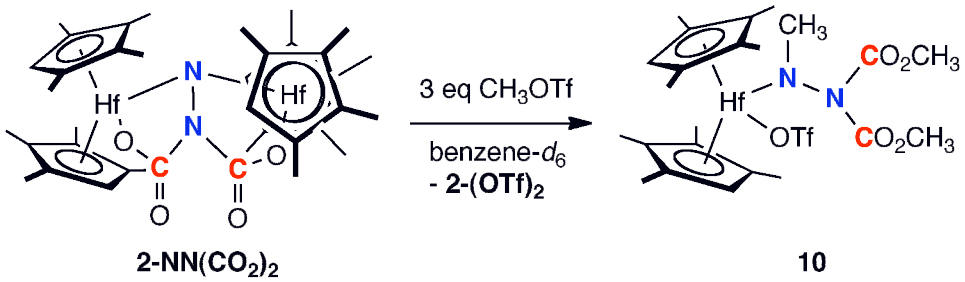

2-NN(CO$_2$)$_2$ **10**

Figure 4.17. Addition of methyl triflate to previously reported hafnocene hydrazide compound **2-NN(CO$_2$)$_2$**.

Similar to **6** and **7** above (Figure 4.16), hydrolysis of **10** afforded the corresponding free dicarboxylated hydrazine, **11** (Figure 4.18), as judged by NMR spectroscopy and mass spectrometry. Addition of iodotrimethylsilane also resulted in liberation of the corresponding silylated hydrazine, **12** (Figure 4.19), along with the diiodide compound **6-I$_2$** and $(CH_3)_3SiOTf$. These results highlight the importance of ligand choice in the CO_2 addition reactions, and demonstrate that a variety of substituted hydrazines are synthetically accessible from atmospheric dinitrogen and small carbon-based feedstocks. A summary of the substituted hydrazines synthesized in this work and accompanying mass spectral data is presented in Figure 4.19.

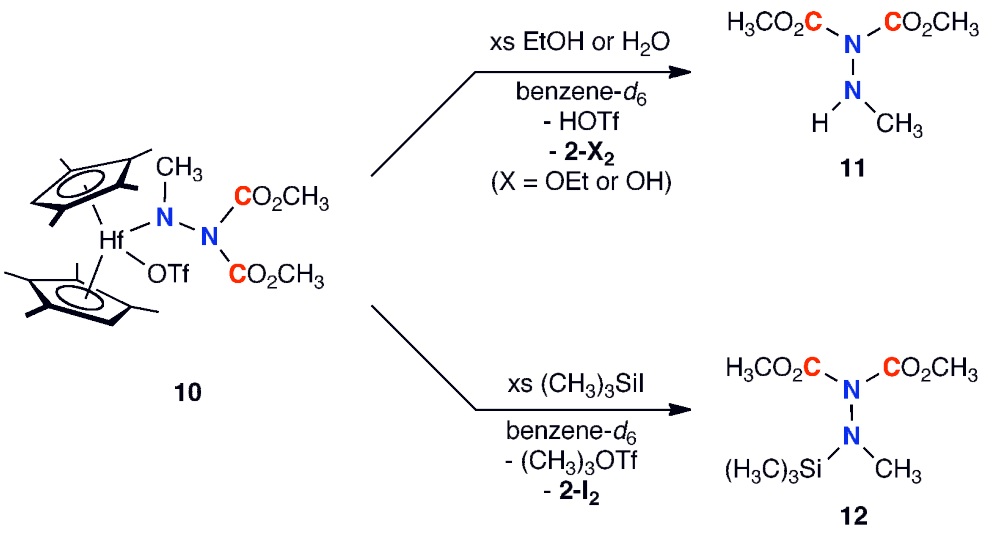

Figure 4.18. Hydrolysis and addition of $(CH_3)_3SiI$ to hafnocene hydrazide complexes **10**.

From **3-N_2 / 4-N_2**:

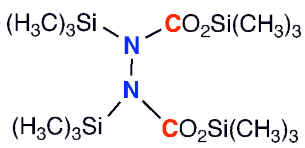

5

Natural Abundance: m/z = 408
^{13}C labeled: m/z = 410
^{13}C, ^{15}N labeled: m/z = 412
^{13}C NMR, d = 157.2, 170.1 ppm
$^{1}J_{C\text{-}N}$ = 16.5 Hz

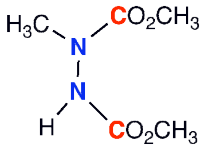

8

Natural Abundance: m/z = 162
All CD_3 groups: m/z = 171
All CD_3 groups, $^{13}CO_2$: m/z = 173
All $^{13}CH_3$ groups: m/z = 165

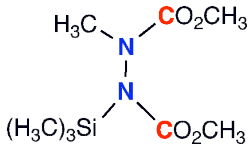

9

Natural Abundance: m/z = 234
Previously reported[31]

From **2-N_2**:[19]

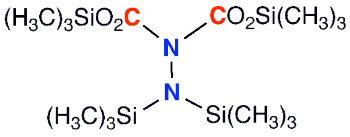

Natural Abundance: m/z = 408
^{13}C labeled: m/z = 410
^{13}C, ^{15}N labeled: m/z = 412
^{13}C NMR, d = 157.7, 157.23 ppm
$^{1}J_{C\text{-}N}$ = 20.6 Hz

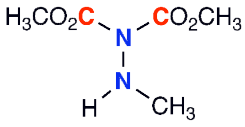

11

Natural Abundance: m/z = 162
All CD_3 groups: m/z = 171
All CD_3 groups, $^{13}CO_2$: m/z = 173
All $^{13}CH_3$ groups: m/z = 165

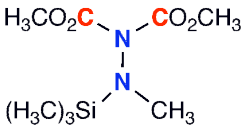

12

Natural Abundance: m/z = 234
3 CD_3 groups: m/z = 243
3 $^{13}CH_3$ groups: m/z = 237

Figure 4.19. Summary of substituted hydrazines synthesized in this work.

Preliminary investigations: Carboxylation of metallocene dinitrogen complexes bearing alternative ligand substituents. Two additional *ansa*-zirconocene dinitrogen complexes, $([Me_2Si(\eta^5\text{-}C_5Me_4)(\eta^5\text{-}C_5H_3\text{-}^{i}Pr)]Zr)_2(\mu_2,\eta^2,\eta^2\text{-}N_2)$ (**5-N_2**) and $([Me_2Si(\eta^5\text{-}C_5Me_4)(\eta^5\text{-}C_5H_3\text{-}^{Cy}Hexyl)]Zr)_2(\mu_2,\eta^2,\eta^2\text{-}N_2)$ (**6-N_2**), were studied for their reactivity with carbon dioxide. We were interested in studying the effect of the cyclopentadienyl substitutent on the regioselectivity of carbon dioxide insertion into the metal nitrogen bonds, as well as the impact on subsequent reactivity with electrophiles such as methyl triflate. Compound **5-N_2** has been previously

reported, and was isolated as a mixture of the *syn*-homochiral and *anti*-homochiral dimers.[33] The cyclohexyl-cyclopentadienyl substituted dinitrogen compound **6-N$_2$** was prepared by sodium amalgam (0.5%, 5 equivalents) reduction of the corresponding diiodide, **6-I$_2$**, for 5 days under an atmosphere of dinitrogen (Figure 4.20). The desired product was recrystallized from diethyl ether, furnishing green crystals of **6-N$_2$** as a single diastereomer, the *syn*-homochiral dimer as determined by multinuclear NMR spectroscopic characterization.

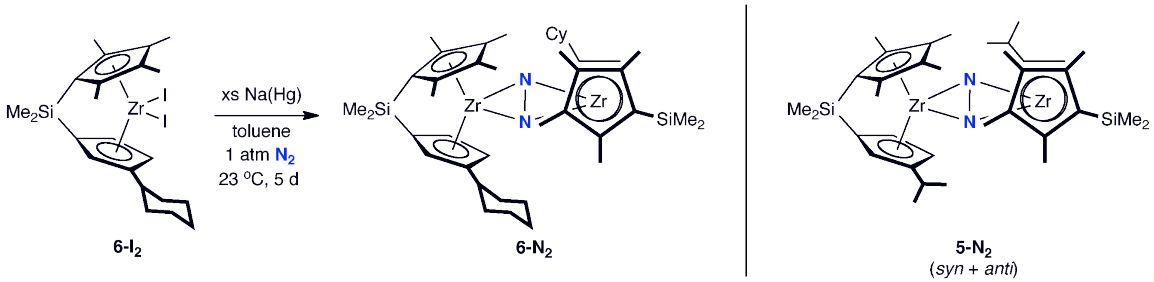

Figure 4.20. Additional *ansa*-zirconocene dinitrogen complexes studied in this work, **5-N$_2$**[33] and **6-N$_2$**.

Addition of carbon dioxide to pentane solutions of **5-N$_2$** and **6-N$_2$** resulted in precipitation of the corresponding carboxylated products, **5-(NCO$_2$)$_2$** and **6-(NCO$_2$)$_2$**, respectively (Figure 4.21). Compound **5-(NCO$_2$)$_2$** exhibits idealized C_2-symmetry in solution as judged by NMR spectroscopy, consistent with *N,N'*-dicarboxylation of the starting nitrogen compounds Unfortunately **6-(NCO$_2$)$_2$** is insoluble in most solvents and is tenuously assigned based on infrared spectroscopic and degradation studies as having a structural configuration analogous to **3-(NCO$_2$)$_2$** and **5-(NCO$_2$)$_2$**. A summary of spectroscopic data for these molecules along with a comparative data for related compounds is presented in Figure 4.22.

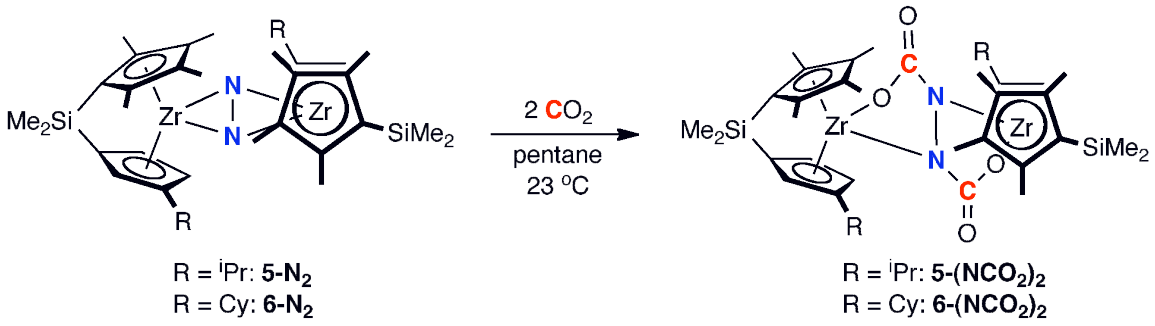

Figure 4.21. Addition of carbon dioxide to *ansa*-zirconocene dinitrogen compounds **5-N_2** and **6-N_2**.

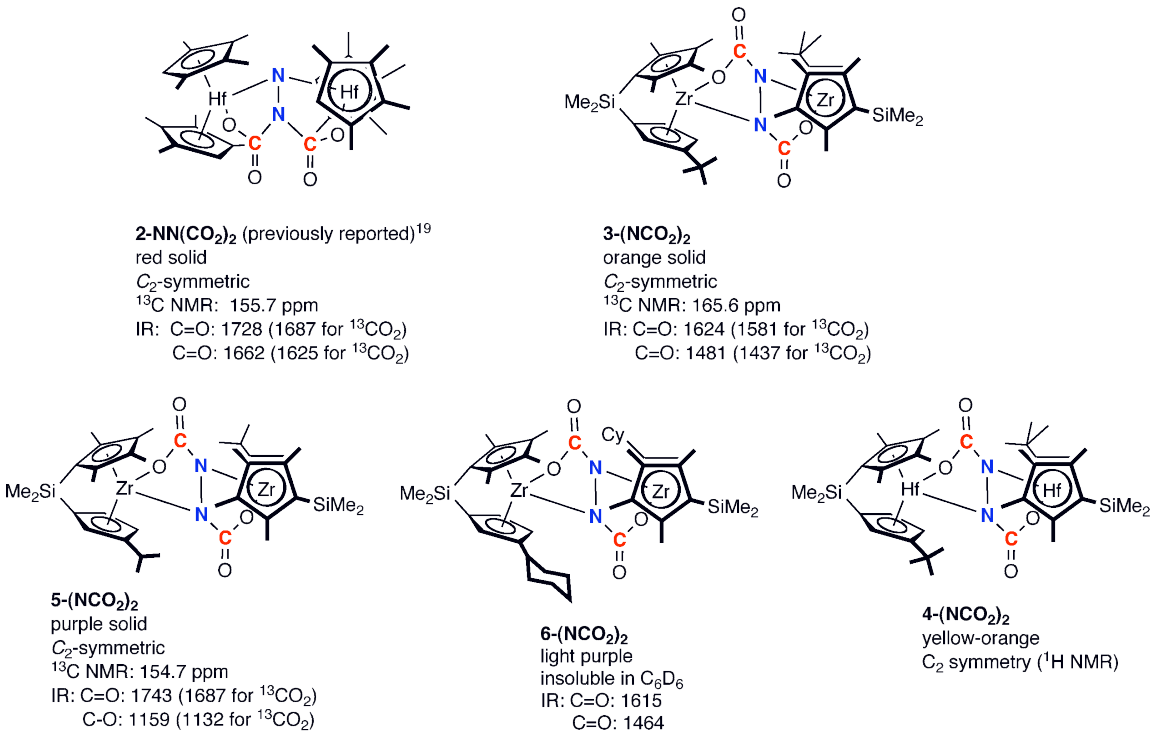

Figure 4.22. Comparison of products formed from dicarboxylation of metallocene dinitrogen compounds.

Conclusions

A series of C_2-symmetric *ansa*-zirconocene dinitrogen complexes promote the selective insertion of 2 equivalents of carbon dioxide into Zr−N bonds resulting in the synthesis of a variety of *N*,*N'*-dicarboxylated hydrazines from two inert atmospheric gases, N_2 and CO_2. In some cases the functionalized product was treated with silyl- and carbon-based electrophiles to form new N−Si and N−C bonds, respectively. The previously reported hafnocene complex **2-NN(CO$_2$)$_2$** was also revisited,[19] and elaboration of this molecule led to additional N-C bond formation and synthesis of several unique *N*,*N*-carboxylated hydrazines. Together these results open new synthetic pathways for the selective synthesis of organic molecules from abundant chemical feedstocks and demonstrate that such N_2 functionalization with heterocumulenes reactions are available to a range of zirconocene and hafnocene dinitrogen complexes.

Experimental Section

General Considerations. All air- and moisture-sensitive manipulations were carried out using standard high vacuum line, Schlenk or cannula techniques or in an M. Braun inert atmosphere drybox containing an atmosphere of purified nitrogen. The M. Braun drybox was equipped with a cold well designed for freezing samples in liquid nitrogen. Solvents for air- and moisture-sensitive manipulations were dried and deoxygenated using literature procedures.[34] Toluene, benzene, pentane and heptane were further dried by distillation from "titanocene".[35] Deuterated solvents for NMR spectroscopy were distilled from sodium metal under an atmosphere of argon and stored over 4 Å molecular sieves. Argon and hydrogen gas were purchased from Airgas Incorporated and passed through a column containing manganese oxide on vermiculite and 4 Å molecular sieves before admission to the high vacuum line.

Carbon dioxide was also dried over 4 Å molecular sieves before admission to the high vacuum line. Trimethylsilyl iodide was purchased from Acros and dried over 4 Å molecular sieves prior to use. The hafnocene dinitrogen complex, **2-N_2**, was prepared according to literature procedures.[17] **3-N_2**[26] was prepared as described previously using the diiodide precursor, **3-I_2**.

^{1}H NMR spectra were recorded on a Varian Inova 400 Spectrometer operating at 399.860 MHz. All chemical shifts are reported relative to $SiMe_4$ using ^{1}H (residual) chemical shifts of the solvent as a secondary standard. ^{2}H, ^{13}C, ^{29}Si, and ^{15}N NMR spectra were recorded on a Varian Inova 500 Spectrometer operating at 76.848, 125.716, 161.83, 99.320 and 50.663 MHz, respectively. ^{2}H, ^{29}Si, and ^{13}C chemical shifts are reported relative to $SiMe_4$ using chemical shifts of the solvent as a secondary standard where applicable. ^{15}N chemical shifts are reported relative liquid to NH_3 using an external standard.

Mass spectra were acquired using a JEOL GCMate II mass spectrometer operating at 500 (LRMS) resolving power (20% FWHM) in positive ion mode and an electron ionization (EI) potential of 70 eV. Samples were introduced via a GC inlet using an Agilent HP 6890N GC equipped with a 30 m (0.25 m i.d.) HP-5ms capillary GC column. The carrier gas is helium with a flow rate of 1 mL/min. Samples were introduced into the GC using a split/splitless injector at 230 ºC with a split ratio of 50:1. Infrared spectroscopy was conducted on a Mattson RS-10500 Research Series FT-IR spectrometer calibrated with a polystyrene standard. Elemental analyses were performed at Robertson Microlit Laboratories, Inc., in Madison, NJ.

Preparation of [$Me_2Si(\eta^5$-$C_5Me_4)(\eta^5$-C_5H_3-3-^{t}Bu)]ZrI_2 (3-I_2). A 20 mL scintillation vial was charged with 1.31 g (0.0028 mol) of [$Me_2Si(\eta^5$-$C_5Me_4)(\eta^5$-C_5H_3-3-^{t}Bu)]$ZrCl_2$ dissolved in approximately 10 mL of toluene. To the vial 4.55 g (0.023 mol) of

iodotrimethylsilane was added with stirring. The reaction was stirred at room temperature for 5 days. Excess iodotrimethylsilane and toluene were removed *in vacuo*, yielding a yellow solid identified as **3-I_2** in quantitative yield. ^{1}H NMR (benzene-d_6): ∂ = 0.25 (s, 3H, SiMe_2), 0.33 (s, 3H, SiMe_2), 1.57 (s, 9H, $C_5H_3CMe_3$), 1.65 (s, 3H, C_5Me_4), 2.28 (s, 3H, C_5Me_4), 2.34 (s, 3H, C_5Me_4), 5.26 (m, 1H, $C_5H_3CMe_3$), 5.58 (m, 1H, $C_5H_3CMe_3$), 7.45 (m, 1H, $C_5H_3CMe_3$). One C_5Me_4 not observed. {^{1}H} ^{13}C NMR (benzene-d_6): ∂ = -0.94 (SiMe_2), 0.46 (SiMe_2), 15.91 (CpMe), 16.58 (CpMe), 16.92 (CpMe), 18.35 (CpMe), 31.78 (CMe_3), 34.60 (CMe$_3$), 96.02, 101.29, 112.17, 113.86, 125.03, 129.23, 130.04, 136.13, 137.54, 151.45 (*Cp*).

Preparation of ([$Me_2Si(\eta^5$-$C_5Me_4)(\eta^5$-C_5H_3-3-^{t}Bu)]Zr)$_2(NCO_2)_2$ (3-$(NCO_2)_2$). A J. Young NMR tube was charged with 0.045 g (0.056 mmol) of **3-N_2** and approximately 1 mL of pentane was added. On a high-vacuum line, two equivalents (0.11 mmol) of CO_2 were admitted to the tube via a calibrated gas bulb. The green color of the starting dinitrogen compound disappeared and an orange precipitate formed over several minutes. The tube was transferred to the dry box and the orange solid was collected by filtration, washed with cold pentane and dried *in vacuo* to obtain **3-$(NCO_2)_2$** in 76% yield. Anal. Calcd for $C_{42}H_{60}O_4N_2Si_2Zr_2$: C, 56.32; H, 6.75; N, 3.13. Found: C, 55.97; H, 6.94; N, 2.99. ^{1}H NMR (benzene-d_6): ∂ = 0.48 (s, 3H, SiMe_2), 0.61 (s, 3H, SiMe_2), 1.39 (s, 9H, $C_5H_3CMe_3$), 1.91 (s, 3H, C_5Me_4), 1.99 (s, 3H, C_5Me_4), 2.10 (s, 3H, C_5Me_4), 2.19 (s, 3H, C_5Me_4), 5.79 (m, 1H, $C_5H_3CMe_3$), 5.91 (m, 1H, $C_5H_3CMe_3$), 6.76 (m, 1H, $C_5H_3CMe_3$). {^{1}H} ^{13}C NMR (benzene-d_6): ∂ = 165.6 (NCO_2). ^{15}N NMR (benzene-d_6): ∂ = 209.5 ($^{15}N_2$). ($^1J_{CN}$=8.4 Hz, $^2J_{CN}$=2.2 Hz, $^1J_{NN}$=17.3 Hz, $^3J_{CC}$=3.8 Hz). IR (KBr): ν = 1481, 1624 cm^{-1} (C=O); n = 1437, 1581 cm^{-1} (^{13}C=O).

Preparation of ([$Me_2Si(\eta^5$-$C_5Me_4)(\eta^5$-C_5H_3-3-^{t}Bu)]Hf)$_2(NCO_2)_2$ (4-$(NCO_2)_2$). This compound was prepared similarly to **3-$(NCO_2)_2$** above, using 0.066 g (0.067 mmol) of **4-N_2** and 2.2 equivalents (0.148 mmol) of CO_2. A yellow-orange precipitate formed after several minutes. Filtration and cold pentane washings furnished the product, **4-$(NCO_2)_2$** as a yellow solid in 73 % yield. ^{1}H NMR (benzene-d_6): ∂ = 0.49 (s, 3H, SiMe_2), 0.61 (s, 3H, SiMe_2), 1.41 (s, 9H, $C_5H_3CMe_3$), 1.96 (s, 3H, C_5Me_4), 2.07 (s, 3H, C_5Me_4), 2.15 (s, 3H, C_5Me_4), 2.27 (s, 3H, C_5Me_4), 5.79 (m, 1H, $C_5H_3CMe_3$), 5.87 (m, 1H, $C_5H_3CMe_3$), 6.77 (m, 1H, $C_5H_3CMe_3$).

Preparation of $[(Me_3Si)(Me_3SiO_2C)N]_2$ (5). A J. Young NMR tube was charged with 0.010 g (0.011 mmol) of **3-$(NCO_2)_2$** and approximately 0.5 mL benzene-d_6. To the solution was added an excess (6.4 mL (0.11 mmol)) of iodotrimethylsilane. The tube was shaken for several minutes, during which time the solution became yellow indicative of zirconium diiodide formation and hydrazine generation. A diastereomeric mixture of the product, **5**, was characterized *in situ* as follows: ^{1}H NMR (benzene-d_6): ∂ = 0.32, 0.42, 0.53 ((CH_3)$_3$SiN, (CH_3)$_3$SiOCO). $\{^1H\}^{13}$C NMR (benzene-d_6): ∂ = 157.2, 170.1 ppm (N^{13}*C*OSi); ($^1J_{CN}$=16.5 Hz). LRMS (m/z) $[(Me_3Si)(Me_3SiO_2C)N]_2$: 408, 393, 147, 73; $[(Me_3Si)(Me_3SiO_2{}^{13}C)N]_2$: 410, 395, 147, 73. $[(Me_3Si)(Me_3SiO_2{}^{13}C)^{15}N]_2$: 412, 398, 147, 73. Free hydrazine **5** was also prepared in a similar manner starting from the hafnocene congener **4-$(NCO_2)_2$**.

Preparation of $Me_2Si(\eta^5$-$C_5Me_4)(\eta^5$-C_5H_3-3-^{t}Bu)Zr(OTf) [N(CO_2Me)N (CO_2Me)(Me)] (6). A 25 mL round bottom flask was charged with 0.080 g (0.089 mmol) **3-$(NCO_2)_2$** and slurried in approximately 10 mL of pentane. On a high vacuum line, the flask assembly was submerged in liquid nitrogen and degassed. At this temperature, 132 torr (0.71 mmol) of methyl triflate were admitted. Upon thawing, a

yellow solution formed after several minutes and was identified as an equimolar mixture of **6** and the corresponding bis(triflate) species, **3-(OTf)$_2$**. Excess methyl triflate and solvent were removed in vacuo and the remaining yellow solid was extracted into approximately 5 mL pentane and recrystallized at -35 ºC (45.1% yield). ^{1}H NMR (benzene-*d$_6$*): ∂ = 0.50 (s, 3H, Si*Me$_2$*), 0.51 (s, 3H, Si*Me$_2$*), 1.03 (s, 9H, C_5H_3C*Me$_3$*), 1.81 (s, 3H, C_5*Me$_4$*), 2.03 (s, 3H, C_5*Me$_4$*), 2.12 (s, 3H, C_5*Me$_4$*), 2.19 (s, 3H, C_5*Me$_4$*), 3.24 (s, 3H, C*H*$_3O_2$CNZr), 3.34 (s, 3H, C*H*$_3$NNZr), 3.47 (s, 3H, C*H*$_3O_2$CNNZr), 5.33 (m, 1H, C_5*H*$_3$CMe$_3$), 6.37 (m, 1H, C_5*H*$_3$CMe$_3$), 7.22 (m, 1H, C_5*H*$_3$CMe$_3$). {^{1}H} ^{13}C NMR (benzene-*d$_6$*): ∂ = 38.26 (N^{13}*C*H$_3$, $^1J_{CN}$=11.5 Hz, $^2J_{CN}$=1.3 Hz, $^3J_{CC}$=6.3 Hz), 53.40 (NCO$_2{}^{13}$*C*H$_3$, $^3J_{CC}$=8.1 Hz), 52.91 (NCO$_2{}^{13}$*C*H$_3$, $^3J_{CC}$=4.5 Hz), 155.20 (N^{13}*C*O$_2$, $^1J_{CN}$=29.4 Hz), 162.61 (N^{13}*C*O$_2$, $^1J_{CN}$=10.4 Hz). IR (KBr): ν = 1518 cm^{-1}, 1720 (C=O); 1489, 1678 (^{13}C=O); 1014, 1364 (SO_3); 1202 (CF_3).

Preparation of Me$_2$Si(*η*^{5}-C$_5$Me$_4$)(*η*^{5}-C$_5$H$_3$-3-^{t}Bu)Hf(OTf) [N(CO$_2$Me)N (CO$_2$Me)(Me)] (7). This compound was prepared similarly to **6** above, using 0.012 (0.011 mmol) g **4-(NCO$_2$)$_2$** and 4 equivalents (0.045 mmol) of methyl triflate admitted *via* calibrated gas bulb. Product **7** was formed in an equimolar ratio with the corresponding bis(triflate) compound **4-(OTf)$_2$**.

Preparation of Me$_2$Si(*η*^{5}-C$_5$Me$_4$)(*η*^{5}-C$_5$H$_3$-3-^{t}Bu)Zr(OTf)$_2$, (3-(OTf)$_2$). 3-(OTf)$_2$ was prepared as a byproduct of the reaction yielding **6**. **6** and **3-(OTf)$_2$** were formed in an equimolar ratio. **3-(OTf)$_2$** was independently prepared by addition of 2.2 equivalents of silver triflate (0.012 g, 0.047 mmol) to a benzene solution containing 0.014 g (0.022 mmol) of **3-I$_2$**. The AgI byproduct was removed via filtration and the solvent was removed in vacuo affording **3-(OTf)$_2$** in quantitative yield. ^{1}H NMR (benzene-*d$_6$*): ∂ = 0.30 (s, 3H, Si*Me$_2$*), 0.39 (s, 3H, Si*Me$_2$*), 1.09 (s, 9H, C_5H_3C*Me$_3$*),

1.62 (s, 3H, C_5Me_4), 1.68 (s, 3H, C_5Me_4), 1.94 (s, 3H, C_5Me_4), 2.00 (s, 3H, C_5Me_4), 5.48 (m, 1H, $C_5H_3CMe_3$), 6.02 (m, 1H, $C_5H_3CMe_3$), 7.11 (m, 1H, $C_5H_3CMe_3$). $\{^1H\}^{13}C$ NMR (benzene-d_6): ∂ = -1.61 ($SiMe_2$), 0.19 ($SiMe_2$), 10.97 (Cp*Me*), 12.75 (Cp*Me*), 15.02 (Cp*Me*), 15.17 (Cp*Me*), 30.26 (CMe_3), 31.44 (CF_3), 31.76 (CF_3), 33.89 (CMe_3), 103.14, 110.80, 113.07, 120.33, 121.75, 125.99, 135.77, 137.52, 144.81, 162.49 (*Cp*). ^{19}F NMR (benzene-d_6): ∂ = -75.27, -74.10 (CF_3). IR (KBr): ν = 997, 1360 cm^{-1} (SO_3); 1198 cm^{-1} (CF_3).

Preparation of $Me_2Si(\eta^5\text{-}C_5Me_4)(\eta^5\text{-}C_5H_3\text{-}3\text{-}^tBu)Hf(OTf)_2$ (4-$(OTf)_2$). This compound was independently synthesized with a procedure similar to that used for the synthesis of **3-$(OTf)_2$** above, using 0.100 g (0.18 mmol) of **4-Cl_2** and 0.103 g (0.40 mmol) AgOTf. The product **4-$(OTf)_2$** was recrystallized from diethyl ether and obtained in 86 % yield. ^1H NMR (benzene-d_6): ∂ = 0.31 (s, 3H, $SiMe_2$), 0.40 (s, 3H, $SiMe_2$), 1.09 (s, 9H, $C_5H_3CMe_3$), 1.75 (s, 3H, C_5Me_4), 1.80 (s, 3H, C_5Me_4), 2.00 (s, 3H, C_5Me_4), 2.09 (s, 3H, C_5Me_4), 5.49 (m, 1H, $C_5H_3CMe_3$), 6.03 (m, 1H, $C_5H_3CMe_3$), 7.05 (m, 1H, $C_5H_3CMe_3$). ^{19}F NMR (benzene-d_6): ∂ = -76.33, -74.93 (CF_3).

Preparation of (H)(CO_2Me)NN(CO_2Me)(Me) (8). The free hydrazine **8** was prepared by treating a benzene-d_6 solution of **6** (0.005g, 0.0078 mmol) with approximately 50 mL of H_2O and shaking for 20 minutes. The resulting mixture was filtered through a thin layer of celite and solvent was removed from the filtrate *in vacuo* leaving a pale yellow oil identified as **8**. Free hydrazine **8** was also prepared in a similar manner starting from the hafnocene congener **4-$(NCO_2)_2$**. ^1H NMR (benzene-d_6): ∂ = 1.09 (s, 3H, N*Me*, $^1J_{HC}$=129.6 Hz), 3.31 (br s, 3H, CO_2Me, $^1J_{HC}$=146.3 Hz), 3.36 (br s, 3H, CO_2Me, $^1J_{HC}$=147.6 Hz), one N-H not observed. $\{^1H\}^{13}C$ NMR (benzene-d_6): ∂ = 31.01 (N*Me*), 52.37 (NCO_2Me), 53.00 (Cp*Me*), 156.03 (CO_2Me),

157.14 (CO$_2$Me). GC-MS: LRMS (m/z) (Me)(MeO$_2$C)N-N(CO$_2$Me)(H): 162, 130, 103, 88, 59; (Me)(MeO$_2$^{13}C)N-N(^{13}CO$_2$Me)(H): 164, 132, 104, 89, 60; (CD$_3$)(CD$_3$O$_2$C)N-N(CO$_2$CD$_3$)(H): 171, 136, 109, 94, 62; (CD$_3$)(CD$_3$O$_2$^{13}C)N-N(^{13}CO$_2$CD$_3$)(H): 173, 138, 110, 95, 63; (^{13}CH$_3$)(^{13}CH$_3$O$_2$C)N-N(CO$_2$^{13}CH$_3$)(H): 165, 132, 105, 90, 60.

Preparation of (Me$_3$Si)(CO$_2$Me)NN(CO$_2$Me)(Me) (9). The free hydrazine **9** was prepared by treating a benzene-d_6 solution of **6** (0.006 g, 0.0089 mmol) with 10 equivalents of iodotrimethylsilane (13 mL, 0.089 mmol) at room temperature. Formation of **9** occurred within 5 minutes in 33.3% yield with concomitant formation of the corresponding zirconium diiodide compound, **3-I$_2$** and trimethylsilyl triflate. Free hydrazine **9** was also prepared in a similar manner starting from the hafnocene congener **4-(NCO$_2$)$_2$**. Characterization of **9** by ^{1}H NMR spectroscopy is consistent with previous literature values.[31] ^{1}H NMR (dichloromethane-d_2): ∂ = 0.25 (s, 9H, SiMe_3), 3.06 (s, 3H, NMe), 3.65 (s, 3H, CO$_2$$Me$), 3.70 (s, 3H, CO$_2$$Me$). GC-MS: LRMS (m/z): 234, 219, 163, 130, 89, 73, 59.

Preparation of (η^5-C$_5$Me$_4$H)$_2$Hf(OTf)[N(Me)N(CO$_2$Me)$_2$] (10). This compound was prepared similarly to **6** above, using 0.015 g (0.017 mmol) of **2-NN(CO$_2$)$_2$** and 4 equivalents (0.069 mmol) of methyl triflate admitted *via* calibrated gas bulb. Product **10** was formed in an equimolar ratio with the corresponding bis(triflate) compound **2-(OTf)$_2$**.[32] ^{1}H NMR (benzene-d_6): ∂ = 1.65 (s, 3H, C$_5$$Me_4$H), 1.70 (s, 3H, C$_5$$Me_4$H), 1.74 (s, 3H, C$_5$$Me_4$H), 2.02 (s, 3H, C$_5$$Me_4$H), 2.05 (s, 3H, C$_5$$Me_4$H), 2.12 (s, 3H, C$_5$$Me_4$H), 2.17 (s, 3H, C$_5$$Me_4$H), 3.18 (s, 3H, C$H_3O_2$CNNHf), 3.29 (s, 3H, C$H_3$NHf), 3.54 (s, 3H, C$H_3O_2$CNNHf), 5.72 (m, 1H, C$_5Me_4$$H$), 6.33 (m, 1H, C$_5Me_4$$H$), One

Cp*Me* resonance not found. $\{^1H\}$ ^{13}C NMR (benzene-d_6): ∂ = 32.99 ($N^{13}CH_3$), 57.50 ($NCO_2{}^{13}CH_3$), 58.55 ($NCO_2{}^{13}CH_3$), 156.02 ($N^{13}CO_2$), 162.34 ($N^{13}CO_2$).

Preparation of 11. The free hydrazine **11** was prepared by treating a benzene-d_6 solution of **10** (0.020 g, 0.028 mmol) with approximately 50 mL of H_2O and shaking for 20 minutes. The resulting mixture was filtered through a thin layer of celite and solvent was removed from the filtrate *in vacuo* leaving a pale yellow oil identified as **11**. GC-MS: LRMS (m/z) (Me)(H)N-N(CO_2Me)$_2$: 162, 130, 103, 88, 59; (Me)(H)N-N($^{13}CO_2Me$)$_2$: 164, 132, 104, 89, 60; (CD_3)(H)N-N(CO_2CD_3)$_2$: 171, 136, 109, 94, 62.

Preparation of 12. The free hydrazine **12** was prepared by treating a benzene-d_6 solution of **10** (0.015 g, 0.021 mmol) with 10 equivalents of iodotrimethylsilane (3.1 μL, 0.21 mmol) at room temperature. Formation of **12** occurred within 5 minutes with concomitant formation of the corresponding hafnocene diiodide compound, **2-I_2** and trimethylsilyl triflate. GC-MS: LRMS (m/z): 234, 219, 163, 130, 89, 73, 59.

Preparation of ([$Me_2Si(\eta^5$-$C_5Me_4)(\eta^5$-C_5H_3-^{Cy}Hexyl)]Zr)$_2(\mu_2,\eta^2,\eta^2$-N_2) (6-N_2). A 100 mL round-bottomed flask was charged with 13.87 g of 0.5% sodium amalgam and 15 mL of toluene. With vigorous stirring, 0.400 g (0.75 mmol) of [$Me_2Si(\eta^5$-$C_5Me_4)(\eta^5$-C_5H_3-^{Cy}Hexyl)]ZrI_2 was added as a yellow toluene solution, and the resulting reaction mixture was stirred for 5 days at ambient temperature. The resulting green solution was filtered through a pad of Celite, and the solvent was removed *in vacuo*, leaving a green solid. Recrystallization from diethyl ether furnished green crystals of **6-N_2** in 64 % yield. ^1H NMR (benzene-d_6): δ = 0.60 (s, 3H, Si*Me*$_2$), 0.71 (s, 3H, Si*Me*$_2$), 1.15-1.95 (m, 10H, $C_5H_3{}^{Cy}$*Hexyl*), 1.75 (s, 3H, C_5Me_4), 1.90 (s, 3H, C_5Me_4), 2.05 (s, 3H, C_5Me_4), 2.23 (s, 3H, C_5Me_4), 2.27 (s, 3H, C_5Me_4), 2.80 (m, 1H,

$C_5H_3(CH)$), 5.65 (m, 1H, $C_5H_3CMe_3$), 5.74 (m, 1H, $C_5H_3CMe_3$), 5.83 (m, 1H, $C_5H_3CMe_3$).

Preparation of ([$Me_2Si(\eta^5$-$C_5Me_4)(\eta^5$-C_5H_3-3-^{i}Pr)]Zr)$_2(NCO_2)_2$ (5-$(NCO_2)_2$). This compound was prepared similarly to **3-$(NCO_2)_2$** above, using 0.070 g (0.090 mmol) of **5-N_2** and 2.2 equivalents (0.20 mmol) of CO_2. A purple precipitate formed after several minutes. Filtration and cold pentane washings furnished the product, **5-$(NCO_2)_2$** as a purple solid in 67 % yield. ^{1}H NMR (benzene-d_6): ∂ = 0.57 (s, 6H, $SiMe_2$), 0.60 (s, 6H, $SiMe_2$), 1.30 (d, 12H, $C_5H_3CHMe_2$), 1.71 (s, 6H, C_5Me_4), 2.11 (s, 6H, C_5Me_4), 2.13 (s, 6H, C_5Me_4), 2.29 (s, 6H, C_5Me_4), 3.27 (m, 2H, $C_5H_3CHMe_2$), 5.61 (m, 4H, $C_5H_3CMe_3$), 6.31 (m, 2H, $C_5H_3CMe_3$). {^{1}H}^{13}C NMR (benzene-d_6): ∂ = 154.73 (NCO_2). IR (KBr): ν = 1159, 1743 cm^{-1} (O-C=O); ν = 1132, 1687 cm^{-1} (O-^{13}C=O).

Preparation of 6-$(NCO_2)_2$. Preparation of ([$Me_2Si(\eta^5$-$C_5Me_4)(\eta^5$-C_5H_3-3-^{Cy}Hexyl)]Zr)$_2(NCO_2)_2$ (6-$(NCO_2)_2$). This compound was prepared similarly to **3-$(NCO_2)_2$** above, using 0.065 g (0.076 mmol) of **6-N_2** and 2.2 equivalents (0.17 mmol) of CO_2. A red-purple precipitate formed after several minutes. Filtration and cold pentane washings furnished the product, **6-$(NCO_2)_2$** as a purple solid in 41 % yield. IR (KBr): ν = 1464, 1615 cm^{-1} (C=O).

REFERENCES

[1] Aresta, M.; Armor, J. N.; Barteau, M. A.; Beckman, E. J.; Bell, A. T.; Bercaw, J. E.; Creutz, C.; Dinjus, E.; Dixon, D. A.; Domen, K.; Dubois, D. L.; Eckert, J.; Fujita, E.; Gibson, D. H.; Goddard, W. A.; Goodman, D. W.; Keller, J.; Kubas, G. J.; Kung, H. H.; Lyons, J. E.; Manzer, L. E.; Marks, T. J.; Morokuma, K.; Nicholas, K. M.; Periana, R.; Que, L.; Rostrup-Nielson, J.; Sachtler, W. M. H.; Schmidt, L. D.; Sen, A.; Somorjai, G. A.; Stair, P. C.; Stults, B. R.; Tumas, W. *Chem. Rev.* **2001**, *101*, 953.

[2] (a) Schlgl, R. *Angew. Chem., Int. Ed.* **2003**, *42*, 2004. (b) Tamaru, K. In *Catalytic Ammonia Synthesis*; Jennings, J. R., Ed.; Plenum: New York, **1991**. (c) Pimentel, D.; Patzek, T. W. *Nat. Resources Res.* **2005**, *14*, 65.

[3] Ertl, G. *Angew. Chem., Int. Ed.* **2008**, *47*, 3524.

[4] Hager, T. *The Alchemy of Air*; Three Rivers Press: New York, **2008**.

[5] Guiducci, A. E.; Cowley, A. R.; Skinner, M. E. G.; Mountford, P. *J. Chem. Soc., Dalton Trans.* **2001**, 1392.

[6] Hazari, N.; Mountford, P. *Acc. Chem. Res.* **2005**, *38*, 839.

[7] Guiducci, A. E.; Boyd, C. L.; Mountford, P. *Organometallics* **2006**, *25*, 1167.

[8] Dunn, S. C.; Hazari, N.; Cowley, A. R.; Green, J. C.; Mountford, P. *Organometallics* **2006**, *25*, 1755.

[9] Clulow, A. J.; Selby, J. D.; Cushion, M. G.; Schwarz, A. D.; Mountford, P. *Inorg. Chem.* **2008**, *47*, 12049.

[10] Trösch, D. J. M.; Collier, P. E.; Bashall, A.; Gade, L. H.; McPartlin, M.; Mountford, P.; Radojevic, S. *Organometallics* **2001**, *20*, 3308.

[11] Weitershaus, K.; Fillol, J. L.; Wadepohl, H.; Gade, L. H. *Organometallics* **2009**, *28*, 4747.

[12] Chisholm, M. H.; Extine, M. W. *J. Am. Chem. Soc.* **1977**, *99*, 792.

[13] Andersen, R. A. *Inorg. Chem.* **1979**, *18*, 2928.

[14] MacLachlan, E. A.; Fryzuk, M. D. *Organometallics* **2006**, *25*, 1530.

[15] Pool, J. A.; Lobkovsky, E.; Chirik, P. J. *Nature* **2004**, *427*, 527.

[16] Chirik, P. J. *Dalton Trans.* **2007**, 16.

[17] Bernskoetter, W. H.; Olmos, A. V.; Lobkovsky, E.; Chirik, P. J. *Organometallics* **2006**, *25*, 1021.

[18] Bernskoetter, W. H.; Olmos, A. V.; Pool, J. A.; Lobkovsky, E.; Chirik, P. J. *J. Am. Chem. Soc.* **2006**, *128*, 10696.

[19] Bernskoetter, W. H.; Lobkovsky, E.; Chirik, P. J. *Angew. Chem., Int. Ed.* **2007**, *46*, 2858.

[20] Evans, W. J.; Lorenz, S. E.; Ziller, J. W. *Inorg. Chem.*, **2009**, *48*, 2001.

[21] Ward, B. D.; Orde, G.; Clot, E.; Cowley, A. R.; Gade, L. H.; Mountford, P. *Organometallics* **2005**, *24*, 2368.

[22] For a full discussion see Chapters 1-3 of this Thesis and references 23-25.

[23] Knobloch, D. J.; Lobkovsky, E.; Chirik, P. J. *Nature Chem.* **2010**, *2*, 30.

[24] Knobloch, D. J.; Lobkovsky, E.; Chirik, P. J. *J. Am. Chem. Soc.* **2010**, *132*, 10553.

[25] Knobloch, D. J.; Lobkovsky, E.; Chirik, P. J. *J. Am. Chem. Soc.* **2010**, *132*, 15340.

[26] Hanna, T. E.; Keresztes, I.; Lobkovsky, E.; Chirik, P. J. *Inorg. Chem.* **2007**, *46*, 1675.

[27] Zachmanoglou, C. E.; Docrat, A.; Bridgewater, B. M.; Parkin, G.; Brandow, C. G.; Bercaw, J. E.; Jardine, C. N.; Lyall, M.; Green, J. C.; Keister, J. B. *J. Am. Chem. Soc.* **2002**, *124*, 9525.

[28] For application of *ansa*-cyclopentadienyl ligands in stereospecific olefin polymerization, see: Coates, G. W. *Chem. Rev.* **2000**, *100*, 1223.

[29] For related discussion, see Yin, X.; Moss, J. R. *Coord. Chem. Rev.* **1999**, *181*, 27 and references therein.

[30] Hirotsu, M.; Fontaine, P. P.; Zavalij, P. Y.; Sita, L. R. *J. Am. Chem. Soc.* **2007**, *129*, 12690.

[31] Kalinin, A. V.; Apasov, E. T.; Bugaeva, S. V.; Ioffe, S. L.; Tartakovskii, V. A. *Bull. Acad. Sci. USSR Div. Chem. Sci.* **1983**, *32*, 1282.

[32] Knobloch, D. J.; Benito-Garagorri, D.; Bernskoetter, W. H.; Keresztes, I.; Lobkovsky, E.; Toomey, H.; Chirik, P. J. *J. Am. Chem. Soc.* **2009**, *131*, 14903.

[33] Hanna, T. E. PhD Dissertation, Cornell University, **2006**.

[34] Pangborn, A. B.; Giardello, M. A.; Grubbs, R. H.; Rosen, R. K.; Timmers, F. J. *Organometallics* **1996**, *15*, 1518.

[35] Marvich, R. H.; Brintzinger, H. H. *J. Am. Chem. Soc.* **1971**, *93*, 2046.

CHAPTER 5

Addition of Carbon-based Electrophiles to a Series of Zirconocene and Hafnocene Dinitrogen Complexes: Stepwise N_2 Methylation and Formation of a Hafnocene Hydrazonato Compound.*

Abstract

A series of metallocene complexes was studied for the direct alkylation of the coordinated dinitrogen ligand. Generally when the metallocene dinitrogen compounds were treated with alkylating substrates such as methyl halides and methyl triflates, products derived from either dinitrogen loss or 1,4-addition chemistry were observed. However, in one exceptional case using $[(\eta^5\text{-}C_5Me_4H)_2Hf]_2(\mu_2,\eta^2,\eta^2\text{-}N_2)$ and methyl triflate, new nitrogen-carbon bond formation was observed, albeit in low yield. The resulting triflate hafnocene diazenido compound, $[(\eta^5\text{-}C_5Me_4H)_2Hf](OTf)(N_2CH_3)$, underwent subsequent protonolysis to furnish free *N*-methylhydrazine, demonstrating alkylated hydrazines can be synthesized directly from N_2. Further exposure of the hafnocene diazenide compound to methyl triflate resulted in additional N-C bond formation and conversion to an equimolar mixture of a rare triflato hafnocene hydrazonato compound, $[(\eta^5\text{-}C_5Me_4H)_2Hf](OTf)(\eta^2\text{-}N(CH_3)N{=}CH_2)$, and the corresponding hafnocene bis(triflate) species, along with release of methane gas. Isotopic labeling studies and other experiments are consistent with a pathway involving initial methylation of the unsubstituted nitrogen in the methyl diazenido ligand followed by deprotonation by a triflate anion.

* Portions of this work were taken with permission from: Knobloch, D. J.; Benito-Garagorri, D.; Bernskoetter, W. H.; Keresztes, I.; Lobkovsky, E.; Toomey, H. E.; Chirik, P. J. *J. Am. Chem. Soc.* **2009**, *131*, 14903.

Introduction

The ubiquity of nitrogen-carbon bonds in pharmaceuticals, commodity chemicals, fuels/fertilizers and materials, has prompted many investigations into new chemically and energetically efficient methods for direct functionalization of dinitrogen with carbon-based feedstocks.[1,2,3] If rendered catalytic, such methods would offer an alternative to the current paradigm whereby Haber-Bosch ammonia functions as the conduit to most nitrogen-containing organic molecules that are produced on an industrial scale.[4,5,6,7]

Well-defined examples of nitrogen−carbon bond formation from coordinated N_2 has been most commonly observed for transition metal complexes of groups 5 and 6.[3,8,9,10,11,] However, recent strides have been made by our research group and others in this area with group 4 complexes. Some of these results have been discussed in the preceding chapters, including CO-induced N-N bond cleavage[12,13,14,15] and CO_2 insertion into M-N bonds,[16,17] all promoted by group 4 metallocene dinitrogen compounds.[18,19,20] Fryzuk and co-workers have also observed N-C formation using terminal alkynes mediated by a zirconium dinitrogen compound.[21] However, dinitrogen functionalization by addition of electrophilic carbon-based substrates is more poorly understood for group 4 transition metal complexes. In an early report by van Tamelen,[22] and later reports by Mori,[23,24] and Sobota,[25] the N_2-derived synthesis of amines, nitriles, amides and even more complex molecules such as pumilotoxin C and lycopodine was achieved, but the titanium complexes involved were ill-defined in all of these cases. Rare well-defined examples until now are limited to a recent report by Sita and co-workers of N_2 alkylation with a group 4 transition metal dinitrogen complex, where addition of ethyl bromide to a cyclopentadienyl amidinate hafnium dinitrogen complex resulted in N−C bond formation.[26] Initial attempts to achieve dinitrogen alkylation were reported recently by our group, but unfortunately were

unsuccessful.[27] Instead of N-C bond formation, the formation of alkyl halide hafnocene dinitrogen complexes with weakly activated end-on dinitrogen ligands was observed (Figure 5.1). Over time, these compounds undergo formal disproportionation with loss of N_2 to regenerate the starting side-on bound hafnocene dinitrogen complex and the hafnocene alkyl halide derivative (Figure 5.1).[27]

In this chapter, the direct alkylation of a series of group 4 metallocene dinitrogen complexes will be probed. A rare example of dinitrogen methylation will be described involving a stepwise N−C bond-forming sequence upon addition of methyl triflate to $(\eta^5\text{-}C_5Me_4H)_2Hf]_2(\mu_2,\eta^2,\eta^2\text{-}N_2)$ (**2-N₂**). The first methylation event forms a hafnocene methyl diazenido complex while the second results in a rare hafnocene hydrazonato compound. The mechanism of the second N−C bond-forming reaction has been investigated with a series of isotopic labeling studies, concentration effects as well as with model reactions.

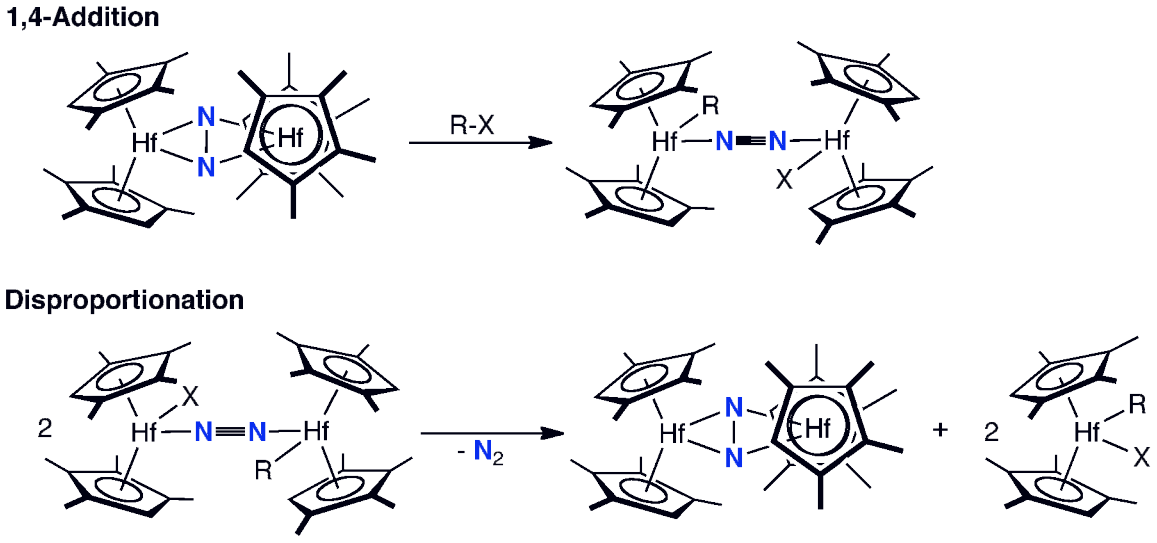

Figure 5.1. Attempted dinitrogen alkylation using group 4 metallocene compounds.

Results and Discussion

Attempted dinitrogen methylation with side-on bound dinitrogen compounds. The functionalization of coordinated dinitrogen by direct alkylation was inspired in part by recently reported examples in the early to mid transition metals by Sita,[26] Kawaguchi,[10] and Schrock[9] as well as by the attempted dinitrogen alkylation studies recently reported by our own group.[27] A series of zirconocene and hafnocene dinitrogen complexes, presented in Figure 5.2, were selected for this study providing a range of formally four electron reduced dinitrogen ligands with varying N-N bond distances. As discussed in previous chapters these complexes exhibit very rich dinitrogen functionalization chemistry with carbon-based substrates such as CO[28] and CO_2.[29]

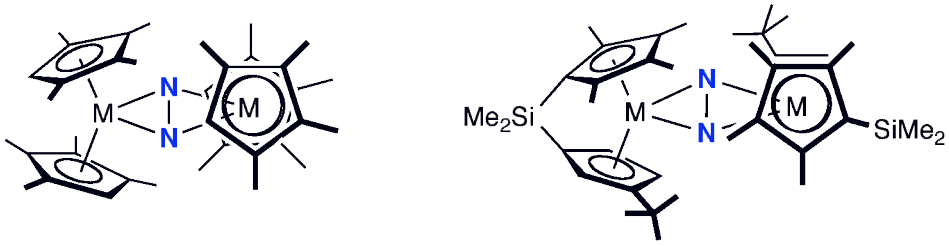

M = Zr, **1-N_2**: d(NN) = 1.377(3) Å
M = Hf, **2-N_2**: d(NN) = 1.423(11) Å

M = Zr, **3-N_2**: d(NN) = 1.406(4) Å
M = Hf, **4-N_2**: d(NN) = 1.457(5) Å

Figure 5.2. Representative metallocene dinitrogen complexes used in alkylation studies.

Previously our laboratory reported that alkyl halide addition to the unlinked variants **1-N_2** and **2-N_2** does not promote dinitrogen functionalization. Instead, either products derived from N_2 loss (in the case of **1-N_2**) or from 1,4-addition of the alkyl halide across the [Hf-N_2-Hf] core (in the case of **2-N_2**) were observed.[27] Following these discoveries, alkyl halide addition to the *ansa*-metallocene N_2 complexes (**3-N_2** and **4-N_2**) was also explored.

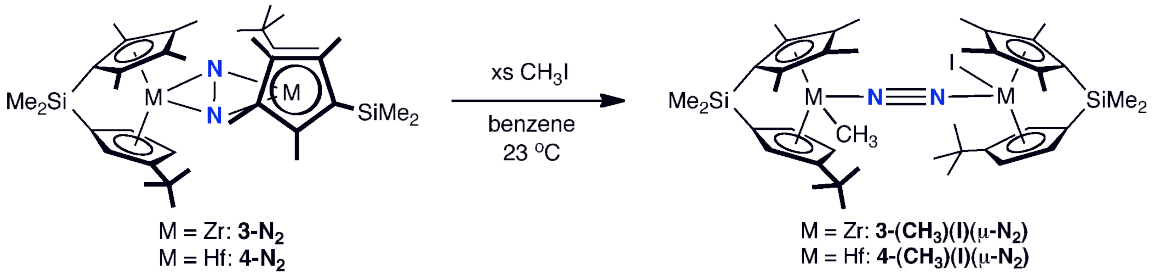

Figure 5.3. Treatment of *ansa*-metallocene dinitrogen complexes with CH_3I.

For both *ansa*-metallocene compounds, reactivity analogous to that of **2-N$_2$** was observed. Treatment of a solution of either **3-N$_2$** or **4-N$_2$** with 2 equivalents of methyl iodide resulted in rapid and complete conversion to a dark green-brown (in the case of **3-N$_2$**) or deep purple compound (in the case of **4-N$_2$**) identified as the bimetallic metallocene end-on dinitrogen complexes, **3-(CH$_3$)(I)(μ-N$_2$)** and **4-(CH$_3$)(I)(μ-N$_2$)**, arising from formal 1,4-addition of the CH_3-I bond across the two metal centers (Figure 5.3). The proposed C_1-symmetric structures were supported by multinuclear (^{1}H, ^{13}C) NMR and infrared spectroscopies. The number of resonances observed by ^{1}H and ^{13}C NMR spectroscopy is consistent with two inequivalent metallocene subunits, with a diagnostic chemical shifts at 0.18 ppm and 0.13 for the zirconium- and hafnium-bound methyl groups, respectively. The ^{1}H NMR signal for the ^{13}C-enriched hafnium methyl group is split into a doublet with $^1J_{CH}$ = 115.8 Hz. Chemical shifts corresponding to the dinitrogen ligand in **4-(CH$_3$)(I)(μ-N$_2$)** were observed in the benzene-d_6 ^{15}N NMR spectrum, presented in Figure 5.4, at 658.9 ppm and 676.2 ppm ($^1J_{NN}$ = 24.3 Hz), consistent with an asymmetric and weakly reduced $[N_2]^0$ group[14,30] bound to two M(III) d^1 centers antiferromagnetically coupled to give an overall S=0 complex. Solution and solid state magnetic measurements (Evans' method and Guoy balance, respectively) also support the S=0 ground states of these molecules. Upon protonolysis of **3-(CH$_3$)(I)(μ-N$_2$)** and **4-(CH$_3$)(I)(μ-N$_2$)** with HCl, no

ammonium chloride was detected by ^{1}H NMR spectroscopy, further supporting weakly activated N_2 ligands. A similar electronic structure has been proposed for the unlinked hafnocene variant, **2-(CH_3)(I)(μ-N_2)**,[27] and in a product reported by Sita and co-workers derived from a strongly activated hafnium dinitrogen compound.[31] Notably **3-(CH_3)(I)(μ-N_2)** and **4-(CH_3)(I)(μ-N_2)** are stable for days in solution at room temperature and do not undergo disproportionation to the starting dinitrogen compounds (**3-N_2** and **4-N_2**) as was observed in the case of **2-N_2**.[27]

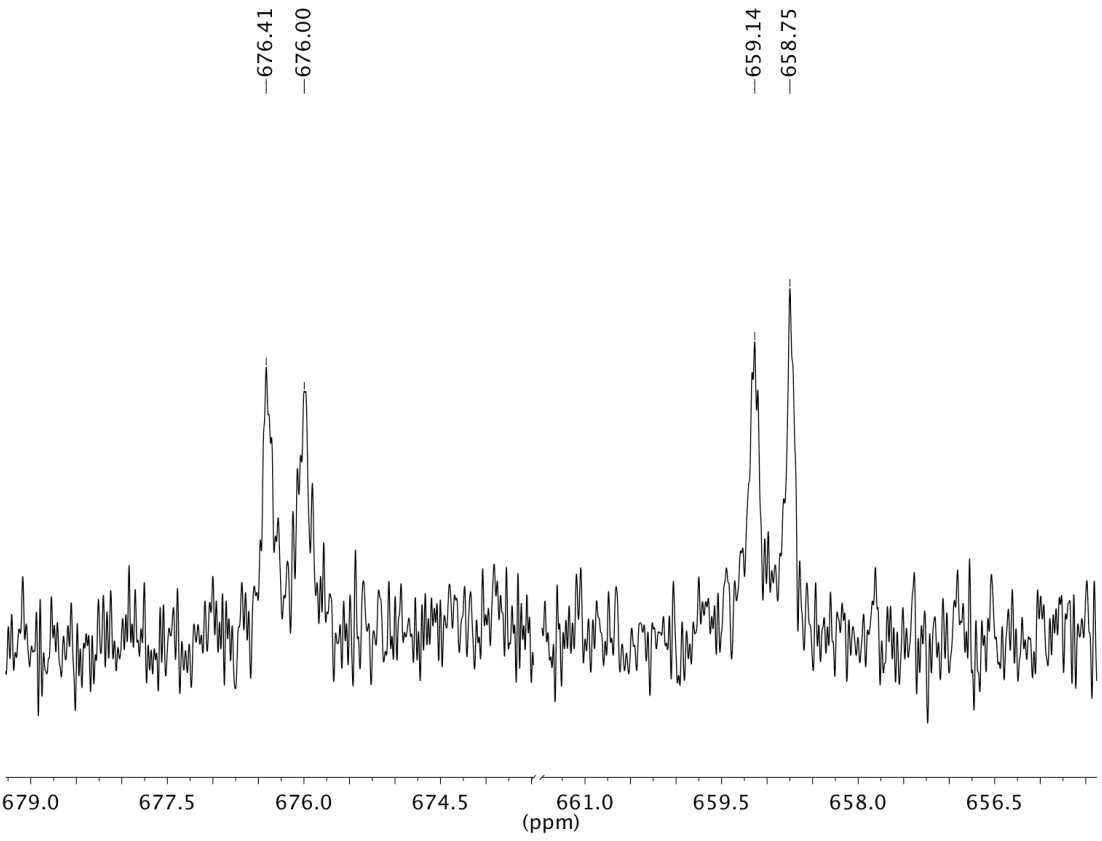

Figure 5.4. Partial benzene-d_6 ^{15}N NMR spectrum of **4-(CH_3)(I)(μ-N_2)** at 23 ºC.

In light of the unsuccessful functionalization attempts using methyl iodide, other electrophiles were explored. In particular, the strong alkylating agent methyl triflate was chosen. As discussed in the previous chapter, methyl triflate has also seen success in our laboratory with the functionalization of coordinated carboxyhydrazide ligands derived from N_2.[29] Treatment of a benzene-d_6 solution of the least activated dinitrogen complex in the series, **1-N$_2$**, with excess methyl triflate resulted in rapid formation of a mixture of predominantly three products (Figure 5.5). Two of these products were derived from N_2 loss, and were identified as the zirconocene methyl triflate complex (**1-(Me)(OTf)**) and the zirconocene methoxy triflate complex (**1-(OMe)(OTf)**), obtained in 25% and 40% yield, respectively. The third product, an insoluble blue precipitate formed in 30% yield, was identified as the end-on bound dinitrogen compound, **(1-OTf)$_2$N$_2$**. In addition to these three major products, several other unidentified zirconocene products were observed totaling less than 5% of the product mixture, as judged by ^{1}H NMR spectroscopy. Likely pathways to the identified species will be discussed in a later section in the context of the hafnocene congener, **2-N$_2$**.

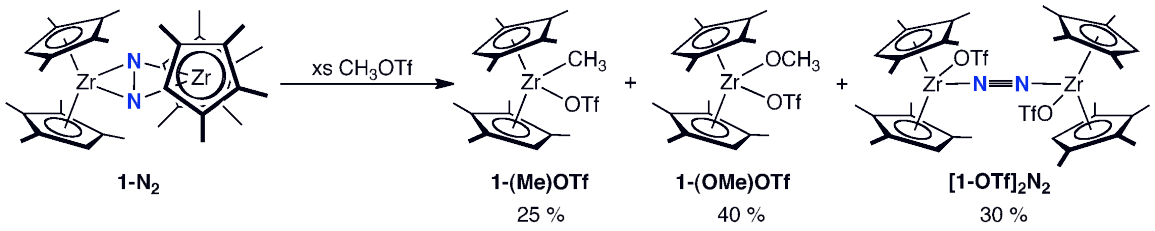

Figure 5.5. Treatment of **1-N$_2$** with CH_3OTf.

Related chemistry was observed with the *ansa*-metallocene dinitrogen complexes, **3-N$_2$** and **4-N$_2$**. In the case of the zirconium congener, exposure to excess CH_3OTf resulted in exclusive formation of the methoxy zirconocene triflate

compound **3-(OMe)(OTf)**, concomitant with dinitrogen loss and no new N-C bond formation (Figure 5.6). The zirconocene product, **3-(OMe)(OTf)**, was fully characterized by multinuclear NMR and vibrational spectroscopy. A diagnostic downfield methyl resonance in the benzene-d_6 ^{1}H NMR spectrum at 3.70 ppm distinguishes the observed product from the corresponding zirconocene methyl triflate complex (**3-(Me)(OTf)**) which was *not* observed. Although the formation of both **1-(OMe)(OTf)** (Figure 5.5) and **3-(OMe)(OTf)** in these reactions ostensibly appears to violate the law of mass action at first glance, this is not the case. Each zirconocene subunit consumes two equivalents of CH_3OTf and forms one equivalent of CH_3Tf as a byproduct.

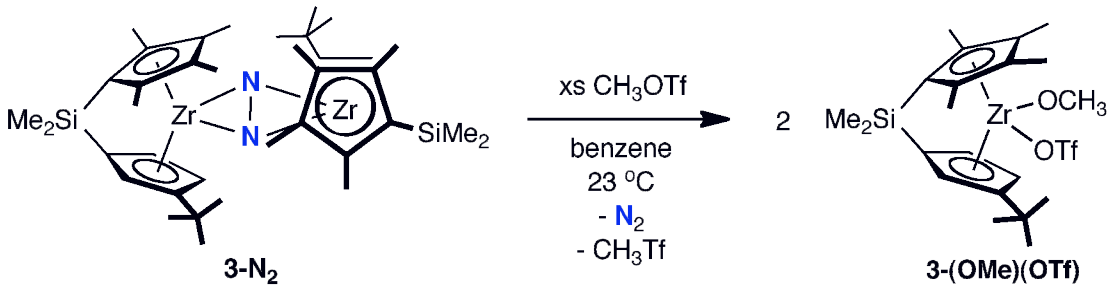

Figure 5.6. Treatment of **3-N_2** with excess methyl triflate.

The hafnocene congener of the *ansa*-zirconocene dinitrogen compound, **4-N_2**, was also treated with methyl triflate. **4-N_2** is notable for having the most activated dinitrogen ligand reported to date by our laboratory. When exposed to two equivalents or excess methyl triflate for 3 hours, **4-N_2** was converted to exclusively the end-on dinitrogen compound, **[4-(OTf)]$_2$(μ_2,η^1,η^1-N_2)**, as indicated by a color change to magenta (Figure 5.7). Disappointingly, no N_2-derived N-C bond formation was observed. This product is analogous to that observed in the addition of methyl triflate to **1-N_2** (Figure 5.5) and **2-N_2** (*vide infra*), although the reaction is cleaner and the

product is soluble in benzene, facilitating spectroscopic characterization. The product was characterized by multinuclear (^{1}H, ^{13}C, ^{19}F, ^{15}N) NMR and infrared spectroscopies. The benzene-d_6 ^{1}H and ^{13}C NMR spectra contain the number of resonances consistent with a molecule of C_2 symmetry. A single diagnostic resonance corresponding to the triflate fluorine atoms was observed at -76.45 ppm in the benzene-d_6 ^{19}F NMR spectrum, presented in Figure 5.8. When the reaction was performed in a sealed J. Young NMR tube, a stoichiometric quantity of ethane was observed, accounting for the loss of the remaining methyl fragments. The presence of a dinitrogen ligand was supported by Toepler pump analysis, which indicated no liberation of N_2 during the reaction. Additionally, a single nitrogen resonance was observed at 750.6 ppm in the benzene-d_6 ^{15}N NMR spectrum of the ^{15}N-enriched isotopologue, **[4-(OTf)]$_2$(μ_2,η^1,η^1-^{15}N$_2$)** (Figure 5.8). This chemical shift is downfield of those observed in highly activated, side-on bound metallocene dinitrogen compounds, and is consistent with a weakly or modestly activated end-on bound, C_2-symmetric dinitrogen compound.[14,30] No ammonium chloride was observed by ^{1}H NMR spectroscopy (DMSO-d_6) upon protonolysis with HCl,[32] further suggesting weak activation of dinitrogen in an end-on binding mode.

The formation of **[4-(OTf)]$_2$(μ_2,η^1,η^1-N$_2$)** likely results from 1,4-addition of MeOTf to **4-N$_2$**,[27] followed by a subsequent reaction with a second molecule of MeOTf at the intermediate [Hf-CH$_3$] bond, as shown in Figure 5.9.

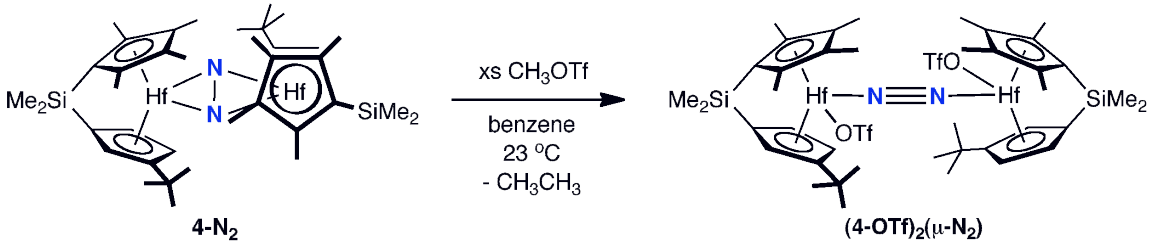

Figure 5.7. Treatment of **4-N$_2$** with excess methyl triflate.

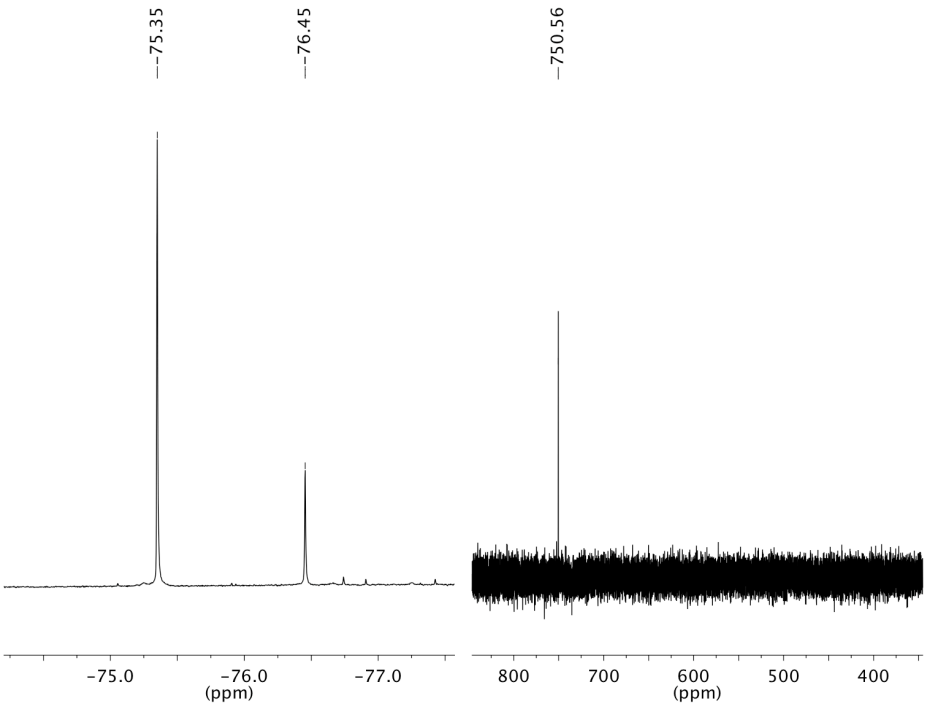

Figure 5.8. Benzene-d_6 ^{19}F NMR (left) and ^{15}N NMR (right) spectra of **[4-(OTf)]$_2$(μ_2,η^1,η^1-N$_2$)** at 23 ºC. Resonance at -75.35 ppm (left) corresponds to the internal standard CH_3OTf.

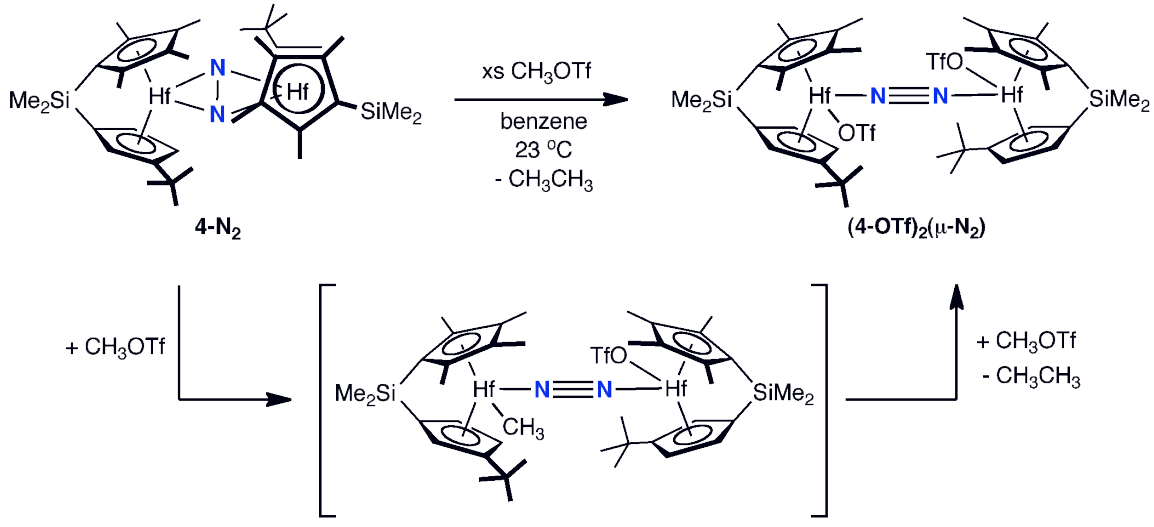

Figure 5.9. Likely route to the formation of **[4-(OTf)]$_2$(μ_2,η^1,η^1-N$_2$)**. A similar pathway is likely for the analogous compound **[2-(OTf)]$_2$(μ_2,η^1,η^1-N$_2$)** (*vida infra*).

To complete the series of dinitrogen compounds, **2-N_2** was targeted for methylation studies. Addition of a slight excess (2.2 equivalents) of methyl triflate to a benzene-d_6 solution of **2-N_2** resulted in formation of a mixture of products (Figure 5.10) arising from three distinct reaction pathways. The major pathway consumed 60% of the starting dinitrogen compound and resulted in conversion of **2-N_2** to the triflato hafnocene dinitrogen compound, **[2-(OTf)]$_2$(μ_2,η^1,η^1-N_2)**, with concomitant liberation of ethane (which was detected by ^{1}H NMR). This compound is similar to products obtained from methyl triflate addition to **1-N_2** and **4-N_2**. A mechanism for the formation of **[2-(OTf)]$_2$(μ_2,η^1,η^1-N_2)** similar to that shown in Figure 5.9 is likely operative. Due to its low solubility **[2-(OTf)]$_2$(μ_2,η^1,η^1-N_2)** was not characterized in solution by NMR spectroscopy but purple crystals suitable for X-ray diffraction were obtained. The solid-state structure of **[2-(OTf)]$_2$(μ_2,η^1,η^1-N_2)** is presented in Figure 5.11 and confirms the end-on hapticity of the dinitrogen ligand. The dinitrogen ligand is weakly activated as judged by the N-N and Hf-N bond distances of d(NN)=1.189(8) Å and d(Hf-N)=2.060(4) Å.

The second pathway accounted for consumption of only 5% of the starting material and led to formation of the hafnocene methoxy triflate compound, **2-(OMe)(OTf)**, arising from dinitrogen loss. The identification of this compound, along with the observation in earlier cases of **1-(OMe)(OTf)** and **3-(OMe)(OTf)**, seemingly violoates the law of mass action, as an additional oxygen atom is present in these molecules. This issue was addressed by independently synthesizing **2-(Me)(OTf)** and **2-(OMe)(OTf)** as well as other relevant hafnocene complexes that may serve to elucidate a pathway to the unusual observed product.

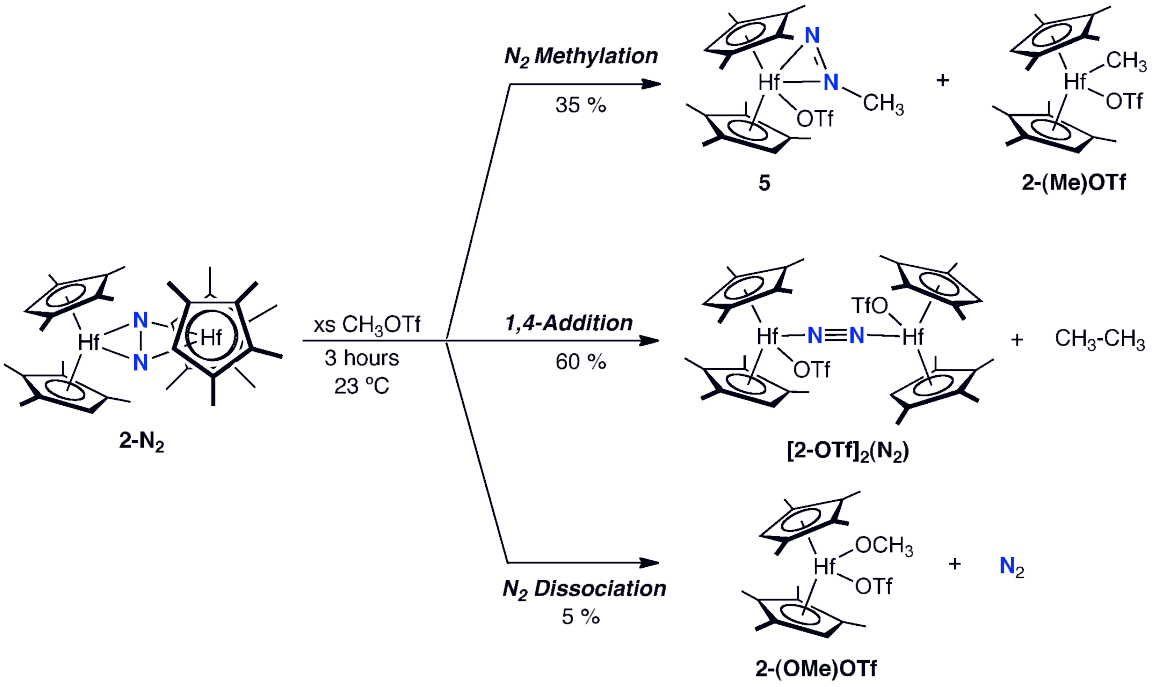

Figure 5.10. Treatment of **2-N_2** with CH_3OTf.

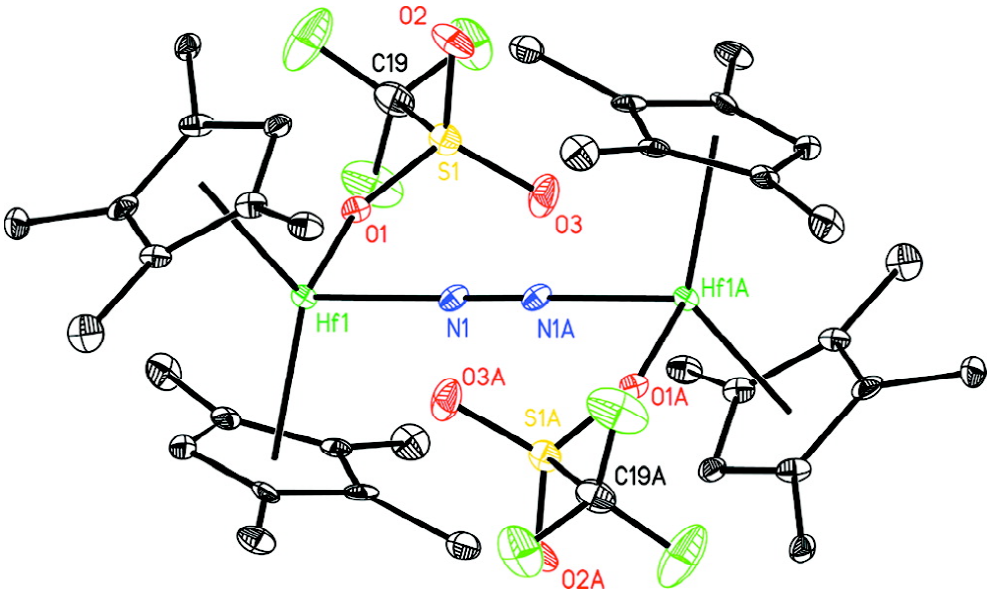

Figure 5.11. Molecular structure of **[2-(OTf)]$_2$(μ_2,η^1,η^1-N_2)** at 30% probability ellipsoids. Hydrogen atoms are omitted for clarity. Single crystals were isolated and obtained by Wesley Bernskoetter.

Addition of one equivalent of silver triflate to $(\eta^5\text{-}C_5Me_4H)_2HfMe_2$ (**2-Me$_2$**) in toluene followed by filtration cleanly furnished $(\eta^5\text{-}C_5Me_4H)_2Hf(Me)OTf$ (**2-(Me)OTf**), establishing its identity as one of the products from methyl triflate addition to **2-N$_2$** (Figure 5.12). Synthesis of **2-(OMe)OTf** was accomplished by treatment of a benzene-d_6 solution of **2-(Me)OTf** with a slight excess of methanol, thereby confirming its formation as a byproduct during dinitrogen methylation (Figure 5.12).*

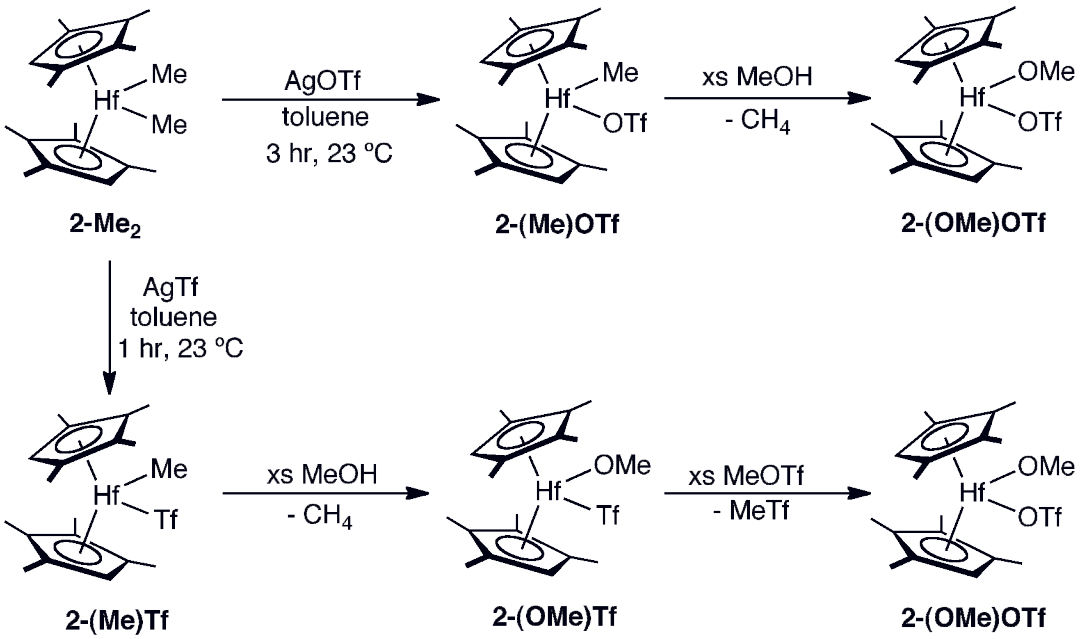

Figure 5.12. Independent syntheses of several relevant hafnocene species.

Possible origins of **2-(OMe)OTf** were also studied. It seems plausible that a hafnocene methoxy sulfone complex, $(\eta^5\text{-}C_5Me_4H)_2Hf(OMe)Tf$ (Tf = −OS(O)CF$_3$) (**2-(OMe)Tf**), could arise from S−O bond cleavage and oxidative addition to "hafnocene". An independent synthesis of **2-(OMe)Tf** was pursued and was inspired

* The independent syntheses described here and depicted in Figure 5.12 were originally carried out by David Benito-Garagorri and are reproduced here with permission.

by the successful synthesis of **2-(OMe)OTf** (Figure 5.12). Treatment of **2-Me$_2$** with one equivalent of silver trifluoromethylsulfone yielded the desired hafnocene methyl sulfone complex, **2-(Me)Tf**. Subsequent addition of methanol resulted in liberation of methane and formation of the hafnocene methoxy sulfone, **2-(OMe)Tf**. This compound has distinct ^{1}H, ^{13}C and ^{19}F spectroscopic features from **2-(OMe)OTf** further substantiating its absence as a byproduct of methyl triflate addition to **2-N$_2$**. Importantly, addition of excess methyl triflate to a benzene-d_6 solution of **2-(OMe)Tf** resulted in rapid and quantitative conversion to **2-(OMe)OTf**. In the observed reaction chemistry, the competing pathways result in a continual excess of methyl triflate being present, meaning that if **2-(Me)Tf** is initially formed, it is likely rapidly converted to **2-(OMe)OTf** and is therefore not observed.

The remaining 35% of the starting dinitrogen compound was consumed by a final pathway (the top pathway in Figure 5.10) that satisfyingly resulted in dinitrogen methylation and formation of the triflate hafnocene diazenide compound, **5**, along with an equimolar amount of the corresponding hafnocene methyl triflate compound, **2-(Me)(OTf)**. Despite its low yield, this result demonstrates our original goal of nitrogen-carbon bond formation ultimately derived from atmospheric N_2.

The remainder of this chapter will focus on the formation and characterization of **5** and subsequent reactivity studies. However, a statement regarding the overall series of studied compounds is first appropriate. The diversity in reactivity among the dinitrogen compounds considered in this work is quite notable, especially with respect to the hafnocene congeners. Specifically, the unlinked hafnocene compound (**2-N$_2$**) exhibits the only instance of productive N-C bond forming chemistry. The N-N bond distance of 1.423(11) Å in this compound is longer than that of the zirconium congener (**1-N$_2$**), although it is shorter than the N-N bond distance in the related *ansa*-hafnocene compound, **4-N$_2$**, which importantly does not undergo dinitrogen alkylation

upon treatment with methyl triflate. These results demonstrate that N-N length is not the only requirement for dinitrogen functionalization and suggest that the cyclopentadienyl substituents also play an important role.

Direct methylation of a hafnocene dinitrogen compound. Compound **5** was of primary interest due to the presence of a functionalized dinitrogen ligand. Unfortunately, attempts to scale the reaction up and separate **5** from the other byproducts via recrystallization were unsuccessful, precluding characterization by X-ray diffraction. Nonetheless, the identity compound was firmly established by multinuclear (^{1}H, ^{13}C, ^{15}N, ^{19}F) and multidimensional NMR spectroscopy, as well as vibrational spectroscopy. Various isotopologues of **5** could be prepared using the appropriate isotopically enriched starting materials (**2-$^{15}N_2$**, $^{13}CH_3OTf$, CD_3OTf).

The benzene-d_6 $\{^{1}H\}^{13}C$ NMR spectrum of the ^{13}C,^{15}N isotopologue (Figure 5.13) of **5** (denoted **5-^{13}C/$^{15}N_2$**) exhibited a doublet of doublets centered at 55.85 ppm and yielded coupling constants of $^{1}J_{N-C}$ = 3.5 and $^{2}J_{N-C}$ = 1.1 Hz. The benzene-d_6 ^{15}N NMR spectrum of ^{15}N isotopologue, **5-$^{15}N_2$** (Figure 5.13), exhibited two doublets centered at 460.1 and 729.8 ppm with a coupling constant of $^{1}J_{N-N}$ = 20.6 Hz, establishing inequivalent nitrogens. Furthermore, the ^{1}H-^{15}N HMBC spectrum of **5-$^{15}N_2$** established coupling between the methyl protons and both nitrogen atoms (Figure 5.14). Based on these data, the structure of **5** was established as the triflato hafnocene diazenide compound, $(\eta^5\text{-}C_5Me_4H)_2Hf(OTf)(N_2CH_3)$.

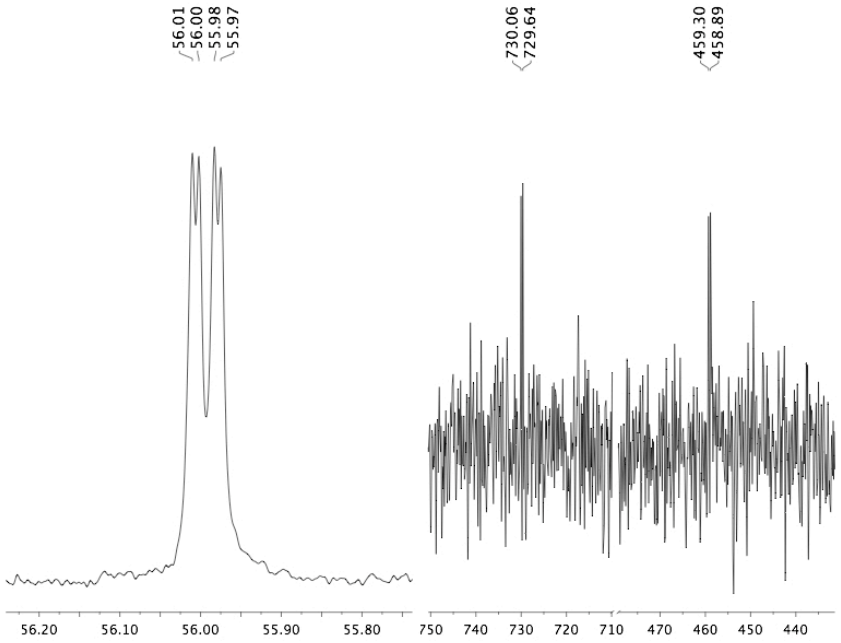

Figure 5.13. Partial benzene-d_6 $\{^1H\}^{13}C$ NMR spectrum of **5-^{13}C/^{15}N$_2$** (left) and ^{15}N NMR spectrum of **5-^{15}N$_2$** (right) at 23 ºC.

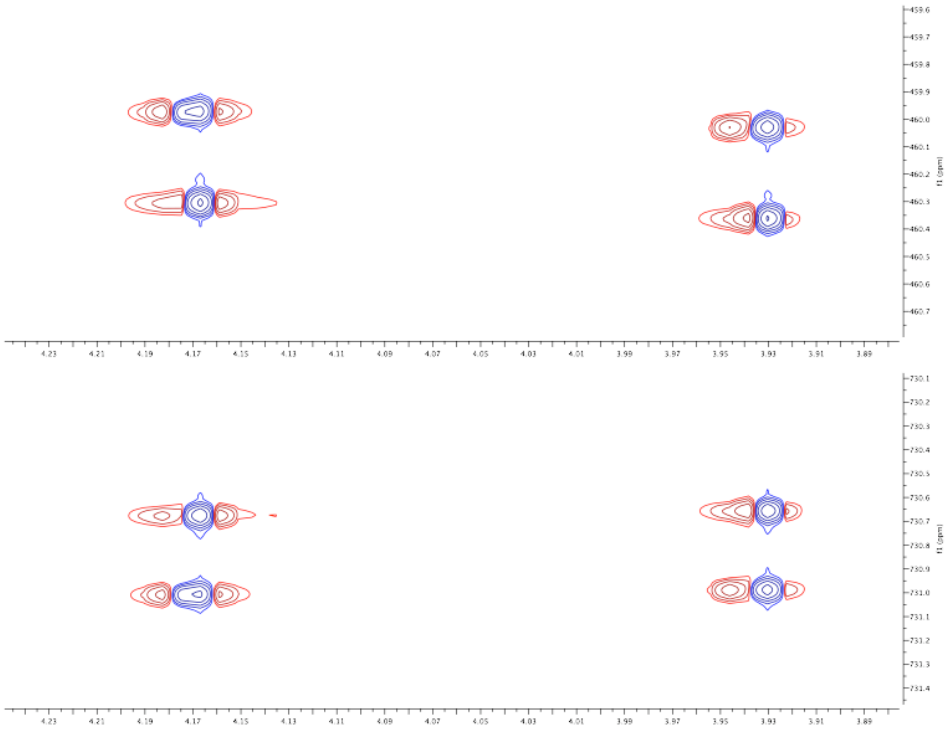

Figure 5.14. ^1H-^{15}N HMBC spectrum of **5-^{13}C/^{15}N$_2$**.

Gade and co-workers have recently reported the synthesis of similar, structurally characterized zirconium diazenido complexes from thermal decomposition of the corresponding hydrazinediide compounds (i.e. non-N_2 derived) (Figure 5.15).[33] In analogy to **5**, both the 1-adamantyl- and mesityl-substituted diazenide ligands exhibit significantly downfield-shifted ^{15}N NMR resonances (804.2 ppm, R = ^{1}Ad; 810.9 ppm, R = Mes) for the unsubstituted nitrogen atom. In Gade's compounds, DFT calculations also confirmed the assignment of the downfield ^{15}N peaks to the unsubstituted nitrogen atoms.

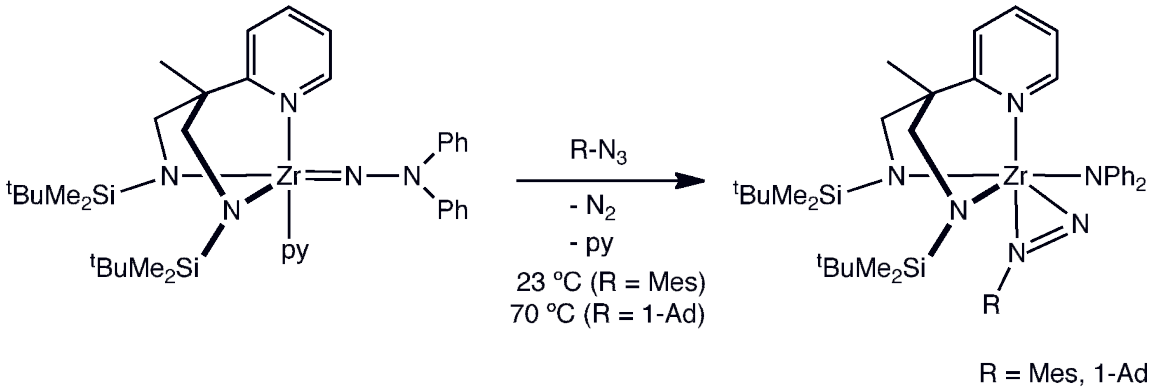

Figure 5.15. Zirconium diazenido formation reported by Gade and coworkers. Reproduced with permission from reference 33.

In the case of compound **5**, to satisfy the hafnium center with formally 18 electrons, and also based on the literature precedent set by Gade and co-workers,[33] we tentatively assign the η^2-haptomer as the ground state. However, it should be noted that the η^1 variant cannot be definitively ruled out on the basis of the NMR data.[34] In the infrared spectrum, no strong bands assignable to an N−N stretch have been observed, also supporting the η^2 assignment.

The reaction of **5** with additional methyl triflate resulted in a second nitrogen−carbon bond-forming event. Treatment of a benzene-d_6 solution of **5** with 1 equivalent or excess CH_3OTf at 23 °C yielded a new hafnocene hydrazonato product, **6**, with concomitant release of methane gas (detected by ^{1}H NMR and infrared spectroscopies, *vide infra*) and formation of an equimolar quantity the hafnocene bis(triflate), **2-(OTf)$_2$** (Figure 5.16). Complete consumption of **5** required approximately 16−18 h under these conditions (i.e. with 1 equivalent of CH_3OTf per equivalent of **5**). The yield of **6** is approximately 50% (per mol of starting material **5**) as judged by ^{1}H NMR spectroscopy. As will be presented during the mechanistic discussion, an equivalent of **5** is sacrificed in the formation of methane and **2-(OTf)$_2$**, rendering the normalized yield of **6** >95%.

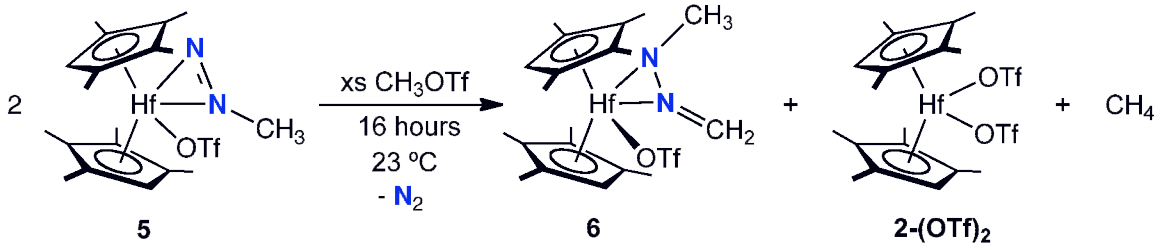

Figure 5.16. Treatment of **5** with additional CH_3OTf.

The structure of the newly formed hafnocene hydrazonato compound was fully assignable by NMR spectroscopy. The benzene-d_6 ^{1}H NMR spectrum of **6** exhibits singlets centered at 2.94 and 5.40 ppm, assigned to N−CH_3 and N=CH_2 groups, respectively. These assignments were confirmed by DEPT, HSQC, and HMBC NMR experiments as well as by preparation of the ^{13}C and ^{2}H isotopologues. The singly or doubly labeled ^{13}C- and ^{15}N-enriched isotopologues were also prepared from **5**-

(^{13}C)(^{15}N$_2$) and $^{13}CH_3OTf$. Representative ^{13}C NMR and ^{15}N NMR spectra are presented in Figure 5.17 and Figure 5.18, respectively.

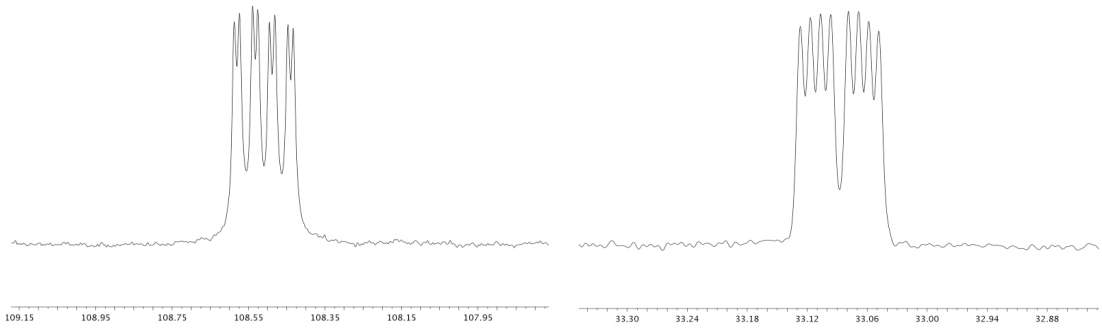

Figure 5.17. Benzene-d_6 ^{13}C NMR spectra of the N-CH_3 signal (right) ($^3J_{CC}$ = 6.1 Hz, $^1J_{CN}$ = 2.3 Hz, $^2J_{CN}$ = 1.2 Hz, $^1J_{NN}$ = 15.0 Hz) and the N=CH_2 signal (left) ($^3J_{CC}$ = 6.1 Hz, $^1J_{CN}$ = 11.5 Hz, $^2J_{CN}$ = 1.9 Hz, $^1J_{NN}$ = 15.0 Hz) of **6-^{13}C$_2$/^{15}N$_2$** at 23 ºC.

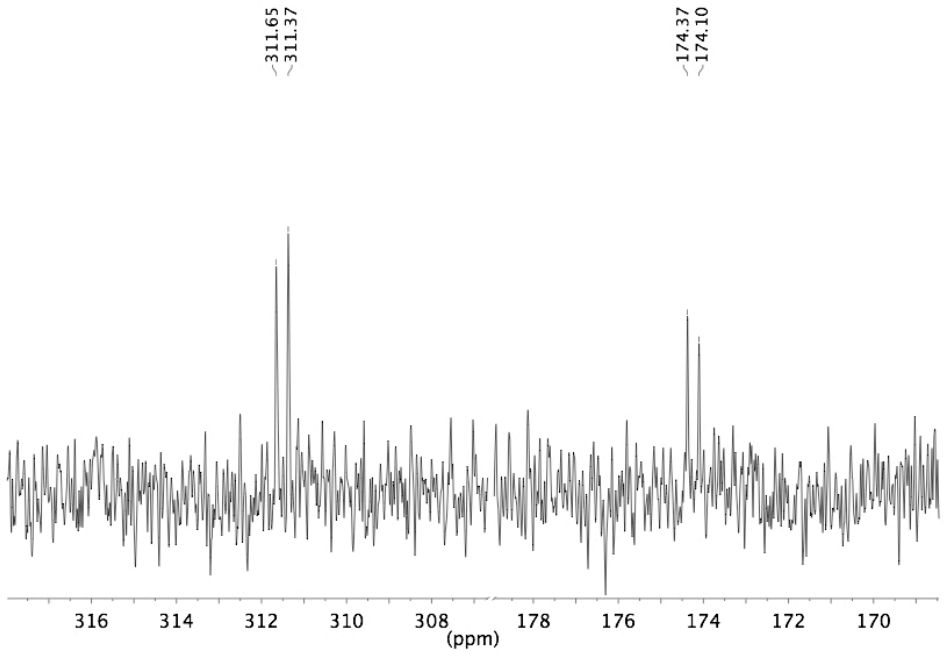

Figure 5.18. Benzene-d_6 ^{15}N NMR of **6-^{15}N$_2$** at 23 ºC.

The ^{13}C NMR spectrum of **6-$^{13}C_2$** exhibits two doublets for the $^{13}CH_3$ and $^{13}CH_2$ groups at 33.13 ppm and 108.43 ppm, respectively, with a coupling of $^{3}J_{CC}$=6.1 Hz. For the doubly labeled isotopologue **6-($^{15}N_2$)($^{13}C_2$)**, more complex splitting was observed due to coupling among all four labeled atoms (Figure 5.17). Coupling constants of $^{1}J_{C-N}$ = 2.3 Hz and $^{2}J_{C-N}$ = 1.2 Hz for the N−*C*H$_3$ signal were measured, and values of $^{1}J_{C-N}$ = 11.5 Hz and $^{2}J_{C-N}$ = 1.9 Hz were determined for the N = *C*H$_2$ peak. In the ^{15}N NMR spectrum of **6-$^{15}N_2$**, two doublets centered at 311.51 (N = CH_2) and 174.23 (N−CH_3) ppm were observed with a coupling of $^{1}J_{NN}$ = 15.0 Hz (Figure 5.18). All of these data support the identity of **6** as the triflato hafnocene hydrazonato compound resulting from a second N−C bond-forming reaction with concomitant loss of methane and formation of **2-(OTf)$_2$**. As with **5**, the NMR data does not distinguish between η^2 and η^1 haptomers of the hydrazonato ligand. We tentatively favor the η^2 structure with the neutral donor occupying the central position in the hafnocene wedge, and all structures are drawn accordingly. Both the benzene solution and solid state (KBr) infrared spectra of **6** were recorded. However, no diagnostic bands assigned to the hydrazonato ligand were identified.

Examples of zirconocene hydrazonato compounds have been previously synthesized by the insertion of diazoalkanes into Zr−C and Zr−H bonds[35,36,37] and mechanisms of their formation have been studied computationally.[38] To further explore the stability of this fragment and to prepare a hafnocene example, the independent syntheses of triflato zirconocene and hafnocene hydrazonato complexes were explored. Treatment of either **1-Me$_2$** or **2-Me$_2$** with commercially available ethyl diazoacetate followed by AgOTf addition furnished (η^5-$C_5Me_4H)_2$Hf(OTf)(η^2-N(CH_3)N=C(H)COOEt) (M = Zr, **7**; Hf, **8**) in moderate yields (Figure 5.19). The ^{1}H and ^{13}C benzene-d_6 NMR spectra of **7** and **8** exhibit features similar to **6** (see the

Experimental Section for details) supporting the evidence of the hafnocene hydrazonato complex from methyl triflate addition to **5**.

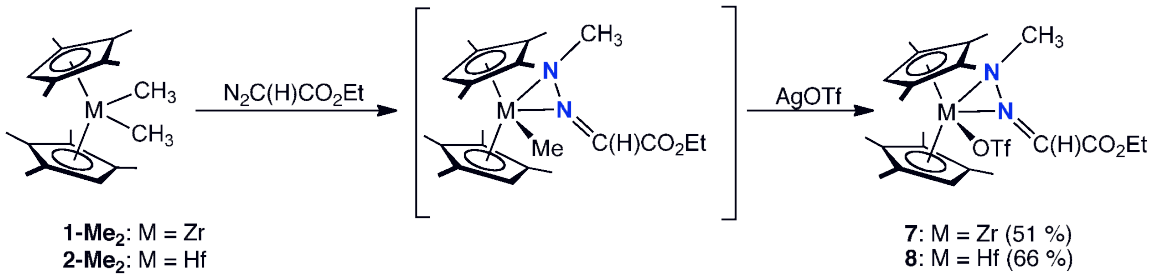

Figure 5.19. Independent syntheses of related metallocene hydrazonato compounds **7** and **8**.

To explore the mechanism of the transformation from **5** to **6**, isotopic labeling experiments were performed. When **5** (natural abundance) was treated with excess $^{13}CH_3OTf$, *both* the methyl and methylene positions of the resulting product (**6**) were enriched with ^{13}C labeling (Figure 5.20). Analysis of the methane gas byproduct by ^{1}H NMR spectroscopy established formation of both $^{13}CH_4$ and CH_4 (Figure 5.21d), with $^{13}CH_4$ predominating. The converse experiment, addition of CH_3OTf to **5-^{13}C**, also yielded a mixture of CH_4 and $^{13}CH_4$, this time with CH_4 predominating (Figure 5.21c). Therefore the predominant methane isotopologue formed during the conversion of **5** to **6** is from the second equivalent of added methyl triflate. The ratio of methane isotopologues also increases with the number of equivalents of CH_3OTf added. In all of the ^{13}C exchange studies, no isotopic incorporation was observed in any of the byproducts formed during the synthesis of **5**.

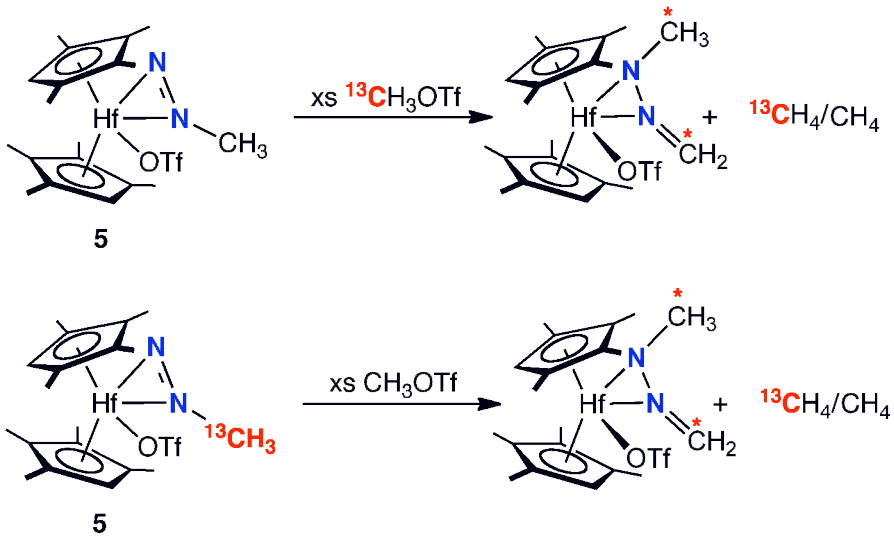

Figure 5.20. Isotopic exchange of **5**/**5**-^{13}**C** with $^{13}CH_3OTf/CH_3OTf$.

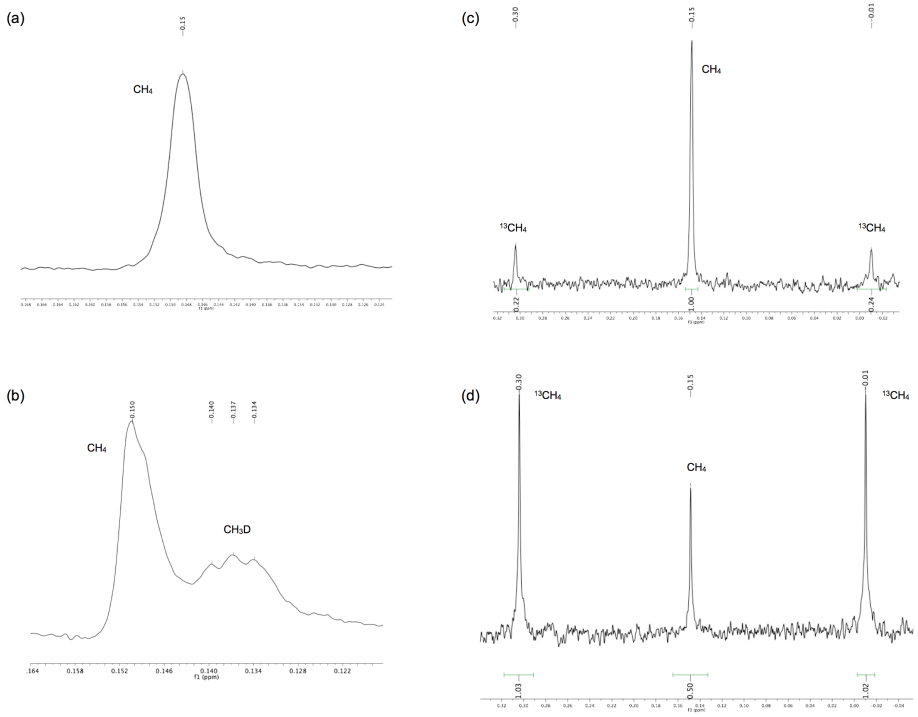

Figure 5.21. ^{1}H NMR spectra of isotopologues of methane obtained during the reaction of (a) **5** with CH_3OTf, (b) **5**-***d*$_3$ with CH_3OTf, (c) **5**-^{13}**C** with CH_3OTf and (d) **5** with $^{13}CH_3OTf$.

Monitoring the above experiments by ^{13}C NMR spectroscopy at shorter reaction times revealed growth of the N–$^{13}CH_3$ peak centered at 55.85 ppm in **5** over the course of 3 h at 23 °C prior to conversion to **6**. Likewise, the converse experiment, addition of natural abundance CH_3OTf to **5-^{13}C**, resulted in partial disappearance of the labeled methyl group as exchange for natural abundance CH_3 took place prior to conversion to **6**.

Similar results were obtained from deuterium labeling. Treatment of **5-*d*$_3$** (as a mixture with **2-(CD$_3$)(OTf)**), prepared from addition of CD_3OTf to **2-N$_2$**, with CH_3OTf resulted in growth of the N–CH_3 peak centered at 4.11 ppm in the ^1H NMR spectrum of **5** prior to conversion to **6**, clearly establishing fast and reversible nitrogen methylation prior to formation of the triflato hafnocene hydrazonato compound, **6** (Figure 5.22). Over time the reaction ultimately yielded **6-*d*$_n$** along with CH_4 and CH_3D as the principal isotopologues of methane as judged by ^1H NMR spectroscopy (Figure 5.21b). It is possible that CD_3H was formed at low concentration but was not detected by ^1H NMR spectroscopy. Analysis of **6-*d*$_n$** by ^1H NMR spectroscopy established hydrogen incorporation into both the N–CD_3 and N=CD_2 positions, consistent with methyl group exchange in **5**.

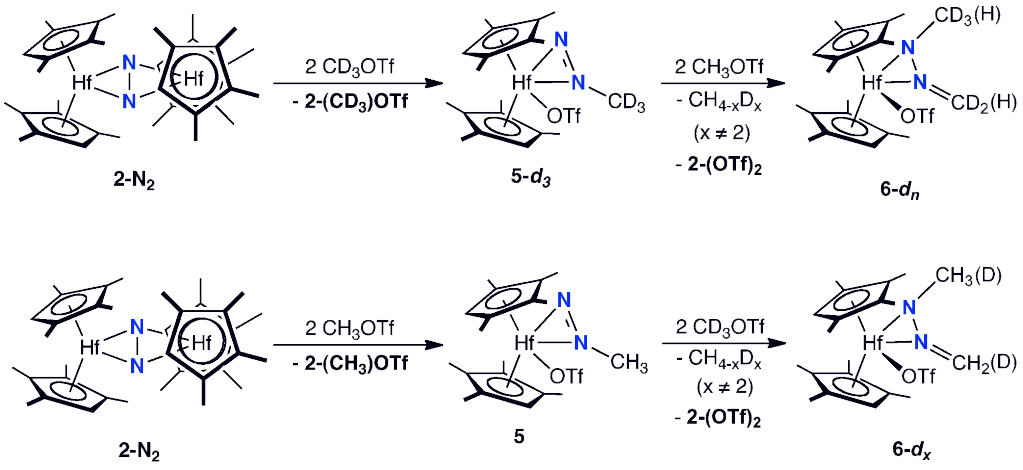

Figure 5.22. Isotopic exchange of **5-*d*$_3$/5** with CH_3OTf/CD_3OTf.

The converse isotopic labeling experiment, addition of CD_3OTf to natural abundance **5**, was also conducted (Figure 5.22). As expected, deuterium incorporation was observed in the N−CH_3 and N═CH_2 positions as judged by ^2H NMR spectroscopy. To definitively characterize the isotopologues of methane produced, gas-phase infrared experiments were conducted. This technique is more sensitive than ^1H NMR spectroscopy for identifying methane isotopologues including CD_4.[39] After the addition of CD_3OTf to **5**, the reaction was stirred overnight, and the volatile components were then removed and collected with a Toepler pump. The methane was collected in a gas-phase IR cell and analyzed. As shown in Figure 5.23, bands for CH_4, CD_4, CH_3D (trace), and CD_3H are observed. Importantly, there is no evidence for formation of CH_2D_2.

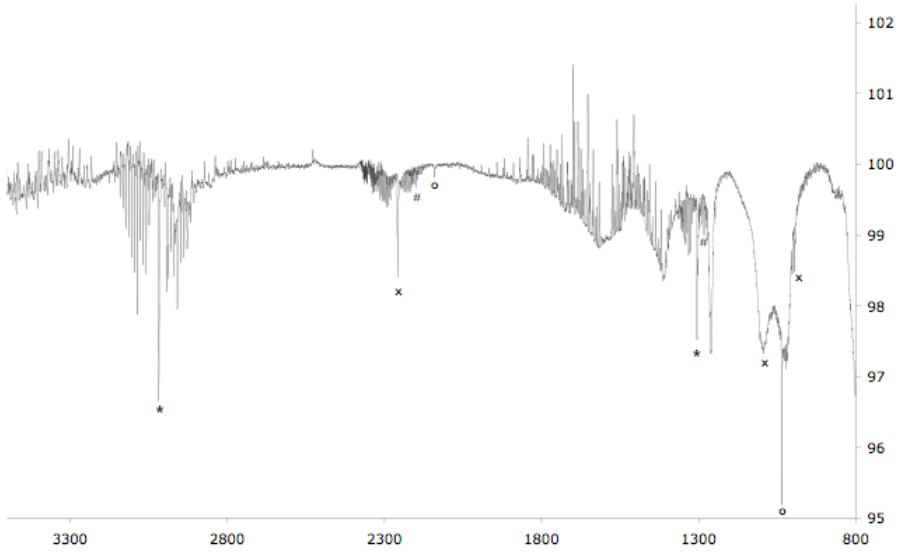

Figure 5.23. Infrared of methane isotopes. Gas phase infrared spectrum of **5** with excess CD_3OTf establishing formation of CH_4 (*, 3019 and 1306 cm^{-1}), CD_4 (x, 2259, 1094 and 996 cm^{-1}), CH_3D (#, 2200 and 1300 cm^{-1}) and CD_3H (o, 2142 and 1036 cm^{-1}). Assignments based on data reported in reference 39.

Since **2-(Me)OTf** could not be separated from **5** before subsequent reactivity with CH_3OTf was studied, control experiments were conducted to establish the behavior of this compound toward various isotopologues of methyl triflate. Addition of methyl triflate to a benzene-d_6 solution of **2-(Me)OTf** produced no reaction over the course of days at 23 °C. Likewise, treatment of **2-(Me)OTf** with excess $^{13}CH_3OTf$ did not result in exchange of the isotopic label into the hafnium compound. By contrast, addition of one equivalent of HOTf to a benzene-d_6 solution of **2-(Me)OTf** resulted in immediate formation of **2-(OTf)$_2$** with concomitant formation of methane. As a side note, these results demonstrate that the methyl triflate used is not detectably contaminated with HOTf. Crossover experiments were also conducted. Mixing benzene solutions of the ^{13}C isotopologue of **6**, **6-$^{13}C_2$**, with a benzene-d_6 solution of **5-*d*$_3$** produced no change over the course of days at 23 °C as judged by ^{13}C NMR spectroscopy. Neither ^{13}C enrichment into **5-*d*$_3$** nor ^{2}H incorporation into **6-$^{13}C_2$** was observed. Therefore, exchange between the starting materials and products was ruled out. An additional crossover experiment was conducted to evaluate the possibility of hafnocene methyl group exchange. A benzene-d_6 solution of **5-^{13}C** was prepared as a mixture including the appropriate amount of **2-($^{13}CH_3$)OTf**. To this mixture was added a stoichiometric amount of (independently prepared) **2-(CH_3)OTf** as well as excess $^{13}CH_3OTf$. The formation of **6-$^{13}C_2$** was monitored by ^{1}H NMR spectroscopy and revealed no incorporation of natural abundance [CH_3] from **2-(CH_3)(OTf)** into the final product. Thus **2-(CH_3)(OTf)** formed *in situ* clearly does not participate in the conversion of **5** to the hafnocene hydrazonato compound **6**.

Finally, qualitative CH_3OTf dependence experiments were performed to evaluate the effect of the concentration of added methyl triflate on the conversion of **5** to **6**. Unfortunately quantitative kinetic analyses could not be carried out due to the complicated mixture of inseparable products formed. With one equivalent of added

methyl triflate, the half-life for the conversion of **5** to **6** at 23 °C was 48 h. At 15 equivalents of added MeOTf, the conversion was complete within 4 h, establishing a rate dependence on added methyl triflate. Representative NMR data from these experiments are presented in the Figure 5.24.

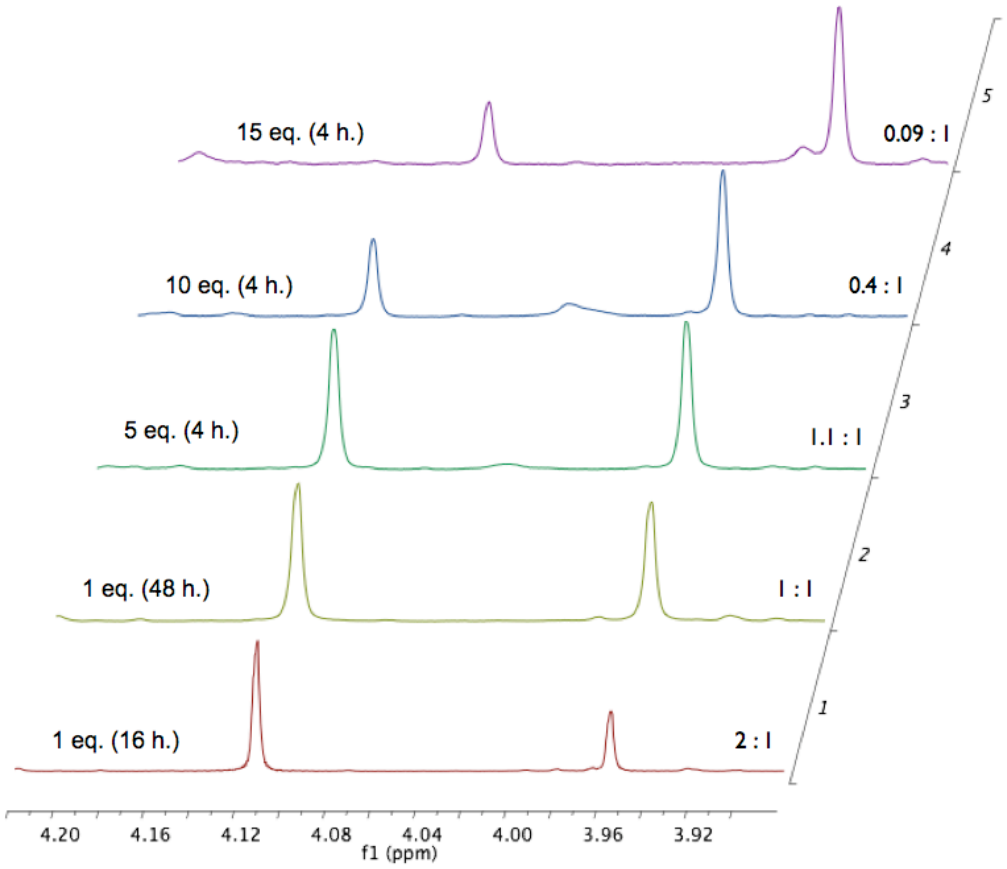

Figure 5.24. ^{1}H NMR spectra of the conversion of **5** to **6** as a function of added CH_3OTf. The peak at 4.11 ppm corresponds to the N-C*H*$_3$ hydrogens of **5** while that at 3.96 ppm is the –O*CH*$_3$ group in **2-(OMe)OTf** used as an internal standard.

Mechanistic proposal. Based on the above experimental data, a mechanistic pathway for the formation of **6** upon addition of methyl triflate to **5** was proposed and is presented in Figure 5.25. Added methyl triflate is denoted in red so it may be tracked and to highlight the results of the isotopic labeling experiments. The mechanism begins with methylation of the unsubstituted nitrogen atom in **5** to form a cationic hafnium dimethyl diazene intermediate. The neutral diazene ligand may rotate or dissociate and recoordinate to exchange the methyl positions in the lateral and central sites in the hafnocene wedge. This exchange accounts for the observation of ^{13}C (or ^{2}H) enrichment in both positions of **6**. Also, the methylation of **5** with MeOTf must be both fast (relative to formation of **6**) and reversible as both ^{13}C- and ^{2}H-labeling experiments demonstrate isotopic incorporation into the starting compound before conversion to **6**. To form **6**, deprotonation of one of the methyl groups of the dimethyl diazene ligand by the triflate anion takes place with concomitant release of HOTf. Distinguishing the site of deprotonation (either lateral or central position of the hafnocene wedge) was not possible on the basis of the available experimental data. The resulting hydrazonato complex can likely undergo η^2,η^1 interconversion to assume the thermodynamically preferred hapticity.

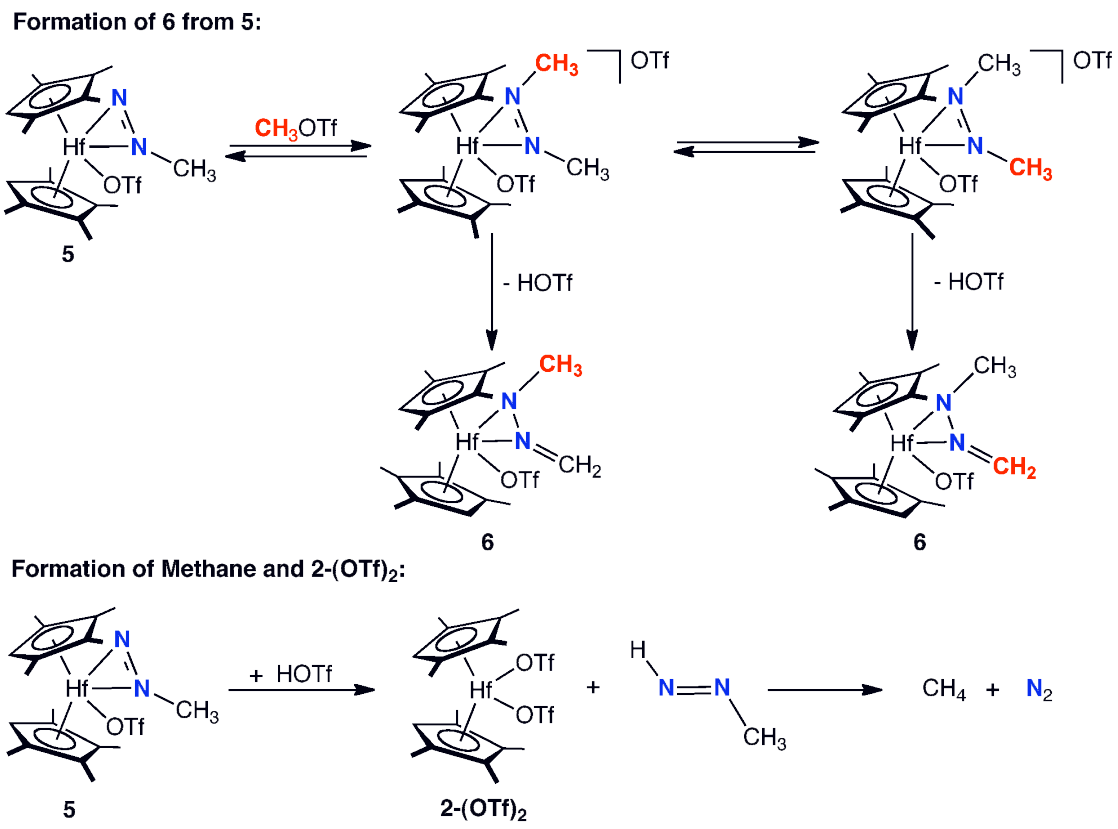

Figure 5.25. Proposed mechanism for hafnocene hydrazonato formation from **5**.

The mechanism proposed in Figure 5.25 also accounts for the observation of the various methane isotopologues and formation of **2-(OTf)$_2$**. Recall that the isotopologue of methane observed depends on the isotopic labeling in **5**. Specifically, the predominant methane isotopologue observed is derived from the added methyl triflate. For instance, when **5** is treated with $^{13}CH_3OTf$, the ratio of the methane isotopologues favors $^{13}CH_4$ over CH_4 (Figure 5.21). Therefore it is most likely that the generated HOTf reacts rapidly with a sacrificial equivalent of **5** to form **2-(OTf)$_2$** and release methyl diazene, which subsequently undergoes the known decomposition to N_2 and CH_4.[40] This is fully consistent with the experimentally observed trend in the formation of methane isotopologues. That is, as the number of equivalents of the

second methyl triflate addition is increased, the predominance of the isotopologue derived from that addition also increases. A mechanistic alternative whereby generated HOTf reacts with the byproduct **2-(Me)(OTf)** to form **2-(OTf)$_2$** and methane would follow the opposite trend, inconsistent with the experimental results. Also in this latter possibility, one would expect consumption of **2-(Me)OTf** during conversion to **6**, and this is not observed. For these reasons this latter possibility cannot be operative.

To experimentally support the proposed mechanism, a benzene-d_6 solution of **5** was treated with HOTf. Immediate formation of **2-(OTf)$_2$** and methane was observed (Figure 5.26). Only trace amounts (<10%) of methylhydrazine were detected from this experiment. Again, it is known that free diazomethane, $CH_3N{=}NH$, undergoes decomposition to methane and N_2[40] and accounts for formation of CH_4 observed from the control experiment and the conversion of **5** to **6**.

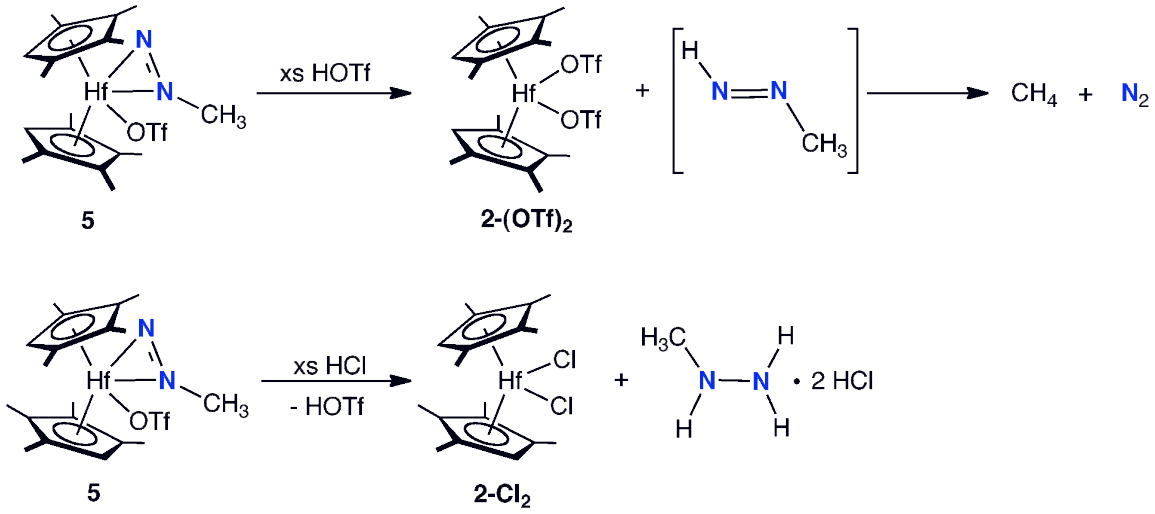

Figure 5.26. Protonolysis of **5** with HOTf (top) and HCl (bottom).

In contrast to the triflic acid addition, treatment of a benzene-d_6 solution of **5** with a large excess (>10 equiv) of the mineral acid HCl yielded the hafnocene

dichloride, **2-Cl$_2$**, along with free *N*-methylhydrazine as its HCl salt (Figure 5.26). The hydrazine derivative was characterized by comparison of the D_2O solution ^1H and $\{^1H\}^{13}C$ NMR spectra to an authentic sample obtained commercially. Other minor products accompany the protonation products and the fate of the triflate from these experiments is unknown. Notably, protonation with HCl demonstrates the synthesis of an alkylated hydrazine directly from atmospheric dinitrogen.

An alternative mechanism to that proposed in Figure 5.25 was also considered and is presented in Figure 5.27. The pathway involves initial reversible β-hydrogen elimination from **5** to form **2-(H)OTf** and diazomethane. The added methyl triflate serves to convert **2-(H)OTf** to **2-(OTf)$_2$**, allowing the diazomethane to insert into the hafnium methyl bond of **2-(Me)OTf** to yield **6**. However, the absence of crossover in the experiment whereby the conversion of **5-^{13}C** with $^{13}CH_3OTf$ was conducted in the presence of natural abundance **2-(Me)OTf** clearly rules out this mechanistic pathway. Additionally β-hydrogen elimination from coordinatively saturated **5** also seems unlikely.

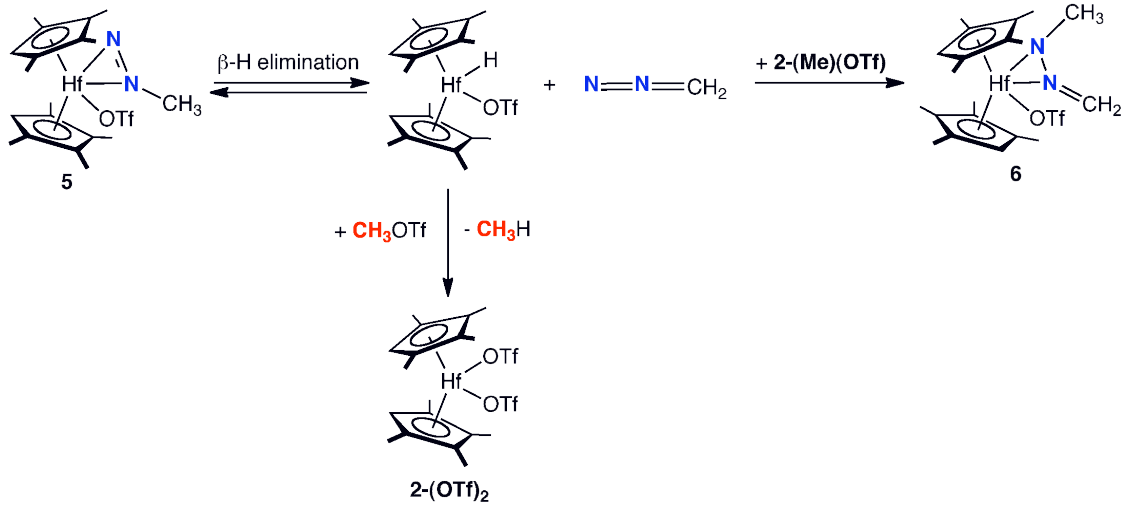

Figure 5.27. Alternative but experimentally inconsistent mechanism for the conversion of **5** to **6**.

Conclusions

A rare example of stepwise formation of nitrogen−carbon bonds to coordinated dinitrogen has been observed with a hafnocene complex bearing a strongly activated, side-on bound N_2 ligand. The success of the N_2 functionalization reaction is specific to the electrophile and the metal dinitrogen complex; N−C bond formation is only observed upon addition of methyl triflate to the hafnocene dinitrogen compound **2-N_2**. Even when dinitrogen methylation occurs, 1,4-addition of the electrophile to yield an end-on hafnocene dinitrogen compound remains competitive. The first addition of methyl triflate yields a rare example of a triflato hafnocene methyl diazenido compound. Addition of excess methyl triflate forms a triflato hafnocene hydrazonato compound along with methane and the hafnocene bis(triflate). Isotopic labeling studies and other experiments establish that the second methyl triflate addition proceeds via reversible methylation of the unsubstituted nitrogen atom followed by deprotonation by triflate. Future development of the early metallocene platform, through modification of the cyclopentadienyl ligands, may potentially afford compounds that promote similar dinitrogen functionalization chemistry with increased selectivity, substrate scope, and yield.

Experimental Section

General Considerations. All air- and moisture-sensitive manipulations were carried out using standard high vacuum line, Schlenk, or cannula techniques or in an M. Braun inert atmosphere drybox containing an atmosphere of purified nitrogen. The M. Braun drybox was equipped with a cold well designed for freezing samples in liquid nitrogen. Solvents for air- and moisture-sensitive manipulations were dried and deoxygenated using literature procedures.[41] Toluene, benzene, pentane, and heptane were further dried by distillation from “titanocene”.[42] Deuterated solvents for NMR

spectroscopy were distilled from sodium metal under an atmosphere of argon and stored over 4 Å molecular sieves. The zirconocene and hafnocene dinitrogen complexes, **1-N_2** and **2-N_2**, were prepared according to literature procedures.[18,19] **2-$^{15}N_2$** was prepared by reduction of **2-I_2** under an atmosphere of $^{15}N_2$.[19] AgTf[43] and **2-Me_2**[19] were also prepared according to literature procedures.

^{1}H NMR spectra were recorded on a Varian Inova 400 spectrometer operating at 399.860 MHz. All chemical shifts were reported relative to $SiMe_4$ using ^{1}H (residual) chemical shifts of the solvent as a secondary standard. ^{2}H, ^{13}C, and ^{15}N NMR spectra were recorded on a Varian Inova 500 spectrometer operating at 76.848, 125.716, and 50.663 MHz, respectively. ^{2}H and ^{13}C chemical shifts were reported relative to $SiMe_4$ using chemical shifts of the solvent as a secondary standard where applicable. ^{15}N chemical shifts were reported relative to liquid NH_3 using an external standard. ^{19}F NMR spectra were recorded on a Varian Inova 400 spectrometer operating at 376.127 MHz and referenced to hexafluorobenzene.

Single crystals suitable for X-ray diffraction were coated with polyisobutylene oil in a drybox transferred to a nylon loop and then quickly transferred to the goniometer head of a Bruker X8 APEX2 diffractometer equipped with a molybdenum X-ray tube (λ = 0.71073 Å). Preliminary data revealed the crystal system. A hemisphere routine was used for data collection and determination of lattice constants. The space group was identified, and the data were processed using the Bruker SAINT+ program and corrected for absorption using SADABS. The structures were solved using direct methods (SHELXS) completed by subsequent Fourier synthesis and refined by full-matrix least-squares procedures. Infrared spectroscopy was conducted on a Mattson RS-10500 Research Series FT-IR spectrometer calibrated with a polystyrene standard. Elemental analyses were performed at Robertson Microlit Laboratories, Inc., in Madison, NJ.

Preparation of ([$Me_2Si(\eta^5$-$C_5Me_4)(\eta^5$-C_5H_3-3-^{t}Bu)]Zr)$_2$(Me)(I)(μ_2,η^1,η^1-N_2 (3-(Me)(I)(μ_2,η^1,η^1-N_2)). A thick-walled glass vessel was charged with 0.076 g (0.094 mmol) of **3-N_2** and approximately 10 mL of toluene. On a high vacuum line, two equivalents of methyl iodide were added via calibrated gas bulb (38 torr in a 100.1 mL bulb). The solution turned to red-brown over the course of 1 h, the solvent was removed *in vacuo* and the resulting oil was recrystallized from pentane at -35 °C affording **3-(Me)(I)(μ_2,η^1,η^1-N_2)** as a red-brown solid in 64% yield. ^{1}H NMR (benzene-d_6): δ = 0.18 (s, 3H, Zr-CH_3), 0.45 (s, 3H, SiMe_2), 0.49 (s, 3H, SiMe_2), 0.65 (s, 3H, SiMe_2), 0.67 (s, 3H, SiMe_2), 1.48 (s, 9H, $C_5H_3CMe_3$), 1.56 (s, 3H, C_5Me_4), 1.64 (s, 9H, $C_5H_3CMe_3$), 1.78 (s, 3H, C_5Me_4), 2.00 (s, 3H, C_5Me_4), 2.01 (s, 3H, C_5Me_4), 2.27 (s, 3H, C_5Me_4), 2.33 (s, 3H, C_5Me_4), 2.71 (s, 3H, C_5Me_4), 2.99 (s, 3H, C_5Me_4), 5.20 (m, 1H, $C_5H_3CMe_3$), 5.27 (m, 1H, $C_5H_3CMe_3$), 5.30 (m, 1H, $C_5H_3CMe_3$), 5.51 (m, 1H, $C_5H_3CMe_3$), 5.58 (m, 1H, $C_5H_3CMe_3$), 7.44 (m, 1H, $C_5H_3CMe_3$).

Preparation of ([$Me_2Si(\eta^5$-$C_5Me_4)(\eta^5$-C_5H_3-3-^{t}Bu)]Hf)$_2$(Me)(I)(μ_2,η^1,η^1-N_2 (4-(Me)(I)(μ_2,η^1,η^1-N_2)). A thick-walled glass vessel was charged with 0.082 g (0.084 mmol) of **4-N_2** and approximately 10 mL of toluene. On a high vacuum line, two equivalents of methyl iodide were added via calibrated gas bulb (34 torr in a 100.1 mL bulb). The solution turned to deep purple over the course of 1 h, the solvent was removed *in vacuo* and the resulting oil was recrystallized from pentane at -35 °C affording **4-(Me)(I)(μ_2,η^1,η^1-N_2)** as a dark purple solid in 68% yield. ^{1}H NMR (benzene-d_6): δ = 0.13 (s, 3H, Hf-CH_3), 0.46 (s, 3H, SiMe_2), 0.47 (s, 3H, SiMe_2), 0.65 (s, 3H, SiMe_2), 0.69 (s, 3H, SiMe_2), 1.42 (s, 9H, $C_5H_3CMe_3$), 1.50 (s, 9H, $C_5H_3CMe_3$), 1.66 (s, 3H, C_5Me_4), 1.85 (s, 3H, C_5Me_4), 1.95 (s, 3H, C_5Me_4), 1.98 (s, 3H, C_5Me_4), 2.03 (s, 3H, C_5Me_4), 2.39 (s, 3H, C_5Me_4), 2.83 (s, 3H, C_5Me_4), 3.11 (s, 3H, C_5Me_4),

5.09 (m, 1H, $C_5H_3CMe_3$), 5.17 (m, 1H, $C_5H_3CMe_3$), 5.25 (m, 1H, $C_5H_3CMe_3$), 5.43 (m, 1H, $C_5H_3CMe_3$), 5.57 (m, 1H, $C_5H_3CMe_3$), 6.02 (m, 1H, $C_5H_3CMe_3$). $\{^1H\}^{13}C$ NMR (benzene-d_6): δ = -1.14 (Hf-CH_3), -0.23 (SiMe_2), -0.14 (SiMe_2), 0.30 (SiMe_2), 0.46 (SiMe_2), 12.13 (CpMe), 12.33 (CpMe), 12.83 (CpMe), 14.11 (CpMe), 15.62 (CpMe), 15.75 (CpMe), 15.85 (CpMe), 16.26 (CpMe), 31.79 (CMe_3), 31.98 (CMe_3), 34.28 (CMe$_3$), 90.96, 99.27, 103.78, 104.02, 104.12, 105.54, 105.94, 106.01, 111.58, 112.92, 116.63, 116.72, 120.01, 121.27, 122.98, 123.53, 126.03, 128.90, 129.67, 134.01, 153.50 (Cp), 1 CMe$_3$ resonance not located. ^{15}N NMR (benzene-d_6): δ = 658.9, 676.2 ($^{15}N_2$, $^1J_{NN}$ = 24.4 Hz).

Characterization data for [(η^5-$C_5Me_4H)_2Zr(OTf)]_2(\mu_2,\eta^1,\eta^1$-$N_2$) ([1-OTf]$_2N_2$). Anal. Calcd for $C_{38}H_{52}Zr_2N_2O_6S_2F_6$: C, 45.95; H, 5.28; N, 2.82. Found: C, 46.09; H, 5.06; N, 2.64.

Preparation of (η^5-$C_5Me_4H)_2ZrMe_2$ (1-Me$_2$). A 20 mL scintillation vial was charged with 0.300 g (0.742 mmol) of (η^5-$C_5Me_4H)_2ZrCl_2$ (**1-Cl$_2$**) and approximately 10 mL of diethyl ether. The solution was chilled to −35 °C, and 1.16 mL (1.85 mmol) of a 1.6 M methyl lithium solution in diethyl ether was added via microsyringe. The reaction mixture was stirred at ambient temperature for 16 h, and the solvent was removed *in vacuo*. The resulting white residue was extracted with pentane and filtered to give 0.166 g (61%) of **1-Me$_2$** as a white solid. Anal. Calcd for $C_{20}H_{32}Zr$: C, 66.05; H, 8.87. Found: C, 66.01; H, 9.00. ^1H NMR (benzene-d_6, 23 °C): δ = −0.54 (s, 6H, Hf−CH_3), 1.68 (s, 12H, C_5Me_4H), 1.94 (s, 12H, C_5Me_4H), 4.73 (s, 2H, C_5Me_4H). $\{^1H\}^{13}C$ NMR (benzene-d_6, 23 °C): δ = 121.79, 116.67, 110.53, 105.75 (Cp), 93.00 (C_5Me$_4$H), 35.32 (Hf−CH_3), 13.67, 11.98 (Cp).

Preparation of (η^5-$C_5Me_4H)_2Zr(O_3SCF_3)Me$ (1-Me(OTf)). A 20 mL scintillation vial was charged with 0.080 g (0.220 mmol) of **1-Me$_2$**, 0.062 g (0.240 mmol) of AgOTf and approximately 5 mL of toluene. The reaction mixture was stirred at ambient temperature for 3 h the solvent removed *in vacuo* and the resulting dark residue extracted with pentane. Following filtration to remove Ag^0 precipitate, recrystallization at −35 °C afforded 0.046 g (42%) of **1-Me(OTf)** as a white powder. Anal. Calcd for $C_{20}H_{29}F_3SO_3Zr$: C, 48.26; H, 5.87. Found: C, 47.98; H, 6.02. ^{1}H NMR (benzene-d_6, 23 °C): δ = 0.23 (s, 3H, Hf−CH_3), 1.40 (s, 6H, C_5Me_4H), 1.79 (s, 6H, C_5Me_4H), 1.82 (s, 6H, C_5Me_4H), 1.85 (s, 6H, C_5Me_4H), 5.05 (s, 2H, C_5Me_4H). $\{^1H\}^{13}$C NMR (benzene-d_6, 23 °C): δ = 125.54, 125.08, 119.00, 117.86 (*Cp*), 108.50 (C_5Me_4H), 40.95 (Hf−CH_3), 11.57, 11.52. 9.93, 9.45 (*Cp*), CF_3 signal not located. ^{19}F NMR (benzene-d_6, 23 °C): δ = −77.07.

Preparation of (η^5-$C_5Me_4H)_2Zr(OMe)OTf$ ((1-OMe)OTf). A J. Young tube was charged with 0.012 g (0.024 mmol) of **1-(Me)OTf** and approximately 0.5 mL of benzene-d_6. On a high vacuum line, two equivalents of methanol were added via calibrated gas bulb (28 Torr in a 31.6 mL bulb). The colorless reaction mixture was transferred to a 20 mL scintillation vial after 1 h and dried, affording 0.012 g (94%) of **1-(OMe)OTf** as a white powder. Anal. Calcd. for $C_{20}H_{29}F_3SO_4Zr$: C, 46.76; H, 5.69. Found: C, 46.55; H, 5.48. ^{1}H NMR (benzene-d_6, 23 °C): δ = 1.67 (s, 6H, C_5Me_4H), 1.72 (s, 6H, C_5Me_4H), 1.78 (s, 6H, C_5Me_4H), 1.94 (s, 6H, C_5Me_4H), 3.90 (s, 3H, OCH_3), 5.57 (s, 2H, C_5Me_4H). $\{^1H\}^{13}$C NMR (benzene-d_6, 23 °C): δ = 113.15 (C_5Me_4H), 60.47 (Hf−OCH_3), 13.07, 11.24 (*Cp*), quaternary signals not located. ^{19}F NMR (benzene-d_6, 23 °C): δ = −77.17.

Preparation of [$Me_2Si(\eta^5\text{-}C_5Me_4)(\eta^5\text{-}C_5H_3\text{-}3\text{-}^tBu)$]Zr(OMe)(OTf) (3-(OMe)(OTf)). A thick-walled glass vessel was charged with 0.075 g (0.093 mmol) of **3-N_2** and approximately 10 mL of toluene. On a high vacuum line, two equivalents of methyl triflate were added via calibrated gas bulb (38 torr in a 100.1 mL bulb). The solution turned from green to orange over the course of several hours, the solvent was removed *in vacuo* and the resulting oil was recrystallized from pentane at -35 °C affording (**[3-(OMe)(OTf)** as a pale yellow solid in 53% yield. ^{1}H NMR (benzene-d_6): δ = 0.40 (s, 3H, SiMe_2), 0.51 (s, 3H, SiMe_2), 1.14 (s, 9H, $C_5H_3C$$Me_3$), 1.63 (s, 3H, $C_5$$Me_4$), 1.80 (s, 3H, $C_5$$Me_4$), 1.82 (s, 3H, $C_5$$Me_4$), 1.92 (s, 3H, $C_5$$Me_4$), 3.70 (s, 3H, Zr-OC$H_3$), 5.55 (m, 1H, $C_5$$H_3$$CMe_3$), 5.86 (m, 1H, $C_5$$H_3$$CMe_3$), 7.02 (m, 1H, $C_5$$H_3$$CMe_3$). {^{1}H}^{13}C NMR (benzene-d_6): δ = −0.91 (SiMe_2), 0.29 (SiMe_2), 10.96 (CpMe), 14.09 (CpMe), 14.16 (CpMe), 14.50 (CpMe), 30.61 (CMe_3), 33.13 ($C$$Me_3$), 60.11 (Zr-O$CH_3$), 108.72, 111.83, 116.79, 116.93, 117.65, 118.24, 120.66, 120.79, 136.84, 154.06 (*Cp*). ^{19}F NMR (benzene-d_6, 23 °C): δ = −77.64 (CF_3).

Preparation of ([$Me_2Si(\eta^5\text{-}C_5Me_4)(\eta^5\text{-}C_5H_3\text{-}3\text{-}^tBu)$]Hf(OTf)]$_2(\mu_2,\eta^1,\eta^1\text{-}N_2$ ([4-(OTf)]$_2(\mu_2,\eta^1,\eta^1\text{-}N_2)$). A thick-walled glass vessel was charged with 0.080 g (0.081 mmol) of **4-N_2** and approximately 10 mL of toluene. On a high vacuum line, two equivalents of methyl triflate were added via calibrated gas bulb (33 torr in a 100.1 mL bulb). The solution turned from purple to magenta over the course of 3 h, the solvent was removed in vacuo and the resulting oil was recrystallized from pentane at -35 °C affording (**[4-(OTf)]$_2(\mu_2,\eta^1,\eta^1\text{-}N_2)$** as a pink solid in 71% yield. ^{1}H NMR (benzene-d_6): δ = 0.50 (s, 6H, SiMe_2), 0.67 (s, 6H, SiMe_2), 1.23 (s, 18H, $C_5H_3C$$Me_3$), 1.96 (s, 6H, $C_5$$Me_4$), 2.01 (s, 6H, $C_5$$Me_4$), 2.12 (s, 6H, $C_5$$Me_4$), 2.33 (s, 6H, $C_5$$Me_4$), 5.54 (m, 2H, $C_5$$H_3$$CMe_3$), 5.68 (m, 2H, $C_5$$H_3$$CMe_3$), 6.22 (m, 2H, $C_5$$H_3$$CMe_3$). {^{1}H}^{13}C NMR (benzene-d_6): δ = -1.68 (SiMe_2), 1.37 (SiMe_2), 11.40 (CpMe), 11.53

(Cp*Me*), 15.29 (Cp*Me*), 15.50 (Cp*Me*), 30.66 (C*Me*$_3$), 31.17 (OSO$_2$*C*F$_3$), 33.46 (*C*Me$_3$), 101.14, 103.85, 107.45, 113.61, 116.83, 118.26, 120.81, 121.44, 136.28, 155.15 (*Cp*). ^{19}F NMR (benzene-d_6, 23 °C): δ = −76.45 (C*F*$_3$). ^{15}N NMR (benzene-d_6, 23 °C): δ = 750.56.

Treatment of [(η^5-C$_5$Me$_4$H)$_2$Hf]$_2$(μ$_2$,η^1,η^1-N$_2$) (2-N$_2$) with Methyl Triflate. A J. Young tube was charged with 0.010 g (0.011 mmol) of **2-N$_2$** and approximately 0.5 mL of benzene-d_6. On a high vacuum line, two equivalents of methyl triflate were added via calibrated gas bulb (32 Torr in a 13.1 mL bulb). Over the course of 1 h the solution turned from violet to deep pink to yellow with some dark-violet precipitate. The dark solid was identified as [(η^5-C$_5$Me$_4$H)$_2$Hf(OTf)]$_2$(μ$_2$,η^1,η^1-N$_2$) by X-ray diffraction and combustion analysis. Benzene-d_6 solution ^{1}H NMR spectroscopy of the soluble products revealed a 1:1 ratio of **2-(Me)OTf** and **5**. Three additional equivalents of methyl triflate were then added to the reaction mixture via calibrated gas bulb (18 Torr in a 31.6 mL bulb). Over the course of 16 h, the solution turned light yellow; analysis of the mixture by NMR spectroscopy revealed complete consumption of **5** along with the formation of **6** and **2-(OTf)$_2$** in a 1:1 ratio.

Characterization data for [(η^5-C$_5$Me$_4$H)$_2$Hf(OTf)](N$_2$Me) (5). ^{1}H NMR (benzene-d_6, 23 °C): δ = 1.24 (s, 6H, C$_5$*Me*$_4$H), 1.66 (s, 6H, C$_5$*Me*$_4$H), 1.83 (s, 6H, C$_5$*Me*$_4$H), 1.87 (s, 6H, C$_5$*Me*$_4$H), 4.11 (s, 3H, N−C*H*$_3$), 5.30 (s, 2H, C$_5$Me$_4$*H*). {^{1}H}^{13}C NMR (benzene-d_6, 23 °C): δ = 10.51, 11.61, 12.06, 12.32 (C$_5$*Me*$_4$H), 55.85 (N−*C*H$_3$; ^{15}N−^{13}CH$_3$, dd, $^1J_{CN}$ = 5.1 Hz, $^2J_{CN}$ = 1.1 Hz), 109.96 (*Cp*H), quaternary signals not located. ^{19}F NMR (benzene-d_6, 23 °C): δ = −75.94. ^{15}N NMR (benzene-d_6, 23 °C): δ = 460.13 (*N*-CH$_3$, d, $^1J_{NN}$ = 20.6 Hz), 729.86 (*N*═N(CH$_3$)).

Characterization data for $[(\eta^5\text{-}C_5Me_4H)_2Hf(OTf)]_2(\mu_2,\eta^1,\eta^1\text{-}N_2)$ ($[2\text{-}OTf]_2(N_2)$). Anal. Calcd for $C_{40}H_{52}Hf_2N_2O_6S_2F_6$: C, 39.08; H, 4.49; N, 2.40. Found: C, 39.10; H, 4.06; N, 2.81. IR (KBr) $\nu_{S-O} = 1335\ cm^{-1}$.

Preparation of $(\eta^5\text{-}C_5Me_4H)_2Hf(O_3SCF_3)Me$ (2-(Me)OTf). A 20 mL scintillation vial was charged with 0.080 g (0.177 mmol) of **2-Me$_2$**, 0.055 g (0.195 mmol) of AgOTf and approximately 5 mL of toluene. The reaction mixture was stirred at ambient temperature for 3 h the solvent removed *in vacuo* and the resulting dark residue extracted with pentane. Following filtration to remove Ag^0 precipitate, recrystallization at −35 °C afforded 0.041 g (39%) of **2-Me(OTf)** as a white powder. Anal. Calcd for $C_{20}H_{29}HfO_3SF_3$: C, 50.36; H, 5.28. Found: C, 49.91; H, 5.10. ^{1}H NMR (benzene-d_6, 23 °C): δ = 0.10 (s, 3H, Hf−CH_3), 1.49 (s, 6H, C$_5$*Me*$_4$H), 1.83 (s, 6H, C$_5$*Me*$_4$H), 1.84 (s, 6H, C$_5$*Me*$_4$H), 1.87 (s, 6H, C$_5$*Me*$_4$H), 5.10 (s, 2H, C$_5$Me$_4$*H*). $\{^1H\}^{13}$C NMR (benzene-d_6, 23 °C): δ = 12.08, 12.73, 14.24, 14.31 (C$_5$*Me*$_4$H), 42.04 (Hf−*C*H$_3$), 110.85, 119.01, 120.14, 126.64, 126.80 (*Cp*), *C*F$_3$ signal not located. ^{19}F NMR (benzene-d_6, 23 °C): δ = −75.71.

Preparation of $(\eta^5\text{-}C_5Me_4H)_2Hf(OMe)OTf$ ((2-OMe)OTf). A J. Young tube was charged with 0.015 g (0.026 mmol) of **2-(Me)OTf** and approximately 0.5 mL of benzene-d_6. On a high vacuum line, two equivalents of methanol were added via calibrated gas bulb (15 Torr in a 31.6 mL bulb). The colorless reaction mixture was transferred to a 20 mL scintillation vial after 1 h and dried, affording 0.014 g (95%) of **2-(OMe)OTf** as a white powder. Anal. Calcd. for $C_{20}H_{29}F_3SO_4Hf$: C, 39.97; H, 4.86. Found: C, 39.78; H, 4.80. ^{1}H NMR (benzene-d_6, 23 °C): δ = 1.73 (s, 6H, C$_5$*Me*$_4$H), 1.77 (s, 6H, C$_5$*Me*$_4$H), 1.82 (s, 6H, C$_5$*Me*$_4$H), 1.99 (s, 6H, C$_5$*Me*$_4$H), 3.96 (s, 3H, OC*H*$_3$), 5.52 (s, 2H, C$_5$Me$_4$*H*). $\{^1H\}^{13}$C NMR (benzene-d_6, 23 °C): δ = 127.46,

126.74, 118.76, 117.09 (*Cp*), 112.02 (C_5Me_4H), 58.57 (Hf-CH_3), 13.05, 12.84. 11.21, 11.10 (Cp*Me*), CF_3 signal not located. ^{19}F NMR (benzene-d_6, 23 °C): $\delta = -76.94$.

Characterization Data for (η^5-$C_5Me_4H)_2Hf(OTf)(\eta^2$-$N(CH_3)N{=}CH_2$) (6). ^1H NMR (benzene-d_6, 23 °C): δ = 1.76 (s, 6H, C_5Me_4H), 1.84 (s, 6H, C_5Me_4H), 1.87 (s, 6H, C_5Me_4H), 1.89 (s, 6H, C_5Me_4H), 2.94 (s, 3H, N−CH_3), 5.40 (s, 2H, CH_2), 5.76 (s, 2H, C_5Me_4H). $\{^1H\}^{13}C$ NMR (benzene-d_6, 23 °C): δ = 10.77, 11.28, 11.44, 13.00 (C_5Me_4H), 33.13 (N-CH_3), 108.47 (CH_2), other signals not located. $\{^1H\}^{15}N$ NMR (benzene-d_6, 23 °C): δ = 174.23 (*N*−CH_3, d, $^1J_{NN}$ = 17.1 Hz), 311.49 (*N*═CH_2).

Procedure for the Liberation of *N*-Methylhydrazine·2 HCl. Approximately 10 mg of **5** (along with associated byproducts) were prepared by methyl triflate addition to **2-N_2** in benzene-d_6. The contents of the tube were frozen in liquid nitrogen, and approximately 10 equivalents of anhydrous HCl (vacuum transferred from a solution in dioxane) were added via calibrated gas volume. The solution was thawed and shaken, and the volatiles were removed *in vacuo*. The resulting solids were dissolved in D_2O, the ^1H and ^{13}C NMR spectra were recorded, and the desired product was confirmed by comparison to an authentic commercial sample.

Preparation of (η^5-$C_5Me_4H)_2Hf(O_3SCF_3)_2$ (2-OTf_2). A 20 mL scintillation vial was charged with 0.050 g (0.102 mmol) of **2-Cl_2**, 0.060 g (0.213 mmol) of AgOTf, and approximately 10 mL of toluene. The reaction mixture was stirred at ambient temperature for 8 h the solvent removed *in vacuo* and the resulting white residue extracted with diethyl ether. Following filtration to remove AgCl precipitate, recrystallization at −35 °C afforded 0.021 g (29%) of **2-$(OTf)_2$** as colorless crystals. Anal. Calcd for $C_{20}H_{26}HfO_6S_2F_6$: C, 33.41; H, 3.46. Found: C, 34.26; H, 3.65. ^1H

NMR (benzene-d_6, 23 °C): δ = 1.78 (s, 12H, C_5Me_4H), 1.89 (s, 12H, C_5Me_4H), 5.80 (s, 2H, C_5Me_4H). $\{^1H\}^{13}C$ NMR (benzene-d_6, 23 °C): δ = 11.57, 12.92 (C_5Me_4H), 116.42, 122.73, 131.91 (*Cp*), *C*F_3 signal not located. ^{19}F NMR (benzene-d_6, 23 °C): δ = −75.00 (CF_3).

Preparation of (η^5-$C_5Me_4H)_2Hf(OMe)(Tf)$ (2-(OMe)Tf). A 20 mL scintillation vial was charged with **2-Me$_2$** (30 mg, 0.067 mmol), $AgSO_2CF_3$ (16 mg, 0.067 mmol), and 5 mL of benzene. The reaction mixture was stirred at ambient temperature for 1 h, the solvent was removed *in vacuo* and the resulting dark residue extracted with pentane. Following filtration to remove the Ag° precipitate, the solvent was removed *in vacuo*, and the remaining solid was dissolved in benzene and transferred to a thick-walled bomb. On a high vacuum line, MeOH (40 Torr in a 100.1 mL calibrated gas bulb, excess) was added, and the mixture was stirred at ambient temperature for 2 h. The solvent was removed *in vacuo* to give 22 mg of (56%) of (η^5-$C_5Me_4H)_2Hf(OMe)(Tf)$ (**2-(OMe)Tf**) as a white solid. Anal. Calcd for $C_{20}H_{29}F_3SO_3Hf$: C, 41.06; H, 5.00. Found: C, 41.12; H, 5.12. ^1H NMR (benzene-d_6, 23 °C): δ = 1.76 (s, 6H, C_5Me_4H), 1.78 (s, 6H, C_5Me_4H), 1.79 (s, 6H, C_5Me_4H), 1.92 (s, 6H, C_5Me_4H), 3.89 (s, 3H, Hf-OCH_3), 5.46 (s, 2H, C_5Me_4H). $\{^1H\}^{13}C$ NMR (benzene-d_6, 23 °C): δ = 11.03, 11.37, 12.90, 13.03 (C_5Me_4H), 57.97 (OCH_3), 111.19, 116.14, 117.58, 123.14, 126.14 (*Cp*), *C*F_3 resonance not located. ^{19}F NMR (benzene-d_6, 23 °C): δ = −85.53 (CF_3).

Preparation of (η^5-$C_5Me_4H)_2Zr(OTf)(\eta^2$-$N(CH_3)N{=}C(H)COOEt)$ (7). In a 20 mL scintillation vial, ethyl diazoacetate (22.3 μL, 0.211 mmol) was added to a solution of 0.070 g of **1-Me$_2$** (0.192 mmol) in approximately 10 mL of toluene. The reaction mixture was stirred at room temperature for 16 h, and the solvent was removed *in vacuo*. The resulting yellow oil was redissolved in approximately 5 mL of toluene and

54.2 mg of AgOTf (0.211 mmol) was added, whereupon the reaction turned dark brown. The reaction mixture was stirred for 30 min, the solvent was removed *in vacuo* and the resulting brown residue extracted with pentane. Following filtration to remove Ag^0 precipitate, recrystallization at −35 °C afforded 0.60 g (51%) of (**7**) as a white solid. Anal. Calcd for $C_{24}H_{35}F_3N_2O_5SZr$: C, 47.11; H, 5.77; N, 4.58. Found: C, 46.84; H, 5.59; N, 4.24. ^{1}H NMR (benzene-d_6, 23 °C): δ = 1.05 (t, $^3J_{HH}$ = 6.7 Hz, 3H, $COOCH_2CH_3$), 1.58 (s, 6H, C_5Me_4H), 1.82 (s, 6H, C_5Me_4H), 1.89 (s, 6H, C_5Me_4H), 1.95 (s, 6H, C_5Me_4H), 2.98 (s, 3H, N−CH_3), 4.08 (q, $^3J_{HH}$ = 6.7 Hz, 2H, $COOCH_2CH_3$), 5.75 (s, 2H, C_5Me_4H), 6.33 (s, 1H, C*H*). {^{1}H}^{13}C NMR (benzene-d_6, 23 °C): δ = 11.27, 11.68, 13.03, 13.77 (C_5Me_4H), 15.14 (CH_3), 32.70 (N-CH_3), 59.76 (CH_2), 108.63 (*Cp*), 111.90 (*C*H), 115.47, 115.98, 118.56, 122.76 (*Cp*), 164.86 (*C*O). ^{19}F NMR (benzene-d_6, 23 °C): δ = −76.53 (CF_3).

Preparation of (η^5-$C_5Me_4H)_2Hf(OTf)(\eta^2$-$N(CH_3)N{=}C(H)COOEt$) (8). In a 20 mL scintillation vial, ethyl diazoacetate (18.0 μL, 0.170 mmol) was added to a solution of 0.070 g of **2-Me$_2$** (0.155 mmol) in approximately 10 mL of toluene. The reaction mixture was stirred at room temperature for 16 h, and the solvent was removed *in vacuo*. The resulting yellow oil was redissolved in approximately 5 mL of toluene, and 43.7 mg of AgOTf (0.170 mmol) was added, whereupon the reaction turned dark brown. The reaction mixture was stirred for 30 min, the solvent was removed *in vacuo* and the resulting brown residue was extracted with pentane. Following filtration to remove Ag^0 precipitate, recrystallization at −35 °C afforded 0.071 g (66%) of (**8**) as a white solid. Anal. Calcd for $C_{24}H_{35}F_3HfN_2O_5S$: C, 41.23; H, 5.05; N, 4.01. Found: C, 40.92; H, 4.79; N, 3.74. ^{1}H NMR (benzene-d_6, 23 °C): δ = 1.04 (t, $^3J_{HH}$ = 7.3 Hz, 3H, $COOCH_2CH_3$), 1.65 (s, 6H, C_5Me_4H), 1.86 (s, 6H, C_5Me_4H), 1.94 (s, 6H, C_5Me_4H), 2.03 (s, 6H, C_5Me_4H), 2.96 (d, $^4J_{HH}$ = 1.1 Hz, 3H, N−CH_3), 4.07 (q, $^3J_{HH}$ = 7.3 Hz, 2H,

COOC*H*$_2$CH$_3$), 5.73 (s, 2H, C$_5$Me$_4$*H*), 6.43 (d, $^4J_{HH}$ = 1.1 Hz, 1H, C*H*). {^{1}H}^{13}C NMR (benzene-d_6, 23 °C): δ = 11.18, 11.72, 12.67, 13.11 (C$_5$*Me*$_4$H), 14.89 (*C*H$_3$), 36.01 (N-*C*H$_3$), 60.37 (*C*H$_2$), 113.03 (*Cp*), 114.44 (*C*H), 116.40, 121.94, 122.23, 128.92 (*Cp*), 164.13 (*C*O). ^{19}F NMR (benzene-d_6, 23 °C): δ = −76.27 (C*F*$_3$).

REFERENCES

[1] Mori, M. *J. Organomet. Chem.* **2004**, *689*, 4210.

[2] Fryzuk, M. D. *Chem. Rec.* **2003**, *3*, 2.

[3] (a) Henderickx, H.; Kwakkenbos, G.; Peters, A.; van der Spoel, J.; de Vries, K. *Chem. Commun.* **2003**, 2050. (b) Komori, K.; Oshita, H.; Mizobe, Y.; Hidai, M. *J. Am. Chem. Soc.* **1989**, *111*, 1939. (c) Rocklage, S. M.; Schrock, R. R. *J. Am. Chem. Soc.* **1982**, *104*, 3077. (d) Betley, T. E.; Peters, J. C. *J. Am. Chem. Soc.* **2003**, *125*, 10782. (e) Figueroa, J. S.; Piro, N. A.; Clough, C. R.; Cummins, C. C. *J. Am. Chem. Soc.* **2006**, *128*, 940.

[4] Smil V. *Enriching the Earth: Fritz Haber, Carl Bosch, and the Transformation of World Food Production*; MIT Press, Cambridge, MA, 2001.

[5] (a) Schlögl, R. *Angew. Chem. Int. Ed.* **2003**, *42*, 2004. (b) Tamaru, K. in *Catalytic Ammonia Synthesis.* J. R. Jennings, Ed.; Plenum, NY 1991. (c) Pimentel, D.; Patzek, T. W. *Nat. Resources Res.* **2005**, *14*, 65.

[6] Ertl, G. *Angew. Chem. Int. Ed.* **2008**, *47*, 3524.

[7] Shaver, M. P.; Fryzuk, M. D. *Adv. Synth. Catal.* **2003**, *345*, 1061.

[8] (a) Hidai, M.; Mizobe, Y. *Pure Appl. Chem.* **2001**, *73*, 261. (b) Hidai, M. *Coord. Chem. Rev.* **1999**, *185-186*, 99. (c) Hidai, M.; Mizobe, Y. *Chem. Rev.* **1995**, *95*, 1115.

[9] Kupfer, T.; Schrock, R. R. *J. Am. Chem. Soc.*, **2009**, *131*, 12829.

[10] Akagi, F.; Matsuo, T.; Kawaguchi, H. *Angew. Chem., Int. Ed.* **2007**, *46*, 8778.

[11] Chatt, J.; Dilworth, J. R.; Richards, R. L. *Chem. Rev.* **1978**, *78*, 589.

[12] For a full discussion see Chapters 1-3 of this Thesis, and References 13-15.

[13] Knobloch, D. J.; Lobkovsky, E.; Chirik, P. J. *Nature Chem.* **2010**, *2*, 30.

[14] Knobloch, D. J.; Lobkovsky, E.; Chirik, P. J. *J. Am. Chem. Soc.* **2010**, *132*, 10553.

[15] Knobloch, D. J.; Lobkovsky, E.; Chirik, P. J. *J. Am. Chem. Soc.* **2010**, *132*, 15340.

[16] Bernskoetter, W. H.; Lobkovsky, E.; Chirik, P. J. *Angew. Chem. Int. Ed.* **2007**, *119*, 2858.

[17] Knobloch, D. J.; Toomey, H. E.; Chirik, P. J. *J. Am. Chem. Soc.* **2008**, *130*, 4248.

[18] Pool, J. A.; Lobkovsky, E.; Chirik, P. J. *Nature* **2004**, *427*, 527.

[19] Bernskoetter, W. H.; Olmos, A. V.; Lobkovsky, E.; Chirik, P. J. *Organometallics* **2006**, *25*, 1021.

[20] Chirik, P. J. *Dalton Trans.* **2007**, 16.

[21] Morello, L.; Love, J. B.; Patrick, B. O.; Fryzuk, M. D. *J. Am. Chem. Soc.* **2004**, *126*, 9480.

[22] van Tamelen, E. E. *Acc. Chem. Res.* **1970**, *11*, 361.

[23] Mori, M. *J. Organomet. Chem.* **2004**, *689*, 4210.

[24] Hori, M.; Mori, M. *J. Org. Chem.* **1995**, *60*, 1480.

[25] Sobota, P.; Janas, Z. J. *Organomet. Chem.* **1984**, *276*, 171.

[26] Hirotsu, M.; Fontaine, P. P.; Zavalij, P. Y.; Sita, L. R. *J. Am. Chem. Soc.* **2007**, *129*, 12690.

[27] Benito-Garagorri, D.; Bernskoetter, W. H.; Lobkovsky, E.; Chirik, P. J. *Organometallics* **2009**, *28*, 4807.

[28] For a full discussion see Chapters 1-3 of this Thesis and References 13-15.

[29] For a full discussion see Chapter 4 of this Thesis and References 16 and 17.

[30] (a) Manriquez, J. M.; Bercaw, J. E. *J. Am. Chem. Soc.* **1974**, *96*, 6229. (b) Manriquez, J. M.; McAlister, D. R.; Rosenberg, E.; Shiller, A. M.; Williamson, K. L.; Chan, S. I.; Bercaw, J. E. *J. Am. Chem. Soc.* **1978**, *100*, 3078.

[31] Hirotsu, M.; Fontaine, P. P.; Zavalij, P. Y.; Sita, L. R. *J. Am. Chem. Soc.* **2007**, *129*, 12690.

[32] Wiberg, N.; Holleman, A. F.; Wiberg, E. *Inorganic Chemistry*; Academic Press, 2002.

[33] Gehrmann, T.; Fillol, J. L.; Wadepohl, H.; Gade, L. H. *Angew. Chem. Int. Ed.* **2009**, *48*, 2152.

[34] Kahlal, S.; Saillard, J. –Y.; Hamon, J. –R.; Manzur, C.; Carrillo, D. *New J. Chem.* **2001**, *25*, 231.

[35] Gambarotta, S.; Floriani, C.; Chiesi-Villa, A.; Guastini, C. *Inorg. Chem.* **1983**, *22*, 2029.

[36] Vaughan, G. A.; Hillhouse, G. L.; Rheingold, A. L. *J. Am. Chem. Soc.* **1990**, *112*, 7994.

[37] Bai, G.; Roesky, H. W.; Hao, H.; Noltenmeyer, M.; Schmidt, H.-G. *Inorg. Chem.* **2001**, *40*, 2424.

[38] Hay, J. P. *Organometallics* **2007**, 26, 4424.

[39] Wilmshurst, J. K; Bernstein, H. J. *Can. J. Chem.* **1957**, *35*, 226.

[40] (a) Tsuji, T.; Kosower, E. M. *J. Am. Chem. Soc.* **1970**, *92*, 1429. (b) Ackermann, M. N.; Ellenson, J. L.; Robison, D. H. *J. Am. Chem. Soc.* **1969**, *91*, 7173.

[41] Pangborn, A. B.; Giardello, M. A.; Grubbs, R. H.; Rosen, R. K.; Timmers, F. J. *Organometallics* **1996**, *15*, 1518.

[42] Marvich, R.H.; Brintzinger, H.H. *J. Am. Chem. Soc.* **1971**, *93*, 2046.

[43] Hendrickson, J. S.; Skipper, P. L. *Tetrahedron* **1976**, *32*, 1627.

APPENDIX A:

Preliminary Investigations: An unusual *ansa*-zirconocene dinitrogen complex bearing a $[\mu_2, \eta^1, \eta^1\text{-}N_2]^{1-}$ ligand.

Results and Discussion

In an effort to study the effect of the cyclopentadienyl substituents on dinitrogen coordination in a series of *ansa*-zirconocene complexes, the adamantyl substituted zirconocene dichloride compound, $Me_2Si(\eta^5\text{-}C_5Me_4)(\eta^5\text{-}C_5H_3\text{-}3\text{-}^2Ad)ZrCl_2$ (**7-Cl$_2$**) (^{2}Ad = 2-adamantyl) was prepared *via* salt metathesis of the corresponding dilithiated species with $ZrCl_4$. Reduction of a toluene solution of **7-Cl$_2$** with 0.5% sodium amalgam under an atmosphere of N_2 for three days resulted in an intractable mixture of unidentified products. Varying the reaction conditions, including the quantity of Na(Hg) used and reaction time, did not produce clean products. The stronger reductant KC_8 was selected in hopes of cleaner reduction chemistry. Dropwise addition of a toluene solution of **7-Cl$_2$** to a stirring toluene slurry of KC_8 resulted in an immediate color change of the solution from yellow to deep red. After 30 min the reaction was filtered and the product was isolated from diethyl ether. The product was identified as the dichloro, end-on dinitrogen *ansa*-zirconocene anion compound, $[(Me_2Si(\eta^5\text{-}C_5Me_4)(\eta^5\text{-}C_5H_3\text{-}3\text{-}^2Ad)Zr(Cl))_2(\mu_2, \eta^1, \eta^1\text{-}N_2)][K(OEt_2)_2]$ (**[7-N$_2$]$^-$**), on the basis of NMR and EPR spectroscopies, X-ray diffraction, and degradation studies (Figure A.1).

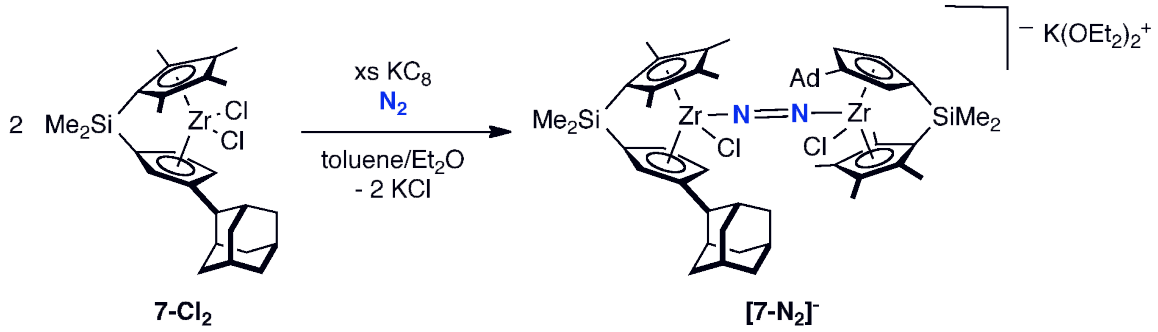

Figure A.1. Synthesis of **[7-N_2]$^-$**.

The product exhibits no signal in the room temperature benzene-d_6 NMR spectrum, consistent with a paramagnetic species. In addition, no stretch assignable to an N_2 ligand was observed by solution or solid-state (KBr) infrared spectroscopy. The room temperature solution (toluene/diethyl ether) EPR spectrum of **[7-N_2]$^-$** exhibits a five line pattern at $g_{iso} = 2.007$ (Figure A.2), resulting from an S = 1/2 spin system with coupling to two chemically equivalent I = 1/2 ^{14}N nuclei. In addition, a small multi-line signal with hyperfine coupling to the two I = 5/2 ^{91}Zr (11.2% natural abundance) nuclei was observed. Simulation of the data established hyperfine coupling to the ^{14}N and ^{91}Zr nuclei of $A_{iso} = 3.3 \times 10^{-4}$ cm^{-1} and $A_{iso} = 3.8 \times 10^{-4}$ cm^{-1}, respectively (Figure A.2).

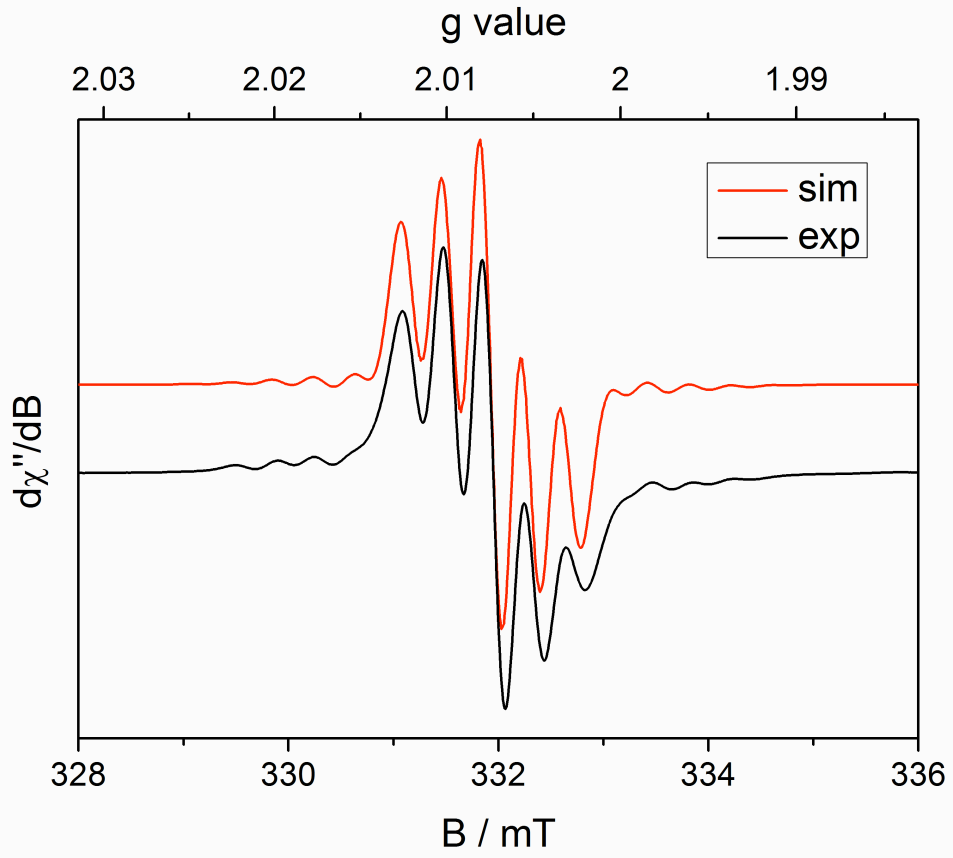

Figure A.2. Experimental (bottom) and simulated (top) toluene/diethyl ether solution EPR spectra of **[7-N_2]**$^-$ at 23 ºC.

The reduction of **7-Cl_2** was repeated under an atmosphere of $^{15}N_2$, furnishing the ^{15}N-labeled isotopologue, **[7-$^{15}N_2$]**$^-$. The room temperature EPR spectrum of **[7-$^{15}N_2$]**$^-$ exhibits a triplet pattern, consistent with electronic coupling to two I = 1 ^{15}N nuclei. The experimental spectrum is presented in Figure A.3, and the simulated spectrum and hyperfine constants are forthcoming. Importantly the EPR data are consistent with an S = 1/2 compound with the spin localized on the dinitrogen ligand.

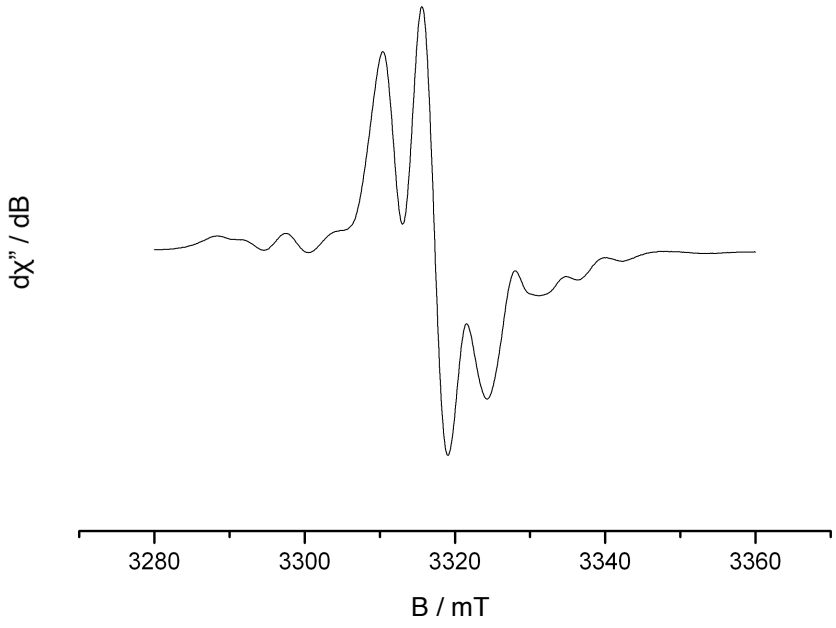

Figure A.3. Toluene/diethyl ether solution EPR spectrum of **[7-$^{15}N_2$]**$^-$ at 23 ºC.

Single crystals of **[7-N_2]**$^-$ suitable for X-ray diffraction were obtained from diethyl ether at -35 ºC and confirm a dimeric chlorozirconocene compound with end-on coordination of the dinitrogen ligand. The crystal structure also confirms the presence of a solvent-chelated potassium counterion in close proximity to and approximately equidistant from the two nitrogen atoms. A representation of the (*S*,*S*)-enantiomer of **[7-$^{15}N_2$]**$^-$ is presented in Figure A.4 and selected distances are reported in Table A.1. The (*R,R*) enantiomer is reported in Appendix C. The N-N bond distance of 1.223(9) Å is consistent with a modestly activated dinitrogen ligand. Overall, the EPR and X-ray crystallographic data are fully consistent with the dimeric zirconocene

dinitrogen anion, which is formally assigned as an $[N_2]^{1-}$ fragment coordinated to two $Zr^{3.5+}$ metal centers.

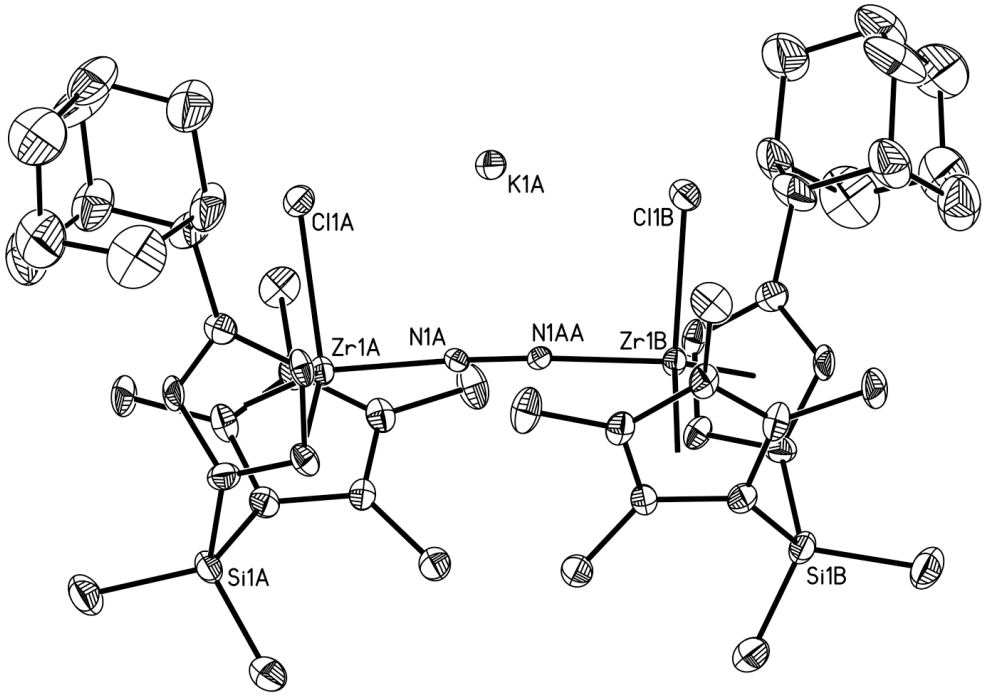

Figure A.4. Molecular structure of **[7-N_2]$^-$** at 30% probability ellipsoids. Hydrogen atoms and the chelated solvent molecule omitted for clarity. The (*S*,*S*)-enantiomer is shown.

Table A.1. Selected crystal structure parameters for **[7-N_2]$^-$**.

Bond / Angle	Distance (Å) / Angle (º)
N1A-N1AA	1.223(9)
Zr1A-N1A	2.007(4)
Zr1A-Cl1A	2.5270(19)
N1A-K1A	2.895(6)
K1A-Cl1A	3.0596(19)
Zr1A-N1A-N1AA	176.99(17)

Interestingly, EPR spectral characteristics very similar to those of **[7-N_2]$^-$** were observed for a monomeric zirconocene compound having a rare side-on bound dinitrogen ligand reported by Lappert in 1978.[1,2] Unfortunately this compound was not crystallographically characterized. We believe that an anionic dimer akin to **[7-N_2]$^-$** is an alternative structural possibility for Lappert's molecule, and is fully consistent with the published spectroscopic data.[1,2]

The modestly activated N_2 ligand in **[7-N_2]$^-$** suggested partial diazenido character, prompting protonolysis studies. Treatment of **[7-N_2]$^-$** with excess gaseous HCl resulted in rapid and quantitative conversion to the corresponding dichloride compound, **7-Cl_2** with concomitant formation of NH_4Cl in 25.8% yield (per N-atom) (Figure A.5). NH_4Cl formation results from liberation of diazene and subsequent known decomposition[3] to NH_3 and N_2 (Figure A.6). The observed yield of NH_4Cl is also consistent with the stoichiometry of this known decomposition. In addition, when the protonolysis was performed in the presence of 20 equivalents of 1-hexene, most of the generated diazene was consumed by hydrogenation of the olefin, and the yield of NH_4Cl decreased to 6.3% (Figure A.6).

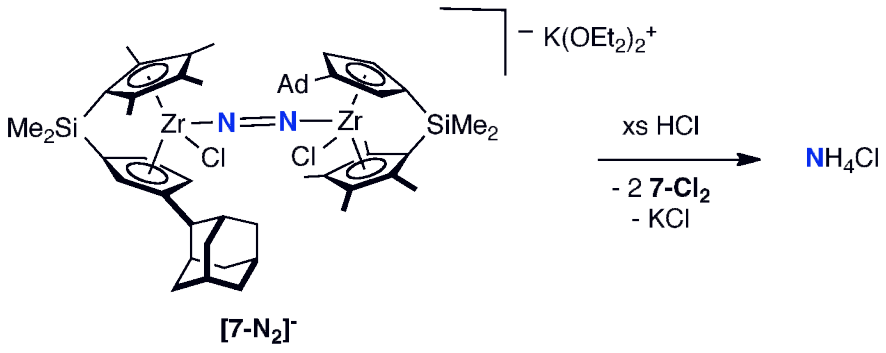

Figure A.5. Protonolysis of **[7-N_2]$^-$** with excess gaseous HCl.

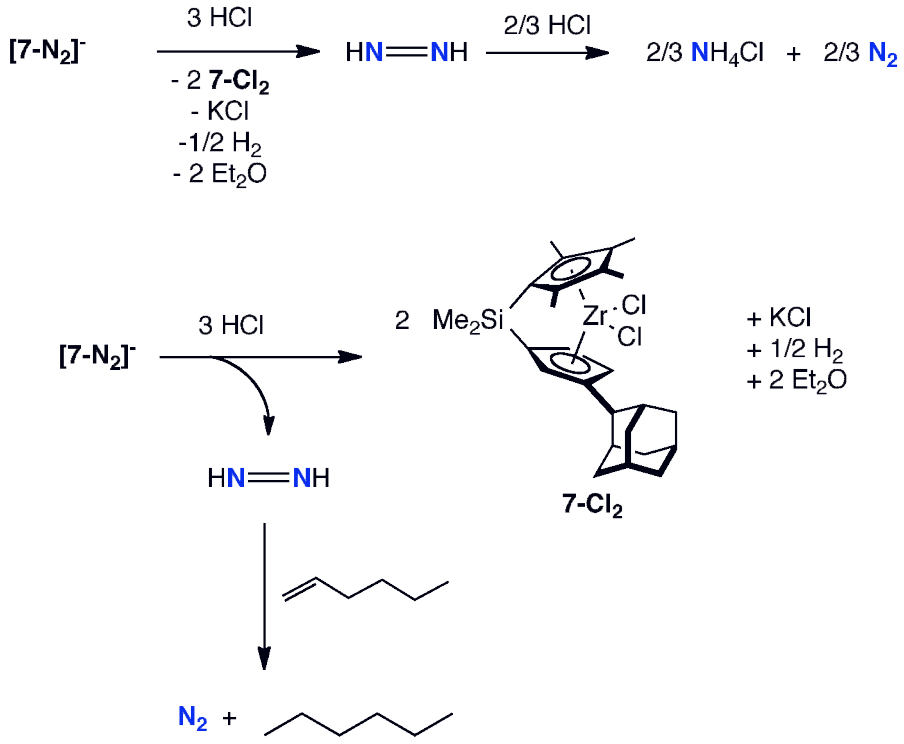

Figure A.6. Protonolysis pathway of **[7-N$_2$]$^-$** in the absence (top) and presence (bottom) of excess 1-hexene.

Oxidation of **[7-N$_2$]$^-$** with $AgBPh_4$ furnished the corresponding neutral dinitrogen compound, $[Me_2Si(\eta^5\text{-}C_5Me_4)(\eta^5\text{-}C_5H_3\text{-}3\text{-}^1Ad)Zr(Cl)]_2(\mu_2, \eta^1, \eta^1\text{-}N_2)$ (**7-N$_2$**) , as a green solid (Figure A.7). This compound was identified on the basis of NMR spectroscopy. To confirm the retention of the dinitrogen ligand, **7-N$_2$** was reduced with KC_8. An immediate color change from green to red signaled formation of **[7-N$_2$]$^-$** and was confirmed by NMR (i.e. complete disappearance of **7-N$_2$**) and EPR spectroscopy.

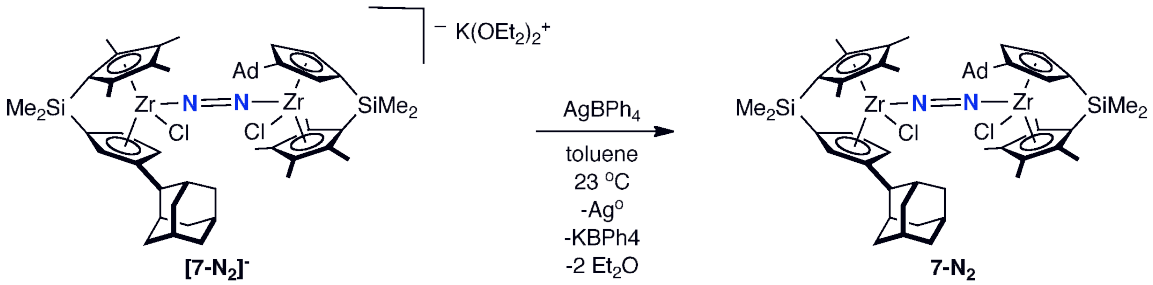

Figure A.7. Oxidation of **[7-N_2]**$^-$.

Overall these results demonstrate a zirconocene dinitrogen compound in which the coordinated dinitrogen ligand adopts the unusual formal oxidation state, $[N_2]^{1-}$.[4] Evans and coworkers have also recently reported the first example of a three electron-reduced dinitrogen ligand.[5] Exploiting the unique properties of the modestly reduced dinitrogen radical fragment **[7-N_2]**$^-$ toward new N_2 functionalization chemistry is the subject of ongoing investigations.

Experimental Section.

Preparation of $Me_2Si(\eta^5\text{-}C_5Me_4)(\eta^5\text{-}C_5H_3\text{-}3\text{-}^1Ad)ZrCl_2$ (7-Cl_2). In a drybox, a 250-mL round bottom flask was charged with 2.68 g $ZrCl_4$ and 4.50 g $Li_2[Me_2Si(\eta^5\text{-}C_5Me_4)(\eta^5\text{-}C_5H_3\text{-}3\text{-}^1Ad)]$. To the solids was added approximately 150 mL toluene, and the reaction flask was fitted with a reflux condenser and needle valve, and transferred to the Schlenk line. The apparatus was purged with argon and refluxed, with stirring, for 3 d. The solvent was removed *in vacuo*, and the salt byproduct was removed *via* filtration through Celite with minimal pentane. The filtrate was concentrated and recrystallized at -35 ºC, furnishing a pale yellow solid identified as **7-Cl_2** in 83% yield. Anal. Calcd for $C_{26}H_{36}Si_1Zr_1Cl_2$: C, 57.96; H, 6.74; N, 0.00. Found: C, 58.21; H, 6.72; N, 0.00. ^{1}H NMR (benzene-d_6): ∂ = 0.40 (s, 3H, Si*Me*$_2$), 0.46 (s, 3H, Si*Me*$_2$), 1.49, 1.82, 2.19-2.41, 3.21 (m, 16H, C_5H_3*Ad*), 1.66 (s, 3H, C_5*Me*$_4$), 1.75 (s, 3H, C_5*Me*$_4$),

1.99 (s, 3H, C_5Me_4), 2.02 (s, 3H, C_5Me_4), 5.37 (m, 1H, $C_5H_3CMe_3$), 5.54 (m, 1H, $C_5H_3CMe_3$), 6.88 (m, 1H, $C_5H_3CMe_3$). $\{^1H\}^{13}C$ NMR (benzene-d_6): ∂ = -0.31 ($SiMe_2$), -0.16 ($SiMe_2$), 12.68 (Cp*Me*), 12.76 (Cp*Me*), 15.20 (Cp*Me*), 15.40 (Cp*Me*), 28.59, 28.65, 32.94, 33.19, 33.42, 33.51, 38.59, 39.29 (Cp*Ad*), 97.22, 105.56, 111.91, 113.44, 125.29, 125.38, 126.24, 135.59, 135.74, 146.18 (*Cp*).

Preparation of [($Me_2Si(\eta^5$-$C_5Me_4)(\eta^5$-C_5H_3-3-^{1}Ad)Zr(Cl))$_2(\mu_2, \eta^1, \eta^1$-$N_2)$][$K(OEt_2)_2$] ([7-N_2]$^-$). In a drybox, a 20-mL scintillation vial was charged with 0.150 (1.11 mmol) of KC_8, 1 mL diethyl ether, and 5 mL of toluene. To this stirring slurry, 0.150 g (0.28 mmol) of **7-Cl_2** as a toluene solution (~5 mL) was added over the course of 1 min. The solution turned deep red immediately, and was stirred for 30 min at 23 ºC. Excess reductant, graphite and salts were removed *via* filtration and the filtrate solvent was removed *in vacuo*. The resulting red solid was dissolved in minimal diethyl ether and recrystallized at -35º C, furnishing **[7-N_2]$^-$** as a red crystalline solid in 51 % yield.

Oxidation of [7-N_2]$^-$ with $AgBPh_4$. In a drybox, a 20-mL scintillation vial was charged with 0.017 g (0.039 mmol) of $AgBPh_4$, and 5 mL of toluene. To this stirring slurry, 0.040 g (0.033 mmol) of **[7-N_2]$^-$** as a diethyl ether solution (~5 mL) was added. The solution turned from red to green over the course of several minutes, and was stirred for 3 h at 23 ºC. Insoluble byproducts were removed *via* filtration and the filtrate solvent was removed *in vacuo*. The resulting brown-green oil was washed with cold pentane, furnishing a green solid identified as the 1e$^-$ oxidized dinitrogen compound, **7-N_2**. ^{1}H NMR (benzene-d_6): ∂ = 0.49 (s, 6H, $SiMe_2$), 0.69 (s, 6H, $SiMe_2$), 1.45-2.40, 2.67 (m, 32H, C_5H_3Ad), 1.46 (s, 6H, C_5Me_4), 1.82 (s, 6H, C_5Me_4), 1.91 (s, 6H, C_5Me_4), 2.86 (s, 6H, C_5Me_4), 5.44 (m, 2H, $C_5H_3CMe_3$), 7.02 (m, 2H, $C_5H_3CMe_3$),

7.13 (m, 2H, $C_5H_3CMe_3$). $\{^1H\}^{13}C$ NMR (benzene-d_6): ∂ = -0.02 (SiMe_2), 0.17 (SiMe_2), 11.85 (Cp*Me*), 12.91 (Cp*Me*), 14.31 (Cp*Me*), 16.50 (Cp*Me*), 28.74, 28.86, 33.02, 34.19, 34.78, 39.32, 39.57, 40.09, 45.44 (Cp*Ad*), 103.79, 105.72, 106.46, 111.33, 115.68, 119.46, 121.79, 126.03, 133.93, 145.51 (*Cp*).

Protonolysis of [7-N_2]$^-$ with HCl. A benzene-d_6 solution of 0.030 g (0.025 mmol) **[7-N_2]$^-$** was treated with excess (20 eq per dimer) gaseous HCl, admitted via calibrated gas bulb. The solution instantly turned yellow, signaling conversion to **7-Cl_2**, with concomitant precipitation of NH_4Cl in 25.8% yield (assuming all N atoms are converted to ammonia). Ammonium chloride was initially identified by DMSO-d_6 ^1H NMR spectroscopy, and quantified in triplicate measurements by phenol-hypochlorite colorometric titration.[6]

Protonolysis of [7-N_2]$^-$ with HCl in the presence of 1-hexene. To a benzene-d_6 solution of 0.030 g (0.025 mmol) **[7-N_2]$^-$** were added 20 equivalents (0.50 mmol) each of 1-hexene and HCl, admitted via calibrated gas bulb. Protonolysis was repeated as above. Ammonium chloride was detected in 6.3 % yield.

REFERENCES

[1] Gynane, M. J. S.; Jeffery, J.; Lappert, M. F. *J. Chem. Soc., Chem. Commun.* **1978**, 34.

[2] Jeffery, J.; Lappert, M. F.; Riley, P. I. *J. Organomet. Chem.* **1979**, *181*, 25.

[3] Wiberg, E.; Wiberg, N.; Holleman, A. F. in *Inorganic Chemistry*, Academic Press, San Diego, CA, 2001.

[4] Chiesa, M.; Giamello, E.; Murphy, D. M.; Pacchioni, G.; Paganini, M. C.; Soave, R.; Sojka, Z. *J. Phys. Chem. B* **2001**, *105*, 497.

[5] (a) Evans, W. J.; Fang, M.; Zucchi, G.; Furche, F.; Ziller, J. W.; Hoekstra, R. M.; Zink, J. I. *J. A. Chem. Soc.* **2009**, *131*, 11195. (b) Kaim, W.; Sarkar, B. *Angew. Chem. Int. Ed.* **2009**, *48*, 9409. (c) Chirik, P. J. *Nature Chem.* **2009**, *1*, 520.

[6] Weatherburn, M. W. *Anal. Chem.* **1967**, *39*, 971.

APPENDIX B:

Plots of Kinetic Data

(See Chapter 1 for Experimental Details)

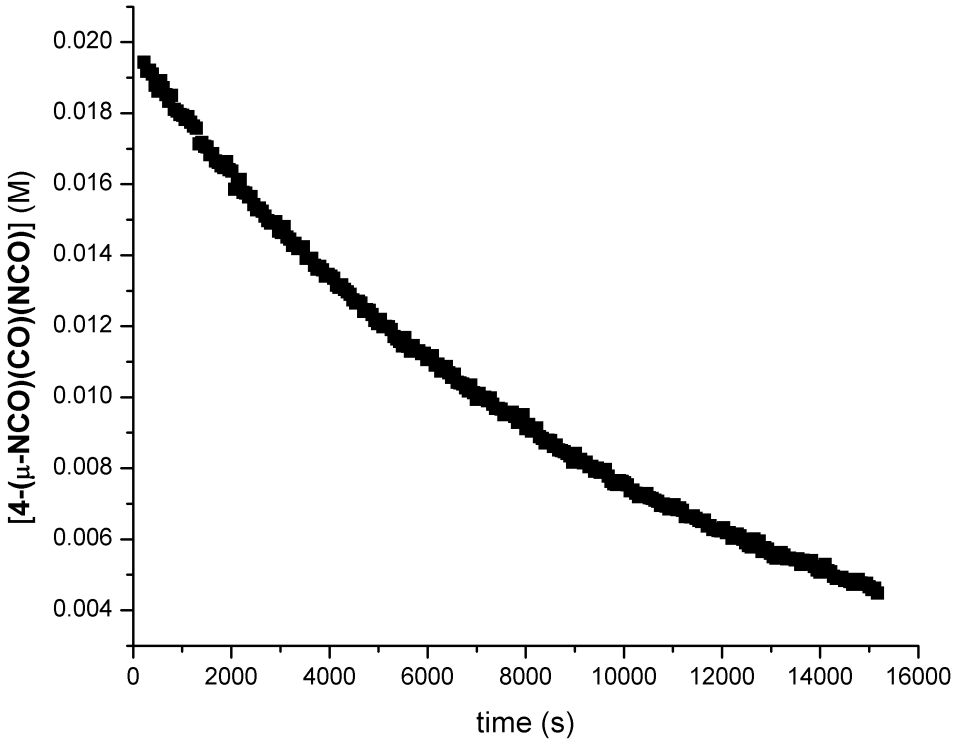

Figure B.1. Representative plot of [**4-(μ-NCO)(CO)(NCO)**] versus time in benzene-d_6 at 10 ºC.

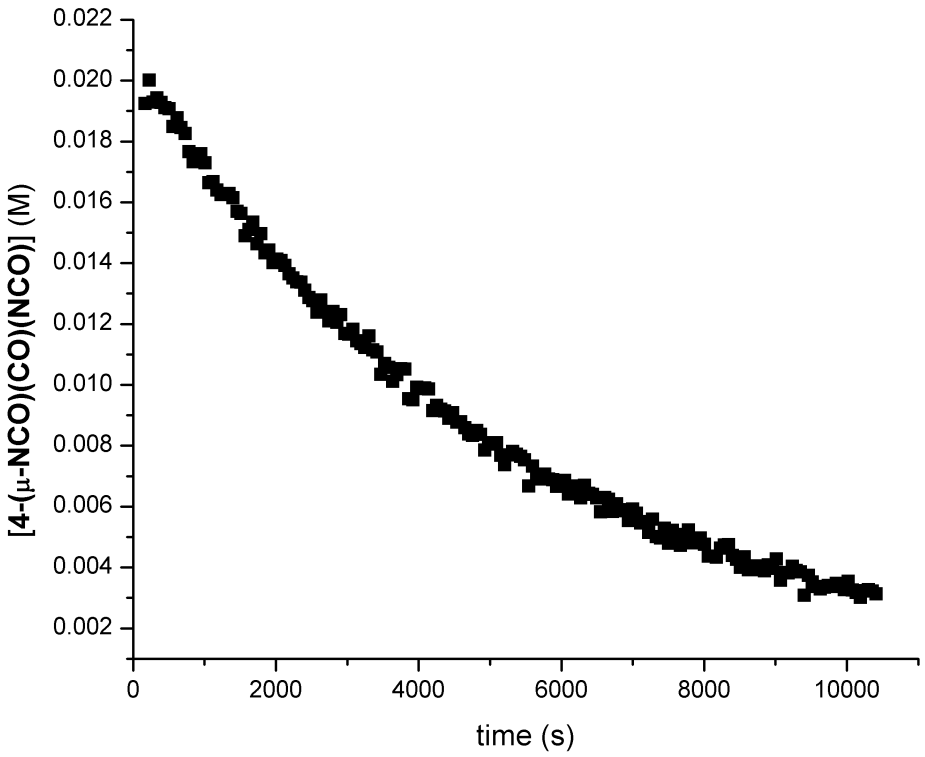

Figure B.2. Representative plot of [**4-(μ-NCO)(CO)(NCO)**] versus time in benzene-d_6 at 15 ºC.

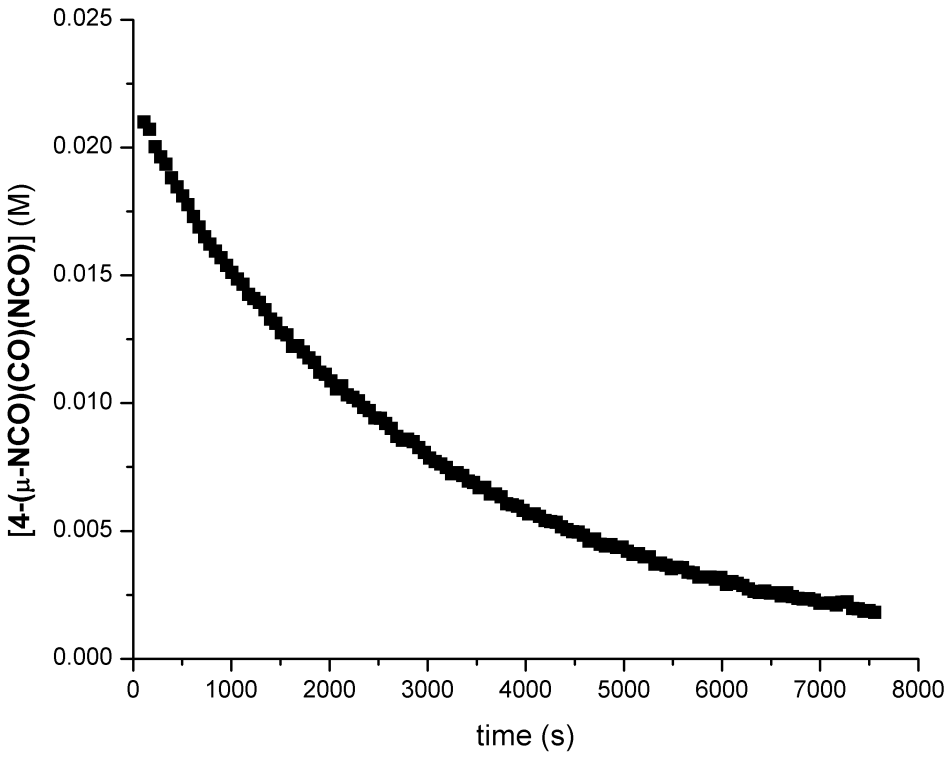

Figure B.3. Representative plot of [**4-(μ-NCO)(CO)(NCO)**] versus time in benzene-d_6 at 20 ºC.

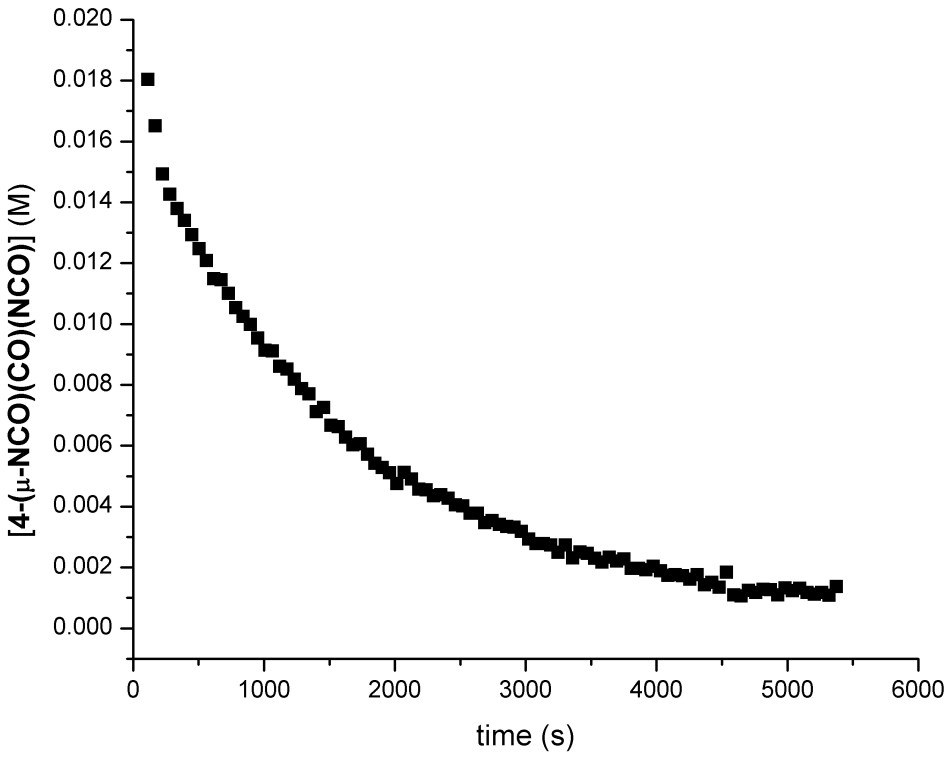

Figure B.4. Representative plot of [**4-(μ-NCO)(CO)(NCO)**] versus time in benzene-d_6 at 25 ºC.

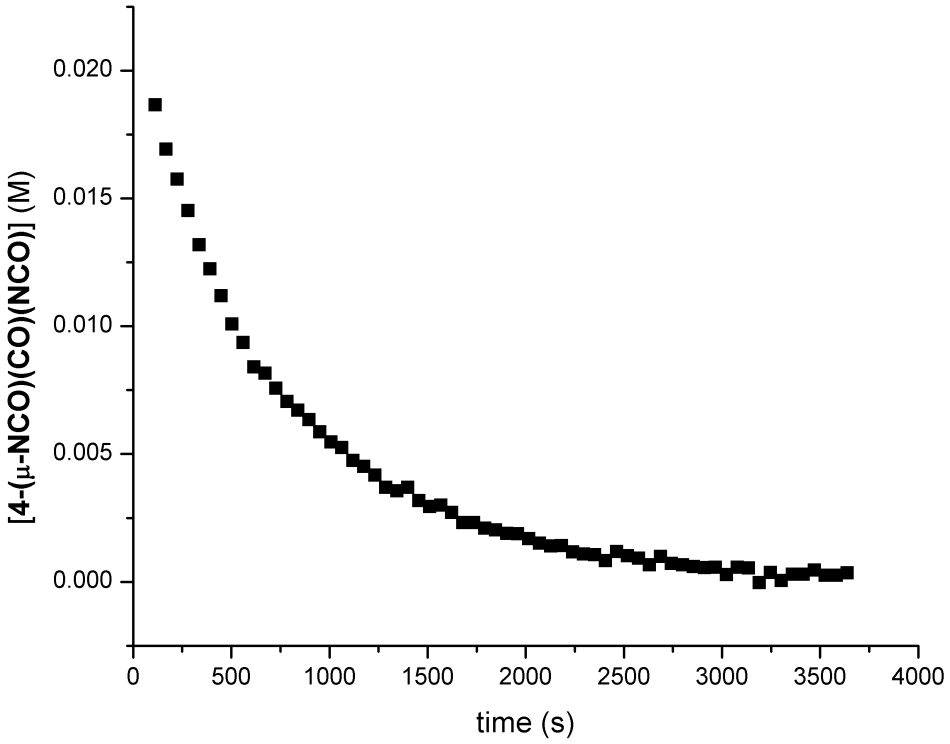

Figure B.5. Representative plot of [**4-(μ-NCO)(CO)(NCO)**] versus time in benzene-d_6 at 30 ºC.

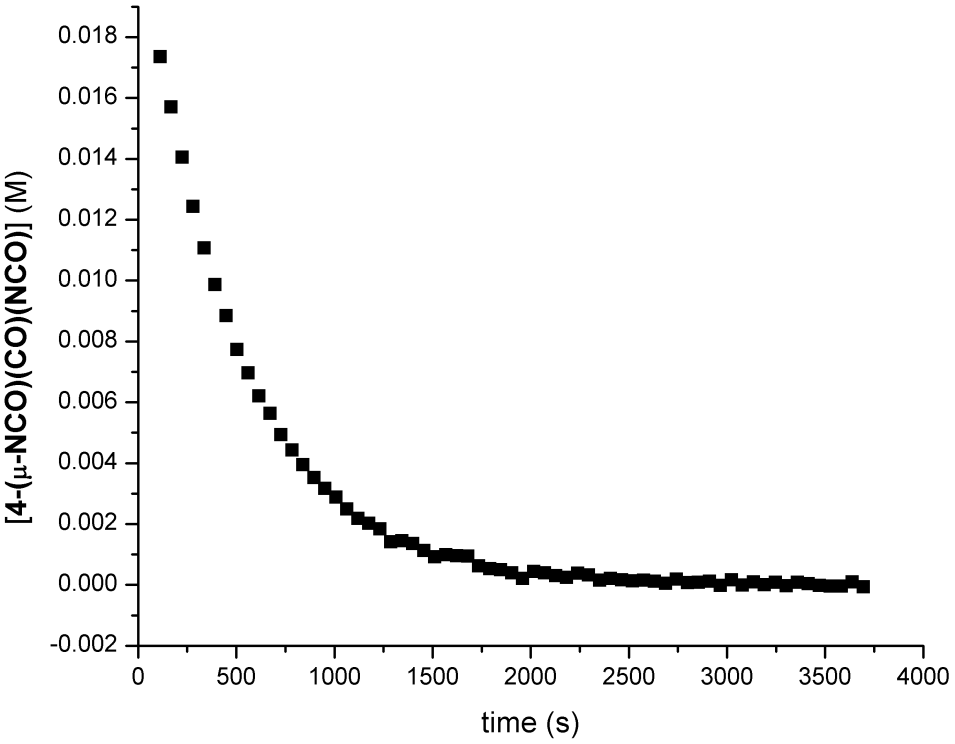

Figure B.6. Representative plot of [**4-(μ-NCO)(CO)(NCO)**] versus time in benzene-d_6 at 35 ºC.

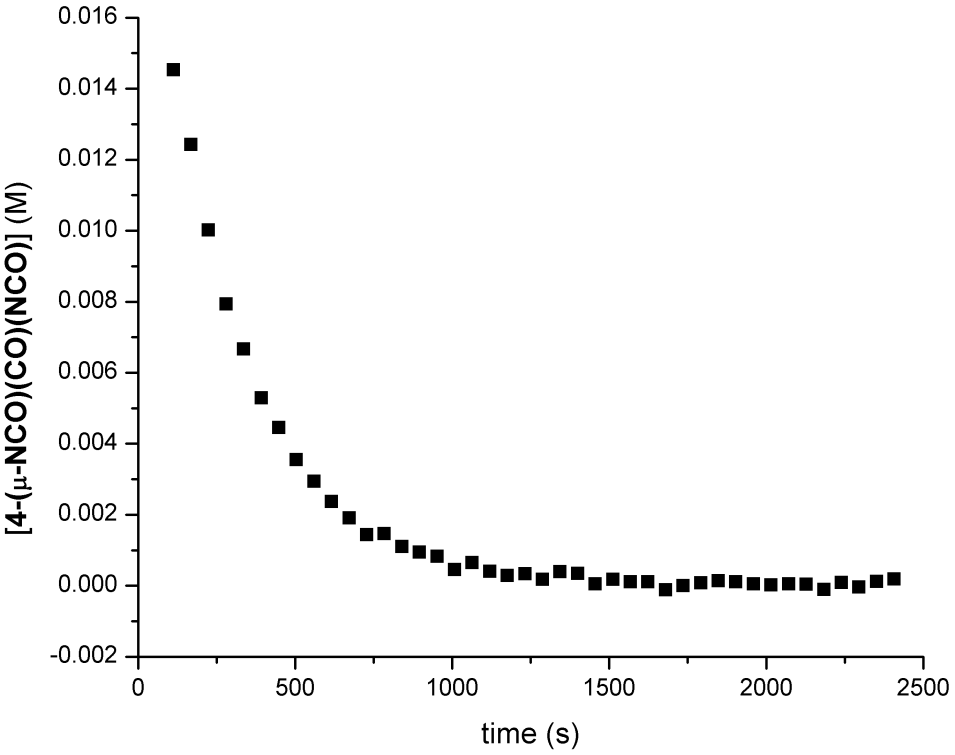

Figure B.7. Representative plot of [**4-(μ-NCO)(CO)(NCO)**] versus time in benzene-d_6 at 40 ºC.

Table B.1. Observed rate constants for the first-order decay of [**4-(μ-NCO)(CO)(NCO)**]. Measured at each temperature in triplicate.

Temp.	k_{obs} (10^4 s^{-1})			Mean	Std. Dev.
(ºC)	Trial 1	Trial 2	Trial 3	(10^4 s^{-1})	(10^4 s^{-1})
10	0.941	0.957	1.15	1.02	0.12
15	1.76	1.80	1.84	1.80	0.04
20	3.37	3.22	3.38	3.32	0.09
25	5.89	5.41	6.25	5.85	0.42
30	11.3	11.3	12.5	11.7	0.7
35	20.3	20.3	20.7	20.4	0.3
40	35.7	37.8	33.6	35.7	2.1

APPENDIX C:

Crystal Structure Data

Table C.1. Compilation of X-ray data for compounds discussed in this manuscript.

Compound	Molecular formula	CU X-Ray ID	CSD Deposition Number
4-Cl_2	$C_{20}H_{30}Cl_2HfSi$	PR01	NA[a]
4-N_2	$C_{40}H_{60}Hf_2N_2Si_2$	djk2	731456
4-$N_2C_2O_2$-*C_2*	$C_{42}H_{60}Hf_2N_2O_2Si_2$	djk9	731457
4-$N_2C_2O_2$-*C_1*	$C_{42}H_{60}Hf_2N_2O_2Si_2$	djk29	NA
2-$N_2C_2O_2$	$C_{38}H_{52}Hf_2N_2O_2$	djk13	805660
5 (Ch. 1)	$C_{44}H_{63}Hf_2N_2Si_2O_3I$	djk32	NA
4-(μ-O)$(NCO)_2$	$C_{42}H_{60}Hf_2N_2Si_2O_3$	djk33	NA
5 (Ch. 2)	$C_{41}H_{60}Hf_2N_2OSi_2$	djk10	731458
6 (Ch. 2)	$C_{37}H_{52}Hf_2N_2O$	djk22	805661
2-(μ-NH)(H)(NCO)	$C_{37}H_{54}Hf_2N_2O$	djk21	805662
4-(μ-NH)(H)(NCO)	$C_{41}H_{62}Hf_2N_2OSi_2$	djk24	805663
3-(μ-NH)(H)(NCO)	$C_{41}H_{62}Zr_2N_2OSi_2$	djk23	805664
4-(μ-O)(H)(NCO)	$C_{41}H_{61}Hf_2NO_2Si_2$	djk19	805665
2-$(CH_3I)_2$	$C_{40}H_{58}Hf_2N_2O_2I_2$	djk12	805658
2-$(PhSiH_3)_2$	$C_{50}H_{68}Hf_2N_2O_2Si_2$	djk14	805659
4-(^{t}BuNCO)$_2$	$C_{52}H_{78}Hf_2N_4O_4Si_2$	djk31	805655
4-$(CO_2)_2$	$C_{44}H_{60}Hf_2N_2O_6Si_2$	djk17	805656
4-(I)(NCO)	$C_{21}H_{30}HfNOI$	djk16	805657
[2-(OTf)]$_2$(μ_2,η^1,η^1-N_2)	$C_{38}H_{52}Hf_2N_2O_6S_2F_6$	wb46	704798
[7-N_2]$^-$	$C_{60}H_{90}Cl_2K_1N_2O_2Si_2Zr_2$	djk8	NA

[a]Details of these structures have not been published and are included in Appendix C.

Table C.2. Crystal data and structure refinement for **4-Cl_2**.

Identification code	**4-Cl_2**	
Chemical formula	$C_{20}H_{30}Cl_2HfSi$	
Formula weight	547.92	
Temperature	100(2) K	
Wavelength	0.71073 Å	
Crystal size	0.23 x 0.36 x 0.53 mm	
Crystal habit	clear pale blue plate	
Crystal system	orthorhombic	
Space group	P b c n	
Unit cell dimensions	a = 24.715(2) Å	α = 90°
	b = 9.6948(10) Å	β = 90°
	c = 17.3292(17) Å	γ = 90°
Volume	4152.2(7) $Å^3$	
Z	8	
Density (calculated)	.753 Mg/cm^3	
Absorption coefficient	5.340 mm^{-1}	
F(000)	2160	

Diffractometer	Bruker APEX II CCD
Radiation source	fine-focus tube, Mo
Theta range for data collection	2.26 to 32.11°
Index ranges	-36<=h<=36, -14<=k<=14, -25<=l<=25
Reflections collected	69099
Independent reflections	7243 [R(int) = 0.0346]
Coverage of independent reflections	99.5%
Absorption correction	multi-scan
Max. and min. transmission	0.3731 and 0.1627
Structure solution technique	direct methods
Structure solution program	SHELXS-97 (Sheldrick, 2008)
Refinement method	Full-matrix least-squares on F^2
Refinement program	SHELXL-97 (Sheldrick, 2008)
Function minimized	$\Sigma w(F_o^2 - F_c^2)^2$
Data / restraints / parameters	7243 / 0 / 227

Goodness-of-fit on F^2	2.180	
Δ/σ_{max}	1.626	
Final R indices	6021 data; $I>2\sigma(I)$	R1 = 0.0238, wR2 = 0.0483
	all data	R1 = 0.0319, wR2 = 0.0496
Weighting scheme	$w=1/[\sigma^2(F_o^2)+(0.0000P)^2+0.0000P]$	
	where $P=(F_o^2+2F_c^2)/3$	
Extinction coefficient	0.0003(0)	
Largest diff. peak and hole	1.217 and -1.072 $eÅ^{-3}$	
R.M.S. deviation from mean	0.105 $eÅ^{-3}$	

Table C.3. Atomic coordinates and equivalent isotropic atomic displacement parameters ($Å^2$) for **4-Cl_2**. U(eq) is defined as one third of the trace of the orthogonalized Uij tensor.

	x/a	y/b	z/c	U(eq)
Hf1	0.621672(3)	0.747573(7)	0.086502(4)	0.01438(3)
Cl1	0.56843(2)	0.92077(5)	0.14984(3)	0.03232(13)
Cl2	0.67324(2)	0.89667(5)	0.00213(3)	0.03141(13)
Si1	0.62460(2)	0.40609(5)	0.10338(3)	0.01806(11)
C1	0.66449(7)	0.54651(18)	0.14996(11)	0.0174(4)
C2	0.70627(8)	0.62525(19)	0.11466(11)	0.0190(4)
C3	0.71291(8)	0.75069(18)	0.15631(12)	0.0173(4)
C4	0.67564(7)	0.75369(16)	0.21757(11)	0.0149(3)
C5	0.64421(7)	0.63083(18)	0.21128(11)	0.0160(4)
C6	0.67665(8)	0.85424(18)	0.28479(11)	0.0170(4)
C7	0.62466(8)	0.8476(2)	0.33223(12)	0.0215(4)
C8	0.68694(8)	0.00197(19)	0.25827(13)	0.0247(4)
C9	0.72397(8)	0.8088(2)	0.33671(13)	0.0269(5)
C10	0.58554(9)	0.3093(2)	0.17709(13)	0.0292(5)
C11	0.66700(9)	0.2830(2)	0.04761(14)	0.0273(5)
C12	0.58341(7)	0.52774(17)	0.04291(11)	0.0149(4)
C13	0.60298(8)	0.59743(18)	0.97522(11)	0.0168(4)
C14	0.56841(8)	0.71126(19)	0.95955(11)	0.0172(4)
C15	0.52859(8)	0.71689(18)	0.01768(11)	0.0164(4)
C16	0.53821(7)	0.60749(18)	0.07007(11)	0.0156(4)
C17	0.64856(8)	0.5544(2)	0.92319(12)	0.0254(4)
C18	0.57102(9)	0.8020(2)	0.88933(12)	0.0242(4)
C19	0.48079(8)	0.8119(2)	0.02021(12)	0.0221(4)
C20	0.50173(8)	0.57847(19)	0.13786(11)	0.0216(4)

Table C.4. Bond lengths [Å] and angles [°] for **4-Cl$_2$**.

Hf1-Cl1	2.3990(5)	C12-Hf1-C13	34.04(6)
Hf1-Cl2	2.4191(5)	C2-Hf1-C13	91.72(6)
Hf1-C12	2.4509(17)	Cl1-Hf1-C1	125.61(5)
Hf1-C2	2.4528(18)	Cl2-Hf1-C1	120.91(5)
Hf1-C13	2.4599(18)	C12-Hf1-C1	67.49(6)
Hf1-C1	2.4757(18)	C2-Hf1-C1	33.54(6)
Hf1-C16	2.4861(18)	C13-Hf1-C1	88.83(4)
Hf1-C5	2.5034(18)	Cl2-Hf1-C16	133.98(5)
Hf1-C3	2.5592(19)	C12-Hf1-C16	33.86(6)
Hf1-C14	2.5879(19)	C2-Hf1-C16	117.77(6)
Hf1-C15	2.6083(19)	C13-Hf1-C16	55.33(6)
Hf1-C4	2.6348(19)	C1-Hf1-C16	88.60(6)
Si1-C10	1.856(2)	Cl1-Hf1-C5	92.48(4)
Si1-C11	1.859(2)	Cl2-Hf1-C5	132.45(4)
Si1-C1	1.8647(19)	C12-Hf1-C5	87.65(6)
Si1-C12	1.8776(19)	C2-Hf1-C5	54.54(6)
C1-C2	1.422(3)	C13-Hf1-C5	116.83(6)
C1-C5	1.431(3)	C1-Hf1-C5	33.41(6)
C2-C3	1.424(2)	C16-Hf1-C5	105.00(4)
C3-C4	1.406(3)	Cl2-Hf1-C3	79.31(5)
C4-C5	1.426(2)	C12-Hf1-C3	119.73(6)
C4-C6	1.519(2)	C2-Hf1-C3	32.92(6)
C6-C7	1.527(3)	C13-Hf1-C3	122.89(6)
C6-C8	1.525(3)	C1-Hf1-C3	54.73(6)
C6-C9	1.540(3)	C16-Hf1-C3	142.35(6)
C12-C16	1.438(2)	C5-Hf1-C3	53.20(6)
C12-C13	1.437(2)	Cl1-Hf1-C14	101.84(5)
C13-C14	1.422(3)	Cl2-Hf1-C14	80.53(4)
C13-C17	1.502(3)	C12-Hf1-C14	54.79(6)
C14-C15	1.409(3)	C2-Hf1-C14	122.48(6)
C14-C18	1.503(3)	C13-Hf1-C14	32.60(6)
C15-C16	1.416(2)	C1-Hf1-C14	119.21(6)
C15-C19	1.498(3)	C16-Hf1-C14	53.57(6)
C16-C20	1.507(3)	C5-Hf1-C14	141.81(6)
		C3-Hf1-C14	148.40(6)
Cl1-Hf1-Cl2	98.47(2)	Cl1-Hf1-C15	78.77(4)
Cl1-Hf1-C12	122.55(4)	Cl2-Hf1-C15	104.86(4)
Cl2-Hf1-C12	122.45(5)	C12-Hf1-C15	54.52(6)
Cl1-Hf1-C2	135.64(5)	C2-Hf1-C15	141.97(6)
Cl2-Hf1-C2	87.71(5)		
C12-Hf1-C2	88.27(6)		
Cl1-Hf1-C13	132.05(5)		
Cl2-Hf1-C13	88.78(5)		

Table C.4. (continued)

C13-Hf1-C15	53.73(6)	C6-C4-Hf1	133.14(12)
C1-Hf1-C15	119.37(6)	C4-C5-C1	110.06(16)
C16-Hf1-C15	32.17(6)	C4-C5-Hf1	79.03(11)
C5-Hf1-C15	122.66(6)	C1-C5-Hf1	72.23(10)
C3-Hf1-C15	174.07(5)	C4-C6-C7	111.85(15)
C14-Hf1-C15	31.47(6)	C4-C6-C8	111.97(16)
Cl1-Hf1-C4	82.39(4)	C7-C6-C8	110.00(15)
Cl2-Hf1-C4	103.94(4)	C4-C6-C9	106.07(15)
C12-Hf1-C4	118.73(6)	C7-C6-C9	108.21(16)
C2-Hf1-C4	53.69(6)	C8-C6-C9	108.54(16)
C13-Hf1-C4	141.65(6)	C16-C12-C13	106.01(15)
C1-Hf1-C4	54.43(6)	C16-C12-Si1	125.19(14)
C16-Hf1-C4	122.08(6)	C13-C12-Si1	124.63(14)
C5-Hf1-C4	32.10(5)	C16-C12-Hf1	74.41(10)
C3-Hf1-C4	31.36(6)	C13-C12-Hf1	73.33(10)
C14-Hf1-C4	173.45(5)	Si1-C12-Hf1	99.50(7)
C15-Hf1-C4	147.49(6)	C14-C13-C12	108.57(16)
C10-Si1-C11	109.07(10)	C14-C13-C17	123.49(17)
C10-Si1-C1	110.25(10)	C12-C13-C17	127.70(17)
C11-Si1-C1	113.30(9)	C14-C13-Hf1	78.66(10)
C10-Si1-C12	114.81(9)	C12-C13-Hf1	72.64(10)
C11-Si1-C12	114.74(9)	C17-C13-Hf1	119.61(13)
C1-Si1-C12	94.00(8)	C15-C14-C13	108.25(17)
C2-C1-C5	105.49(16)	C15-C14-C18	125.88(18)
C2-C1-Si1	126.12(14)	C13-C14-C18	125.67(18)
C5-C1-Si1	123.59(14)	C15-C14-Hf1	75.06(11)
C2-C1-Hf1	72.35(10)	C13-C14-Hf1	68.75(10)
C5-C1-Hf1	74.36(10)	C18-C14-Hf1	125.93(13)
Si1-C1-Hf1	99.00(8)	C14-C15-C16	108.18(16)
C3-C2-C1	108.91(17)	C14-C15-C19	126.53(18)
C3-C2-Hf1	77.65(11)	C16-C15-C19	125.01(18)
C1-C2-Hf1	74.11(10)	C14-C15-Hf1	73.47(11)
C4-C3-C2	108.97(16)	C16-C15-Hf1	69.16(10)
C4-C3-Hf1	77.28(11)	C19-C15-Hf1	127.73(13)
C2-C3-Hf1	69.43(10)	C15-C16-C12	108.86(16)
C3-C4-C5	106.37(16)	C15-C16-C20	122.62(16)
C3-C4-C6	125.57(16)	C12-C16-C20	128.28(16)
C5-C4-C6	127.12(17)	C15-C16-Hf1	78.67(10)
C3-C4-Hf1	68.87(10)	C12-C16-Hf1	71.73(10)
		C20-C16-Hf1	120.60(13)

Table C.5. Crystal data and structure refinement for **4-$N_2C_2O_2$-C_1**.

Identification code	**4-$N_2C_2O_2$-C_1**	
Empirical formula	C42 H60 Hf2 N2 O2 Si2	
Formula weight	1038.08	
Temperature	173(2) K	
Wavelength	0.71073 Å	
Crystal system	Triclinic	
Space group	P-1	
Unit cell dimensions	a = 10.2531(6) Å	α= 95.947(3)°.
	b = 13.9891(9) Å	β= 107.780(3)°.
	c = 15.2353(9) Å	γ = 97.433(3)°.
Volume	2039.5(2) $Å^3$	
Z	2	
Density (calculated)	1.690 Mg/m^3	
Absorption coefficient	5.182 mm^{-1}	
F(000)	1028	
Crystal size	0.35 x 0.15 x 0.05 mm^3	
Theta range for data collection	1.89 to 28.52°.	
Index ranges	-13<=h<=13, -18<=k<=18, -20<=l<=20	
Reflections collected	41113	
Independent reflections	10092 [R(int) = 0.0333]	
Completeness to theta = 28.52°	97.5 %	
Absorption correction	Semi-empirical from equivalents	
Max. and min. transmission	0.7817 and 0.2642	
Refinement method	Full-matrix least-squares on F^2	
Data / restraints / parameters	10092 / 0 / 463	
Goodness-of-fit on F^2	1.077	
Final R indices [I>2sigma(I)]	R1 = 0.0244, wR2 = 0.0514	
R indices (all data)	R1 = 0.0321, wR2 = 0.0539	
Largest diff. peak and hole	0.682 and -0.757 $e.Å^{-3}$	

Table C.6. Atomic coordinates (x 10^4) and equivalent isotropic displacement parameters (Å^{2}x 10^3) for **4-$N_2C_2O_2$-*C*$_1$**. U(eq) is defined as one third of the trace of the orthogonalized U^{ij} tensor.

	x	y	z	U(eq)
Hf(1)	3120(1)	9893(1)	2016(1)	19(1)
Hf(2)	1648(1)	6135(1)	2508(1)	20(1)
Si(1)	3089(1)	11807(1)	933(1)	26(1)
Si(2)	-64(1)	3892(1)	2044(1)	29(1)
E(1)	1768(2)	8640(2)	1293(2)	21(1)
N(1)	1768(2)	8640(2)	1293(2)	21(1)
E(2)	2981(3)	7383(2)	3225(2)	22(1)
N(2)	2981(3)	7383(2)	3225(2)	22(1)
E(3)	3674(3)	8984(2)	2995(2)	22(1)
N(3)	3674(3)	8984(2)	2995(2)	22(1)
E(4)	1157(3)	7023(2)	1503(2)	22(1)
N(4)	1157(3)	7023(2)	1503(2)	22(1)
C(1)	2241(4)	11456(2)	1801(2)	25(1)
C(2)	1062(4)	10711(3)	1606(2)	25(1)
C(3)	1042(4)	10358(3)	2438(2)	25(1)
C(4)	2206(4)	10879(3)	3184(2)	25(1)
C(5)	2940(4)	11525(3)	2779(3)	28(1)
C(6)	4215(3)	10838(2)	1076(2)	22(1)
C(7)	3829(3)	9855(2)	590(2)	21(1)
C(8)	4660(3)	9254(2)	1135(2)	23(1)
C(9)	5569(3)	9845(3)	1953(2)	25(1)
C(10)	5299(3)	10807(3)	1930(2)	25(1)
C(11)	4108(4)	13059(3)	1228(3)	43(1)
C(12)	1770(4)	11699(3)	-228(3)	38(1)
C(13)	2532(4)	10820(3)	4215(3)	34(1)
C(14)	1991(5)	9815(3)	4386(3)	47(1)
C(15)	4090(5)	11088(4)	4712(3)	47(1)
C(16)	1793(5)	11560(3)	4614(3)	49(1)
C(17)	2757(4)	9471(3)	-345(2)	26(1)
C(18)	4598(4)	8187(3)	858(3)	30(1)
C(19)	6694(4)	9513(3)	2689(3)	35(1)
C(20)	6176(4)	11654(3)	2643(3)	39(1)
C(21)	1667(4)	4399(3)	1960(3)	26(1)
C(22)	2882(4)	4702(3)	2746(3)	26(1)
C(23)	3853(3)	5394(2)	2550(2)	24(1)
C(24)	3211(3)	5554(3)	1623(3)	25(1)
C(25)	1885(3)	4949(2)	1270(2)	23(1)

Table C.6. (continued)

C(26)	-318(3)	5038(3)	2677(2)	25(1)
C(27)	560(4)	5454(3)	3618(3)	29(1)
C(28)	505(4)	6461(3)	3759(3)	29(1)
C(29)	-369(4)	6697(3)	2924(3)	26(1)
C(30)	-881(3)	5837(3)	2271(2)	25(1)
C(31)	-1353(4)	3472(3)	866(3)	46(1)
C(32)	13(4)	2857(3)	2719(3)	44(1)
C(33)	5313(3)	5798(3)	3188(3)	27(1)
C(34)	5348(4)	6008(3)	4199(3)	36(1)
C(35)	6229(4)	5027(3)	3106(3)	38(1)
C(36)	5901(4)	6735(3)	2909(3)	35(1)
C(37)	1329(4)	4920(3)	4371(3)	38(1)
C(38)	1214(4)	7148(3)	4651(3)	41(1)
C(39)	-700(4)	7696(3)	2780(3)	33(1)
C(40)	-1873(4)	5799(3)	1308(3)	31(1)
C(41)	2927(3)	8119(2)	2746(2)	21(1)
C(42)	1858(3)	7907(2)	1762(2)	21(1)

Table C.7. Bond lengths [Å] and angles [°] for **4-$N_2C_2O_2$-C_1**.

Hf(1)-E(3)	2.056(2)	C(8)-C(18)	1.495(5)
Hf(1)-E(1)	2.060(2)	C(9)-C(10)	1.411(5)
Hf(1)-C(6)	2.459(3)	C(9)-C(19)	1.503(5)
Hf(1)-C(2)	2.474(3)	C(10)-C(20)	1.502(5)
Hf(1)-C(10)	2.474(3)	C(13)-C(15)	1.521(6)
Hf(1)-C(1)	2.486(3)	C(13)-C(14)	1.522(6)
Hf(1)-C(7)	2.490(3)	C(13)-C(16)	1.538(6)
Hf(1)-C(5)	2.508(4)	C(21)-C(22)	1.418(5)
Hf(1)-C(3)	2.547(3)	C(21)-C(25)	1.420(5)
Hf(1)-C(8)	2.551(3)	C(22)-C(23)	1.417(5)
Hf(2)-E(2)	2.046(3)	C(23)-C(24)	1.420(5)
Hf(2)-E(4)	2.056(2)	C(23)-C(33)	1.511(5)
Hf(2)-C(26)	2.466(3)	C(24)-C(25)	1.419(5)
Hf(2)-C(25)	2.470(3)	C(26)-C(30)	1.435(5)
Hf(2)-C(30)	2.479(3)	C(26)-C(27)	1.452(5)
Hf(2)-C(21)	2.489(4)	C(27)-C(28)	1.415(5)
Hf(2)-C(27)	2.494(3)	C(27)-C(37)	1.508(5)
Hf(2)-C(22)	2.505(3)	C(28)-C(29)	1.413(5)
Hf(2)-C(29)	2.534(3)	C(28)-C(38)	1.497(6)
Hf(2)-C(24)	2.544(4)	C(29)-C(30)	1.408(5)
Si(1)-C(12)	1.847(4)	C(29)-C(39)	1.502(5)
Si(1)-C(11)	1.854(4)	C(30)-C(40)	1.500(5)
Si(1)-C(1)	1.864(4)	C(33)-C(36)	1.527(5)
Si(1)-C(6)	1.879(3)	C(33)-C(34)	1.527(5)
Si(2)-C(31)	1.856(4)	C(33)-C(35)	1.538(5)
Si(2)-C(32)	1.857(4)	C(41)-C(42)	1.535(4)
Si(2)-C(21)	1.871(4)		
Si(2)-C(26)	1.873(4)	E(3)-Hf(1)-E(1)	81.21(9)
E(1)-C(42)	1.306(4)	E(3)-Hf(1)-C(6)	137.84(10)
E(2)-C(41)	1.320(4)	E(1)-Hf(1)-C(6)	115.03(11)
E(3)-C(41)	1.297(4)	E(3)-Hf(1)-C(2)	129.06(11)
E(4)-C(42)	1.302(4)	E(1)-Hf(1)-C(2)	85.75(11)
C(1)-C(2)	1.424(5)	C(6)-Hf(1)-C(2)	92.08(11)
C(1)-C(5)	1.429(5)	E(3)-Hf(1)-C(10)	107.03(11)
C(2)-C(3)	1.412(5)	E(1)-Hf(1)-C(10)	135.60(11)
C(3)-C(4)	1.422(5)	C(6)-Hf(1)-C(10)	33.92(11)
C(4)-C(5)	1.410(5)	C(2)-Hf(1)-C(10)	116.30(11)
C(4)-C(13)	1.517(5)	E(3)-Hf(1)-C(1)	141.54(11)
C(6)-C(7)	1.437(5)	E(1)-Hf(1)-C(1)	116.52(11)
C(6)-C(10)	1.439(5)	C(6)-Hf(1)-C(1)	68.19(11)
C(7)-C(8)	1.421(4)	C(2)-Hf(1)-C(1)	33.37(11)
C(7)-C(17)	1.503(5)	C(10)-Hf(1)-C(1)	84.36(11)
C(8)-C(9)	1.409(5)	E(3)-Hf(1)-C(7)	124.09(10)

Table C.7. (continued)

E(1)-Hf(1)-C(7)	83.78(10)	C(30)-Hf(2)-C(21)	93.15(12)
C(6)-Hf(1)-C(7)	33.75(11)	E(2)-Hf(2)-C(27)	106.49(11)
C(2)-Hf(1)-C(7)	102.83(11)	E(4)-Hf(2)-C(27)	136.59(11)
C(10)-Hf(1)-C(7)	54.98(11)	C(26)-Hf(2)-C(27)	34.03(12)
C(1)-Hf(1)-C(7)	92.85(11)	C(25)-Hf(2)-C(27)	116.54(12)
E(3)-Hf(1)-C(5)	110.30(11)	C(30)-Hf(2)-C(27)	54.94(11)
E(1)-Hf(1)-C(5)	136.64(11)	C(21)-Hf(2)-C(27)	84.63(12)
C(6)-Hf(1)-C(5)	84.90(12)	E(2)-Hf(2)-C(22)	109.59(11)
C(2)-Hf(1)-C(5)	53.95(12)	E(4)-Hf(2)-C(22)	136.47(11)
C(10)-Hf(1)-C(5)	82.56(12)	C(26)-Hf(2)-C(22)	84.59(11)
C(1)-Hf(1)-C(5)	33.24(11)	C(25)-Hf(2)-C(22)	53.80(11)
C(7)-Hf(1)-C(5)	117.22(11)	C(30)-Hf(2)-C(22)	116.95(11)
E(3)-Hf(1)-C(3)	96.93(11)	C(21)-Hf(2)-C(22)	32.99(12)
E(1)-Hf(1)-C(3)	84.69(11)	C(27)-Hf(2)-C(22)	82.31(11)
C(6)-Hf(1)-C(3)	122.08(11)	E(2)-Hf(2)-C(29)	92.29(11)
C(2)-Hf(1)-C(3)	32.64(11)	E(4)-Hf(2)-C(29)	83.34(10)
C(10)-Hf(1)-C(3)	134.91(12)	C(26)-Hf(2)-C(29)	55.36(12)
C(1)-Hf(1)-C(3)	54.77(11)	C(25)-Hf(2)-C(29)	135.31(12)
C(7)-Hf(1)-C(3)	134.74(11)	C(30)-Hf(2)-C(29)	32.62(12)
C(5)-Hf(1)-C(3)	53.11(12)	C(21)-Hf(2)-C(29)	123.02(11)
E(3)-Hf(1)-C(8)	91.86(10)	C(27)-Hf(2)-C(29)	54.19(11)
E(1)-Hf(1)-C(8)	82.68(11)	C(22)-Hf(2)-C(29)	135.70(11)
C(6)-Hf(1)-C(8)	55.26(11)	E(2)-Hf(2)-C(24)	96.16(11)
C(2)-Hf(1)-C(8)	134.94(11)	E(4)-Hf(2)-C(24)	84.25(10)
C(10)-Hf(1)-C(8)	54.07(11)	C(26)-Hf(2)-C(24)	122.50(12)
C(1)-Hf(1)-C(8)	122.72(11)	C(25)-Hf(2)-C(24)	32.84(11)
C(7)-Hf(1)-C(8)	32.72(10)	C(30)-Hf(2)-C(24)	135.47(12)
C(5)-Hf(1)-C(8)	135.87(11)	C(21)-Hf(2)-C(24)	54.90(11)
C(3)-Hf(1)-C(8)	163.33(11)	C(27)-Hf(2)-C(24)	135.02(11)
E(2)-Hf(2)-E(4)	81.17(9)	C(22)-Hf(2)-C(24)	53.30(11)
E(2)-Hf(2)-C(26)	137.71(11)	C(29)-Hf(2)-C(24)	163.74(11)
E(4)-Hf(2)-C(26)	116.25(10)	C(12)-Si(1)-C(11)	108.2(2)
E(2)-Hf(2)-C(25)	128.59(11)	C(12)-Si(1)-C(1)	110.16(18)
E(4)-Hf(2)-C(25)	85.94(11)	C(11)-Si(1)-C(1)	114.44(19)
C(26)-Hf(2)-C(25)	92.36(12)	C(12)-Si(1)-C(6)	115.37(18)
E(2)-Hf(2)-C(30)	124.54(11)	C(11)-Si(1)-C(6)	112.85(17)
E(4)-Hf(2)-C(30)	85.03(10)	C(1)-Si(1)-C(6)	95.56(15)
C(26)-Hf(2)-C(30)	33.73(11)	C(31)-Si(2)-C(32)	108.4(2)
C(25)-Hf(2)-C(30)	103.34(12)	C(31)-Si(2)-C(21)	110.79(19)
E(2)-Hf(2)-C(21)	140.56(11)	C(32)-Si(2)-C(21)	112.72(17)
E(4)-Hf(2)-C(21)	116.82(11)	C(31)-Si(2)-C(26)	115.02(18)
C(26)-Hf(2)-C(21)	68.40(12)	C(32)-Si(2)-C(26)	113.42(19)
C(25)-Hf(2)-C(21)	33.27(11)	C(21)-Si(2)-C(26)	96.11(16)

Table C.7. (continued)

C(42)-E(1)-Hf(1)	113.3(2)	C(8)-C(9)-C(10)	108.3(3)
C(41)-E(2)-Hf(2)	113.9(2)	C(8)-C(9)-C(19)	125.4(3)
C(41)-E(3)-Hf(1)	113.2(2)	C(10)-C(9)-C(19)	126.2(3)
C(42)-E(4)-Hf(2)	113.7(2)	C(8)-C(9)-Hf(1)	73.96(19)
C(2)-C(1)-C(5)	104.8(3)	C(10)-C(9)-Hf(1)	70.72(19)
C(2)-C(1)-Si(1)	124.7(3)	C(19)-C(9)-Hf(1)	124.3(2)
C(5)-C(1)-Si(1)	124.9(3)	C(9)-C(10)-C(6)	109.2(3)
C(2)-C(1)-Hf(1)	72.86(19)	C(9)-C(10)-C(20)	122.8(3)
C(5)-C(1)-Hf(1)	74.25(19)	C(6)-C(10)-C(20)	127.5(3)
Si(1)-C(1)-Hf(1)	97.13(15)	C(9)-C(10)-Hf(1)	76.71(19)
C(3)-C(2)-C(1)	109.5(3)	C(6)-C(10)-Hf(1)	72.48(18)
C(3)-C(2)-Hf(1)	76.52(19)	C(20)-C(10)-Hf(1)	123.6(3)
C(1)-C(2)-Hf(1)	73.78(19)	C(4)-C(13)-C(15)	110.1(3)
C(2)-C(3)-C(4)	108.6(3)	C(4)-C(13)-C(14)	112.0(3)
C(2)-C(3)-Hf(1)	70.84(19)	C(15)-C(13)-C(14)	110.1(3)
C(4)-C(3)-Hf(1)	76.3(2)	C(4)-C(13)-C(16)	107.5(3)
C(5)-C(4)-C(3)	105.9(3)	C(15)-C(13)-C(16)	109.1(4)
C(5)-C(4)-C(13)	126.6(3)	C(14)-C(13)-C(16)	107.8(4)
C(3)-C(4)-C(13)	127.3(3)	C(22)-C(21)-C(25)	105.0(3)
C(5)-C(4)-Hf(1)	70.2(2)	C(22)-C(21)-Si(2)	123.5(3)
C(3)-C(4)-Hf(1)	71.7(2)	C(25)-C(21)-Si(2)	125.6(3)
C(13)-C(4)-Hf(1)	126.6(2)	C(22)-C(21)-Hf(2)	74.1(2)
C(4)-C(5)-C(1)	111.1(3)	C(25)-C(21)-Hf(2)	72.7(2)
C(4)-C(5)-Hf(1)	77.9(2)	Si(2)-C(21)-Hf(2)	96.70(15)
C(1)-C(5)-Hf(1)	72.5(2)	C(23)-C(22)-C(21)	111.2(3)
C(7)-C(6)-C(10)	105.6(3)	C(23)-C(22)-Hf(2)	77.29(19)
C(7)-C(6)-Si(1)	126.3(2)	C(21)-C(22)-Hf(2)	72.88(19)
C(10)-C(6)-Si(1)	123.1(3)	C(22)-C(23)-C(24)	106.0(3)
C(7)-C(6)-Hf(1)	74.30(18)	C(22)-C(23)-C(33)	125.6(3)
C(10)-C(6)-Hf(1)	73.60(18)	C(24)-C(23)-C(33)	128.2(3)
Si(1)-C(6)-Hf(1)	97.58(14)	C(22)-C(23)-Hf(2)	70.49(19)
C(8)-C(7)-C(6)	108.9(3)	C(24)-C(23)-Hf(2)	72.10(19)
C(8)-C(7)-C(17)	122.8(3)	C(33)-C(23)-Hf(2)	125.9(2)
C(6)-C(7)-C(17)	128.3(3)	C(25)-C(24)-C(23)	108.1(3)
C(8)-C(7)-Hf(1)	75.98(19)	C(25)-C(24)-Hf(2)	70.71(19)
C(6)-C(7)-Hf(1)	71.95(18)	C(23)-C(24)-Hf(2)	75.8(2)
C(17)-C(7)-Hf(1)	119.2(2)	C(24)-C(25)-C(21)	109.7(3)
C(9)-C(8)-C(7)	108.1(3)	C(24)-C(25)-Hf(2)	76.5(2)
C(9)-C(8)-C(18)	126.7(3)	C(21)-C(25)-Hf(2)	74.1(2)
C(7)-C(8)-C(18)	125.2(3)	C(30)-C(26)-C(27)	105.3(3)
C(9)-C(8)-Hf(1)	74.0(2)	C(30)-C(26)-Si(2)	127.0(3)
C(7)-C(8)-Hf(1)	71.30(19)	C(27)-C(26)-Si(2)	122.6(3)
C(18)-C(8)-Hf(1)	122.1(2)	C(30)-C(26)-Hf(2)	73.61(18)

Table C.7. (continued)

C(27)-C(26)-Hf(2)	74.06(19)	C(28)-C(29)-Hf(2)	74.8(2)
Si(2)-C(26)-Hf(2)	97.43(14)	C(39)-C(29)-Hf(2)	120.4(2)
C(28)-C(27)-C(26)	108.8(3)	C(29)-C(30)-C(26)	109.6(3)
C(28)-C(27)-C(37)	123.7(4)	C(29)-C(30)-C(40)	123.5(3)
C(26)-C(27)-C(37)	127.4(4)	C(26)-C(30)-C(40)	126.9(3)
C(28)-C(27)-Hf(2)	76.2(2)	C(29)-C(30)-Hf(2)	75.84(19)
C(26)-C(27)-Hf(2)	71.91(19)	C(26)-C(30)-Hf(2)	72.65(18)
C(37)-C(27)-Hf(2)	122.0(2)	C(40)-C(30)-Hf(2)	118.6(2)
C(29)-C(28)-C(27)	108.2(3)	C(23)-C(33)-C(36)	111.4(3)
C(29)-C(28)-C(38)	126.1(4)	C(23)-C(33)-C(34)	110.9(3)
C(27)-C(28)-C(38)	125.7(3)	C(36)-C(33)-C(34)	108.8(3)
C(29)-C(28)-Hf(2)	73.0(2)	C(23)-C(33)-C(35)	107.8(3)
C(27)-C(28)-Hf(2)	71.3(2)	C(36)-C(33)-C(35)	108.7(3)
C(38)-C(28)-Hf(2)	123.1(2)	C(34)-C(33)-C(35)	109.2(3)
C(30)-C(29)-C(28)	108.2(3)	E(3)-C(41)-E(2)	128.3(3)
C(30)-C(29)-C(39)	126.7(3)	E(3)-C(41)-C(42)	116.6(3)
C(28)-C(29)-C(39)	125.1(3)	E(2)-C(41)-C(42)	115.1(3)
C(30)-C(29)-Hf(2)	71.54(19)	E(4)-C(42)-E(1)	128.4(3)
		E(4)-C(42)-C(41)	116.1(3)
		E(1)-C(42)-C(41)	115.5(3)

Table C.8. Crystal data and structure refinement for **5** (Ch. 1).

Identification code	**5** (Ch. 1)	
Empirical formula	C44 H63 Hf2 I N2 O3 Si2	
Formula weight	1208.02	
Temperature	173(2) K	
Wavelength	0.71073 Å	
Crystal system	Triclinic	
Space group	P-1	
Unit cell dimensions	a = 11.2581(6) Å	a= 80.324(3)°.
	b = 13.9369(9) Å	b= 86.219(3)°.
	c = 17.4621(10) Å	g = 89.165(3)°.
Volume	2695.0(3) $Å^3$	
Z	2	
Density (calculated)	1.489 Mg/m^3	
Absorption coefficient	4.500 mm^{-1}	
F(000)	1180	
Crystal size	0.40 x 0.30 x 0.20 mm^3	
Theta range for data collection	1.74 to 31.74°.	
Index ranges	-16<=h<=16, -20<=k<=20, -25<=l<=25	
Reflections collected	58124	
Independent reflections	18120 [R(int) = 0.0260]	
Completeness to theta = 31.74°	98.9 %	
Absorption correction	Semi-empirical from equivalents	
Max. and min. transmission	0.4664 and 0.2662	
Refinement method	Full-matrix least-squares on F^2	
Data / restraints / parameters	18120 / 0 / 505	
Goodness-of-fit on F^2	1.009	
Final R indices [I>2sigma(I)]	R1 = 0.0224, wR2 = 0.0661	
R indices (all data)	R1 = 0.0281, wR2 = 0.0685	
Largest diff. peak and hole	1.245 and -0.737 $e.Å^{-3}$	

Table C.9. Atomic coordinates (x 10^4) and equivalent isotropic displacement parameters ($Å^2$x 10^3) for **5** (Ch. 1). U(eq) is defined as one third of the trace of the orthogonalized U^{ij} tensor.

	x	y	z	U(eq)
Hf(1)	2018(1)	5867(1)	1706(1)	22(1)
Hf(2)	2335(1)	2539(1)	4484(1)	19(1)
I(1)	1878(1)	3453(1)	5915(1)	31(1)
Si(1)	2687(1)	5323(1)	-29(1)	36(1)
Si(2)	2879(1)	182(1)	4540(1)	32(1)
O(1)	1126(2)	8541(2)	2651(2)	54(1)
O(2)	1764(2)	4802(1)	2635(1)	28(1)
O(3)	3014(2)	2957(1)	2536(1)	30(1)
N(1)	1661(2)	7044(2)	2280(1)	33(1)
N(2)	1798(2)	4134(1)	3938(1)	23(1)
C(1)	3622(2)	5654(2)	729(2)	30(1)
C(2)	3881(2)	5019(2)	1430(2)	30(1)
C(3)	4206(2)	5592(2)	1977(2)	29(1)
C(4)	4163(2)	6582(2)	1641(2)	29(1)
C(5)	3763(2)	6616(2)	885(2)	28(1)
C(6)	1240(2)	5597(2)	486(2)	29(1)
C(7)	864(2)	6566(2)	582(2)	31(1)
C(8)	2(2)	6499(2)	1211(2)	29(1)
C(9)	-151(2)	5507(2)	1537(2)	29(1)
C(10)	595(2)	4950(2)	1093(2)	28(1)
C(11)	1479(2)	924(2)	4479(2)	28(1)
C(12)	1084(2)	1505(2)	3791(2)	29(1)
C(13)	264(2)	2207(2)	4013(2)	28(1)
C(14)	139(2)	2067(2)	4830(2)	28(1)
C(15)	893(2)	1286(2)	5122(2)	28(1)
C(16)	3848(2)	1221(2)	4633(2)	26(1)
C(17)	3802(2)	1642(2)	5322(2)	29(1)
C(18)	4327(2)	2578(2)	5142(2)	26(1)
C(19)	4665(2)	2773(2)	4344(2)	23(1)
C(20)	4332(2)	1948(2)	4023(2)	24(1)
C(21)	1194(3)	7514(2)	70(2)	41(1)
C(22)	-694(3)	7330(2)	1452(2)	40(1)
C(23)	-1019(3)	5152(2)	2202(2)	37(1)
C(24)	650(3)	3856(2)	1225(2)	36(1)
C(25)	4649(3)	7418(2)	1971(2)	37(1)
C(26)	4421(3)	7289(3)	2857(2)	46(1)
C(27)	6010(3)	7386(4)	1793(3)	68(1)

Table C.9. (continued)

C(28)	4173(3)	8391(2)	1593(2)	45(1)
C(29)	1301(3)	1300(2)	2981(2)	40(1)
C(30)	-433(2)	2905(2)	3476(2)	37(1)
C(31)	-759(2)	2570(2)	5302(2)	36(1)
C(32)	876(3)	839(2)	5972(2)	38(1)
C(33)	5420(2)	3644(2)	3969(2)	25(1)
C(34)	6547(2)	3621(2)	4413(2)	36(1)
C(35)	5775(3)	3600(2)	3119(2)	35(1)
C(36)	4771(2)	4598(2)	4041(2)	27(1)
C(37)	3040(3)	6100(4)	-986(2)	57(1)
C(38)	2894(3)	4034(3)	-134(3)	56(1)
C(39)	2885(3)	-777(2)	5413(2)	47(1)
C(40)	3333(3)	-356(3)	3670(3)	52(1)
C(41)	1391(2)	7774(2)	2468(2)	32(1)
C(42)	1300(3)	5024(2)	4171(2)	35(1)
C(43)	2003(2)	4120(2)	3203(1)	21(1)
C(44)	2587(2)	3140(2)	3151(2)	23(1)

Table C.10. Bond lengths [Å] and angles [°] for **5** (Ch. 1).

Hf(1)-O(2)	2.0149(19)	C(4)-C(25)	1.508(4)
Hf(1)-N(1)	2.083(2)	C(6)-C(10)	1.436(4)
Hf(1)-C(6)	2.443(2)	C(6)-C(7)	1.443(4)
Hf(1)-C(1)	2.451(3)	C(7)-C(8)	1.408(4)
Hf(1)-C(2)	2.453(3)	C(7)-C(21)	1.502(4)
Hf(1)-C(10)	2.468(2)	C(8)-C(9)	1.412(4)
Hf(1)-C(7)	2.478(3)	C(8)-C(22)	1.492(4)
Hf(1)-C(5)	2.488(3)	C(9)-C(10)	1.418(4)
Hf(1)-C(9)	2.545(3)	C(9)-C(23)	1.489(4)
Hf(1)-C(3)	2.550(3)	C(10)-C(24)	1.503(4)
Hf(1)-C(8)	2.572(2)	C(11)-C(15)	1.426(4)
Hf(1)-C(4)	2.614(3)	C(11)-C(12)	1.425(4)
Hf(2)-C(44)	2.338(3)	C(12)-C(13)	1.419(4)
Hf(2)-N(2)	2.354(2)	C(12)-C(29)	1.493(4)
Hf(2)-C(17)	2.464(3)	C(13)-C(14)	1.407(4)
Hf(2)-C(11)	2.464(2)	C(13)-C(30)	1.486(4)
Hf(2)-C(15)	2.474(2)	C(14)-C(15)	1.418(4)
Hf(2)-C(16)	2.479(2)	C(14)-C(31)	1.501(4)
Hf(2)-C(20)	2.512(2)	C(15)-C(32)	1.509(4)
Hf(2)-C(12)	2.529(2)	C(16)-C(17)	1.421(4)
Hf(2)-C(14)	2.575(2)	C(16)-C(20)	1.426(4)
Hf(2)-C(18)	2.591(2)	C(17)-C(18)	1.418(4)
Hf(2)-C(13)	2.597(2)	C(18)-C(19)	1.403(4)
Hf(2)-C(19)	2.638(2)	C(19)-C(20)	1.426(3)
Si(1)-C(38)	1.847(4)	C(19)-C(33)	1.521(3)
Si(1)-C(37)	1.855(4)	C(25)-C(28)	1.513(5)
Si(1)-C(1)	1.864(3)	C(25)-C(26)	1.533(5)
Si(1)-C(6)	1.874(3)	C(25)-C(27)	1.544(5)
Si(2)-C(40)	1.846(4)	C(33)-C(35)	1.522(4)
Si(2)-C(39)	1.852(4)	C(33)-C(34)	1.528(4)
Si(2)-C(16)	1.860(3)	C(33)-C(36)	1.528(3)
Si(2)-C(11)	1.872(3)	C(43)-C(44)	1.521(3)
O(1)-C(41)	1.195(4)		
O(2)-C(43)	1.292(3)	O(2)-Hf(1)-N(1)	97.62(9)
O(3)-C(44)	1.214(3)	O(2)-Hf(1)-C(6)	117.22(9)
N(1)-C(41)	1.151(4)	N(1)-Hf(1)-C(6)	127.13(9)
N(2)-C(43)	1.293(3)	O(2)-Hf(1)-C(1)	117.89(9)
N(2)-C(42)	1.462(3)	N(1)-Hf(1)-C(1)	129.31(10)
C(1)-C(5)	1.425(4)	C(6)-Hf(1)-C(1)	68.28(9)
C(1)-C(2)	1.429(4)	O(2)-Hf(1)-C(2)	85.76(9)
C(2)-C(3)	1.411(4)	N(1)-Hf(1)-C(2)	131.55(9)
C(3)-C(4)	1.407(4)	C(6)-Hf(1)-C(2)	91.69(9)
C(4)-C(5)	1.416(4)	C(1)-Hf(1)-C(2)	33.88(9)

Table C.10. (continued)

O(2)-Hf(1)-C(10)	85.08(9)	C(9)-Hf(1)-C(8)	32.03(9)
N(1)-Hf(1)-C(10)	127.73(9)	C(3)-Hf(1)-C(8)	166.47(9)
C(6)-Hf(1)-C(10)	33.99(9)	O(2)-Hf(1)-C(4)	110.54(8)
C(1)-Hf(1)-C(10)	92.29(9)	N(1)-Hf(1)-C(4)	80.48(9)
C(2)-Hf(1)-C(10)	100.72(9)	C(6)-Hf(1)-C(4)	117.57(9)
O(2)-Hf(1)-C(7)	135.81(9)	C(1)-Hf(1)-C(4)	54.62(8)
N(1)-Hf(1)-C(7)	93.27(9)	C(2)-Hf(1)-C(4)	53.85(9)
C(6)-Hf(1)-C(7)	34.08(9)	C(10)-Hf(1)-C(4)	146.86(9)
C(1)-Hf(1)-C(7)	85.54(9)	C(7)-Hf(1)-C(4)	113.47(9)
C(2)-Hf(1)-C(7)	117.43(9)	C(5)-Hf(1)-C(4)	32.10(8)
C(10)-Hf(1)-C(7)	55.31(9)	C(9)-Hf(1)-C(4)	167.04(9)
O(2)-Hf(1)-C(5)	135.95(8)	C(3)-Hf(1)-C(4)	31.59(9)
N(1)-Hf(1)-C(5)	95.84(9)	C(8)-Hf(1)-C(4)	135.44(9)
C(6)-Hf(1)-C(5)	85.85(9)	C(44)-Hf(2)-N(2)	57.17(8)
C(1)-Hf(1)-C(5)	33.52(9)	C(44)-Hf(2)-C(17)	127.40(9)
C(2)-Hf(1)-C(5)	54.80(9)	N(2)-Hf(2)-C(17)	141.26(8)
C(10)-Hf(1)-C(5)	117.92(9)	C(44)-Hf(2)-C(11)	101.35(9)
C(7)-Hf(1)-C(5)	84.67(9)	N(2)-Hf(2)-C(11)	133.70(8)
O(2)-Hf(1)-C(9)	82.14(9)	C(17)-Hf(2)-C(11)	84.99(9)
N(1)-Hf(1)-C(9)	95.53(9)	C(44)-Hf(2)-C(15)	126.41(9)
C(6)-Hf(1)-C(9)	55.42(9)	N(2)-Hf(2)-C(15)	123.88(8)
C(1)-Hf(1)-C(9)	122.63(9)	C(17)-Hf(2)-C(15)	86.04(9)
C(2)-Hf(1)-C(9)	132.59(9)	C(11)-Hf(2)-C(15)	33.56(9)
C(10)-Hf(1)-C(9)	32.80(9)	C(44)-Hf(2)-C(16)	101.44(9)
C(7)-Hf(1)-C(9)	54.17(9)	N(2)-Hf(2)-C(16)	149.25(8)
C(5)-Hf(1)-C(9)	137.77(9)	C(17)-Hf(2)-C(16)	33.40(9)
O(2)-Hf(1)-C(3)	83.15(8)	C(11)-Hf(2)-C(16)	67.39(8)
N(1)-Hf(1)-C(3)	99.42(9)	C(15)-Hf(2)-C(16)	86.16(8)
C(6)-Hf(1)-C(3)	121.90(9)	C(44)-Hf(2)-C(20)	73.24(8)
C(1)-Hf(1)-C(3)	54.81(9)	N(2)-Hf(2)-C(20)	116.32(8)
C(2)-Hf(1)-C(3)	32.68(9)	C(17)-Hf(2)-C(20)	54.43(9)
C(10)-Hf(1)-C(3)	132.51(9)	C(11)-Hf(2)-C(20)	90.10(8)
C(7)-Hf(1)-C(3)	136.89(9)	C(15)-Hf(2)-C(20)	116.90(8)
C(5)-Hf(1)-C(3)	53.29(9)	C(16)-Hf(2)-C(20)	33.19(8)
C(9)-Hf(1)-C(3)	160.24(9)	C(44)-Hf(2)-C(12)	72.53(9)
O(2)-Hf(1)-C(8)	110.15(8)	N(2)-Hf(2)-C(12)	102.76(8)
N(1)-Hf(1)-C(8)	76.90(9)	C(17)-Hf(2)-C(12)	115.35(9)
C(6)-Hf(1)-C(8)	55.01(9)	C(11)-Hf(2)-C(12)	33.14(9)
C(1)-Hf(1)-C(8)	117.51(9)	C(15)-Hf(2)-C(12)	54.43(9)
C(2)-Hf(1)-C(8)	146.61(9)	C(16)-Hf(2)-C(12)	89.20(8)
C(10)-Hf(1)-C(8)	53.98(9)	C(20)-Hf(2)-C(12)	97.01(8)
C(7)-Hf(1)-C(8)	32.32(9)	C(44)-Hf(2)-C(14)	108.98(9)
C(5)-Hf(1)-C(8)	113.72(9)	N(2)-Hf(2)-C(14)	91.46(8)

Table C.10. (continued)

C(17)-Hf(2)-C(14)	116.28(9)	C(40)-Si(2)-C(16)	111.74(15)
C(11)-Hf(2)-C(14)	54.48(8)	C(39)-Si(2)-C(16)	111.46(15)
C(15)-Hf(2)-C(14)	32.53(8)	C(40)-Si(2)-C(11)	115.57(16)
C(16)-Hf(2)-C(14)	117.88(8)	C(39)-Si(2)-C(11)	113.69(14)
C(20)-Hf(2)-C(14)	144.54(8)	C(16)-Si(2)-C(11)	94.60(11)
C(12)-Hf(2)-C(14)	53.28(9)	C(43)-O(2)-Hf(1)	159.86(17)
C(44)-Hf(2)-C(18)	110.77(8)	C(41)-N(1)-Hf(1)	167.5(2)
N(2)-Hf(2)-C(18)	109.41(7)	C(43)-N(2)-C(42)	118.0(2)
C(17)-Hf(2)-C(18)	32.45(8)	C(43)-N(2)-Hf(2)	101.56(15)
C(11)-Hf(2)-C(18)	116.78(8)	C(42)-N(2)-Hf(2)	140.38(17)
C(15)-Hf(2)-C(18)	115.90(9)	C(5)-C(1)-C(2)	105.7(2)
C(16)-Hf(2)-C(18)	54.02(8)	C(5)-C(1)-Si(1)	124.9(2)
C(20)-Hf(2)-C(18)	52.85(8)	C(2)-C(1)-Si(1)	124.7(2)
C(12)-Hf(2)-C(18)	143.22(8)	C(5)-C(1)-Hf(1)	74.67(15)
C(14)-Hf(2)-C(18)	140.24(9)	C(2)-C(1)-Hf(1)	73.13(14)
C(44)-Hf(2)-C(13)	78.15(8)	Si(1)-C(1)-Hf(1)	98.11(11)
N(2)-Hf(2)-C(13)	80.20(8)	C(3)-C(2)-C(1)	108.4(2)
C(17)-Hf(2)-C(13)	137.24(9)	C(3)-C(2)-Hf(1)	77.47(15)
C(11)-Hf(2)-C(13)	54.14(8)	C(1)-C(2)-Hf(1)	72.99(15)
C(15)-Hf(2)-C(13)	53.49(9)	C(4)-C(3)-C(2)	109.3(2)
C(16)-Hf(2)-C(13)	119.60(8)	C(4)-C(3)-Hf(1)	76.71(15)
C(20)-Hf(2)-C(13)	127.87(8)	C(2)-C(3)-Hf(1)	69.85(14)
C(12)-Hf(2)-C(13)	32.09(8)	C(3)-C(4)-C(5)	106.4(2)
C(14)-Hf(2)-C(13)	31.56(9)	C(3)-C(4)-C(25)	126.1(3)
C(18)-Hf(2)-C(13)	169.30(8)	C(5)-C(4)-C(25)	126.8(3)
C(44)-Hf(2)-C(19)	80.19(8)	C(3)-C(4)-Hf(1)	71.71(15)
N(2)-Hf(2)-C(19)	97.82(7)	C(5)-C(4)-Hf(1)	69.04(15)
C(17)-Hf(2)-C(19)	53.33(8)	C(25)-C(4)-Hf(1)	131.81(18)
C(11)-Hf(2)-C(19)	119.95(8)	C(1)-C(5)-C(4)	110.1(2)
C(15)-Hf(2)-C(19)	137.68(8)	C(1)-C(5)-Hf(1)	71.80(15)
C(16)-Hf(2)-C(19)	53.95(8)	C(4)-C(5)-Hf(1)	78.85(16)
C(20)-Hf(2)-C(19)	32.04(7)	C(10)-C(6)-C(7)	105.8(2)
C(12)-Hf(2)-C(19)	128.16(8)	C(10)-C(6)-Si(1)	126.1(2)
C(14)-Hf(2)-C(19)	169.60(8)	C(7)-C(6)-Si(1)	123.6(2)
C(18)-Hf(2)-C(19)	31.10(8)	C(10)-C(6)-Hf(1)	73.99(14)
C(13)-Hf(2)-C(19)	155.31(8)	C(7)-C(6)-Hf(1)	74.32(14)
C(38)-Si(1)-C(37)	108.9(2)	Si(1)-C(6)-Hf(1)	98.11(11)
C(38)-Si(1)-C(1)	111.43(16)	C(8)-C(7)-C(6)	108.8(2)
C(37)-Si(1)-C(1)	111.13(16)	C(8)-C(7)-C(21)	122.8(3)
C(38)-Si(1)-C(6)	114.53(16)	C(6)-C(7)-C(21)	128.1(3)
C(37)-Si(1)-C(6)	115.59(16)	C(8)-C(7)-Hf(1)	77.49(15)
C(1)-Si(1)-C(6)	94.58(11)	C(6)-C(7)-Hf(1)	71.60(15)
C(40)-Si(2)-C(39)	109.15(18)	C(21)-C(7)-Hf(1)	122.23(19)

Table C.10. (continued)

C(7)-C(8)-C(9)	108.4(2)	C(14)-C(15)-C(32)	123.1(2)
C(7)-C(8)-C(22)	125.5(3)	C(11)-C(15)-C(32)	127.6(2)
C(9)-C(8)-C(22)	125.9(3)	C(14)-C(15)-Hf(2)	77.65(14)
C(7)-C(8)-Hf(1)	70.19(14)	C(11)-C(15)-Hf(2)	72.83(14)
C(9)-C(8)-Hf(1)	72.96(14)	C(32)-C(15)-Hf(2)	123.73(19)
C(22)-C(8)-Hf(1)	126.10(19)	C(17)-C(16)-C(20)	106.2(2)
C(8)-C(9)-C(10)	108.0(2)	C(17)-C(16)-Si(2)	121.7(2)
C(8)-C(9)-C(23)	123.8(3)	C(20)-C(16)-Si(2)	127.4(2)
C(10)-C(9)-C(23)	128.1(3)	C(17)-C(16)-Hf(2)	72.72(14)
C(8)-C(9)-Hf(1)	75.01(15)	C(20)-C(16)-Hf(2)	74.67(13)
C(10)-C(9)-Hf(1)	70.61(14)	Si(2)-C(16)-Hf(2)	98.78(10)
C(23)-C(9)-Hf(1)	123.22(19)	C(18)-C(17)-C(16)	108.6(2)
C(9)-C(10)-C(6)	108.9(2)	C(18)-C(17)-Hf(2)	78.70(15)
C(9)-C(10)-C(24)	124.8(3)	C(16)-C(17)-Hf(2)	73.88(15)
C(6)-C(10)-C(24)	126.3(2)	C(19)-C(18)-C(17)	108.9(2)
C(9)-C(10)-Hf(1)	76.59(15)	C(19)-C(18)-Hf(2)	76.29(14)
C(6)-C(10)-Hf(1)	72.02(14)	C(17)-C(18)-Hf(2)	68.85(14)
C(24)-C(10)-Hf(1)	119.57(18)	C(18)-C(19)-C(20)	106.9(2)
C(15)-C(11)-C(12)	106.8(2)	C(18)-C(19)-C(33)	123.2(2)
C(15)-C(11)-Si(2)	124.1(2)	C(20)-C(19)-C(33)	129.2(2)
C(12)-C(11)-Si(2)	125.4(2)	C(18)-C(19)-Hf(2)	72.60(13)
C(15)-C(11)-Hf(2)	73.61(14)	C(20)-C(19)-Hf(2)	69.12(13)
C(12)-C(11)-Hf(2)	75.96(14)	C(33)-C(19)-Hf(2)	130.81(15)
Si(2)-C(11)-Hf(2)	99.01(10)	C(19)-C(20)-C(16)	109.2(2)
C(13)-C(12)-C(11)	108.4(2)	C(19)-C(20)-Hf(2)	78.84(13)
C(13)-C(12)-C(29)	124.6(3)	C(16)-C(20)-Hf(2)	72.14(13)
C(11)-C(12)-C(29)	126.0(3)	C(4)-C(25)-C(28)	112.3(3)
C(13)-C(12)-Hf(2)	76.59(14)	C(4)-C(25)-C(26)	112.1(3)
C(11)-C(12)-Hf(2)	70.91(14)	C(28)-C(25)-C(26)	110.3(3)
C(29)-C(12)-Hf(2)	127.42(18)	C(4)-C(25)-C(27)	105.3(2)
C(14)-C(13)-C(12)	108.2(2)	C(28)-C(25)-C(27)	109.1(3)
C(14)-C(13)-C(30)	125.6(3)	C(26)-C(25)-C(27)	107.5(3)
C(12)-C(13)-C(30)	125.9(3)	C(35)-C(33)-C(19)	111.5(2)
C(14)-C(13)-Hf(2)	73.35(14)	C(35)-C(33)-C(34)	108.8(2)
C(12)-C(13)-Hf(2)	71.32(13)	C(19)-C(33)-C(34)	107.6(2)
C(30)-C(13)-Hf(2)	125.62(18)	C(35)-C(33)-C(36)	110.4(2)
C(13)-C(14)-C(15)	108.0(2)	C(19)-C(33)-C(36)	111.0(2)
C(13)-C(14)-C(31)	125.4(2)	C(34)-C(33)-C(36)	107.4(2)
C(15)-C(14)-C(31)	126.2(3)	N(1)-C(41)-O(1)	178.6(4)
C(13)-C(14)-Hf(2)	75.09(14)	O(2)-C(43)-N(2)	126.9(2)
C(15)-C(14)-Hf(2)	69.81(13)	O(2)-C(43)-C(44)	127.6(2)
C(31)-C(14)-Hf(2)	127.01(18)	N(2)-C(43)-C(44)	105.5(2)
C(14)-C(15)-C(11)	108.6(2)	O(3)-C(44)-C(43)	121.0(2)

O(3)-C(44)-Hf(2)	143.63(19)	C(43)-C(44)-Hf(2)	95.26(15)

Table C.11. Crystal data and structure refinement for **4-(μ-O)(NCO)$_2$**.

Identification code	**4-(μ-O)(NCO)$_2$**	
Empirical formula	C45 H63 Hf2 N2 O3 Si2	
Formula weight	1093.13	
Temperature	173(2) K	
Wavelength	0.71073 Å	
Crystal system	Triclinic	
Space group	P-1	
Unit cell dimensions	a = 9.3309(7) Å	a= 85.677(3)°.
	b = 10.2407(8) Å	b= 87.437(3)°.
	c = 24.575(2) Å	g = 68.155(3)°.
Volume	2173.1(3) Å^3	
Z	2	
Density (calculated)	1.671 Mg/m^3	
Absorption coefficient	4.870 mm^{-1}	
F(000)	1086	
Crystal size	0.30 x 0.15 x 0.10 mm^3	
Theta range for data collection	1.66 to 30.51°.	
Index ranges	-12<=h<=13, -14<=k<=14, -35<=l<=35	
Reflections collected	37372	
Independent reflections	13133 [R(int) = 0.0218]	
Completeness to theta = 30.51°	99.0 %	
Absorption correction	Semi-empirical from equivalents	
Max. and min. transmission	0.6416 and 0.3228	
Refinement method	Full-matrix least-squares on F^2	
Data / restraints / parameters	13133 / 0 / 505	
Goodness-of-fit on F^2	1.017	
Final R indices [I>2sigma(I)]	R1 = 0.0199, wR2 = 0.0414	
R indices (all data)	R1 = 0.0266, wR2 = 0.0440	
Largest diff. peak and hole	0.711 and -0.547 e.Å^{-3}	

Table C.12. Atomic coordinates (x 10^4) and equivalent isotropic displacement parameters ($Å^2$x 10^3) for **4-(μ-O)(NCO)$_2$**. U(eq) is defined as one third of the trace of the orthogonalized U^{ij} tensor.

	x	y	z	U(eq)
Hf(1)	6430(1)	12193(1)	3436(1)	15(1)
Hf(2)	5275(1)	12582(1)	1894(1)	15(1)
Si(1)	7403(1)	14736(1)	3814(1)	21(1)
Si(2)	7729(1)	10550(1)	1019(1)	21(1)
O(1)	5492(2)	8449(2)	4124(1)	44(1)
O(2)	514(2)	15812(3)	1975(1)	74(1)
O(3)	5786(2)	12371(1)	2671(1)	18(1)
N(1)	6184(2)	10289(2)	3709(1)	25(1)
N(2)	3075(2)	14198(2)	1899(1)	26(1)
C(1)	9393(2)	10490(2)	3629(1)	19(1)
C(2)	9262(2)	11014(2)	3077(1)	19(1)
C(3)	8793(2)	12502(2)	3063(1)	19(1)
C(4)	8596(2)	12933(2)	3604(1)	20(1)
C(5)	8931(2)	11672(2)	3948(1)	20(1)
C(6)	5552(2)	14405(2)	3904(1)	21(1)
C(7)	5337(3)	13386(2)	4304(1)	22(1)
C(8)	4134(3)	12993(2)	4135(1)	23(1)
C(9)	3586(2)	13742(2)	3630(1)	23(1)
C(10)	4433(2)	14616(2)	3490(1)	21(1)
C(11)	5854(2)	14740(2)	1330(1)	20(1)
C(12)	6873(2)	14202(2)	1768(1)	20(1)
C(13)	7797(2)	12774(2)	1688(1)	19(1)
C(14)	7348(2)	12391(2)	1196(1)	19(1)
C(15)	6097(2)	13613(2)	994(1)	21(1)
C(16)	6000(2)	10419(2)	1395(1)	19(1)
C(17)	4432(3)	11248(2)	1243(1)	23(1)
C(18)	3455(3)	11274(2)	1699(1)	25(1)
C(19)	4371(3)	10500(2)	2143(1)	23(1)
C(20)	5932(2)	9974(2)	1959(1)	19(1)
C(21)	10154(2)	8969(2)	3846(1)	22(1)
C(22)	9549(3)	8698(2)	4416(1)	31(1)
C(23)	11885(3)	8701(3)	3887(1)	31(1)
C(24)	9961(3)	7949(2)	3460(1)	33(1)
C(25)	6093(3)	12919(2)	4850(1)	28(1)
C(26)	3437(3)	12064(3)	4452(1)	32(1)
C(27)	2264(3)	13682(3)	3322(1)	30(1)
C(28)	4113(3)	15652(2)	2998(1)	26(1)

Table C.12. (continued)

C(29)	4864(3)	16278(2)	1187(1)	26(1)
C(30)	3552(3)	16394(3)	812(1)	35(1)
C(31)	5920(3)	16948(3)	879(1)	40(1)
C(32)	4193(3)	17106(2)	1692(1)	35(1)
C(33)	3828(3)	11864(3)	684(1)	33(1)
C(34)	1727(3)	11904(3)	1703(1)	36(1)
C(35)	3778(3)	10160(3)	2688(1)	31(1)
C(36)	7240(3)	9017(2)	2307(1)	26(1)
C(37)	7405(3)	16002(2)	3230(1)	31(1)
C(38)	8166(3)	15167(3)	4435(1)	33(1)
C(39)	9634(3)	9337(2)	1282(1)	34(1)
C(40)	7746(3)	10338(3)	276(1)	37(1)
C(41)	5835(3)	9385(2)	3919(1)	25(1)
C(42)	1797(3)	14995(3)	1940(1)	35(1)
C(1S)	10017(4)	15542(4)	491(2)	59(1)
C(2S)	9523(3)	14453(4)	466(2)	55(1)
C(3S)	9502(3)	13912(3)	-20(2)	57(1)

Table C.13. Bond lengths [Å] and angles [°] for **4-(μ-O)(NCO)$_2$**.

Hf(1)-O(3)	1.9747(14)	C(6)-C(7)	1.441(3)
Hf(1)-N(1)	2.1035(19)	C(7)-C(8)	1.413(3)
Hf(1)-C(6)	2.4598(19)	C(7)-C(25)	1.505(3)
Hf(1)-C(4)	2.468(2)	C(8)-C(9)	1.418(3)
Hf(1)-C(3)	2.470(2)	C(8)-C(26)	1.497(3)
Hf(1)-C(10)	2.4970(19)	C(9)-C(10)	1.414(3)
Hf(1)-C(7)	2.519(2)	C(9)-C(27)	1.499(3)
Hf(1)-C(5)	2.558(2)	C(10)-C(28)	1.510(3)
Hf(1)-C(9)	2.579(2)	C(11)-C(12)	1.405(3)
Hf(1)-C(8)	2.604(2)	C(11)-C(15)	1.415(3)
Hf(1)-C(2)	2.607(2)	C(11)-C(29)	1.523(3)
Hf(1)-C(1)	2.704(2)	C(12)-C(13)	1.418(3)
Hf(2)-O(3)	1.9647(14)	C(13)-C(14)	1.424(3)
Hf(2)-N(2)	2.1034(18)	C(14)-C(15)	1.431(3)
Hf(2)-C(13)	2.461(2)	C(16)-C(20)	1.431(3)
Hf(2)-C(16)	2.4679(19)	C(16)-C(17)	1.442(3)
Hf(2)-C(14)	2.490(2)	C(17)-C(18)	1.408(3)
Hf(2)-C(20)	2.5018(19)	C(17)-C(33)	1.507(3)
Hf(2)-C(17)	2.509(2)	C(18)-C(19)	1.415(3)
Hf(2)-C(15)	2.589(2)	C(18)-C(34)	1.497(3)
Hf(2)-C(19)	2.594(2)	C(19)-C(20)	1.418(3)
Hf(2)-C(18)	2.602(2)	C(19)-C(35)	1.491(3)
Hf(2)-C(12)	2.606(2)	C(20)-C(36)	1.503(3)
Hf(2)-C(11)	2.732(2)	C(21)-C(24)	1.525(3)
Si(1)-C(38)	1.860(2)	C(21)-C(22)	1.530(3)
Si(1)-C(37)	1.861(2)	C(21)-C(23)	1.541(3)
Si(1)-C(4)	1.865(2)	C(29)-C(30)	1.529(3)
Si(1)-C(6)	1.880(2)	C(29)-C(32)	1.531(3)
Si(2)-C(40)	1.855(3)	C(29)-C(31)	1.540(4)
Si(2)-C(39)	1.860(2)	C(1S)-C(2S)	1.363(5)
Si(2)-C(16)	1.867(2)	C(1S)-C(3S)#1	1.377(5)
Si(2)-C(14)	1.866(2)	C(2S)-C(3S)	1.359(5)
O(1)-C(41)	1.190(3)	C(3S)-C(1S)#1	1.377(5)
O(2)-C(42)	1.182(3)		
N(1)-C(41)	1.169(3)	O(3)-Hf(1)-N(1)	100.66(7)
N(2)-C(42)	1.173(3)	O(3)-Hf(1)-C(6)	115.42(6)
C(1)-C(5)	1.411(3)	N(1)-Hf(1)-C(6)	127.52(7)
C(1)-C(2)	1.412(3)	O(3)-Hf(1)-C(4)	116.38(7)
C(1)-C(21)	1.517(3)	N(1)-Hf(1)-C(4)	127.56(7)
C(2)-C(3)	1.419(3)	C(6)-Hf(1)-C(4)	68.41(7)
C(3)-C(4)	1.416(3)	O(3)-Hf(1)-C(3)	86.23(7)
C(4)-C(5)	1.428(3)	N(1)-Hf(1)-C(3)	127.18(7)
C(6)-C(10)	1.438(3)	C(6)-Hf(1)-C(3)	93.42(7)

Table C.13. (continued)

C(4)-Hf(1)-C(3)	33.32(7)	C(5)-Hf(1)-C(2)	51.98(7)
O(3)-Hf(1)-C(10)	84.78(6)	C(9)-Hf(1)-C(2)	168.22(7)
N(1)-Hf(1)-C(10)	126.66(7)	C(8)-Hf(1)-C(2)	158.56(7)
C(6)-Hf(1)-C(10)	33.72(7)	O(3)-Hf(1)-C(1)	115.29(6)
C(4)-Hf(1)-C(10)	93.96(7)	N(1)-Hf(1)-C(1)	78.40(7)
C(3)-Hf(1)-C(10)	106.03(7)	C(6)-Hf(1)-C(1)	114.47(7)
O(3)-Hf(1)-C(7)	136.87(6)	C(4)-Hf(1)-C(1)	53.23(6)
N(1)-Hf(1)-C(7)	94.24(7)	C(3)-Hf(1)-C(1)	52.45(7)
C(6)-Hf(1)-C(7)	33.63(7)	C(10)-Hf(1)-C(1)	146.14(7)
C(4)-Hf(1)-C(7)	83.47(7)	C(7)-Hf(1)-C(1)	107.25(7)
C(3)-Hf(1)-C(7)	115.90(7)	C(5)-Hf(1)-C(1)	30.94(6)
C(10)-Hf(1)-C(7)	54.53(7)	C(9)-Hf(1)-C(1)	159.38(7)
O(3)-Hf(1)-C(5)	137.46(6)	C(8)-Hf(1)-C(1)	128.03(7)
N(1)-Hf(1)-C(5)	94.89(7)	C(2)-Hf(1)-C(1)	30.76(6)
C(6)-Hf(1)-C(5)	83.64(7)	O(3)-Hf(2)-N(2)	101.07(7)
C(4)-Hf(1)-C(5)	32.94(7)	O(3)-Hf(2)-C(13)	87.81(7)
C(3)-Hf(1)-C(5)	53.53(7)	N(2)-Hf(2)-C(13)	128.57(7)
C(10)-Hf(1)-C(5)	116.43(7)	O(3)-Hf(2)-C(16)	117.69(6)
C(7)-Hf(1)-C(5)	80.14(7)	N(2)-Hf(2)-C(16)	125.35(7)
O(3)-Hf(1)-C(9)	84.97(6)	C(13)-Hf(2)-C(16)	91.77(7)
N(1)-Hf(1)-C(9)	94.77(7)	O(3)-Hf(2)-C(14)	119.00(6)
C(6)-Hf(1)-C(9)	54.78(7)	N(2)-Hf(2)-C(14)	125.34(7)
C(4)-Hf(1)-C(9)	122.80(7)	C(13)-Hf(2)-C(14)	33.43(7)
C(3)-Hf(1)-C(9)	138.04(7)	C(16)-Hf(2)-C(14)	67.52(7)
C(10)-Hf(1)-C(9)	32.30(7)	O(3)-Hf(2)-C(20)	86.27(6)
C(7)-Hf(1)-C(9)	53.39(7)	N(2)-Hf(2)-C(20)	128.24(7)
C(5)-Hf(1)-C(9)	133.06(7)	C(13)-Hf(2)-C(20)	102.63(7)
O(3)-Hf(1)-C(8)	113.82(7)	C(16)-Hf(2)-C(20)	33.47(7)
N(1)-Hf(1)-C(8)	76.98(7)	C(14)-Hf(2)-C(20)	92.03(7)
C(6)-Hf(1)-C(8)	54.53(7)	O(3)-Hf(2)-C(17)	136.71(7)
C(4)-Hf(1)-C(8)	115.35(7)	N(2)-Hf(2)-C(17)	91.75(7)
C(3)-Hf(1)-C(8)	146.74(7)	C(13)-Hf(2)-C(17)	115.75(7)
C(10)-Hf(1)-C(8)	53.41(7)	C(16)-Hf(2)-C(17)	33.67(7)
C(7)-Hf(1)-C(8)	31.97(7)	C(14)-Hf(2)-C(17)	83.66(7)
C(5)-Hf(1)-C(8)	108.17(7)	C(20)-Hf(2)-C(17)	54.58(7)
C(9)-Hf(1)-C(8)	31.74(7)	O(3)-Hf(2)-C(15)	137.61(6)
O(3)-Hf(1)-C(2)	87.10(6)	N(2)-Hf(2)-C(15)	92.72(7)
N(1)-Hf(1)-C(2)	95.25(7)	C(13)-Hf(2)-C(15)	53.48(7)
C(6)-Hf(1)-C(2)	122.05(7)	C(16)-Hf(2)-C(15)	83.77(7)
C(4)-Hf(1)-C(2)	54.00(7)	C(14)-Hf(2)-C(15)	32.66(6)
C(3)-Hf(1)-C(2)	32.30(6)	C(20)-Hf(2)-C(15)	115.79(7)
C(10)-Hf(1)-C(2)	138.09(7)	C(17)-Hf(2)-C(15)	81.80(7)
C(7)-Hf(1)-C(2)	131.76(7)	O(3)-Hf(2)-C(19)	83.91(7)

Table C.13. (continued)

N(2)-Hf(2)-C(19)	97.00(7)	C(40)-Si(2)-C(16)	114.21(12)
C(13)-Hf(2)-C(19)	134.42(7)	C(39)-Si(2)-C(16)	115.81(11)
C(16)-Hf(2)-C(19)	54.46(7)	C(40)-Si(2)-C(14)	114.00(11)
C(14)-Hf(2)-C(19)	121.29(7)	C(39)-Si(2)-C(14)	110.33(11)
C(20)-Hf(2)-C(19)	32.26(7)	C(16)-Si(2)-C(14)	95.14(9)
C(17)-Hf(2)-C(19)	53.37(7)	Hf(2)-O(3)-Hf(1)	175.91(8)
C(15)-Hf(2)-C(19)	134.21(7)	C(41)-N(1)-Hf(1)	167.71(18)
O(3)-Hf(2)-C(18)	111.57(7)	C(42)-N(2)-Hf(2)	172.4(2)
N(2)-Hf(2)-C(18)	77.12(7)	C(5)-C(1)-C(2)	106.66(18)
C(13)-Hf(2)-C(18)	145.52(7)	C(5)-C(1)-C(21)	125.1(2)
C(16)-Hf(2)-C(18)	54.22(7)	C(2)-C(1)-C(21)	127.35(18)
C(14)-Hf(2)-C(18)	115.31(7)	C(5)-C(1)-Hf(1)	68.82(11)
C(20)-Hf(2)-C(18)	53.24(7)	C(2)-C(1)-Hf(1)	70.83(11)
C(17)-Hf(2)-C(18)	31.91(7)	C(21)-C(1)-Hf(1)	133.50(14)
C(15)-Hf(2)-C(18)	110.53(7)	C(1)-C(2)-C(3)	108.44(18)
C(19)-Hf(2)-C(18)	31.60(7)	C(1)-C(2)-Hf(1)	78.41(12)
O(3)-Hf(2)-C(12)	86.69(6)	C(3)-C(2)-Hf(1)	68.53(11)
N(2)-Hf(2)-C(12)	97.08(7)	C(4)-C(3)-C(2)	109.02(19)
C(13)-Hf(2)-C(12)	32.33(6)	C(4)-C(3)-Hf(1)	73.24(12)
C(16)-Hf(2)-C(12)	120.73(7)	C(2)-C(3)-Hf(1)	79.17(12)
C(14)-Hf(2)-C(12)	53.81(7)	C(3)-C(4)-C(5)	105.68(17)
C(20)-Hf(2)-C(12)	134.65(7)	C(3)-C(4)-Si(1)	125.41(16)
C(17)-Hf(2)-C(12)	132.85(7)	C(5)-C(4)-Si(1)	124.67(17)
C(15)-Hf(2)-C(12)	51.68(7)	C(3)-C(4)-Hf(1)	73.44(12)
C(19)-Hf(2)-C(12)	164.35(7)	C(5)-C(4)-Hf(1)	77.01(12)
C(18)-Hf(2)-C(12)	161.50(7)	Si(1)-C(4)-Hf(1)	96.88(9)
O(3)-Hf(2)-C(11)	113.75(6)	C(1)-C(5)-C(4)	110.09(19)
N(2)-Hf(2)-C(11)	78.63(7)	C(1)-C(5)-Hf(1)	80.23(12)
C(13)-Hf(2)-C(11)	52.18(6)	C(4)-C(5)-Hf(1)	70.04(12)
C(16)-Hf(2)-C(11)	114.19(7)	C(10)-C(6)-C(7)	105.88(19)
C(14)-Hf(2)-C(11)	52.71(6)	C(10)-C(6)-Si(1)	126.15(17)
C(20)-Hf(2)-C(11)	144.33(7)	C(7)-C(6)-Si(1)	123.46(17)
C(17)-Hf(2)-C(11)	109.25(7)	C(10)-C(6)-Hf(1)	74.56(11)
C(15)-Hf(2)-C(11)	30.69(6)	C(7)-C(6)-Hf(1)	75.44(11)
C(19)-Hf(2)-C(11)	162.26(7)	Si(1)-C(6)-Hf(1)	96.73(8)
C(18)-Hf(2)-C(11)	131.65(7)	C(8)-C(7)-C(6)	108.9(2)
C(12)-Hf(2)-C(11)	30.41(6)	C(8)-C(7)-C(25)	123.4(2)
C(38)-Si(1)-C(37)	110.60(12)	C(6)-C(7)-C(25)	127.3(2)
C(38)-Si(1)-C(4)	111.76(11)	C(8)-C(7)-Hf(1)	77.34(12)
C(37)-Si(1)-C(4)	107.35(11)	C(6)-C(7)-Hf(1)	70.93(11)
C(38)-Si(1)-C(6)	116.45(11)	C(25)-C(7)-Hf(1)	123.84(14)
C(37)-Si(1)-C(6)	114.03(11)	C(7)-C(8)-C(9)	108.0(2)
C(4)-Si(1)-C(6)	95.40(9)	C(7)-C(8)-C(26)	126.6(2)
C(40)-Si(2)-C(39)	107.17(12)	C(9)-C(8)-C(26)	125.1(2)

Table C.13. (continued)

C(7)-C(8)-Hf(1)	70.68(12)	Si(2)-C(16)-Hf(2)	98.19(8)
C(9)-C(8)-Hf(1)	73.15(12)	C(18)-C(17)-C(16)	108.5(2)
C(26)-C(8)-Hf(1)	126.41(14)	C(18)-C(17)-C(33)	122.8(2)
C(8)-C(9)-C(10)	108.2(2)	C(16)-C(17)-C(33)	128.3(2)
C(8)-C(9)-C(27)	125.3(2)	C(18)-C(17)-Hf(2)	77.71(13)
C(10)-C(9)-C(27)	126.3(2)	C(16)-C(17)-Hf(2)	71.61(12)
C(8)-C(9)-Hf(1)	75.11(12)	C(33)-C(17)-Hf(2)	122.56(15)
C(10)-C(9)-Hf(1)	70.65(11)	C(17)-C(18)-C(19)	108.63(19)
C(27)-C(9)-Hf(1)	123.25(14)	C(17)-C(18)-C(34)	125.9(2)
C(9)-C(10)-C(6)	108.9(2)	C(19)-C(18)-C(34)	125.3(2)
C(9)-C(10)-C(28)	124.0(2)	C(17)-C(18)-Hf(2)	70.38(12)
C(6)-C(10)-C(28)	127.0(2)	C(19)-C(18)-Hf(2)	73.87(12)
C(9)-C(10)-Hf(1)	77.04(11)	C(34)-C(18)-Hf(2)	125.68(16)
C(6)-C(10)-Hf(1)	71.72(11)	C(18)-C(19)-C(20)	107.8(2)
C(28)-C(10)-Hf(1)	120.32(14)	C(18)-C(19)-C(35)	125.8(2)
C(12)-C(11)-C(15)	106.83(18)	C(20)-C(19)-C(35)	126.1(2)
C(12)-C(11)-C(29)	127.25(19)	C(18)-C(19)-Hf(2)	74.53(13)
C(15)-C(11)-C(29)	125.2(2)	C(20)-C(19)-Hf(2)	70.30(12)
C(12)-C(11)-Hf(2)	69.86(12)	C(35)-C(19)-Hf(2)	126.10(15)
C(15)-C(11)-Hf(2)	69.06(12)	C(19)-C(20)-C(16)	108.90(19)
C(29)-C(11)-Hf(2)	133.24(14)	C(19)-C(20)-C(36)	123.4(2)
C(11)-C(12)-C(13)	108.89(19)	C(16)-C(20)-C(36)	127.56(19)
C(11)-C(12)-Hf(2)	79.73(13)	C(19)-C(20)-Hf(2)	77.44(12)
C(13)-C(12)-Hf(2)	68.18(12)	C(16)-C(20)-Hf(2)	71.97(11)
C(12)-C(13)-C(14)	108.65(18)	C(36)-C(20)-Hf(2)	120.64(14)
C(12)-C(13)-Hf(2)	79.49(12)	C(1)-C(21)-C(24)	111.69(19)
C(14)-C(13)-Hf(2)	74.39(12)	C(1)-C(21)-C(22)	112.53(18)
C(13)-C(14)-C(15)	105.66(17)	C(24)-C(21)-C(22)	109.4(2)
C(13)-C(14)-Si(2)	125.18(16)	C(1)-C(21)-C(23)	105.86(18)
C(15)-C(14)-Si(2)	124.87(16)	C(24)-C(21)-C(23)	108.98(19)
C(13)-C(14)-Hf(2)	72.18(12)	C(22)-C(21)-C(23)	108.25(19)
C(15)-C(14)-Hf(2)	77.48(12)	C(11)-C(29)-C(30)	110.90(19)
Si(2)-C(14)-Hf(2)	97.47(9)	C(11)-C(29)-C(32)	112.77(19)
C(11)-C(15)-C(14)	109.80(19)	C(30)-C(29)-C(32)	109.4(2)
C(11)-C(15)-Hf(2)	80.25(13)	C(11)-C(29)-C(31)	107.00(18)
C(14)-C(15)-Hf(2)	69.86(12)	C(30)-C(29)-C(31)	108.6(2)
C(20)-C(16)-C(17)	106.15(18)	C(32)-C(29)-C(31)	108.0(2)
C(20)-C(16)-Si(2)	126.03(16)	N(1)-C(41)-O(1)	178.6(3)
C(17)-C(16)-Si(2)	123.67(17)	N(2)-C(42)-O(2)	179.0(4)
C(20)-C(16)-Hf(2)	74.56(11)	C(2S)-C(1S)-C(3S)#1	119.6(3)
C(17)-C(16)-Hf(2)	74.71(11)	C(3S)-C(2S)-C(1S)	120.2(3)
		C(2S)-C(3S)-C(1S)#1	120.3(3)

Symmetry transformations used to generate equivalent atoms:
#1 -x+2,-y+3,-z

Table C.14. Crystal data and structure refinement for **[7-N_2]$^-$**.

Identification code	**[7-N_2]$^-$**	
Empirical formula	C60 H90 Cl2 K N2 O2 Si2 Zr2	
Formula weight	1219.96	
Temperature	173(2) K	
Wavelength	0.71073 Å	
Crystal system	Orthorhombic	
Space group	Fdd2	
Unit cell dimensions	a = 36.721(4) Å	a= 90°.
	b = 10.7165(11) Å	b= 90°.
	c = 32.744(4) Å	g = 90°.
Volume	12885(2) Å^3	
Z	8	
Density (calculated)	1.258 Mg/m^3	
Absorption coefficient	0.547 mm^{-1}	
F(000)	5128	
Crystal size	0.10 x 0.05 x 0.03 mm^3	
Theta range for data collection	1.67 to 23.26°.	
Index ranges	-39<=h<=40, -11<=k<=11, -36<=l<=32	
Reflections collected	10445	
Independent reflections	4356 [R(int) = 0.0768]	
Completeness to theta = 23.26°	100.0 %	
Absorption correction	Semi-empirical from equivalents	
Max. and min. transmission	0.9864 and 0.9473	
Refinement method	Full-matrix least-squares on F^2	
Data / restraints / parameters	4356 / 169 / 321	

Goodness-of-fit on F^2	1.032
Final R indices [I>2sigma(I)]	R1 = 0.0602, wR2 = 0.1347
R indices (all data)	R1 = 0.0800, wR2 = 0.1454
Absolute structure parameter	-0.09(8)
Largest diff. peak and hole	0.730 and -0.382 e.$Å^{-3}$

Table C.15. Atomic coordinates (x 10^4) and equivalent isotropic displacement parameters (Å^{2}x 10^3) for **[7-N_2]$^-$**. U(eq) is defined as one third of the trace of the orthogonalized U^{ij} tensor.

	x	y	z	U(eq)
Zr(1)	664(1)	5896(1)	4174(1)	26(1)
Cl(1)	705(1)	6455(2)	4923(1)	37(1)
Si(1)	1144(1)	6002(2)	3324(1)	36(1)
K(1)	0	5000	5070(1)	41(1)
N(1)	157(1)	5208(4)	4206(2)	21(1)
C(1)	1127(2)	4813(7)	3745(2)	36(2)
C(2)	841(2)	3953(6)	3818(2)	34(2)
C(3)	858(2)	3586(6)	4233(2)	33(2)
C(4)	1148(2)	4189(7)	4413(2)	36(2)
C(5)	1309(2)	4964(6)	4122(2)	35(2)
C(6)	852(2)	7199(6)	3578(2)	34(2)
C(7)	458(2)	7197(6)	3592(2)	28(2)
C(8)	339(2)	7908(6)	3927(2)	33(2)
C(9)	660(2)	8370(5)	4128(2)	35(2)
C(10)	966(2)	7924(7)	3925(2)	39(2)
C(11)	206(2)	6629(7)	3279(2)	40(2)
C(12)	-50(2)	8199(7)	4032(3)	50(2)
C(13)	658(2)	9275(7)	4492(3)	48(2)
C(14)	1347(2)	8278(7)	4059(2)	45(2)
C(15)	951(2)	5393(8)	2848(2)	49(2)
C(16)	1617(2)	6492(8)	3216(3)	59(3)
C(17)	1267(2)	3930(7)	4866(3)	60(2)
C(18)	1262(2)	2520(8)	4987(2)	77(2)
C(19)	1322(3)	2454(11)	5441(3)	102(3)
C(20)	1681(2)	3011(8)	5563(3)	88(3)
C(21)	1948(3)	2225(12)	5342(3)	121(3)
C(22)	1939(3)	2454(8)	4883(3)	102(3)
C(23)	1931(3)	3812(8)	4783(4)	95(3)
C(24)	1628(2)	4475(9)	4984(2)	78(3)
C(25)	1669(4)	4353(8)	5441(3)	106(3)
C(26)	1587(3)	1849(8)	4794(4)	104(3)
O(1S)	347(2)	3594(5)	5680(2)	54(2)
C(1S)	180(3)	1786(9)	5272(3)	80(4)
C(2S)	278(3)	2256(8)	5718(4)	81(4)
C(3S)	480(3)	4059(8)	6058(3)	72(3)
C(4S)	576(3)	5415(9)	5995(3)	74(3)

Table C.16. Bond lengths [Å] and angles [°] for **[7-N_2]$^-$**.

Zr(1)-N(1)	2.007(4)	C(19)-C(20)	1.501(10)
Zr(1)-C(2)	2.473(7)	C(20)-C(21)	1.482(11)
Zr(1)-C(7)	2.481(7)	C(20)-C(25)	1.494(10)
Zr(1)-C(1)	2.493(7)	C(21)-C(22)	1.522(11)
Zr(1)-C(6)	2.499(7)	C(22)-C(26)	1.475(10)
Zr(1)-Cl(1)	2.5270(19)	C(22)-C(23)	1.492(10)
Zr(1)-C(10)	2.572(7)	C(23)-C(24)	1.476(10)
Zr(1)-C(5)	2.576(6)	C(24)-C(25)	1.508(10)
Zr(1)-C(3)	2.583(6)	O(1S)-C(3S)	1.420(10)
Zr(1)-C(8)	2.594(7)	O(1S)-C(2S)	1.461(10)
Zr(1)-C(9)	2.656(6)	C(1S)-C(2S)	1.586(14)
Zr(1)-C(4)	2.667(7)	C(3S)-C(4S)	1.508(12)
Cl(1)-K(1)	3.0596(19)		
Si(1)-C(15)	1.832(8)	N(1)-Zr(1)-C(2)	87.6(2)
Si(1)-C(16)	1.850(8)	N(1)-Zr(1)-C(7)	87.9(2)
Si(1)-C(6)	1.867(8)	C(2)-Zr(1)-C(7)	101.0(2)
Si(1)-C(1)	1.878(7)	N(1)-Zr(1)-C(1)	119.4(2)
K(1)-O(1S)	2.808(6)	C(2)-Zr(1)-C(1)	33.2(2)
K(1)-O(1S)#1	2.808(6)	C(7)-Zr(1)-C(1)	92.0(2)
K(1)-N(1)	2.895(6)	N(1)-Zr(1)-C(6)	120.2(2)
K(1)-N(1)#1	2.895(6)	C(2)-Zr(1)-C(6)	91.7(2)
K(1)-Cl(1)#1	3.0597(19)	C(7)-Zr(1)-C(6)	33.8(2)
K(1)-Zr(1)#1	3.9337(19)	C(1)-Zr(1)-C(6)	68.3(2)
N(1)-N(1)#1	1.233(9)	N(1)-Zr(1)-Cl(1)	95.25(16)
C(1)-C(2)	1.417(10)	C(2)-Zr(1)-Cl(1)	129.89(17)
C(1)-C(5)	1.415(10)	C(7)-Zr(1)-Cl(1)	129.07(17)
C(2)-C(3)	1.417(10)	C(1)-Zr(1)-Cl(1)	128.12(17)
C(3)-C(4)	1.376(10)	C(6)-Zr(1)-Cl(1)	127.54(17)
C(4)-C(5)	1.396(10)	N(1)-Zr(1)-C(10)	136.6(2)
C(4)-C(17)	1.571(10)	C(2)-Zr(1)-C(10)	116.6(2)
C(6)-C(10)	1.438(10)	C(7)-Zr(1)-C(10)	54.0(2)
C(6)-C(7)	1.448(10)	C(1)-Zr(1)-C(10)	85.4(2)
C(7)-C(8)	1.405(10)	C(6)-Zr(1)-C(10)	32.9(2)
C(7)-C(11)	1.510(10)	Cl(1)-Zr(1)-C(10)	94.73(18)
C(8)-C(9)	1.439(10)	N(1)-Zr(1)-C(5)	135.6(2)
C(8)-C(12)	1.500(10)	C(2)-Zr(1)-C(5)	53.2(2)
C(9)-C(10)	1.391(10)	C(7)-Zr(1)-C(5)	116.6(2)
C(9)-C(13)	1.535(10)	C(1)-Zr(1)-C(5)	32.4(2)
C(10)-C(14)	1.517(10)	C(6)-Zr(1)-C(5)	84.9(2)
C(17)-C(24)	1.499(10)	Cl(1)-Zr(1)-C(5)	95.85(18)
C(17)-C(18)	1.563(9)	C(10)-Zr(1)-C(5)	84.9(2)
C(18)-C(19)	1.505(10)	N(1)-Zr(1)-C(3)	84.27(19)
C(18)-C(26)	1.533(10)	C(2)-Zr(1)-C(3)	32.5(2)

Table C.16. (continued)

C(7)-Zr(1)-C(3)	132.9(2)	O(1S)-K(1)-O(1S)#1	89.4(2)
C(1)-Zr(1)-C(3)	53.7(2)	O(1S)-K(1)-N(1)	130.23(15)
C(6)-Zr(1)-C(3)	121.2(2)	O(1S)#1-K(1)-N(1)	138.04(15)
Cl(1)-Zr(1)-C(3)	97.95(18)	O(1S)-K(1)-N(1)#1	138.04(14)
C(10)-Zr(1)-C(3)	135.6(2)	O(1S)#1-K(1)-N(1)#1	130.23(15)
C(5)-Zr(1)-C(3)	51.7(2)	N(1)-K(1)-N(1)#1	24.58(18)
N(1)-Zr(1)-C(8)	83.9(2)	O(1S)-K(1)-Cl(1)	90.09(12)
C(2)-Zr(1)-C(8)	132.3(2)	O(1S)#1-K(1)-Cl(1)	102.88(12)
C(7)-Zr(1)-C(8)	32.0(2)	N(1)-K(1)-Cl(1)	68.82(10)
C(1)-Zr(1)-C(8)	121.6(2)	N(1)#1-K(1)-Cl(1)	93.03(11)
C(6)-Zr(1)-C(8)	54.5(2)	O(1S)-K(1)-Cl(1)#1	102.88(12)
Cl(1)-Zr(1)-C(8)	97.66(17)	O(1S)#1-K(1)-Cl(1)#1	90.09(12)
C(10)-Zr(1)-C(8)	52.9(2)	N(1)-K(1)-Cl(1)#1	93.03(11)
C(5)-Zr(1)-C(8)	136.5(2)	N(1)#1-K(1)-Cl(1)#1	68.82(10)
C(3)-Zr(1)-C(8)	161.2(2)	Cl(1)-K(1)-Cl(1)#1	161.84(11)
N(1)-Zr(1)-C(9)	111.4(2)	O(1S)-K(1)-Zr(1)	112.31(12)
C(2)-Zr(1)-C(9)	144.6(2)	O(1S)#1-K(1)-Zr(1)	132.91(11)
C(7)-Zr(1)-C(9)	52.6(2)	N(1)-K(1)-Zr(1)	29.49(9)
C(1)-Zr(1)-C(9)	115.9(2)	N(1)#1-K(1)-Zr(1)	54.07(9)
C(6)-Zr(1)-C(9)	53.1(2)	Cl(1)-K(1)-Zr(1)	39.96(4)
Cl(1)-Zr(1)-C(9)	79.58(18)	Cl(1)#1-K(1)-Zr(1)	122.08(7)
C(10)-Zr(1)-C(9)	30.8(2)	O(1S)-K(1)-Zr(1)#1	132.90(11)
C(5)-Zr(1)-C(9)	112.9(2)	O(1S)#1-K(1)-Zr(1)#1	112.31(12)
C(3)-Zr(1)-C(9)	164.3(2)	N(1)-K(1)-Zr(1)#1	54.07(9)
C(8)-Zr(1)-C(9)	31.8(2)	N(1)#1-K(1)-Zr(1)#1	29.49(9)
N(1)-Zr(1)-C(4)	110.5(2)	Cl(1)-K(1)-Zr(1)#1	122.07(7)
C(2)-Zr(1)-C(4)	52.1(2)	Cl(1)#1-K(1)-Zr(1)#1	39.96(4)
C(7)-Zr(1)-C(4)	144.5(2)	Zr(1)-K(1)-Zr(1)#1	83.56(5)
C(1)-Zr(1)-C(4)	52.6(2)	N(1)#1-N(1)-Zr(1)	176.99(17)
C(6)-Zr(1)-C(4)	115.4(2)	N(1)#1-N(1)-K(1)	77.71(9)
Cl(1)-Zr(1)-C(4)	80.73(16)	Zr(1)-N(1)-K(1)	105.27(19)
C(10)-Zr(1)-C(4)	112.7(2)	C(2)-C(1)-C(5)	106.0(6)
C(5)-Zr(1)-C(4)	30.8(2)	C(2)-C(1)-Si(1)	126.2(6)
C(3)-Zr(1)-C(4)	30.3(2)	C(5)-C(1)-Si(1)	123.2(5)
C(8)-Zr(1)-C(4)	165.5(2)	C(2)-C(1)-Zr(1)	72.7(4)
C(9)-Zr(1)-C(4)	134.9(2)	C(5)-C(1)-Zr(1)	77.1(4)
Zr(1)-Cl(1)-K(1)	88.99(7)	Si(1)-C(1)-Zr(1)	96.9(3)
C(15)-Si(1)-C(16)	107.6(4)	C(3)-C(2)-C(1)	108.1(6)
C(15)-Si(1)-C(6)	113.7(4)	C(3)-C(2)-Zr(1)	78.0(4)
C(16)-Si(1)-C(6)	115.4(4)	C(1)-C(2)-Zr(1)	74.2(4)
C(15)-Si(1)-C(1)	111.7(3)	C(4)-C(3)-C(2)	108.4(6)
C(16)-Si(1)-C(1)	111.3(4)	C(4)-C(3)-Zr(1)	78.2(4)
C(6)-Si(1)-C(1)	96.9(3)	C(2)-C(3)-Zr(1)	69.5(4)

Table C.16. (continued)

C(3)-C(4)-C(5)	108.4(6)	C(13)-C(9)-Zr(1)	125.9(5)
C(3)-C(4)-C(17)	122.5(7)	C(9)-C(10)-C(6)	109.3(6)
C(5)-C(4)-C(17)	129.1(7)	C(9)-C(10)-C(14)	121.4(7)
C(3)-C(4)-Zr(1)	71.5(4)	C(6)-C(10)-C(14)	129.2(7)
C(5)-C(4)-Zr(1)	71.0(4)	C(9)-C(10)-Zr(1)	77.9(4)
C(17)-C(4)-Zr(1)	125.7(5)	C(6)-C(10)-Zr(1)	70.8(4)
C(4)-C(5)-C(1)	109.1(6)	C(14)-C(10)-Zr(1)	121.1(5)
C(4)-C(5)-Zr(1)	78.2(4)	C(24)-C(17)-C(4)	114.9(7)
C(1)-C(5)-Zr(1)	70.6(4)	C(24)-C(17)-C(18)	108.8(7)
C(10)-C(6)-C(7)	105.3(6)	C(4)-C(17)-C(18)	114.0(6)
C(10)-C(6)-Si(1)	123.8(5)	C(19)-C(18)-C(26)	105.7(8)
C(7)-C(6)-Si(1)	125.9(5)	C(19)-C(18)-C(17)	107.1(8)
C(10)-C(6)-Zr(1)	76.3(4)	C(26)-C(18)-C(17)	109.8(7)
C(7)-C(6)-Zr(1)	72.4(4)	C(18)-C(19)-C(20)	112.0(8)
Si(1)-C(6)-Zr(1)	97.0(3)	C(21)-C(20)-C(25)	115.9(10)
C(8)-C(7)-C(6)	109.6(6)	C(21)-C(20)-C(19)	103.0(9)
C(8)-C(7)-C(11)	123.8(6)	C(25)-C(20)-C(19)	106.5(8)
C(6)-C(7)-C(11)	126.3(6)	C(20)-C(21)-C(22)	112.2(9)
C(8)-C(7)-Zr(1)	78.4(4)	C(26)-C(22)-C(23)	111.5(8)
C(6)-C(7)-Zr(1)	73.8(4)	C(26)-C(22)-C(21)	98.3(9)
C(11)-C(7)-Zr(1)	118.8(4)	C(23)-C(22)-C(21)	112.0(9)
C(7)-C(8)-C(9)	106.8(6)	C(24)-C(23)-C(22)	112.8(8)
C(7)-C(8)-C(12)	126.0(7)	C(23)-C(24)-C(17)	111.3(8)
C(9)-C(8)-C(12)	127.1(7)	C(23)-C(24)-C(25)	109.0(8)
C(7)-C(8)-Zr(1)	69.5(4)	C(17)-C(24)-C(25)	108.1(8)
C(9)-C(8)-Zr(1)	76.5(4)	C(20)-C(25)-C(24)	110.7(8)
C(12)-C(8)-Zr(1)	122.6(5)	C(22)-C(26)-C(18)	113.3(8)
C(10)-C(9)-C(8)	108.9(6)	C(3S)-O(1S)-C(2S)	109.3(7)
C(10)-C(9)-C(13)	126.3(7)	C(3S)-O(1S)-K(1)	125.9(5)
C(8)-C(9)-C(13)	124.7(7)	C(2S)-O(1S)-K(1)	120.5(5)
C(10)-C(9)-Zr(1)	71.3(4)	O(1S)-C(2S)-C(1S)	105.8(8)
C(8)-C(9)-Zr(1)	71.7(3)	O(1S)-C(3S)-C(4S)	107.5(7)

Symmetry transformations used to generate equivalent atoms:
#1 -x,-y+1,z

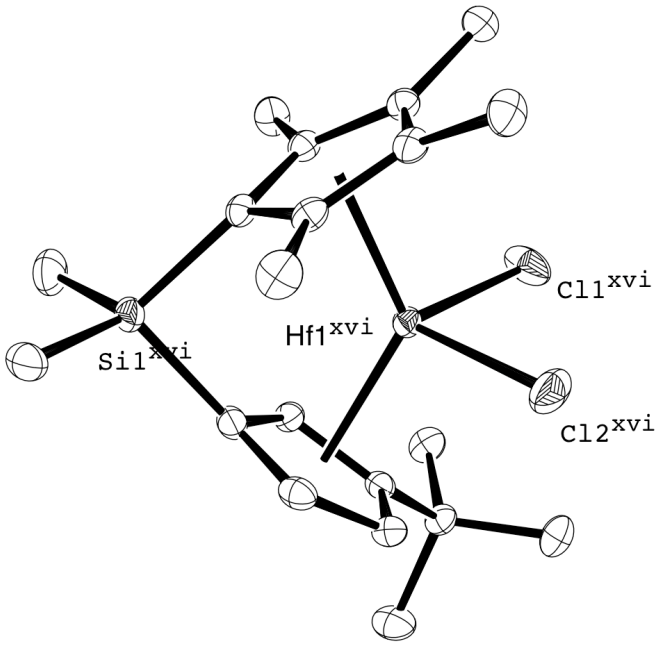

Figure C.1. Molecular structure of the (*R*,*R*) enantiomer of **4-Cl$_2$** at 30% probability ellipsoids. Hydrogen atoms omitted for clarity.

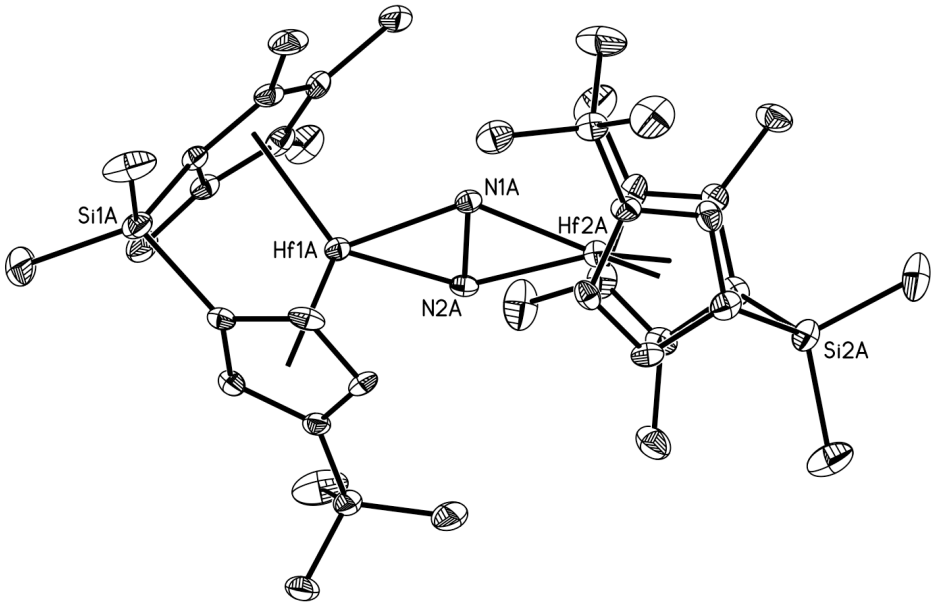

Figure C.2. Molecular structure of the (*R*,*R*) enantiomer of **4-N$_2$** at 30% probability ellipsoids. Hydrogen atoms omitted for clarity.

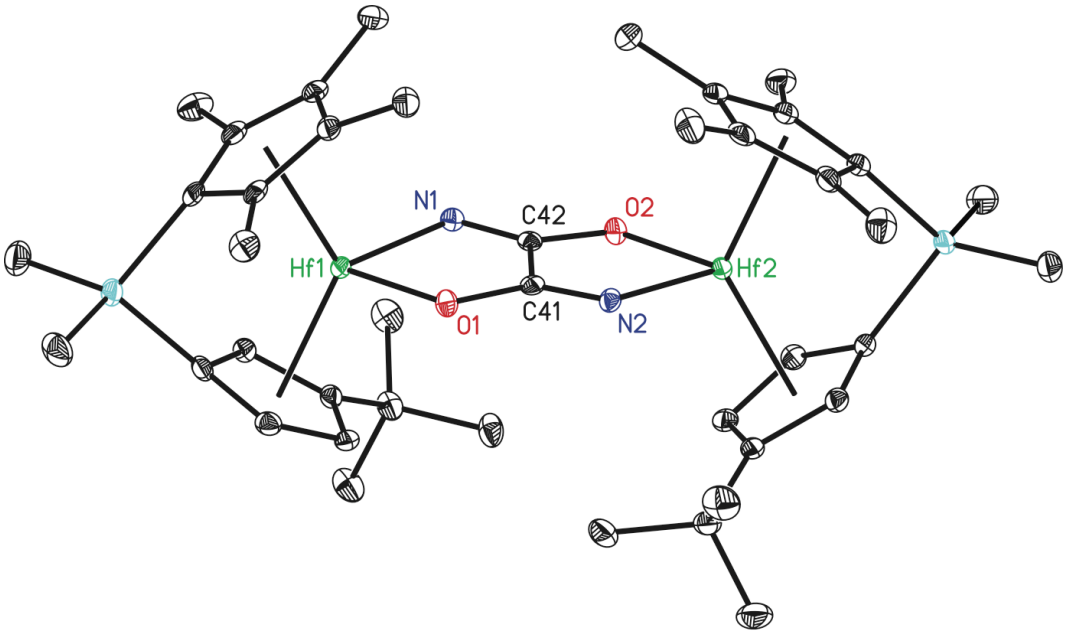

Figure C.3. Molecular structure of the (*R*,*R*) enantiomer of **4-$N_2C_2O_2$-*C_2*** at 30% probability ellipsoids. Hydrogen atoms omitted for clarity.

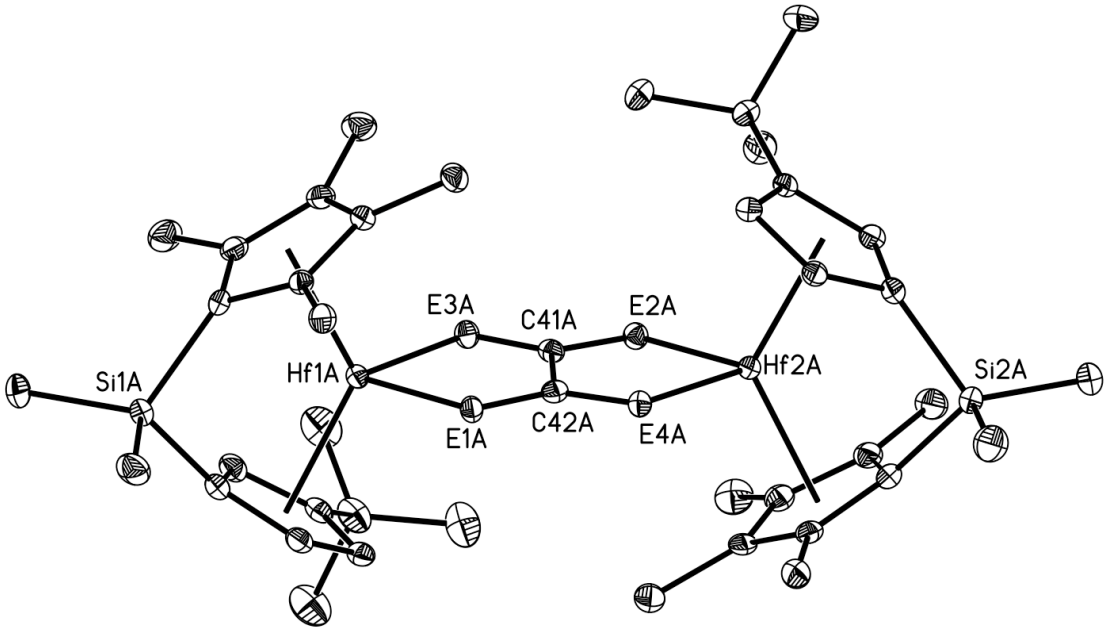

Figure C.4. Molecular structure of the (*R*,*R*) enantiomer of **4-$N_2C_2O_2$-*C_1*** at 30% probability ellipsoids. Hydrogen atoms omitted for clarity.

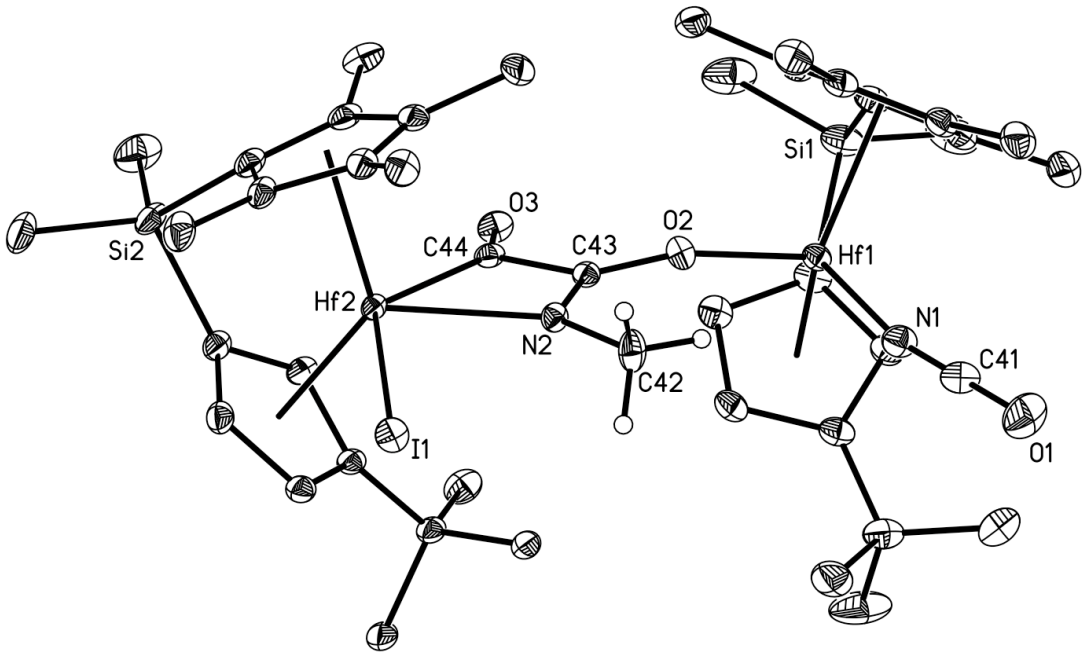

Figure C.5. Molecular structure of the (*R*,*R*) enantiomer of **5** (Ch. 1) at 30% probability ellipsoids. Hydrogen atoms (except N-CH_3 hydrogens) omitted for clarity.

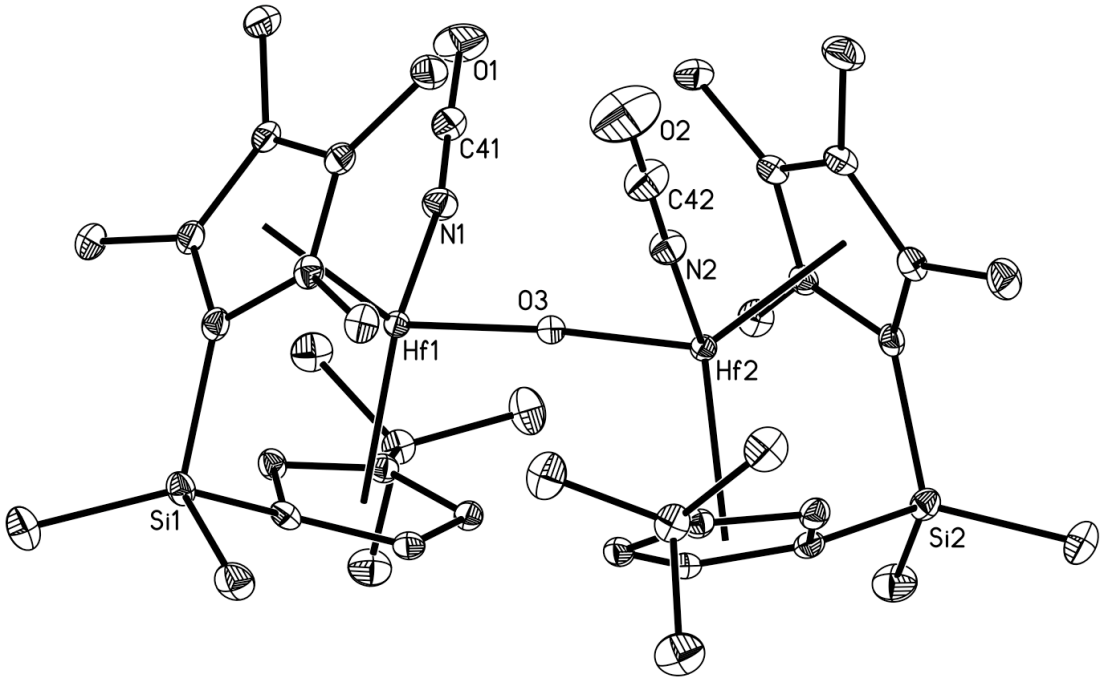

Figure C.6. Molecular structure of the (*R*,*R*) enantiomer of **4-(μ-O)(NCO)$_2$** at 30% probability ellipsoids. Hydrogen atoms omitted for clarity.

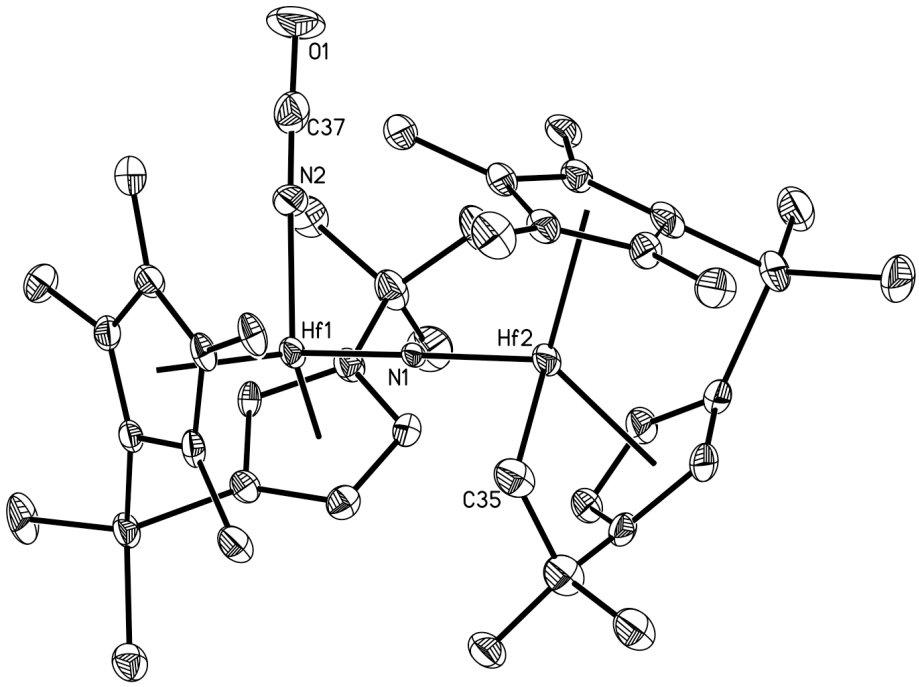

Figure C.7. Molecular structure of the (*R*,*R*) enantiomer of **5** (Ch. 2) at 30% probability ellipsoids. Hydrogen atoms omitted for clarity.

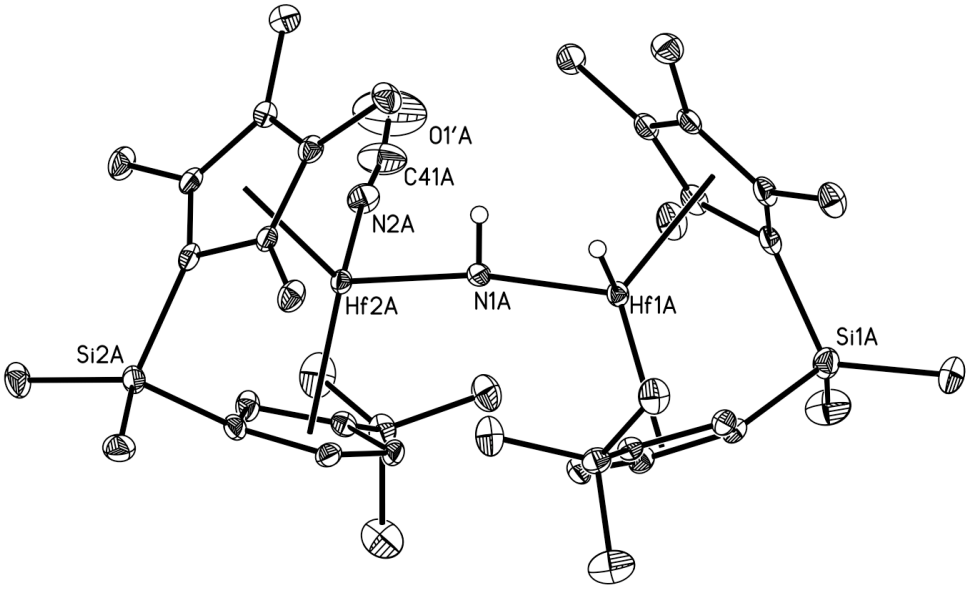

Figure C.8. Molecular structure of the (*R*,*R*) enantiomer of **4-(μ-NH)(H)(NCO)** at 30% probability ellipsoids. Hydrogen atoms (except Hf-H and N-H) omitted for clarity.

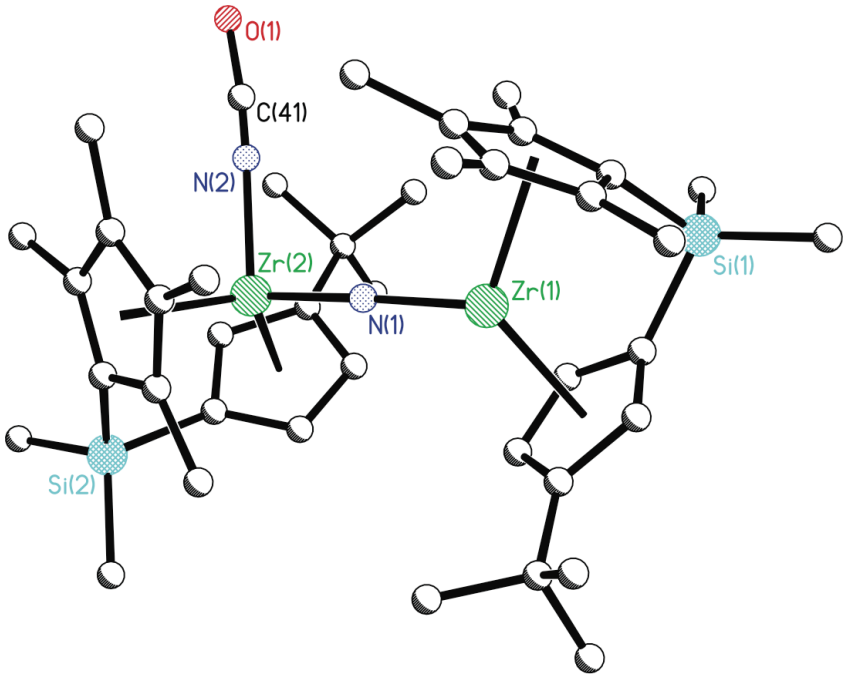

Figure C.9. Structural representation of the (*R*,*R*) enantiomer of **3-(μ-NH)(H)(NCO)**. Hydrogen atoms omitted for clarity.

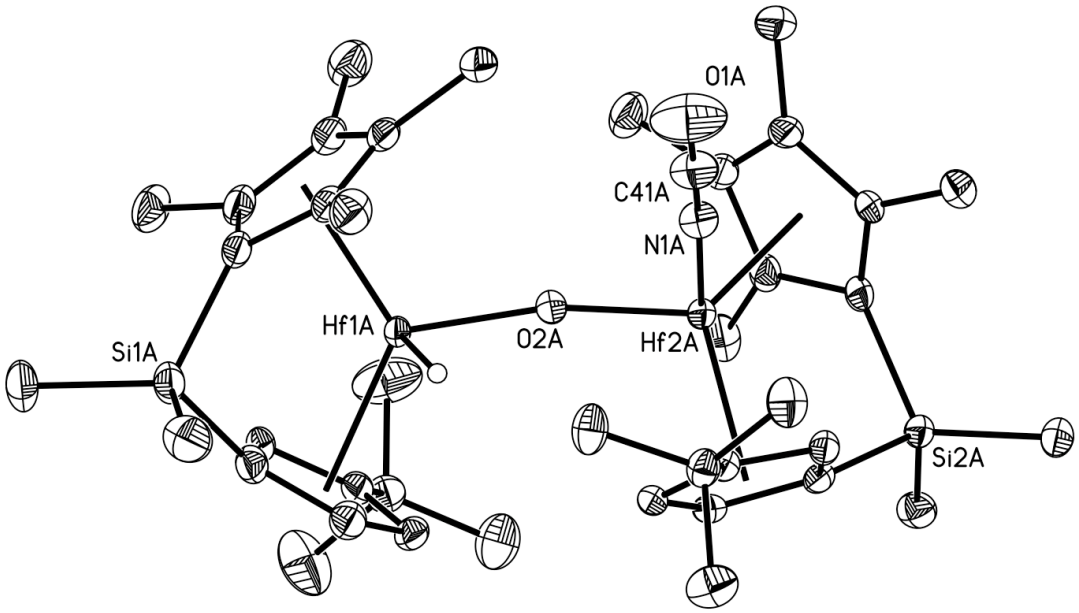

Figure C.10. Molecular structure of the (*R*,*R*) enantiomer of **4-(μ-O)(H)(NCO)** at 30% probability ellipsoids. Hydrogen atoms (except Hf-H) omitted for clarity.

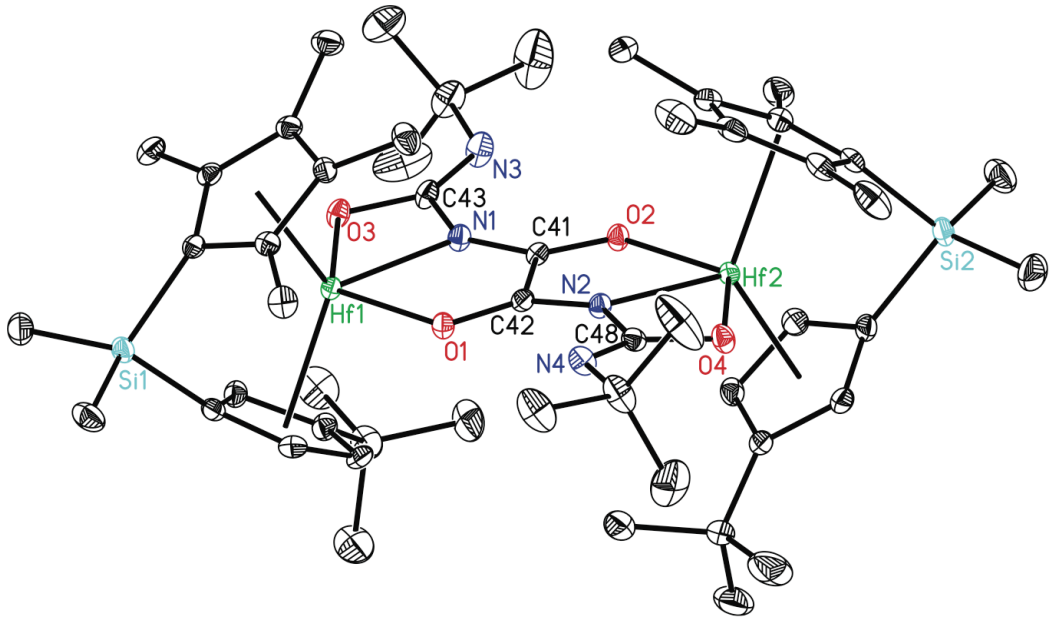

Figure C.11. Molecular structure of the (*R*,*R*) enantiomer of **4-(^{t}BuNCO)$_2$** at 30% probability ellipsoids. Hydrogen atoms omitted for clarity.

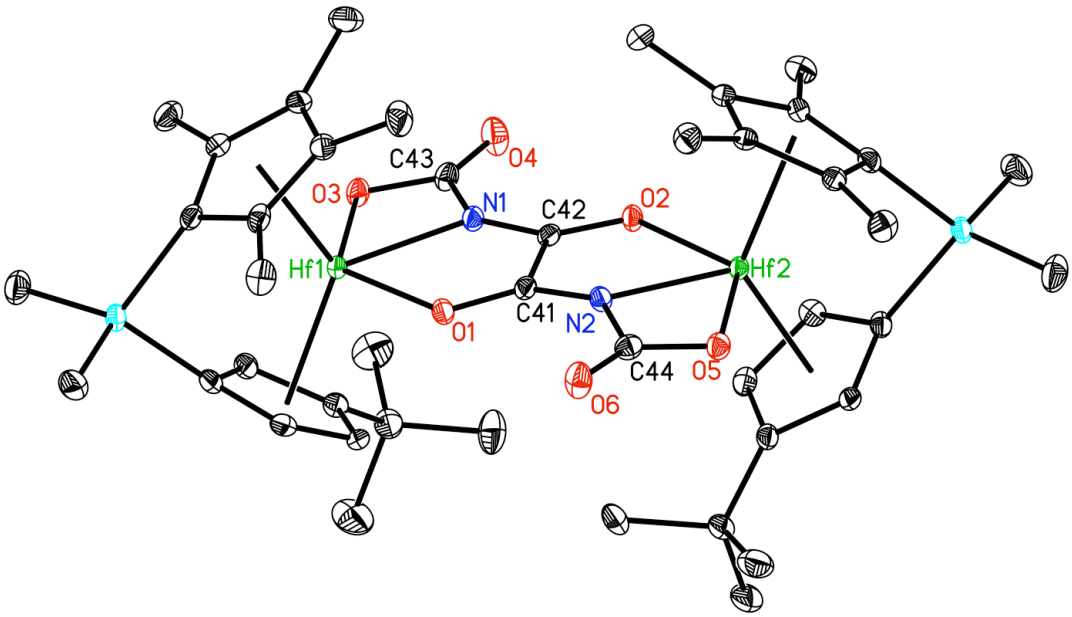

Figure C.12. Molecular structure of the (*R*,*R*) enantiomer of **4-(CO$_2$)$_2$** at 30% probability ellipsoids. Hydrogen atoms omitted for clarity.

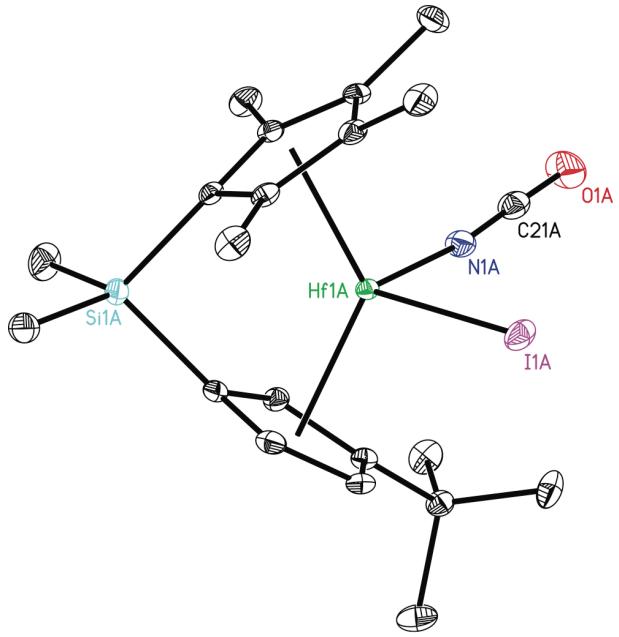

Figure C.13. Molecular structure of the (*R*) enantiomer of **4-(I)(NCO)** at 30% probability ellipsoids. Hydrogen atoms omitted for clarity.

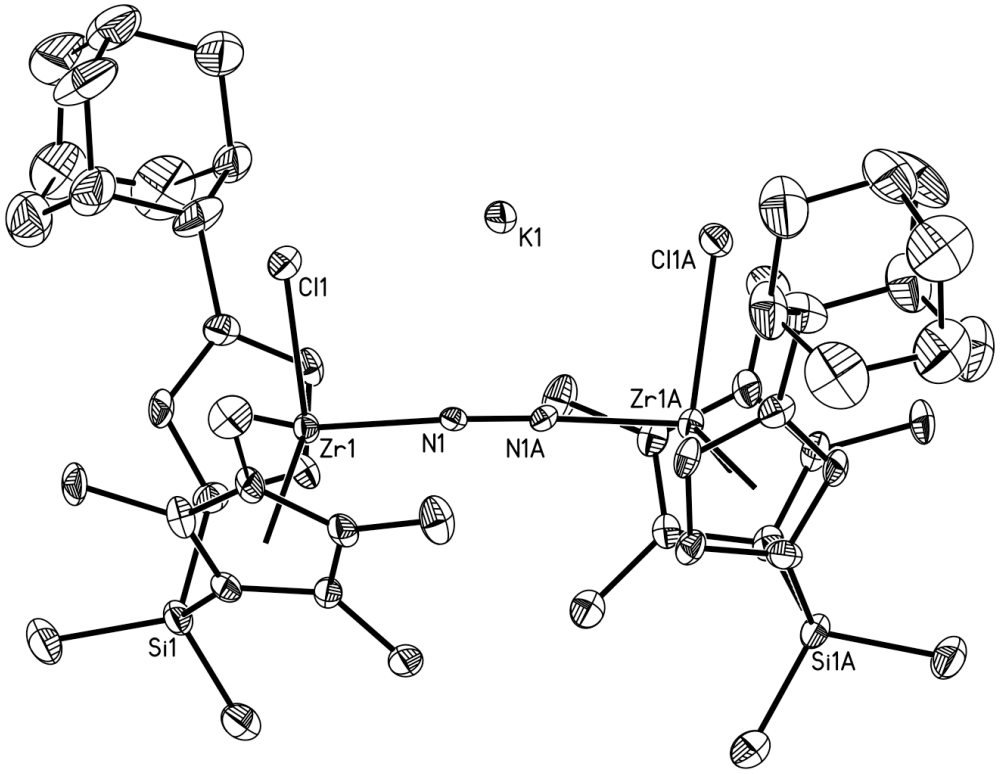

Figure C.14. Molecular structure of the (*R*,*R*) enantiomer of $[\mathbf{7\text{-}N_2}]^-$ at 30% probability ellipsoids. Hydrogen atoms and chelated solvent atoms omitted for clarity.